NASA/TM-2000-210300

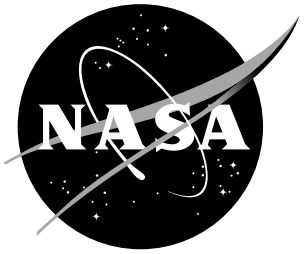

Static Performance of Six Innovative Thrust Reverser Concepts for Subsonic Transport Applications

Summary of the NASA Langley Innovative Thrust Reverser Test Program

Scott C. Asbury and Jeffrey A. Yetter
Langley Research Center, Hampton, Virginia

July 2000

The NASA STI Program Office ... in Profile

Since its founding, NASA has been dedicated to the advancement of aeronautics and space science. The NASA Scientific and Technical Information (STI) Program Office plays a key part in helping NASA maintain this important role.

The NASA STI Program Office is operated by Langley Research Center, the lead center for NASA's scientific and technical information. The NASA STI Program Office provides access to the NASA STI Database, the largest collection of aeronautical and space science STI in the world. The Program Office is also NASA's institutional mechanism for disseminating the results of its research and development activities. These results are published by NASA in the NASA STI Report Series, which includes the following report types:

- TECHNICAL PUBLICATION. Reports of completed research or a major significant phase of research that present the results of NASA programs and include extensive data or theoretical analysis. Includes compilations of significant scientific and technical data and information deemed to be of continuing reference value. NASA counter-part of peer reviewed formal professional papers, but having less stringent limitations on manuscript length and extent of graphic presentations.

- TECHNICAL MEMORANDUM. Scientific and technical findings that are preliminary or of specialized interest, e.g., quick release reports, working papers, and bibliographies that contain minimal annotation. Does not contain extensive analysis.

- CONTRACTOR REPORT. Scientific and technical findings by NASA-sponsored contractors and grantees.

- CONFERENCE PUBLICATION. Collected papers from scientific and technical conferences, symposia, seminars, or other meetings sponsored or co-sponsored by NASA.

- SPECIAL PUBLICATION. Scientific, technical, or historical information from NASA programs, projects, and missions, often concerned with subjects having substantial public interest.

- TECHNICAL TRANSLATION. English-language translations of foreign scientific and technical material pertinent to NASA's mission.

Specialized services that help round out the STI Program Office's diverse offerings include creating custom thesauri, building customized databases, organizing and publishing research results ... even providing videos.

For more information about the NASA STI Program Office, see the following:

- Access the NASA STI Program Home Page at ***http://www.sti.nasa.gov***

- E-mail your question via the Internet to help@sti.nasa.gov

- Fax your question to the NASA Access Help Desk at (301) 621-0134

- Phone the NASA Access Help Desk at (301) 621-0390

- Write to:
  NASA Access Help Desk
  NASA Center for AeroSpace Information
  7121 Standard Drive
  Hanover, MD 21076-1320

NASA/TM-2000-210300

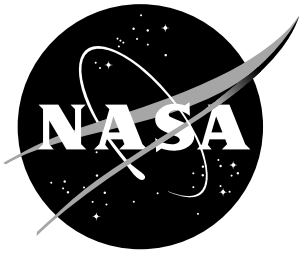

Static Performance of Six Innovative Thrust Reverser Concepts for Subsonic Transport Applications

Summary of the NASA Langley Innovative Thrust Reverser Test Program

Scott C. Asbury and Jeffrey A. Yetter
Langley Research Center, Hampton, Virginia

National Aeronautics and
Space Administration

Langley Research Center
Hampton, Virginia 23681-2199

July 2000

The use of trademarks or names of manufacturers in the report is for accurate reporting and does not constitute an official endorsement, either expressed or implied, of such products or manufacturers by the National Aeronautics and Space Administration.

Available from:

NASA Center for AeroSpace Information (CASI)
7121 Standard Drive
Hanover. MD 21076-1320
(301) 621-0390

National Technical Information Service (NTIS)
5285 Port Royal Road
Springfield, VA 22161-2171
(703) 605-6000

Abstract

The NASA Langley Configuration Aerodynamics Branch, in cooperation with Allison, BF Goodrich Aerospace, Boeing, General Electric, Northrop-Grumman, Pratt & Whitney, and Rolls-Royce, has completed an experimental investigation to study the static aerodynamic performance of innovative thrust reverser concepts applicable to high-bypass-ratio turbofan engines. Testing was conducted on a conventional separate-flow exhaust system configuration (forward thrust baseline), a conventional cascade thrust reverser configuration (reverse thrust baseline), and six innovative thrust reverser configurations. The innovative thrust reverser configurations tested consisted of a cascade thrust reverser with porous fan-duct blocker, a blockerless thrust reverser, two core-mounted target thrust reversers, a multi-door crocodile thrust reverser, and a wing-mounted thrust reverser. Each of the innovative thrust reverser concepts investigated offer potential weight savings and/or design simplifications over a conventional cascade thrust reverser design. Testing was conducted in the Jet-Exit Test Facility at NASA Langley Research Center using a 7.9%-scale exhaust system model with a fan-to-core bypass ratio of approximately 9.0. All tests were conducted with no external flow and cold, high-pressure air was used to simulate core and fan exhaust flows. Results show that the innovative thrust reverser concepts achieved thrust reverser performance levels which, when taking into account the potential for system simplification and reduced weight, may make them competitive with, or potentially more cost effective than current state-of-the-art thrust reverser systems.

Introduction

Although used for only a fraction of airplane operating time, the impact of thrust reverser systems on commercial aircraft nacelle design, weight, engine maintenance, airplane cruise performance, and overall operating and maintenance costs is significant. For example, the weight of a conventional cascade thrust reverser system installed in a bypass ratio (BPR) 9 engine nacelle is approximately 1,500 pounds per engine. During cruise flight, losses due to flow leakage and pressure drops across stowed reverser hardware are estimated to reduce specific fuel consumption by 0.5% to 1.0%. Furthermore, the amortized cost of a thrust reverser system on a 767 aircraft is approximately $125,000 per airplane per year (ref. 1).

While their penalties may be significant, thrust reverser systems remain a necessary commodity for most commercial aircraft. This is because thrust reverser systems provide additional stopping force, added safety margins, and increased directional control during landing rolls, rejected takeoffs, and ground operations on contaminated runways where wheel braking effectiveness is diminished. In fact, airlines consider thrust reverser systems essential to achieving the maximum level of aircraft operating safety (ref. 1).

The conventional cascade thrust reverser is commonly used on commercial aircraft equipped with high-bypass-ratio (5<BPR<9) turbofan engines. Cascade thrust reversers are known for their high degree of structural integrity, reliability, and their tolerance to various aircraft applications. Cascade thrust reversers are typically used to block engine fan flow (the fan accounts for approximately 80% of engine thrust for a BPR 9 engine) to produce reverse thrust. Cascade thrust reversers can also be used to block engine core flow; however, such applications are rare due to operation and maintenance difficulties associated with a cascade thrust reverser operating in a hot core exhaust environment. As illustrated in figure 1, the cascade thrust reverser uses blocker doors, actuated by the motion of a translating sleeve, to block the engine fan flow. The sleeve translates aft to expose cascade vanes (mounted around the perimeter of the engine nacelle) that redirect the engine fan flow forward to produce reverse thrust. Photographs of a conventional cascade thrust reverser installed on the NASA 757-200 aircraft are presented in figure 2.

In response to demands for increased thrust levels and/or higher propulsive efficiency, the current trend in engine design is progressing towards very-high-bypass-ratios (BPR on the order of 12 to 15). Designers are faced with the reality that conventional cascade thrust reversers may become exceedingly heavy and difficult to integrate into nacelles housing such large engines. The interest in innovative thrust reverser systems is based on the premise that high thrust reverser effectiveness levels may not be required with very-high-bypass-ratio engines to achieve the necessary aircraft stopping force. This is because a substantial amount of the aircraft stopping force is achieved from the ram drag of the large engine nacelles when the thrust is spoiled. In light of this, there is tremendous incentive to investigate the potential for simpler, lighter weight thrust reverser systems.

In response to a challenge from industry to provide a "technology injection" to thrust reverser design, the NASA Langley Configuration Aerodynamics Branch conducted a cooperative test program with industry to investigate innovative thrust reverser concepts that offer potential weight savings and/or design simplifications over conventional cascade thrust reverser systems. Industry partners in this test program included Allison, BF Goodrich Aerospace, Boeing, General Electric, Northrop-Grumman, Pratt & Whitney, and Rolls-Royce. Candidate thrust reverser concepts for the NASA Innovative Thrust Reverser Test Program were proposed with industry partners. Six of the most promising concepts, presented in figure 3, were downselected for testing. The concepts tested consisted of a cascade thrust reverser with porous fan-duct blocker, a blockerless thrust reverser, two core-mounted target thrust reversers, a multi-door crocodile thrust reverser, and a wing-mounted thrust reverser. These innovative concepts attempt to simplify thrust reverser design, reduce weight, and/or improve overall propulsion system performance by eliminating some of the mechanisms and nacelle design compromises that cause engine performance losses during cruise operation. These loss mechanisms include leakage, blocker scrubbing drag, linkage complexities and weight associated with the cascades, translating sleeve, blocker doors, etc.

The cascade thrust reverser with porous blocker is intended to simulate a blocker concept that would be lightweight, yet still spoil the thrust of the flow which leaks through the porous blocker door. The blockerless thrust reverser offers additional weight savings by eliminating the blocker doors and replacing them with diverter jets (powered by core bleed air) to block the engine fan flow. The annular (metal) target thrust reverser relocates the reverser hardware to the core cowl, offering potential reductions in reverser and nacelle weight while allowing the nacelle lines to be optimized for cruise aerodynamics. The fabric target thrust reverser is also core-mounted, but offers additional weight savings by utilizing a lightweight fabric target. Each of the core-mounted thrust reverser concepts utilize a post-exit target that deploys out of the core cowl to capture the fan flow and redirect it forward to produce reverse thrust. The multi-door crocodile thrust reverser has a set of inner and outer fan-cowl mounted doors, hinged at the door trailing edge, that rotate to block the fan duct and redirect the fan flow forward to produce reverse thrust. The wing-mounted thrust reverser uses one or more flow deflectors deployed from the wing to capture and reverse the engine exhaust flow. By removing the thrust reverser system from the nacelle, the wing-mounted thrust reverser concept offers the nacelle designer more options for improving nacelle aerodynamics and propulsion-airframe integration, simplifying nacelle structural designs, reducing nacelle weight, and improving engine maintenance access.

No attempt has been made to address the practicality of these thrust reverser concepts in regards to mechanical complexity (such as actuation linkages and kinematics, structural/thermal considerations, and integration with the airframe and aircraft/engine systems) other than to acknowledge that these issues do exist and represent challenges to the successful implementation of these concepts.

The purpose of this report is to document the results from testing each of the six innovative thrust

reverser concepts. Parametric variations of key design parameters were investigated for each concept. The cascade thrust reverser configurations included conventional blocker mechanisms with varying leakage and innovative blockers with up to 50% porosity. Geometric variations for the blockerless thrust reverser included diverter jet type, number, location, size, and angle. Coanda flow turning surfaces were also tested in lieu of the cascade vanes for the blockerless thrust reverser concept. Parametric variables for the annular (metal) target thrust reverser included target angle, target to nozzle exit spacing (reverser flow area) and a target kicker plate. The fabric target thrust reverser design variables included the nominal target angle and fabric length. The multi-door crocodile thrust reverser design variables included reverser port size, door deployment angle, outer door cutback (size), kicker plates, fences, bullnose radius, and axial leakage. The wing-mounted thrust reverser design variables included flow deflector angles and chord length, optional deflector fences, and the mount angle of the deflector system (normal to the engine centerline or parallel to the trailing edge of the wing).

Symbols

All forces and moments are referred to the model centerline (body axis). The model (balance) moment reference center was located at model station 5.500. A discussion of the data reduction procedure, definitions of force and moment terms, and propulsion relationships used herein can be found in reference 2.

A_{core} core nozzle throat area, 6.76 in^2

A_{fan} fan nozzle throat area, 33.90 in^2

A_{port} multi-door crocodile thrust reverser port minimum area, in^2

A_{rev} thrust reverser exit area, in^2

AR reverser area ratio, A_{rev}/A_{fan}

b wingspan, 199.71 in.

C_A axial force coefficient, $F_A/(p_oS/2)$

C_l rolling moment coefficient, Rolling moment/$(p_o(b/2)(S/2))$

C_m pitching moment coefficient, Pitching moment/$(p_o \bar{c} S/2)$

C_N normal force coefficient, $F_N/(p_oS/2)$

CNPR core nozzle pressure ratio, $p_{t,core}/p_o$

C_n yawing moment coefficient, Yawing moment/$(p_o(b/2)(S/2))$

C_r root chord length, 34.14 in.

C_t tip chord length, 10.25 in.

C_Y side force coefficient, $F_S/(p_oS/2)$

c local chord length, in.

$\bar{c}$ mean aerodynamic chord, 24.33 in.

d_{max} maximum nacelle diameter, 11.42 in.

F_A corrected balance axial force, lbf

F_{core} core nozzle forward thrust, lbf

F_{fan} fan nozzle forward thrust, lbf

F_i sum of ideal isentropic core and fan nozzle thrusts, $F_{i,core}+F_{i,fan}$, lbf

$F_{i,core}$ ideal isentropic core nozzle thrust,

$$w_{p,core}\sqrt{\frac{R_j T_{t,core}}{g^2}\frac{2\gamma}{\gamma-1}\left[1-\left(\frac{1}{CNPR}\right)^{(\gamma-1)/\gamma}\right]},\ \text{lbf}$$

$F_{i,fan}$ ideal isentropic fan nozzle thrust,

$$w_{p,fan}\sqrt{\frac{R_j T_{t,fan}}{g^2}\frac{2\gamma}{\gamma-1}\left[1-\left(\frac{1}{FNPR}\right)^{(\gamma-1)/\gamma}\right]},\ \text{lbf}$$

F_N corrected balance normal force, positive upward, lbf

FNPR fan nozzle pressure ratio, $p_{t,fan}/p_o$

$F_{i,rev}$ isentropic gross reverse thrust, $F_A+F_{i,core}$, lbf

F_r resultant thrust, $\sqrt{F_A^2+F_N^2+F_S^2}$, lbf

F_{rev} gross reverse thrust, F_A+F_{core}, lbf

F_S corrected balance side force, positive to right when looking upstream, lbf

F_{total} total nozzle (fan+core) forward thrust, lbf

g acceleration due to gravity, 32.17 ft/sec^2

h_d upstream fan duct height (used herein as a reference length), 2.25 in.

h_{gp} ground plane height, in.

h_t blockerless thrust reverser tab height, in.

IPR blockerless thrust reverser injection pressure ratio, same as CNPR, $p_{t,core}/p_o$

l_c multi-door crocodile thrust reverser outer door cutback length, in.

l_f wing-mounted thrust reverser deflector chord length, in.

l_o multi-door crocodile thrust reverser kicker plate overhang length, in.

l_p multi-door crocodile thrust reverser port length, in.

l_s target thrust reverser shim length, in.

p_o test cell ambient pressure, psia

$p_{t,core}$ average jet total pressure for core flow, psia

$p_{t,fan}$ average jet total pressure for fan flow, psia

R_j gas constant (for γ=1.3997), 1716ft^2/sec^2-°R

r multi-door crocodile thrust reverser port bullnose radius, in.

S full-span wing reference area, 4431.27 in^2

$T_{t,core}$ average jet total temperature for core flow, °R

$T_{t,fan}$ average jet total temperature for fan flow, °R

w_a multi-door crocodile thrust reverser port aft width, in.

w_b multi-door crocodile thrust reverser bullnose width, in.

w_{bl} core bleed weight-flow rate, lbf/sec

w_{cas} blockerless thrust reverser cascade vane weight flow-rate, $w_{p,tot}$-w_{noz}, lbf/sec

w_f multi-door crocodile thrust reverser port forward width, in.

$w_{i,core}$ computed ideal isentropic core weight-flow rate,

$$(A_{core})(p_{t,core})\left(\frac{2}{\gamma+1}\right)^{\frac{\gamma+1}{2(\gamma-1)}}\sqrt{\frac{\gamma g^2}{T_{t,core}\ R_j}} \quad \text{for CNPR} > 1.89,$$

$$(A_{core})(p_{t,core})\left(\frac{1}{CNPR}\right)^{\frac{1}{\gamma}}\sqrt{\frac{2\gamma g}{(\gamma-1)\ T_{t,core}\ R_j}\left[1-\left(\frac{1}{CNPR}\right)^{\sqrt{(\gamma-1)/\gamma}}\right]} \quad \text{for CNPR} \le 1.89, \text{ lbf/sec}$$

$w_{i,fan}$ computed ideal isentropic fan weight-flow rate in forward thrust,

$$(A_{fan})(p_{t,fan})\left(\frac{2}{\gamma+1}\right)^{\frac{\gamma+1}{2(\gamma-1)}}\sqrt{\frac{\gamma g^2}{T_{t,fan}\ R_j}} \quad \text{for FNPR} > 1.89,$$

$$(A_{fan})(p_{t,fan})\left(\frac{1}{FNPR}\right)^{\frac{1}{\gamma}}\sqrt{\frac{2\gamma g}{(\gamma-1)\ T_{t,fan}\ R_j}\left[1-\left(\frac{1}{FNPR}\right)^{\sqrt{(\gamma-1)\ \gamma}}\right]} \quad \text{for FNPR} \le 1.89, \text{ lbf/sec}$$

$w_{i,rev}$ computed ideal isentropic fan weight-flow rate in reverse thrust,

$$(A_{rev})(p_{t,fan})\left(\frac{2}{\gamma+1}\right)^{\frac{\gamma+1}{2(\gamma-1)}}\sqrt{\frac{\gamma g^2}{T_{t,fan}\ R_j}} \quad \text{for FNPR} > 1.89,$$

$$(A_{rev})(p_{t,fan})\left(\frac{1}{FNPR}\right)^{\frac{1}{\gamma}}\sqrt{\frac{2\gamma g}{(\gamma-1)\ T_{t,fan}\ R_j}\left[1-\left(\frac{1}{FNPR}\right)^{\sqrt{(\gamma-1)/\gamma}}\right]} \quad \text{for FNPR} \le 1.89, \text{ lbf/sec}$$

w_{inj} blockerless thrust reverser injection weight-flow rate, equal to $w_{p,core}$, lbf/sec

w_{noz} blockerless thrust reverser fan exhaust nozzle weight-flow rate (computed from total pressure measurements taken at fan nozzle exit), lbf/sec

$w_{p,core}$ measured core (primary) weight-flow rate, lbf/sec

$w_{p,fan}$ measured fan (secondary) weight-flow rate, lbf/sec

$w_{p,tot}$ sum of measured core and fan weight-flow rates, $w_{p,core}+w_{p,fan}$, lbf/sec

w_s blockerless thrust reverser injection slot width, in.

w_{sp} multi-door crocodile thrust reverser port spacer width, in.

x axial distance measured from MS 33.75, positive downstream, in.

x_t axial distance measured from MS 33.75 to core-mounted target, in.

y lateral distance measured from model centerline, positive to right when looking upstream, in.

z vertical distance measured from WL 0.00, positive upward, in.

Λ local wing sweep, deg

β thrust reverser area match parameter

γ ratio of specific heats, 1.3997 for air

η	wing semi-span location, y/(b/2)
η_{fan}	fan reverser effectiveness, F_{rev}/F_{fan}
$\eta_{fan_{id}}$	fan reverser effectiveness based on ideal thrust, $F_{i,rev}/F_{i,fan}$
η_{rev}	overall thrust reverser effectiveness, F_A/F_{total}
λ	wing taper ratio, 0.30
θ	blockerless thrust reverser injection slot angle (measured from vertical, positive counter-clockwise), deg
ρ	angular location of static pressure taps (see figs. 18 and 20), deg
ψ	wing-mounted thrust reverser deflector angle, deg

Subscripts:

c/4	quarter chord
1	wing-mounted thrust reverser deflector 1
2	wing-mounted thrust reverser deflector 2
3	wing-mounted thrust reverser deflector 3

Abbreviations:

BPR	bypass-ratio
CB	cutback
CCW	counter-clockwise
CL	model centerline
Config.	configuration number
LE	leading edge
MAC	mean aerodynamic chord
MS	model station, in.
PSATR	annular (metal) target thrust reverser static pressure, psi
PSBAS	blockerless thrust reverser base static pressure, psi

PSCID	multi-door crocodile thrust reverser inner door centerline static pressure, psi
PSCOD	multi-door crocodile thrust reverser outer door centerline static pressure, psi
PSCORE	blockerless thrust reverser core static pressure, psi
PSEID	multi-door crocodile thrust reverser inner door edge static pressure, psi
PSEOD	multi-door crocodile thrust reverser outer door edge static pressure, psi
PSFEN	fan exhaust nozzle static pressure, psi
PSFL	wing-mounted thrust reverser deflector static pressure, psi
PSFP	wing-mounted thrust reverser back of deflector static pressure, psi
PSIFD	inner fan duct static pressure, psi
PSINJ	blockerless thrust reverser injection plenum static pressure, psi
PSOFD	outer fan duct static pressure, psi
PSPBD	porous blocker diffuser static pressure, psi
PSRB	multi-door crocodile thrust reverser barrel static pressure, psi
PSPYL	pylon static pressure, psi
PSWL	wing-section lower surface static pressure, psi
PSWU	wing-section upper surface static pressure, psi
PTFNE	fan nozzle exit total pressure, psi
R	radius, in.
TE	trailing edge
WL	waterline, in
X-Long	extra long

Apparatus and Procedure

Jet-Exit Test Facility

This investigation was conducted in the Jet-Exit Test Facility at NASA Langley Research Center. Tests are conducted in a large room where the jet from a dual-flow propulsion simulation system vents to the atmosphere through acoustically treated exhaust passages. A control room is remotely located from

the test room and a closed-circuit television is used to observe the model when the jet is operating. The Jet-Exit Test Facility has an air control system that is similar to that of the NASA Langley Research Center 16-Foot Transonic Tunnel and includes valves, filters, and a heat exchanger to maintain the jet flow at a constant stagnation temperature. The air system uses the same clean, dry air supply that is used by the 16-Foot Transonic Tunnel (ref. 3).

Dual-Flow Propulsion Simulation System

The separate-flow exhaust system (forward thrust) and thrust reverser models were tested on a dual-flow propulsion simulation system consisting of an axisymmetric air-powered model mounted on a six-component strain-gauge balance. A photograph and sketch of the separate-flow exhaust system model with wing section installed on the dual-flow propulsion simulation system is presented in figure 4. An external high-pressure air system supplies the simulator with a continuous flow of clean, dry air at a constant stagnation temperature of about 540°R at the model instrumentation section, located just upstream of MS 33.75.

Independently controlled primary and secondary flow systems provide pressurized air to isolated plenum chambers on the dual-flow system through two pairs of semi-rigid, thin-walled (0.021-in. wall thickness), 1-in. diameter, S-shaped, stainless steel tubes (S-tubes). These tubes provide flexible connections that transfer air from the non-metric to the metric (supported by the force balance) part of the system. The geometric design of the airflow system attempts to minimize any balance force and moment tares that can be generated by the flexure of the S-tubes as air pressure is increased or by transfer of axial momentum as pressurized air passes into the plenum. The primary and secondary air systems can be used separately or combined for dual-flow operation. For the current investigation, the primary system was used to simulate engine core flow and the secondary system was used to simulate engine fan flow.

High-pressure air supplied to the primary plenum is delivered by a 15 lbf/sec air system that contains dual in-line venturis for weight-flow measurements. From the primary plenum, air is then discharged radially into the annular low-pressure primary duct (on the model centerline) through eight equally spaced sonic nozzles. The primary airflow then passes over a bullet fairing, through the primary choke plate (used as a flow straightener), and through the facility primary instrumentation section before entering the primary adapter at MS 21.75.

High-pressure air supplied to the secondary plenum is delivered by a 30 lbf/sec air system that also contains dual in-line venturis for weight-flow measurements. From the secondary plenum, air is then discharged radially into an annular low-pressure secondary duct (surrounding the primary duct and located on the model centerline) through twelve equally spaced sonic nozzles. The secondary airflow then passes through the annular secondary choke plate (used as a flow straightener), and through the facility secondary instrumentation section before entering the secondary adapter at MS 21.75.

Thrust Reverser Concepts and Models

High-Bypass-Ratio Separate-Flow Exhaust System

A 7.9%-scale, high-bypass-ratio, separate-flow exhaust system model designed for the dual-flow propulsion simulation system was built for the Innovative Thrust Reverser Test Program. The model core and fan nozzle contours (internal/external) were based on a preliminary BPR≈9.0 separate-flow exhaust system design provided by General Electric. The maximum nacelle diameter (d_{max}) of the model was 11.42 in, the core nozzle throat area (A_{core}) was 6.76 in^2, and the fan nozzle throat area (A_{fan}) was 33.90

in^2. A fully metric, instrumented, 7.9%-scale supercritical left-hand wing section, attached via a pylon, was fabricated for use with this model. A typical test setup of the high-bypass-ratio separate-flow exhaust system model with the wing section installed is presented in figure 4. The separate-flow exhaust system model was tested in the forward thrust mode (with and without the wing-section installed) to provide reference forward thrust levels for assessing the effectiveness of innovative thrust reverser configurations.

Adapter sections at MS 21.75 were used to attach the separate-flow exhaust system model to the facility hardware and provide smooth transitions to the model instrumentation sections. Choke plates installed at the downstream end of the adapter sections provided for low flow distortion in the instrumentation sections. The inner/outer duct diameters of the instrumentation sections were matched to the starting diameters of the core and fan exhaust nozzles. The separate-flow exhaust system model was installed on the downstream end of the instrumentation section at MS 33.75.

Details of the separate-flow exhaust system model are presented in figure 5. A photograph of the separate-flow exhaust system model is presented in figure 5(a). As shown in figure 5(b), the fan section consisted of the forward fan nozzle (fig. 5(c)) and the aft fan nozzle (fig. 5(d)). The fan nozzle was split into forward and aft pieces to facilitate installation of cascade vane sections for testing of cascade thrust reverser configurations. The core section consisted of the core nozzle (fig. 5(e)), core nozzle insert #1 (fig. 5(f)), and core plug assembly (fig. 5(g)). The removable core nozzle insert permitted installation of a fan-duct blocker for cascade thrust reverser testing and facilitated modifications of the core cowl section for testing of the core-mounted thrust reverser configurations which utilized as much of the separate-flow exhaust system model hardware as possible. For structural integrity, the pylon assembly (fig. 5(h)) interfaced directly with the fan nozzle. A complete list of separate-flow exhaust system model configurations tested is presented in table 1.

7.9%-Scale Supercritical Left-Hand Wing Section

A fully metric, instrumented, 7.9%-scale supercritical left-hand wing section, attached via a pylon, was fabricated for use with the separate-flow exhaust system model to facilitate testing of wing-mounted thrust reverser configurations. Details of the separate-flow exhaust system model with the wing-section installed are presented in figure 6. A photograph and sketch of the separate-flow exhaust system model with the wing-section installed are presented in figures 6(a) and 6(b), respectively. Wing geometry is presented in figure 6(c), with the wing-section used in this investigation denoted by the heavy dashed line. The wing geometry was based on a design which, at model scale, had a full-span wing reference area (S) of 4431.27 in^2, wing span (b) of 199.70 in., mean aerodynamic chord ($\bar{c}$) of 24.33 in., aspect ratio of 9.00, taper ratio (λ) of 0.30, and a dihedral angle of 3°. The separate-flow exhaust system model centerline was located at a wing semi-span location (b/2) of 0.35 and the wing section (fig. 6(d)) extended span-wise from b/2=0.18 to b/2=0.52. The wing section was sized to extend $1.5d_{max}$ on either side of the nacelle centerline. A sketch showing wing section geometry at b/2=0.18, b/2=0.35, and b/2=0.52 is presented in figure 6(e). Wing section ordinates are provided in figure 6(f).

Cascade Thrust Reverser

Details of the cascade thrust reverser model are presented in figure 7. The cascade thrust reverser model (fig. 7(a)) was used to represent a conventional cascade thrust reverser system and the innovative cascade thrust reverser with porous blocker. All cascade thrust reverser configurations were tested without the wing-section installed on the pylon.

Conventional Cascade Thrust Reverser. The conventional cascade thrust reverser model (fig. 7(b))

was tested with a variable leakage fan-duct blocker door set to leakage areas equivalent to 0% (no leakage), 5%, or 11% of the fan nozzle throat area. Test results for the 5% blocker leakage configuration are used as a baseline in this report to assess the effectiveness of innovative thrust reverser configurations.

To assemble the conventional cascade thrust reverser model, core nozzle insert #1 and the aft fan nozzle were removed from the separate-flow exhaust system model. A variable leakage blocker, consisting of blocker door #1 (fig. 7(c)) and the blocker door restrictor plate (fig. 7(d)), was installed to block the fan duct and provide a mount for the cascade vane sections and aft fan nozzle (translated 3.340 in. aft from MS 35.750), as shown in figure 7(b). Holes drilled through blocker door #1 were used to simulate leakage past the blocker. The blocker door restrictor plate, located on the downstream side of blocker door #1, was used to set blocker door leakage to 0% (no leakage), 5%, or 11% of the fan nozzle throat area. The blocker door restrictor plate was assembled in different circumferential locations so that varying amounts of holes in blocker door #1 were covered in order to obtain the different leakage amounts. As shown in figure 7(b), a bullnose fairing (fig. 7(e)) was installed in the forward fan nozzle to smoothly turn the fan flow into the cascades. Twelve cascade vanes segments were mounted around the circumference of the fan nozzle (see fig. 7(f)) to direct the fan flow forward for reverse thrust. Details of the cascade vanes segments are presented in figures 7(g) to 7(n). The cascade vanes (provided by Pratt & Whitney) were configured with an array of 7 longitudinal ports having cant and skew angles representative of a left-hand wing installation. The nominal flow area of the cascade vanes with all ports open was 104% of the fan nozzle throat area. A cascade aft port blocker plate (fig. 7(o)) was available to close off the aft cascade port to vary the cascade area to 90% of the fan nozzle throat area. The shortened core nozzle insert #2 (fig. 7(p)) and the aft fan nozzle were installed to complete the configuration. The two primary design parameters investigated for the conventional cascade thrust reverser model were blocker leakage and cascade area. A complete list of conventional cascade thrust reverser configurations tested is presented in table 2.

Cascade Thrust Reverser with Porous Blocker. The cascade thrust reverser with porous blocker concept offers a reduction in blocker weight. Functionally, blocker door #2 (fig. 7(q)) replaced blocker door #1 that was used with the conventional cascade thrust reverser model. The blocker door restrictor plate and cascade aft port blocker plate were not used for porous blocker configurations. Blocker door #2 was designed with a porosity representing 50% of the fan duct cross-sectional area at the blocker. Button-head screws were inserted into every other hole in blocker door #2 and secured with nuts to reduce the blocker porosity to 25%. Core nozzle insert #2 was replaced with core nozzle insert #3 (fig. 7(r)) to complete the configuration. Core nozzle insert #3 created a diffuser downstream of the porous blocker (eliminating the core surface contour) to help spoil the thrust of flow which leaked through the porous blocker door. The primary design parameter investigated was blocker porosity. A complete list of cascade thrust reverser with porous blocker model configurations tested is presented in table 3.

Blockerless Thrust Reverser

The blockerless thrust reverser concept eliminates the blocker doors from the conventional cascade thrust reverser and uses diverter jets powered by core bleed air to block the fan flow. This concept offers a potential weight savings over a conventional cascade thrust reverser system by eliminating the blocker door hardware. A forward thrust performance improvement would also result from elimination of losses associated with blocker door hardware.

Details of the blockerless thrust reverser model are presented in figure 8. A photograph and sketch of the blockerless thrust reverser model are presented in figures 8(a) and 8(b), respectively. To assemble the blockerless thrust reverser model, all hardware except for the forward fan nozzle was removed from the

separate-flow exhaust system model. A fluidic injector assembly (fig. 8(c)) was installed in place of the core hardware. As shown in figure 8(b), the bullnose fairing was added to the forward fan nozzle to smoothly turn the fan flow into the cascades. Twelve cascade vanes segments, discussed previously, were mounted (via the forward fan nozzle and support strut assembly) around the circumference of the fan nozzle to direct the fan flow forward for reverse thrust. The alternate pylon assembly (fig. 8(d)) and the aft fan nozzle were installed to complete the configuration. The primary design parameter investigated for blockerless thrust reverser configurations was fluidic injection port geometry. A complete list of blockerless thrust reverser model configurations tested is presented in table 4.

The fluidic injector assembly (fig. 8(c)) used a series of interchangeable injector rings to vary the fluidic injection port geometry at each of five injection locations. The fluidic injection locations were designated "duct", "forward", "mid", "aft", and "throat" and were located at MS 35.263, MS 36.713, MS 37.113, MS 37.513, and MS 40.207, respectively. Injector ring #1 (fig. 8(e)) set the "duct" injection port geometry to either blank (no injection) or a continuous slot width (w_s) of 0.025 in. with a slot angle (θ) of 0° (perpendicular to the model centerline). Injector rings #2 (fig. 8(f)), #3 (fig. 8(g)), and #4 (fig. 8(h)) could respectively set the "fwd", "mid", and "aft" injection port geometries to either blank, w_s=0.013 in. with θ=0°, w_s=0.013 in. with θ=45°, w_s=0.025 in. with θ=0°, or w_s=0.025 in. with θ=45°. In addition, injector ring #4 could set the "aft" injection port geometry to discrete 0.025 in. holes located 0.0375 in. apart on centerline or add injection tabs with heights (h_t) of 0.20 in., 0.40 in., or 0.60 in. to the w_s=0.025 in. with θ=45° geometry. The tab created a partial blocker (equivalent to a fan duct area blockage of 7%, 14%, and 21% at h_t of 0.20 in., 0.40 in., or 0.60 in., respectively) at the aft injection location. Injector ring #5 (fig. 8(i)) set the "throat" injection port geometry to either blank, w_s=0.013 in. with θ=45°, w_s=0.025 in. with θ=0°, or w_s=0.025 in. with θ=45°. The support strut assembly (fig. 8(j)) was an integral part of the fluidic injector assembly and provided support for the cascade vanes and aft fan nozzle in place of the blocker door. An aft cascade port fairing was attached to the upstream end of the support strut assembly (see fig. 8(b)) to help smoothly turn the fan flow into the cascades. Two different aft cascade port fairing geometries, shown in figures 8(k) and 8(l), were tested. The blockerless thrust reverser assembly in figure 8(b) is shown with the aft cascade port fairing #1 installed.

To help reduce flow separation from the bullnose fairing (fan cowl lip just upstream of the cascades), several coanda turning surfaces were fabricated to replace the bullnose fairing. Coanda fairing #1 (fig. 8(m)) had a surface definition that was potentially more favorable to attached flow than the original bullnose fairing. Coanda fairing #2 (fig. 8(n)) had a surface definition that blocked off the forward cascade port, reducing the cascade area to 90% of the fan nozzle throat area, to potentially provide an even more favorable geometry. Coanda fairing #3 (fig. 8(o)), tested without the cascade vanes installed, had a surface definition with the largest radius of curvature of the coanda fairings.

Annular (Metal) Target Thrust Reverser

The annular (metal) target thrust reverser concept relocates the reverser hardware to the core cowl, allowing the nacelle lines to be optimized for cruise operation while offering potential reductions in reverser and nacelle weight. Although this concept is not new (ref. 4), an attempt was made in the model design process to define target geometries (size, spacing) which had areas consistent with the potential design constraints of a core-mounted system. The annular targets covered the full circumference of the fan exit and represented a blocker arrangement with no leakage. The internal surface contour of the targets was based on a nominal shape of the fabric target thrust reverser concept (discussed later).

Details of the annular target thrust reverser model are presented in figure 9. A photograph and sketch of the annular (metal) target thrust reverser model are presented in figures 9(a) and 9(b), respectively. To

assemble the annular (metal) target thrust reverser, core nozzle insert #1 was removed from the separate-flow exhaust system model (see fig. 5(b)). Core nozzle insert #4 (fig. 9(c)) was installed, along with either the 20° annular target assembly (fig. 9(d)) (with an optional kicker) or the 40° annular target assembly (fig. 9(e)) (with an optional extension), to complete the configuration. The two primary design parameters investigated for the annular (metal) target thrust reverser configurations were reverser area ratio (AR) and target angle. A complete list of annular (metal) target thrust reverser configurations tested is presented in table 5.

The reverser area ratio is defined as the ratio of the thrust reverser exit area (A_{rev}) and the fan nozzle throat area (A_{fan}). The reverser exit (a conic surface) is defined by a line drawn perpendicular to the inner (forward) surface of the target that intersects the fan cowl. The reverser exit area is the minimum area downstream of the fan nozzle exit as shown in figure 9(b). The fan nozzle throat area is the minimum area in the fan duct, upstream of the fan nozzle exit. The target angle is defined as the angle between the inner surface of the target and a plane perpendicular to the centerline of the nozzle (thrust axis). This is also the nominal reverser efflux angle, the angle of the vector drawn normal to the reverser exit.

Reverser area ratios of 1.05, 1.15, and 1.25 were tested for the annular (metal) target thrust reverser configurations. Each of the annular target assemblies (figs. 9(d) and 9(e)) had shims of varying length (l_s) to reposition the targets on the core nozzle and set the reverser exit area. The outer diameters of the 20° and 40° targets were established by the AR=1.25 target position, since the AR=1.25 target position required the largest target diameter. To evaluate the effect of target length (diameter), an extension piece was built for the 40° target and tested with the target in the AR=1.25 position.

One reason for testing a 20° annular target was to evaluate the performance impact if longer target panels could not be installed in the core nozzle cowl. In addition, the shorter target lengths offer a lighter weight installation and more options in the core section installation. For the 20° target, an attempt to obtain additional flow turning was made by adding a kicker plate at the target exit. Kicker plates (endplates) have been shown to increase reverser effectiveness on conventional low-bypass-ratio target reverser systems. Endplates also offer performance advantages on concepts which use short targets that do not have exit areas perpendicular to the target panel (ref. 5). The kicker plate could also possibly be used to locally trim the reverser efflux pattern. The length of the kicker plate was selected to reduce the reverser area ratio to 1.05 when the target was located in the AR=1.25 position on the core cowl.

Fabric Target Thrust Reverser

The fabric target thrust reverser concept represents a lightweight design based on the annular (metal) target thrust reverser, with consideration given to how the device might be deployed and stowed. This concept has been patented by Pratt & Whitney.

Details of the fabric target thrust reverser model are presented in figure 10. A photograph and sketch of the fabric target thrust reverser model are presented in figures 10(a) and 10(b), respectively. To assemble the fabric target thrust reverser, core nozzle insert #1 was removed from the separate-flow exhaust system model. Core nozzle insert #4 was installed, along with either the short fabric target thrust reverser assembly (fig. 10(c)) or the long fabric target thrust reverser assembly (fig. 10(d)) to complete the configuration. The fabric target thrust reverser configurations were designed for a reverser area ratio (AR) of 1.15 and nominal exit angles of 20° and 40°. A complete list of fabric target thrust reverser configurations tested is presented in table 6.

Each fabric target thrust reverser assembly consisted of the standoff mount (fig. 10(e)), standoffs

(vertical and radial, as shown in figure 10(f)), fabric attachment fingers (fig. 10(f)), and a fabric target. For test purposes, the fabric target was supported from behind at 22.5° increments, instead of using support ribs in front of the fabric as shown conceptually in figure 3. The inside edge (along the core) of the fabric target was secured below the core surface; no attempt was made to attach the fabric target to the pylon. The nominal fabric target shape was established by the reverser exit angle and a circular arc matched to the slope of the core surface and the nominal target exit angle. Short (fig. 10(g)) and long (fig. 10(h)) fabric lengths were tested at target angles of 20° and 40°. At the 40° target angle, the longer fabric length required the use standoff shims (fig. 10(f)) with the attachment finger repositioned forward. The fabric material was KEVLAR 840 with a porosity of 1.08 $ft^3/min/ft^2$ and a weight of 7 oz/yd^2.

The nominal fabric contours were used to define the internal surface geometry of the annular (metal) target thrust reverser configurations discussed in the previous section. The unloaded (jet-off) shape of the fabric targets were essentially the same as the metal targets described previously. The inflation characteristics (loaded shape) of the fabric target are important to the operation of this concept. The interchangeable "short" and "long" fabric sections were tested with the 20° and 40° target angles to provide information on the effects of fabric length. These data, along with data from the annular (metal) target thrust reverser concepts, provide insight into the effects of fabric inflation.

Multi-Door Crocodile Thrust Reverser

The multi-door crocodile thrust reverser concept uses 8 inner and outer door sets located symmetrically around the circumference of the fan cowl. The doors are hinged at the trailing edge and rotate open to expose reverser ports; the inner doors block the fan duct and the outer doors redirect the fan flow forward to produce reverse thrust. In an actual application, the outer doors would simultaneously act as an airbrake, because of expected low pressures on the aft side of the doors, to increase aircraft stopping force generated by the thrust reverser. From both the structural and mechanical viewpoints, this concept is potentially simpler than a conventional cascade thrust reverser. Advantages over a conventional cascade thrust reverser are the simpler actuation system (non-interdependence of doors), improved maintenance access, and reduction in manufacturing cost due to the elimination of the cascades.

Details of the multi-door crocodile thrust reverser model are presented in figure 11. A photograph, side view cutaway sketch, and end view sketch of the crocodile thrust reverser model are presented in figures 11(a), 11(b), and 11(c), respectively. To assemble the crocodile thrust reverser model, the forward and aft fan nozzles were removed from the separate-flow exhaust system model. The reverser barrel (fig. 11(d) and fig. 11(e)) was installed, along with the port inserts (fig. 11(f)), optional port spacers, and bullnose inserts (fig. 11(g)). A lower fan-duct bifurcator (fig. 11(h)) was installed between doors D and E. The inner doors (fig. 11(i)) mounted to the inside surface of the reverser barrel using inner door brackets (fig. 11(j)) to set the inner door angle. The outer doors (fig. 11(k)) mounted to the outside surface of the reverser barrel using outer door brackets (fig. 11(l)) to set the outer door angle. The two upper (A and H) and two lower (D and E) outer doors were tested with no cutback, partial cutback, and full cutback angles (for wing and ground clearance). Port covers (fig. 11(m)) were used for the cutback configurations to match the port geometry to the door. Optional outer door kicker plates (fig. 11(n)) and outer door fences (fig. 11(o)) were evaluated. Upper and lower filler pieces (fig. 11(p)) were used to investigate the effects of inner door (blocker) leakage. Design variables investigated for multi-door crocodile thrust reverser configurations with inner and outer doors fully deployed included inner door leakage, reverser port bullnose radius, reverser port area, kicker plates, door fences, and outer door cutback (size). Partially deployed reverser configurations were also tested. A complete list of multi-door crocodile thrust reverser configurations tested is presented in table 7.

To investigate the effects of inner door (blocker) leakage, configurations were tested without the pylon/bifurcator filler pieces. In effect, the filler pieces closed, but did not seal, the gap between the inner doors and the pylon and lower fan-duct bifurcator. A "no leak" configuration was tested that sealed the gaps between the inner doors and the pylon and lower fan duct bifurcator and the gaps between the individual inner doors. Aluminum tape was used on the downstream surfaces to effectively seal these gaps.

A bullnose insert could be located at the forward edge of each reverser port to control the flow turning into the reverser port. See figure 11(b). Three different bullnose shapes with radius-to-height ratios (r/h_d) of 0.22, 0.18, and 0.13 were tested (see fig. 11(g)). The bullnose inserts were designed so that changes in reverser port length between bullnose insert geometries were minimal. Multi-door crocodile thrust reverser configurations were also tested without the bullnose inserts installed.

The shape of the reverser port is trapezoidal, with the width larger at the aft end. The geometry of the reverser port can be seen in figure 11(c). The reverser port minimum area is defined as the product of the port length (l_p) and average port width ($1/2(w_f+w_a)$). Variations in reverser port area were achieved by installing a spacer and/or the bullnose, thereby reducing the length of the reverser port. The largest reverser port area tested had neither the bullnose or port spacer installed. As shown in figure 11(c), six different port geometries (area ratios) were investigated by using spacer and bullnose combinations. The port length-to-height ratios (l_p/h_d) for the six port geometries were 1.67, 1.58, 1.49, 1.45, 1.36, and 1.27. The corresponding forward port width-to-height ratios (w_f/h_d) were 0.84, 0.84, 0.84, 0.77, 0.80, and 0.83. The aft port width-to-height ratio (w_a/h_d) was constant at 1.26. With these combinations of port width and length, six reverser area ratios (A_{rev}/A_{fan}) were investigated: 1.91, 1.81, 1.71, 1.60, 1.53, and 1.45. The smaller area ratios correspond to a 5.2%, 10.4%, 16.5%, 20.3%, and 24.2% reduction in port area relative to the A_{rev}/A_{fan}=1.91 configuration.

In an actual aircraft application, fences and/or kicker plates on the outer doors may be required for effective thrust reverser efflux control. A typical kicker installation on the multi-door crocodile thrust reverser model is shown in figure 11(b). Selected configurations were tested without kicker plates or fences and with long and extra-long (X-long) kickers and fences. The effect of kicker plate cutback (fig. 11(n)) was also evaluated. Kicker plate size is defined by the amount of overhang from edge of the door (l_o, see figure 11(b)). Expressed as a ratio to the fan duct height (l_o/h_d), the lengths of the long and extra long kicker plates were 0.18 and 0.24, respectively.

For a conventional subsonic transport nacelle installation, it is likely that the outer doors at the top (doors A and H) and bottom (doors D and E) of the nacelle will require cutback to provide clearance with the ground and wing leading edge slats (when deployed). The relative amount of cutback investigated is depicted in figure 11(c) as dashed lines on these doors. The door cutback is made along a waterline, essentially cutting off a corner of the door. The amount of cutback is defined by the ratio of the cutback length (l_c) to the fan-duct height (h_d). An external reverser port cover is installed at each cutback to match the port geometry to the door. The port cover reduces the reverser port area. The following terminology is used to describe the cutback combinations investigated:

Partial - Outer doors A, D, E, and H cutback to a cutback ratio (l_c/h_d) of 0.36.

Full - Outer doors panels A, D, E, and H cutback to a cutback ratio of 0.83.

Mixed - A mixture of partial and full cutbacks. Partial cutback doors installed at the top of the nacelle (doors A and H) and full cutback doors installed at the bottom of the nacelle (doors D and E).

Combinations of outer and inner door deployment angles were tested. Fixed door brackets were used to vary the outer door deployment angle from 10° to 60° in 10° increments, and the inner door deployment angle from 6° to 36° in 6° increments. The majority of testing was done with the inner doors set to the fully deployed 36° position, while the outer door position was varied between 40°, 50°, and 60° to determine the optimum door position. Combinations of inner and outer door positions were also tested to simulate partial deployment configurations.

Wing-Mounted Thrust Reverser

One of the limitations of fan-cowl mounted (cascade or multi-door) and core-mounted (target) thrust reverser systems is that only the fan flow is reversed. With the wing-mounted thrust reverser concept, both the core and fan flows can be captured and reversed, and thrust reverser effectiveness can be improved. By removing the thrust reverser system from the nacelle, the wing-mounted thrust reverser concept offers the nacelle designer more options for improving nacelle aerodynamics and propulsion-airframe integration, simplifying nacelle structural designs, reducing nacelle weight, and improving engine maintenance access.

Conceptually, the wing-mounted thrust reverser concept would use one or more flow deflectors deployed from the wing to capture and reverse the engine exhaust flow. Kinematically, these flow deflectors could operate in a variety of different ways. One possibility would be to use the airplane high-lift system to form flow deflectors by either splitting (as shown in figure 3) or overturning one or more of the flap elements. Another possibility would be to deploy the deflector(s) from the lower wing surface. The model used in this investigation is representative of a typical wing-mounted thrust reverser system. Geometric variations of key design parameters investigated for the wing-mounted thrust reverser concept included flow deflector angles and chord length, optional deflector fences, and the mount angle of the deflector system (normal to the engine centerline or parallel to the wing trailing edge). A complete description of wing-mounted thrust reverser configurations tested is presented in table 8.

Details of the wing-mounted thrust reverser model are presented in figure 12. A photograph and sketch of the wing-mounted thrust reverser model are presented in figures 12(a) and 12(b), respectively. To assemble the wing-mounted thrust reverser model, the wing-section was first installed on the separate-flow exhaust system model. A portion of the wing section, extending chordwise from 0.64c to 1.00c and span-wise from b/2=0.225 to b/2=0.475, was removed. This established a reverser port in the wing through which exhaust flow could be turned. As shown in figure 12(b), a smooth wing bullnose (fig. 12(c)) which terminated at 0.69c, helped to efficiently turn the exhaust flow through the reverser port. The deflector assembly (fig. 12(d)) was mounted to the wing section in either the normal or parallel mount positions as shown in figure 12(e).

The deflector assembly consisted of a cross bar (fig. 12(f)), upper (fig. 12(g)) and lower (fig. 12(h)) brackets held together by bracket ties (fig. 12(i)), and deflectors equipped with optional fences (fig. 12(j)). The deflectors were sized to a width twice that of the maximum nacelle diameter, or $2.0d_{max}$. For deflector 1 (upper) and deflector 2 (middle), short and long deflector chord lengths (l_f) were tested. Brackets holding each deflector allowed testing over a range of deflector angles (ψ). The angle of each deflector is defined relative to a plane perpendicular to the nozzle centerline (thrust axis) as shown in figure 12(d). The design of the deflector system allowed ψ_1 and ψ_3 to be independently varied, but changes in ψ_2 at constant ψ_3 resulted in deflector 2 and deflector 3 acting as a "bucket" that moved together as a unit to capture exhaust flow. The deflector assembly was attached to the wing section using wing mounts (fig. 12(k)) and interchangeable links (fig. 12(l)), which allowed the mount angle of deflector assembly to be set in two positions (see fig. 12(e)): (1) normal to the nozzle centerline (thrust

axis) and (2) parallel to the trailing edge of the wing section.

A ground plane was tested with selected wing-mounted thrust reverser configurations to determine the effect of ground proximity on wing-mounted thrust reverser performance. Details of the ground-plane setup are presented in figure 13.

Instrumentation

All forces and moments generated by the model were measured by a six-component strain-gauge balance located on the centerline of the dual-flow propulsion simulation system. The weight-flow rate of high-pressure air supplied to the model was calculated from static-pressure and total-temperature measurements taken in two calibrated, multiple-critical venturis (one for the primary air system and one for the secondary air system) located upstream of the dual-flow propulsion simulation system. The multiple-critical venturi is the standard high-pressure airflow measurement system used in the NASA Langley Research Center 16-Foot Transonic Tunnel and is rated to be 99.9% accurate in weight-flow measurements. Jet total-pressure was determined at a fixed station in the model instrumentation section by averaging measurements taken with nine area-weighted total pressure probes in the primary duct and twelve area-weighted total pressure probes in the secondary duct. Jet total temperature was determined at the same station using iron-constantan thermocouples located in each duct.

Static pressures were measured inside the core and fan nozzles and on model external surfaces (such as the pylon, targets, wing, wing-mounted deflectors, and multi-door crocodile thrust reverser doors) for each configuration using 0.060-inch diameter static pressure orifices. Total pressures were measured downstream of the fan nozzle exit for selected configurations using 0.060-inch diameter total pressure probes. The location of the pressure orifices and probes are shown for each model as follows:

Note that the fabric target thrust reverser model did not have pressure orifices on the fabric target; however, all other pressure orifices for the fabric target thrust reverser model were in the same location as on the annular (metal) target thrust reverser model.

Individual pressure transducers were used to measure pressures in the air supply systems and multiple-critical venturis. The transducers were selected and sized to allow the highest accuracy over each required measurement range. All other pressures were measured by electronically scanning pressure modules located in the JETF test chamber in an acoustically shielded cabinet.

Test Procedures

All configurations were tested at a nominal fan/core nozzle pressure ratio schedule representative of current technology high-bypass-ratio turbofan engines. Procedurally, a core nozzle pressure ratio (CNPR) was set and then the fan nozzle pressure ratio (FNPR) was varied about the nominal pressure ratio

schedule shown in the following table:

CNPR	FNPR
1.10	1.10
	1.20
	1.30
1.20	1.30
	1.40
	1.50
1.30	1.50
	1.60
	1.70
1.40	1.70
	1.80
	1.90
1.50	1.90
	2.00
	2.10

Each configuration was tested up to a maximum fan weight-flow rate of approximately 23 lb/sec.

Data Reduction

Each data point is the average steady-state value computed from 50 frames of data taken at a rate of 10 frames per second. Calibration constants were applied to the data to obtain corrected forces, moments, pressures, and temperatures. A detailed description of the procedures used for data reduction in this investigation can be found in reference 2.

Core nozzle pressure ratio (CNPR) is defined as the average jet total pressure for core flow ($p_{t,core}$), measured in the primary instrumentation section, divided by test cell ambient pressure (p_o):

$$CNPR = p_{t,core}/p_o$$

For blockerless thrust reverser configurations, the injection pressure ratio (IPR) is equal to CNPR. Fan nozzle pressure ratio (FNPR) is defined as the average jet total pressure for fan flow ($p_{t,fan}$), measured in the secondary instrumentation section, divided by the test cell ambient pressure:

$$FNPR = p_{t,fan}/p_o$$

Forward thrust

Core nozzle thrust efficiency ($F_A/F_{i,core}$) is the ratio of corrected balance axial force (F_A) with the core nozzle operating (no fan flow) to the ideal isentropic core nozzle thrust ($F_{i,core}$). Fan nozzle thrust efficiency ($F_A/F_{i,fan}$) is the ratio of corrected balance axial force with the fan nozzle operating (no core flow) to the ideal isentropic fan nozzle thrust ($F_{i,fan}$). Overall nozzle thrust efficiency (F_A/F_i) is the ratio of balance measured axial force with both the core and fan nozzles operating to the sum of ideal core and fan nozzle isentropic thrust (F_i):

$$F_i = F_{i,core}+F_{i,fan}$$

Ideal isentropic thrust values for the core and fan nozzles were computed using the measured weight-flow rate, total pressure, and total temperature of the core and fan flows, respectively. Weight-flow rate was measured using multiple-critical venturi systems, one for the core (primary) air supply and one for the fan (secondary) air supply, located in each air supply line upstream of the dual-flow propulsion simulation system.

Reverse thrust

Three thrust ratios are used to define thrust reverser performance with both the fan and core nozzles operating (dual flow). The overall thrust reverser effectiveness (η_{rev}) is defined as the ratio of corrected balance axial force during reverse thrust operation to the total nozzle (fan+core) forward thrust (F_{total}) that is produced at corresponding core and fan nozzle pressure ratios:

$$F_{total} = F_{core}+F_{fan}$$
$$\eta_{rev} = F_A/F_{total}$$

Core nozzle forward thrust (F_{core}) is based on balance measurements obtained with the core flow operating (no fan flow) in the forward thrust mode. Fan nozzle forward thrust (F_{fan}) is based on balance measurements obtained with the fan flow operating (no core flow) in the forward thrust mode. It was assumed that no thrust interactions occurred when both flows were operating. Curve fits made to the measured force data were used to compute the reference core and fan nozzle forward thrust at the corresponding nozzle pressure ratios.

The fan reverser effectiveness (η_{fan}) is defined as the ratio of gross reverse thrust (F_{rev}) to the fan nozzle forward thrust:

$$\eta_{fan} = F_{rev}/F_{fan}$$

To determine the gross reverse thrust, core nozzle forward thrust is added to the corrected balance axial force in reverse thrust:

$$F_{rev} = F_A + F_{core}$$

The fan reverser effectiveness based on ideal thrust ($\eta_{fan_{id}}$) is defined as the ratio of isentropic gross reverse thrust ($F_{i,rev}$) to the ideal isentropic fan nozzle thrust:

$$\eta_{fan_{id}} = F_{i,rev}/F_{i,fan}$$

To determine the isentropic gross reverse thrust, the ideal isentropic core nozzle thrust is added to the balance corrected axial force in reverse thrust:

$$F_{i,rev} = F_A + F_{i,core}$$

It should be noted that fan reverser effectiveness is not applicable to the wing-mounted thrust reverser configurations that reverse both the core and fan exhaust flows. Most thrust reverser configurations were tested with both the fan and core nozzle operating (dual flow). This was done to ensure that the effects of the core nozzle flow on the blocker base region (downstream side) were properly simulated. For the

blockerless thrust reverser configurations, which were not tested with core flow, base pressure corrections were applied to remove the effects of the blanked core nozzle section.

The thrust reverser area match parameter (β) is defined as the ratio of the effective area of the thrust reverser to the effective area of the fan nozzle operating in the forward thrust mode:

$$\beta = [(w_{p,rev}/w_{i,rev})(A_{rev})]/[(w_{p,fan}/w_{i,fan})*(A_{fan})]$$

Ideally, the thrust reverser area match parameter should be close to 1 to minimize any adverse effects of reverser operation on fan operation. As nozzle operation transitions from forward thrust to reverse thrust, a reduction in the fan effective flow area ($\beta<1$) could shift the fan operating point into a surge condition.

Weight-flow rates through the injectors, fan exhaust nozzle, and cascade vanes are used in the discussion of blockerless thrust reverser performance. The injection weight-flow rate (w_{inj}) is equal to the measured core weight-flow rate ($w_{p,core}$). The fan exhaust nozzle weight-flow rate (w_{noz}) was computed from total pressure measurements taken at the fan nozzle exit using a fan exit rake (see fig. 8(b)). The cascade vane weight-flow rate (w_{cas}) is the difference of the sum of measured core and fan weight-flow rates ($w_{p,tot}=w_{p,core}+w_{p,fan}$) and the computed fan exhaust nozzle weight-flow rate (w_{noz}):

$$w_{cas} = w_{p,tot} - w_{noz}$$

The cascade vane weight-flow rate (w_{cas}) and computed fan exhaust nozzle weight-flow rate (w_{noz}) are ratioed to the sum of the measured core and fan weight-flow rates ($w_{p,tot}$). The injection (w_{inj}) weight-flow rate is ratioed to the measured fan weight-flow rate ($w_{p,fan}$). These ratios (e.g., $w_{cas}/w_{p,tot}$, $w_{noz}/w_{p,tot}$, and $w_{inj}/w_{p,fan}$) are important to establishing the performance of the blockerless thrust reverser configurations, especially when no reverse thrust is generated. The injection weight-flow ratio is an important parameter because it indicates the amount of core bleed air (in percentage of fan weight-flow rate) used to divert the fan flow. It is estimated that modern turbofan engines are capable of supplying a maximum core bleed weight-flow rate to fan weight-flow rate ($w_{bl}/w_{p,fan}$) of 0.05 (ref. 6). Assuming all core bleed air is available for the injectors during reverse thrust operation, then an injection weight-flow ratio ($w_{inj}/w_{p,fan}$) of 0.05 is used as the practical limit for the blockerless thrust reverser concept. Note that the total amount of core bleed air is a function of the BPR:

$$w_{bl}/w_{p,core} = (w_{bl}/w_{p,fan})(w_{p,fan}/w_{p,core}) = (w_{bl}/w_{p,fan})*BPR$$

For a BPR 9 engine, 45% of the total core weight-flow must be bled to provide $w_{bl}/w_{p,fan}=0.05$; for a BPR10 engine, 50% of the total core weight-flow must be bled to provide $w_{bl}/w_{p,fan}=0.05$; and so on.

Model force (C_N and C_Y) and moment (C_m and C_n) coefficients were computed using corrected balance force and moments nondimensionalized by wing reference area (S), wing span (b), and mean aerodynamic chord ($\bar{c}$) as follows:

$C_N = F_N/(p_oS/2)$
$C_Y = F_S/(p_oS/2)$
C_m = Pitching Moment/$(p_o \bar{c} S/2)$
C_n = Yawing Moment/$(p_o(b/2)(S/2))$

Values of b/2 and S/2 were used so that the test setup would more accurately reflect a twin-engine test

on a full-span wing.

Results and Discussion

The data contained in this report were taken in three different operating modes: (1) core only, (2) fan only, and (3) dual flow (both the core and fan operating). The majority of data were taken in the dual flow operation mode with both the core and fan nozzles operating over a nominal core/fan nozzle pressure ratio schedule representative of current technology, high-bypass-ratio turbofan engines. Data were taken up to the maximum operating capability of either the JETF dual-flow system (reached at FNPR≈2.1 in forward thrust) or the force balance (reached at FNPR≈1.6 in reverse thrust). The sawtooth characteristic of some of the graphical data presentation is due to the variation in fan nozzle pressure ratio at several constant values of core nozzle pressure ratio (see table in the section entitled "Test Procedures"). To facilitate machine data plotting, the data fairing is joined at the common FNPR tested a two different values of CNPR and the sawtooth characteristic results. All data gathered in this investigation are contained in a CD-ROM accompanying this report. The description of configurations tested is presented in tables 1 to 8. The names and corresponding symbols or abbreviations for all data contained in the CD-ROM are presented in table 9.

Forward Thrust

Separate-flow exhaust system performance characteristics for all forward thrust configurations tested are presented in Appendix A. Separate-flow exhaust system performance for the same configuration during two separate test entries is presented in figure 22. Overall nozzle thrust efficiency in forward thrust (F_A/F_i) is plotted against fan nozzle pressure ratio (FNPR). The overall nozzle thrust efficiency is typical of a separate-flow exhaust system, varying with FNPR from a low of about 0.95 to a high of about 0.98. Repeatability between the two test entries is better than one percent.

Reverse Thrust

The three most common parameters used in this report to define the performance of innovative thrust reverser configurations are: overall thrust reverser effectiveness (η_{rev}, which includes core nozzle forward thrust), fan reverser effectiveness based on ideal thrust ($\eta_{fan_{id}}$, which does not include core nozzle forward thrust), and the thrust reverser area match parameter (β). For detailed definition of these parameters, see the section entitled "Data Reduction". For configurations that reverse only the fan flow (all except the wing-mounted thrust reverser configurations), $\eta_{fan_{id}}$ is the thrust reverser performance parameter typically used in the discussion of results. For the wing-mounted thrust reverser configurations (which reverse both the core and fan flow), η_{rev} is the thrust reverser performance parameter typically used in the discussion of results.

Conventional Cascade Thrust Reverser

Thrust reverser performance characteristics for all conventional cascade reverser configurations tested are presented in Appendix B. A summary of cascade thrust reverser performance is presented in figure 23. The overall thrust reverser effectiveness (η_{rev}), fan reverser effectiveness based on ideal thrust ($\eta_{fan_{id}}$), and thrust reverser area match parameter (β) are plotted against fan nozzle pressure ratio (FNPR). The performance of the baseline cascade thrust reverser with the aft port open and no blocker leakage (configuration 203) is shown in figure 23(a). The overall thrust reverser effectiveness level is about 0.31, which is typical of cascade thrust reversers (ref. 7). The fan reverser effectiveness level is about 0.54. The thrust reverser area match parameter, which is a measure of the change in effective flow exit area

from forward thrust to reverse thrust, varies between 95 to 98 percent, or 0.02 to 0.05 percent lower than that of the fan nozzle in the forward thrust mode ($\beta = 1.0$). Recall, that β should be close to 1 to minimize any adverse effects of reverser operation on fan operation. As nozzle operation transitions from forward thrust to reverse thrust, a reduction in the fan effective flow area ($\beta<1$) could shift the fan operating point into a surge condition.

Effects of Cascade Port Area. The effects of cascade port area on cascade thrust reverser performance with no blocker leakage are also shown in figure 23(a). Closing off the aft port of the cascade vanes (from configuration 203 to configuration 201) reduces η_{rev} because of the lower gross reverse thrust (smaller reverser port); however, there is little change in $\eta_{fan_{id}}$. The reduction in cascade port area results in an approximate 10 percent reduction in β.

Effects of Blocker Leakage. The effects of blocker leakage (low values of porosity) on cascade thrust reverser performance are shown in figure 23(b). Blocker leakage causes small reductions in η_{rev}. Blocker leakages equivalent to 5% and 12% of the fan duct area result in an approximate 0.03 and 0.07 drop in $\eta_{fan_{id}}$, respectively. The configuration with 5% blocker leakage best matches the effective area of the forward thrust nozzle. At 12% blocker leakage, β is over 1.0.

Cascade Thrust Reverser with Porous Blocker

The effects of blocker porosity (high values of porosity) on cascade thrust reverser performance are also shown in figure 23(b). The porous blocker increases the leakage through the blocker system with little increase in forward thrust due to the diffusion of the leakage flow within the diffused fan nozzle. A blocker porosity (blocker open area/fan duct area) of about 25% results in an approximate 0.14 drop in $\eta_{fan_{id}}$, as compared to the no leak (0% porosity) configuration. Increasing the porosity to 50% reduced $\eta_{fan_{id}}$ an additional 0.20 to value of about 0.20. The effect of flow leakage through the porous blocker on β is significant. To bring the effective area back to that of the forward thrust nozzle ($\beta=1$), a reduction in the cascade port area would be required. Based on the effect of port area discussed previously, reducing cascade port area would not be expected to impact $\eta_{fan_{id}}$ significantly, but would reduce η_{rev} by reducing gross reverse thrust. Even if reverse thrust were reduced to zero (thrust completely spoiled), the blocker door weight reduction resulting from high values of porosity may still be a favorable trade for the entire system. The data obtained from this investigation provides a basis for evaluating these blocker leakage/reverser effectiveness trades.

Blockerless Thrust Reverser

Thrust reverser performance characteristics for all blockerless thrust reverser configurations tested are presented in Appendix D. A summary of blockerless thrust reverser performance is presented in figure 24. The fan reverser effectiveness based on ideal thrust ($\eta_{fan_{id}}$), cascade vane total weight-flow ratio ($w_{cas}/w_{p,tot}$), fan nozzle total weight-flow ratio ($w_{noz}/w_{p,tot}$), and the injection weight-flow ratio ($w_{inj}/w_{p,fan}$) are plotted against fan nozzle pressure ratio (FNPR). Recall that core flow was not simulated and that the practical injection weight-flow ratio for blockerless thrust reverser configurations is assumed to be 0.05.

Effects of Single Injection Location. The effects of a single injection location (mid, aft, or throat) on blockerless thrust reverser performance at an injection pressure ratio (IPR) of 12 for configurations with a 0.025 in. slot width (w_s) and 45° injection angle (θ) are shown in figure 24(a). For these configurations, only the throat injection location provides reverse thrust ($\eta_{fan_{id}}>0$) for FNPR≥1.2; however, injection weight-flow ratios at these conditions are substantially higher than the 0.05 practical limit.

Effects of Multiple Injection Locations. The effects of multiple injection locations (fwd/aft, mid/aft, or fwd/mid/aft) on blockerless thrust reverser performance at IPR=12 for configurations with w_s=0.013 in. and θ=45° are shown in figure 24(b). For these configurations, a substantial amount of reverse thrust is achieved at low FNPR's, although $\eta_{fan_{id}}$ decreases rapidly with increasing FNPR. The trend of decreasing $\eta_{fan_{id}}$ with increasing FNPR was expected for the blockerless thrust reverser concept, which relies on the momentum of injected flow to turn the fan flow through the cascade port. Thus, as fan flow momentum is increased (increasing FNPR) for a constant value of injection momentum, the flow turning capability of the injected flow decreases. Unfortunately, injection weight-ratios are above the practical limit of 0.05 at all conditions.

Effects of Slot Size. The effects of slot size (w_s=0.013 in. and w_s=0.025 in.) on blockerless thrust reverser performance at IPR=12 for configurations with throat injection and θ=45° are shown in figure 24(c). These configurations achieve levels of $\eta_{fan_{id}}$ as high as 0.38; as expected, the amount of reverse thrust generated decreases with increasing FNPR. Reverse thrust levels are highest for w_s=0.025 in., but the required injection weight-flow ratio is well above the practical limit of 0.05. Configuration 617 (w_s=0.013 in.) has injection weight-flow ratios approaching the practical limit at the highest FNPR values; however, the amount of reverse thrust generated at these conditions is small.

Effects of Slot Angle. The effects of slot angle (θ=45° and θ=90°) on blockerless thrust reverser performance at IPR=12 for configurations with fwd, mid, and aft injection and w_s=0.013 in. are shown in figure 24(d). For these configurations, the effect of θ shows the dramatic benefit of canting the injection slots forward at a 45° angle. Reverse thrust is achieved for configuration 603 (θ=45°); but, configuration 606 (θ=90°) does not achieve reverse thrust. Unfortunately, the injection weight-flow ratio for configuration 603 is well above the practical limit of 0.05.

Effects of Injection Tab. The effects of the injection tab on blockerless thrust reverser performance at IPR=12 for configurations with a w_s=0.013 in., θ=45°, and aft injection are shown in figure 24(e). The injection tab is a partial annular blocker that, when deployed, locally reduces the fan duct height. While the tab adds a degree of mechanical complexity to the blockerless thrust reverser design, it reduces the distance the injection flow must penetrate in order to block the fan exhaust flow and turn it out the cascade vanes. It was hypothesized during the experimental design phase that the injection flow penetration distance may be critical in high-bypass-ratio applications and a mechanism (e.g., a tab) to reduce this distance might be necessary to achieve effective reverser performance at practical injection weight-flow ratios. As shown in figure 24(e), the effect of the tab (compare configurations 611 and 614) is to substantially increase the reverse thrust performance of the blockerless thrust reverser concept. However, the injection weight-flow ratio for these configurations is still above the practical limit of 0.05.

Effects of IPR. The effects of IPR on blockerless thrust reverser performance for configuration 611 are shown in figure 24(f). A notable finding from this figure is that levels of $\eta_{fan_{id}}$ between 0.15 and 0.38 are achieved at IPR=4.0 within the practical injection weight-flow ratio limit of 0.05. It is also notable that, with no injection, up to 45% of the fan flow went out of the cascade vanes (denoted by $w_{cas}/w_{p,tot}\approx 0.45$) and the thrust was completely spoiled ($\eta_{fan_{id}}\approx 0$). Because most of the engine generated retarding force on high BPR engines comes from inlet ram drag, thrust spoiling may be sufficient to generate the necessary stopping force on aircraft equipped with high BPR engines; however, for aircraft equipped with low BPR engines (lower inlet ram drag), it is more critical to produce reverse thrust. A review of the figures presented in Appendix D indicates that the tab configurations (611 and 612) are the only configurations capable of providing reverse thrust for FNPR≥1.2 at practical injection weight-flow ratios. This finding supports the earlier hypothesis that the injection flow penetration distance is critical to the success of the blockerless thrust reverser concept. This finding is further supported by the research

documented in reference 6, which demonstrated that, for a BPR=5.0 application, the blockerless thrust reverser concept can achieve levels of $\eta_{fan_{id}}$ in the range of 0.30 to 0.40 with injection flow-ratios at or below the practical limit of 0.05.

Annular (Metal) Target Thrust Reverser

Thrust reverser performance characteristics for all annular (metal) target thrust reverser configurations tested are presented in Appendix E. A summary of annular target thrust reverser performance is presented in figure 25. The overall thrust reverser effectiveness (η_{rev}), fan reverser effectiveness based on ideal thrust ($\eta_{fan_{id}}$), and thrust reverser area match parameter (β) are plotted against the fan nozzle pressure ratio (FNPR). Compared to the conventional cascade thrust reverser with 5% porous blocker (configuration 204), the annular (metal) target thrust reverser concepts investigated achieve somewhat lower levels of fan reverser effectiveness. Fan reverser effectiveness levels for the 40° annular target vary from about 0.30 to 0.40 (fig. 25(a)). An increase in the reverser area ratio (AR) results in a decrease in $\eta_{fan_{id}}$. Extending the length of the 40° target (configuration 308) improves $\eta_{fan_{id}}$ approximately 0.10 to the highest thrust reverser effectiveness levels for the annular (metal) target thrust reverser configurations. The levels of $\eta_{fan_{id}}$ for the 40° annular target configurations are approximately 0.35 to 0.40 higher than the 20° targets (fig. 25(b)). The 20° annular (metal) target thrust configurations only achieve reverse thrust when the kicker plate is installed (configuration 304). The kicker plate increases $\eta_{fan_{id}}$ for the 20° target by about 0.07 when compared to the same AR without the kicker plate. Recall that the length of the 20° target kicker plate was selected to set an AR=1.05 when installed in the AR=1.25 position. Results show that with the kicker installed, β is nearly the same as that of the AR=1.05 target location (fig. 25(b)).

The thrust reverser area match parameter for both target angles is about half that of the forward thrust nozzle. Increasing the exit area ratio increases the effective reverser area. The 20° target configurations exhibit a 0.02 to 0.05 higher effective flow area than the 40° targets. The significant reduction in the effective exit area of the annular (metal) target thrust reverser results from very inefficient flow turning around the sharp edge of the fan cowl trailing edge.

The decrease in $\eta_{fan_{id}}$ with increasing AR is attributed to a decrease in the reverser efflux angle (more vertical) caused by a flattening of the reverser exit plane. To increase the reverser exit area, the annular (metal) target is moved aft on the core nozzle. As the target is moved aft with a fixed target height (diameter), the geometric exit plane formed by the fan cowl trailing edge and forward edge of the target becomes more horizontal (thrust vector more vertical). This reduces the nominal reverser efflux angle and the reverse thrust component.

The effect of the target extension (length) provides support for this explanation. As shown in figure 25(a), for the 40° target with AR=1.25, extending the target length improves $\eta_{fan_{id}}$ by 0.09, with little or no effect on β. This result indicates that the effect of reverser area ratio on reverser effectiveness is primarily due to changes in the orientation of the effective reverser exit plane.

These results indicate that the range of area ratios selected for the annular (metal) target thrust reverser concepts are much too low. Either the aerodynamic shape of the fan cowl trailing edge must be improved (to promote Coanda flow turning and prevent separation) or the annular target needs to be moved aft to properly match the annular reverser concept with the forward thrust nozzle. The amount of effective reverser flow area that can be set for a given target angle is limited by the length of the core cowl downstream of the fan exit. The separate-flow nozzle design used for this investigation does not have sufficient length to install hinged target panels farther aft. The target could be refined to include an additional degree of mechanical articulation to produce an annular target having a larger diameter and

greater reverser exit area; however, increases in weight and mechanical complexity would result.

Fabric Target Thrust Reverser

Thrust reverser performance characteristics for all fabric target thrust reverser configurations tested are presented in Appendix F. A summary of fabric target thrust reverser performance is presented in figure 26. The overall thrust reverser effectiveness (η_{rev}), fan reverser effectiveness based on ideal thrust ($\eta_{fan_{id}}$), and thrust reverser area match parameter (β) are plotted against the fan nozzle pressure ratio (FNPR). The highest fan reverser effectiveness achieved for the fabric target thrust reverser is about 0.25, obtained with the 40° target angle and long fabric length. For both the 20° and 40° target angles, the configuration with the long fabric length demonstrates the best performance. Increasing the fabric length from short to long with the target angle set at 40° results in about a 0.13 increase in $\eta_{fan_{id}}$.

Recall that the nominal (unloaded) shape/length of the short and long fabrics are the same as the internal surface contours of the 20° and 40° metal targets, respectively. If the inflated shape of the fabric reversers matched the internal contours of the metal targets, then the performance of the 20° target with short fabric length should match that of the 20° annular (metal) target, and the performance of the 40° target with long fabric length should match that of the 40° annular (metal) target. The comparisons of the annular (metal) and fabric target thrust reverser performance characteristics presented in figure 27 show that this is not the case. For both the 20° and 40° target angles, the fabric target reverser effectiveness levels are about 0.07 to 0.09 lower than the metal target reverser effectiveness levels. This result can be attributed to three factors: (1) uporting of the fabric near the pylon (fabric is not attached at the pylon), (2) the fabric assuming a shape under operating air pressure loads which reduces the effective reverser efflux angle (more vertical), thereby producing a smaller reverse thrust component, and (3) leakage of the air flow through the porous fabric.

The variation in β with target angle for the fabric target thrust reversers (fig. 26) are similar to those obtained with the annular (metal) target thrust reversers in that an increase in target angle results in a decrease in β. For the 40° target, an increase in β was obtained with the longer fabric (fig 26). Compared to the metal target (fig. 27), the effective area of both the 20° and 40° fabric thrust reversers is about 0.04 higher than that of the metal (with no leakage) annular target. The cause of this increase in flow can be attributed to a combination of leakage through the porous fabric and unporting of the fabric adjacent to the pylon. In addition, the section of fabric between the support brackets billows out under air pressure loads, affecting an increase in the reverser exit area. The demonstrated performance improvement of the long fabric length over the short fabric length indicates that longer fabric lengths (than those tested) may be beneficial.

Multi-Door Crocodile Thrust Reverser

Thrust reverser performance characteristics for all multi-door crocodile thrust reverser configurations tested are presented in Appendix G. A summary of multi-door crocodile thrust reverser performance is presented in figure 28. The overall thrust reverser effectiveness (η_{rev}), fan reverser effectiveness based on ideal thrust ($\eta_{fan_{id}}$), and thrust reverser area match parameter (β) are plotted against the fan nozzle pressure ratio (FNPR).

Effects of Inner Door Leakage. The effects of inner door leakage on multi-door crocodile thrust reverser performance are shown in figure 28(a) for multi-door crocodile thrust reverser configurations with the inner doors at 36° and the outer doors at 60° (inner and outer doors fully deployed). With the inner doors fully deployed, fan flow is able to leak through small gaps between the inner doors; inner

doors and the pylon; and inner doors and the lower fan-duct bifurcator (see fig. 11(c)). It is estimated that this "maximum leakage" configuration (configuration 511) allows approximately 2% of the fan flow to leak past the inner doors. The fan reverser effectiveness for the "maximum leakage" configuration ranges from approximately 0.21 to 0.24 across the range of FNPR tested. By adding filler pieces (fig. 11(p)) adjacent to the pylon and lower fan-duct bifurcator, a "partial leakage" configuration (configuration 512) is created. The addition of the filler pieces eliminates the majority of the leakage between the inner doors and pylon and inner doors and lower fan-duct bifurcator, resulting in a 0.08 increase in $\eta_{fan_{id}}$ (fig. 28(a)). The associated reduction in leakage due to the addition of the filler pieces results in a 0.06 decrease in β. To provide a "no leak" data base for CFD code validation, all of the gaps between the inner doors; inner doors and pylon; and inner doors and lower fan-duct bifurcator were sealed with aluminum tape (configuration 543). As shown in figure 28(a), the effect of completely sealing the joints in the inner doors is about a 0.01 increase in $\eta_{fan_{id}}$ and a 0.04 decrease in β.

Effects of Reverser Port Bullnose Radius. Typical results showing the effects of reverser port bullnose radius (r, see figure 11(g)) are presented in figure 28(b) for multi-door crocodile thrust reverser configurations with the inner and outer door fully deployed. The effects of r on $\eta_{fan_{id}}$ are very small (less than 0.01); however, decreasing r results in a decrease in the effective reverser port area (A_{port}). The trends show about a 0.02 reduction in β for each decrement in r. These results are typical of those obtained for all of the configurations tested.

Effects of Reverser Port Area Ratio. Typical results showing the effect of reverser port area ratio (AR) are presented in figure 28(c) for multi-door crocodile thrust reverser configurations with the inner and outer door fully deployed. The relative magnitude of the port area reductions represented by the area ratios tested (1.60, 1.53, and 1.45) is about 4.4 and 9.4 percent, relative to AR=1.60 (configuration 519). For each decrement in AR, a 0.01 to 0.02 increase in $\eta_{fan_{id}}$ is realized. Each decrement in AR also results in an approximate 0.04 reduction in β.

Effects of Outer Door Kicker Plate. Typical results showing the effects of outer door kicker plates are presented in figure 28(d) for multi-door crocodile configurations with the inner doors fully deployed and the outer doors deployed at 50°. The effects of the "long/cutback" kicker plate (configuration 517) are to increase $\eta_{fan_{id}}$ by approximately 0.03 over configuration 518 (no kicker plate) with a small (about 0.01) increase in β. A further increase in kicker plate size to the "X-long/cutback" kicker plate geometry (configuration 516) tends to overturn the fan exhaust flow towards the engine centerline as indicated by a 0.01 decrease in $\eta_{fan_{id}}$ from the long/cutback kicker geometry (configuration 517). These kicker plate effects are consistent with those obtained when the outer doors are positioned to 40° (configurations 514 and 515) and 60° (configurations 519 and 520), although the performance decrement in $\eta_{fan_{id}}$ associated with the "X-long/cutback" kicker is smaller with the 60° door angle (see data presented in Appendix G). These results indicate that there is an optimum length for the kicker plate and that this length is likely a function of the outer door angle.

Effects of Outer Door Cutback. Typical results showing the effects of outer door cutback are presented in figure 28(e) for multi-door crocodile thrust reverser configurations with the inner and outer doors fully deployed. The effects of the "partial", "mixed", and "full" cutbacks are similar; each cutback results in a small decrease (about 0.02) in $\eta_{fan_{id}}$. With the outer doors positioned to 50° (configurations 526, 525, and 524) and 40° (configurations 527 and 528), the variation in $\eta_{fan_{id}}$ between the full size doors and the doors with full cutback was even less (about 0.01, see data presented in Appendix G). The effect of cutback on β is small at both the 60° (fig. 28(e)) and 50° (see data presented in Appendix G) outer door angles, despite the installation of the reverser port door covers at the leading edge of the port. For the 40° outer door angle (see data presented in Appendix G) the minimum outer door cutback results in a

reduction in β of about 0.03.

Effects of Outer Door Angle with Full Size Outer Doors (No Cutback). Typical results showing the effects of outer door deployment angle with full size outer doors (no cutback) are presented in figure 28(f) for multi-door crocodile thrust reverser configurations with the inner doors fully deployed. These configurations show only small changes in $\eta_{fan_{id}}$ with outer door deployment angles between 30° and 60°. Reducing the outer door angle to 20° (configuration 575) actually increases $\eta_{fan_{id}}$ by about 0.02, but reduces η_{rev} by about the same amount. The area match parameter is similar with the outer doors at 60° (configuration 579) and 50° (configuration 578); however, a substantial reduction in effective port area can be noted from the reduction in β at lower outer door deployment angles. This result was not unexpected. In actual operation, the inner door deployment angle would be scheduled with the outer door deployment angle in order to maintain a constant value of β. See the "Effects of Inner and Outer Door Deployment Schedule" discussion below.

Effects of Outer Door Angle with Full Cutback Outer Doors. Typical results showing the effects of outer door angle with full cutback outer doors are presented in figure 28(g) for multi-door crocodile thrust reverser configurations with the inner doors fully deployed. For the full cutback outer door configurations, increasing the outer door deployment angle from 40° (configuration 528) to 50° (configuration 524) results in a small (about 0.01) decrease in $\eta_{fan_{id}}$ and a 0.02 increase in β. Further increasing the outer door deployment angle from 50° (configuration 524) to 60° (configuration 523) results in a reduction in $\eta_{fan_{id}}$ of about 0.04 with little change in β. These trends are typical of all bullnose shapes and port sizes (bullnose spacer) investigated. The relative magnitudes of the difference in multi-door crocodile thrust reverser performance are the same. In all cases investigated, the value of $\eta_{fan_{id}}$ was obtained with a 50° outer door deployment angle.

Effects of Inner and Outer Door Deployment Schedule. Combinations of inner and outer door deployment angles were tested to provide a data base from which to evaluate blocker door deployment schedules. The variations in η_{rev}, $\eta_{fan_{id}}$, and β during a nominal schedule of the inner and outer doors are shown in figure 28(h). The results presented indicate that:

a) Deploying the inner door 6° and the outer door 10° results in a significant decrease in β. Refinements in the reverser kinematics are required to maintain β within acceptable limits.

b) Further deployment of the inner and outer doors through the intermediate angles increases β to values greater than 1.

c) Due to leakage past the inner blocker door, no reverse thrust is achieved until the inner doors are nearly fully deployed.

d) With the inner doors fully deployed, β drops back below 1 at low FNPR and the maximum value of $\eta_{fan_{id}}$ is obtained.

These results demonstrate the operating characteristics of the multi-door crocodile thrust reverser concept and highlight some of the concerns that must be addressed to develop the blocker door deployment schedule. Results obtained from this investigation provide a data base from which to assess the effects of configuration geometry and door deployment options.

Wing-Mounted Thrust Reverser

A summary of overall thrust reverser effectiveness (η_{rev}) plotted against fan nozzle pressure ratio (FNPR) for the wing-mounted thrust reverser configurations with parallel deflector mount angle, long deflector chord length, and deflector edge fences installed is presented in figure 29 for all deflector angles (ψ) tested. Data for these configurations show that the highest value of η_{rev} occurs for configurations with ψ_3=30°, while the ψ_2 has the most substantial effect on η_{rev}; the highest values of η_{rev} generally occur for configurations with ψ_2 of 0° or less. The overall thrust reverser effectiveness level for configurations with $\psi_2 \leq 0°$ ranges from about 0.30 to 0.44 at FNPR≈1.1 and decreases with increasing FNPR. This performance is competitive with cascade-type thrust reverser systems, which have η_{rev} values on the order of 0.35 to 0.40 (ref. 7).

There are three deflector angle combinations that, depending on FNPR, produce the highest values of η_{rev}. At FNPR values from 1.1 to about 1.25, the configuration with ψ_1=60°, ψ_2=-15°, and ψ_3=30° has the highest η_{rev}. At FNPR values from 1.25 to about 1.5, the configuration with ψ_1=60°, ψ_2=0°, and ψ_3=30° has the highest η_{rev}. At the remaining FNPR values from 1.5 to about 1.6, the configuration with ψ_1=45°, ψ_2=0°, and ψ_3=30° has the highest values of η_{rev}. Therefore, with a parallel deflector mount angle, long deflector chord length, and deflector edge fences installed, these three geometries can be considered the optimum deflector "bucket" shapes for producing the maximum level of reverse thrust over the FNPR range tested. In order to understand the effect of deflector angle and other geometry variations, these configurations will be used (whenever possible) for relative comparisons in the following discussion.

Although not shown in figure 29, large lateral force (C_Y) and moment (C_n) coefficients are generated by the wing-mounted thrust reverser configurations at the parallel (to wing trailing edge) deflector mount angle. This is a result of the deflector system being positioned at a yaw angle with respect to the exhaust flow (where the exhaust flow is not only reversed, but is also thrust vectored in the yaw plane). Note that lateral forces and moments would cancel on a twin engine aircraft configuration with both engines operating at the same reverse thrust condition. A single engine failure in reverse thrust would result in large unopposed C_Y and C_n values that would have to be compensated for by the vertical tail or other control surfaces.

Effects of Deflector 1 Angle (ψ_1). The effects of ψ_1 on wing-mounted thrust reverser performance with parallel deflector mount angle, long deflector chord length, and deflector edge fences installed are presented in figure 30 for configurations with ψ_3=30°. The effect of ψ_1 on η_{rev} is most substantial at FNPR values of about 1.4 or less, with η_{rev} increasing with increasing ψ_1. This is not surprising, since the increased flow turning angle provided by larger values of ψ_1 would be expected to provide higher values of η_{rev}. The smaller area for thru-wing flow turning that results from larger values of ψ_1 does not appear to degrade η_{rev}.

At higher values of FNPR, differences in η_{rev} are very small and there is no consistent trend in η_{rev} with changing ψ_1. The effect of ψ_1 on longitudinal and lateral force and moment coefficients is generally small; the only significant changes with ψ_1 occur in pitching moment coefficient (C_m). The small differences in C_m between configurations most likely result from changes in the reverser efflux pattern and differences in the pressure distributions across the deflectors and wing surfaces.

Effects of Deflector 2 Angle (ψ_2). The effects of ψ_2 on wing-mounted thrust reverser performance with parallel deflector mount angle, long deflector chord length, and deflector edge fences installed are presented in figure 31 for configurations with ψ_1=45°. The highest values of η_{rev} typically occur for configurations with ψ_2=0° and the differences between other values of ψ_2 increase with increasing FNPR.

Although not shown in figure 31, it is obvious from the data presented previously in figure 29 that further increases in ψ_2 (to positive values) would result in reduced η_{rev}. For deflection angles where ψ_2 is negative, a lift force is produced on deflector 2 which increases C_N and C_m. This is attributed to pressure differences acting on the horizontal component of the deflector. The effects of ψ_2 on lateral force and moment coefficients are generally small.

Note that increased values of C_N and C_m are indicative of a tendency of many wing-mounted thrust reverser configurations to generate lift forces. Generally, this is undesirable for a thrust reverser concept since it would act to reduce the amount of airplane weight on the wheels, thereby reducing wheel braking effectiveness. Conversely, reduced values of C_N would be desirable since this would tend to increase wheel braking effectiveness by putting more of the aircraft weight on the wheels.

Effects of Deflector 3 Angle (ψ_3). The effects of ψ_3 on wing-mounted thrust reverser performance with parallel deflector mount angle, long deflector chord length, and deflector edge fences installed are presented in figure 32 for configurations with ψ_1=60°. The effects of ψ_3 for configurations with ψ_2=-15° (fig. 32(a)) show significantly increased η_{rev} and reduced C_N and C_m occurring for the larger values of ψ_3. Increasing ψ_3 results in a larger horizontal surface component on which exhaust pressures may act, resulting in more negative lift forces and pitching moments.

The effects of ψ_3 for configurations with ψ_1=60° and ψ_2=0° (fig. 32(b)) are smaller than that shown for configurations with ψ_2=-15° (figure 32(a)), with increased η_{rev} and reduced C_m occurring at the smaller value of ψ_3. As discussed previously, configurations with ψ_3=30° generally provide the highest values of η_{rev} regardless of the other flap deflection values. The effects of ψ_3 on the other force and moment coefficients are similar to those discussed above.

Effects of Deflector Edge Fences. The effects of deflector edge fences (installed vs. removed) on wing-mounted thrust reverser performance with parallel deflector mount angle and long deflector chord length are presented in figure 33 for configurations with ψ_1=60° and ψ_3=30°. Removing the deflector edge fences results in a substantial drop in overall reverser effectiveness but produces only small changes in force and moment coefficients. The drastic reduction in η_{rev} that occurs when the fences are removed is a result of increased exhaust flow spreading/spillage in the lateral direction. This results in a reduced amount of exhaust flow that is turned by the deflector toward the upstream direction to produce reverse thrust. Although the deflector edge fences are relatively small (approximately 12% of the deflector chord length), their substantial flow turning benefit significantly improves η_{rev}.

Effects of Deflector Chord Length. The effects of deflector chord length (long vs. short) on wing-mounted thrust reverser performance with parallel deflector mount angle and deflector edge fences installed are presented in figure 34 for configurations with ψ_1=60° and ψ_3=30°. The short chord length has substantially lower η_{rev} than the long chord length. The effects of chord length on force and moment coefficients are generally small. The reduction in η_{rev} that occurs when deflector chord length is reduced is most likely caused by some of the exhaust flow passing below the bucket formed by deflectors 2 and 3. Exhaust flow which is not captured by the deflectors would produce forward thrust and reduce η_{rev}.

Effects of Deflector Mount Angle. The effects of deflector mount angle (parallel vs. normal) on wing-mounted thrust reverser performance with long deflector chord length and deflector edge fences installed is presented in figure 35 for configurations with ψ_3=30°. There are substantial increases in η_{rev} and reductions in C_Y and C_n when the deflector system is positioned normal to the exhaust flow. This is a result of eliminating the thrust vectoring effect that acts to reduce η_{rev} and generate C_Y and C_n when the deflectors are mounted parallel to the wing trailing edge.

Besides the obvious advantage of increasing η_{rev} to values as high as 60%, the normal deflector mount configuration would eliminate some of the concern over large asymmetric lateral forces and moments that would occur during a single engine failure in reverse thrust. A disadvantage for the normal mount configuration would be the additional degree of articulation (rotation of the deflector flap system) that could be required. The fact that a parallel deflector mount provides reverser performance competitive with a conventional cascade thrust reverser system indicates that a normal deflector mount position may not be required for the wing-mount thrust reverser concept to be viable.

Concluding Remarks

Test results have shown that several innovative thrust reverser concepts achieve thrust reverser effectiveness levels which, when considering the potential for system simplification and reduced weight, may make them competitive with the current state-of-art thrust reverser systems. Although the configurations investigated were primarily conceptual, the results obtained provide a data base from which to assess thrust reverser performance and conduct preliminary design tradeoffs for some of the more important geometric parameters. The favorable results obtained also justify further concept refinement and more detailed systems studies to better identify and assess the actual system tradeoffs.

References

1. Yetter, Jeffrey A.: *Why Do Airlines Want and Use Thrust Reversers?* NASA TM-109158, January 1995.

2. Mercer, Charles E.; Berrier, Bobby L.; Capone, Francis J.; and Grayston, Alan M.: *Data Reduction Formulas for the 16-Foot Transonic Tunnel-NASA Langley Research Center. Revision 2.* NASA TM-107646, 1992.

3. Staff of the Propulsion Aerodynamics Branch: *A User's Guide to the Langley 16-Foot Transonic Tunnel Complex, Revision 1.* NASA TM-102750, 1990.

4. Poland, Dyckman T.: The Aerodynamics of Thrust Reversers for High Bypass Turbofans. AIAA 67-418, July 1967.

5. J. van Hengst, J.: *Aerodynamic Integration of Thrust Reversers on the Fokker 100.* AGARD-CP-498, 1992.

6. Tindell, R.H.; Marconi, F.; Kalkhoran, I.; and Yetter, J.: Deflection of Turbofan Engine Exhaust Streams for Enhanced Engine/Nacelle Integration. AIAA 97-3152, July 1997.

7. Romine, B.M., Jr.; and Johnson, W.A.: Performance Investigation of a Fan Thrust Reverser for a High By-Pass Turbofan Engine. AIAA-84-1178, June 1984.

Table 1. Description of Separate-Flow Exhaust System Model Configurations Tested

Test	Run	Config.	Operation Mode	Configuration Description	
				Fan-Duct Bifurcator Installed	Wing Installed
987	5	101	Core Only	No	No
987	6	101	Core Only	No	No
992	2	101	Core Only	No	No
992	3	101	Fan Only	No	No
992	5	101	Dual Flow	No	No
994	1	501	Dual Flow	Yes	No
1001	1	101	Core Only	No	No
1001	2	101	Fan Only	No	No
1001	3	101	Dual Flow	No	No
1001	13	701	Core Only	No	Yes
1001	14	701	Fan Only	No	Yes
1001	15	701	Dual Flow	No	Yes
1001	81	501	Core Only	Yes	No
1001	82	501	Fan Only	Yes	No
1001	83	501	Dual Flow	Yes	No

Table 2. Description of Conventional Cascade Thrust Reverser Model Configurations Tested

Test	Run	Config.	Operation Mode	Configuration Description			
				Cascade Aft Port	Blocker Porosity	Fan-Duct Bifurcator Installed	Wing Installed
987	14	201	Dual Flow	Closed	0%	No	No
987	17	202	Dual Flow	Closed	5%	No	No
987	18	203	Dual Flow	Open	0%	No	No
987	19	204	Dual Flow	Open	5%	No	No
987	20	205	Dual Flow	Open	12%	No	No
992	6	206	Fan Only	Open	0%	No	No

Table 3. Description of Cascade Thrust Reverser with Porous Blocker Model Configurations Tested

Test	Run	Config.	Operation Mode	Configuration Description			
				Cascade Aft Port	Blocker Porosity	Fan-Duct Bifurcator Installed	Wing Installed
987	24	208	Dual Flow	Open	50%	No	No
987	25	209	Dual Flow	Open	25%	No	No

Table 4. Description of Blockerless Thrust Reverser Model Configurations Tested

Test	Run	Config.	Operation Mode	Configuration Description							
				Cascades Installed	Injection Location and Geometry					Fwd Bullnose	Port Fairing
					Duct	Fwd	Mid	Aft	Throat		
993	1	601	Injection Only	Yes			0.013”@45°	0.025” holes		Bullnose	#1
993	2	601	Fan+Injection	Yes			0.013”@45°	0.025” holes		Bullnose	#1
993	3	601	Fan Only	Yes			0.013”@45°	0.025” holes		Bullnose	#1
993	4	602	Fan Only	Yes			0.013”@45°	0.025” holes		Bullnose	#2
993	5	602	Fan+Injection	Yes			0.013”@45°	0.025” holes		Bullnose	#2
993	6	603	Fan Only	Yes		0.013”@45°	0.013”@45°	0.013”@45°		Bullnose	#2
993	7	603	Fan+Injection	Yes		0.013”@45°	0.013”@45°	0.013”@45°		Bullnose	#2
993	8	604	Fan Only	Yes		0.013”@45°		0.013”@45°		Bullnose	#2
993	9	604	Fan+Injection	Yes		0.013”@45°		0.013”@45°		Bullnose	#2
993	10	605	Fan Only	Yes		0.013”@90°		0.013”@90°		Bullnose	#2
993	11	605	Fan+Injection	Yes		0.013”@90°		0.013”@90°		Bullnose	#2
993	12	606	Fan Only	Yes		0.013”@90°	0.013”@90°	0.013”@90°		Bullnose	#2
993	13	606	Fan+Injection	Yes		0.013”@90°	0.013”@90°	0.013”@90°		Bullnose	#2
993	14	607	Fan Only	Yes		0.025”@90°				Bullnose	#2
993	15	607	Fan+Injection	Yes		0.025”@90°				Bullnose	#2
993	17	608	Fan Only	No		0.025”@90°				Coanda #3	#2
993	19	608	Fan+Injection	No		0.025”@90°				Coanda #3	#2
993	21	609	Fan Only	Yes		0.025”@90°				Coanda #1	#2
993	23	609	Fan+Injection	Yes		0.025”@90°				Coanda #1	#2
993	24	609	Fan+Injection	Yes		0.025”@90°				Coanda #1	#2
993	25	610	Fan Only	Yes		0.025”@90°				Coanda #2	#2
993	26	610	Fan+Injection	Yes		0.025”@90°				Coanda #2	#2
993	27	611	Fan Only	Yes				0.025” tab 3		Bullnose	#2
993	28	611	Fan+Injection	Yes				0.025” tab 3		Bullnose	#2
993	29	612	Fan Only	Yes				0.025” tab 1		Bullnose	#2
993	30	612	Fan+Injection	Yes				0.025” tab 1		Bullnose	#2
993	31	613	Fan Only	Yes					0.025”@45°	Bullnose	#2
993	32	613	Fan+Injection	Yes					0.025”@45°	Bullnose	#2
993	33	614	Fan Only	Yes				0.025”@45°		Bullnose	#2

Note: Lower fan-duct bifurcator and wing section not installed.

Table 4. Concluded

Test	Run	Config.	Operation Mode	Configuration Description							
				Cascades Installed	Injection Location and Geometry					Fwd Bullnose	Port Fairing
					Duct	Fwd	Mid	Aft	Throat		
993	34	614	Fan+Injection	Yes				0.025”@45°		Bullnose	#2
993	35	615	Fan Only	Yes			0.025”@45°			Bullnose	#2
993	36	615	Fan+Injection	Yes			0.025”@45°			Bullnose	#2
993	37	616	Fan Only	Yes			0.013”@45°	0.013”@45°		Bullnose	#2
993	38	616	Fan+Injection	Yes			0.013”@45°	0.013”@45°		Bullnose	#2
993	39	617	Fan Only	Yes					0.013”@45°	Bullnose	#2
993	40	617	Fan+Injection	Yes					0.013”@45°	Bullnose	#2

Note: Lower fan-duct bifurcator and wing section not installed.

Table 5. Description of Annular (Metal) Target Thrust Reverser Model Configurations Tested

Test	Run	Config.	Operation Mode	Configuration Description				
				Target Angle	Area Ratio	Kicker or Extension	Fan-Duct Bifurcator Installed	Wing Installed
987	28	301	Dual Flow	20°	1.05	None	No	No
987	30	302	Dual Flow	20°	1.15	None	No	No
987	31	303	Dual Flow	20°	1.25	None	No	No
987	32	304	Dual Flow	20°	1.25	Kicker	No	No
987	33	305	Dual Flow	40°	1.05	None	No	No
987	34	306	Dual Flow	40°	1.15	None	No	No
987	35	307	Dual Flow	40°	1.25	None	No	No
987	36	308	Dual Flow	40°	1.25	Extension	No	No

Table 6. Description of Fabric Target Thrust Reverser Model Configurations Tested

Test	Run	Config.	Operation Mode	Configuration Description				
				Target Angle	Area Ratio	Fabric Length	Fan-Duct Bifurcator Installed	Wing Installed
987	37	401	Dual Flow	20°	1.15	Short	No	No
987	38	402	Dual Flow	40°	1.15	Short	No	No
987	39	403	Dual Flow	40°	1.15	Long	No	No
987	40	404	Dual Flow	20°	1.15	Long	No	No

Table 7. Description of Multi-Door Crocodile Thrust Reverser Model Configurations Tested

Test	Run	Config.	Operation Mode	Configuration Description										
				Reverser Port			Outer Door				Inner Door		Door	
				Bullnose	Spacer	Cover	Angle	Cutback	Kicker	Fence	Angle	Fillers	Struts	Leakage
988	1	502	Dual Flow	#1	None	None	60°	None	Long/CB	None	36°	None	Yes	Maximum
988	2	503	Fan Only	#1	None	None	60°	None	None	None	36°	None	Yes	Maximum
988	3	504	Fan Only	#1	0.20”	None	60°	None	Long/CB	None	36°	None	Yes	Maximum
988	4	505	Fan Only	#1	0.40”	None	60°	None	Long/CB	None	36°	None	Yes	Maximum
988	5	506	Fan Only	#2	0.40”	None	60°	None	Long/CB	None	36°	None	Yes	Maximum
988	6	507	Fan Only	#3	0.40”	None	60°	None	Long/CB	None	36°	None	Yes	Maximum
988	7	508	Fan Only	#1	None	None	60°	None	Long/CB	None	36°	All	Yes	Partial
988	8	509	Fan Only	#1	None	None	60°	None	Long/CB	None	36°	Upper	Yes	Partial
988	9	510	Dual Flow	#1	None	Full	60°	Full	None	None	36°	Upper	Yes	Partial
994	2	511	Fan Only	#1	None	None	60°	None	Long/CB	None	36°	None	No	Maximum
994	3	511	Core Only	#1	None	None	60°	None	Long/CB	None	36°	None	No	Maximum
994	4	511	Dual Flow	#1	None	None	60°	None	Long/CB	None	36°	None	No	Maximum
994	5	512	Dual Flow	#1	None	None	60°	None	Long/CB	None	36°	All	No	Partial
994	6	513	Dual Flow	#1	None	None	40°	None	Long/CB	None	36°	All	No	Partial
994	7	514	Dual Flow	#3	None	None	40°	None	Long/CB	None	36°	All	No	Partial
994	8	515	Dual Flow	#3	None	None	40°	None	X-Long/CB	None	36°	All	No	Partial
994	10	516	Dual Flow	#3	None	None	50°	None	X-Long/CB	None	36°	All	No	Partial

Note: Lower fan-duct bifurcator installed; wing section not installed.

Table 7. Continued

Test	Run	Config.	Operation Mode	Configuration Description										
				Reverser Port			Outer Door				Inner Door		Door	
				Bullnose	Spacer	Cover	Angle	Cutback	Kicker	Fence	Angle	Fillers	Struts	Leakage
994	11	517	Dual Flow	#3	None	None	50°	None	Long/CB	None	36°	All	No	Partial
994	12	518	Dual Flow	#3	None	None	50°	None	None	None	36°	All	No	Partial
994	13	519	Dual Flow	#3	None	None	60°	None	Long/CB	None	36°	All	No	Partial
994	14	520	Dual Flow	#3	None	None	60°	None	X-Long/CB	None	36°	All	No	Partial
994	15	521	Dual Flow	#3	None	Partial	60°	Partial	Long/CB	None	36°	All	No	Partial
994	16	522	Dual Flow	#3	None	Mixed	60°	Mixed	Long/CB	None	36°	All	No	Partial
994	17	523	Dual Flow	#3	None	Full	60°	Full	Long/CB	None	36°	All	No	Partial
994	18	524	Dual Flow	#3	None	Full	50°	Full	Long/CB	None	36°	All	No	Partial
994	19	525	Dual Flow	#3	None	Mixed	50°	Mixed	Long/CB	None	36°	All	No	Partial
994	20	526	Dual Flow	#3	None	Partial	50°	Partial	Long/CB	None	36°	All	No	Partial
994	21	527	Dual Flow	#3	None	Partial	40°	Partial	Long/CB	None	36°	All	No	Partial
994	22	528	Dual Flow	#3	None	Full	40°	Full	Long/CB	None	36°	All	No	Partial
994	23	519	Dual Flow	#3	None	None	60°	None	Long/CB	None	36°	All	No	Partial
994	24	529	Dual Flow	#3	0.40”	None	60°	None	Long/CB	None	36°	All	No	Partial
994	25	530	Dual Flow	#3	0.40”	None	50°	None	Long/CB	None	36°	All	No	Partial
994	26	531	Dual Flow	#3	0.40”	None	40°	None	Long/CB	None	36°	All	No	Partial
994	27	532	Dual Flow	#3	0.20”	None	40°	None	Long/CB	None	36°	All	No	Partial
994	29	533	Dual Flow	#3	0.20”	None	50°	None	Long/CB	None	36°	All	No	Partial
994	30	534	Dual Flow	#3	0.20”	None	60°	None	Long/CB	None	36°	All	No	Partial
994	31	535	Dual Flow	#1	0.40”	None	60°	None	Long/CB	None	36°	All	No	Partial
994	32	536	Dual Flow	#2	None	None	60°	None	Long/CB	None	36°	All	No	Partial
994	33	537	Dual Flow	#2	None	None	50°	None	Long/CB	None	36°	All	No	Partial
994	34	538	Dual Flow	#3	None	Mixed	50°	Mixed	Long/CB	None	30°	All	No	Partial
994	35	539	Dual Flow	#3	None	Mixed	40°	Mixed	Long/CB	None	24°	All	No	Partial
994	36	540	Dual Flow	#3	None	Mixed	30°	Mixed	Long/CB	None	18°	All	No	Partial
994	37	519	Dual Flow	#3	None	None	60°	None	Long/CB	None	36°	All	No	Partial
994	38	541	Dual Flow	#1	0.20”	None	60°	None	Long/CB	None	36°	All	No	Partial
994	39	542	Dual Flow	#2	0.20”	None	50°	None	Long/CB	None	36°	All	No	Partial
994	40	543	Dual Flow	#1	None	None	60°	None	Long/CB	None	36°	All+Tape	No	None
994	41	544	Dual Flow	#3	None	None	60°	None	Long/CB	None	36°	All+Tape	No	None
994	43	545	Dual Flow	#3	None	Mixed	10°	Mixed	Long/CB	None	6°	All	No	Partial

Note: Lower fan-duct bifurcator installed; wing section not installed.

Table 7. Continued

Test	Run	Config.	Operation Mode	Configuration Description										
				Reverser Port			Outer Door				Inner Door		Door	
				Bullnose	Spacer	Cover	Angle	Cutback	Kicker	Fence	Angle	Fillers	Struts	Leakage
994	44	546	Dual Flow	#3	None	Mixed	20°	Mixed	Long/CB	None	12°	All	No	Partial
1002	47	547	Core Only	#1	None	None	60°	None	Long/CB	None	36°	All	No	Partial
1002	48	547	Fan Only	#1	None	None	60°	None	Long/CB	None	36°	All	No	Partial
1002	49	547	Dual Flow	#1	None	None	60°	None	Long/CB	None	36°	All	No	Partial
1002	20	543	Dual Flow	#1	None	None	60°	None	Long/CB	None	36°	All+Tape	No	None
1002	21	548	Dual Flow	#1	None	None	60°	None	Long	Yes	36°	All+Tape	No	None
1002	22	549	Dual Flow	#3	None	None	60°	None	Long	Yes	36°	All+Tape	No	None
1002	23	544	Dual Flow	#3	None	None	60°	None	Long/CB	None	36°	All+Tape	No	None
1002	4	544	Dual Flow	#3	None	None	60°	None	Long/CB	None	36°	All+Tape	No	None
1002	9	550	Dual Flow	#2	None	None	60°	None	Long/CB	None	36°	All+Tape	No	None
1002	10	543	Dual Flow	#1	None	None	60°	None	Long/CB	None	36°	All+Tape	No	None
1002	11	551	Dual Flow	None	None	None	60°	None	Long/CB	None	36°	All+Tape	No	None
1002	12	552	Dual Flow	None	0.20”	None	60°	None	Long/CB	None	36°	All+Tape	No	None
1002	13	553	Dual Flow	#1	0.20”	None	60°	None	Long/CB	None	36°	All+Tape	No	None
1002	14	554	Dual Flow	#2	0.20”	None	60°	None	Long/CB	None	36°	All+Tape	No	None
1002	15	555	Dual Flow	#3	0.20”	None	60°	None	Long/CB	None	36°	All+Tape	No	None
1002	16	556	Dual Flow	None	0.40”	None	60°	None	Long/CB	None	36°	All+Tape	No	None
1002	17	557	Dual Flow	#1	0.40”	None	60°	None	Long/CB	None	36°	All+Tape	No	None
1002	18	558	Dual Flow	#2	0.40”	None	60°	None	Long/CB	None	36°	All+Tape	No	None
1002	19	559	Dual Flow	#3	0.40”	None	60°	None	Long/CB	None	36°	All+Tape	No	None
1002	8	544	Dual Flow	#3	None	None	60°	None	Long/CB	None	36°	All+Tape	No	None
1002	5	560	Dual Flow	#3	None	None	60°	None	X-Long	Yes	36°	All+Tape	No	None
1002	7	561	Dual Flow	#3	None	None	60°	None	X-Long/CB	None	36°	All+Tape	No	None
1002	33	562	Dual Flow	#3	None	None	10°	None	Long/CB	None	12°	All	No	Partial
1002	34	563	Dual Flow	#3	None	None	20°	None	Long/CB	None	12°	All	No	Partial
1002	35	564	Dual Flow	#3	None	None	30°	None	Long/CB	None	12°	All	No	Partial
1002	36	565	Dual Flow	#3	None	None	40°	None	Long/CB	None	12°	All	No	Partial
1002	37	566	Dual Flow	#3	None	None	50°	None	Long/CB	None	12°	All	No	Partial
1002	38	567	Dual Flow	#3	None	None	60°	None	Long/CB	None	12°	All	No	Partial
1002	32	568	Dual Flow	#3	None	None	10°	None	Long/CB	None	24°	All	No	Partial
1002	31	569	Dual Flow	#3	None	None	20°	None	Long/CB	None	24°	All	No	Partial

Note: Lower fan-duct bifurcator installed; wing section not installed.

Table 7. Concluded

Test	Run	Config.	Operation Mode	Configuration Description										
				Reverser Port			Outer Door				Inner Door		Door	
				Bullnose	Spacer	Cover	Angle	Cutback	Kicker	Fence	Angle	Fillers	Struts	Leakage
1002	30	570	Dual Flow	#3	None	None	30°	None	Long/CB	None	24°	All	No	Partial
1002	29	571	Dual Flow	#3	None	None	40°	None	Long/CB	None	24°	All	No	Partial
1002	28	572	Dual Flow	#3	None	None	50°	None	Long/CB	None	24°	All	No	Partial
1002	27	573	Dual Flow	#3	None	None	60°	None	Long/CB	None	24°	All	No	Partial
1002	46	574	Dual Flow	#3	None	None	10°	None	Long/CB	None	36°	All	No	Partial
1002	45	575	Dual Flow	#3	None	None	20°	None	Long/CB	None	36°	All	No	Partial
1002	44	576	Dual Flow	#3	None	None	30°	None	Long/CB	None	36°	All	No	Partial
1002	43	577	Dual Flow	#3	None	None	40°	None	Long/CB	None	36°	All	No	Partial
1002	42	578	Dual Flow	#3	None	None	50°	None	Long/CB	None	36°	All	No	Partial
1002	24	579	Dual Flow	#3	None	None	60°	None	Long/CB	None	36°	All	No	Partial
1002	41	580	Dual Flow	#3	None	None	60°	None	Long/CB	None	6°	All	No	Partial
1002	40	581	Dual Flow	#3	None	None	60°	None	Long/CB	None	18°	All	No	Partial
1002	25	581	Dual Flow	#3	None	None	60°	None	Long/CB	None	30°	All	No	Partial

Note: Lower fan-duct bifurcator installed; wing section not installed.

Table 8. Description of Wing-Mounted Thrust Reverser Model Configurations Tested

Test	Run	Config.	Operation Mode	Deflector Geometry							Ground Plane	
				Mount Angle	Chord Length			Angle, ψ			Fences	Installed	Height, FSE
					#1	#2	#3	#1	#2	#3			
1001	47	701	Dual Flow	Parallel	Long	Long	Long	45°	-30°	15°	Yes	No	-
1001	48	702	Dual Flow	Parallel	Long	Long	Long	45°	-30°	30°	Yes	No	-
1001	49	703	Dual Flow	Parallel	Long	Long	Long	45°	-30°	45°	Yes	No	-
1001	50	704	Dual Flow	Parallel	Long	Long	Long	60°	-30°	45°	Yes	No	-
1001	46	705	Dual Flow	Parallel	Long	Long	Long	30°	-15°	15°	Yes	No	-
1001	38	706	Dual Flow	Parallel	Long	Long	Long	30°	-15°	30°	Yes	No	-
1001	45	707	Dual Flow	Parallel	Long	Long	Long	30°	-15°	45°	Yes	No	-
1001	42	708	Dual Flow	Parallel	Long	Long	Long	45°	-15°	15°	Yes	No	-
1001	43	709	Dual Flow	Parallel	Long	Long	Long	45°	-15°	30°	Yes	No	-
1001	44	710	Dual Flow	Parallel	Long	Long	Long	45°	-15°	45°	Yes	No	-
1001	41	711	Dual Flow	Parallel	Long	Long	Long	60°	-15°	15°	Yes	No	-
1001	39	712	Dual Flow	Parallel	Long	Long	Long	60°	-15°	30°	Yes	No	-
1001	40	713	Dual Flow	Parallel	Long	Long	Long	60°	-15°	45°	Yes	No	-
1001	31	714	Dual Flow	Parallel	Long	Long	Long	30°	0°	30°	Yes	No	-
1001	32	715	Dual Flow	Parallel	Long	Long	Long	30°	0°	45°	Yes	No	-
1001	33	716	Dual Flow	Parallel	Long	Long	Long	30°	0°	60°	Yes	No	-
1001	35	717	Dual Flow	Parallel	Long	Long	Long	45°	0°	30°	Yes	No	-
1001	34	718	Dual Flow	Parallel	Long	Long	Long	45°	0°	45°	Yes	No	-
1001	36	719	Dual Flow	Parallel	Long	Long	Long	60°	0°	30°	Yes	No	-
1001	37	720	Dual Flow	Parallel	Long	Long	Long	60°	0°	45°	Yes	No	-
1001	28	721	Dual Flow	Parallel	Long	Long	Long	15°	15°	15°	Yes	No	-
1001	26	722	Dual Flow	Parallel	Long	Long	Long	15°	15°	30°	Yes	No	-
1001	27	723	Dual Flow	Parallel	Long	Long	Long	15°	15°	45°	Yes	No	-
1001	25	724	Dual Flow	Parallel	Long	Long	Long	30°	15°	30°	Yes	No	-
1001	51	725	Dual Flow	Parallel	Long	Long	Long	45°	15°	15°	Yes	No	-
1001	52	726	Dual Flow	Parallel	Long	Long	Long	45°	15°	30°	Yes	No	-
1001	53	727	Dual Flow	Parallel	Long	Long	Long	45°	15°	45°	Yes	No	-
1001	54	728	Dual Flow	Parallel	Long	Long	Long	30°	15°	60°	Yes	No	-
1001	30	729	Dual Flow	Parallel	Long	Long	Long	15°	30°	30°	Yes	No	-
1001	29	730	Dual Flow	Parallel	Long	Long	Long	15°	45°	45°	Yes	No	-

Note: Lower fan-duct bifurcator not installed; wing section installed.

Table 8. Concluded.

Test	Run	Config.	Operation Mode	Deflector Geometry								Ground Plane	
				Mount Angle	Chord Length			Angle, ψ			Fences	Installed	Height, FSE
					#1	#2	#3	#1	#2	#3			
Effect of Flap Fences													
1001	55	731	Dual Flow	Parallel	Long	Long	Long	30°	15°	30°	No	No	-
1001	56	732	Dual Flow	Parallel	Long	Long	Long	45°	0°	30°	No	No	-
1001	57	733	Dual Flow	Parallel	Long	Long	Long	60°	0°	30°	No	No	-
1001	58	734	Dual Flow	Parallel	Long	Long	Long	60°	-15°	30°	No	No	-
1001	59	735	Dual Flow	Parallel	Long	Long	Long	45°	-15°	30°	No	No	-
Effect of Deflector Mount Position													
1001	64	736	Dual Flow	Normal	Long	Long	Long	30°	15°	30°	Yes	No	-
1001	61	737	Dual Flow	Normal	Long	Long	Long	45°	0°	30°	Yes	No	-
1001	62	738	Dual Flow	Normal	Long	Long	Long	60°	0°	30°	Yes	No	-
1001	63	739	Dual Flow	Normal	Long	Long	Long	60°	-15°	30°	No	No	-
1001	60	740	Dual Flow	Normal	Long	Long	Long	45°	-15°	30°	Yes	No	-
Effect of Deflector Height													
1001	70	741	Dual Flow	Parallel	Short	Short	Long	60°	-15°	30°	Yes	No	-
1001	71	742	Dual Flow	Parallel	Short	Short	Long	45°	-15°	30°	Yes	No	-
1001	72	743	Dual Flow	Parallel	Short	Short	Long	60°	0°	30°	Yes	No	-
Effect of Ground Plane													
1001	67	744	Dual Flow	Parallel	Long	Long	Long	60°	-15°	45°	Yes	Yes	36”
1001	68	745	Dual Flow	Parallel	Short	Short	Long	60°	-15°	30°	Yes	Yes	36”
1001	69	746	Dual Flow	Parallel	Short	Short	Long	60°	-15°	30°	Yes	Yes	18”

Note: Lower fan-duct bifurcator not installed; wing section installed.

Table 9. Definition of Data Names with Corresponding Symbols or Abbreviations

Data Names	Symbol or Abbreviation	Units	Definition
AF1.4	F_A	lbf	corrected balance axial force
AMPARM	β		thrust reverser area match parameter
AT1	A_{core}	in^2	core nozzle throat area
AT2	A_{fan}	in^2	fan nozzle throat area
BATCH	BATCH		batch number
CA1	C_A		axial force coefficient
CMX1	C_l		rolling moment coefficient
CMY1	C_m		pitching moment coefficient
CMZ1	C_n		yawing moment coefficient
CN1	C_N		normal force coefficient
CNPR	CNPR		core nozzle pressure ratio
CONFIG	CONFIG		configuration number
CY1	C_Y		side force coefficient
ETAFAN	η_{fan}		fan reverser effectiveness
ETAFANI	$\eta_{fan_{id}}$		fan reverser effectiveness based on ideal thrust
ETAREV	η_{rev}		overall thrust reverser effectiveness
FCORE	F_{core}	lbf	core nozzle forward thrust
FFAN	F_{fan}	lbf	fan nozzle forward thrust
FREV	F_{rev}	lbf	gross reverse thrust
FREVID	$F_{i,rev}$	lbf	isentropic gross reverse thrust
FTOTAL	F_{total}	lbf	total nozzle (fan+core) forward thrust
FGT/FI	F_r/F_i		resultant thrust ratio
FJ1/FI	F_A/F_i		thrust ratio
FI1	$F_{i,core}$	lbf	ideal isentropic core nozzle thrust
FI2	$F_{i,fan}$	lbf	ideal isentropic fan nozzle thrust
FNPR	FNPR		fan nozzle pressure ratio
NF1.4	F_N	lbf	corrected balance normal force, positive upward
PM1.4	Pitching	in-lbs	corrected balance pitching moment
PO	p_o	psia	test cell ambient pressure
POINT	POINT		point number
PSATR	PSATR	psi	annular (metal)target thrust reverser static pressure
PSBAS	PSBAS	psi	blockerless thrust reverser base static pressure
PSCID	PSCID	psi	multi-door crocodile thrust reverser inner door centerline static pressure
PSCOD	PSCOD	psi	multi-door crocodile thrust reverser outer door centerline static pressure

Table 9. Concluded

Data Names	Symbol or Abbreviation	Units	Definition
PSCORE	PSCORE	psi	blockerless thrust reverser core static pressure
PSEID	PSEID	psi	multi-door crocodile thrust reverser inner door edge static pressure
PSEOD	PSEOD	psi	multi-door crocodile thrust reverser outer door edge static pressure
PSFEN	PSFEN	psi	fan exhaust nozzle static pressure
PSFL	PSFL	psi	wing-mounted thrust reverser deflector static pressure
PSFP	PSFP	psi	wing-mounted thrust reverser back of deflector static pressure
PSIFD	PSIFD	psi	inner fan duct static pressure
PSINJ	PSINJ	psi	blockerless thrust reverser injection plenum static pressure
PSOFD	PSOFD	psi	outer fan duct static pressure
PSPBD	PSPBD	psi	porous blocker diffuser static pressure
PSRB	PSRB	psi	multi-door crocodile thrust reverser barrel static pressure
PSPYL	PSPYL	psi	pylon static pressure
PSWL	PSWL	psi	wing-section lower surface static pressure
PSWU	PSWU	psi	wing-section upper surface static pressure
PTFNE	PTFNE	psi	fan nozzle exit total pressure
RM1.4	Rolling	in-lbs	corrected balance rolling moment
RUN	RUN		run number
SF1.4	F_S	lbf	corrected balance side force
TEST	TEST		test number
WCAS	w_{cas}	lbf/sec	blockerless thrust reverser cascade vane weight-flow rate
WCZWF	$w_{cas}/w_{p,fan}$		blockerless thrust reverser cascade-to-fan weight-flow ratio
WCZWT	$w_{cas}/w_{p,tot}$		blockerless thrust reverser cascade vane total weight-flow ratio
WEXZWF	$w_{noz}/w_{p,fan}$		blockerless thrust reverser fan nozzle weight-flow ratio
WEXZWT	$w_{noz}/w_{p,tot}$		blockerless thrust reverser fan nozzle total weight-flow ratio
WFNETO	w_{noz}	lbf/sec	blockerless thrust reverser fan nozzle weight-flow rate
WINJZWT	$w_{inj}/w_{p,fan}$		blockerless thrust reverser injection weight-flow ratio
WP1	$w_{p,core}$	lbf/sec	measured core (primary) weight-flow rate
WP2	$w_{p,fan}$	lbf/sec	measured fan (secondary) weight-flow rate
WPRAT	$w_{p,core}/w_{p,fan}$		blockerless thrust reverser core-to-fan weight-flow ratio
WPTOT	$w_{p,tot}$	lbf/sec	sum of measured core and fan weight-flow rates
WP/WI1	$w_{p,core}/w_{i,core}$		discharge coefficient of core (primary) air flow
WP/WI2	$w_{p,fan}/w_{i,fan}$		discharge coefficient of fan (secondary) air flow
YM1.4	Yawing	in-lbs	corrected balance yawing moment

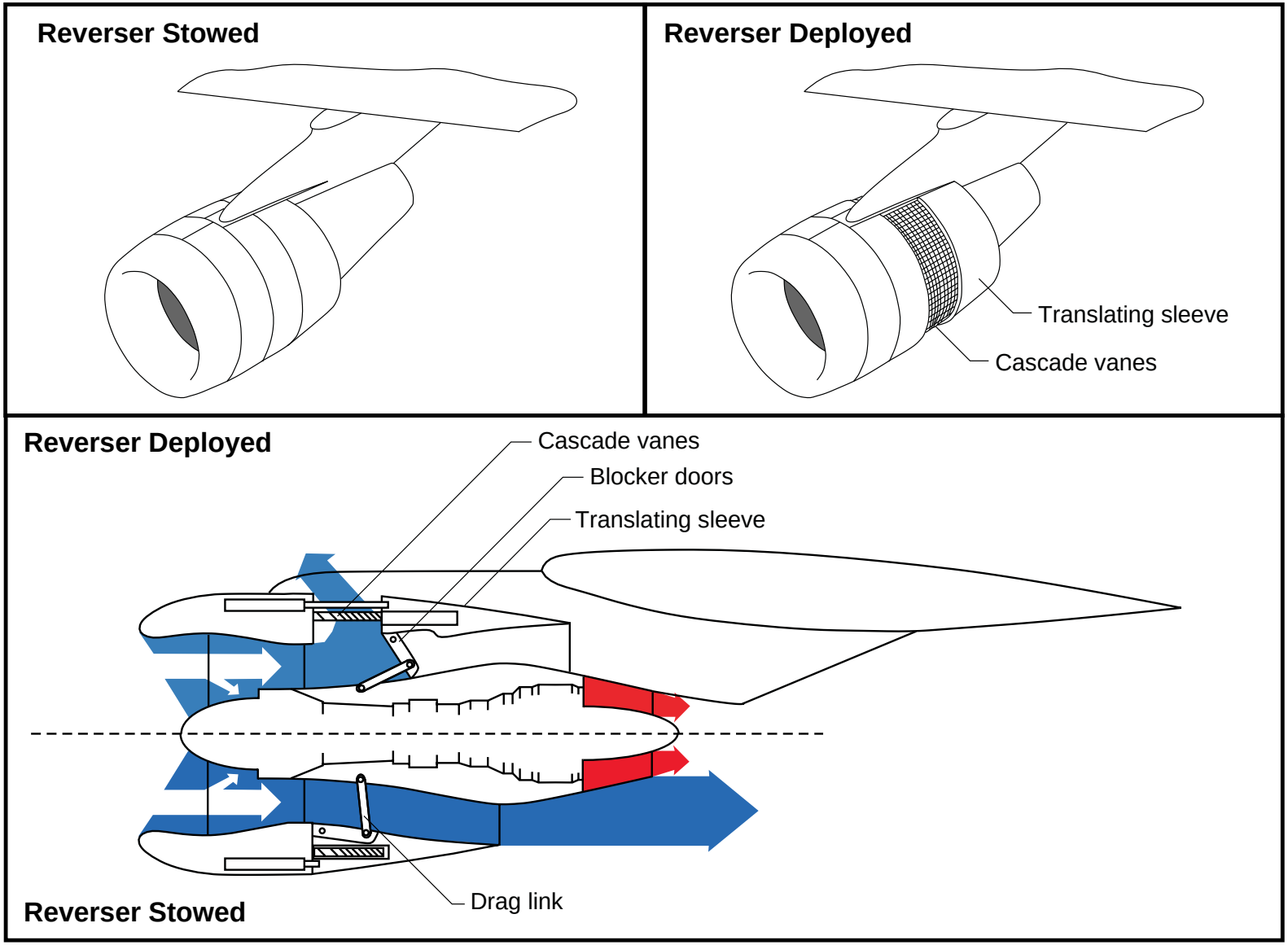

Figure 1. Sketch of a typical cascade thrust reverser.

L96-01925

(a) Side view showing cascade thrust reverser deployed.

Figure 2. Photographs of a cascade thrust reverser installed on the NASA 757-200 aircraft equipped with Rolls-Royce RB-211-535 turbofan engines.

L96-01924

(b) Rear view showing cascade thrust reverser deployed.

Figure 2. Concluded.

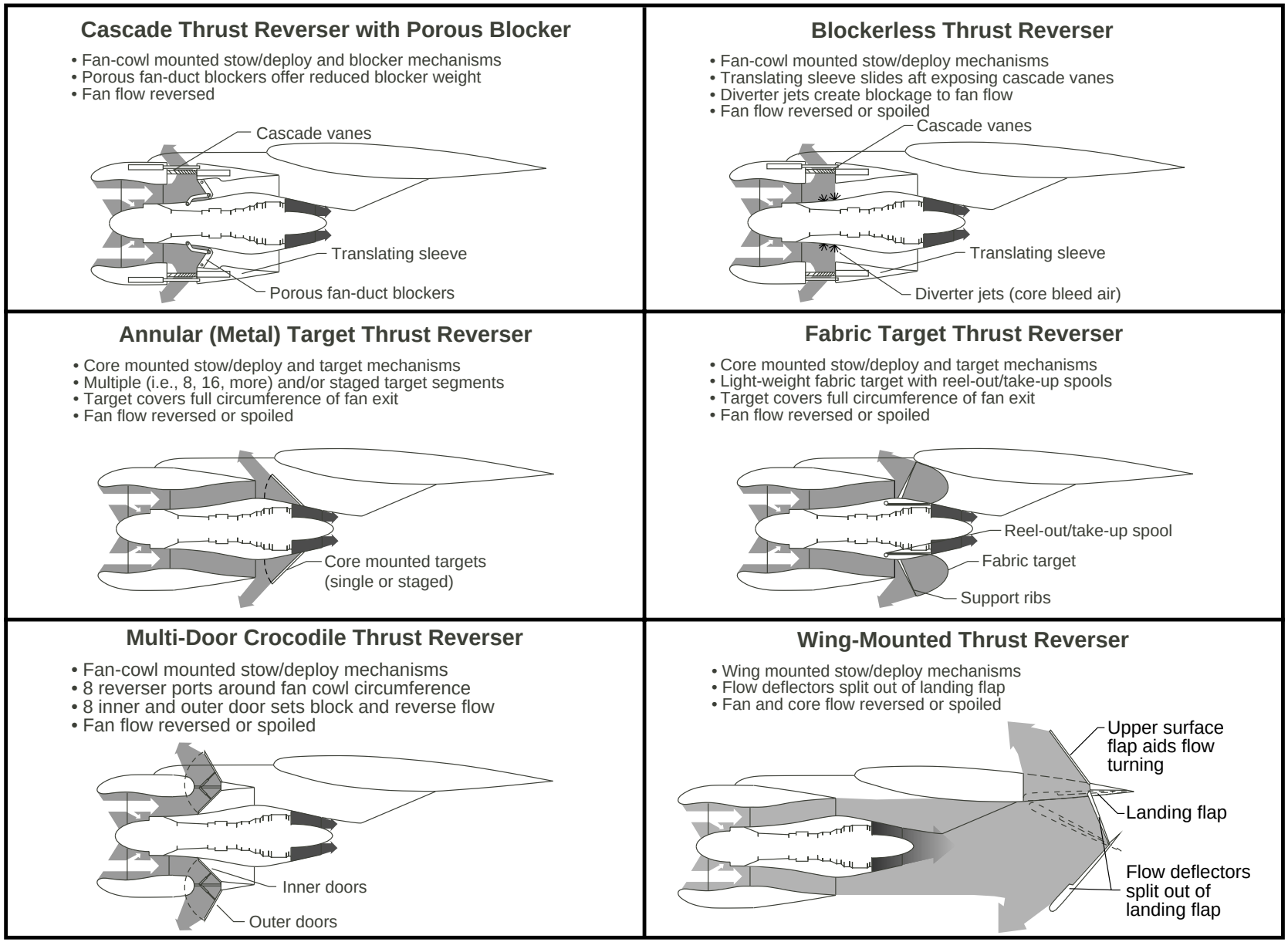

Figure 3. Sketch showing the six thrust reverser concepts tested during the Innovative Thrust Reverser Test Program.

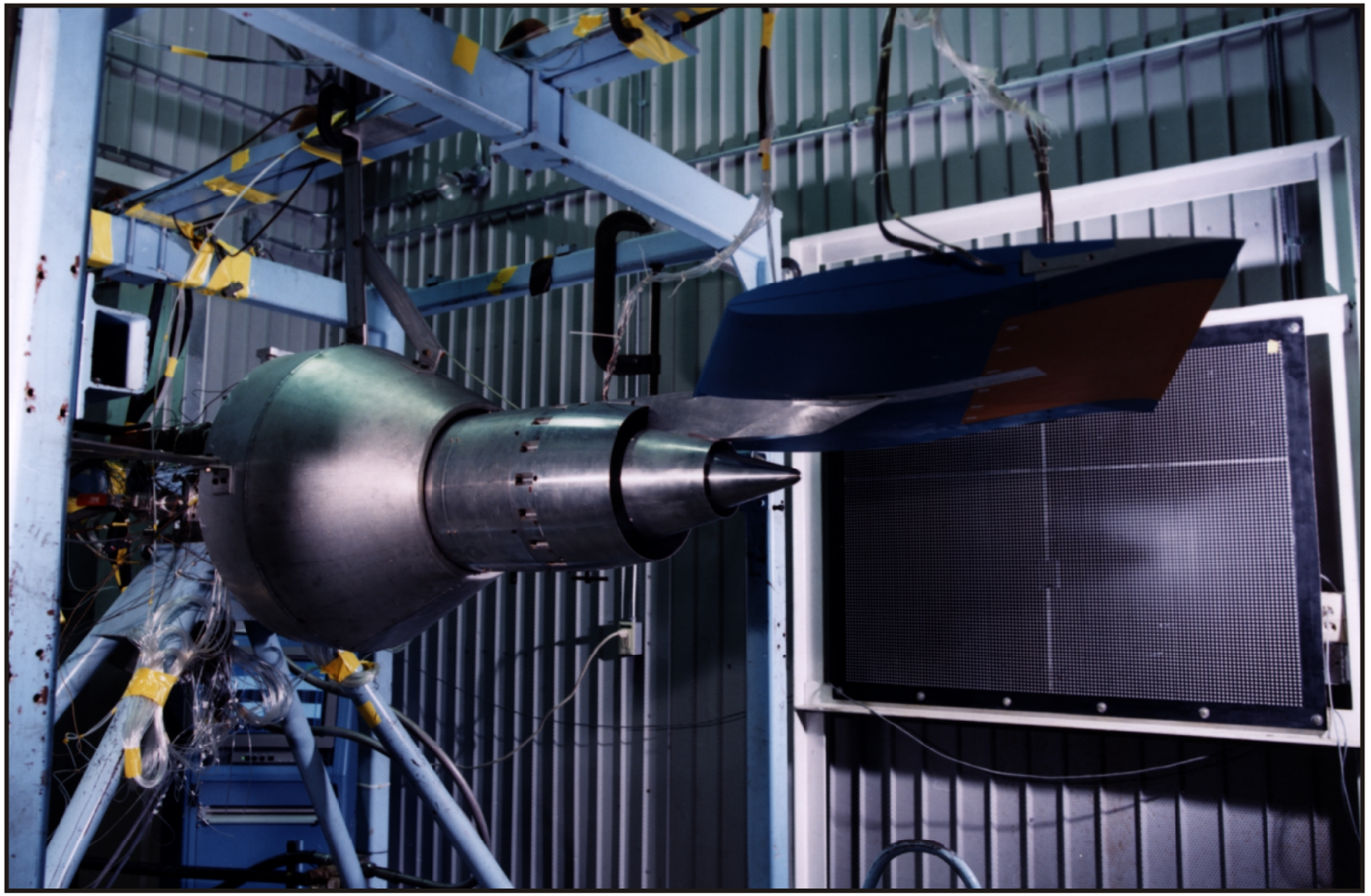

L97-546

(a) Photograph of model installation.

Figure 4. Typical setup of separate-flow exhaust system model and wing section installed on the dual-flow propulsion simulation system.

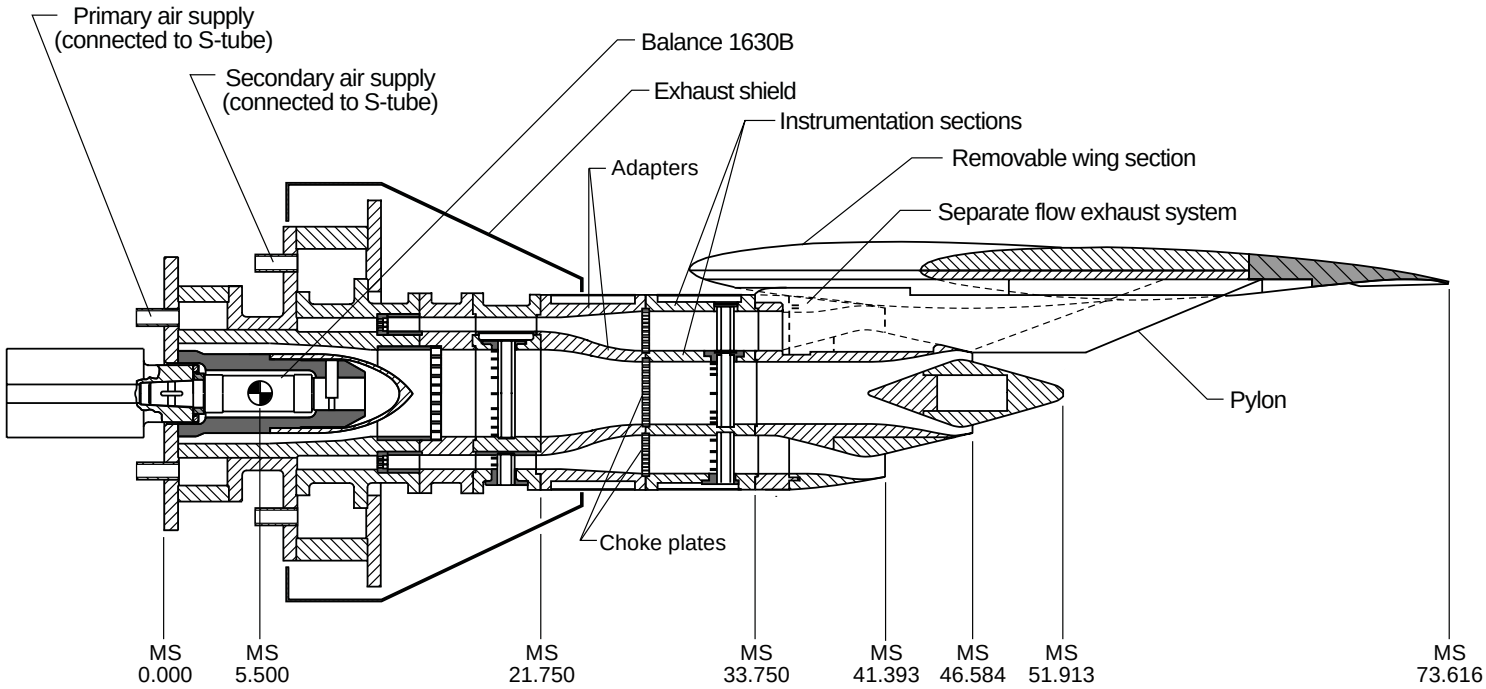

(b) Partial cutaway sketch showing details of model installation.

Figure 4. Concluded.

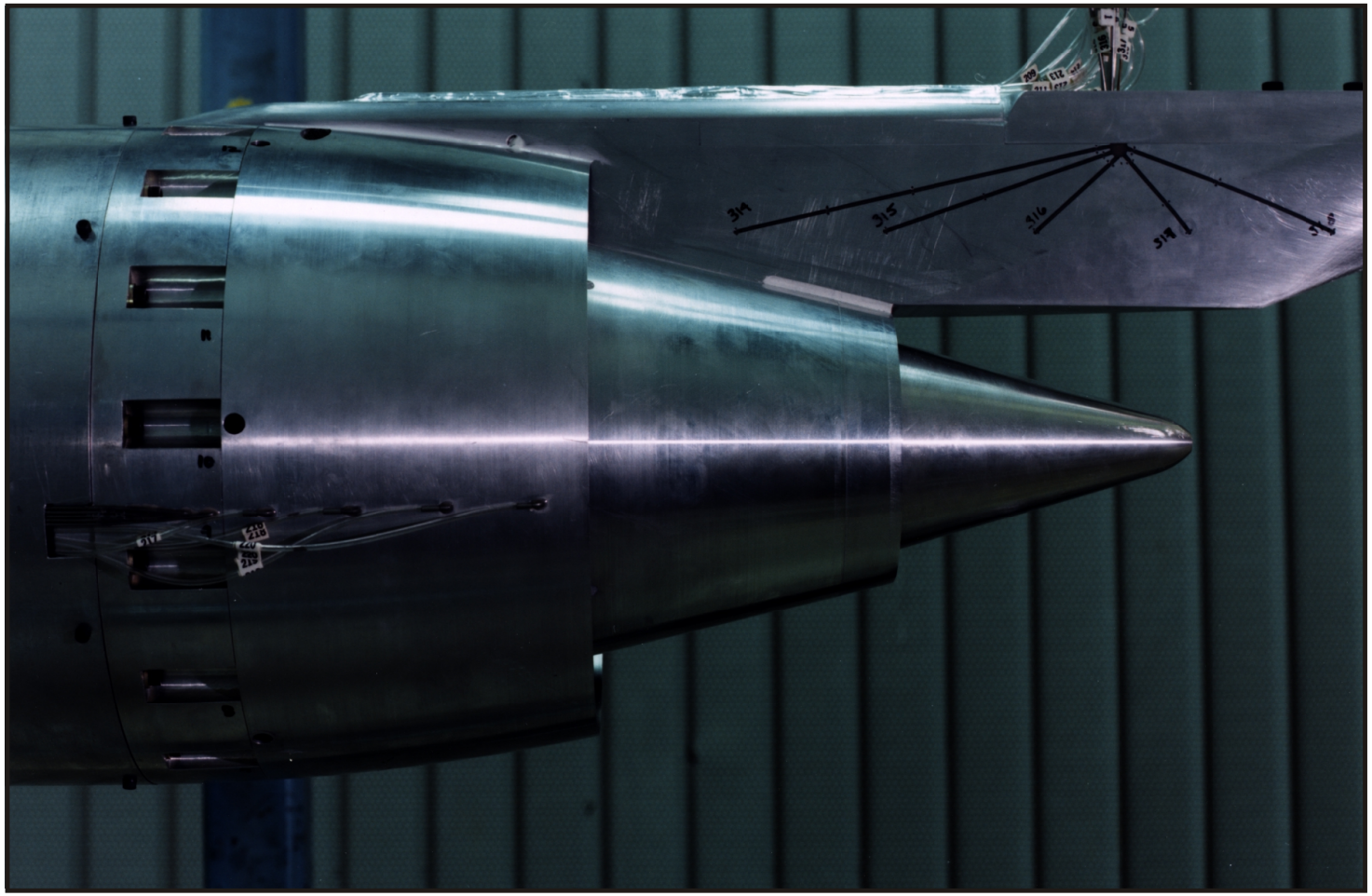

L95-4523

(a) Photograph of separate-flow exhaust system model.

Figure 5. Details of separate-flow exhaust system model. Dimensions are in inches.

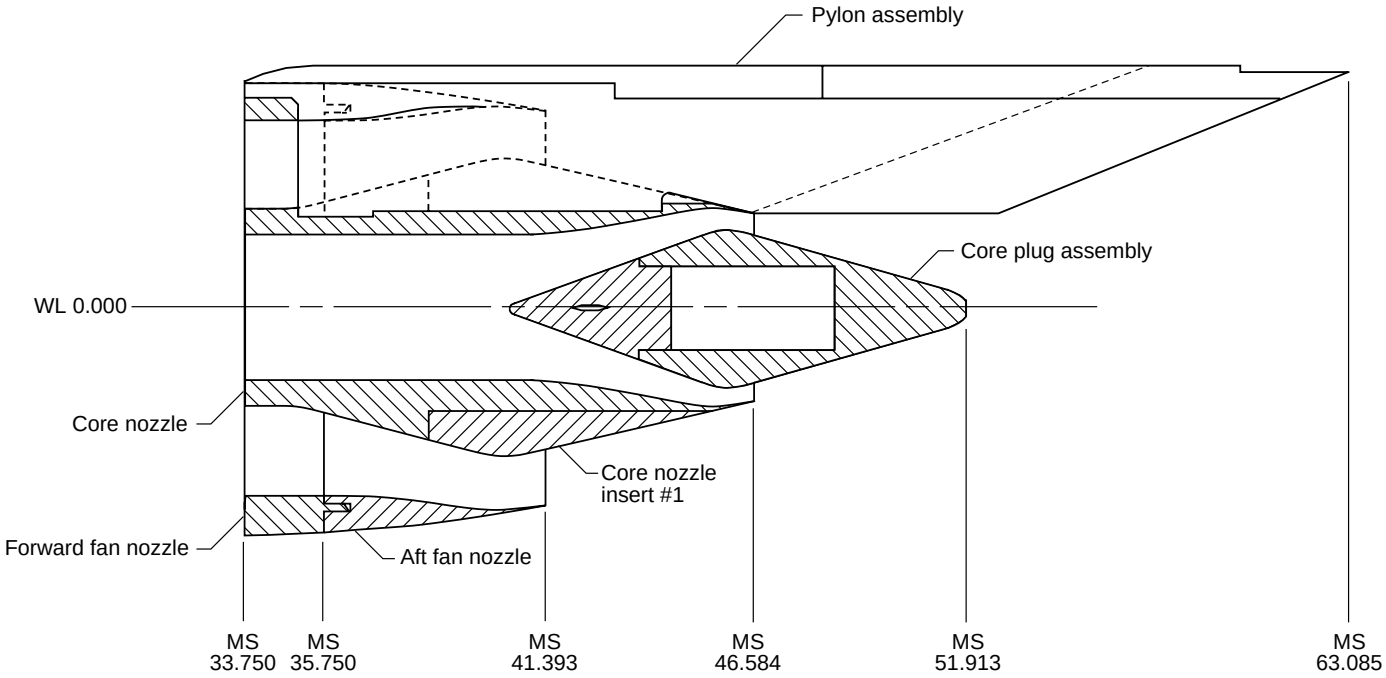

(b) Partial cutaway sketch of separate-flow exhaust system model.

Figure 5. Continued.

x, in.	R, in.
0.000	5.710
0.150	5.709
0.300	5.708
0.450	5.706
0.599	5.704
0.749	5.701
0.899	5.698
1.049	5.694
1.199	5.689
1.349	5.683
1.499	5.678
1.649	5.671
1.798	5.664
1.948	5.657
2.000	5.654

x, in.	R', in.
0.000	4.710
1.268	4.710
1.668	4.707
1.859	4.699
2.000	4.693

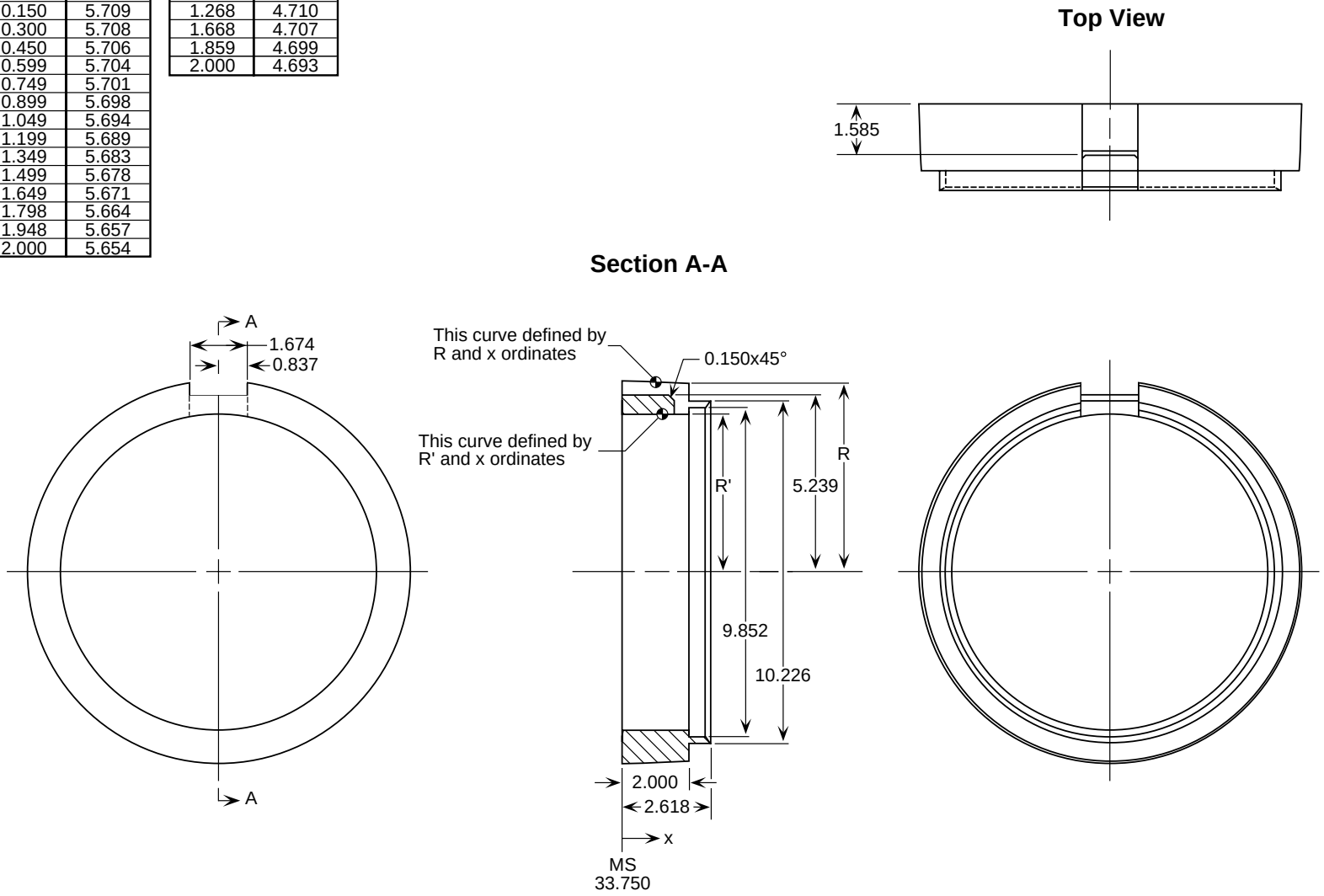

(c) Sketch of forward fan nozzle.

Figure 5. Continued.

x, in.	R, in.
2.000	5.654
2.098	5.649
2.248	5.640
2.398	5.631
2.548	5.621
2.698	5.611
2.847	5.600
2.997	5.589
3.147	5.577
3.297	5.564
3.447	5.551
3.597	5.538
3.747	5.523
3.897	5.509
4.046	5.493
4.196	5.478
4.346	5.461
4.496	5.445
4.646	5.427
4.796	5.409
4.946	5.391
5.096	5.372
5.245	5.352
5.395	5.332
5.545	5.311
5.695	5.290
5.845	5.268
5.995	5.246
6.145	5.223
6.294	5.200
6.444	5.176
6.594	5.151
6.744	5.126
6.894	5.101
7.044	5.075
7.194	5.048
7.344	5.021
7.493	4.993
7.643	4.965

x, in.	R', in.
2.000	4.693
2.156	4.688
2.304	4.685
2.452	4.683
2.601	4.683
2.749	4.685
2.897	4.690
3.046	4.697
3.194	4.705
3.342	4.716
3.491	4.728
3.639	4.743
3.787	4.758
3.935	4.775
4.084	4.794
4.232	4.813
4.380	4.834
4.529	4.856
4.677	4.879
4.825	4.902
4.974	4.926
5.107	4.948
5.270	4.974
5.419	4.998
5.567	5.020
5.715	5.039
5.864	5.057
6.012	5.071
6.160	5.080
6.308	5.085
6.457	5.085
6.605	5.081
6.753	5.070
6.902	5.056
7.050	5.038
7.198	5.016
7.347	4.993
7.495	4.970
7.643	4.946

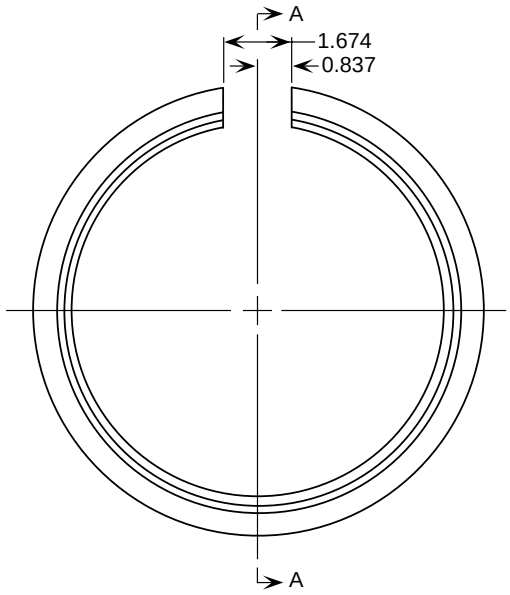

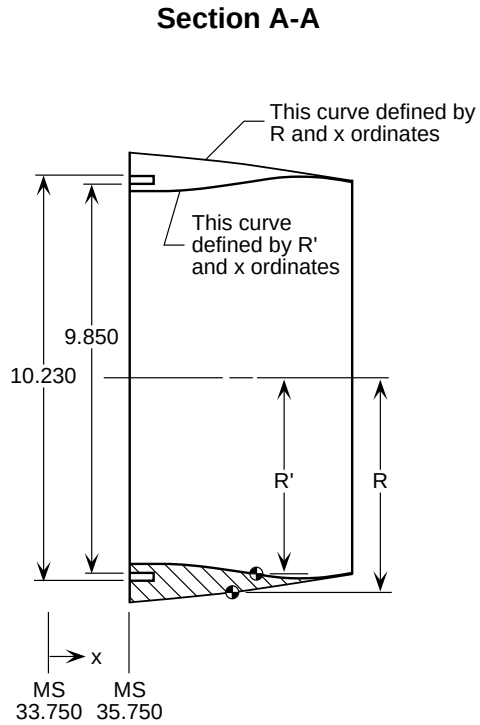

(d) Sketch of aft fan nozzle.

Figure 5. Continued.

x, in.	R, in.
0.0000	2.4630
0.5000	2.4680
1.0000	2.4980
1.5000	2.5430
2.0000	2.6230
2.2300	2.6790
2.4802	2.7460
2.7305	2.8130
2.9807	2.8800
3.2310	2.9470
3.4812	3.0140
3.7315	3.0810
3.9817	3.1480
4.2320	3.2150
4.5290	3.3020
4.6030	3.3248
4.6030	2.6000
5.0000	2.6000
5.5000	2.6000
6.0000	2.6000
6.5000	2.6000
7.0000	2.6000
7.5000	2.6000
8.0000	2.6000
8.5000	2.6000
9.0000	2.6000
9.5000	2.6000
10.0000	2.6000
10.5000	2.6000
11.0000	2.6000
11.5000	2.6000
11.8770	2.6000
12.0214	2.5670
12.2922	2.5050
12.5631	2.4430
12.8340	2.3810

x, in.	R', in.
0.0000	1.7930
0.6200	1.7930
1.2400	1.7930
1.8600	1.7930
2.4800	1.7930
3.1000	1.7930
3.7200	1.7930
4.3400	1.7930
4.9600	1.7930
5.5800	1.7930
6.7000	1.7930
7.2000	1.8230
8.2000	1.8600
8.7000	1.9790
9.2000	2.0610
9.4504	2.1096
9.7007	2.1582
9.9511	2.2069
10.2015	2.2555
10.4519	2.3041
10.7022	2.3527
10.9526	2.4014
11.2030	2.4500
11.3510	2.4790
11.4990	2.5050
11.6480	2.5210
11.7960	2.5270
11.9440	2.5210
12.0930	2.5070
12.2410	2.4860
12.3890	2.4600
12.5380	2.4320
12.6860	2.4020
12.8340	2.3720

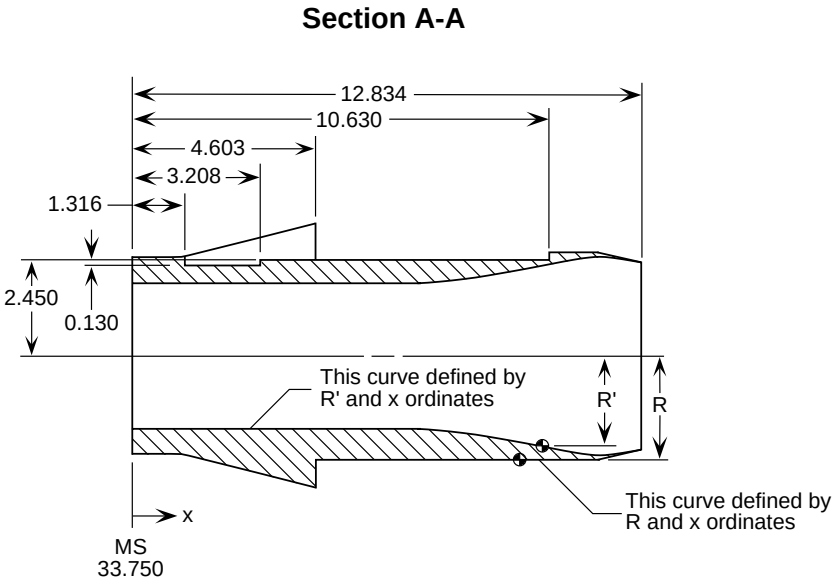

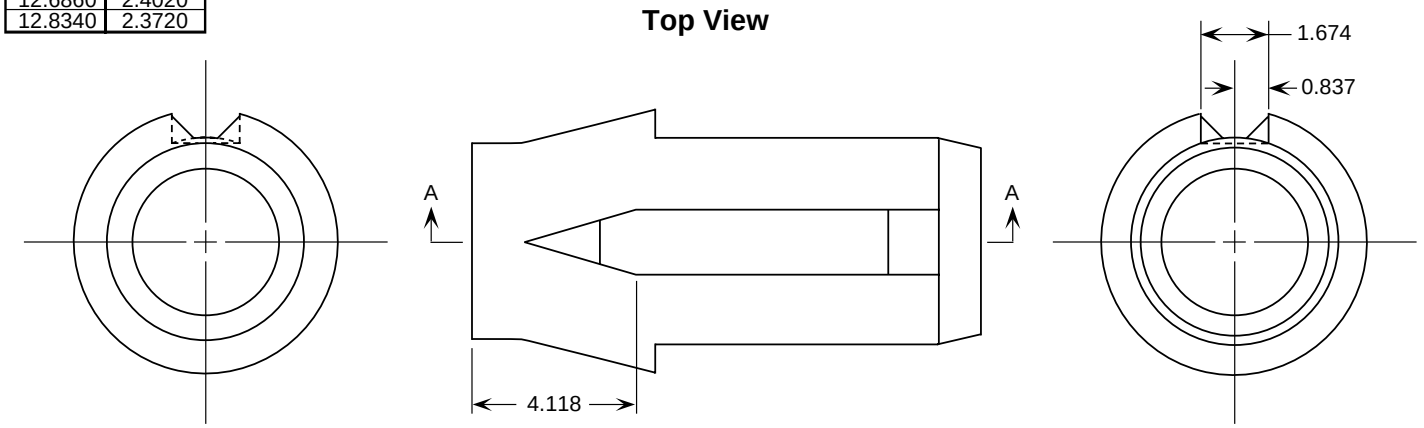

(e) Sketch of core nozzle.

Figure 5. Continued.

x, in.	R, in.
4.6030	3.3248
4.8250	3.3930
5.1220	3.4830
5.2700	3.5270
5.5670	3.6080
5.7150	3.6440
5.8640	3.6770
6.0120	3.7050
6.1600	3.7270
6.3080	3.7440
6.4570	3.7530
6.6050	3.7530
6.7530	3.7450
6.9020	3.7270
7.0500	3.7020
7.1980	3.6700
7.3470	3.6370
7.6430	3.5690
8.5000	3.3730
8.7709	3.3110
9.0417	3.2490
9.3126	3.1870
9.5835	3.1250
9.8544	3.0630
10.1253	3.0110
10.3961	2.9390
10.6670	2.8770
10.9379	2.8150
11.2087	2.7530
11.4796	2.6910
11.7505	2.6290
11.8770	2.6000

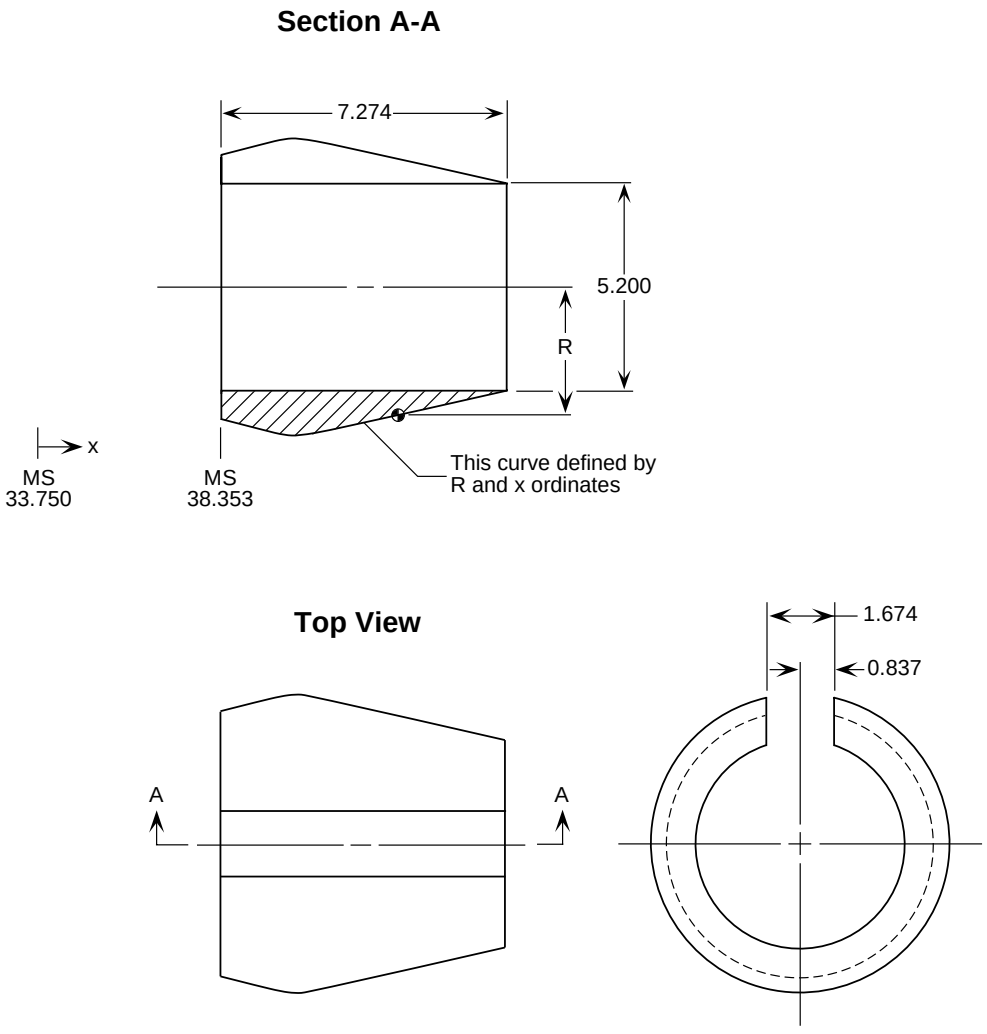

(f) Sketch of core nozzle insert #1.

Figure 5. Continued.

x, in.	R, in.
6.7540	0.0000
6.7110	0.1175
7.0012	0.2230
7.2912	0.3286
7.5812	0.4341
7.8712	0.5396
8.1612	0.6451
8.4512	0.7507
8.7411	0.8562
9.0311	0.9617
9.3211	1.0673
9.6110	1.1728
9.9011	1.2783
10.1911	1.3839
10.4810	1.4896
10.7710	1.5949
11.0610	1.7005
11.3510	1.8060
11.4990	1.8580
11.6480	1.9060
11.7960	1.9440
11.9440	1.9690
12.0930	1.9790
12.2410	1.9750
12.3890	1.9560
12.5380	1.9250
12.6880	1.8870

x, in.	R, in.
12.8340	1.8460
13.1272	1.7646
13.4204	1.6832
13.7136	1.6019
14.0067	1.5205
14.2999	1.4391
14.5931	1.3577
14.8863	1.2764
15.1795	1.1950
15.4727	1.1136
15.7659	1.0322
16.0591	0.9509
16.3522	0.8695
16.6454	0.7881
16.9386	0.7067
17.2318	0.6254
17.5250	0.5440
17.5990	0.5210
17.6730	0.4930
17.7470	0.4610
17.8220	0.4230
17.8960	0.3790
17.9700	0.3300
18.0440	0.2740
18.1180	0.2100
18.1630	0.1670
18.1630	0.0000

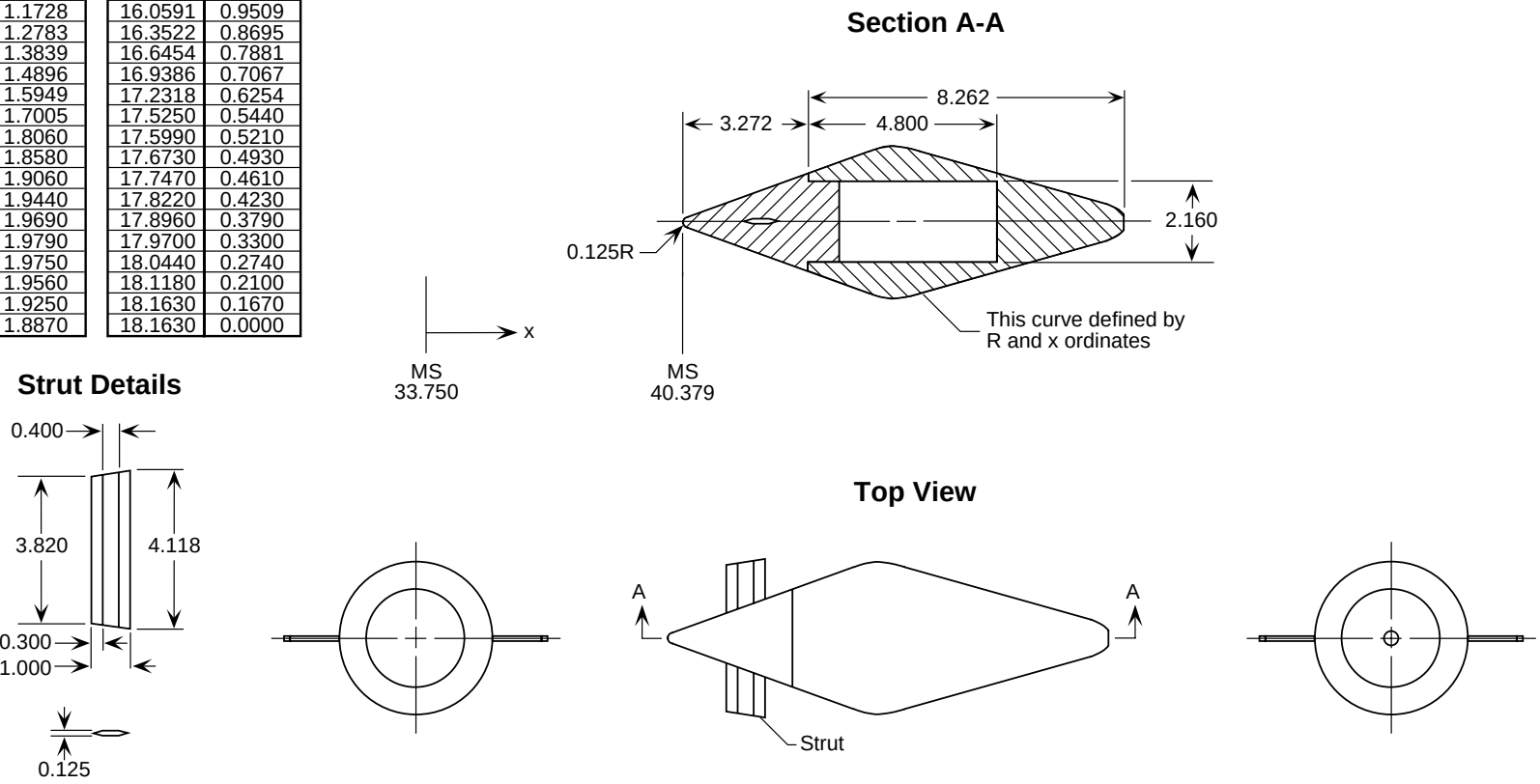

(g) Sketch of core plug assembly.

Figure 5. Continued.

Leading Edge Contour	
x, in.	y, in.
1.5850	0.0000
1.6350	0.0779
1.6850	0.0914
1.7850	0.1134
1.8850	0.1365
1.9850	0.1610
2.0850	0.1865
2.1850	0.2127
2.2850	0.2397
2.3850	0.2675
2.4850	0.2964
2.5850	0.3260
2.6850	0.3556
2.7850	0.3862
2.8850	0.4194
2.9850	0.4540
3.0850	0.4878
3.1850	0.5228
3.2850	0.5610
3.3845	0.5930
3.4850	0.6183
3.5850	0.6418
3.6850	0.6639
3.7850	0.6846
3.8850	0.7039
3.9850	0.7218
4.0850	0.7384
4.1850	0.7536
4.2850	0.7674
4.3850	0.7798
4.4850	0.7910
4.5850	0.8007
4.6850	0.8092
4.7850	0.8163
4.8850	0.8221
4.9850	0.8266
5.0850	0.8297
5.1850	0.8315
5.2730	0.8320

Leading Edge Contour Limit	
x, in.	y, in.
1.5850	-0.9580
1.9850	-0.9733
2.3850	-0.9836
2.7850	-0.9813
3.1850	-0.9625
3.5850	-0.9292
3.9850	-0.8845
4.3850	-0.8303
4.7850	-0.7683
5.1850	-0.7026
5.3850	-0.6701

Pylon Closure	
x, in.	y, in.
12.8340	0.8320
13.7756	0.8040
14.7164	0.7335
15.6579	0.6325
16.5993	0.5075
17.5407	0.3635
18.4817	0.2005
18.9526	0.1115
19.4232	0.0175

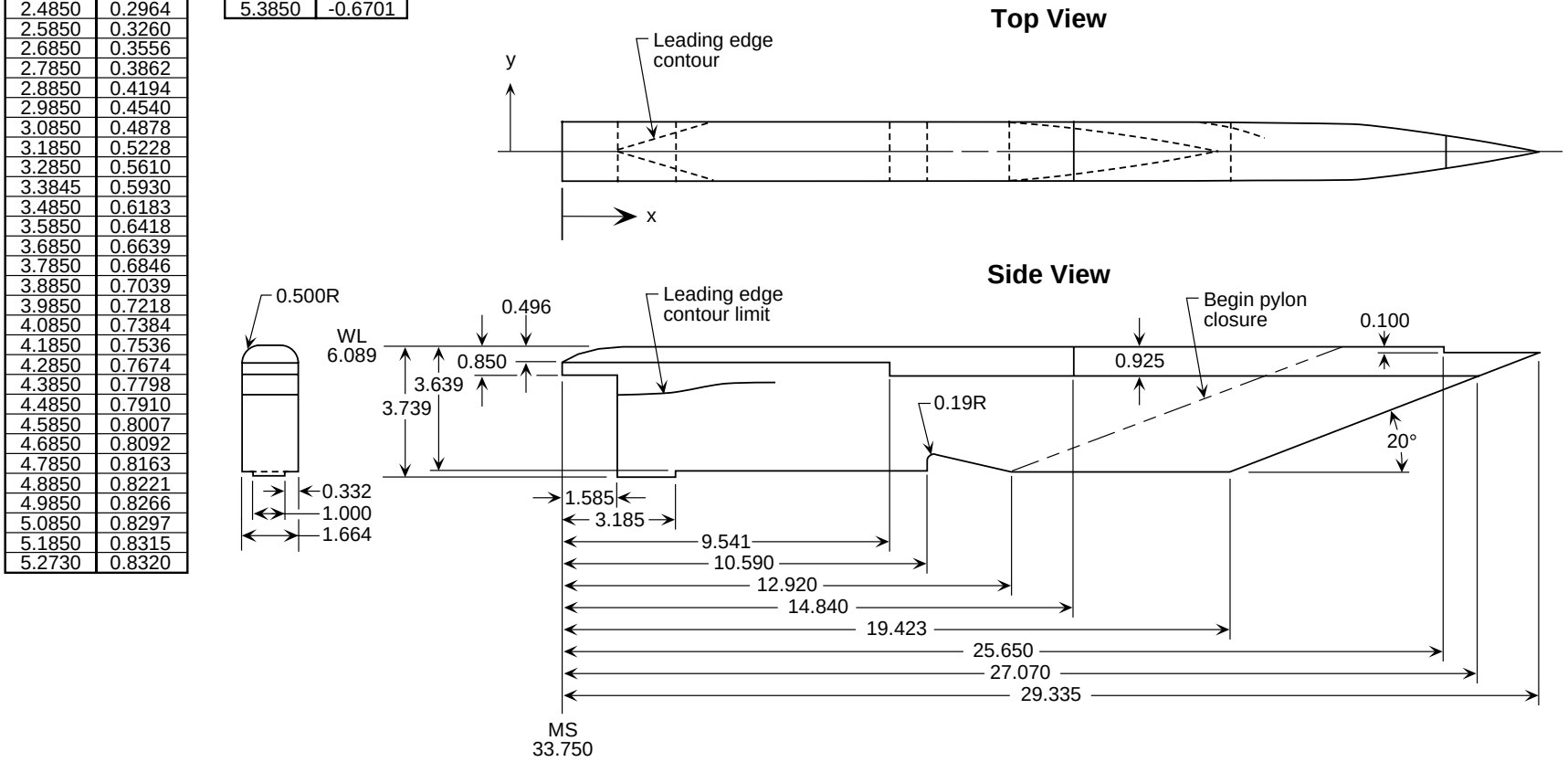

(h) Sketch of pylon assembly.

Figure 5. Concluded.

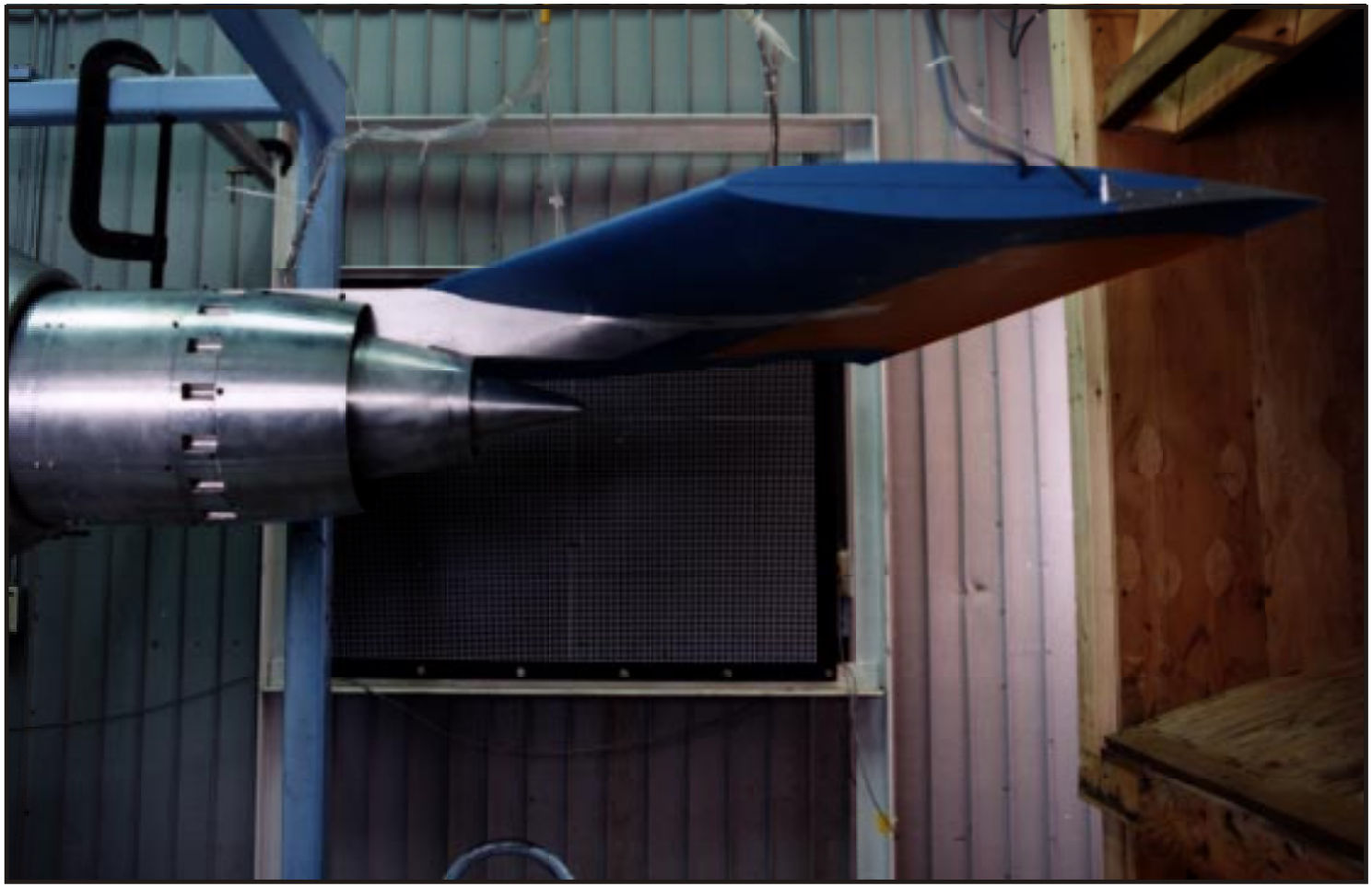

L97-547

(a) Photograph of separate-flow exhaust system model with wing section installed.

Figure 6. Details of separate-flow exhaust system model with wing section installed. Dimensions are in inches.

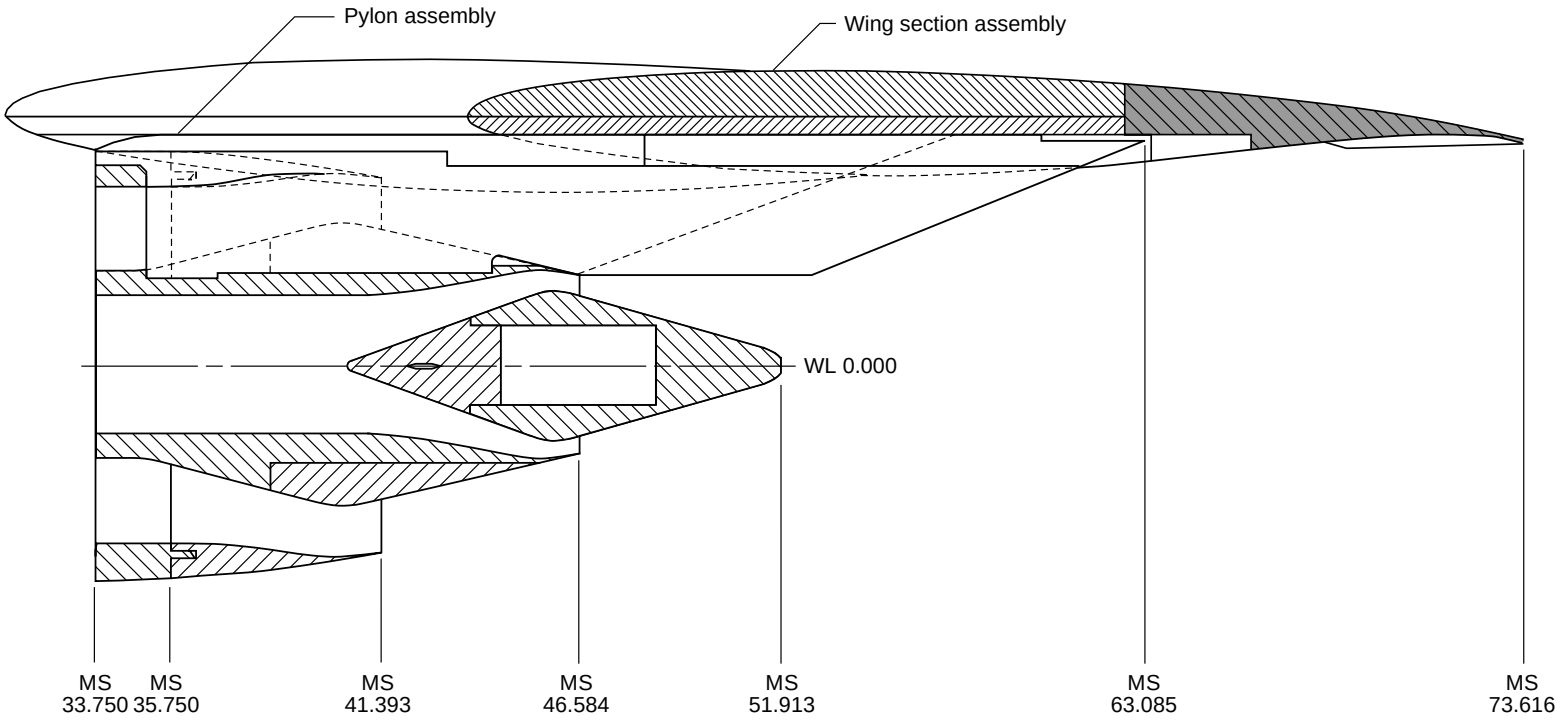

(b) Partial cutaway sketch of separate-flow exhaust system model with wing section installed.

Figure 6. Continued.

Parameter	Unit	Full Scale	Model Scale
S	in^2	712,368.000	4431.269
b/2	in	1266.024	99.852
MAC	in	308.532	24.336
C_r	in	432.828	34.140
C_t	in	129.852	10.248
λ	---	0.300	0.300
Aspect ratio	---	9.000	9.000
MAC η	---	0.410	0.410
LE break η	---	0.350	0.350
Inboard TE break	---	0.300	0.300
Outboard TE break η	---	0.500	0.500
$\Lambda_{inboard\ LE}$	deg	40.236	40.236
$\Lambda_{outboard\ LE}$	deg	37.236	37.236
$\Lambda_{inboard\ TE}$	deg	3.000	3.000
$\Lambda_{mid\ TE}$	deg	15.990	15.990
$\Lambda_{outboard\ TE}$	deg	27.507	27.507
$\Lambda_{c/4}$	deg	35.000	35.000

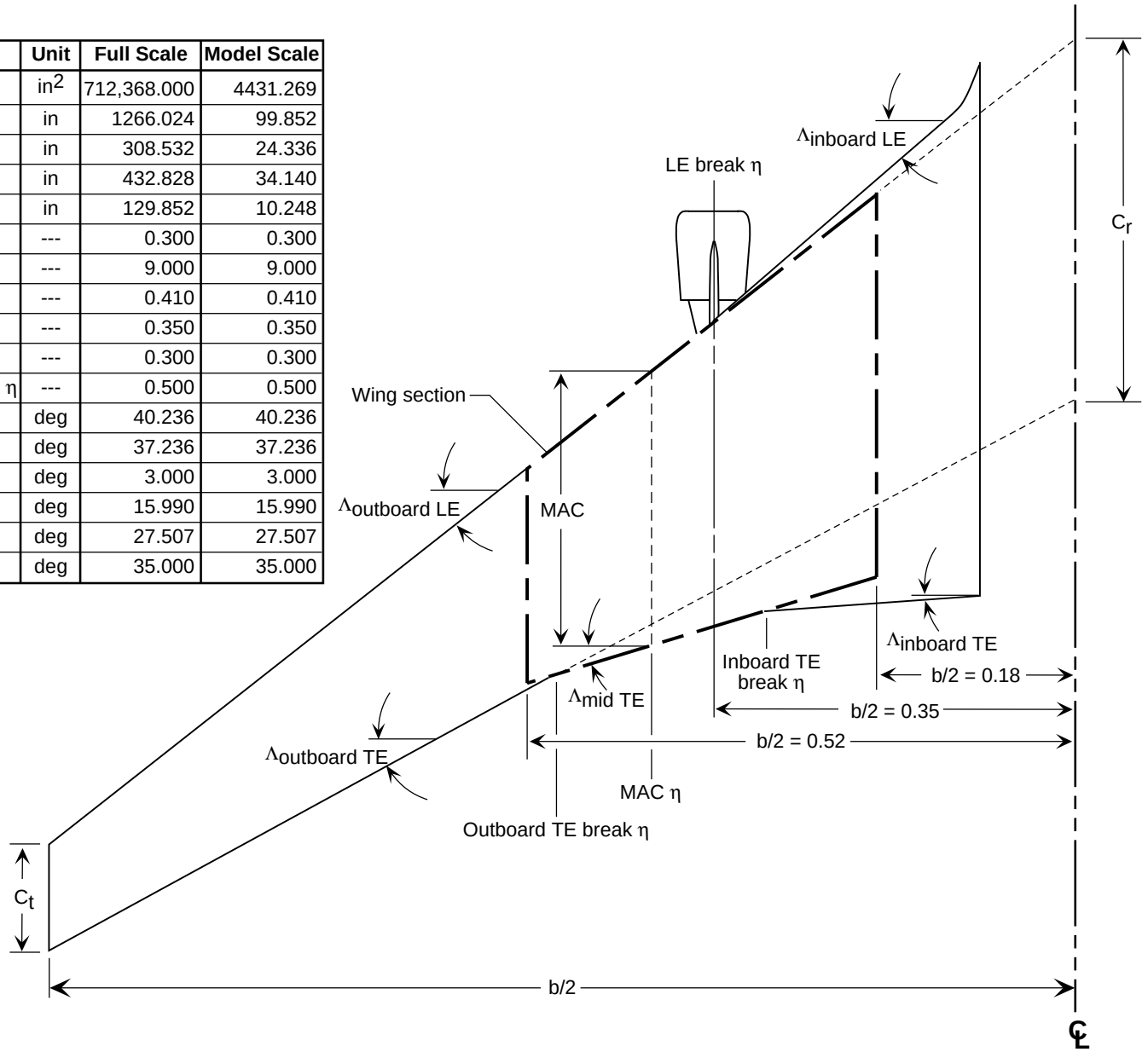

(c) Sketch showing wing planform.

Figure 6. Continued.

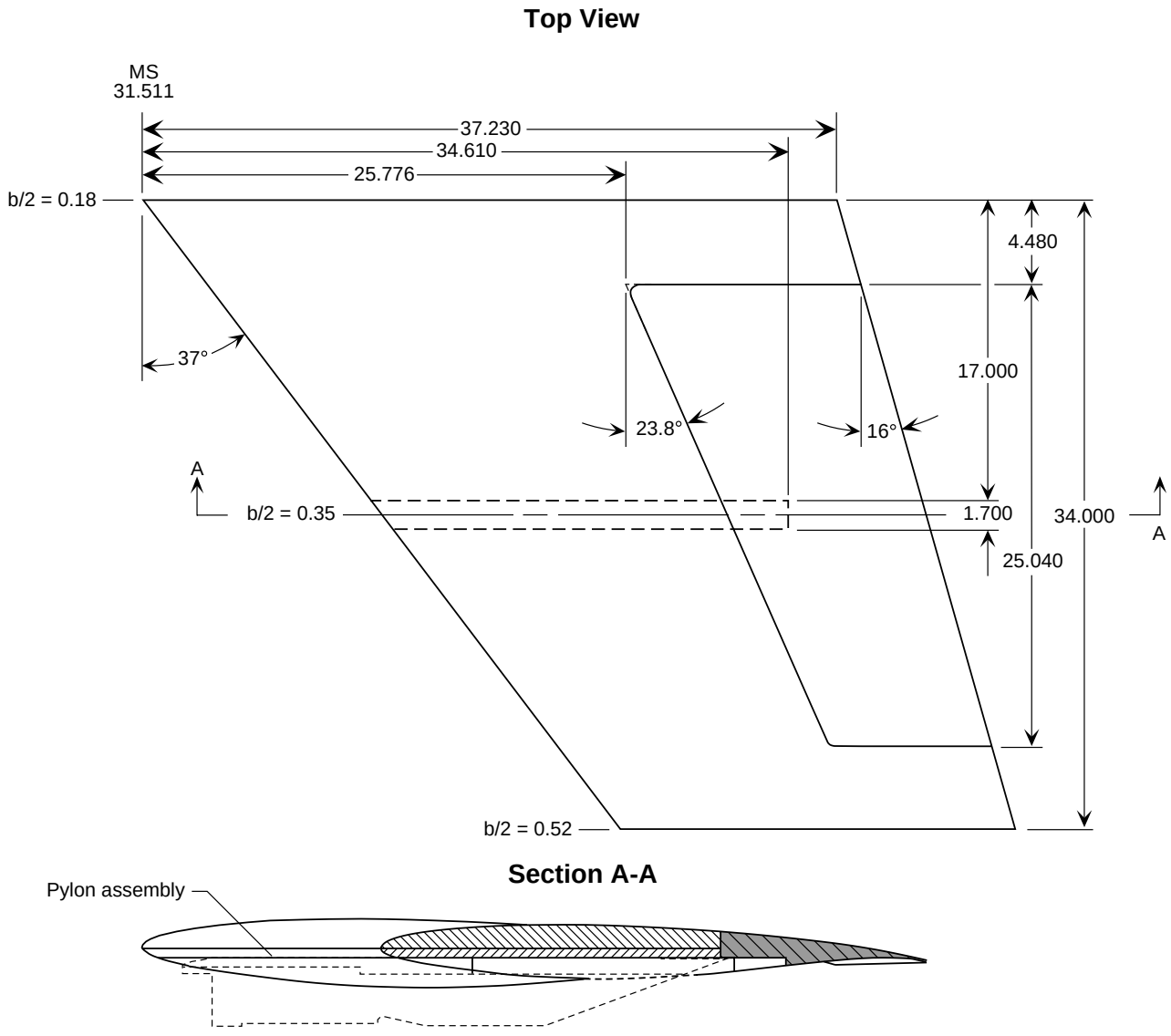

(d) Sketch showing wing section.

Figure 6. Continued.

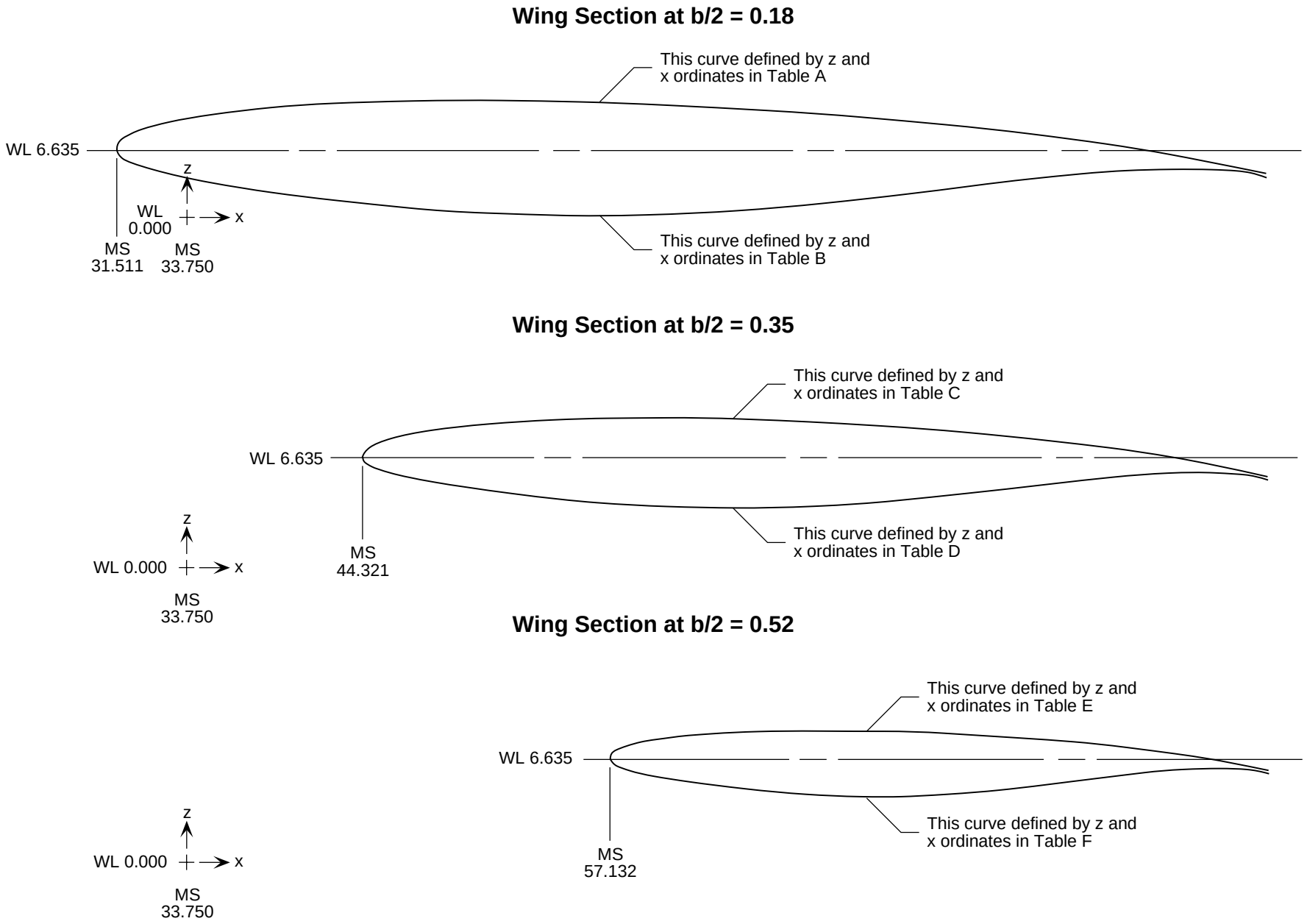

(e) Sketch showing wing sections at b/2 = 0.18, b/2 = 0.35, and b/2 = 0.52. See figure 6(f) for wing ordinates.

Figure 6. Continued.

Table A	
x, in.	z, in.
-2.2390	6.635
-2.0521	6.956
-1.7288	7.157
-1.3764	7.303
-1.0127	7.417
-0.5648	7.529
1.3948	7.852
3.3715	8.051
5.3546	8.172
7.3403	8.238
9.3269	8.266
11.3136	8.256
13.3001	8.216
15.2858	8.150
17.2703	8.054
19.2533	7.931
21.2342	7.778
23.2131	7.601
25.1901	7.404
27.1642	7.179
29.1355	6.931
31.1011	6.642
33.0554	6.284
34.9913	5.839

Table B	
x, in.	z, in.
-2.2390	6.635
-2.0259	6.337
-1.6870	6.167
-1.3262	6.047
-0.9582	5.950
-0.5091	5.848
1.4424	5.502
3.4049	5.224
5.3739	4.997
7.3478	4.817
9.3255	4.686
11.3060	4.605
13.2880	4.584
15.2698	4.617
17.2499	4.707
19.2268	4.850
21.2003	5.035
23.1711	5.247
25.1405	5.471
27.1100	5.695
29.0826	5.888
31.0611	6.007
33.0428	6.003
34.9913	5.701

Table C	
x, in.	z, in.
10.5710	6.635
10.7181	6.888
10.9725	7.046
11.2497	7.160
11.5359	7.251
11.8830	7.338
13.4302	7.593
14.9856	7.749
16.5460	7.844
18.1084	7.896
19.6716	7.919
21.2348	7.910
22.7979	7.879
24.3603	7.827
25.9218	7.752
27.4821	7.655
29.0408	7.535
30.5979	7.395
32.1535	7.240
33.7068	7.063
35.2579	6.868
36.8045	6.640
38.3422	6.359
39.8655	6.009

Table D	
x, in.	z, in.
10.5710	6.635
10.7387	6.401
11.0053	6.267
11.2893	6.172
11.5788	6.096
11.9322	6.016
13.4677	5.744
15.0118	5.525
16.5612	5.346
18.1143	5.205
19.6705	5.101
21.2288	5.038
22.7884	5.021
24.3477	5.047
25.9057	5.118
27.4612	5.231
29.0141	5.376
30.5648	5.543
32.1144	5.719
33.6641	5.895
35.2163	6.048
36.7730	6.141
38.3323	6.138
39.8655	5.900

Table E	
x, in.	z, in.
23.3820	6.635
23.4892	6.819
23.6746	6.934
23.8767	7.018
24.0852	7.084
24.3421	7.148
25.4658	7.333
26.5994	7.447
27.7366	7.516
28.8753	7.554
30.0145	7.571
31.1539	7.564
32.2930	7.542
33.4317	7.504
34.5697	7.449
35.7069	7.378
36.8429	7.291
37.9777	7.189
39.1114	7.076
40.2435	6.947
41.3739	6.805
42.5011	6.639
43.6218	6.434
44.7320	6.179

Table F	
x, in.	z, in.
23.3820	6.635
23.5042	6.464
23.6986	6.367
23.9055	6.298
24.1165	6.242
24.3740	6.184
25.4931	5.985
26.6185	5.826
27.7477	5.696
28.8796	5.592
30.0138	5.517
31.1495	5.471
32.2861	5.459
33.4226	5.478
34.5581	5.529
35.6917	5.612
36.8234	5.717
37.9536	5.839
39.0830	5.967
40.2124	6.096
41.3436	6.207
42.4782	6.275
43.6146	6.273
44.7320	6.100

(f) Wing section ordinates at b/2 = 0.18, b/2 = 0.35, and b/2 = 0.52.

Figure 6. Concluded.

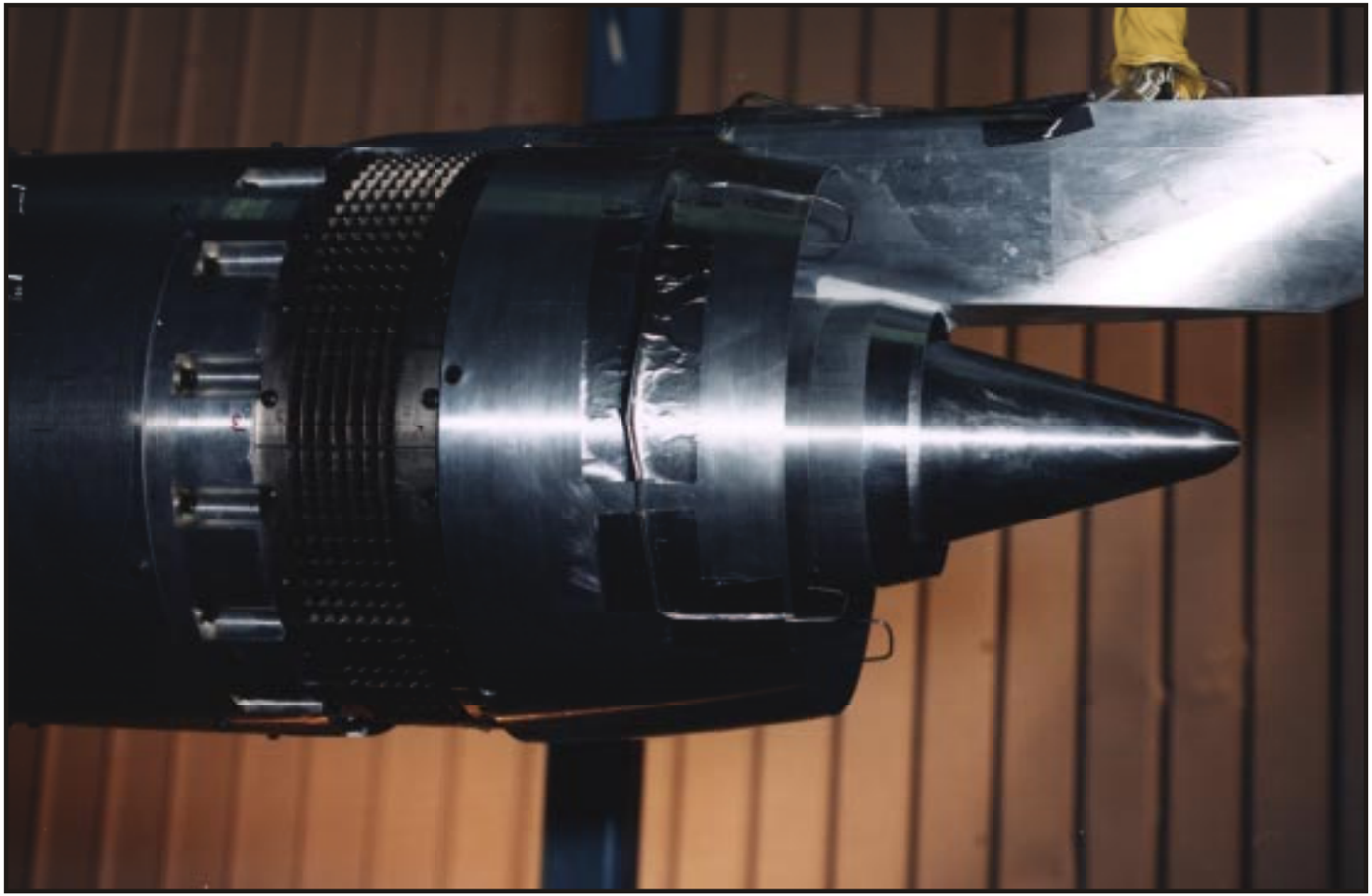

L95-04810

(a) Photograph of cascade thrust reverser model.

Figure 7. Details of cascade thrust reverser model. Dimensions are in inches.

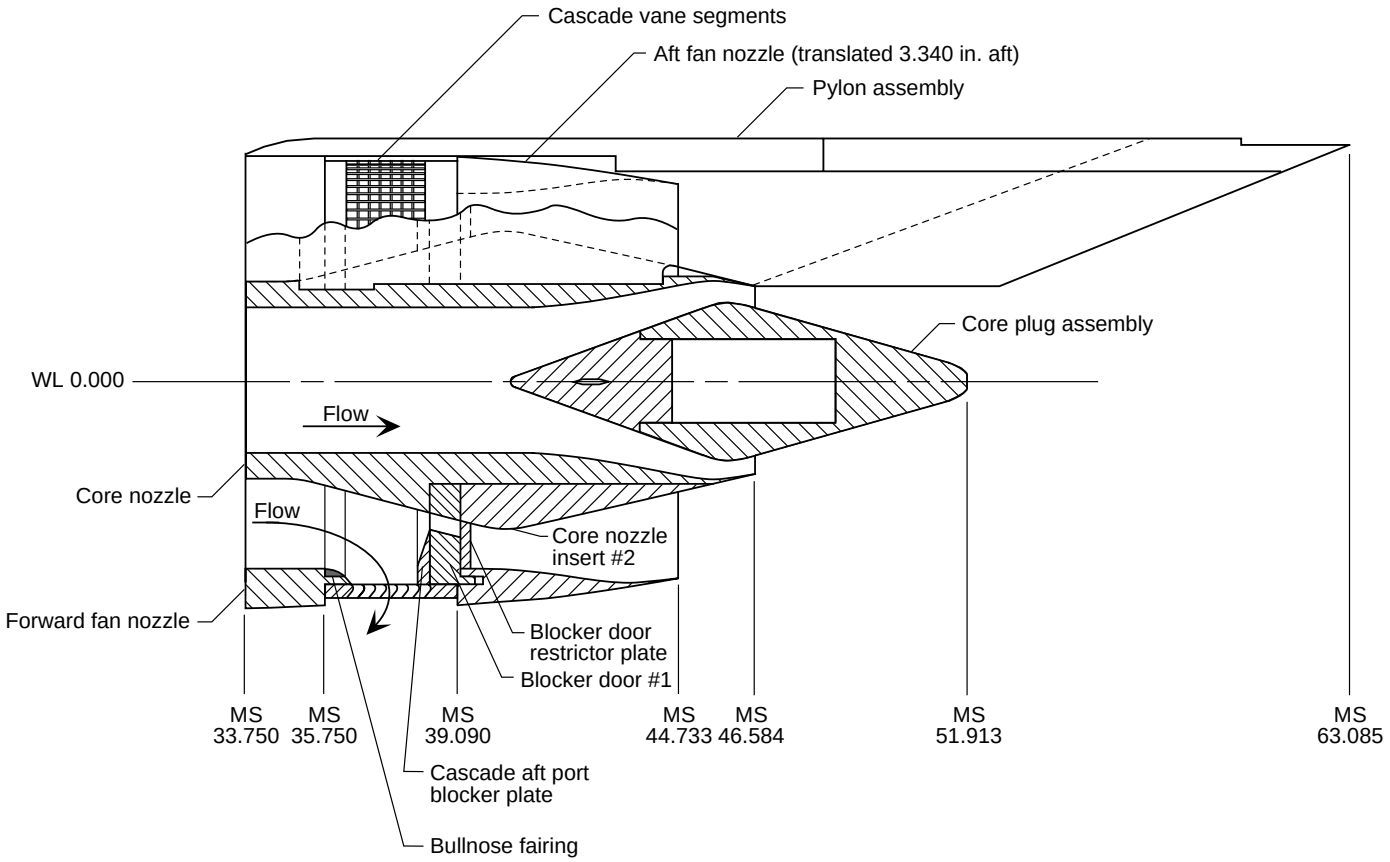

(b) Partial cutaway sketch of conventional cascade thrust reverser model.

Figure 7. Continued.

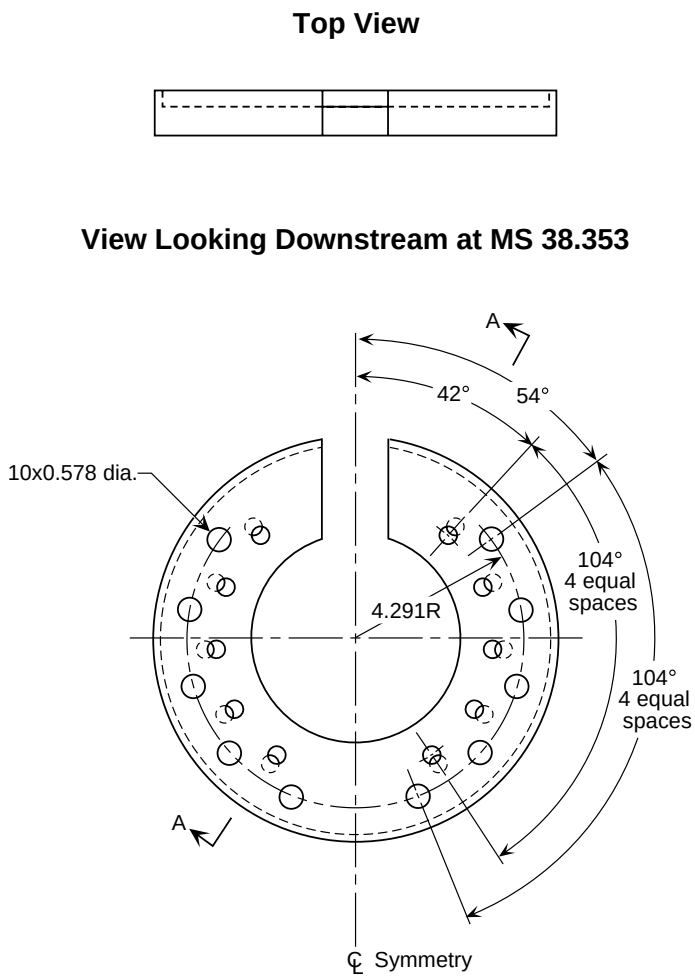

(c) Sketch of blocker door #1.

Figure 7. Continued.

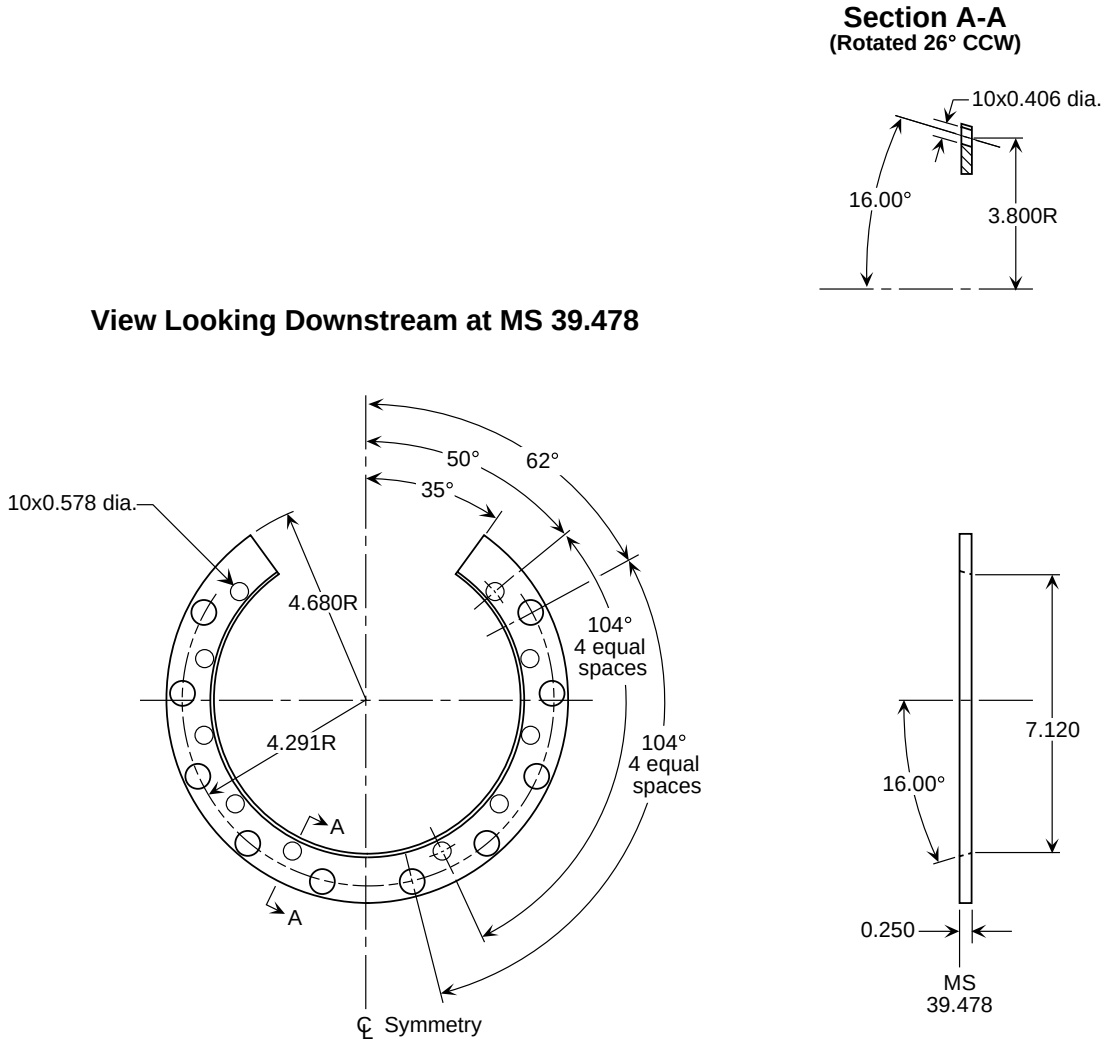

(d) Sketch of blocker door restrictor plate.

Figure 7. Continued.

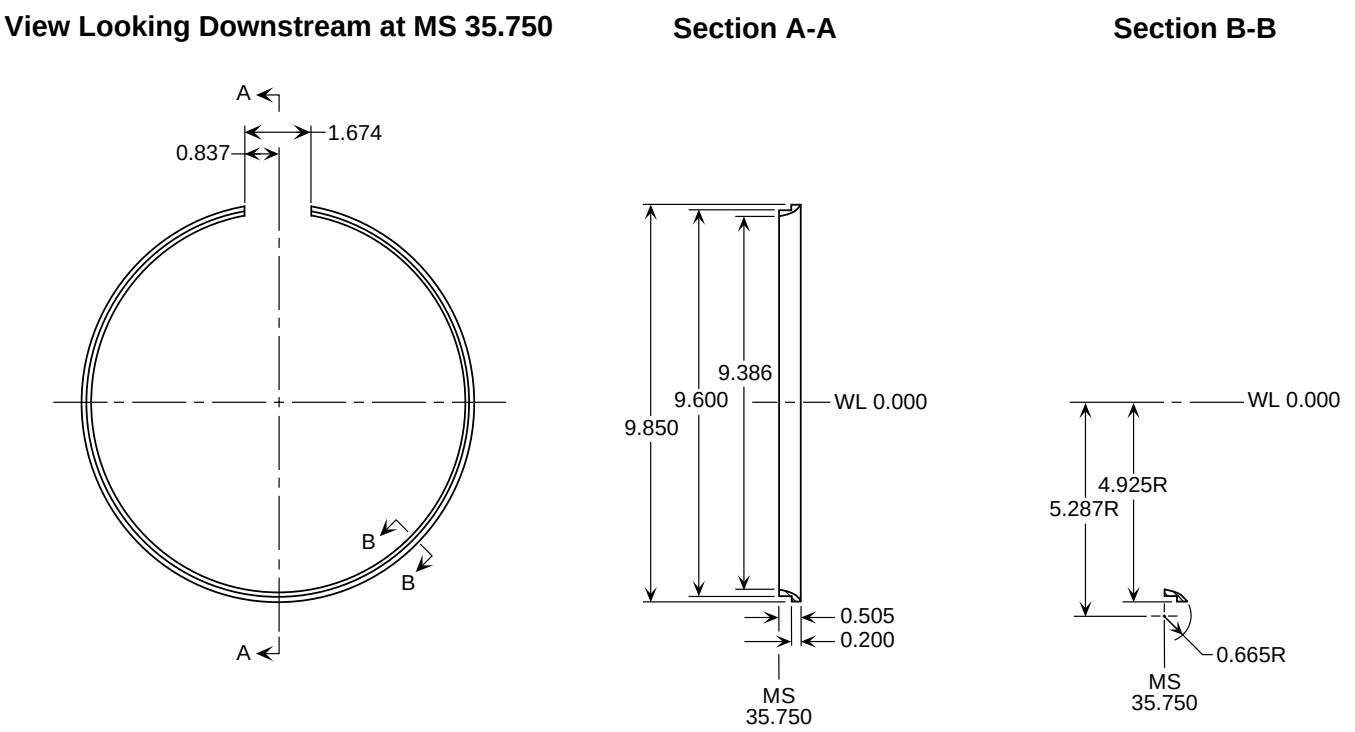

(e) Sketch of bullnose fairing.

Figure 7. Continued.

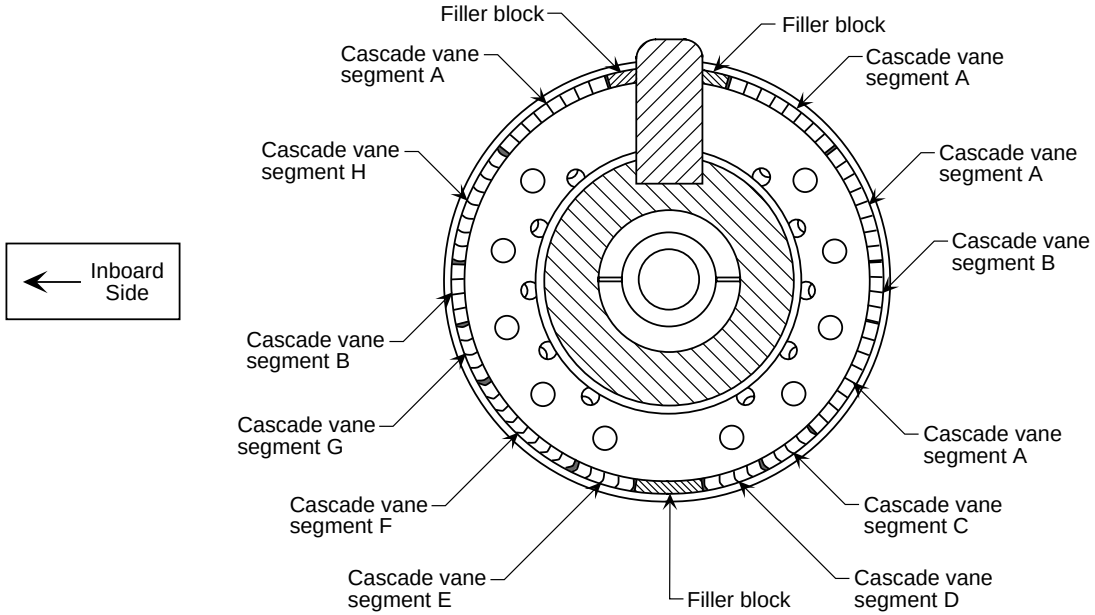

(f) View looking downstream at MS 37.750 showing cascade vane installation.

Figure 7. Continued.

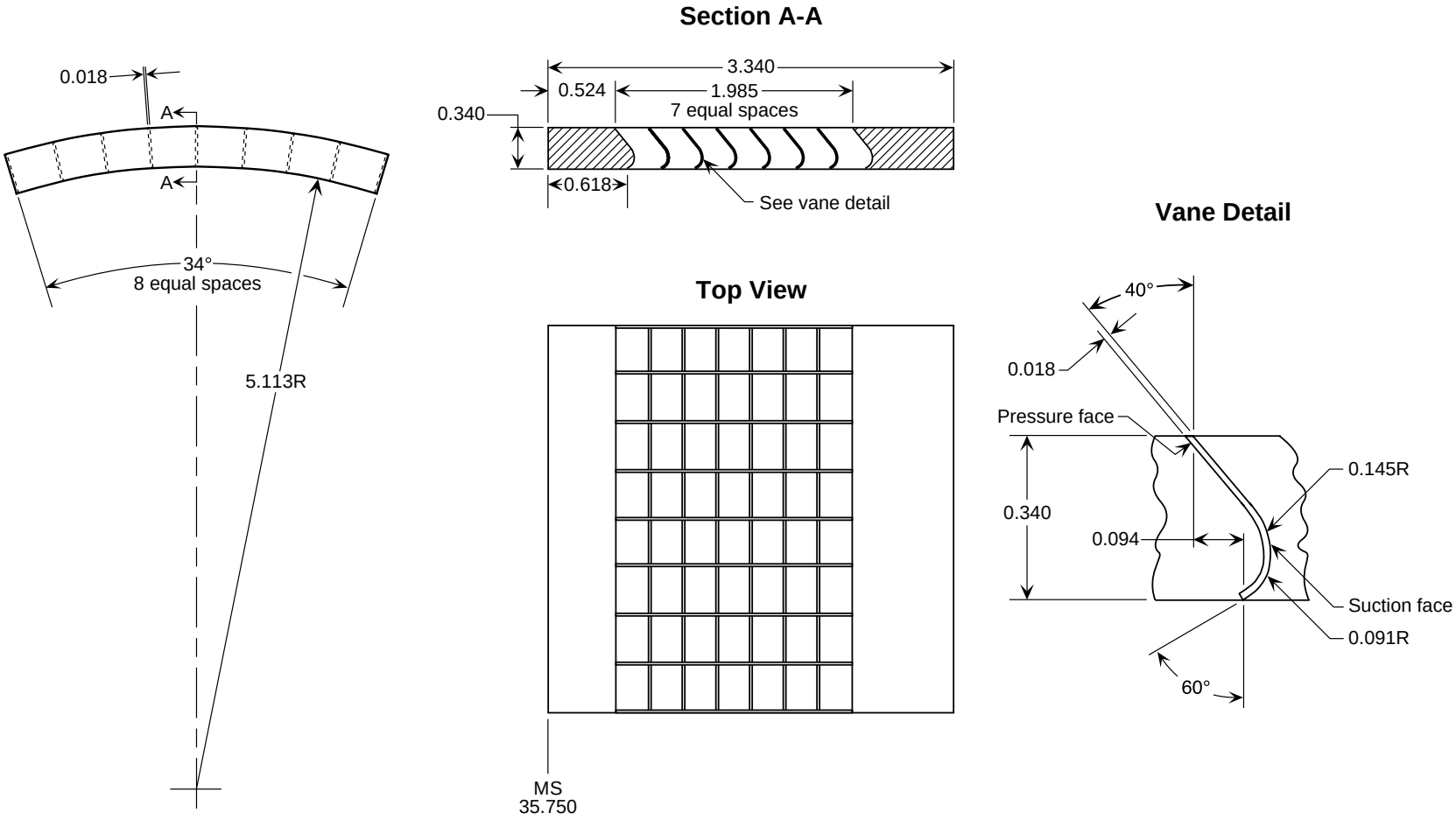

(g) Sketch of cascade vane segment A.

Figure 7. Continued.

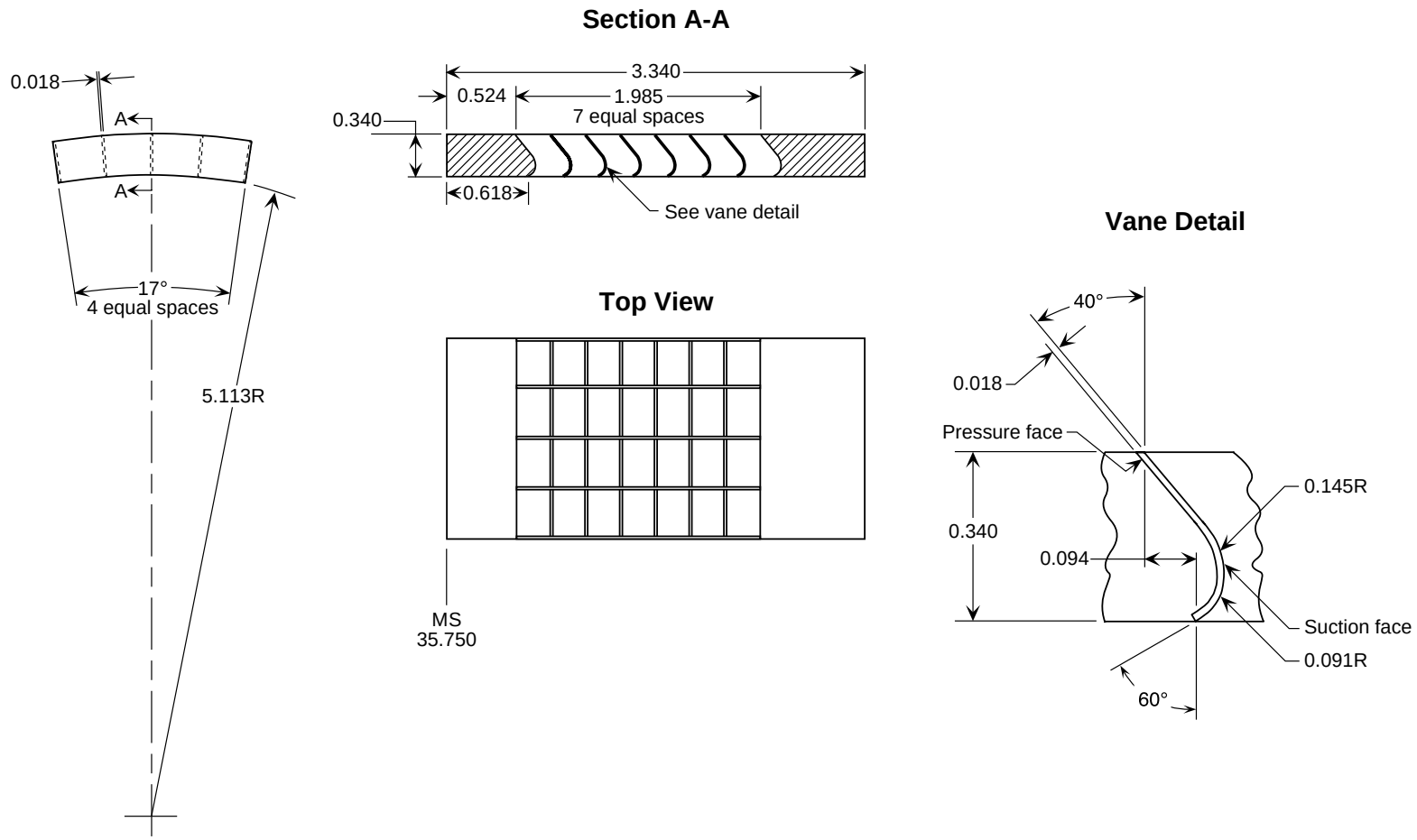

(h) Sketch of cascade vane segment B.

Figure 7. Continued.

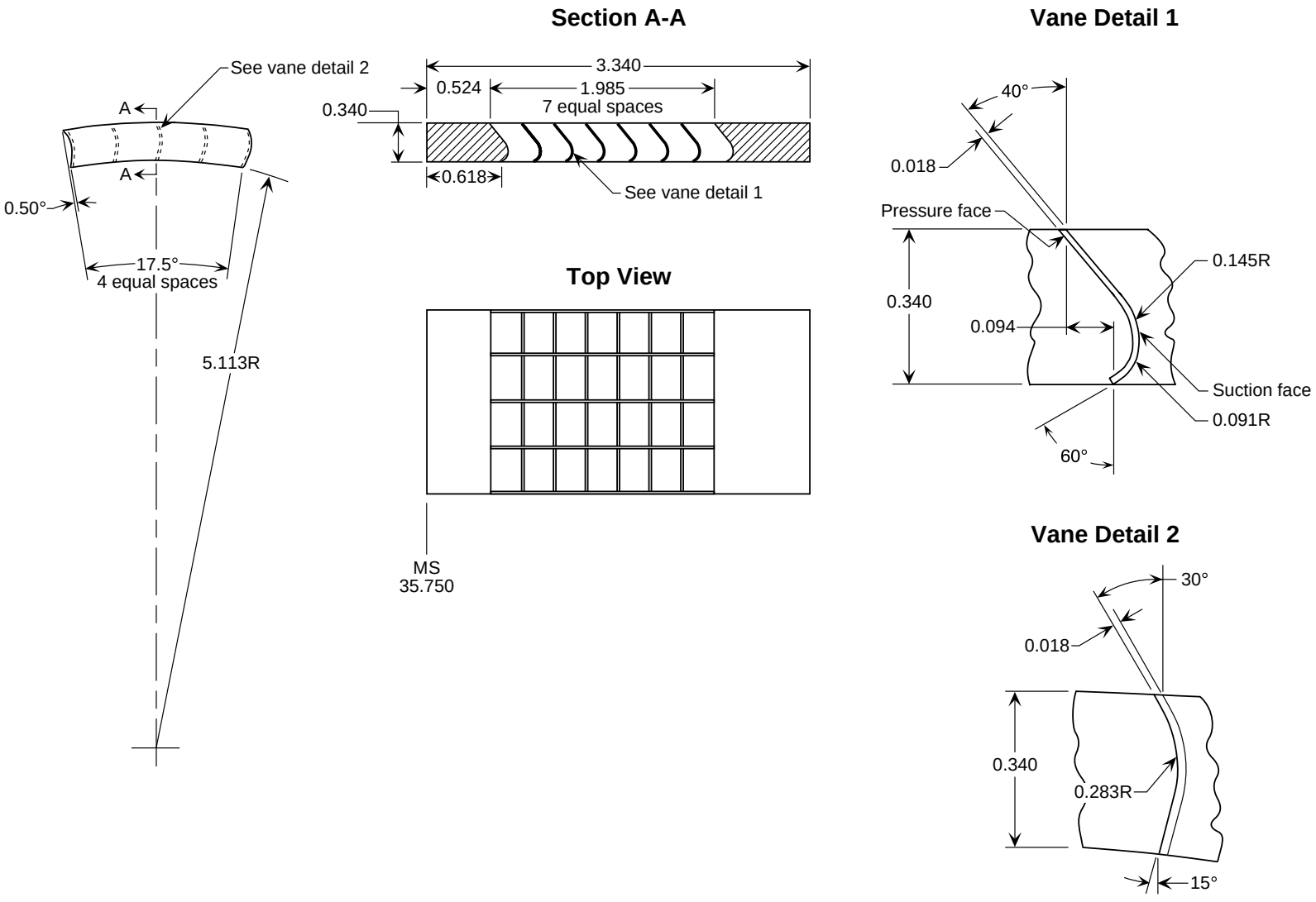

(i) Sketch of cascade vane segment C.

Figure 7. Continued.

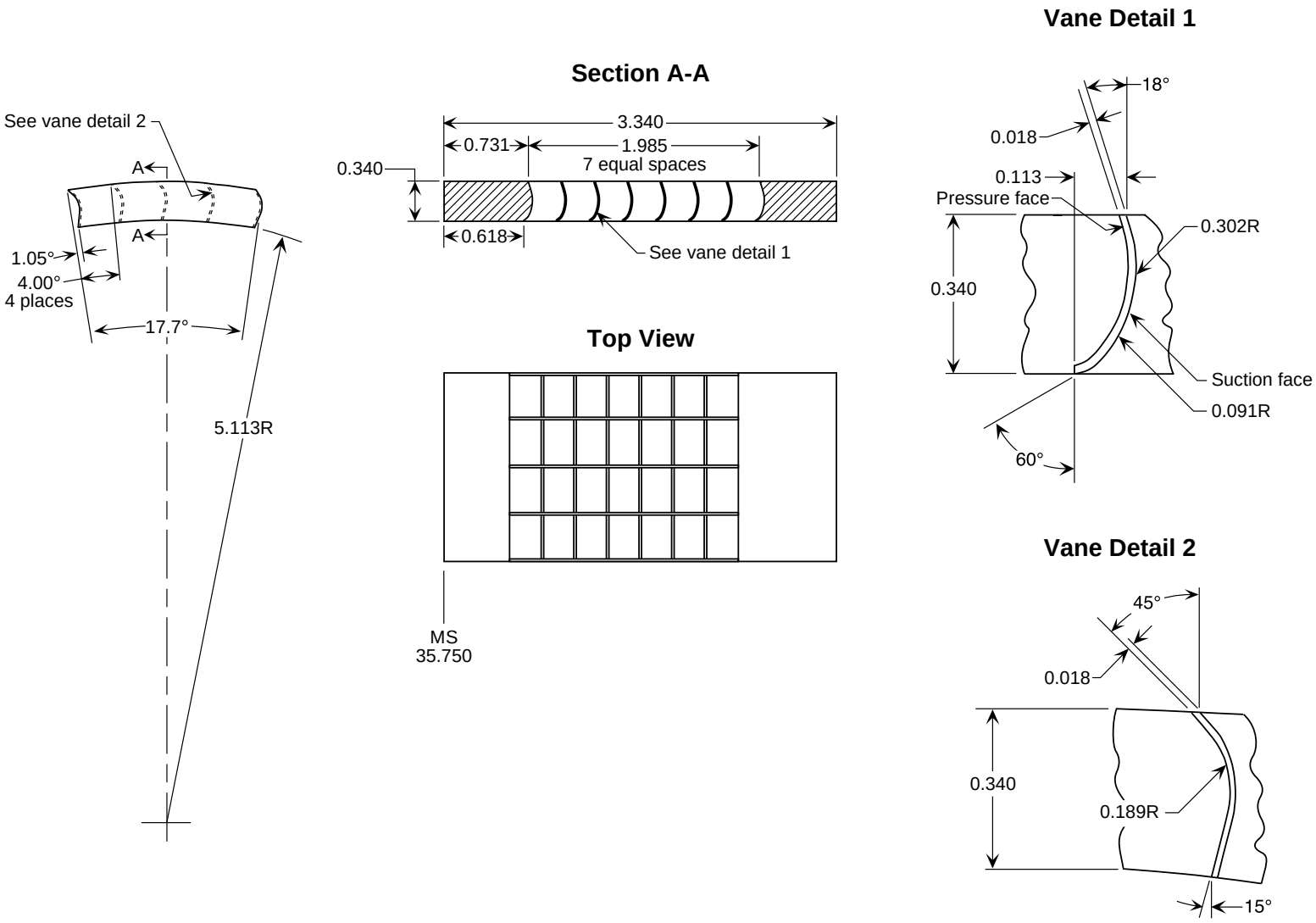

(j) Sketch of cascade vane segment D.

Figure 7. Continued.

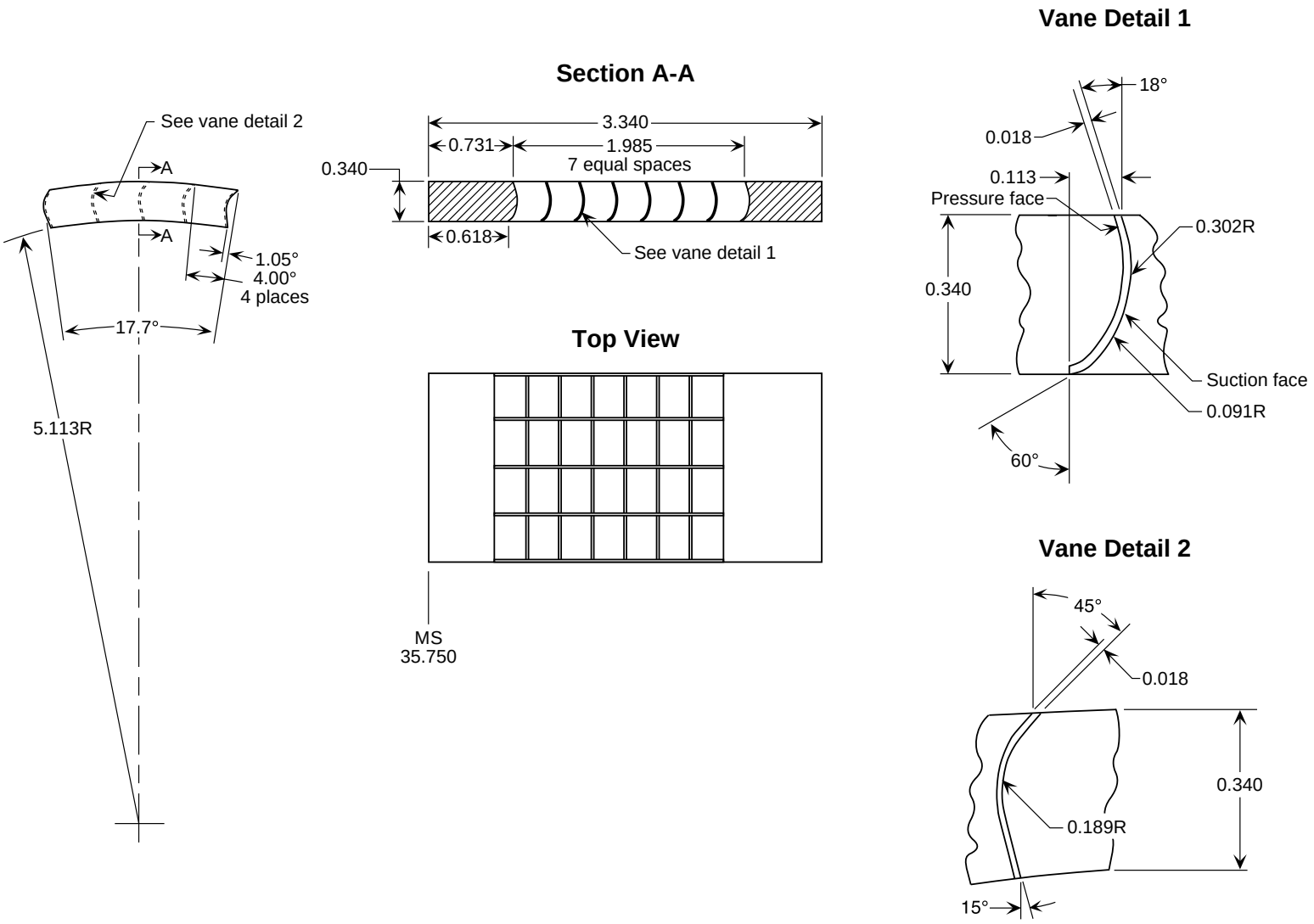

(k) Sketch of cascade vane segment E.

Figure 7. Continued.

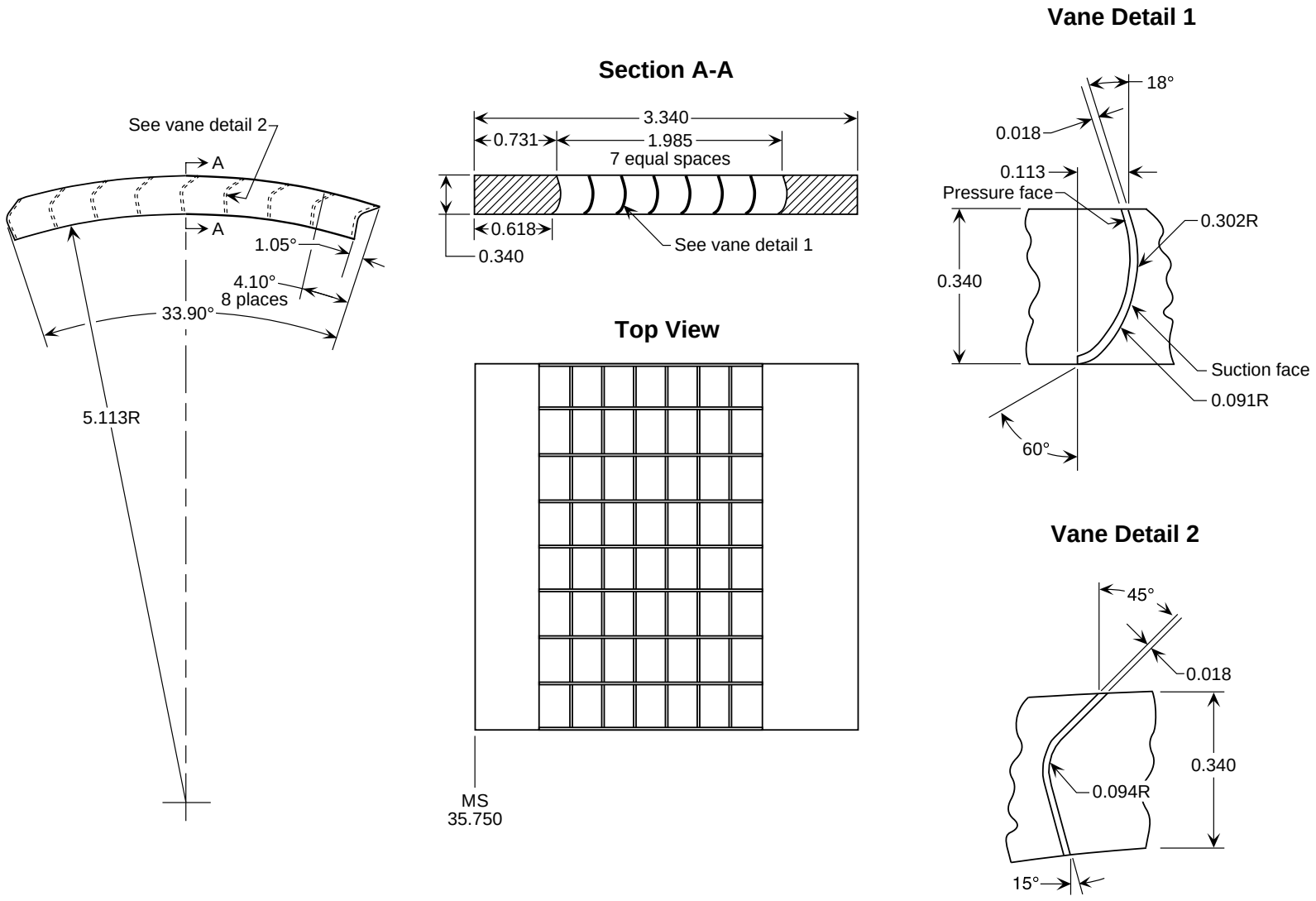

(l) Sketch of cascade vane segment F.

Figure 7. Continued.

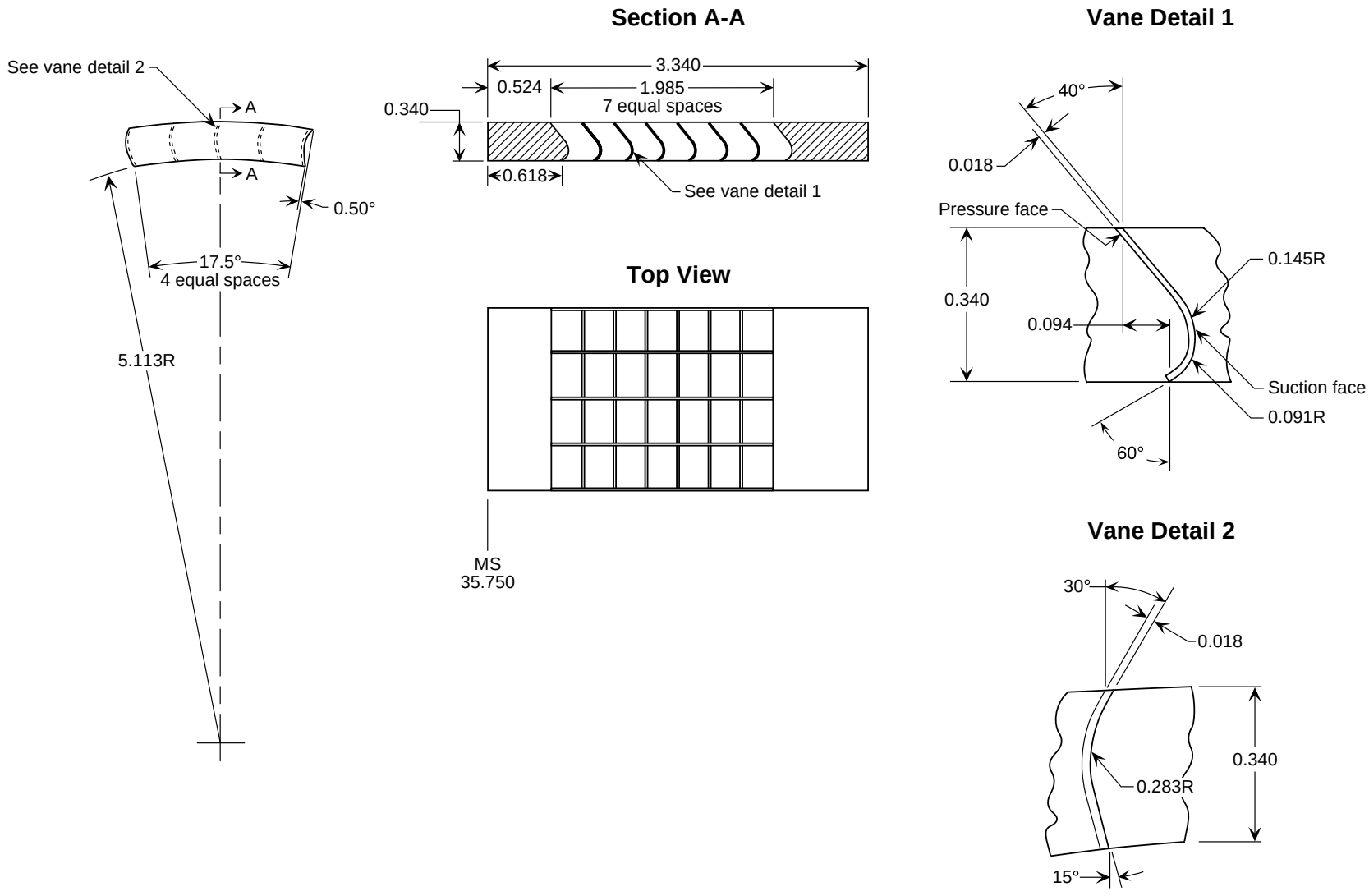

(m) Sketch of cascade vane segment G.

Figure 7. Continued.

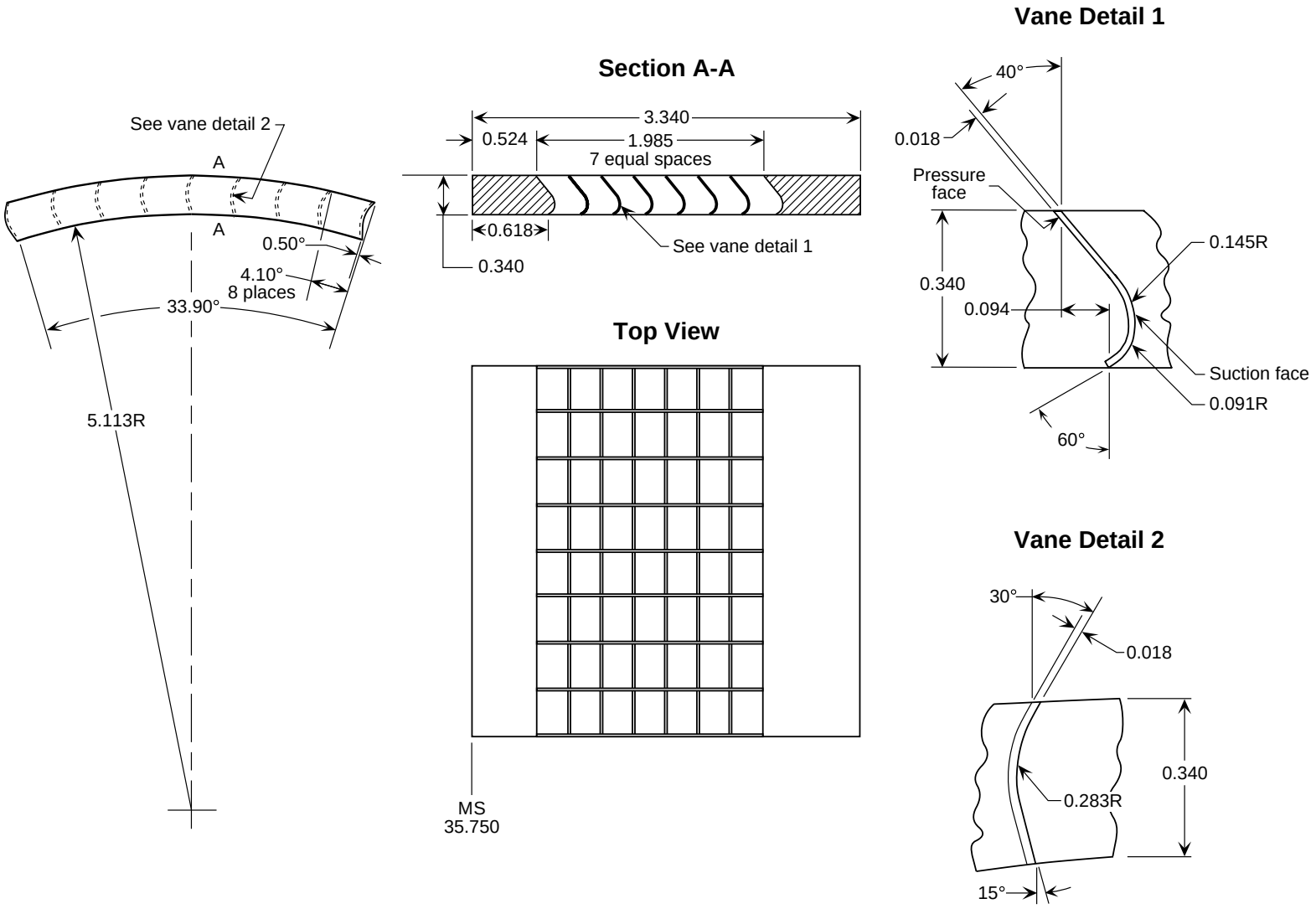

(n) Sketch of cascade vane segment H.

Figure 7. Continued.

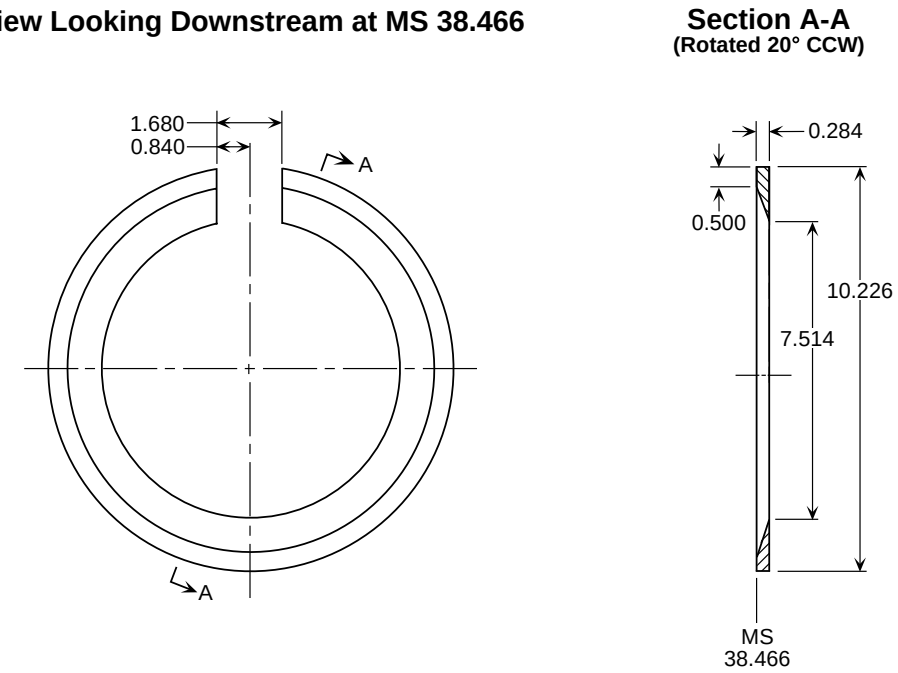

(o) Sketch of cascade aft port blocker plate.

Figure 7. Continued.

x, in.	R, in.
5.3400	3.5461
5.5670	3.6080
5.7150	3.6440
5.8640	3.6770
6.0120	3.7050
6.1600	3.7270
6.3080	3.7440
6.4570	3.7530
6.6050	3.7530
6.7530	3.7450
6.9020	3.7270
7.0500	3.7020
7.1980	3.6700
7.3470	3.6370
7.6430	3.5690
8.5000	3.3730
8.7709	3.3110
9.0417	3.2490
9.3126	3.1870
9.5835	3.1250
9.8544	3.0630
10.1253	3.0110
10.3961	2.9390
10.6670	2.8770
10.9379	2.8150
11.2087	2.7530
11.4796	2.6910
11.7505	2.6290
11.8770	2.6000

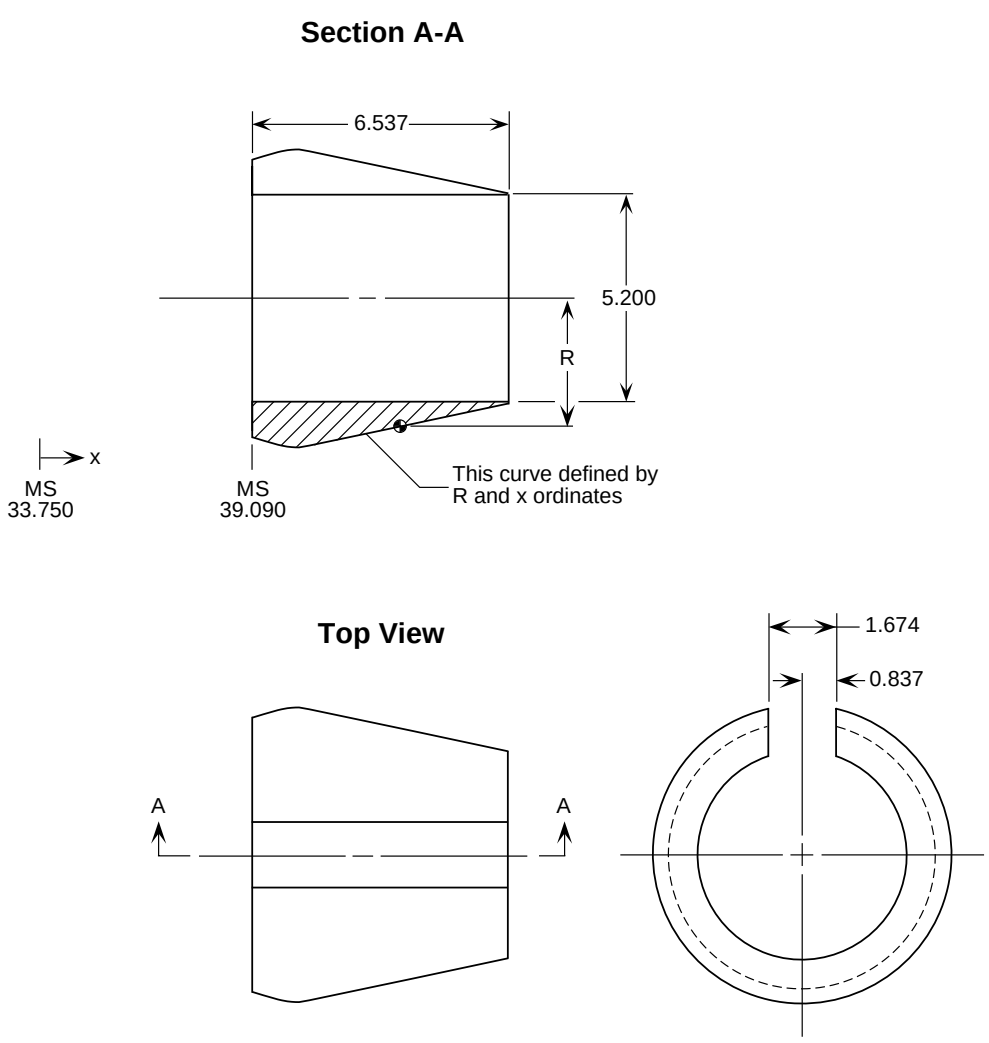

(p) Sketch of core nozzle insert #2.

Figure 7. Continued.

View Looking Downstream at MS 38.353

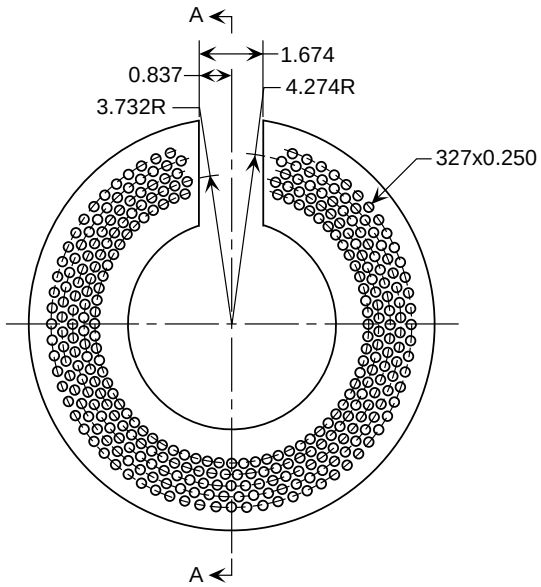

Section A-A

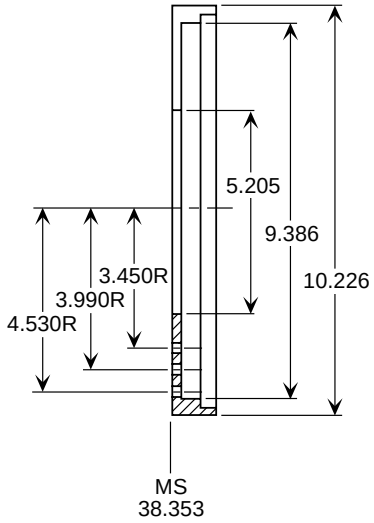

(q) Sketch of blocker door #2.

Figure 7. Continued.

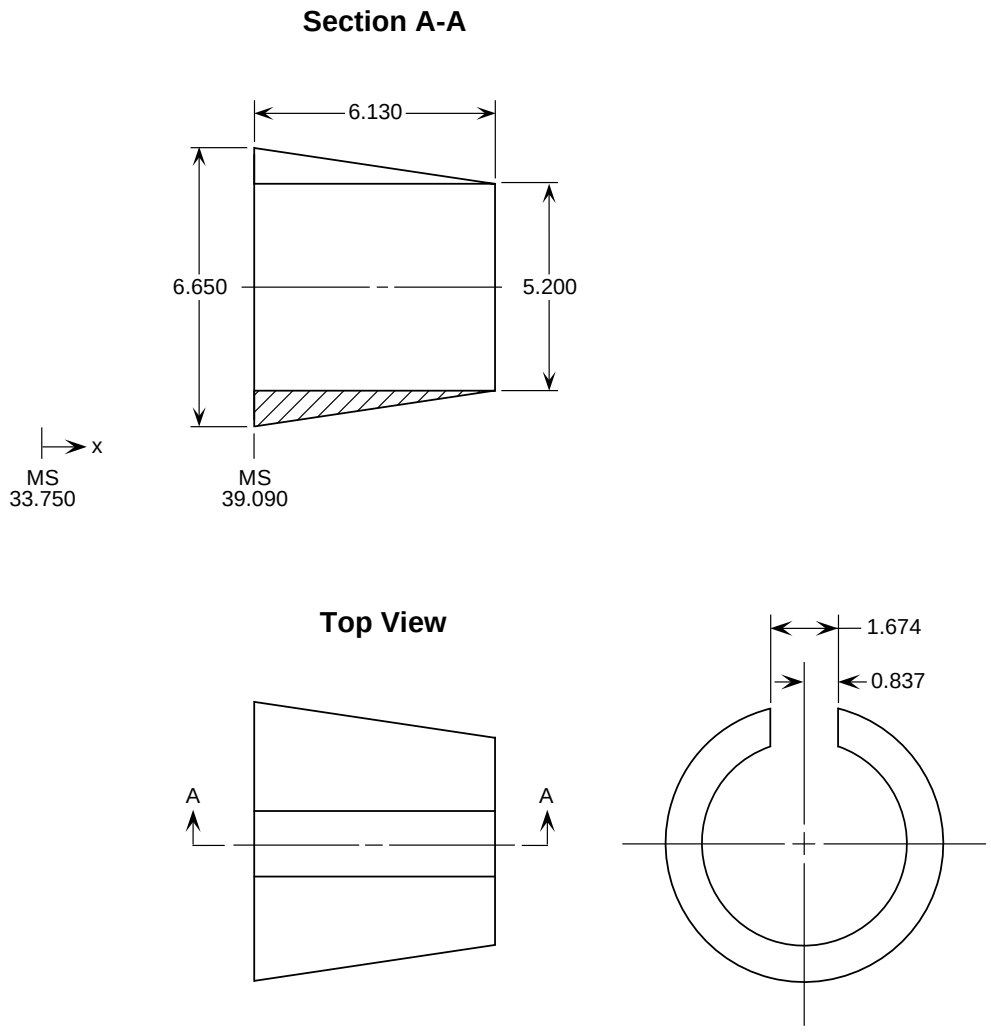

(r) Sketch of core nozzle insert #3.

Figure 7. Concluded.

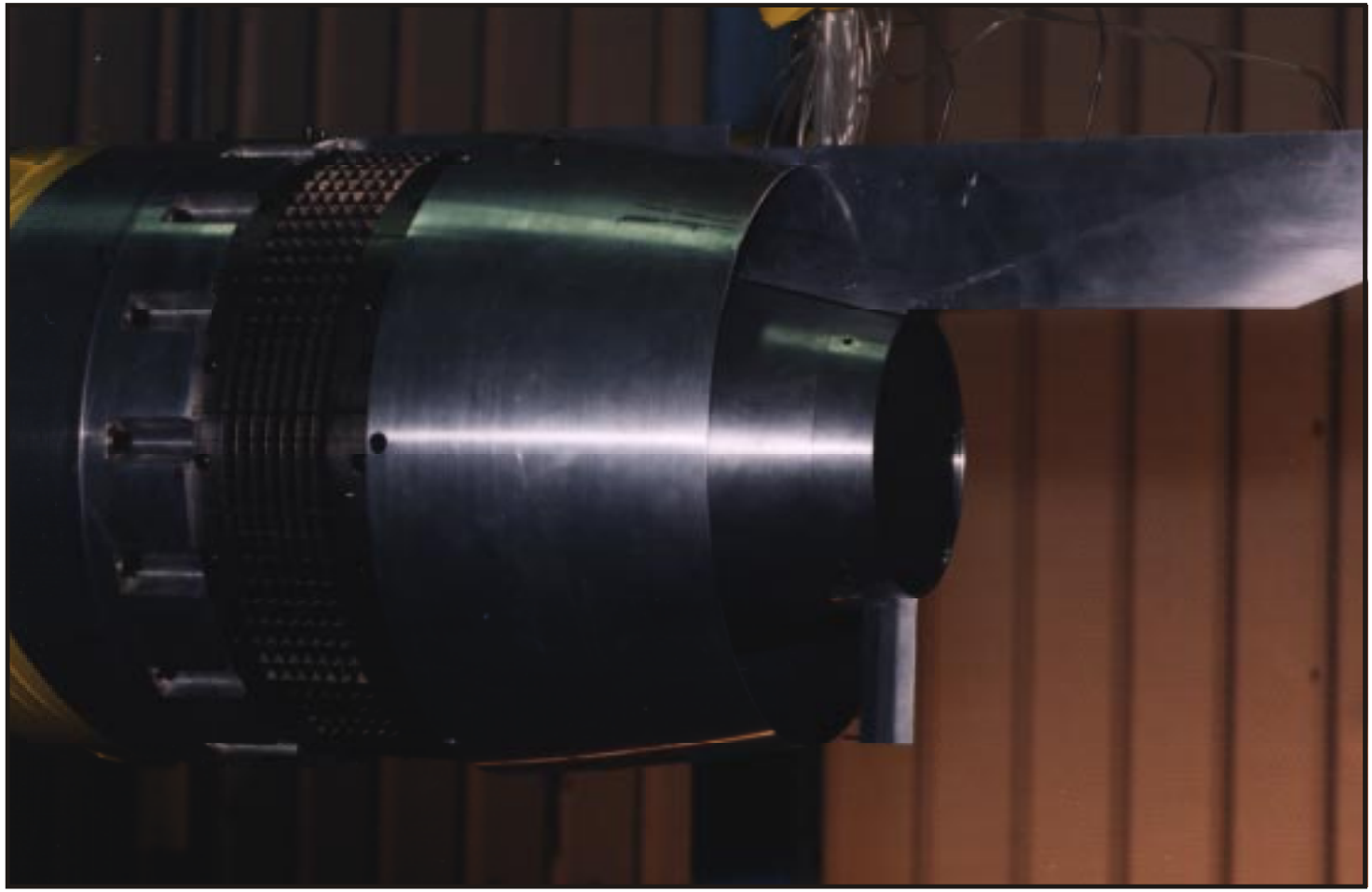

L96-00980

(a) Photograph of blockerless thrust reverser model.

Figure 8. Details of blockerless thrust reverser model. Dimensions are in inches.

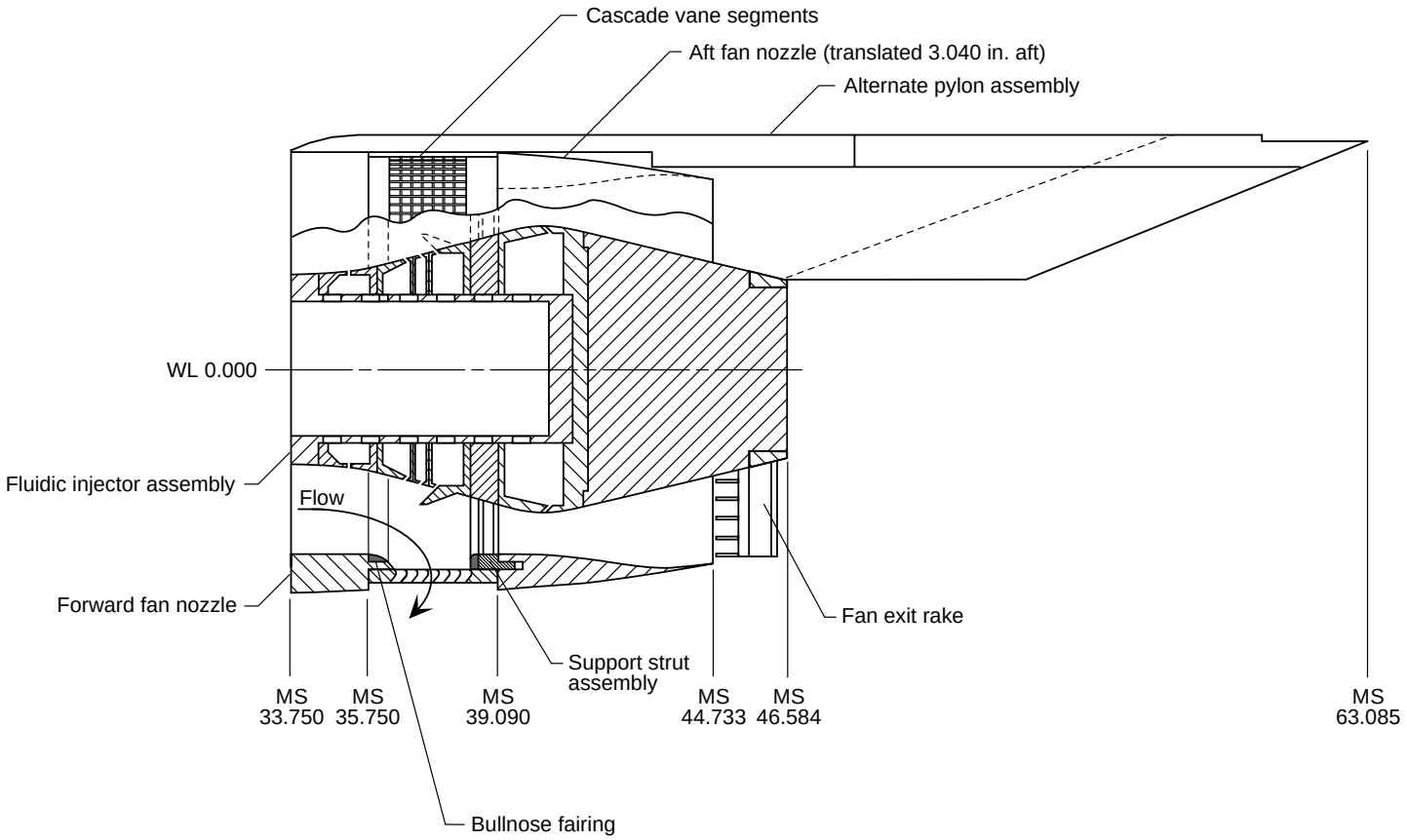

(b) Partial cutaway sketch of blockerless thrust reverser model.

Figure 8. Continued.

x, in.	R, in.
0.0000	2.4630
0.5000	2.4680
1.0000	2.4980
1.5000	2.5430
2.0000	2.6230
2.2300	2.6790
2.4802	2.7460
2.7305	2.8130
2.9807	2.8800
3.2310	2.9470
3.4812	3.0140
3.7315	3.0810
3.9817	3.1480
4.2320	3.2150
4.5290	3.3020
4.8250	3.3930
5.1220	3.4830
5.2700	3.5270
5.5670	3.6080
5.7150	3.6440
5.8640	3.6770
6.0120	3.7050
6.1600	3.7270
6.3080	3.7440
6.4570	3.7530
6.6050	3.7530
6.7530	3.7450
6.9020	3.7270
7.0500	3.7020
7.1980	3.6700
7.3470	3.6370
7.6430	3.5690
8.5000	3.3730
8.7709	3.3110
9.0417	3.2490
9.3126	3.1870
9.5835	3.1250
9.8544	3.0630
10.1253	3.0110
10.3961	2.9390
10.6670	2.8770
10.9379	2.8150
11.2087	2.7530
11.4796	2.6910
11.7505	2.6290
12.0214	2.5670
12.2922	2.5050
12.5631	2.4430
12.8340	2.3810

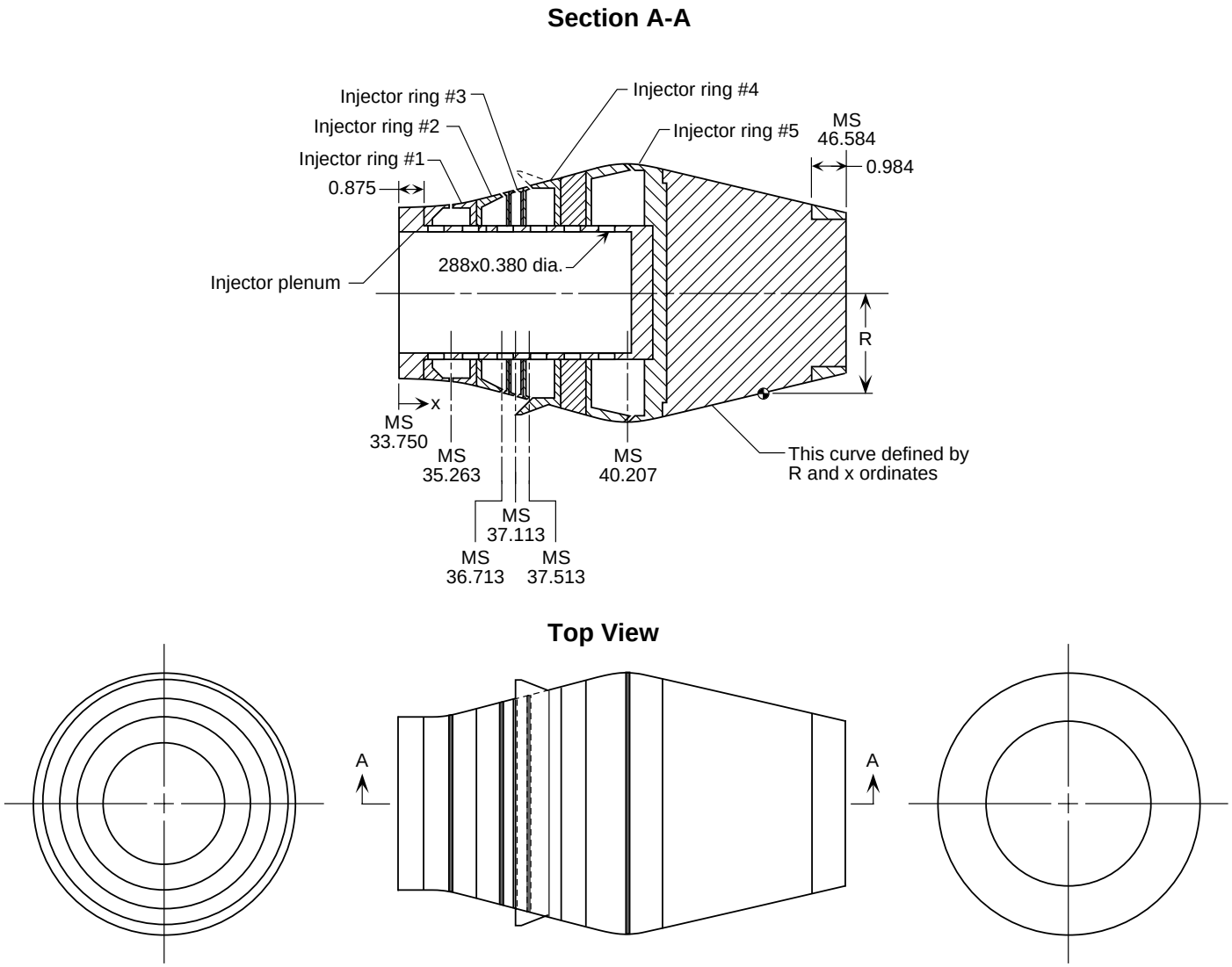

(c) Sketch of fluidic injector assembly.

Figure 8. Continued.

Leading Edge Contour	
x, in.	y, in.
1.5850	0.0000
1.6350	0.0779
1.6850	0.0914
1.7850	0.1134
1.8850	0.1365
1.9850	0.1610
2.0850	0.1865
2.1850	0.2127
2.2850	0.2397
2.3850	0.2675
2.4850	0.2964
2.5850	0.3260
2.6850	0.3556
2.7850	0.3862
2.8850	0.4194
2.9850	0.4540
3.0850	0.4878
3.1850	0.5228
3.2850	0.5610
3.3845	0.5930
3.4850	0.6183
3.5850	0.6418
3.6850	0.6639
3.7850	0.6846
3.8850	0.7039
3.9850	0.7218
4.0850	0.7384
4.1850	0.7536
4.2850	0.7674
4.3850	0.7798
4.4850	0.7910
4.5850	0.8007
4.6850	0.8092
4.7850	0.8163
4.8850	0.8221
4.9850	0.8266
5.0850	0.8297
5.1850	0.8315
5.2730	0.8320

Core Contour	
x, in.	z, in.
1.5850	2.5566
2.0000	2.6230
2.4802	2.7460
2.9807	2.8800
3.4812	3.0140
3.9817	3.1480
4.5290	3.3020
5.1220	3.4830
5.5670	3.6080
5.8640	3.6770
6.1600	3.7270
6.4570	3.7530
6.7530	3.7450
7.0500	3.7020
7.3470	3.6370
8.5000	3.3730
9.0417	3.2490
9.5835	3.1250
10.1253	3.0110
10.6670	2.8770
11.2087	2.7530
11.7505	2.6290
12.2922	2.5050
12.9200	2.3613

Leading Edge Contour Limit	
x, in.	y, in.
1.5850	-0.9580
1.9850	-0.9733
2.3850	-0.9836
2.7850	-0.9813
3.1850	-0.9625
3.5850	-0.9292
3.9850	-0.8845
4.3850	-0.8303
4.7850	-0.7683
5.1850	-0.7026
5.3850	-0.6701

Pylon Closure	
x, in.	y, in.
12.8340	0.8320
13.7756	0.8040
14.7164	0.7335
15.6579	0.6325
16.5993	0.5075
17.5407	0.3635
18.4817	0.2005
18.9526	0.1115
19.4232	0.0175

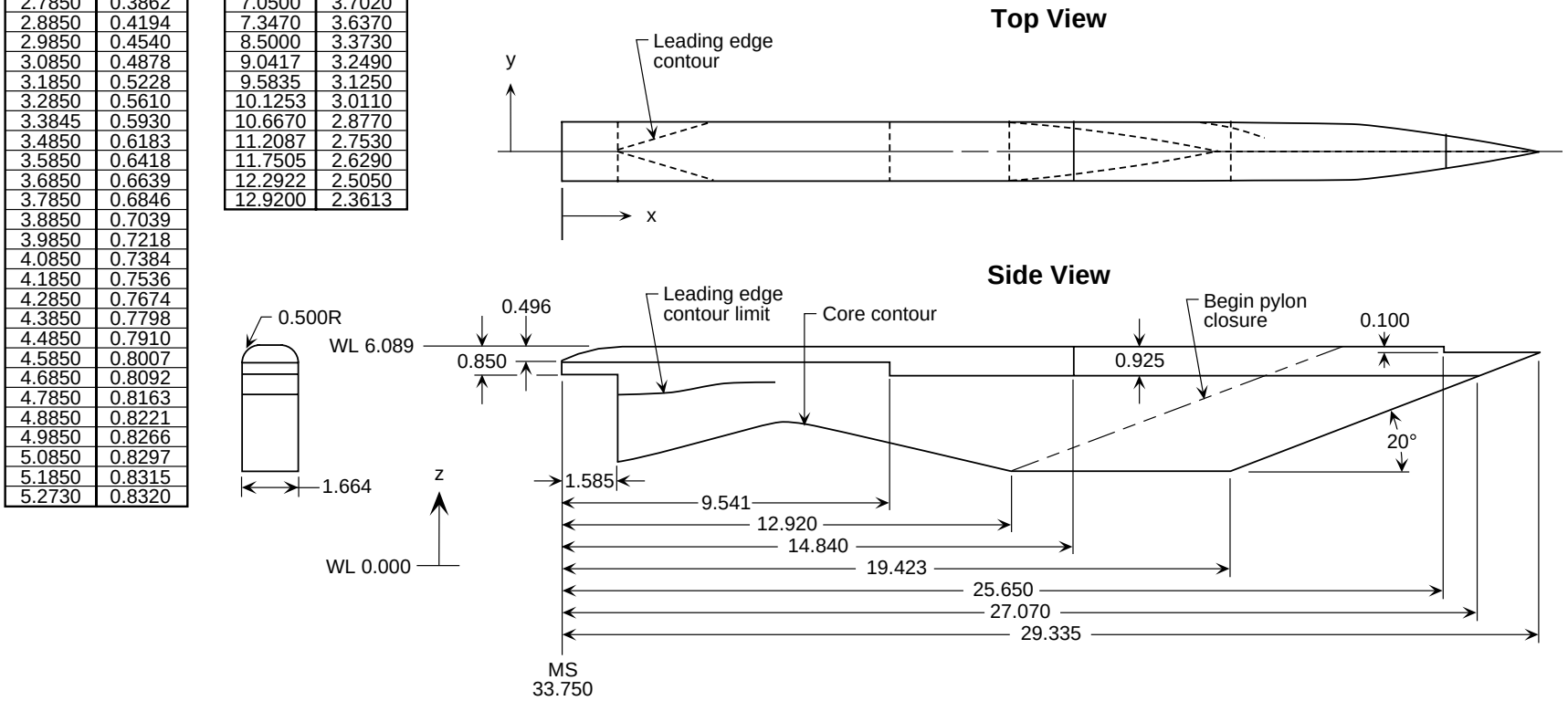

(d) Sketch of alternate pylon assembly.

Figure 8. Continued.

Side View

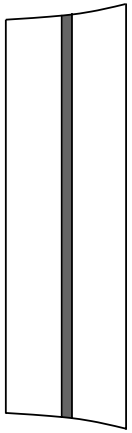

Section A-A

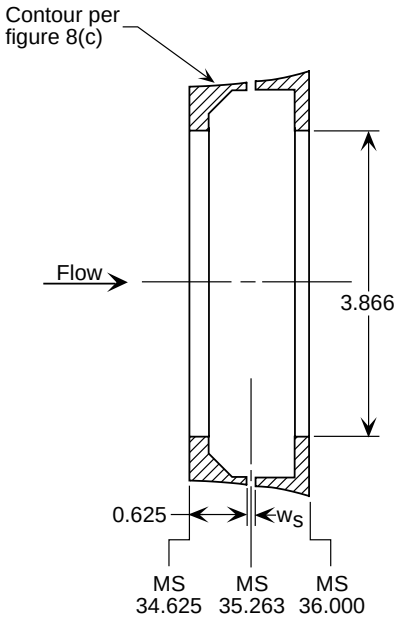

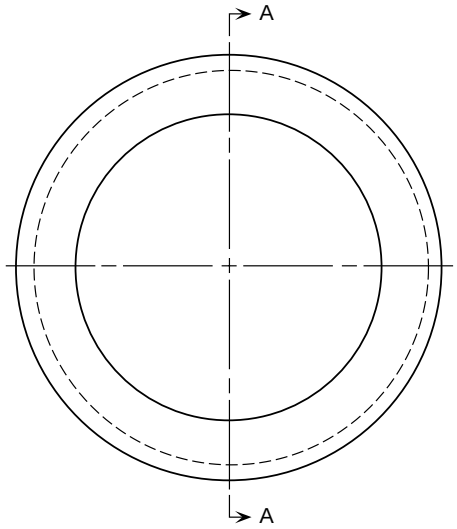

Slot Type	Slot Width (w_S), in.
Blank	0.000
0.025	0.025

(e) Sketch of injector ring #1.

Figure 8. Continued.

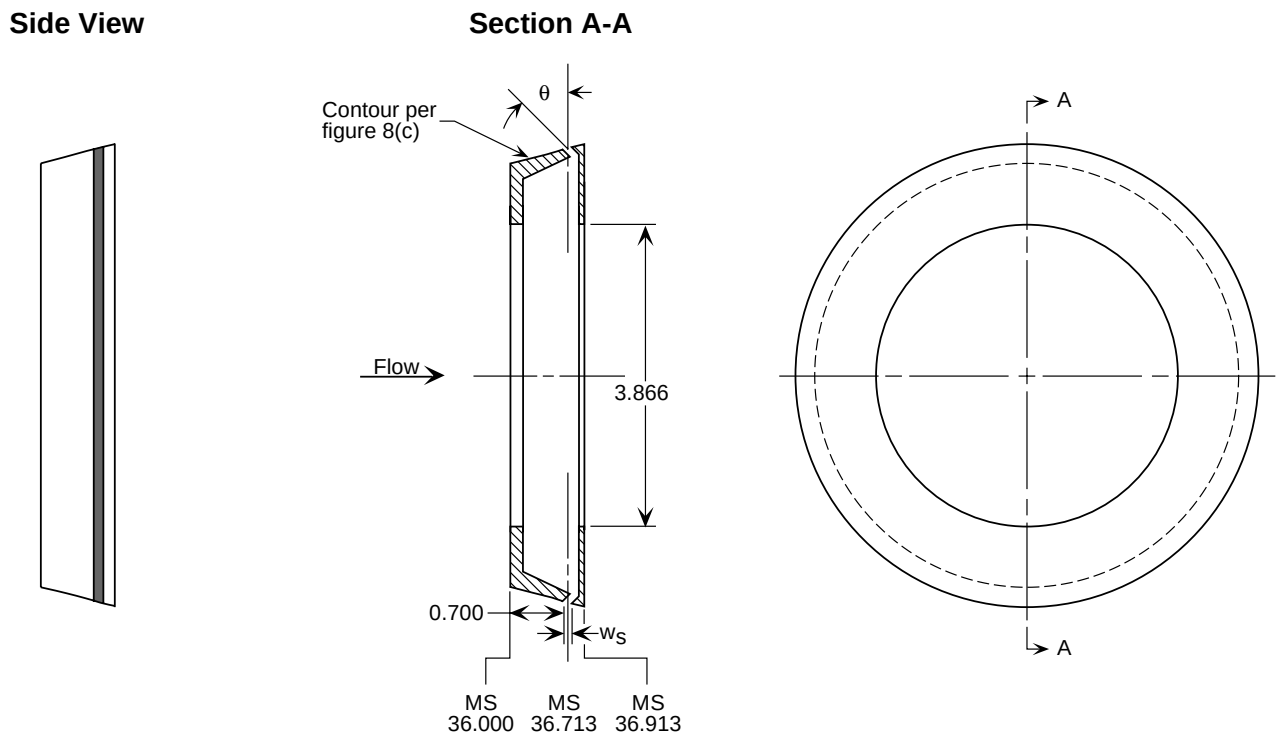

Slot Type	Slot Width (w_S), in.	Slot Angle (θ), deg
Blank	0.000	0
0.013	0.013	0
0.013@45°	0.013	45
0.025	0.025	0
0.025@45°	0.025	45

(f) Sketch of injector ring #2.

Figure 8. Continued.

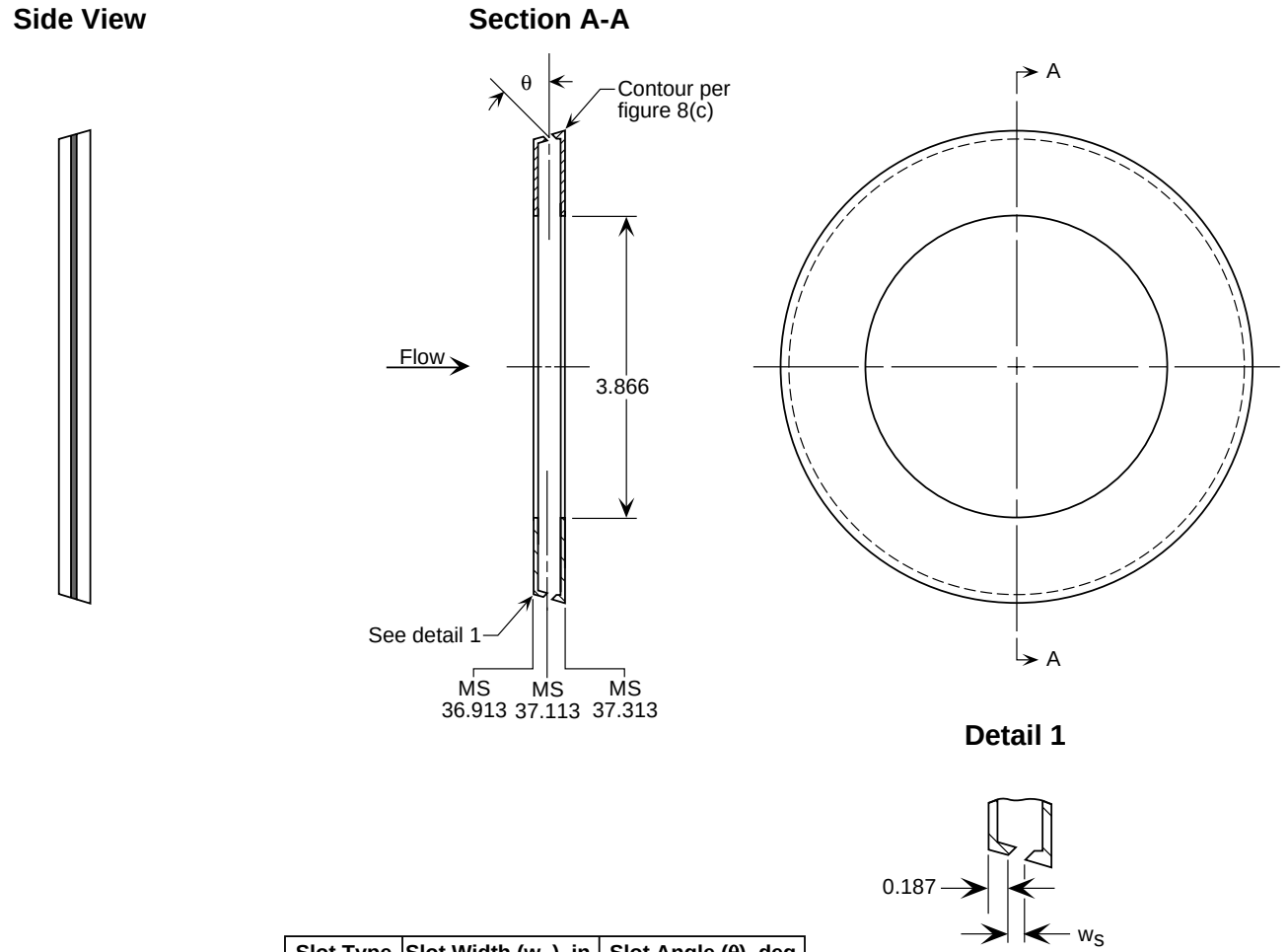

Slot Type	Slot Width (w_S), in.	Slot Angle (θ), deg
Blank	0.000	0
0.013	0.013	0
0.013@45°	0.013	45
0.025	0.025	0
0.025@45°	0.025	45

(g) Sketch of injector ring #3.

Figure 8. Continued.

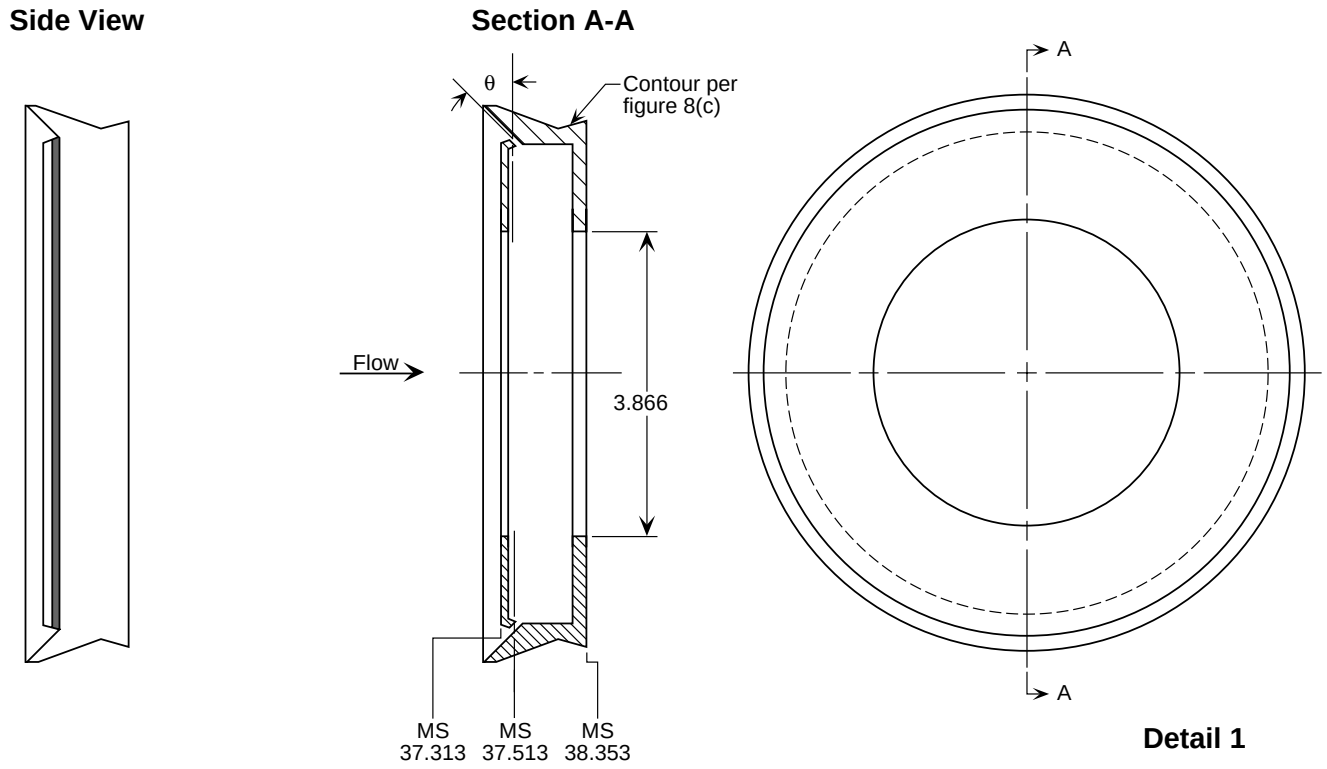

Slot Type	Slot Width (w_S), in.	Slot Angle (θ), deg	Hole Diameter, in.	Tab Height (h_t), in.
Blank	0.000	0	--	0
0.013	0.013	0	--	0
0.013@45°	0.013	45	--	0
0.025	0.025	0	--	0
0.025@45°	0.025	45	--	0
0.025 holes	--	0	0.025	0
0.025 tab 1	0.025	45	--	0.20
0.025 tab 2	0.025	45	--	0.40
0.025 tab 3	0.025	45	--	0.60

(h) Sketch of injector ring #4.

Figure 8. Continued.

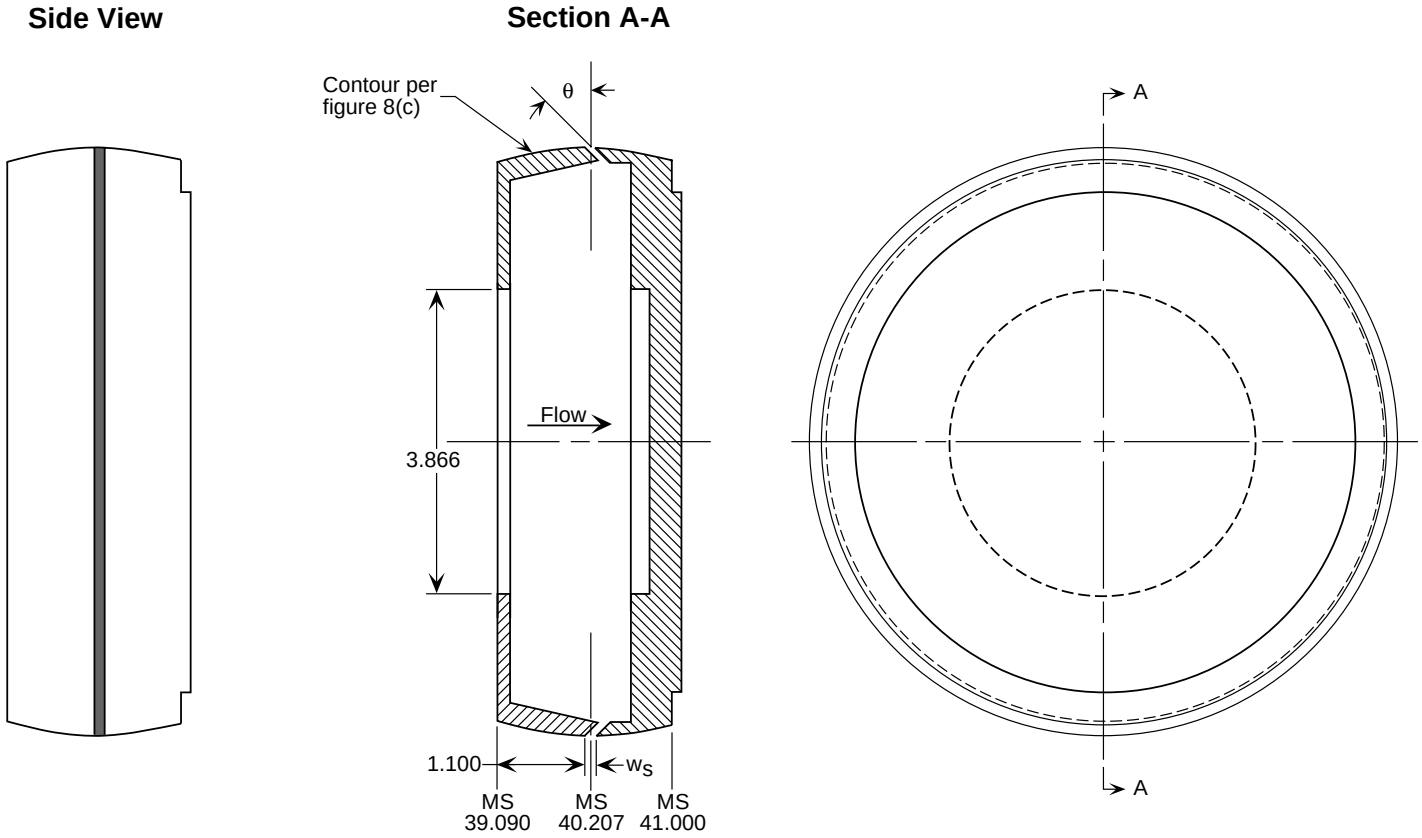

Slot Type	Slot Width (w_S), in.	Slot Angle (θ), deg
Blank	0.000	0
0.013@45°	0.013	45
0.025	0.025	0
0.025@45°	0.025	45

(i) Sketch of injector ring #5.

Figure 8. Continued.

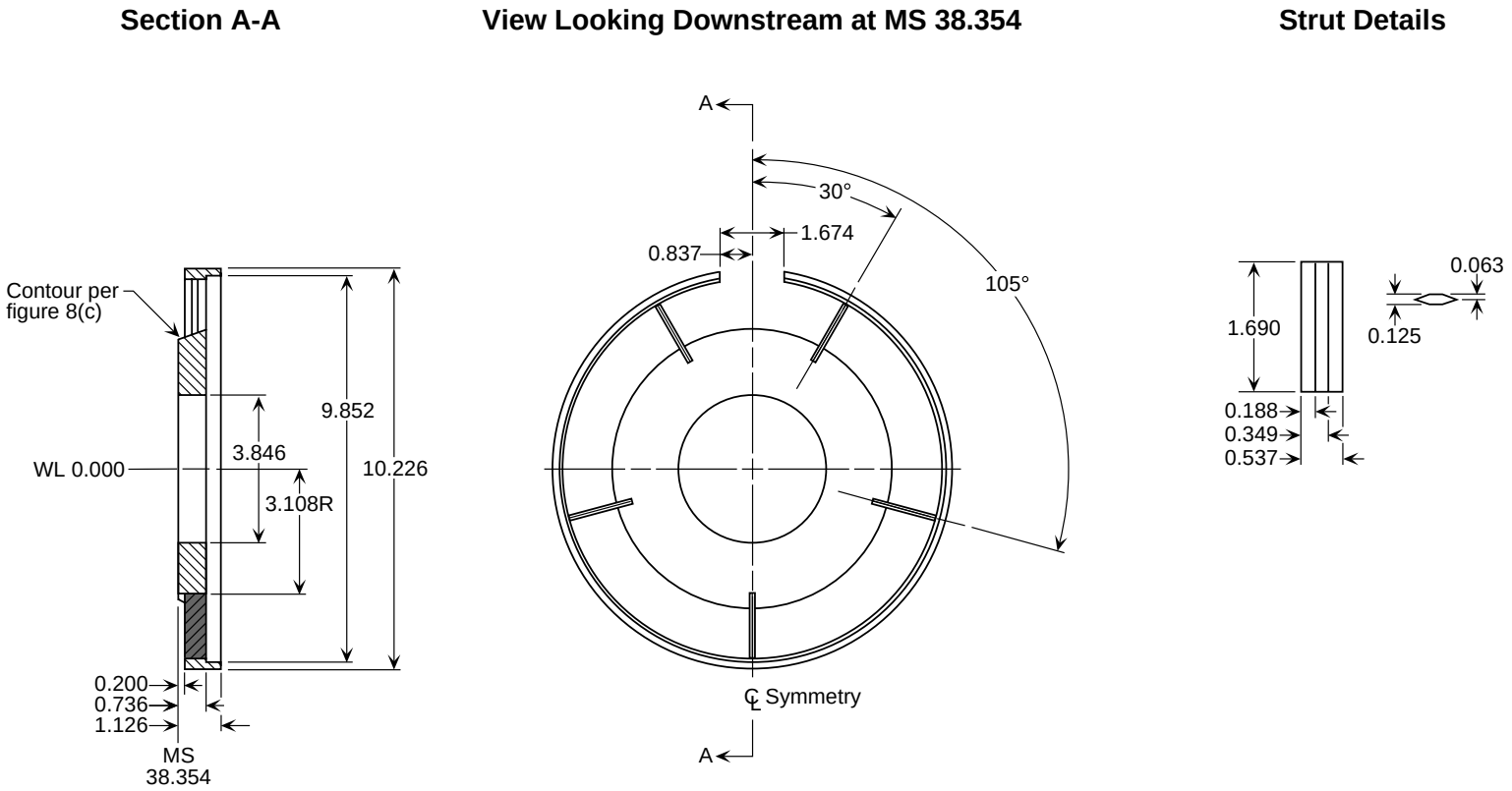

(j) Sketch of support strut assembly.

Figure 8. Continued.

x, in.	R, in.
4.603	5.115
4.653	4.880
4.703	4.780
4.753	4.720
4.803	4.693

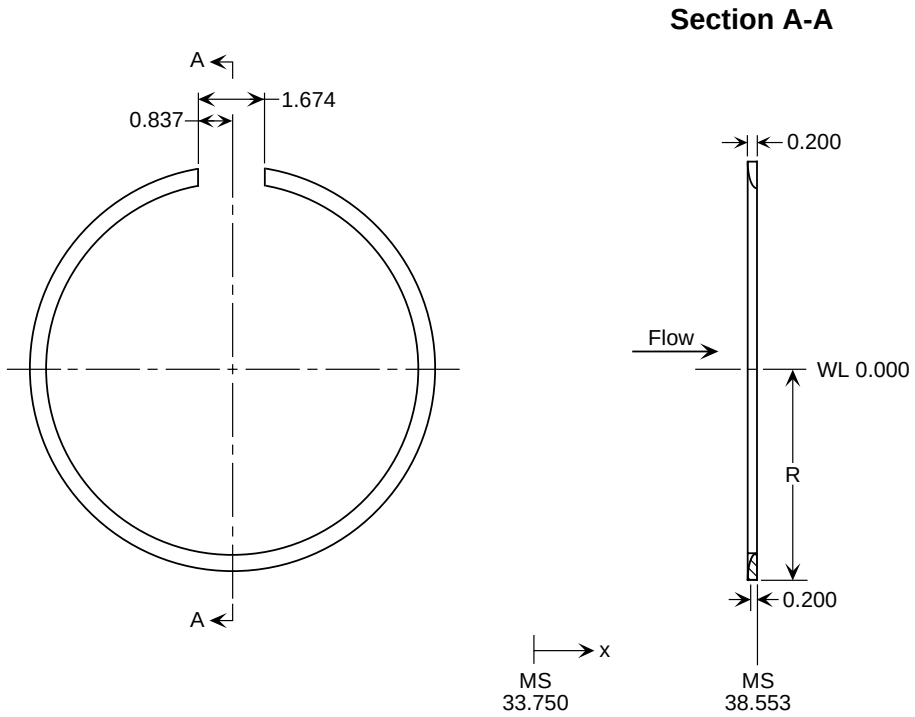

(k) Sketch of port fairing #1.

Figure 8. Continued.

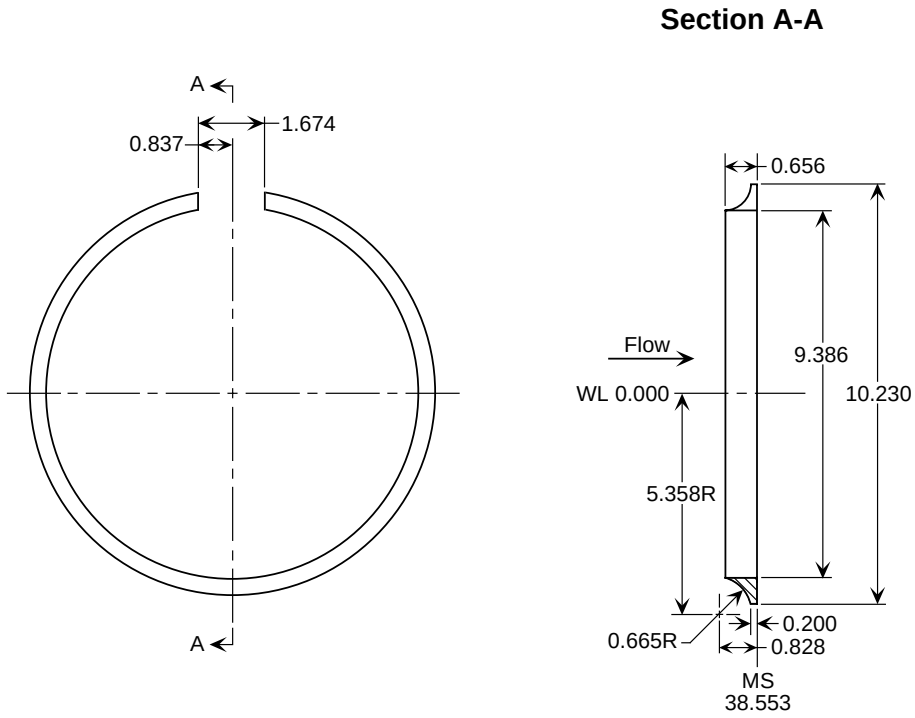

(l) Sketch of port fairing #2.

Figure 8. Continued.

x, in.	R, in.
2.0000	4.6930
2.1655	4.6988
2.2333	4.7093
2.2843	4.7229
2.3260	4.7388
2.3611	4.7567
2.3911	4.7761
2.4168	4.7969
2.4387	4.8188
2.4572	4.8415
2.4724	4.8649
2.4845	4.8888
2.4938	4.9128
2.5003	4.9370

View Looking Downstream at MS 35.750

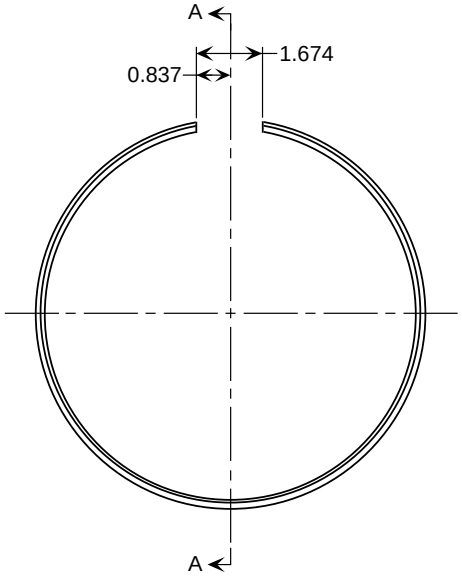

Section A-A

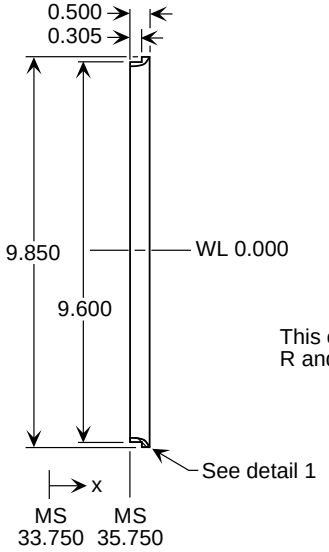

Detail 1

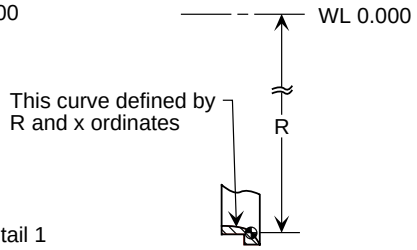

(m) Sketch of coanda fairing #1.

Figure 8. Continued.

x, in.	R, in.
2.0000	4.6930
2.3167	4.7041
2.4466	4.7242
2.5442	4.7502
2.6239	4.7807
2.6911	4.8149
2.7486	4.8521
2.7978	4.8919
2.8397	4.9338
2.8750	4.9773
2.9041	5.0221
2.9164	5.0448

View Looking Downstream at MS 35.750

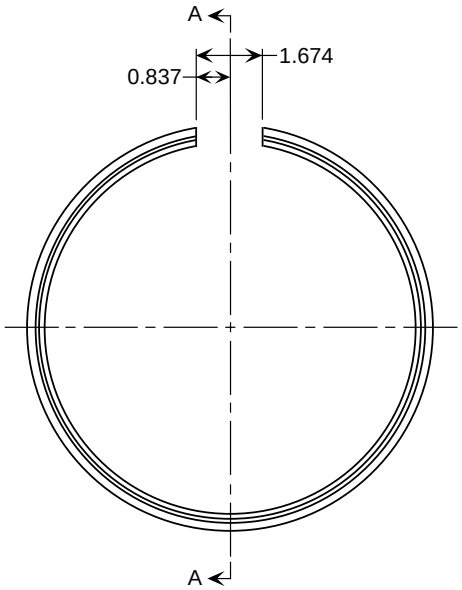

Section A-A

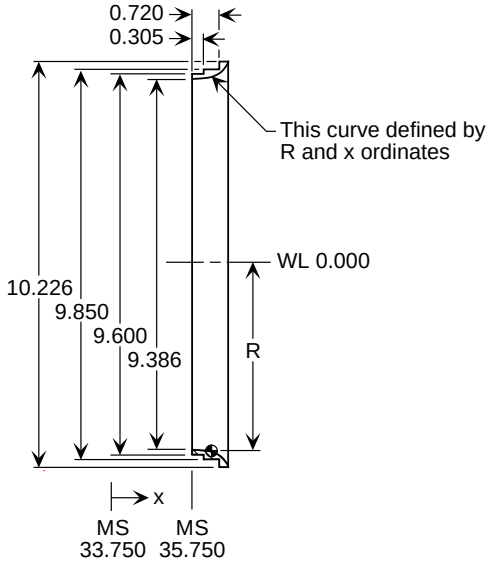

(n) Sketch of coanda fairing #2.

Figure 8. Continued.

x, in.	R, in.
2.0000	4.6930
2.2288	4.6970
2.3955	4.7137
2.5085	4.7375
2.5980	4.7664
2.6726	4.7995
2.7360	4.8361
2.7903	4.8755
2.8144	4.8961
2.8572	4.9388
2.8760	4.9608
2.9088	5.0059
2.9355	5.0521
2.9564	5.0990
2.9717	5.1461
2.9817	5.1932
2.9867	5.2399
2.9873	5.2630
2.9867	5.2858
2.9820	5.3307
2.9779	5.3526
2.9665	5.3952
2.9509	5.4359
2.9312	5.4744
2.9079	5.5104
2.8809	5.5437
2.8507	5.5739
2.8174	5.6009
2.7814	5.6242
2.7429	5.6439
2.7022	5.6595
2.6596	5.6709
2.6154	5.6779
2.5700	5.6803

View Looking Downstream at MS 35.750

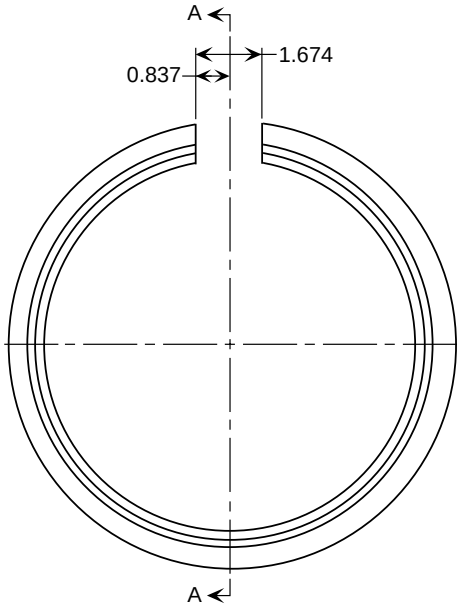

Section A-A

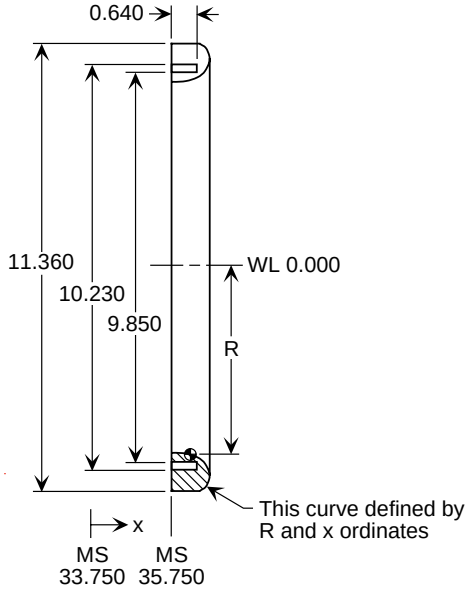

(o) Sketch of coanda fairing #3.

Figure 8. Concluded.

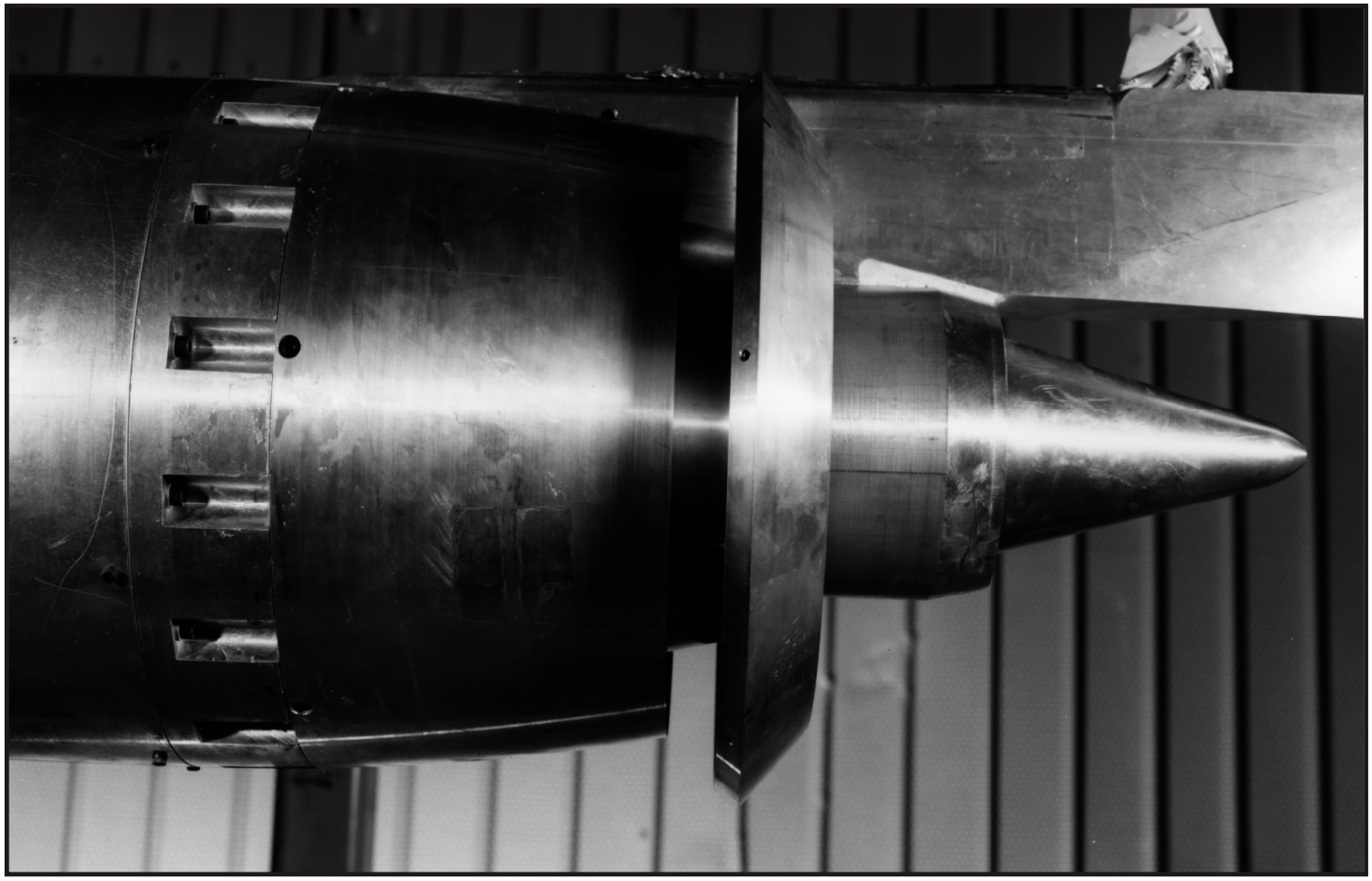

L95-04825

(a) Photograph of annular (metal) target thrust reverser model.

Figure 9. Details of annular (metal) target thrust reverser model. Dimensions are in inches.

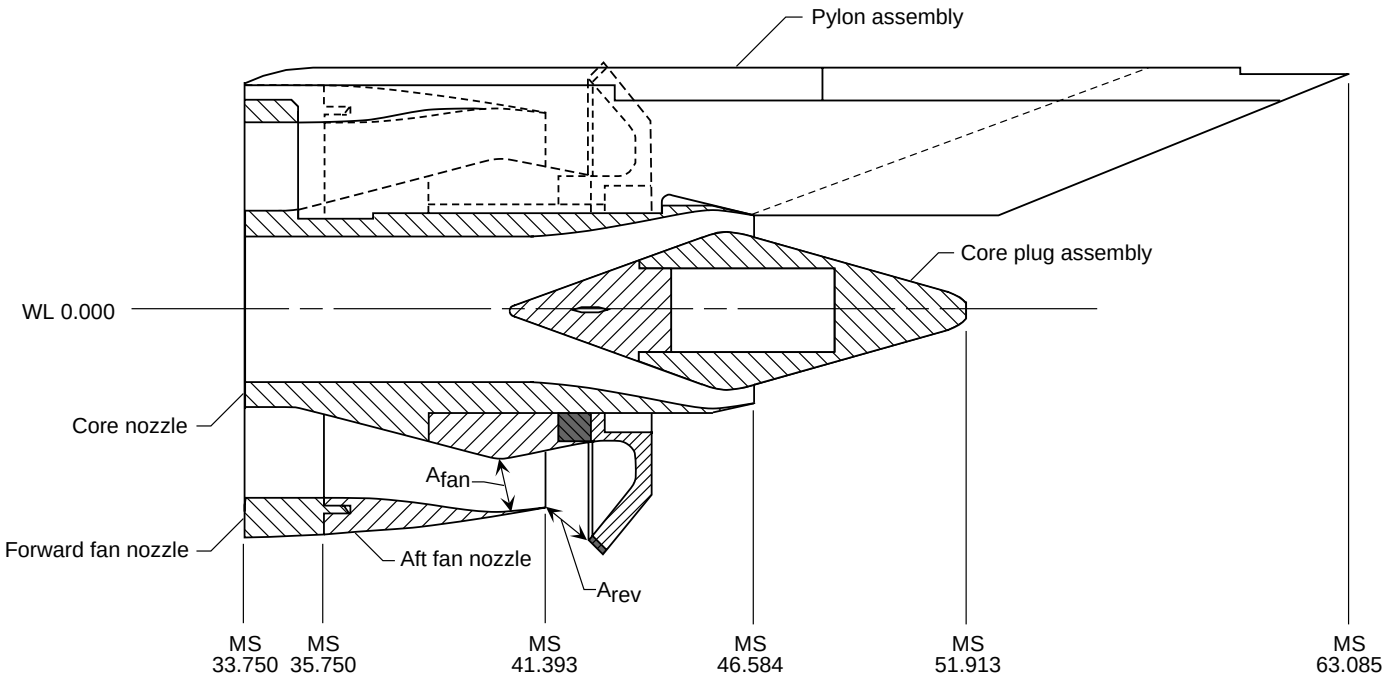

(b) Partial cutaway sketch of annular (metal) target reverser thrust model.

Figure 9. Continued.

x, in.	R, in.
4.6030	3.3248
4.8250	3.3930
5.1220	3.4830
5.2700	3.5270
5.5670	3.6080
5.7150	3.6440
5.8640	3.6770
6.0120	3.7050
6.1600	3.7270
6.3080	3.7440
6.4570	3.7530
6.6050	3.7530
6.7530	3.7450
6.9020	3.7270
7.0500	3.7020
7.1980	3.6700
7.3470	3.6370
7.6430	3.5690
8.5000	3.3730
8.6010	3.3499

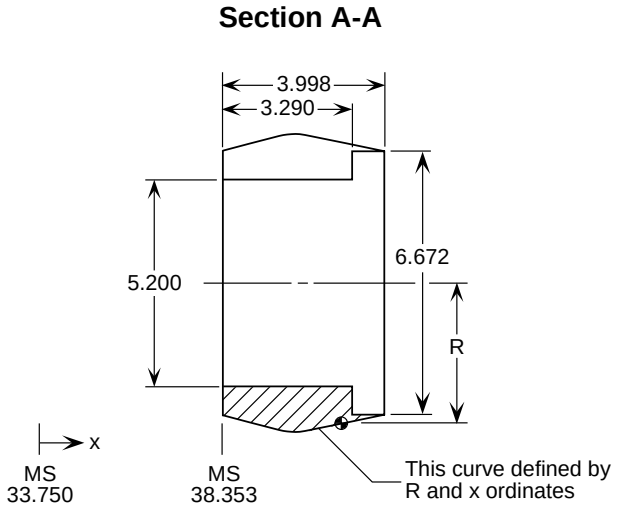

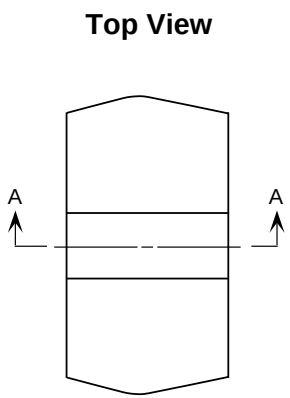

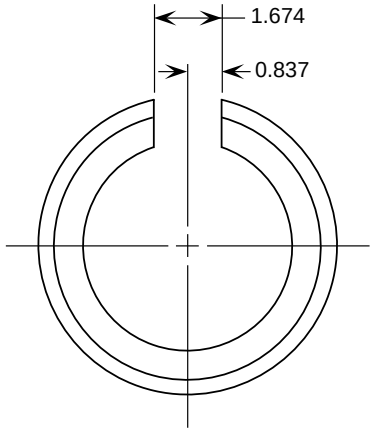

(c) Sketch of core nozzle insert #4.

Figure 9. Continued.

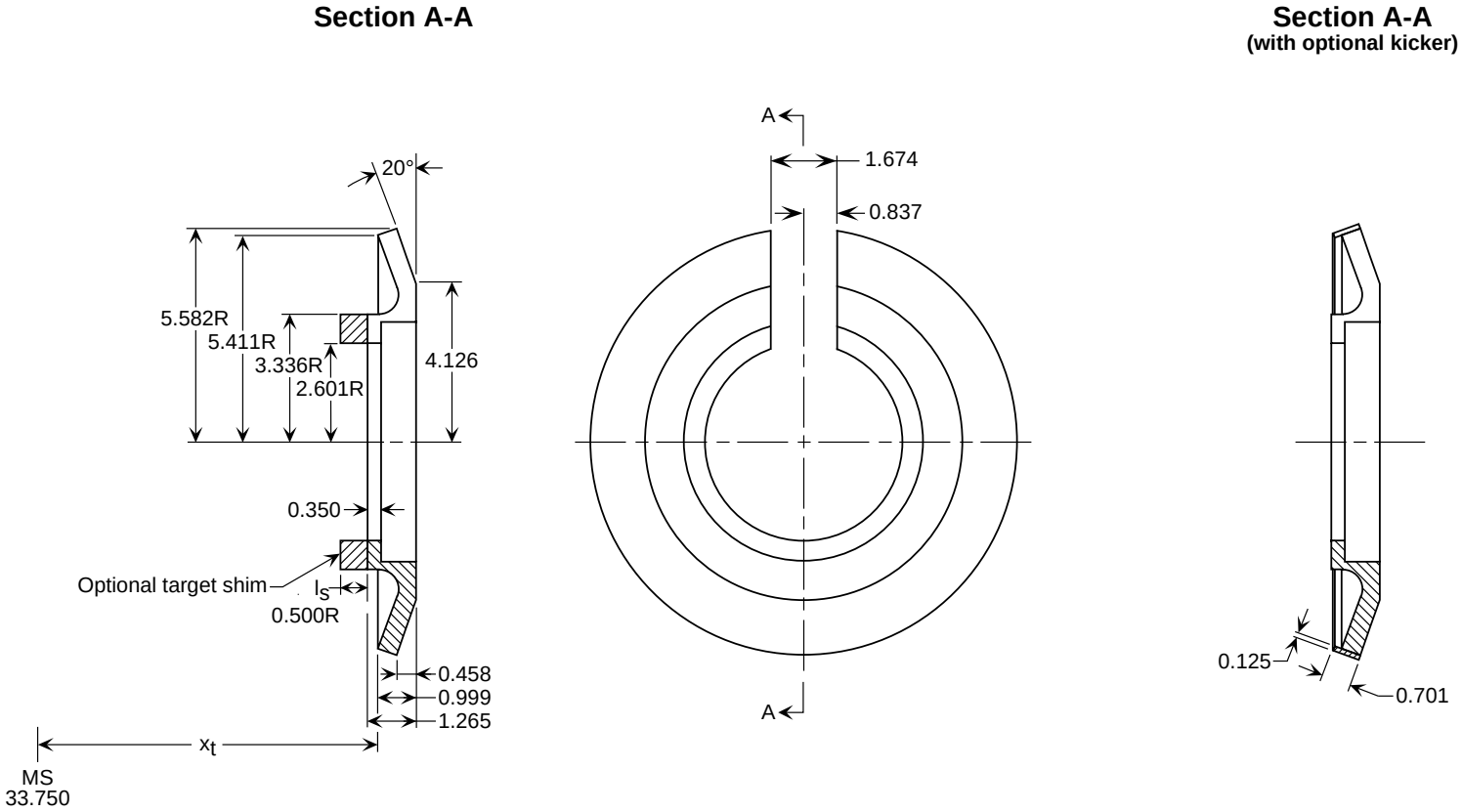

Target Shim	Shim Length (l_S), in.	Distance to Target (x_t), in.
None	0.000	8.159
Short	0.511	8.670
Medium	0.606	8.765
Long	0.700	8.859

(d) Sketch of 20° annular target assembly.

Figure 9. Continued.

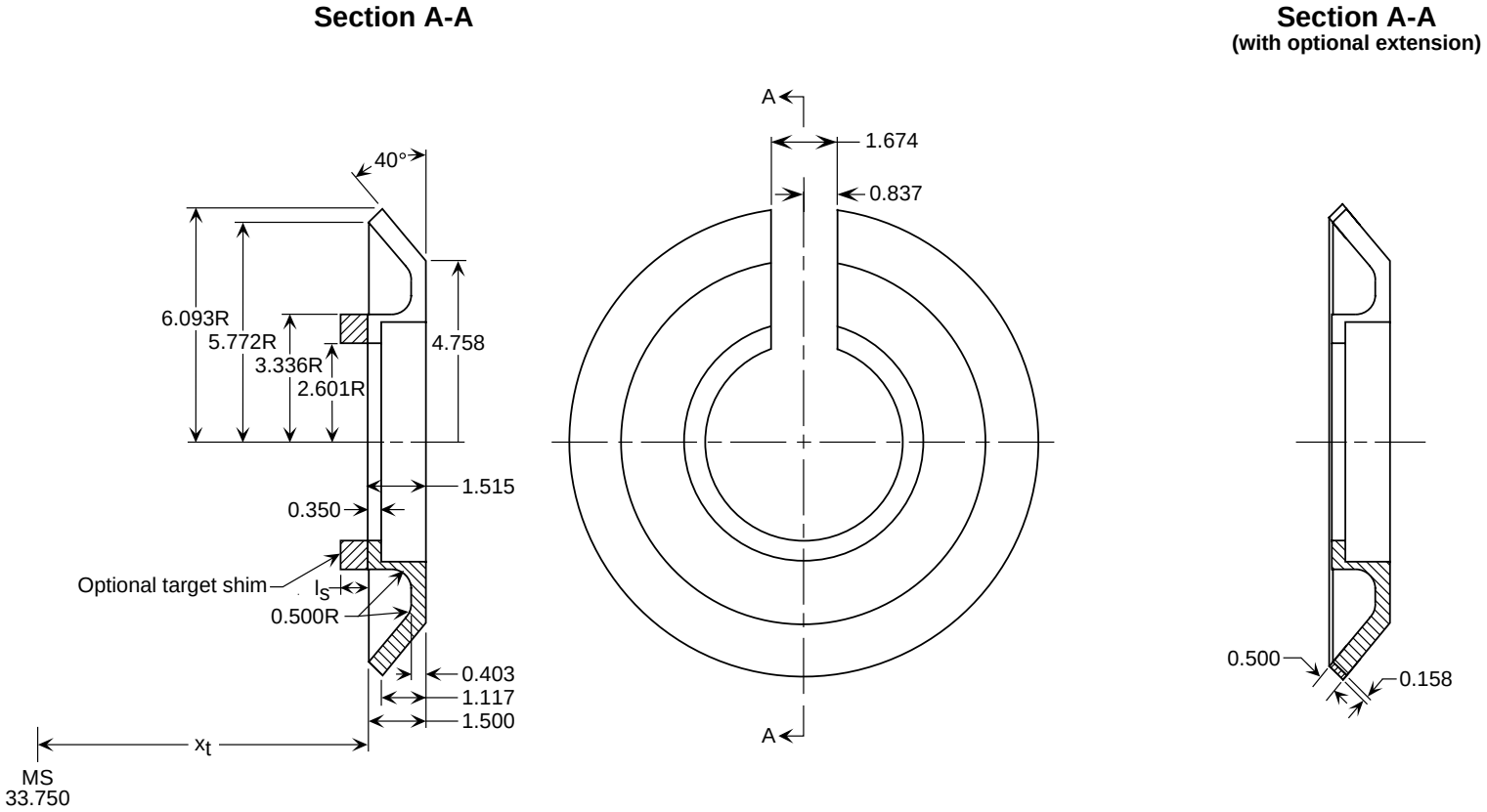

Target Shim	Shim Length (l_S), in.	Distance to Target (x_t), in.
None	0.000	7.908
Short	0.511	8.419
Medium	0.606	8.514
Long	0.700	8.608

(e) Sketch of 40° annular target assembly.

Figure 9. Concluded.

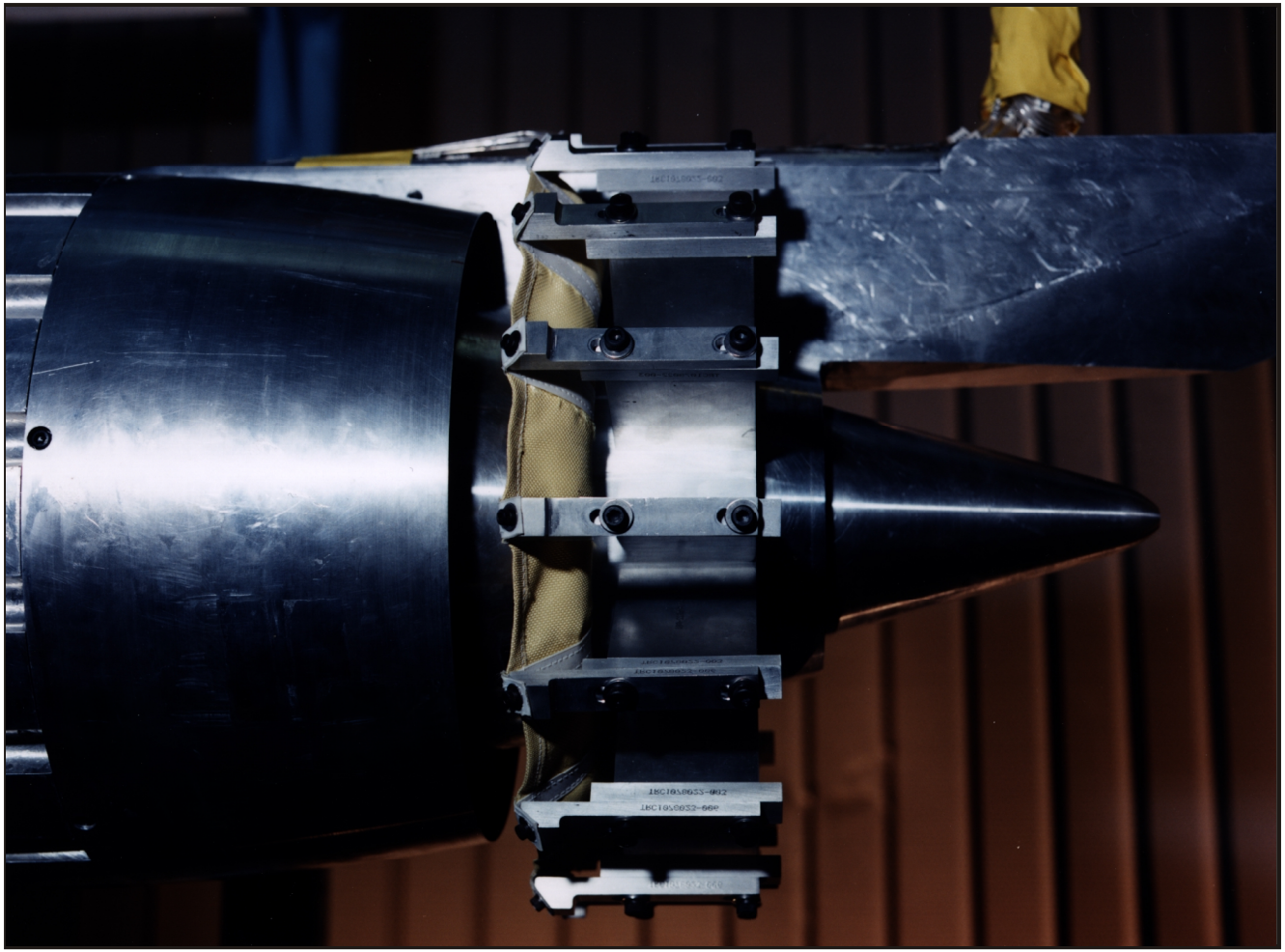

L95-04814

(a) Photograph of fabric target thrust reverser model.

Figure 10. Details of fabric target thrust reverser model. Dimensions are in inches.

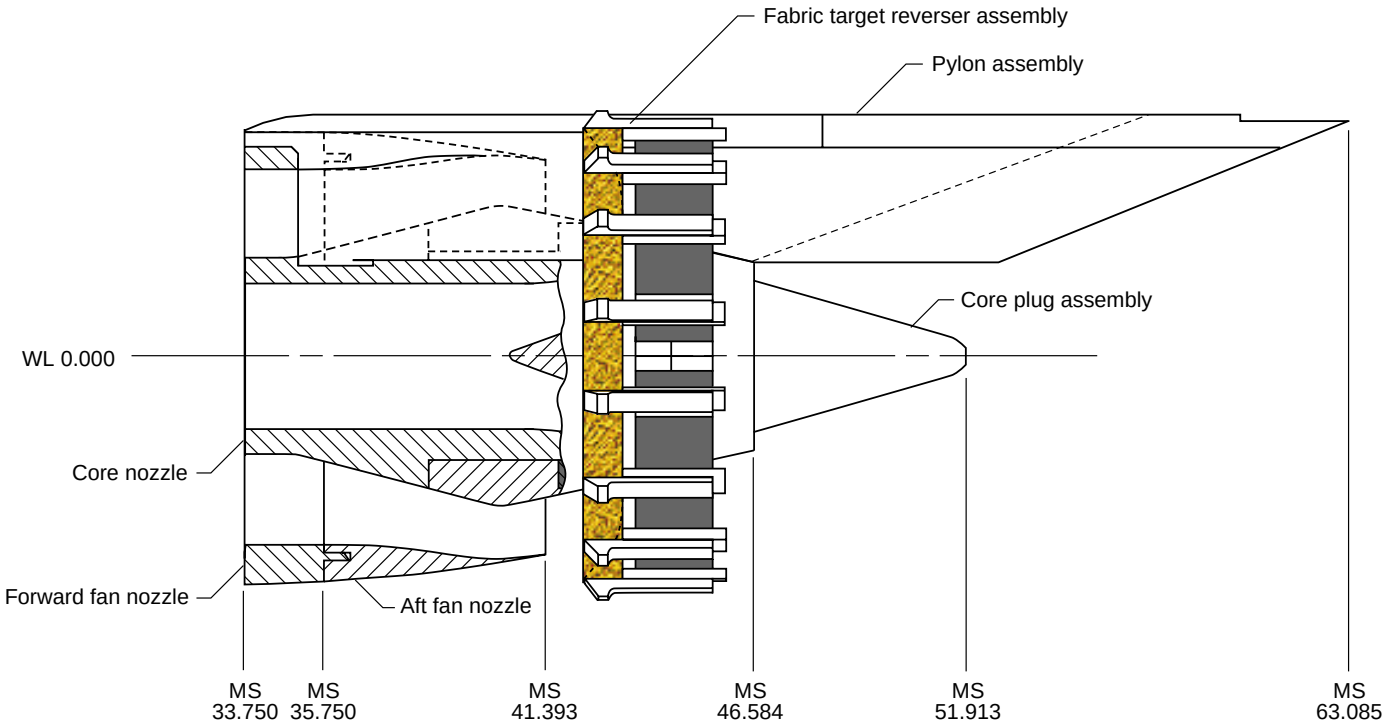

(b) Partial cutaway sketch of fabric target thrust reverser model.

Figure 10. Continued.

Side View

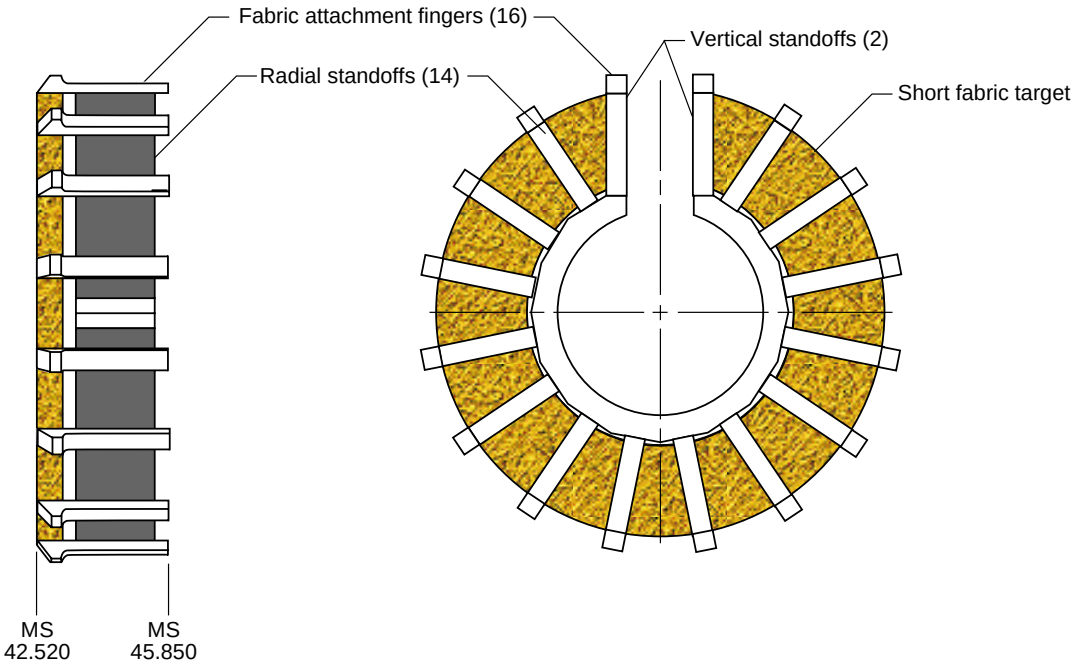

(c) Sketch of short fabric target reverser assembly.

Figure 10. Continued.

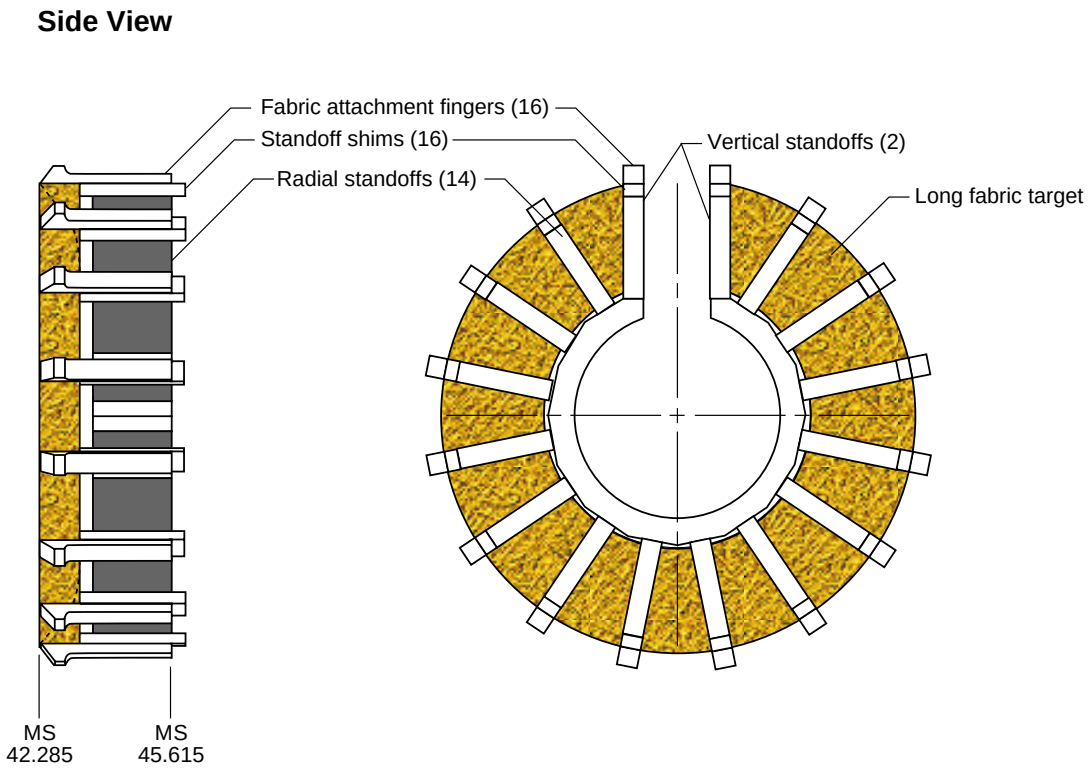

(d) Sketch of long fabric target reverser assembly.

Figure 10. Continued.

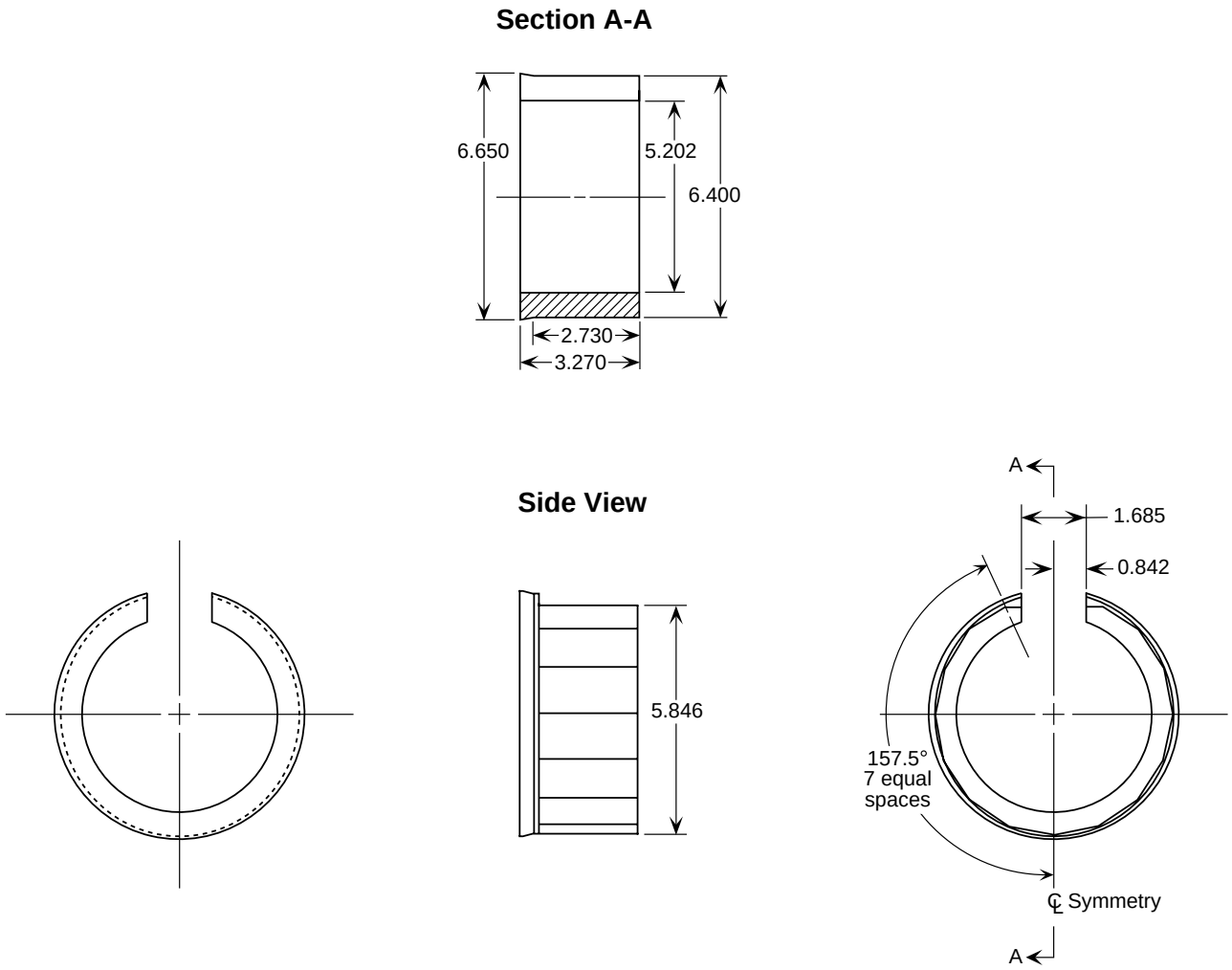

(e) Sketch of standoff mount.

Figure 10. Continued.

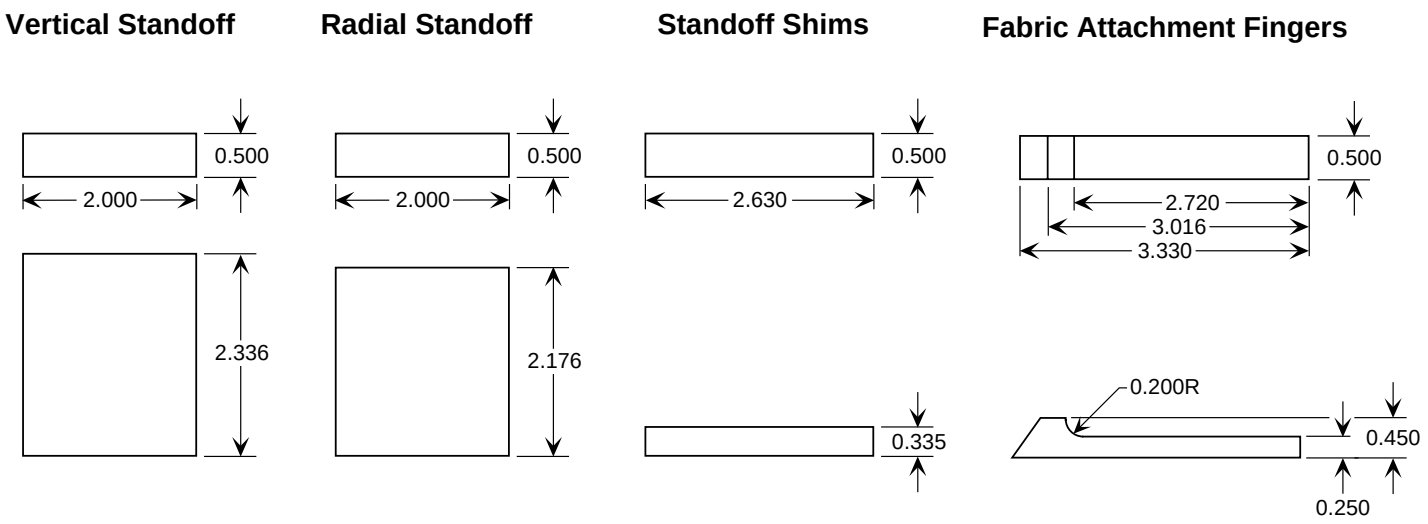

(f) Sketch of standoffs, standoff shims, and fabric attachment fingers.

Figure 10. Continued.

Installed/Inflated Geometry

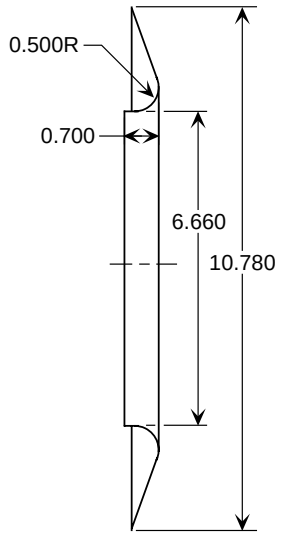

Side View

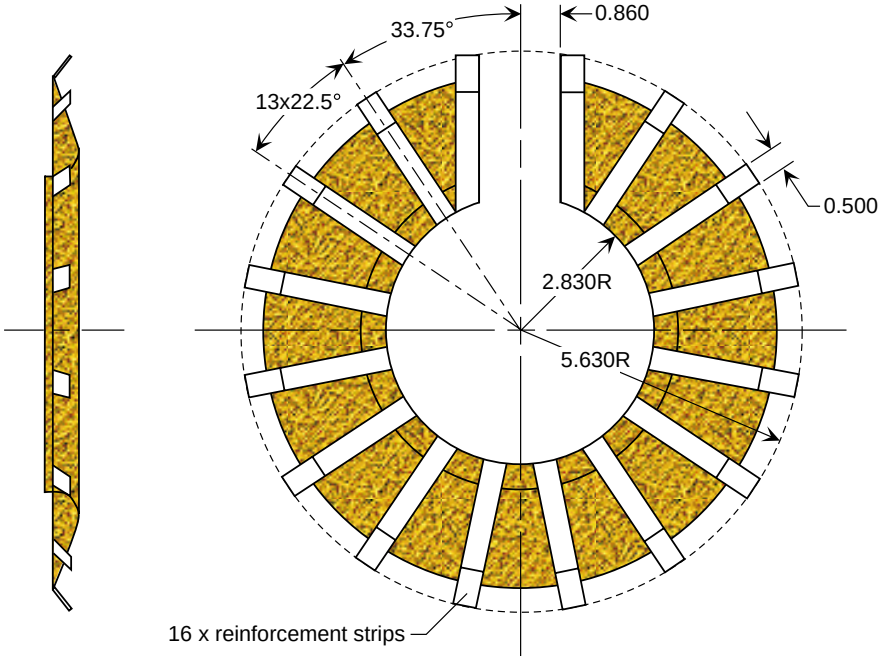

(g) Sketch of short fabric target.

Figure 10. Continued.

Installed/Inflated Geometry

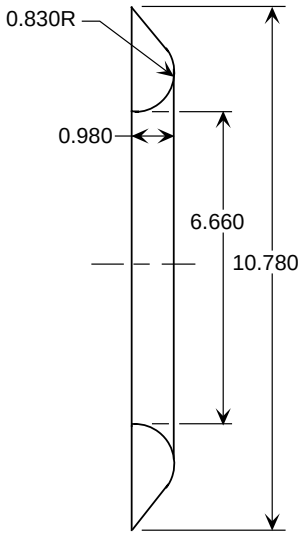

Side View

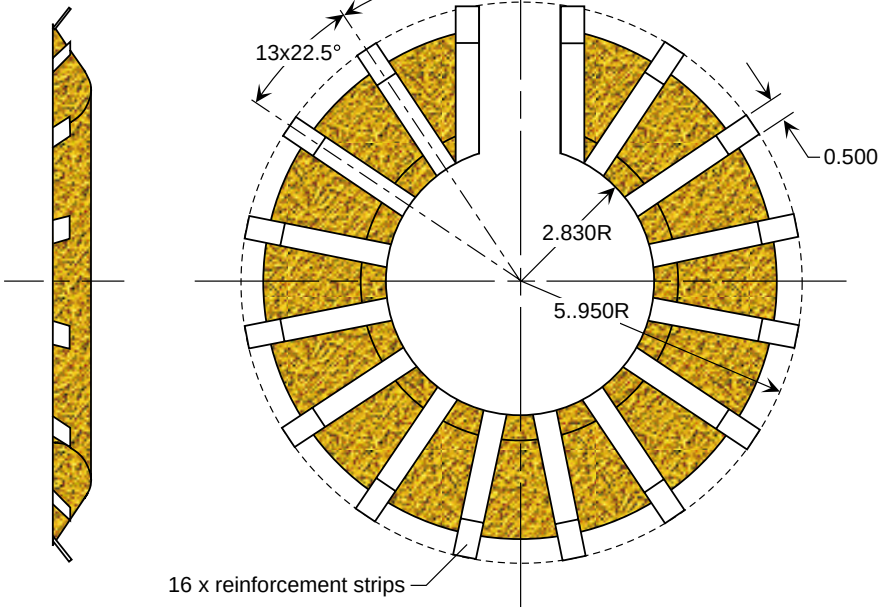

(h) Sketch of long fabric target.

Figure 10. Concluded.

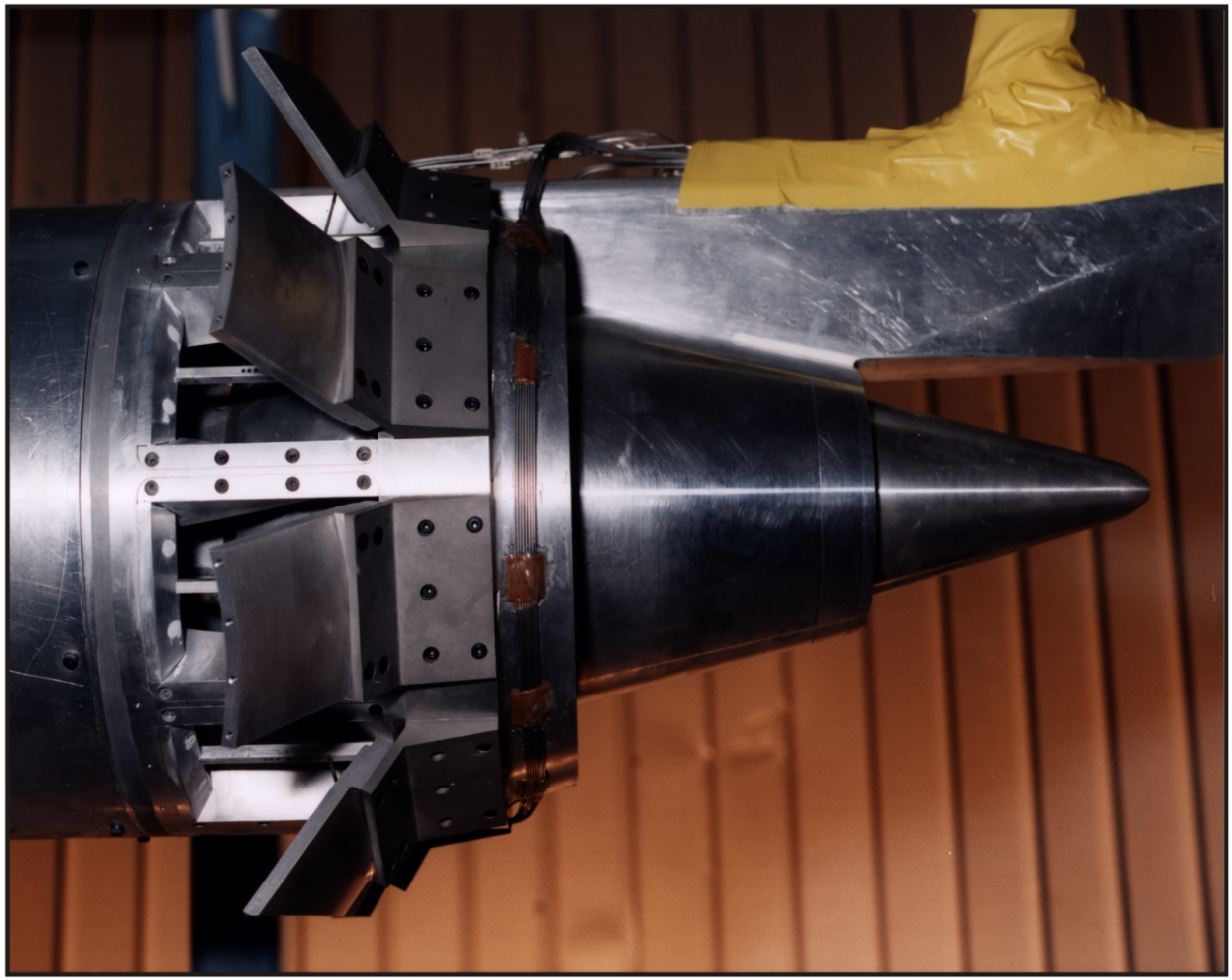

L95-04973

(a) Photograph of multi-door crocodile thrust reverser model.

Figure 11. Details of multi-door crocodile thrust reverser model. Dimensions are in inches.

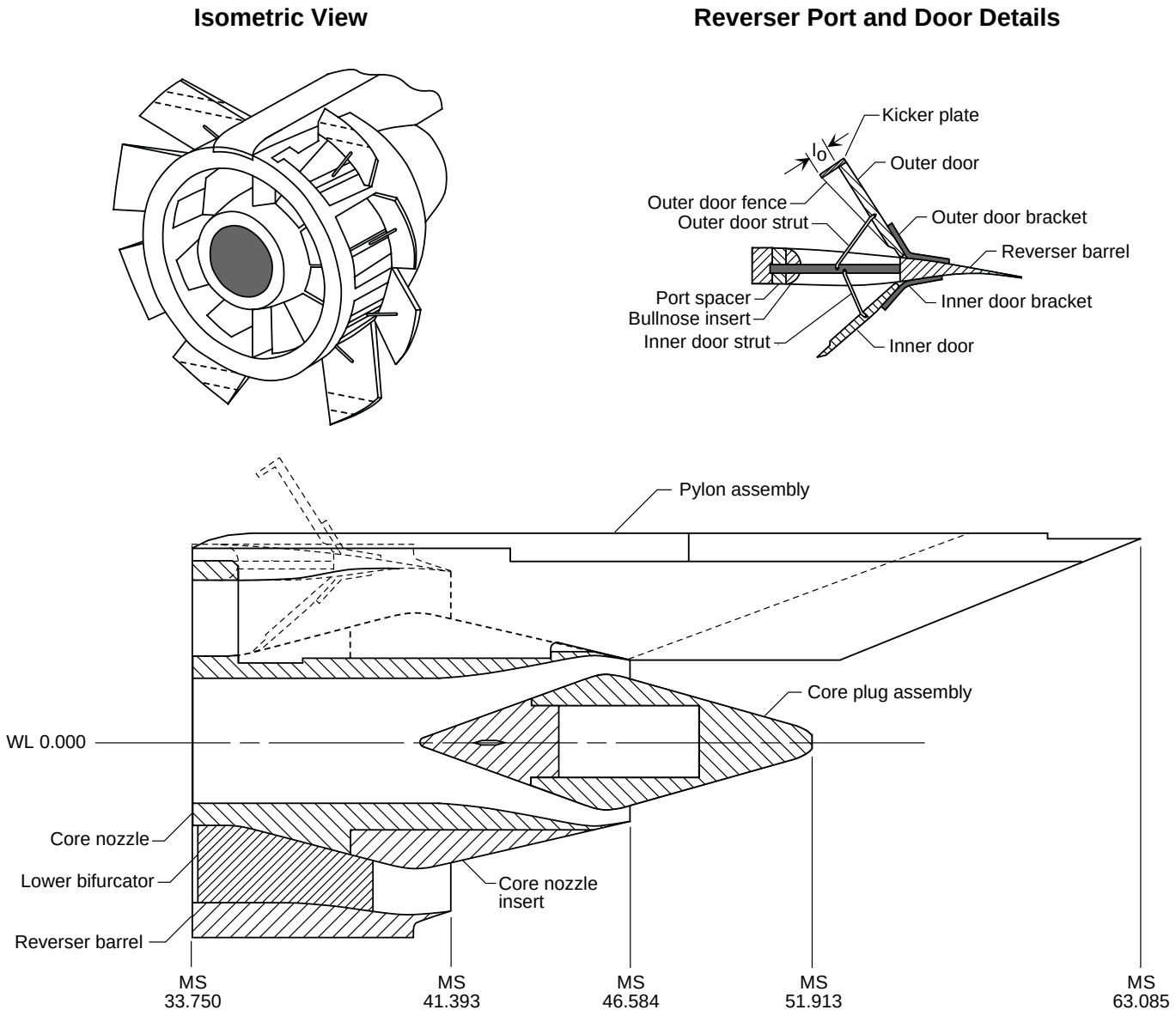

(b) Partial cutaway sketch of multi-door crocodile thrust reverser model.

Figure 11. Continued.

View Looking Downstream at MS 33.750

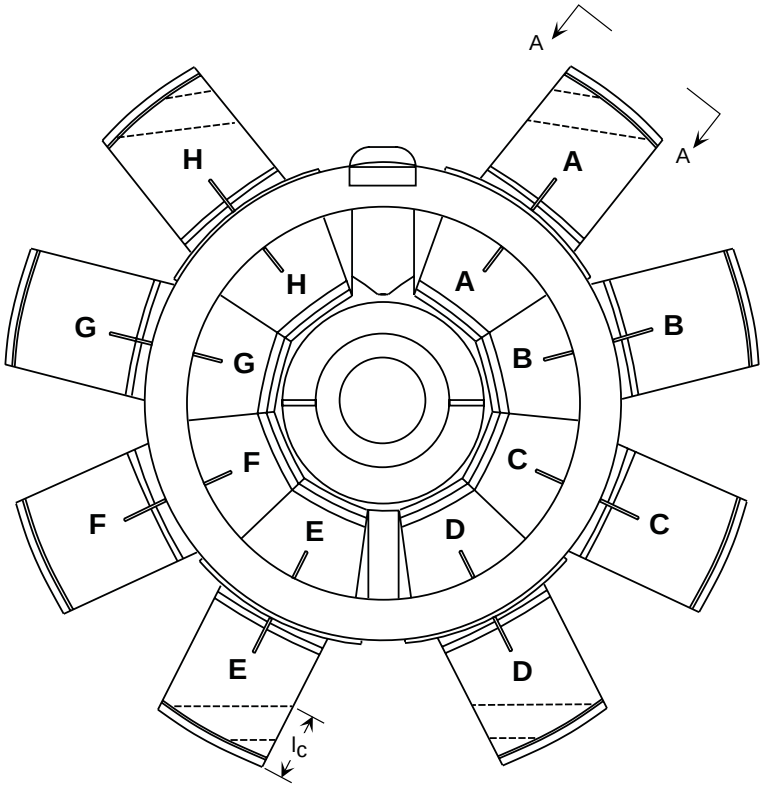

View A-A
(Reverser port details)

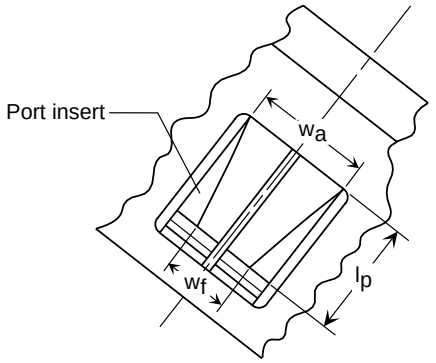

Bullnose	Port Spacer, in.	l_p, in.	w_f, in.	w_a, in.	Port Min. Area (A_{port}), in^2	Reverser Exit Area (A_{rev}), in^2	Reverser Port Area Ratio (A_{rev}/A_{fan})
None	0.000	3.750	1.879	2.822	8.109	64.875	1.914
None	0.200	3.550	1.884	2.822	7.686	61.486	1.814
None	0.400	3.350	1.890	2.822	7.263	58.102	1.714
1, 2, or 3	0.000	3.250	1.720	2.822	6.770	54.160	1.598
1, 2, or 3	0.200	3.050	1.795	2.822	6.468	51.740	1.526
1, 2, or 3	0.400	2.850	1.869	2.822	6.149	49.190	1.451

(c) Crocodile thrust reverser details.

Figure 11. Continued.

x, in.	R, in.
6.400	5.710
6.444	5.176
6.594	5.151
6.744	5.126
6.894	5.101
7.044	5.075
7.194	5.048
7.344	5.021
7.493	4.993
7.643	4.965

x, in.	R', in.
0.000	4.710
1.268	4.710
1.668	4.707
1.859	4.699
2.000	4.693
2.156	4.688
2.304	4.685
2.452	4.683
2.601	4.683
2.749	4.685
2.897	4.690
3.046	4.697
3.194	4.705
3.342	4.716
3.491	4.728
3.639	4.743
3.787	4.758
3.935	4.775
4.084	4.794
4.232	4.813
4.380	4.834
4.529	4.856
4.677	4.879
4.825	4.902
4.974	4.926
5.107	4.948
5.270	4.974
5.419	4.998
5.567	5.020
5.715	5.039
5.864	5.057
6.012	5.071
6.160	5.080
6.308	5.085
6.457	5.085
6.605	5.081
6.753	5.070
6.902	5.056
7.050	5.038
7.198	5.016
7.347	4.993
7.495	4.970
7.643	4.946

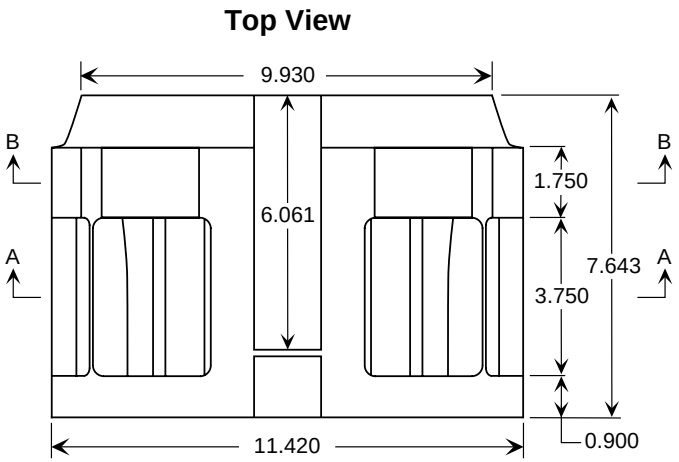

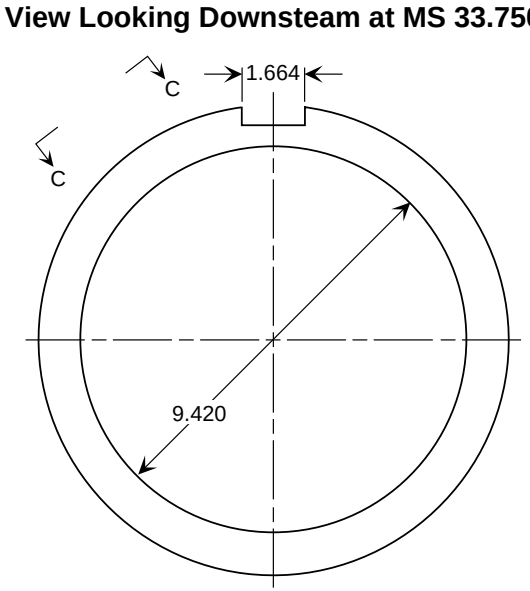

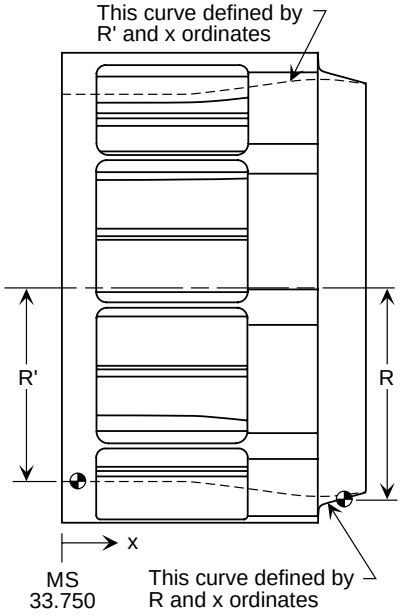

(d) Sketch of reverser barrel.

Figure 11. Continued.

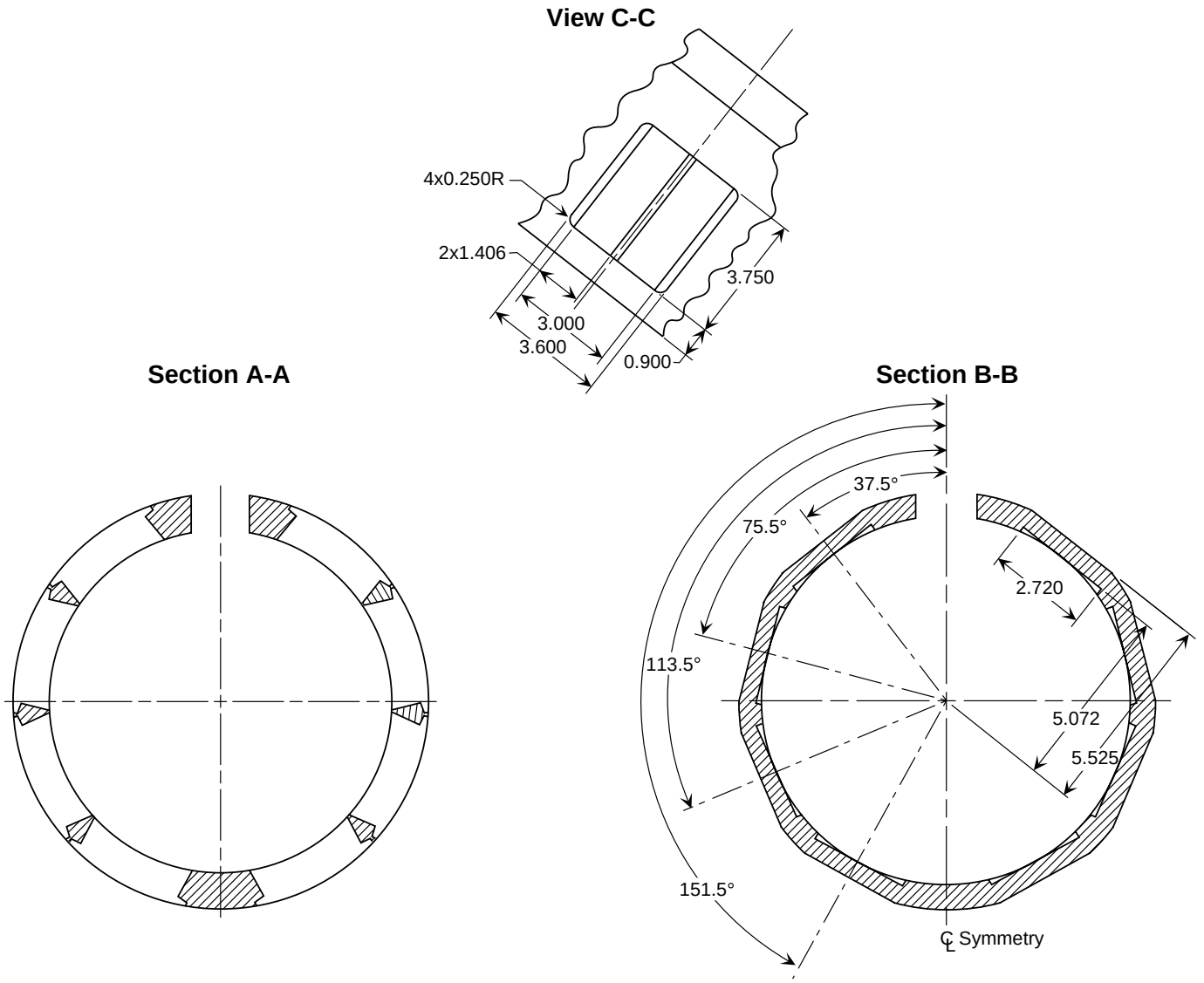

(e) Reverser barrel details.

Figure 11. Continued.

Table A	
x', in.	y', in.
0.000	0.885
0.200	0.893
0.400	0.900
0.600	0.908
0.800	0.917
1.000	0.926
1.200	0.937
1.400	0.950
1.600	0.965
1.800	0.970
2.000	0.968
2.200	0.962
2.400	0.950
2.600	0.937
2.800	0.922
3.000	0.911
3.200	0.903
3.250	0.902
3.400	0.900
3.600	0.900
3.750	0.900

Table B	
x', in.	y', in.
0.000	0.887
0.200	0.927
0.400	0.961
0.600	0.991
0.800	1.017
1.000	1.048
1.200	1.054
1.400	1.066
1.600	1.076
1.800	1.082
2.000	1.091
2.200	1.091
2.400	1.088
2.600	1.083
2.800	1.077
3.000	1.072
3.200	1.068
3.400	1.065
3.600	1.062
3.750	1.061

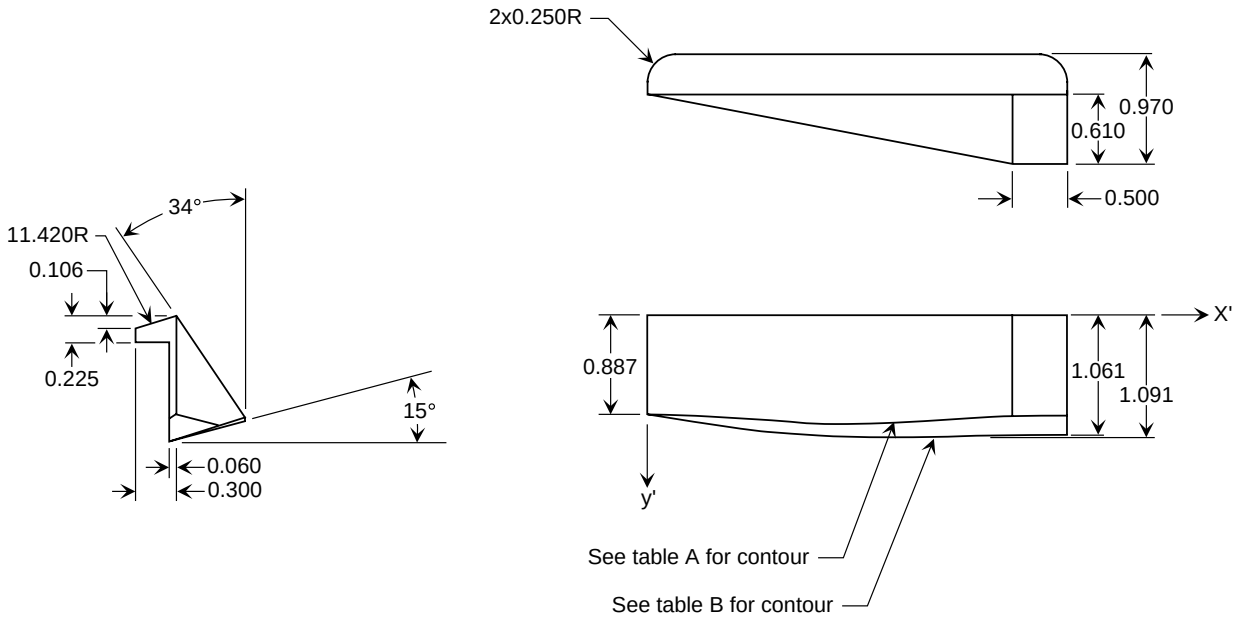

(f) Sketch showing port inserts. Right insert shown; left insert opposite.

Figure 11. Continued.

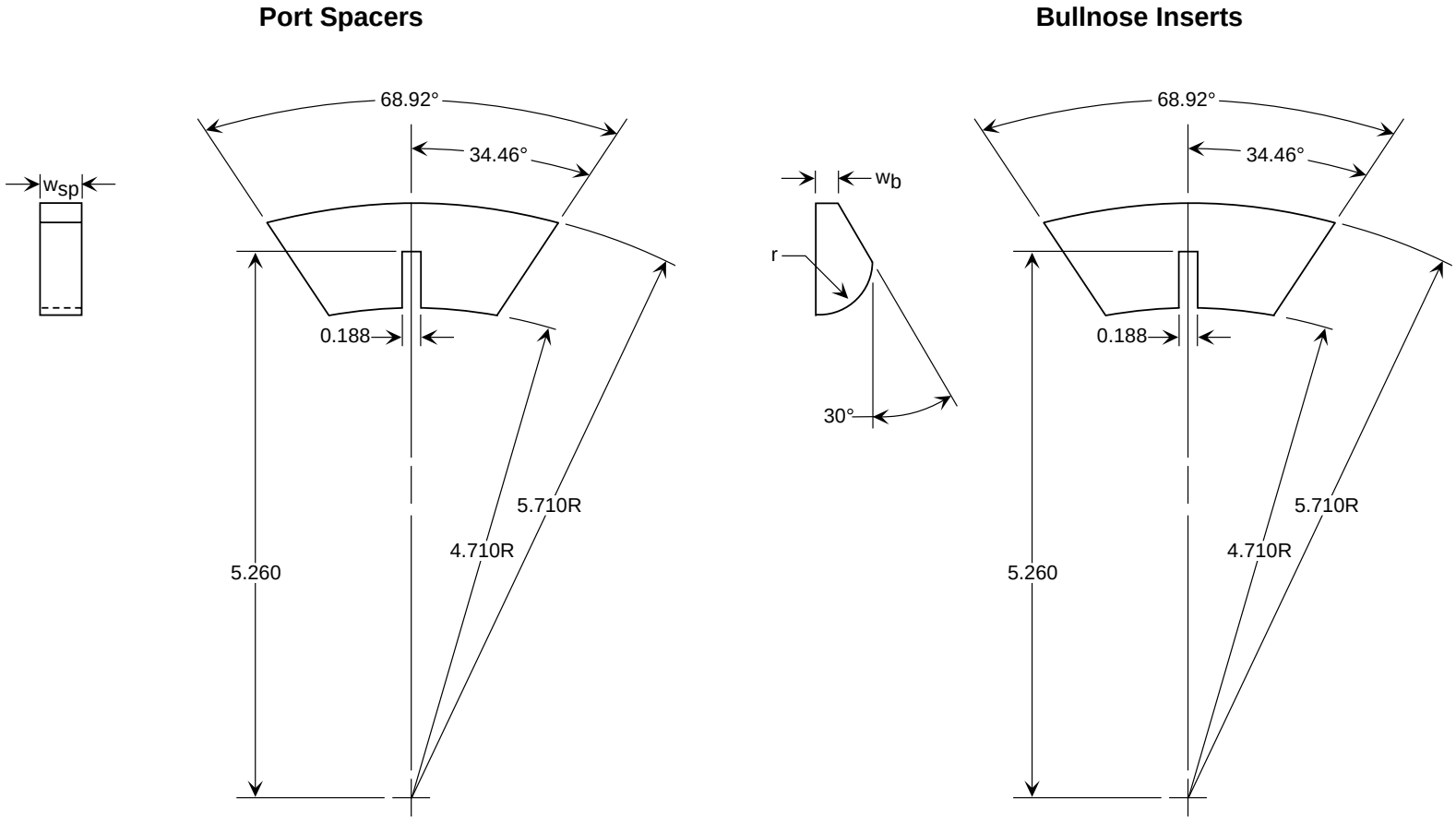

Item	w_{sp}, in.	r, in.	w_b, in.	r/h_d
0.200 in. spacer	0.200	–	–	–
0.400 in. spacer	0.400	–	–	–
Bullnose insert #1	–	0.500R	0.210	0.222
Bullnose insert #2	–	0.400R	0.152	0.178
Bullnose insert #3	–	0.300R	0.094	0.133

(g) Sketch showing port spacers and bullnose inserts.

Figure 11. Continued.

x, in.	R, in.
0.250	0.000
0.300	0.120
0.350	0.200
0.400	0.256
0.450	0.300
0.500	0.328
0.550	0.350
0.600	0.366
0.650	0.380
0.700	0.390
0.750	0.400
0.800	0.406
0.850	0.412
0.900	0.416
0.950	0.419
1.000	0.420
1.050	0.422
1.125	0.425
1.500	0.425
2.000	0.425
2.500	0.425
3.000	0.425
3.200	0.425
3.300	0.421
3.400	0.413
3.500	0.404
3.600	0.395
3.700	0.384
3.800	0.371
3.900	0.358
4.000	0.342
4.100	0.328
4.200	0.311
4.300	0.291
4.400	0.271
4.500	0.251
4.600	0.227
4.700	0.204
4.800	0.180
4.900	0.142
5.000	0.125
5.100	0.096
5.190	0.060

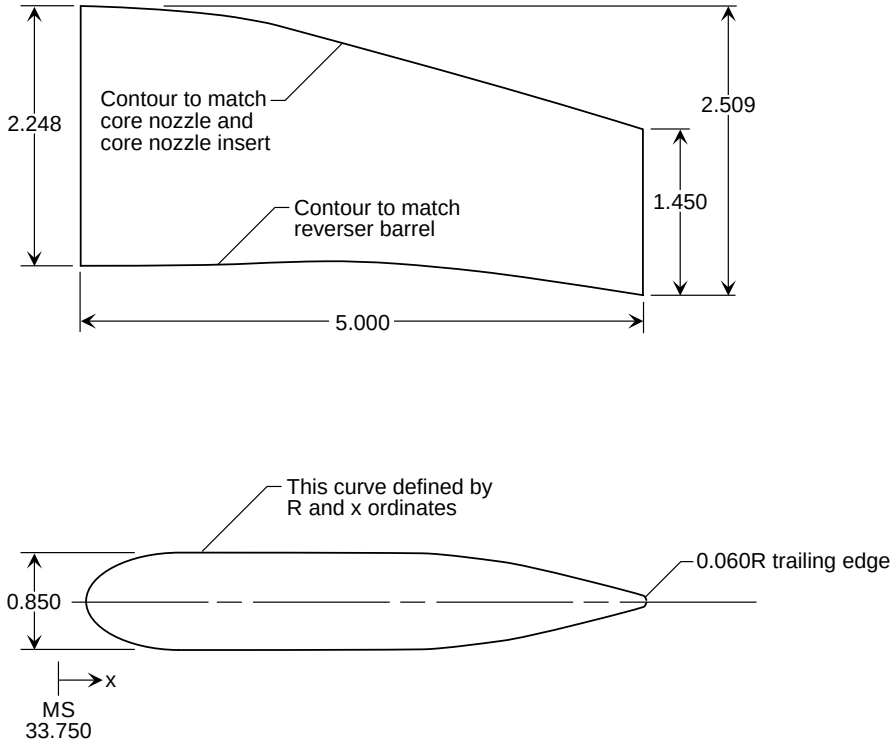

(h) Sketch of lower bifurcator.

Figure 11. Continued.

Side View

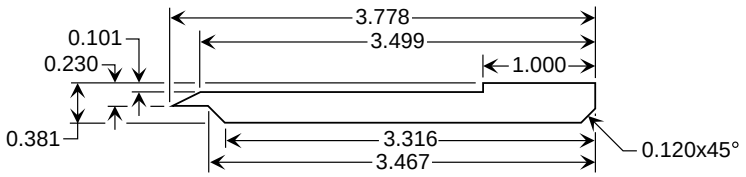

Top View

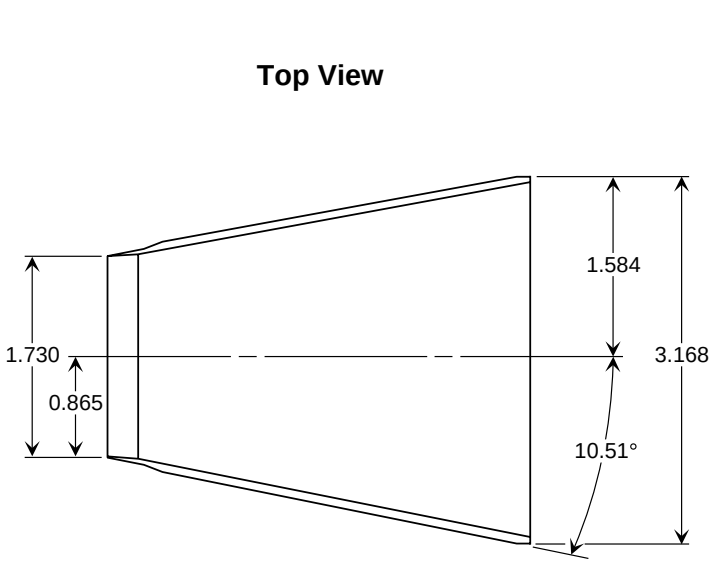

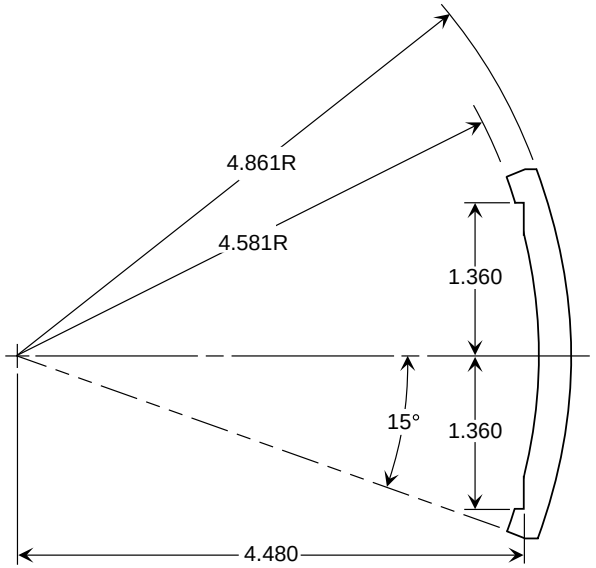

(i) Sketch of inner door.

Figure 11. Continued.

Top View

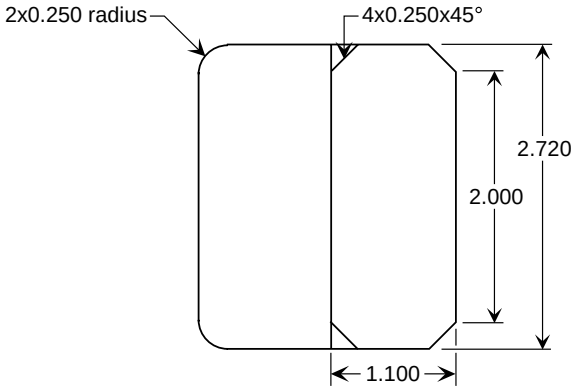

Side View

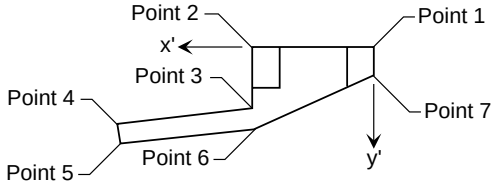

Angle, deg	Point 1		Point 2		Point 3		Point 4		Point 5		Point 6		Point 7	
	x', in.	y', in.	x', in.	y', in.	x', in.	y', in.	x', in.	y', in.	x', in.	y', in.	x', in.	y', in.	x', in.	y', in.
6	0.000	0.000	1.100	0.000	1.100	0.556	2.321	0.684	2.302	0.863	1.092	0.736	0.000	0.244
12	0.000	0.000	1.100	0.000	1.100	0.524	2.257	0.770	2.219	0.946	1.100	0.708	0.000	0.244
18	0.000	0.000	1.100	0.000	1.100	0.496	2.184	0.848	2.128	1.020	1.100	0.685	0.000	0.244
24	0.000	0.000	1.100	0.000	1.100	0.472	2.103	0.919	2.030	1.083	0.145	0.244	0.000	0.244
30	0.000	0.000	1.100	0.000	1.100	0.452	2.016	0.981	1.926	1.137	0.380	0.244	0.000	0.244
36	0.000	0.000	1.100	0.000	1.100	0.435	1.923	1.033	1.817	1.179	0.530	0.244	0.000	0.244

(j) Sketch of inner door brackets.

Figure 11. Continued.

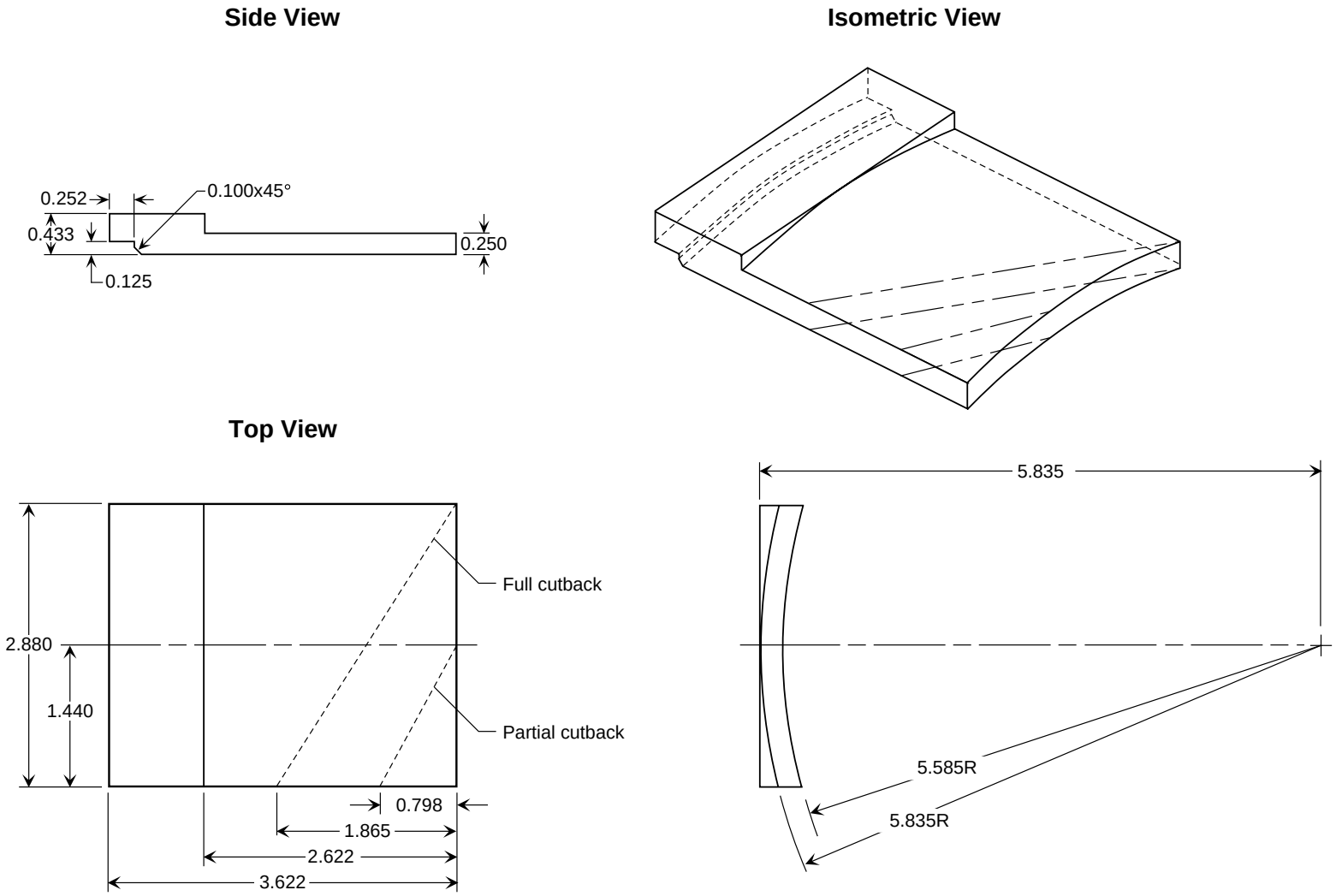

(k) Sketch of outer door. Cutback shown for doors A and H; doors D and E are opposite.

Figure 11. Continued.

Top View

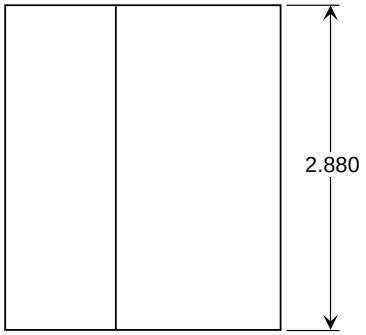

Side View

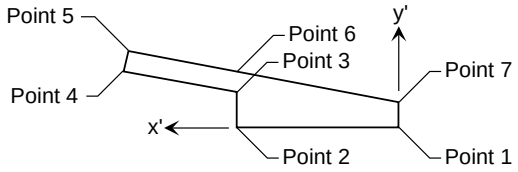

Angle, deg	Point 1		Point 2		Point 3		Point 4		Point 5		Point 6		Point 7	
	x', in.	y', in.	x', in.	y', in.	x', in.	y', in.	x', in.	y', in.	x', in.	y', in.	x', in.	y', in.	x', in.	y', in.
10	0.000	0.000	1.500	0.000	1.500	0.307	2.516	0.487	2.485	0.664	1.501	0.490	0.000	0.226
20	0.000	0.000	1.500	0.000	1.500	0.298	2.503	0.664	2.442	0.833	1.501	0.490	0.000	0.226
30	0.000	0.000	1.500	0.000	1.500	0.281	2.460	0.835	2.370	0.991	1.501	0.490	0.000	0.226
40	0.000	0.000	1.500	0.000	1.500	0.253	2.387	0.997	2.271	1.135	1.501	0.490	0.000	0.226
50	0.000	0.000	1.500	0.000	1.500	0.206	2.287	1.144	2.149	1.260	1.501	0.490	0.000	0.226
60	0.000	0.000	1.500	0.000	1.500	0.123	2.163	1.271	2.007	1.361	1.501	0.490	0.000	0.226

(l) Sketch of outer door brackets.

Figure 11. Continued.

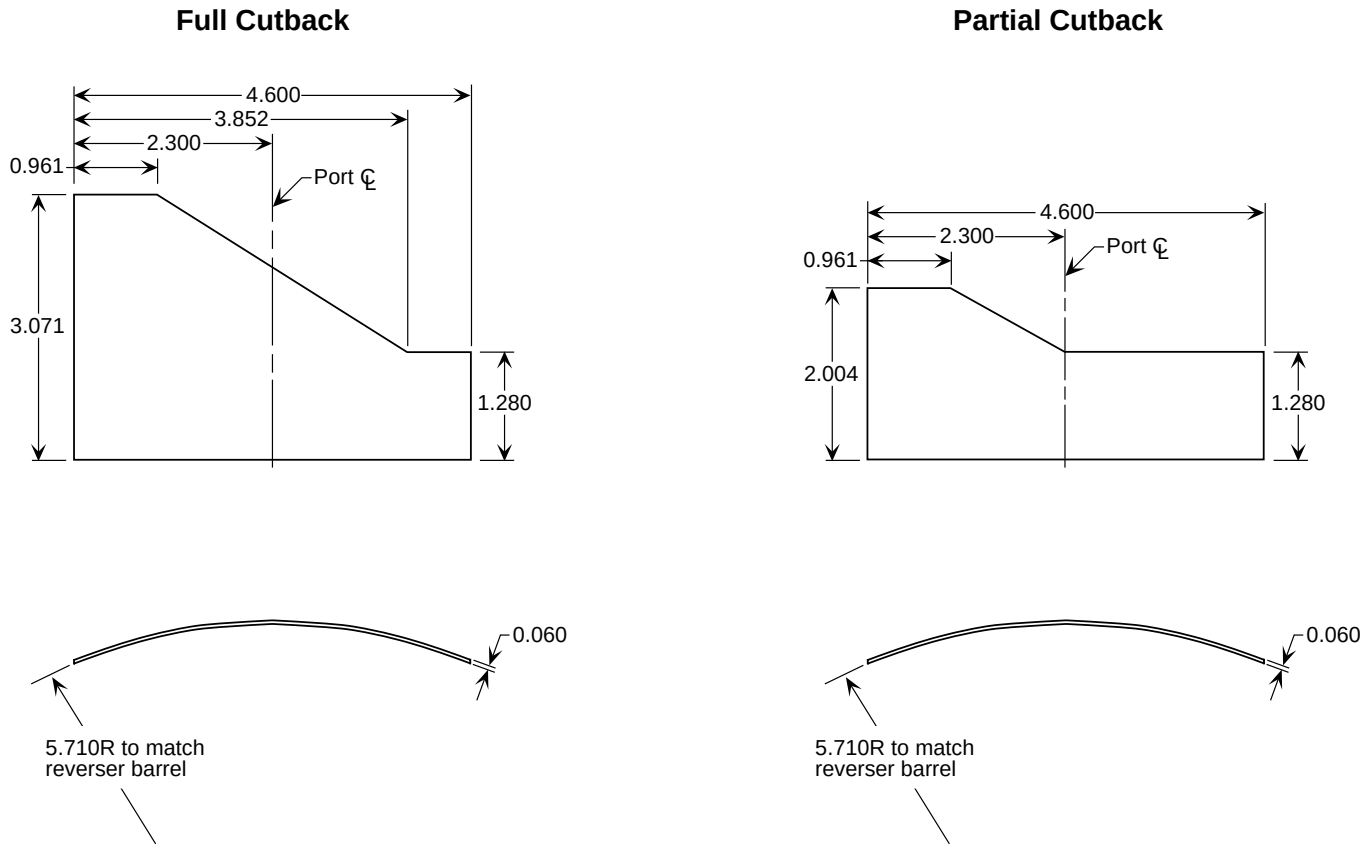

(m) Sketch of port covers. Port covers for doors D and H shown; Port covers for doors A and E are opposite.

Figure 11. Continued.

Long Kicker Plate

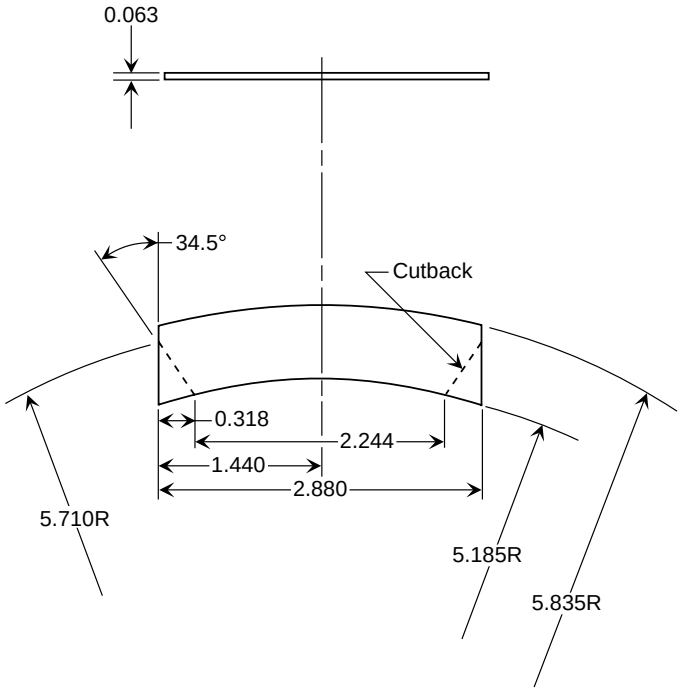

Extra Long Kicker Plate

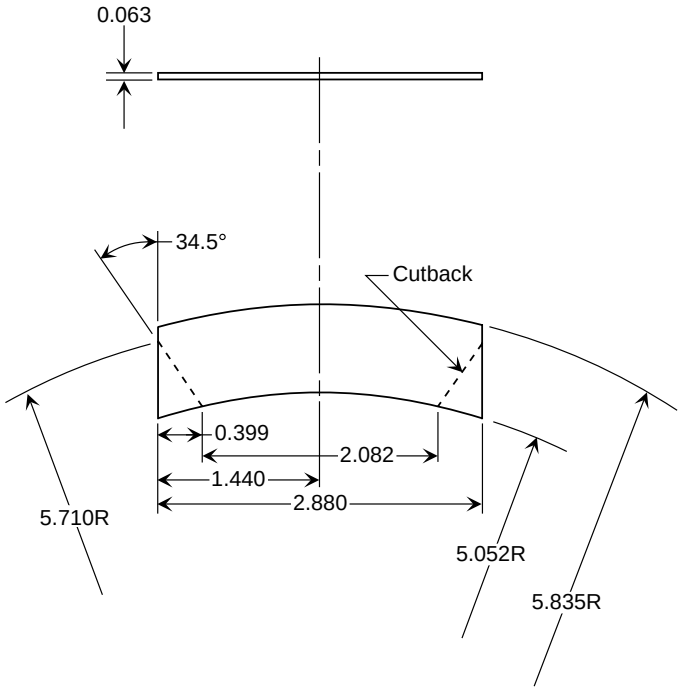

(n) Sketch of outer door kicker plates.

Figure 11. Continued.

Long Fence

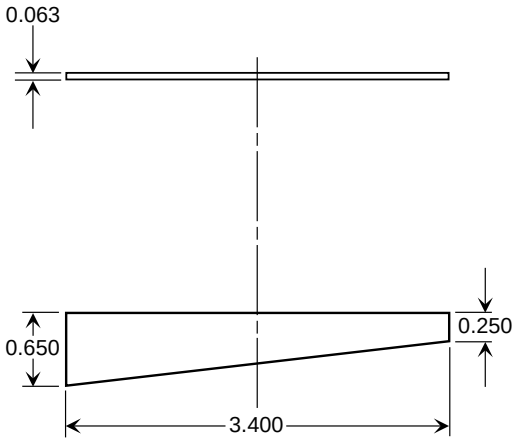

Extra Long Fence

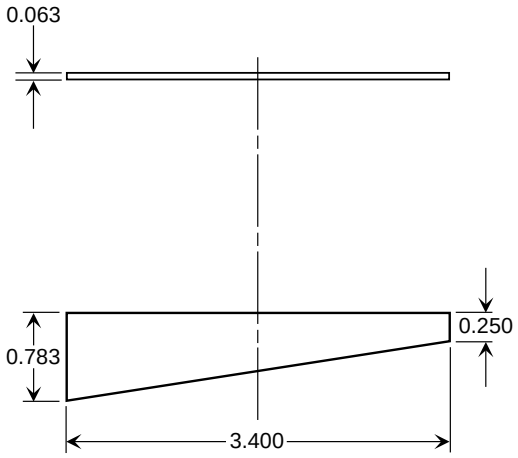

(o) Sketch of outer door fences. Left hand fences shown; right hand fences are opposite.

Figure 11. Continued.

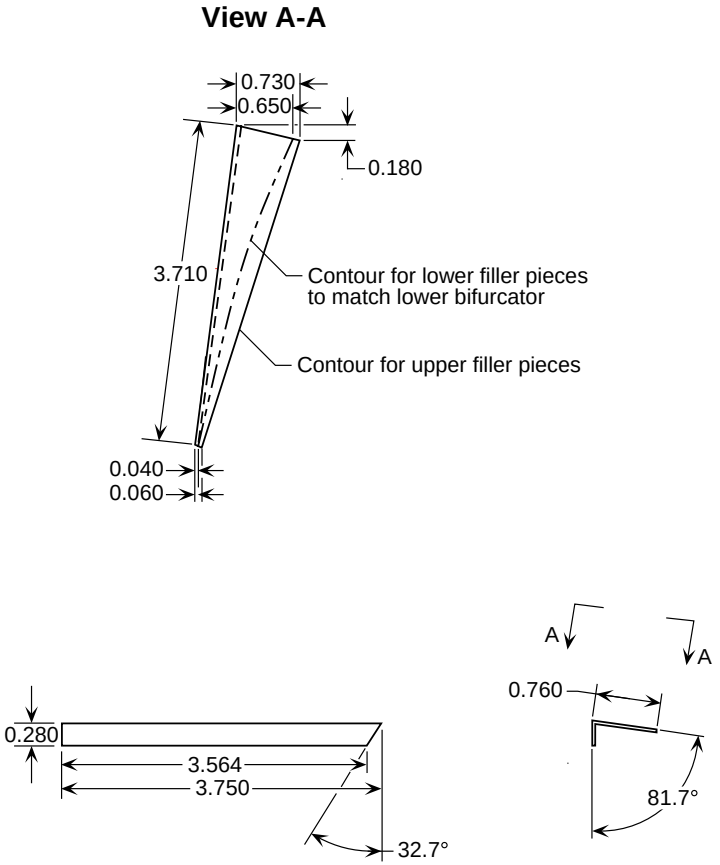

(p) Sketch of upper and lower filler pieces.

Figure 11. Concluded.

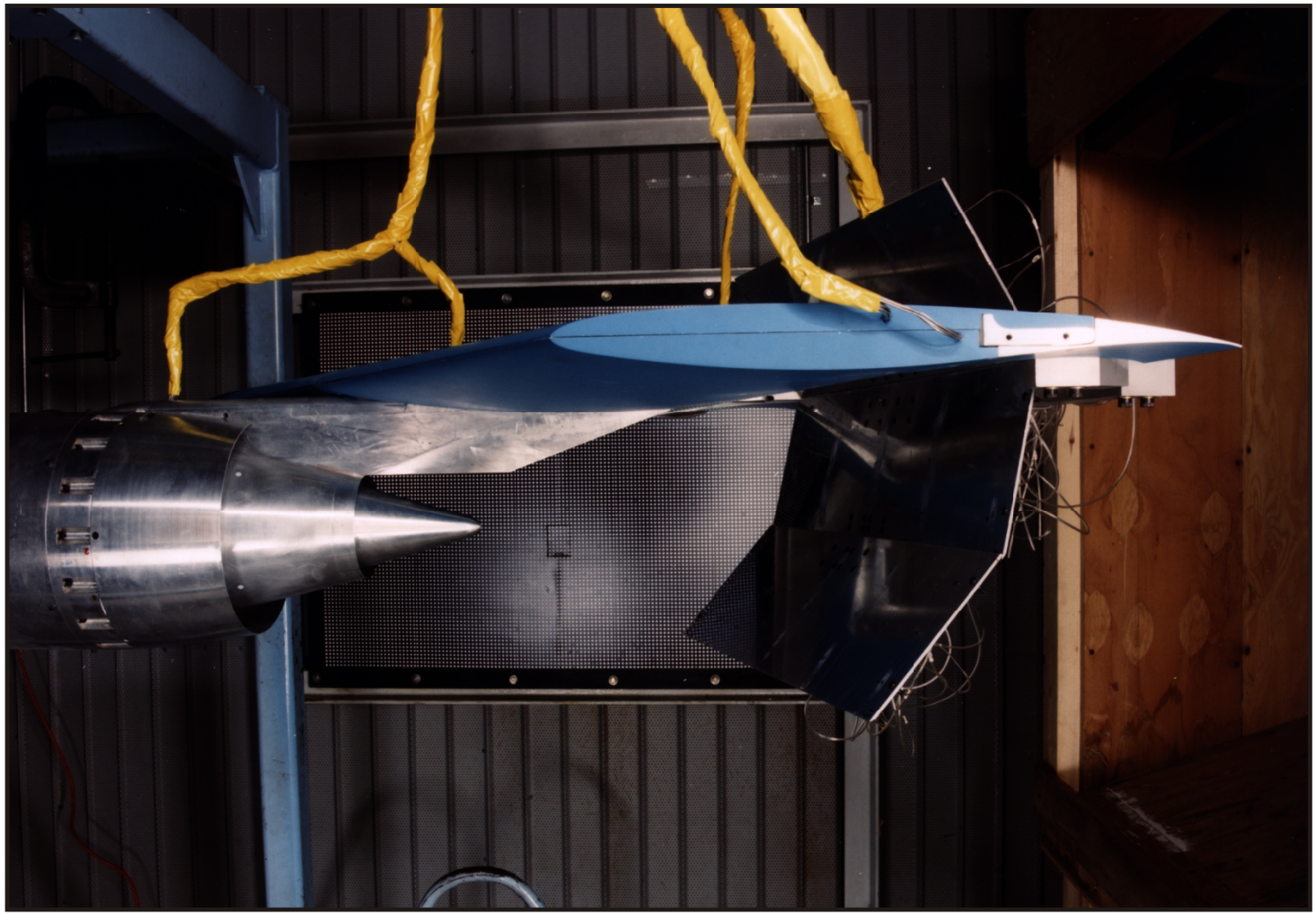

L97-971

(a) Photograph of wing-mounted thrust reverser model.

Figure 12. Details of wing-mounted thrust reverser model. Dimensions are in inches.

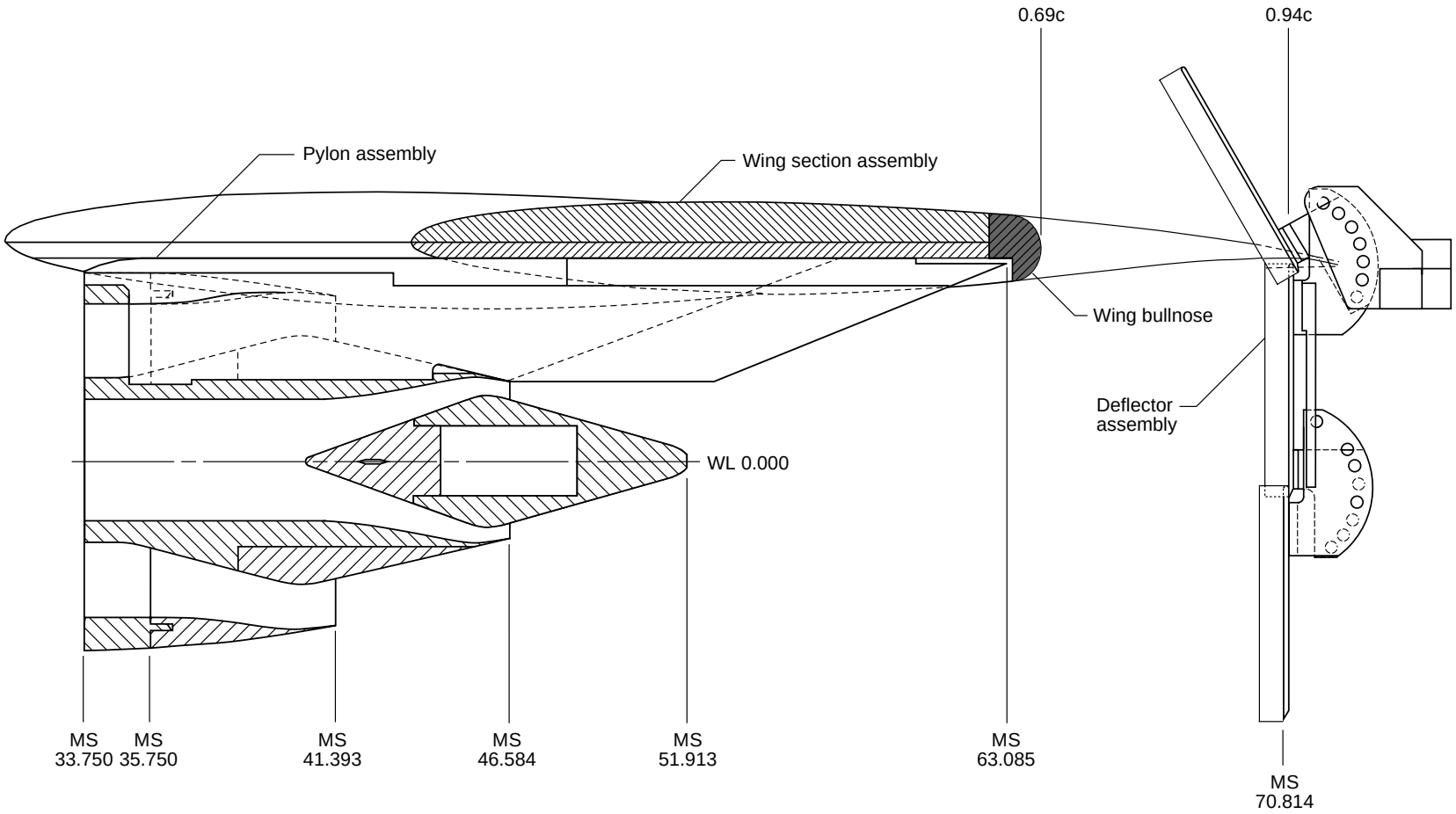

(b) Partial cutaway sketch of wing-mounted thrust reverser model.

Figure 12. Continued.

Section A-A

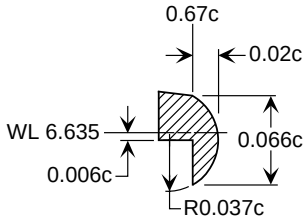

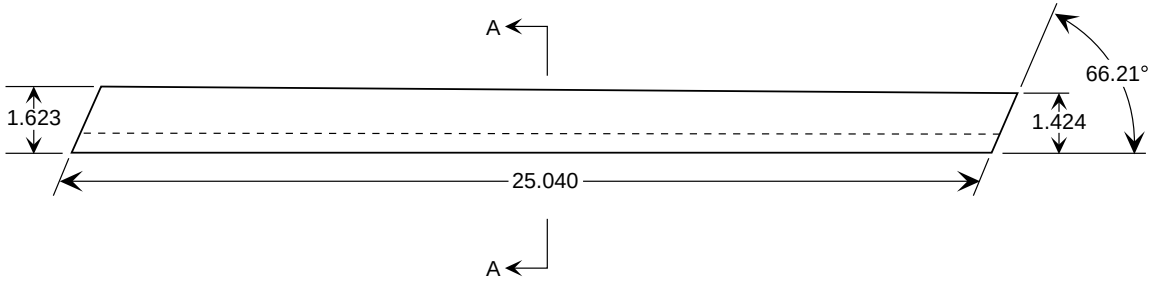

(c) Sketch showing wing bullnose.

Figure 12. Continued.

Deflector Assembly

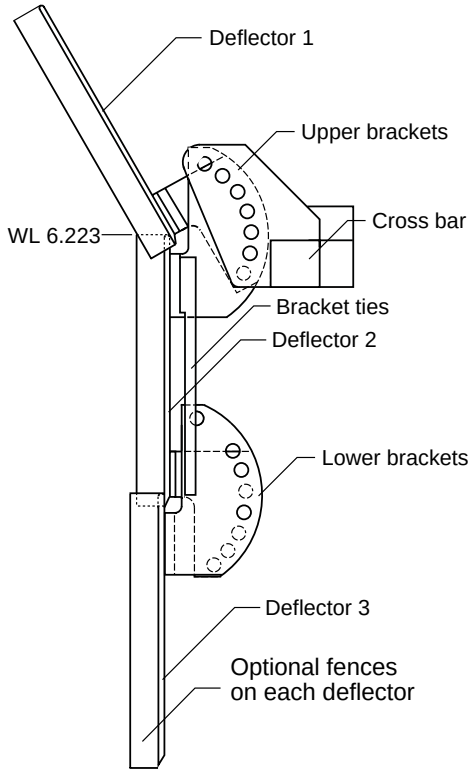

Definition of Deflector Angles

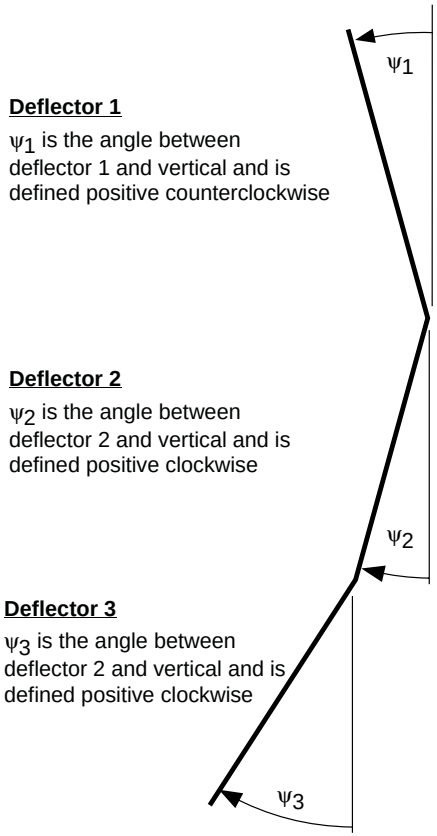

Deflector 1

ψ_1 is the angle between deflector 1 and vertical and is defined positive counterclockwise

Deflector 2

ψ_2 is the angle between deflector 2 and vertical and is defined positive clockwise

Deflector 3

ψ_3 is the angle between deflector 2 and vertical and is defined positive clockwise

Center of Rotation for Deflectors

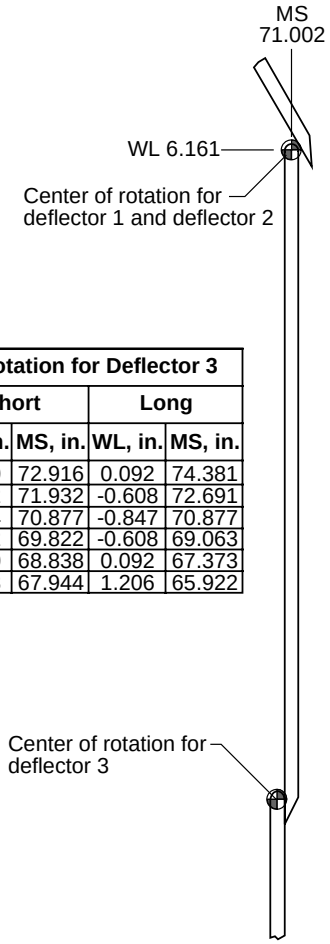

Center of Rotation for Deflector 3				
	Short		Long	
ψ_2, deg	WL, in.	MS, in.	WL, in.	MS, in.
-30	2.630	72.916	0.092	74.381
-15	2.222	71.932	-0.608	72.691
0	2.084	70.877	-0.847	70.877
15	2.222	69.822	-0.608	69.063
30	2.630	68.838	0.092	67.373
45	3.278	67.944	1.206	65.922

(d) Details of deflector assembly.

Figure 12. Continued.

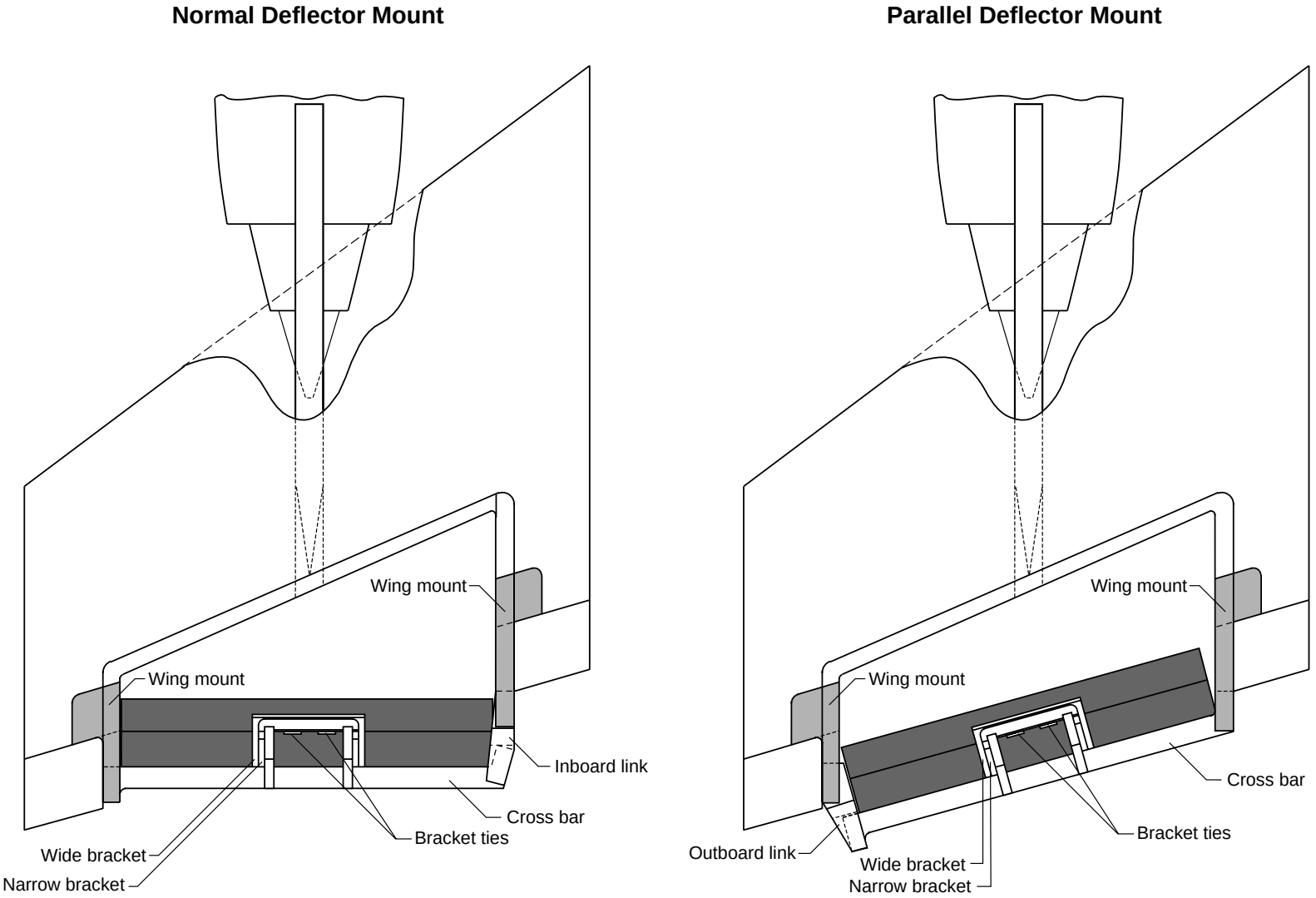

(e) Sketch of parallel and normal deflector mount positions.

Figure 12. Continued.

Flange Details

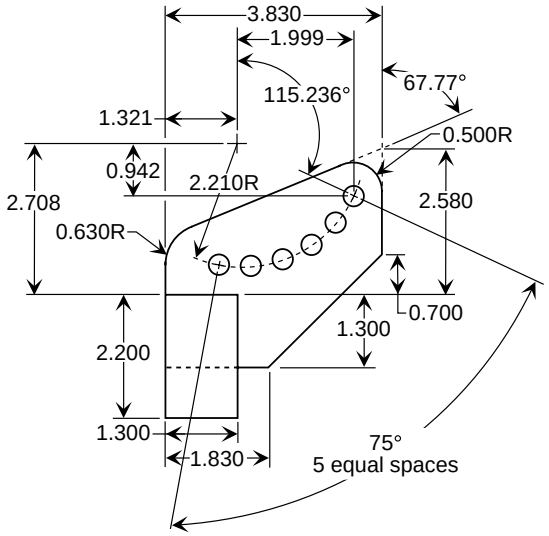

Crossbar

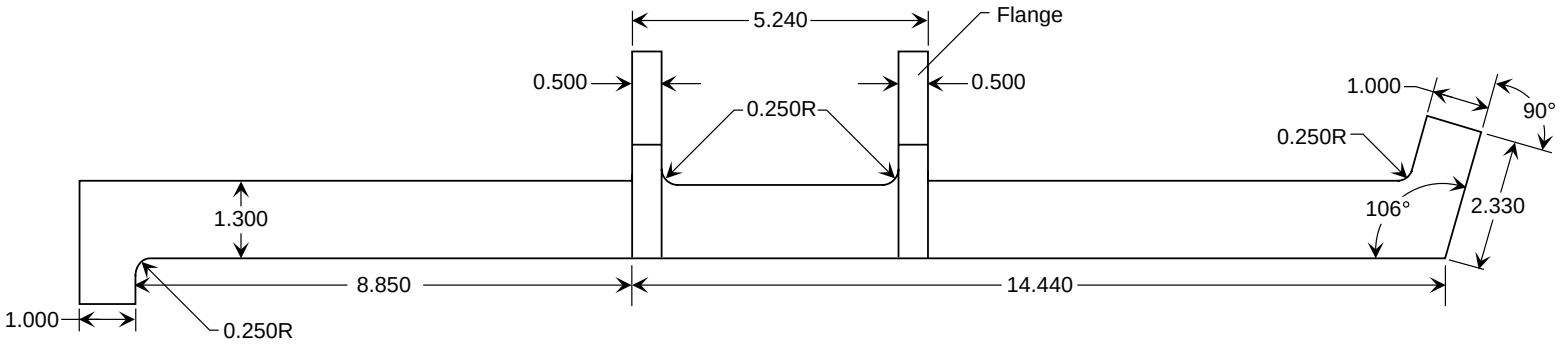

(f) Sketch showing crossbar.

Figure 12. Continued.

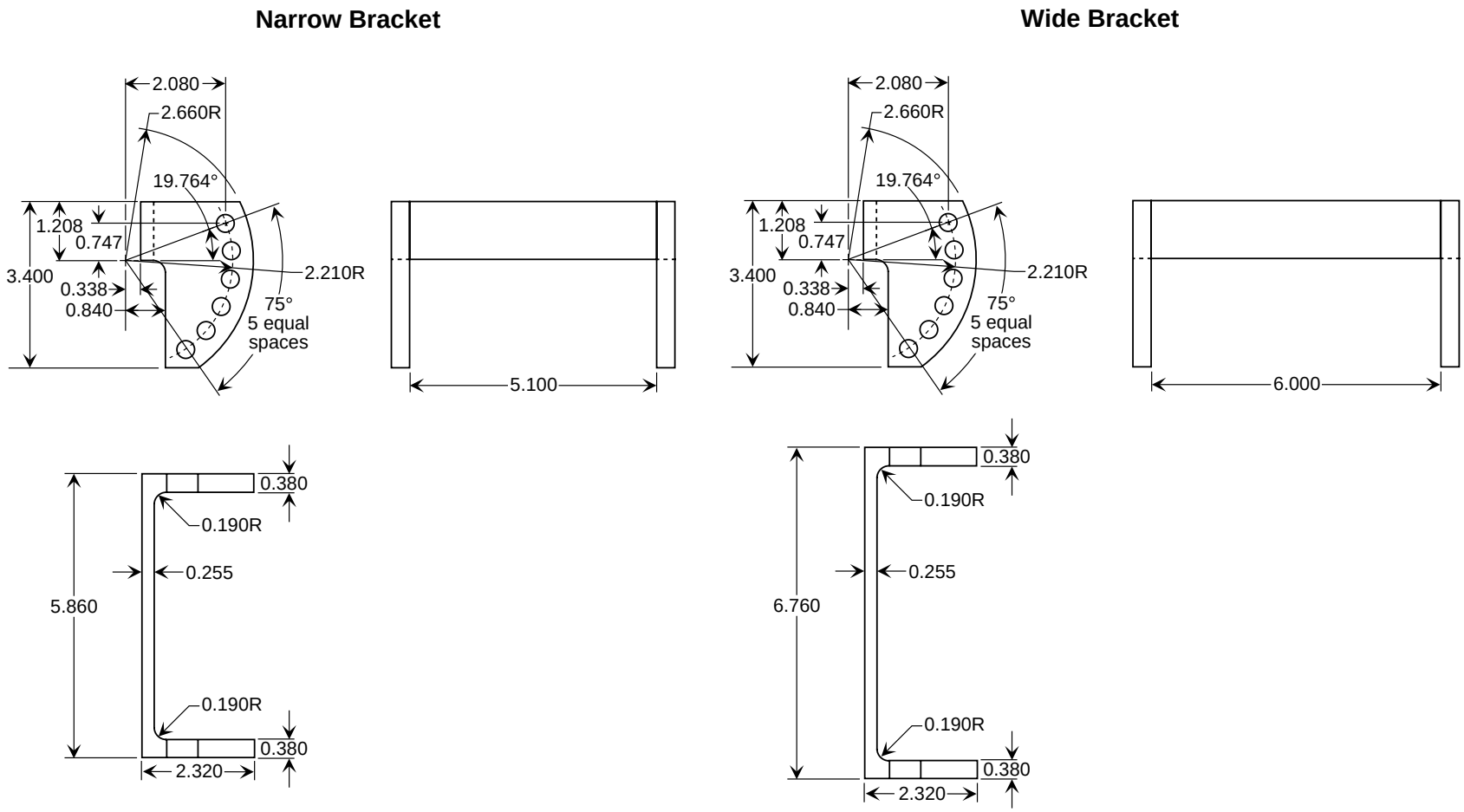

(g) Sketch showing upper brackets.

Figure 12. Continued.

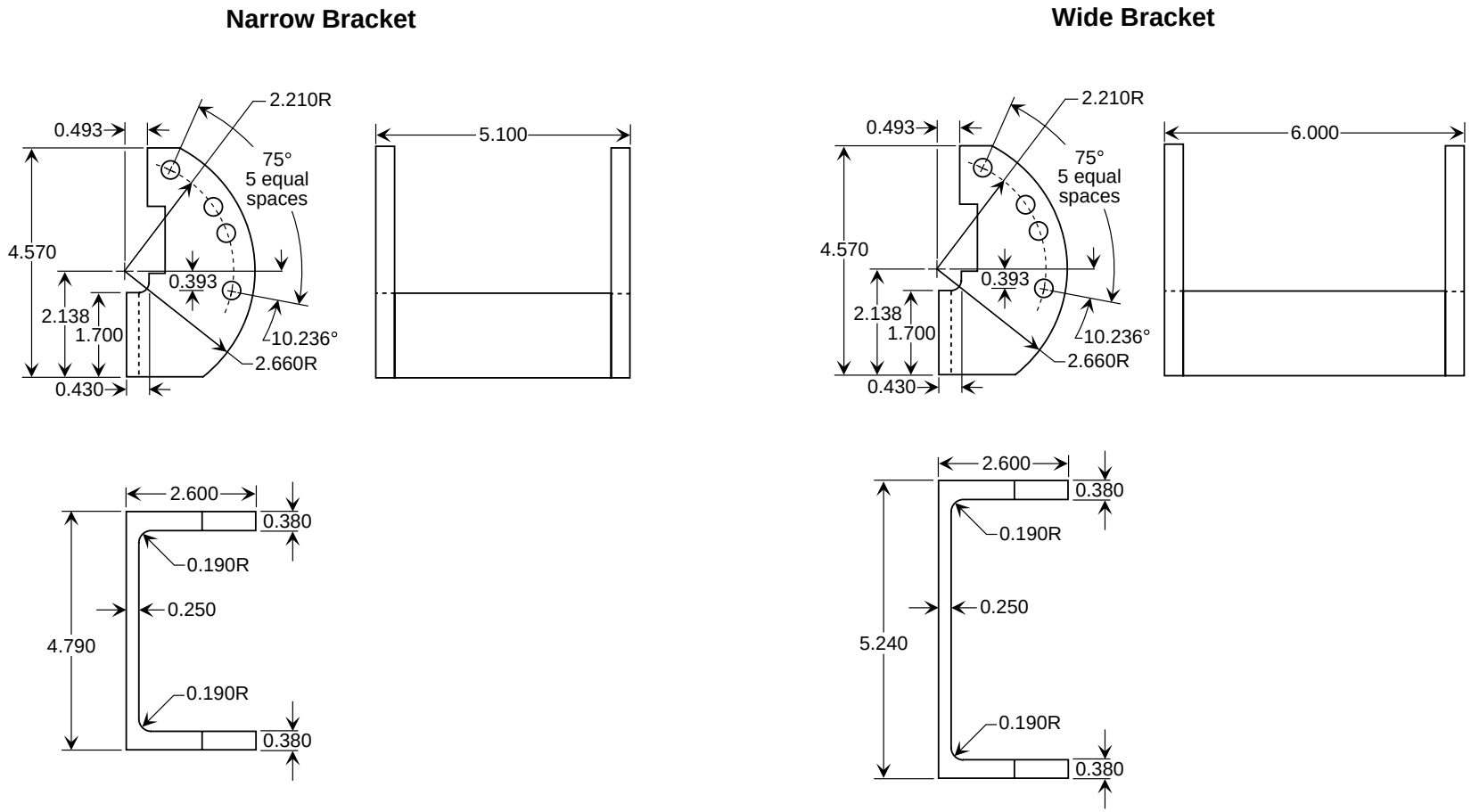

(h) Sketch showing lower brackets.

Figure 12. Continued.

Short Bracket Tie

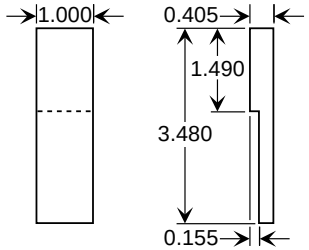

Long Bracket Tie

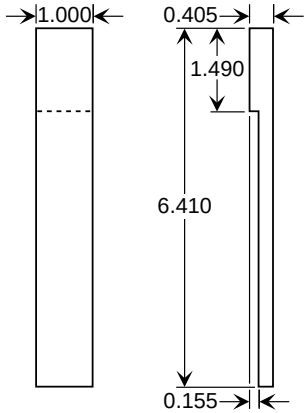

(i) Sketch showing bracket ties. Left hand bracket ties shown; right hand bracket ties are opposite.

Figure 12. Continued.

Deflector

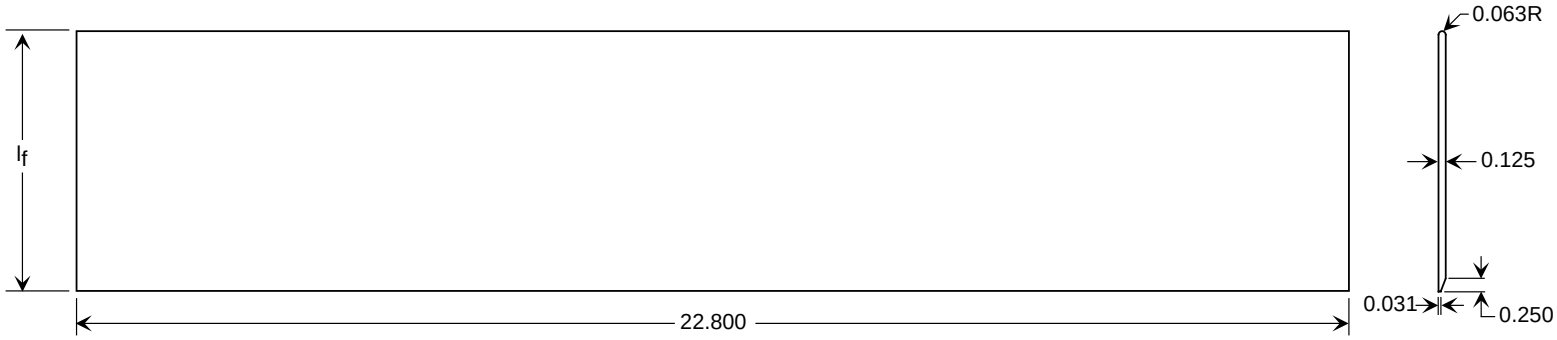

Deflector Chord Length (l_f), in.		
Deflector	Short	Long
1	4.640	7.590
2	4.390	7.320
3	–	7.590

Optional Fence Installation

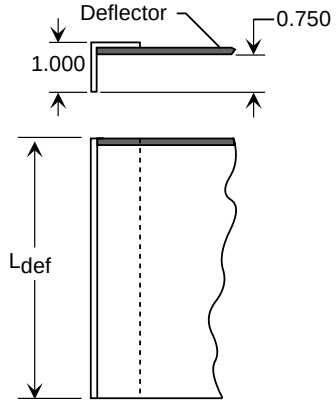

(j) Sketch showing deflectors and optional deflector fences.

Figure 12. Continued.

Outboard Wing Mount

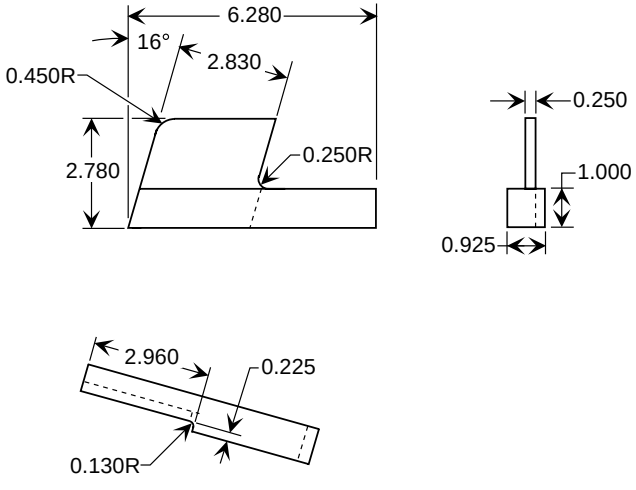

Inboard Wing Mount

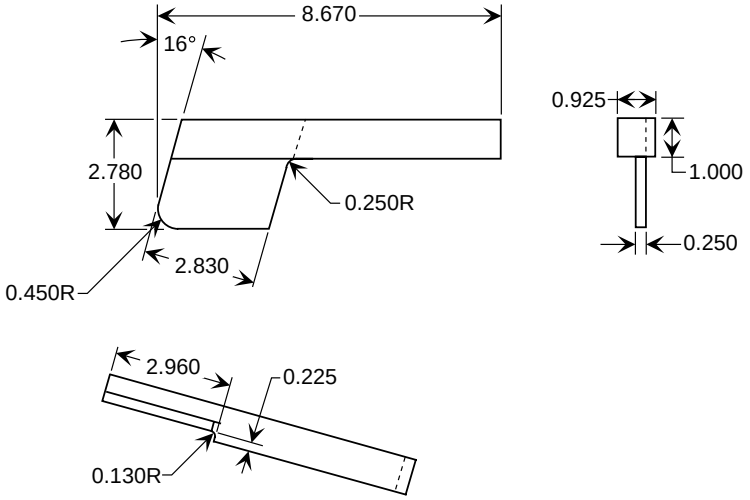

(k) Sketch showing wing mounts.

Figure 12. Continued.

Outboard Link

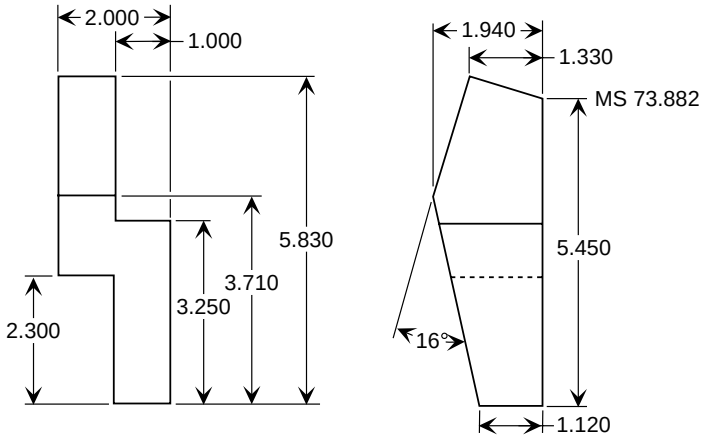

Inboard Link

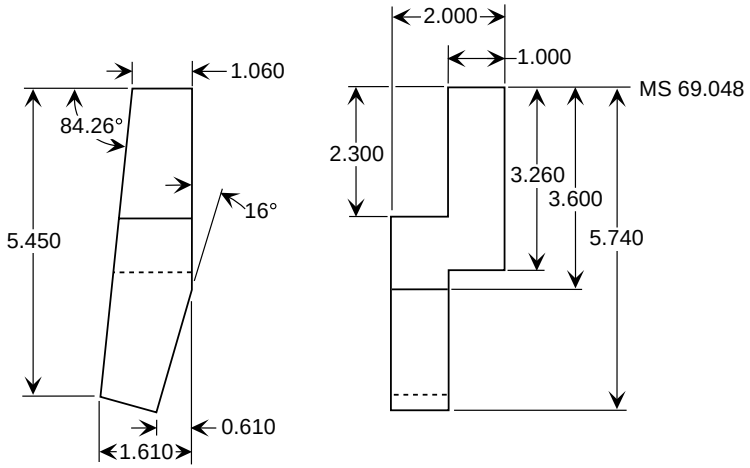

(l) Sketch showing links.

Figure 12. Concluded.

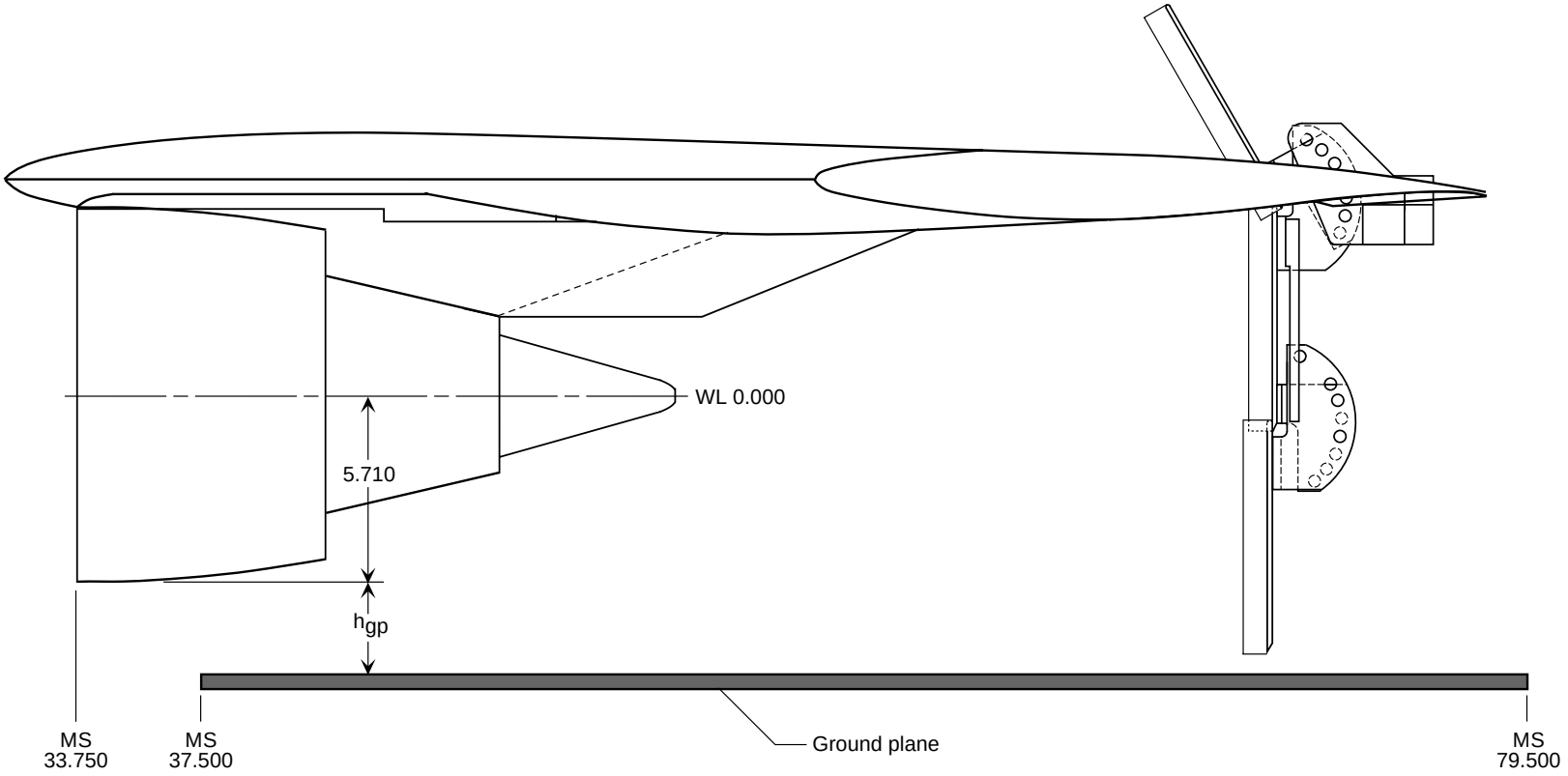

Ground Plane Setup		
	h_{gp}, in.	
Full Scale	18.00	36.00
Model Scale	1.42	2.84

(a) Side view.

Figure 13. Details of ground plane setup for wing-mounted thrust reverser model. Dimensions are in inches.

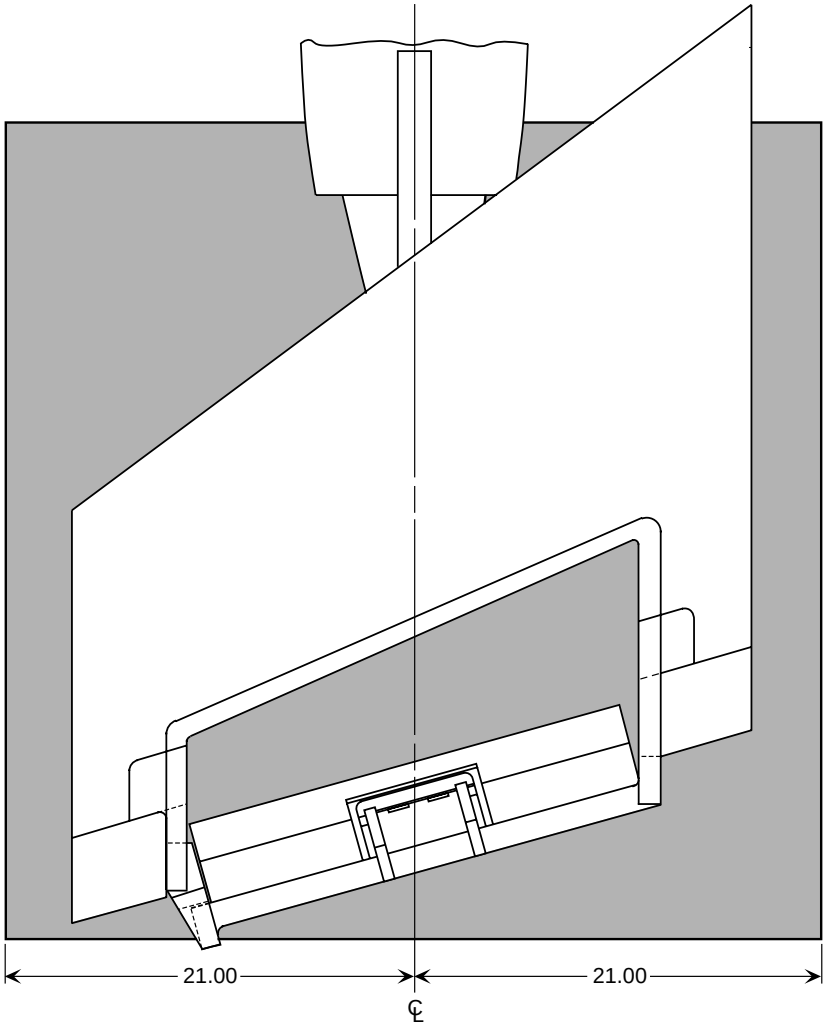

(b) Top view.

Figure 13. Concluded.

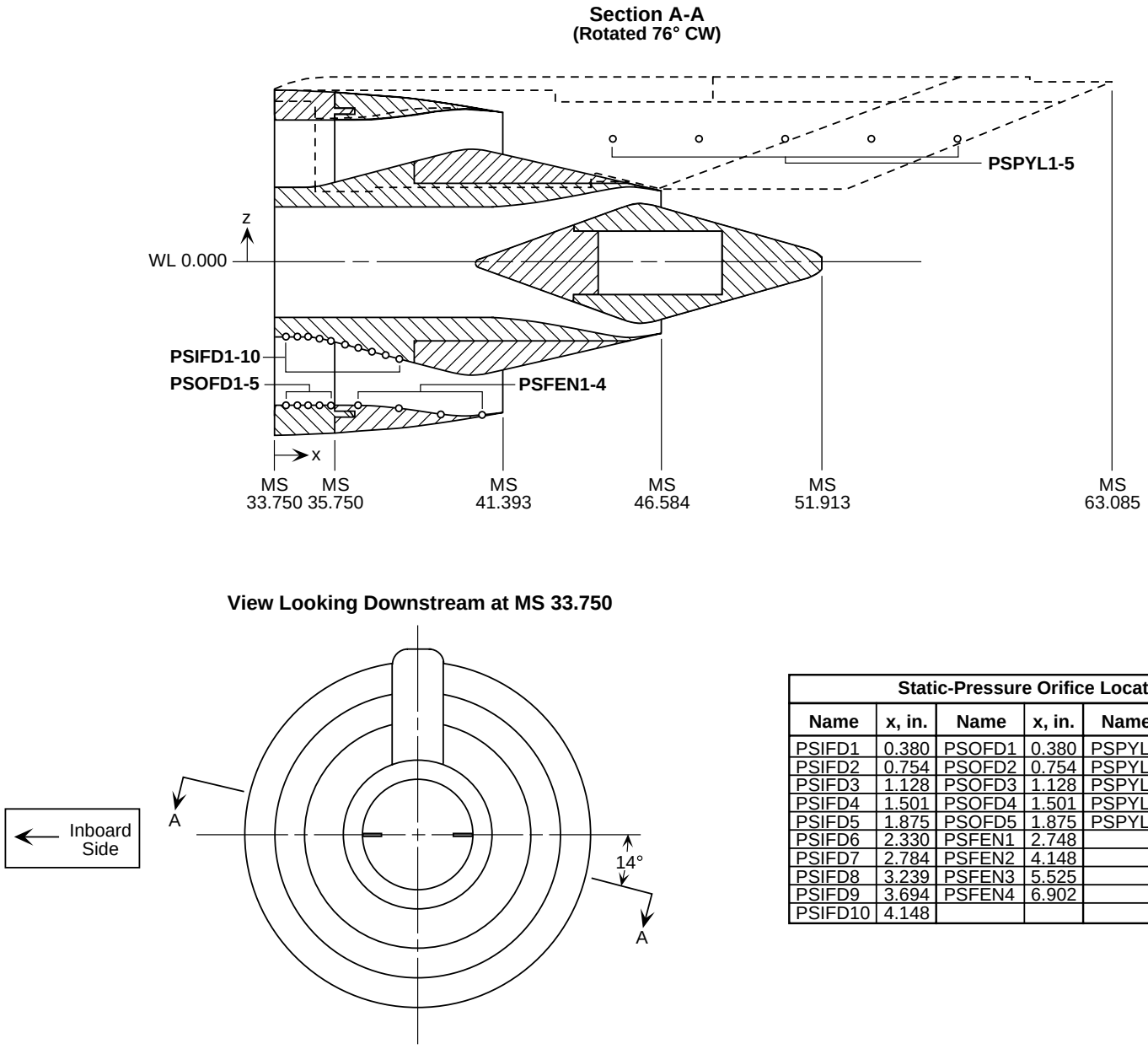

Static-Pressure Orifice Locations						
Name	**x, in.**	**Name**	**x, in.**	**Name**	**x, in.**	**z, in.**
PSIFD1	0.380	PSOFD1	0.380	PSPYL1	10.136	3.676
PSIFD2	0.754	PSOFD2	0.754	PSPYL2	12.739	3.665
PSIFD3	1.128	PSOFD3	1.128	PSPYL3	15.359	3.631
PSIFD4	1.501	PSOFD4	1.501	PSPYL4	18.099	3.621
PSIFD5	1.875	PSOFD5	1.875	PSPYL5	20.728	3.662
PSIFD6	2.330	PSFEN1	2.748			
PSIFD7	2.784	PSFEN2	4.148			
PSIFD8	3.239	PSFEN3	5.525			
PSIFD9	3.694	PSFEN4	6.902			
PSIFD10	4.148					

Figure 14. Details of separate-flow exhaust system model showing static pressure orifice locations (denoted by circles).

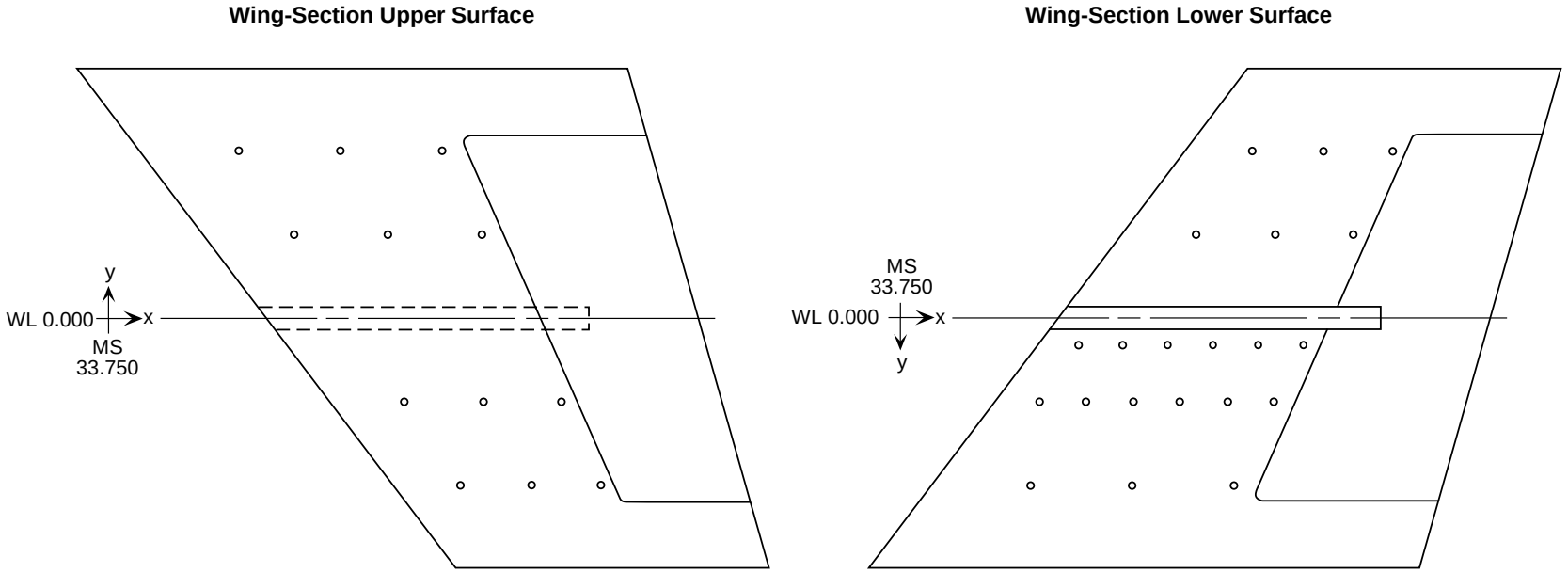

Wing-Section Upper Surface					
Static-Pressure Orifice Locations					
Name	x, in.	y, in.	Name	x, in.	y, in.
PSWU1	8.891	11.420	PSWU7	20.199	-5.710
PSWU2	15.816	11.420	PSWU8	25.524	-5.710
PSWU3	22.741	11.420	PSWU9	30.848	-5.710
PSWU4	12.660	5.710	PSWU10	23.969	-11.420
PSWU5	19.052	5.710	PSWU11	28.760	-11.420
PSWU6	25.443	5.710	PSWU12	33.551	-11.420

Wing-Section Lower Surface								
Static-Pressure Orifice Locations								
Name	x, in.	y, in.	Name	x, in.	y, in.	Name	x, in.	y, in.
PSWL1	8.891	11.420	PSWL8	22.248	5.710	PSWL15	27.227	1.941
PSWL2	15.816	11.420	PSWL9	25.443	5.710	PSWL16	20.199	-5.710
PSWL3	22.741	11.420	PSWL10	12.129	1.941	PSWL17	25.524	-5.710
PSWL4	9.465	5.710	PSWL11	15.148	1.941	PSWL18	30.848	-5.710
PSWL5	12.660	5.710	PSWL12	18.168	1.941	PSWL19	23.969	-11.420
PSWL6	15.856	5.710	PSWL13	21.188	1.941	PSWL20	28.760	-11.420
PSWL7	19.052	5.710	PSWL14	24.207	1.941	PSWL21	33.551	-11.420

Figure 15. Details of wing-section showing static pressure orifice locations (denoted by circles).

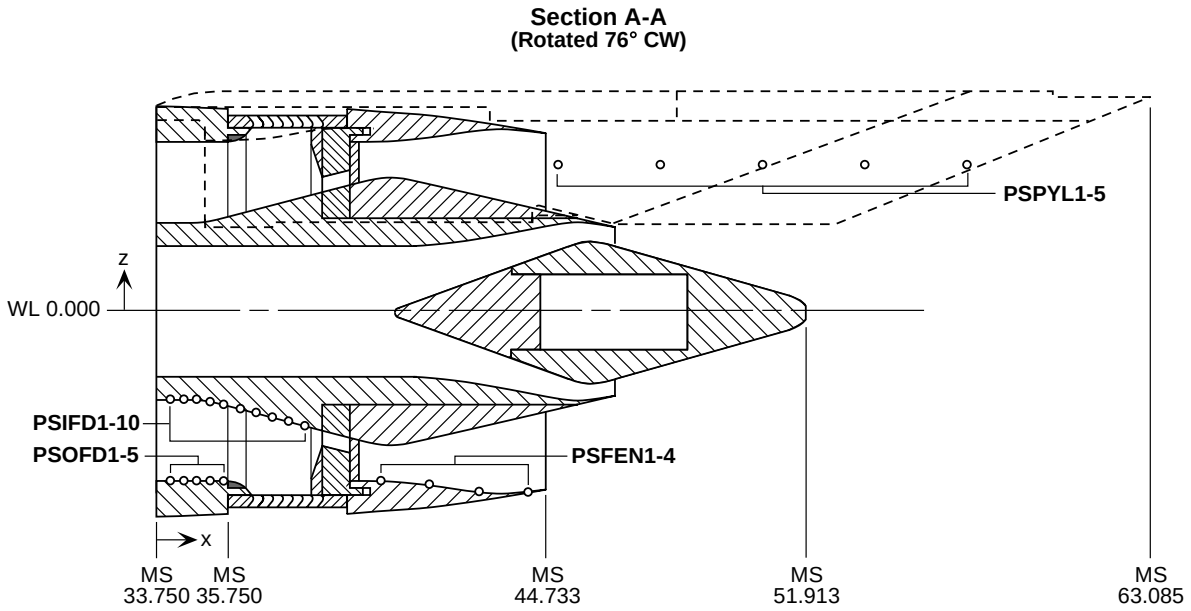

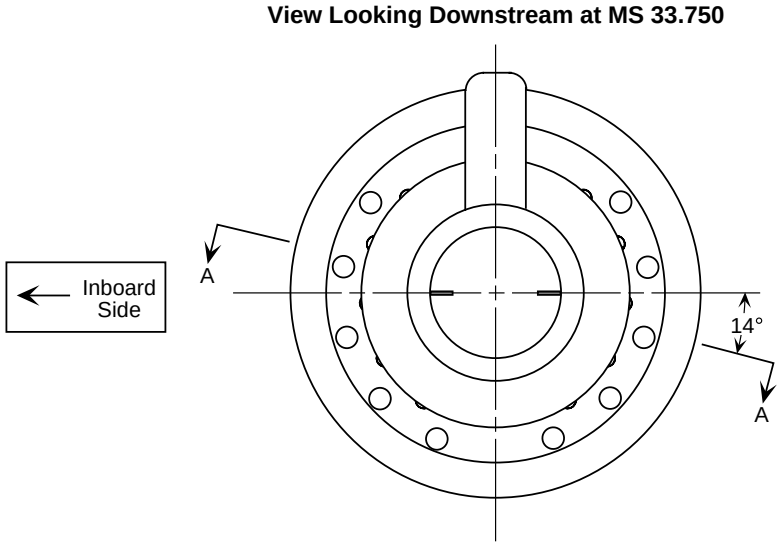

Static-Pressure Orifice Locations						
Name	x, in.	Name	x, in.	Name	x, in.	z, in.
PSIFD1	0.380	PSOFD1	0.380	PSPYL1	10.136	3.676
PSIFD2	0.754	PSOFD2	0.754	PSPYL2	12.739	3.665
PSIFD3	1.128	PSOFD3	1.128	PSPYL3	15.359	3.631
PSIFD4	1.501	PSOFD4	1.501	PSPYL4	18.099	3.621
PSIFD5	1.875	PSOFD5	1.875	PSPYL5	20.728	3.662
PSIFD6	2.330	PSFEN1	6.088			
PSIFD7	2.784	PSFEN2	7.488			
PSIFD8	3.239	PSFEN3	8.865			
PSIFD9	3.694	PSFEN4	10.242			
PSIFD10	4.148					

Figure 16. Details of conventional cascade thrust reverser model showing static pressure orifice locations (denoted by circles).

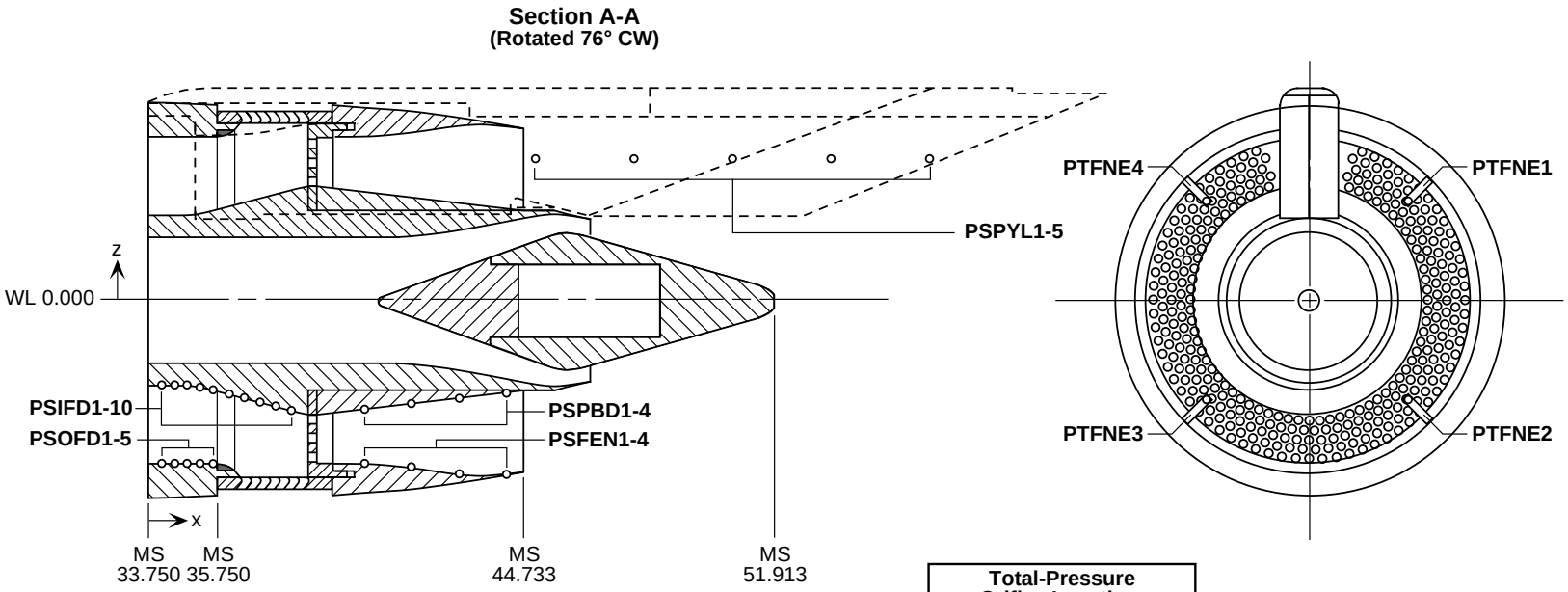

Total-Pressure Orifice Locations		
Name	**x, in.**	**R, in.**
PTFNE1	10.983	4.000
PTFNE2	10.983	4.000
PTFNE3	10.983	4.000
PTFNE4	10.983	4.000

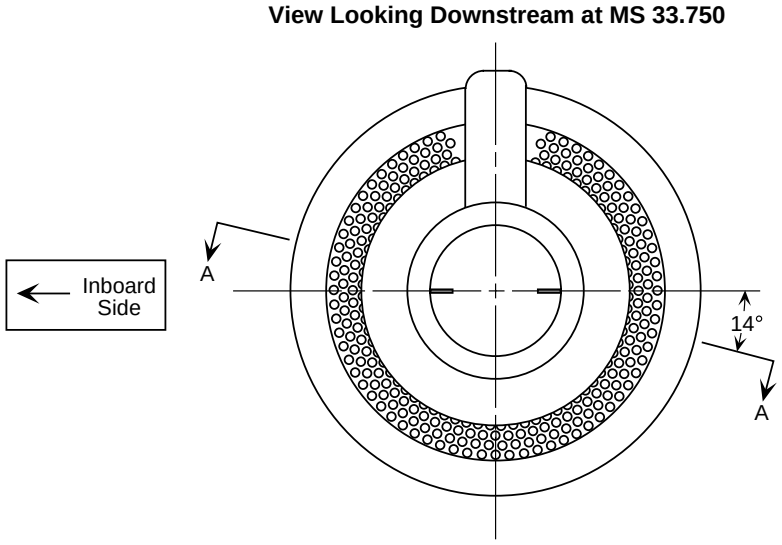

Static-Pressure Orifice Locations						
Name	**x, in.**	**Name**	**x, in.**	**Name**	**x, in.**	**z, in.**
PSIFD1	0.380	PSOFD1	0.380	PSPBD1	6.088	-
PSIFD2	0.754	PSOFD2	0.754	PSPBD2	7.488	-
PSIFD3	1.128	PSOFD3	1.128	PSPBD3	8.865	-
PSIFD4	1.501	PSOFD4	1.501	PSPBD4	10.242	-
PSIFD5	1.875	PSOFD5	1.875	PSPYL1	10.136	3.676
PSIFD6	2.330	PSFEN1	6.088	PSPYL2	12.739	3.665
PSIFD7	2.784	PSFEN2	7.488	PSPYL3	15.359	3.631
PSIFD8	3.239	PSFEN3	8.865	PSPYL4	18.099	3.621
PSIFD9	3.694	PSFEN4	10.242	PSPYL5	20.728	3.662
PSIFD10	4.148					

Figure 17. Details of cascade thrust reverser with porous blocker model showing static and total pressure orifice locations (denoted by circles).

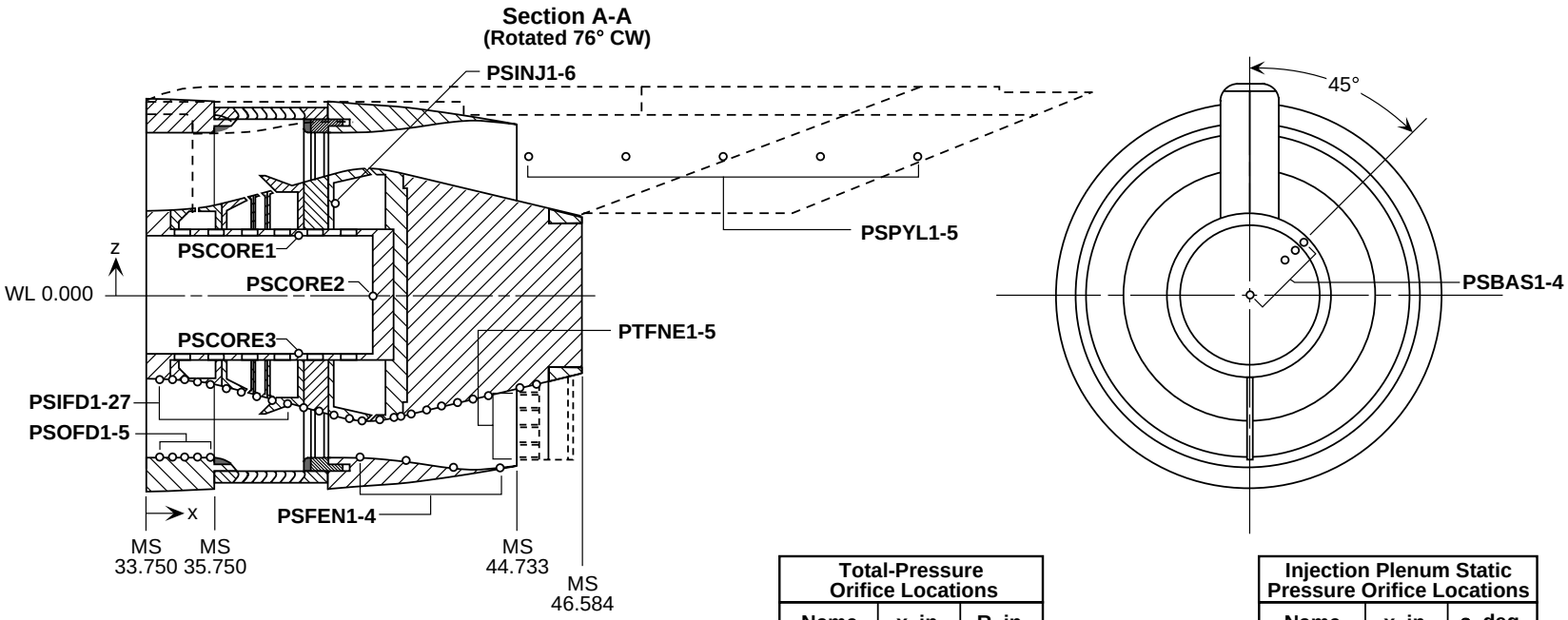

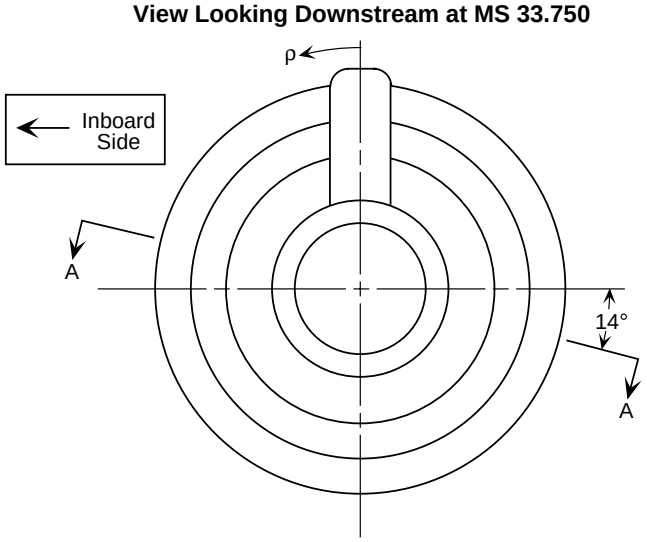

Total-Pressure Orifice Locations		
Name	**x, in.**	**R, in.**
PTFNE1	10.983	3.075
PTFNE2	10.983	3.577
PTFNE3	10.983	4.016
PTFNE4	10.983	4.410
PTFNE5	10.983	4.772

Injection Plenum Static Pressure Orifice Locations		
Name	**x, in.**	**ρ, deg.**
PSINJ1	6.250	0
PSINJ2	6.250	300
PSINJ3	6.250	240
PSINJ4	6.250	180
PSINJ5	6.250	120
PSINJ6	6.250	60

Static-Pressure Orifice Locations								
Name	**x, in.**	**Name**	**x, in.**	**Name**	**x, in.**	**z, in.**	**Name**	**R, in.**
PSIFD1	0.460	PSIFD14	5.964	PSOFD1	0.380	-	PSBAS1	0.000
PSIFD2	0.754	PSIFD15	6.338	PSOFD2	0.754	-	PSBAS2	1.432
PSIFD3	1.128	PSIFD16	6.872	PSOFD3	1.128	-	PSBAS3	1.866
PSIFD4	1.581	PSIFD17	7.326	PSOFD4	1.501	-	PSBAS4	2.213
PSIFD5	1.875	PSIFD18	7.500	PSOFD5	1.875	-		
PSIFD6	2.330	PSIFD19	7.780	PSFEN1	6.088	-		
PSIFD7	2.784	PSIFD20	8.234	PSFEN2	7.488	-		
PSIFD8	3.239	PSIFD21	8.688	PSFEN3	8.865	-		
PSIFD9	3.694	PSIFD22	9.142	PSFEN4	10.242	-		
PSIFD10	4.148	PSIFD23	9.596	PSPYL1	10.136	3.676		
PSIFD11	4.602	PSIFD24	10.050	PSPYL2	12.739	3.665		
PSIFD12	5.056	PSIFD25	10.504	PSPYL3	15.359	3.631		
PSIFD13	5.510	PSIFD26	10.958	PSPYL4	18.099	3.621		
		PSIFD27	11.412	PSPYL5	20.728	3.662		

Figure 18. Details of blockerless thrust reverser model showing static (denoted by circles) and total pressure orifice locations .

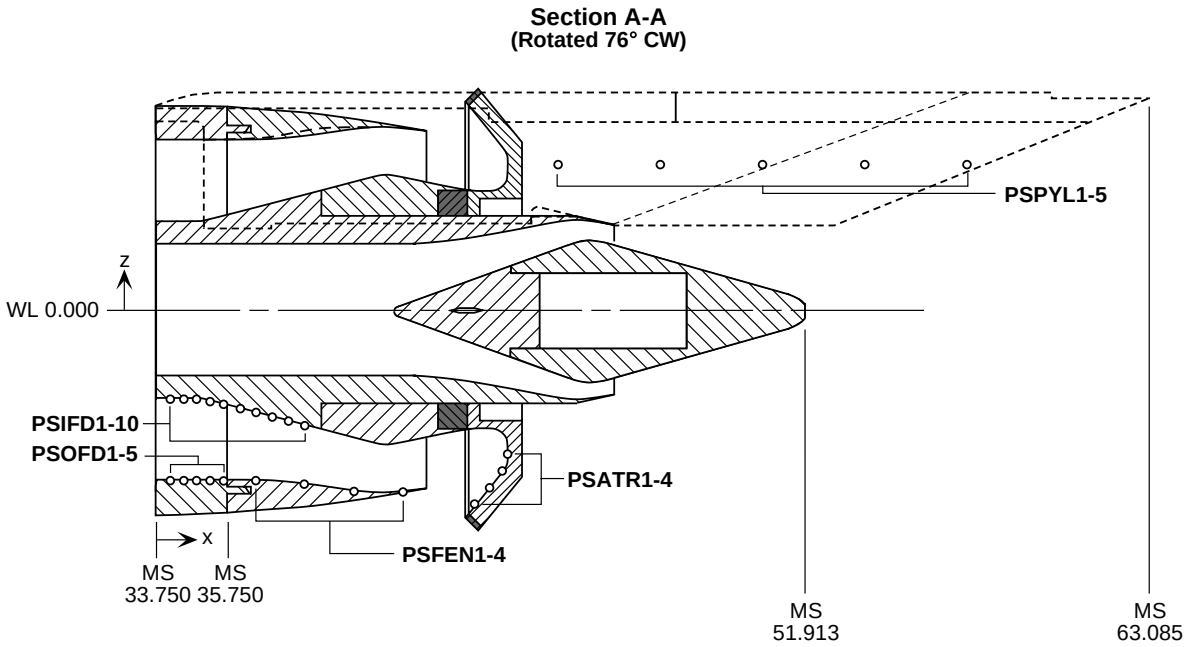

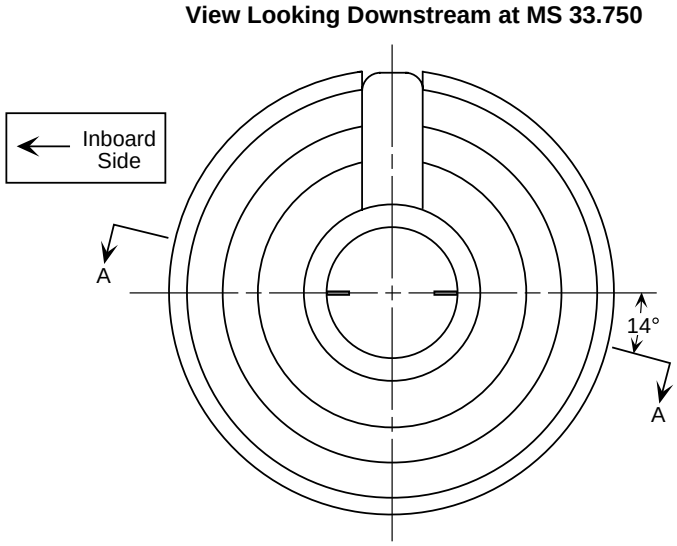

Static-Pressure Orifice Locations								
Name	x, in.	Name	x, in.	Name	x, in.	z, in.	Name	R, in.
PSIFD1	0.380	PSOFD1	0.380	PSPYL1	10.136	3.676	PSATR1	3.835
PSIFD2	0.754	PSOFD2	0.754	PSPYL2	12.739	3.665	PSATR2	4.281
PSIFD3	1.128	PSOFD3	1.128	PSPYL3	15.359	3.631	PSATR3	4.727
PSIFD4	1.501	PSOFD4	1.501	PSPYL4	18.099	3.621	PSATR4	5.173
PSIFD5	1.875	PSOFD5	1.875	PSPYL5	20.728	3.662		
PSIFD6	2.330	PSFEN1	2.748					
PSIFD7	2.784	PSFEN2	4.148					
PSIFD8	3.239	PSFEN3	5.525					
PSIFD9	3.694	PSFEN4	6.902					
PSIFD10	4.148							

Figure 19. Details of annular (metal) target thrust reverser model showing static pressure orifice locations (denoted by circles).

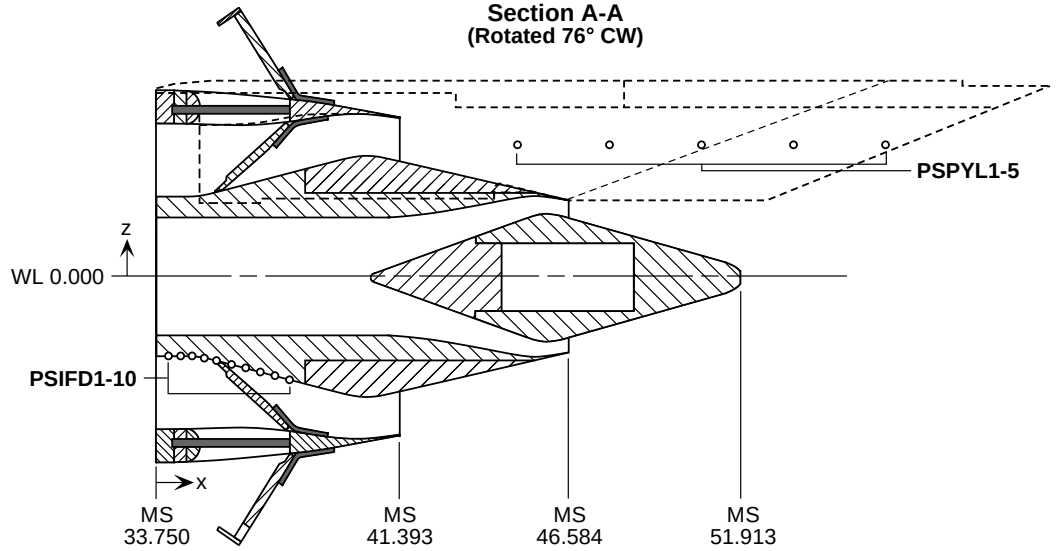

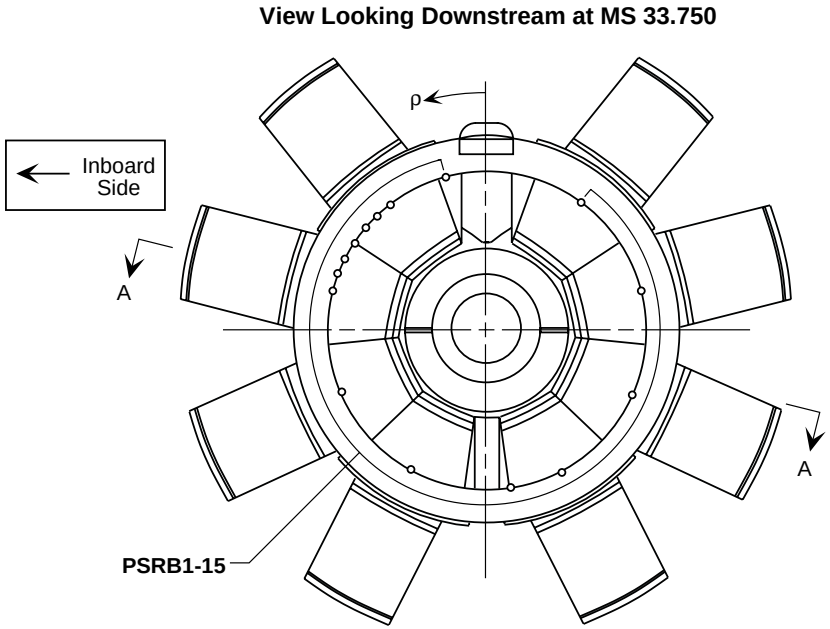

Static-Pressure Orifice Locations					
Name	**x, in.**	**z, in.**	**Name**	**x, in.**	**ρ, deg.**
PSIFD1	0.380	-	PSRB1	34.350	14.540
PSIFD2	0.754	-	PSRB2	34.350	37.500
PSIFD3	1.128	-	PSRB3	34.350	43.830
PSIFD4	1.501	-	PSRB4	34.350	50.160
PSIFD5	1.875	-	PSRB5	34.350	56.490
PSIFD6	2.330	-	PSRB6	34.350	62.820
PSIFD7	2.784	-	PSRB7	34.350	69.150
PSIFD8	3.239	-	PSRB8	34.350	75.500
PSIFD9	3.694	-	PSRB9	34.350	113.500
PSIFD10	4.148	-	PSRB10	34.350	151.500
PSPYL1	10.136	3.676	PSRB11	34.350	189.500
PSPYL2	12.739	3.665	PSRB12	34.350	208.500
PSPYL3	15.359	3.631	PSRB13	34.350	246.500
PSPYL4	18.099	3.621	PSRB14	34.350	284.500
PSPYL5	20.728	3.662	PSRB15	34.350	322.500

(a) Reverser barrel, fan duct, and pylon details.

Figure 20. Details of crocodile thrust reverser model showing static pressure orifice locations (denoted by circles). Dimensions are in inches.

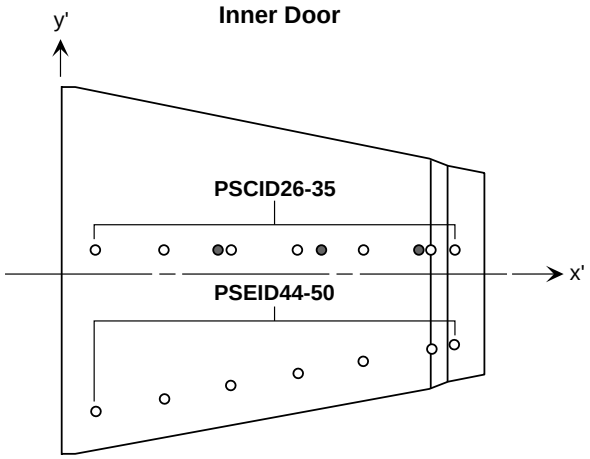

Inner Door Static-Pressure Orifice Locations					
NAME	x', in.	y', in.	NAME	x', in.	y', in.
PSCID26	0.300	0.216	PSEID44	0.300	-1.208
PSCID27	0.900	0.216	PSEID45	0.900	-1.097
PSCID28	1.500	0.216	PSEID46	1.500	-0.986
PSCID29	2.100	0.216	PSEID47	2.100	-0.875
PSCID30	2.700	0.216	PSEID48	2.700	-0.763
PSCID31	3.300	0.216	PSEID49	3.300	-0.652
PSCID32	3.450	0.216	PSEID50	3.450	-0.624
PSCID33*	3.200	0.216			
PSCID34*	2.300	0.216			
PSCID35*	1.400	0.216			

* Indicates pressure orifice (shaded) located on back of door.

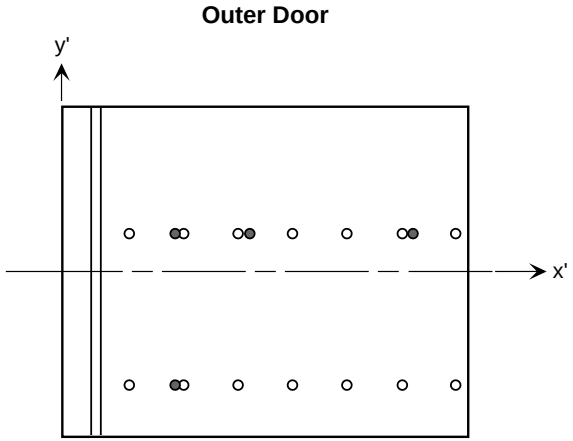

Outer Door Static-Pressure Orifice Locations					
NAME	x', in.	y', in.	NAME	x', in.	y', in.
PSCOD16*	1.000	0.341	PSEOD36*	1.000	-1.024
PSCOD17*	1.674	0.341	PSEOD37	1.674	-1.024
PSCOD18*	3.135	0.341	PSEOD38	3.135	-1.024
PSCOD19	0.600	0.341	PSEOD39	0.600	-1.024
PSCOD20	1.087	0.341	PSEOD40	1.087	-1.024
PSCOD21	1.574	0.341	PSEOD41	1.574	-1.024
PSCOD22	2.061	0.341	PSEOD42	2.061	-1.024
PSCOD23	2.548	0.341	PSEOD43	2.548	-1.024
PSCOD24	3.035	0.341			
PSCOD25	3.522	0.341			

* Indicates pressure orifice (shaded) located on back of door.

(b) Inner and outer door details.

Figure 20. Concluded.

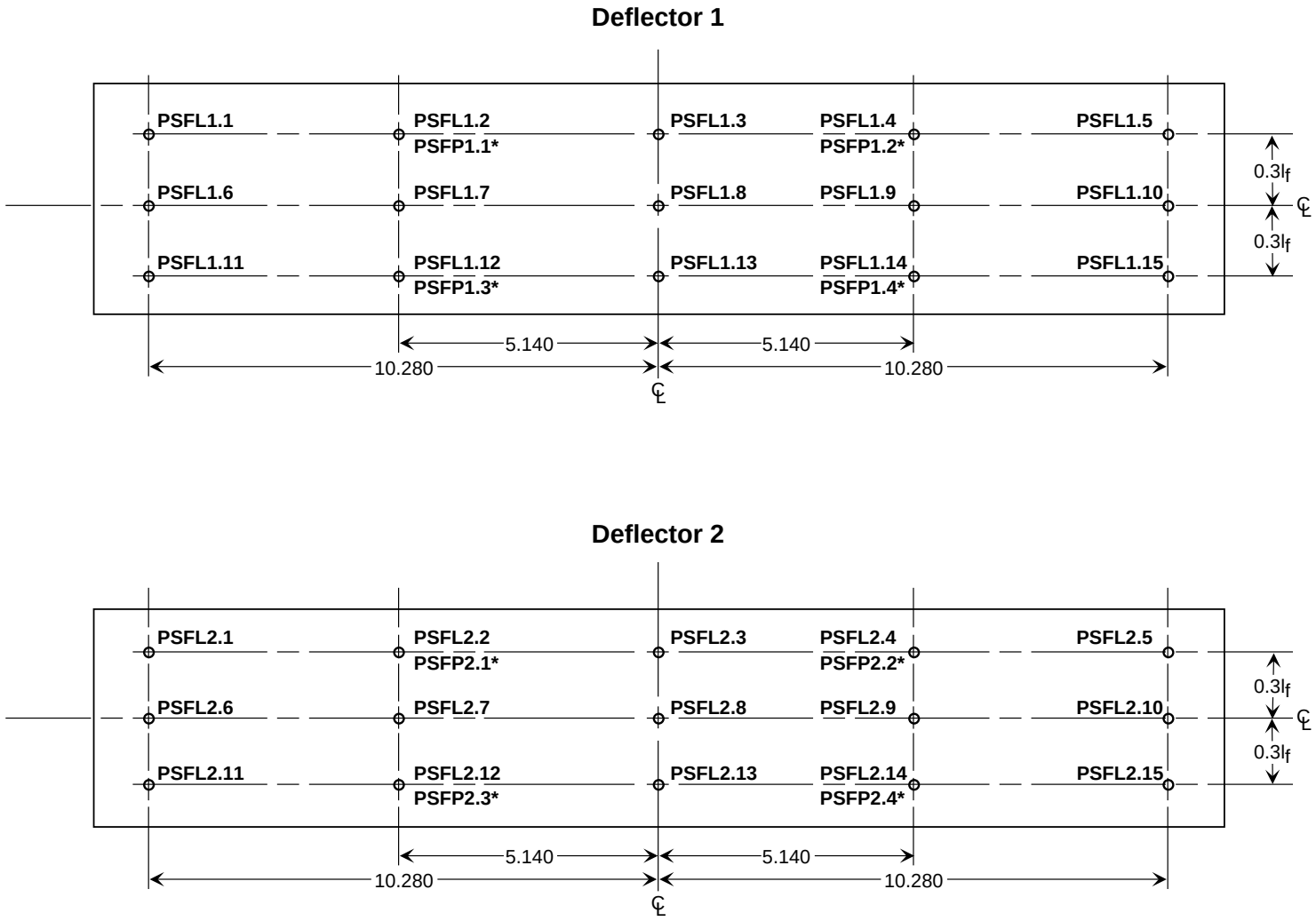

(a) Details of deflectors 1 and 2.

Figure 21. Details of wing mounted thrust reverser model showing deflector static pressure orifice locations (denoted by circles). Dimensions are in inches. A"*" indicates pressure orifice located on back of deflector.

Deflector 3

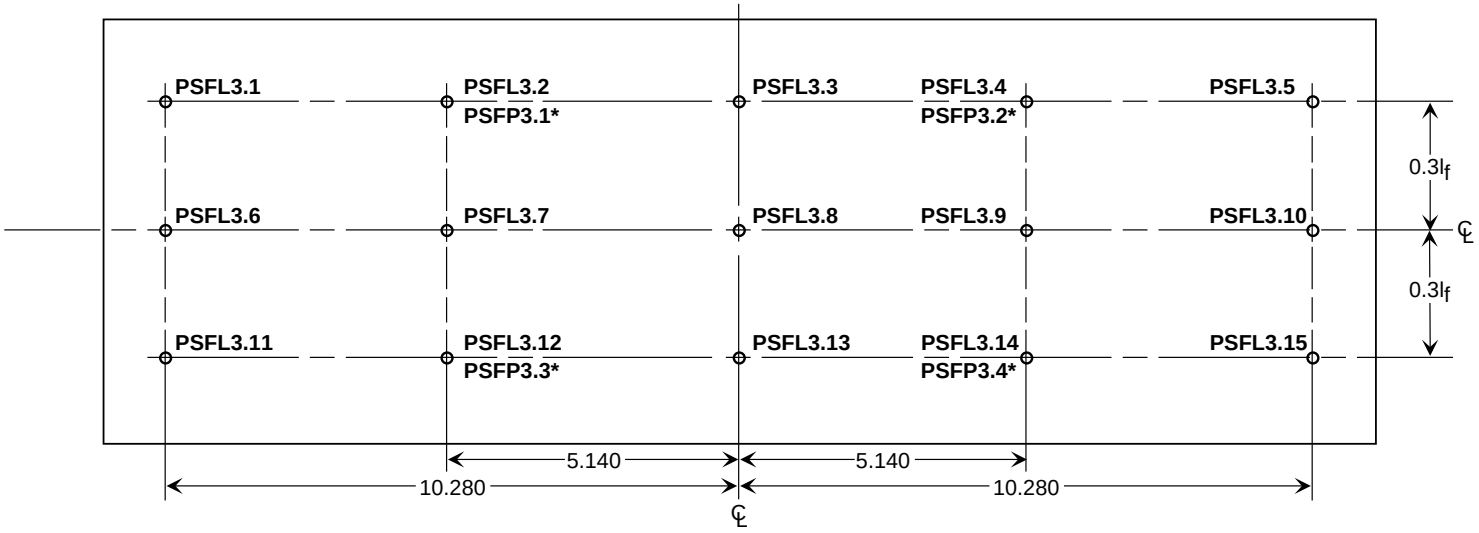

(b) Details of deflector 3.

Figure 21. Concluded.

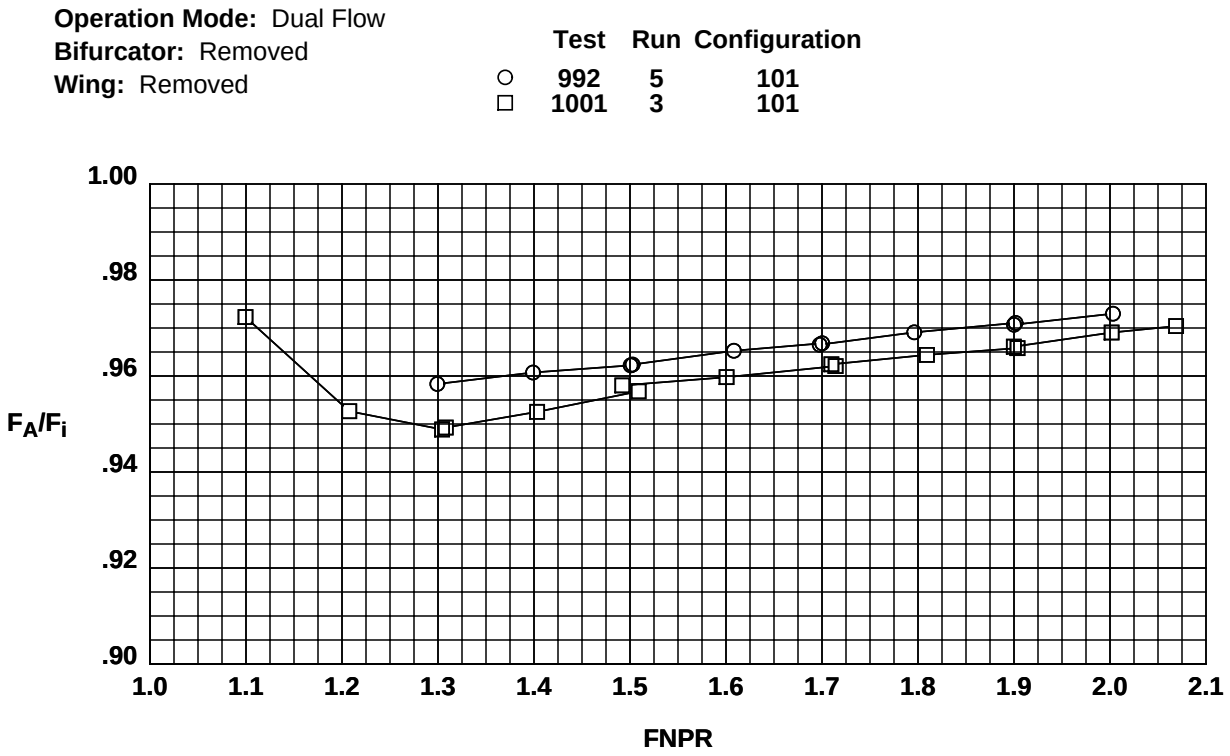

Figure 22. Separate-flow exhaust system performance in forward thrust.

Operation Mode: Dual Flow
Blocker Porosity: 0%
Bifurcator: Removed
Wing: Removed

	Test	Run	Configuration	Aft Port
○	987	18	203	Open
□	987	14	201	Closed

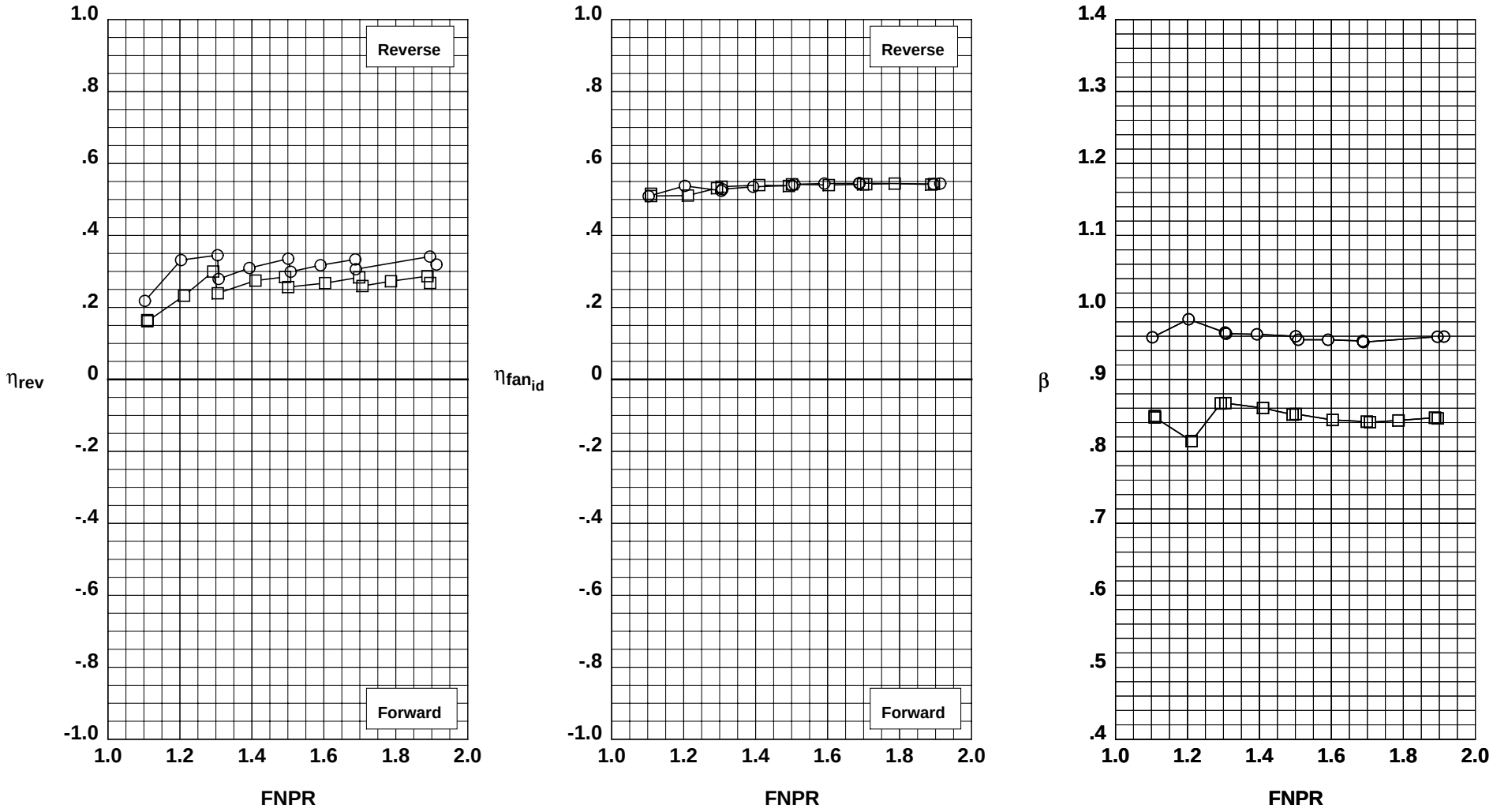

(a) Effects of cascade aft port.

Figure 23. Summary of cascade thrust reverser performance.

Operation Mode: Dual Flow
Cascade Aft Port: Open
Bifurcator: Removed
Wing: Removed

	Test	Run	Configuration	Porosity
○	987	18	203	0%
□	987	19	204	5%
◇	987	20	205	12%
△	987	25	209	25%
◺	987	24	208	50%

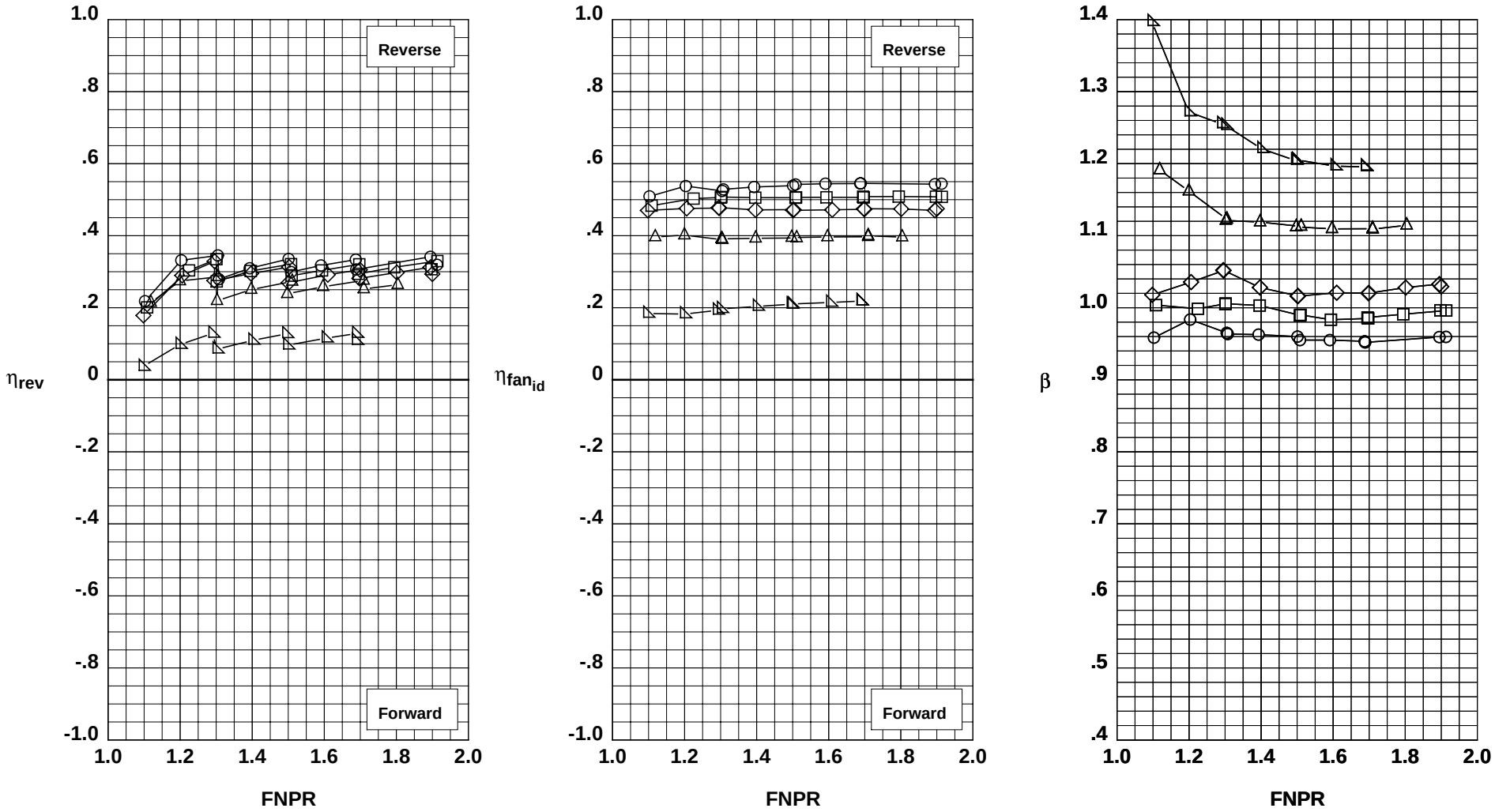

(b) Effects of blocker leakage and blocker porosity.

Figure 23. Concluded.

	Test	Run	Configuration	IPR	Injection Location	w_s, in.	θ, deg
○	993	36	615	12.00	Mid	0.025	45
□	993	34	614	11.98	Aft	0.025	45
◇	993	32	613	12.03	Throat	0.025	45

Operation Mode: Fan + Injection
Cascades: Installed
Fwd Bullnose: Bullnose
Port Fairing: #2
Bifurcator: Removed
Wing: Removed

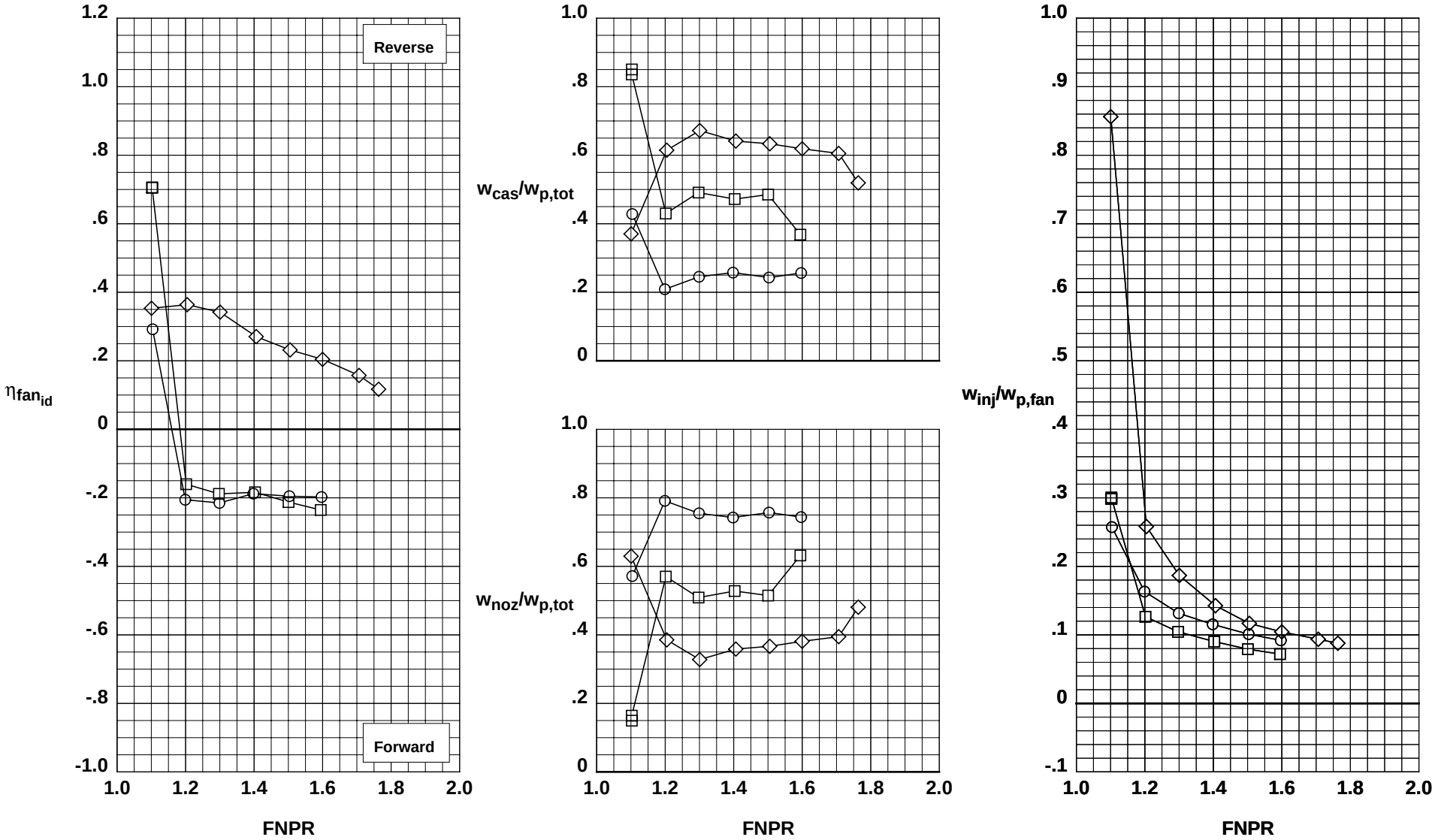

(a) Effects of single injection location.

Figure 24. Summary of blockerless thrust reverser performance.

	Test	Run	Configuration	IPR	Injection Location	w_s, in.	θ, deg
○	993	9	604	12.08	Fwd/Aft	0.013	45
□	993	38	616	12.00	Mid/Aft	0.013	45
◇	993	7	603	12.04	Fwd/Mid/Aft	0.013	45

Operation Mode: Fan + Injection
Cascades: Installed
Fwd Bullnose: Bullnose
Port Fairing: #2
Bifurcator: Removed
Wing: Removed

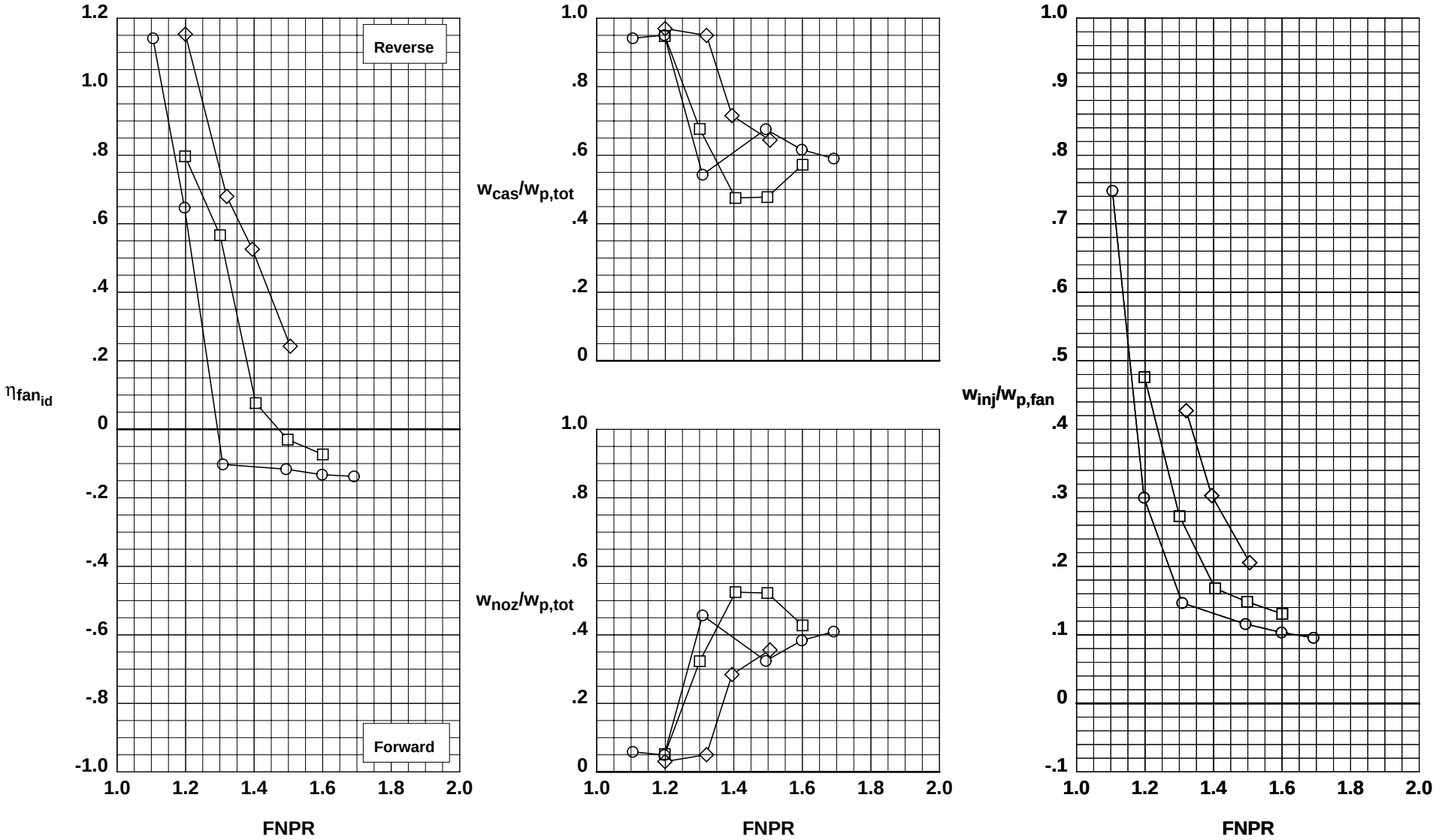

(b) Effects of multiple injection locations.

Figure 24. Continued.

	Test	Run	Configuration	IPR	Injection Location	w_s, in.	θ, deg
○	993	40	617	11.99	Throat	0.013	45
□	993	32	613	12.03	Throat	0.025	45

Operation Mode: Fan + Injection
Cascades: Installed
Fwd Bullnose: Bullnose
Port Fairing: #2
Bifurcator: Removed
Wing: Removed

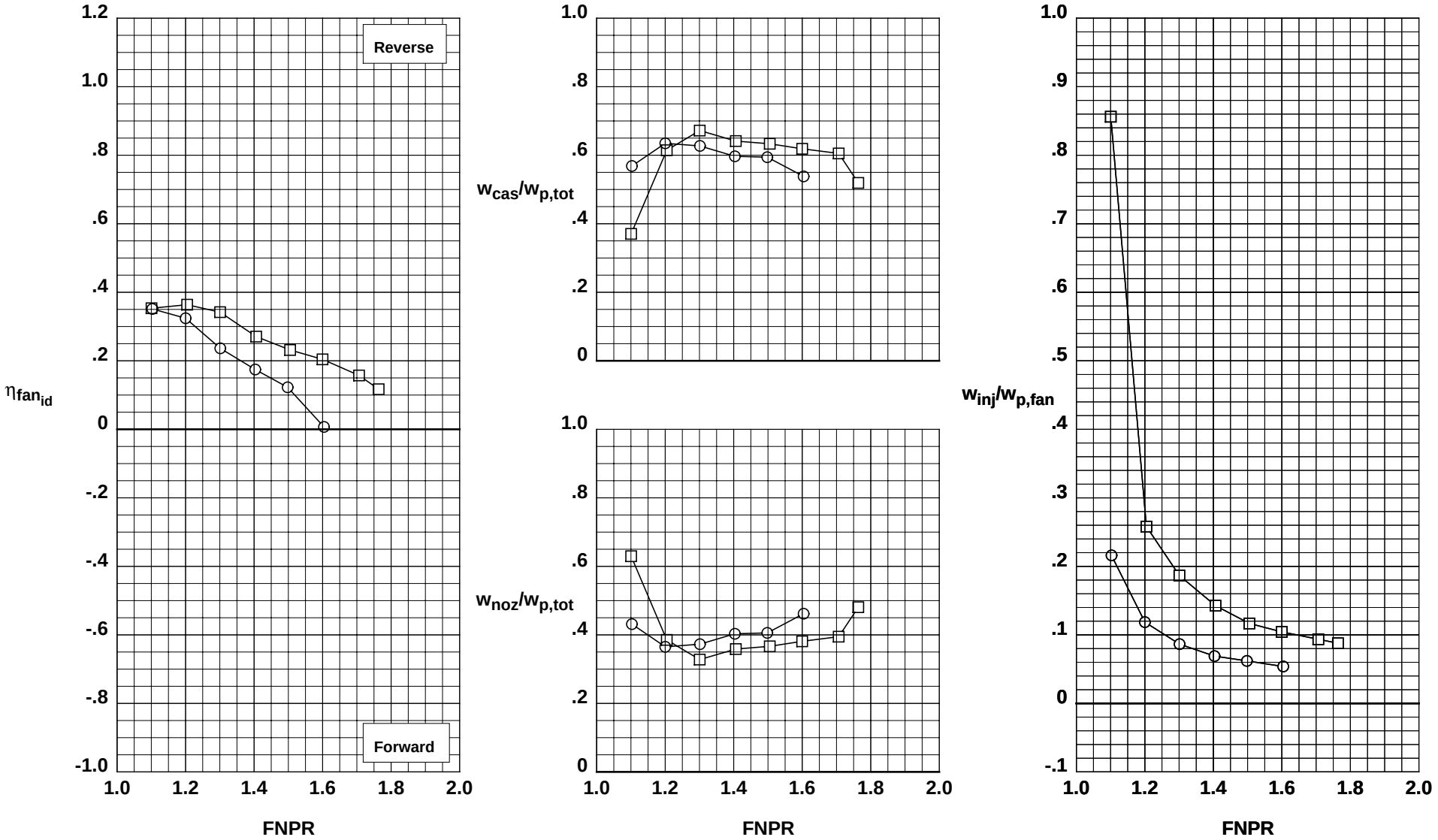

(c) Effects of slot size w_s.

Figure 24. Continued.

	Test	Run	Configuration	IPR	Injection Location	w_s, in.	θ, deg
○	993	7	603	12.04	Fwd/Mid/Aft	0.013	45
□	993	13	606	12.05	Fwd/Mid/Aft	0.013	90

Operation Mode: Fan + Injection
Cascades: Installed
Fwd Bullnose: Bullnose
Port Fairing: #2
Bifurcator: Removed
Wing: Removed

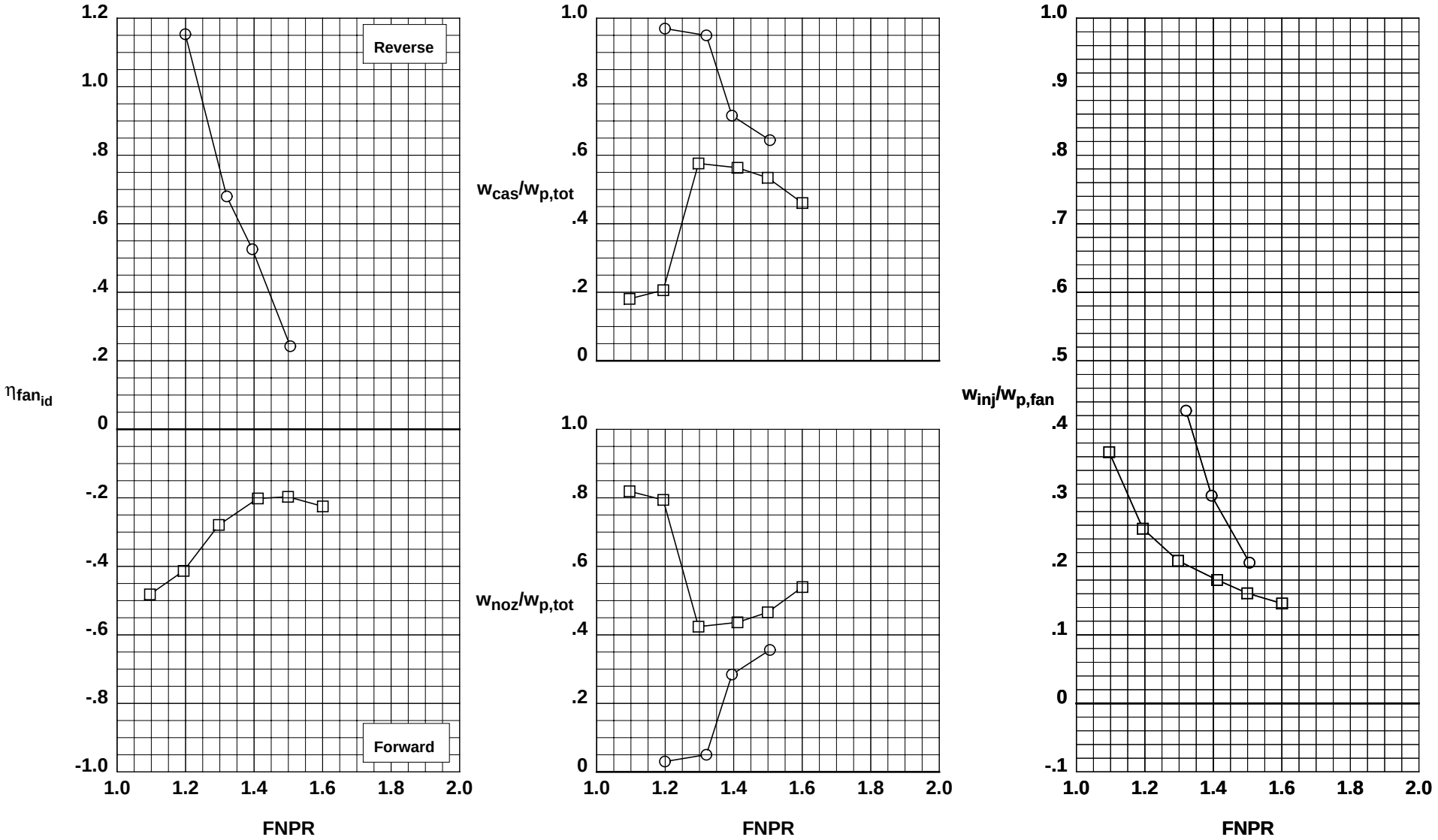

(d) Effects of slot angle θ.

Figure 24. Continued.

	Test	Run	Configuration	IPR	Injection Location	w_s, in.	θ, deg	Tab
○	993	34	614	11.98	Aft	0.025	45	None
□	993	30	612	11.99	Aft	0.025	45	#1
◇	993	28	611	12.01	Aft	0.025	45	#3

Operation Mode: Fan + Injection
Cascades: Installed
Fwd Bullnose: Bullnose
Port Fairing: #2
Bifurcator: Removed
Wing: Removed

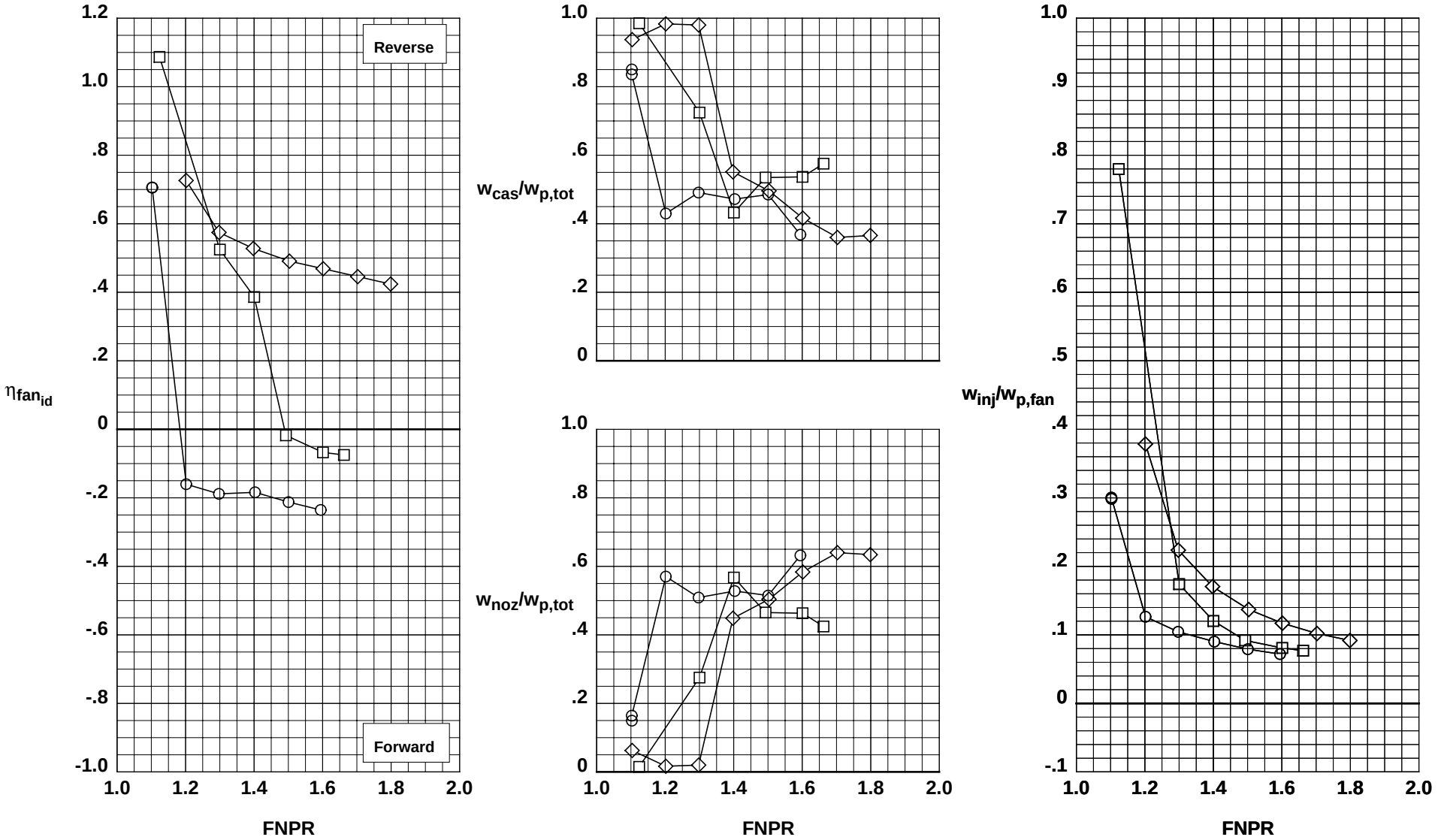

(e) Effects of injection tab.

Figure 24. Continued.

	Test	Run	Configuration	IPR	Injection Location	w_s, in.	θ, deg	Tab No.
○	993	27	611	0.00	Aft	0.025	45	None
□	993	28	611	3.99	Aft	0.025	45	#3
◇	993	28	611	8.00	Aft	0.025	45	#3
△	993	28	611	12.01	Aft	0.025	45	#3
◺	993	28	611	15.99	Aft	0.025	45	#3

Operation Mode: Fan+Injection
Cascades: Installed
Fwd Bullnose: Bullnose
Port Fairing: #2
Bifurcator: Removed
Wing: Removed

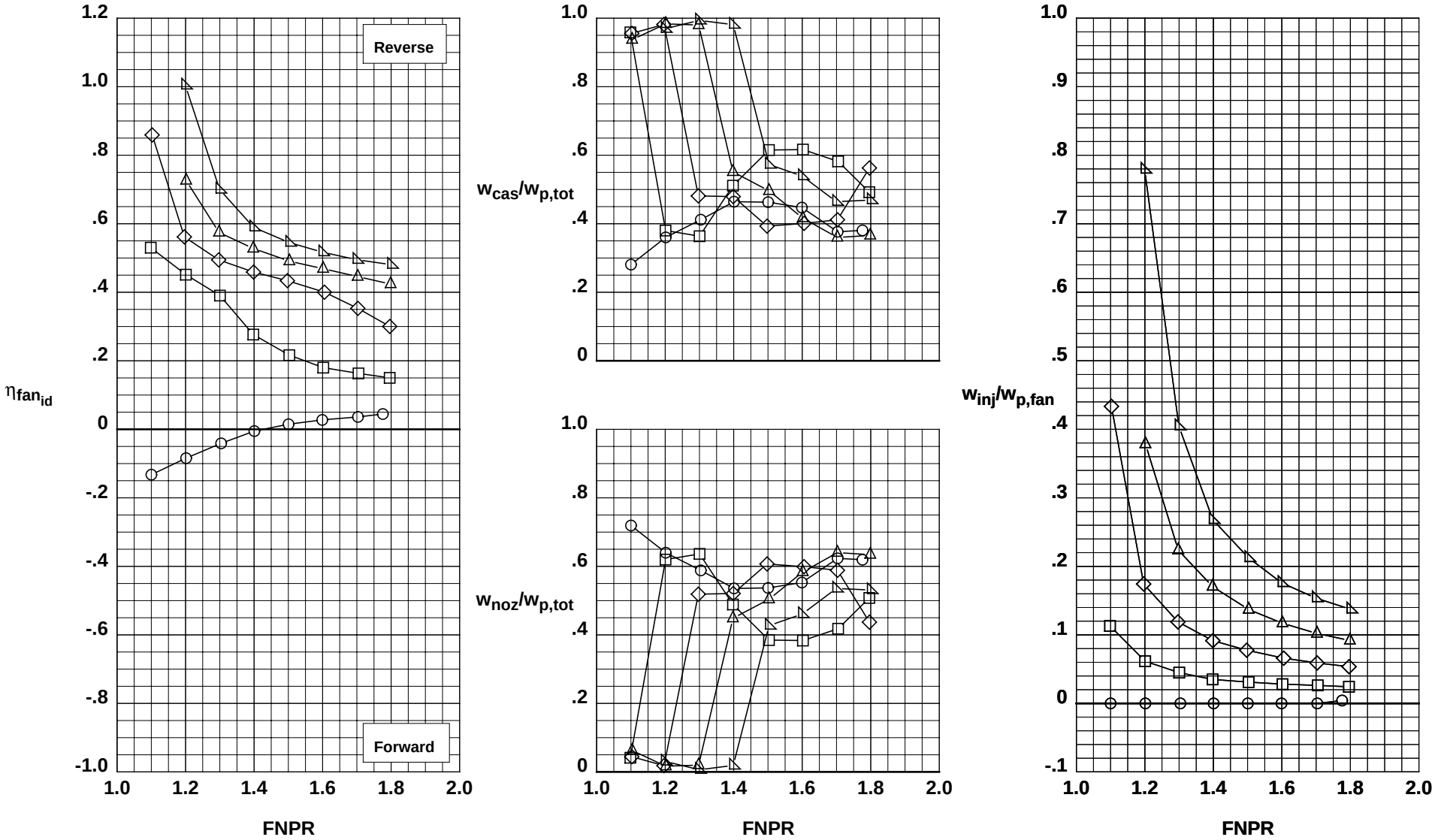

(f) Effects of IPR for configuration 611.

Figure 24. Concluded.

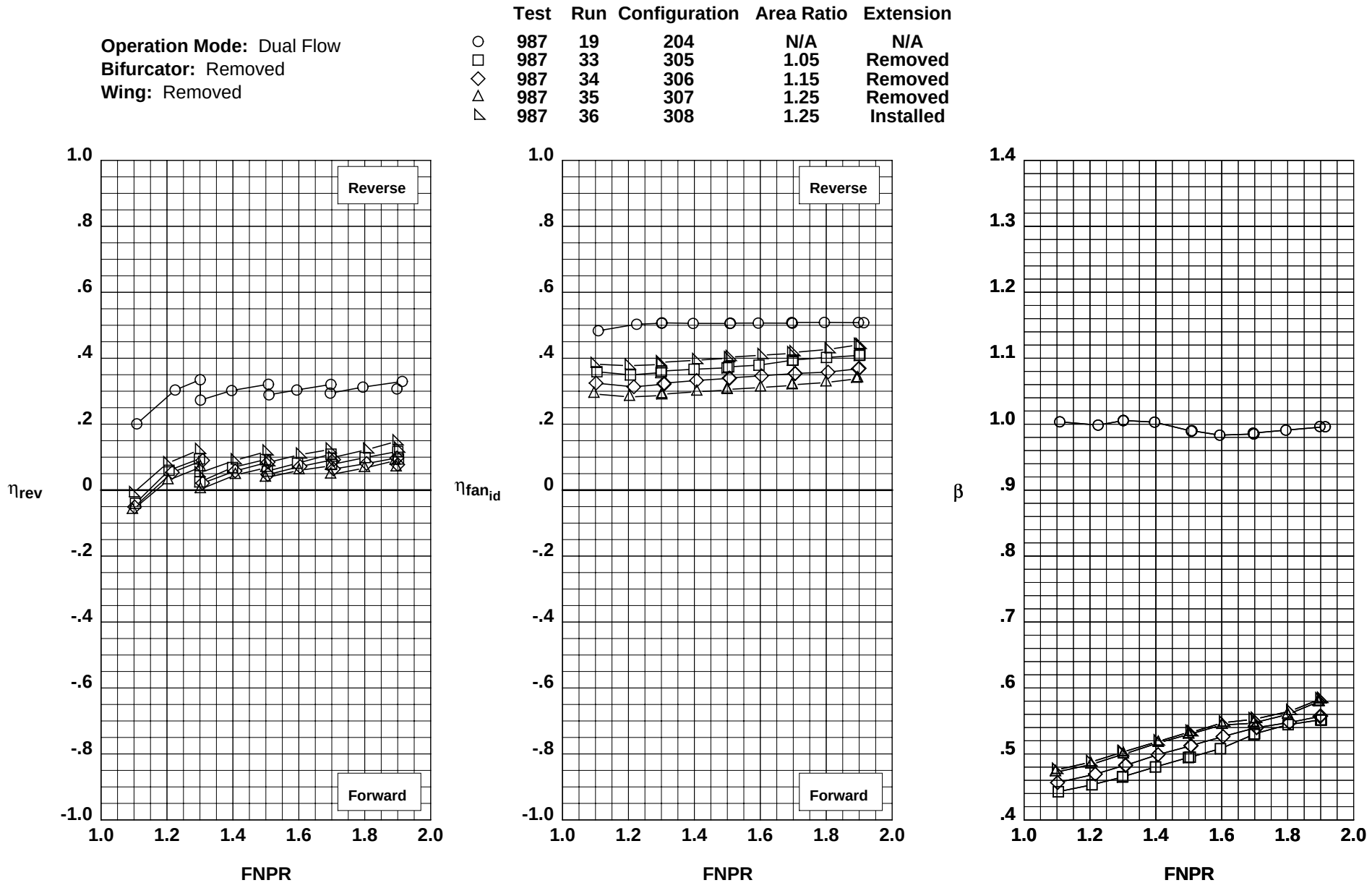

(a) Effect of area ratio for 40° target.

Figure 25. Summary of annular (metal) target thrust reverser performance.

Operation Mode: Dual Flow
Bifurcator: Removed
Wing: Removed

	Test	Run	Configuration	Area Ratio	Kicker
○	987	19	204	N/A	N/A
□	987	28	301	1.05	Removed
◇	987	30	302	1.15	Removed
△	987	31	303	1.25	Removed
◺	987	32	304	1.25	Installed

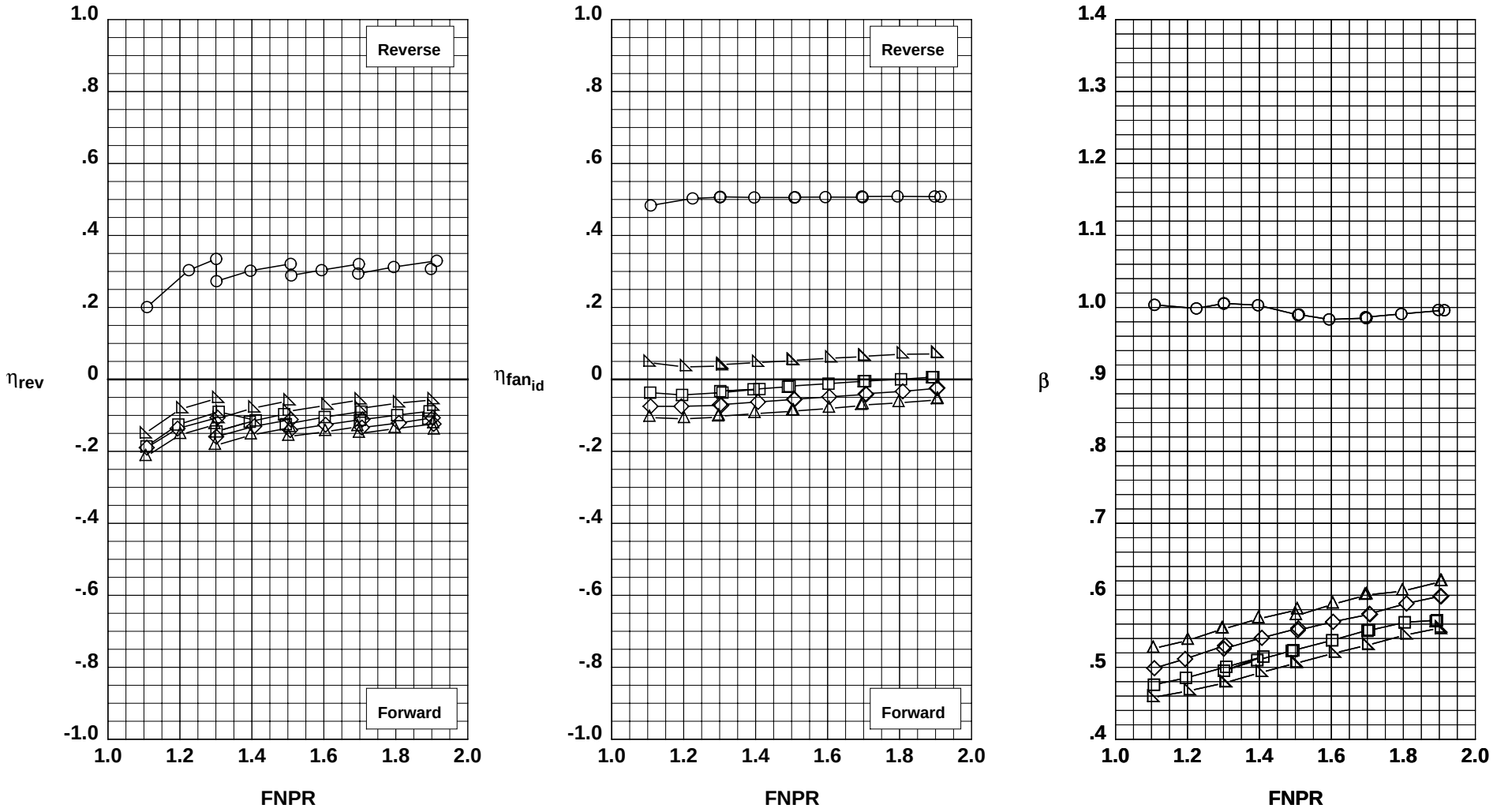

(b) Effect of area ratio for 20° target.

Figure 25. Concluded.

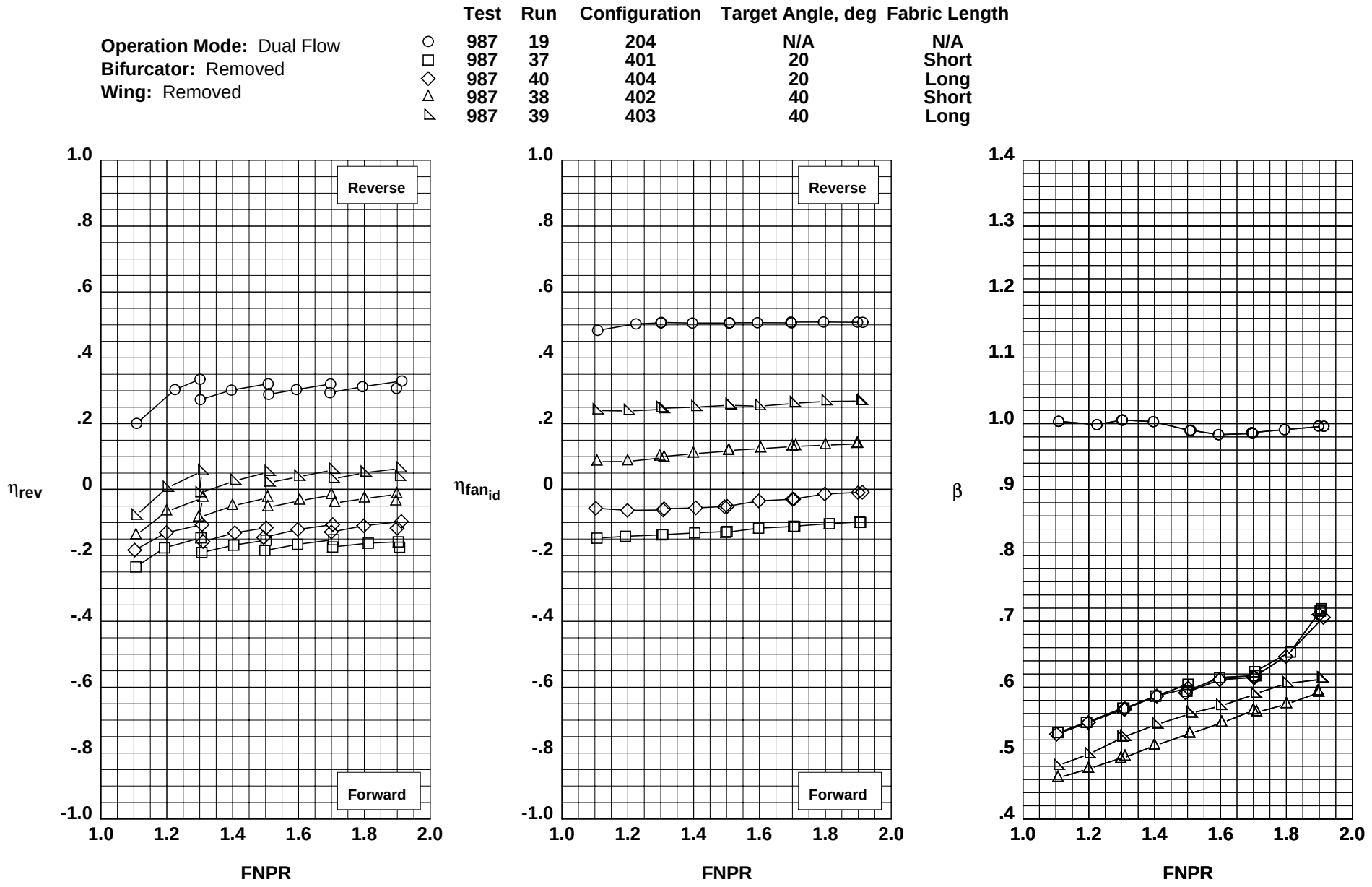

Figure 26. Summary of fabric target thrust reverser performance showing effects of target angle and fabric length.

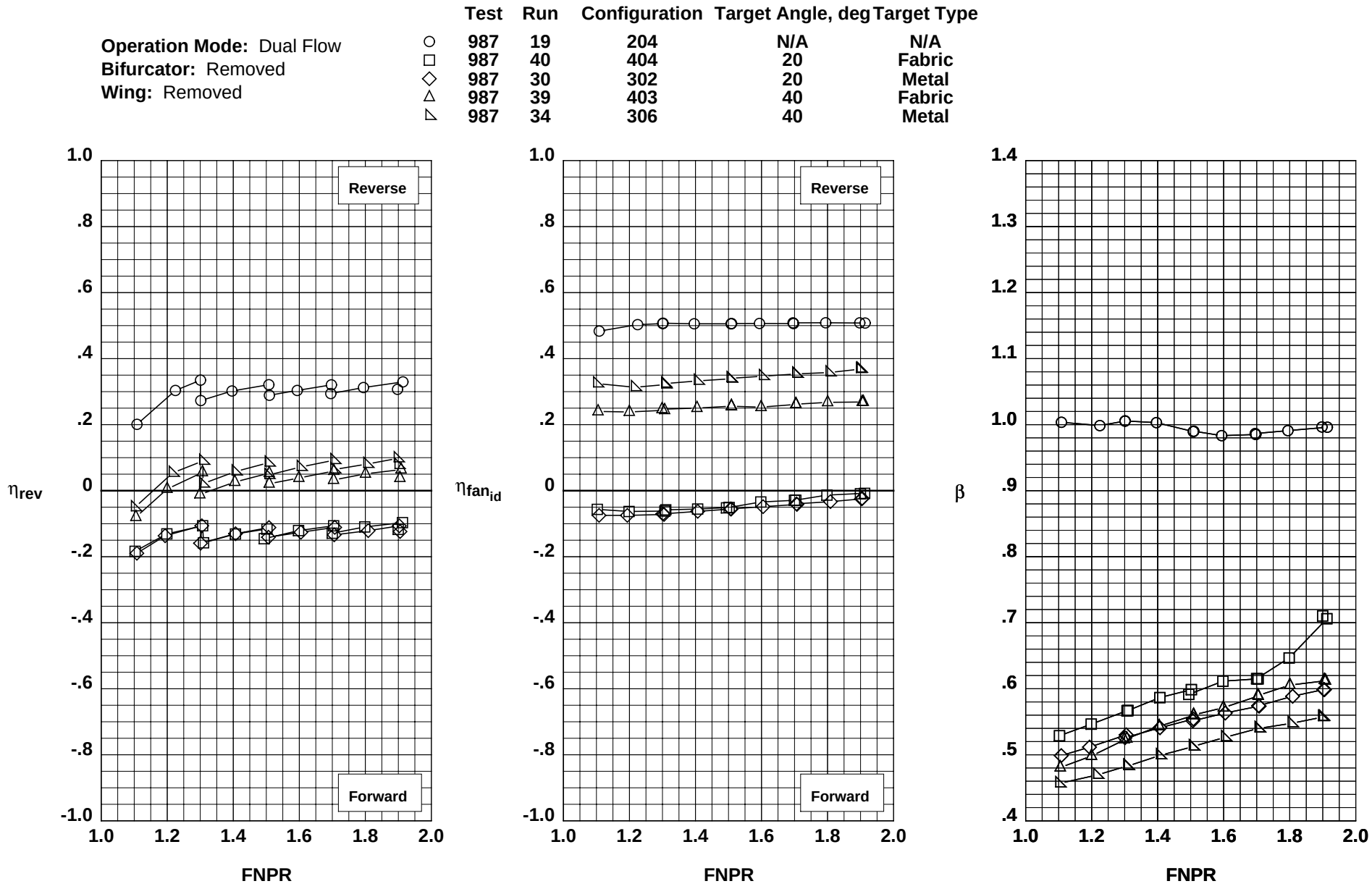

Figure 27. Comparison of annular (metal) and fabric target thrust reverser performance.

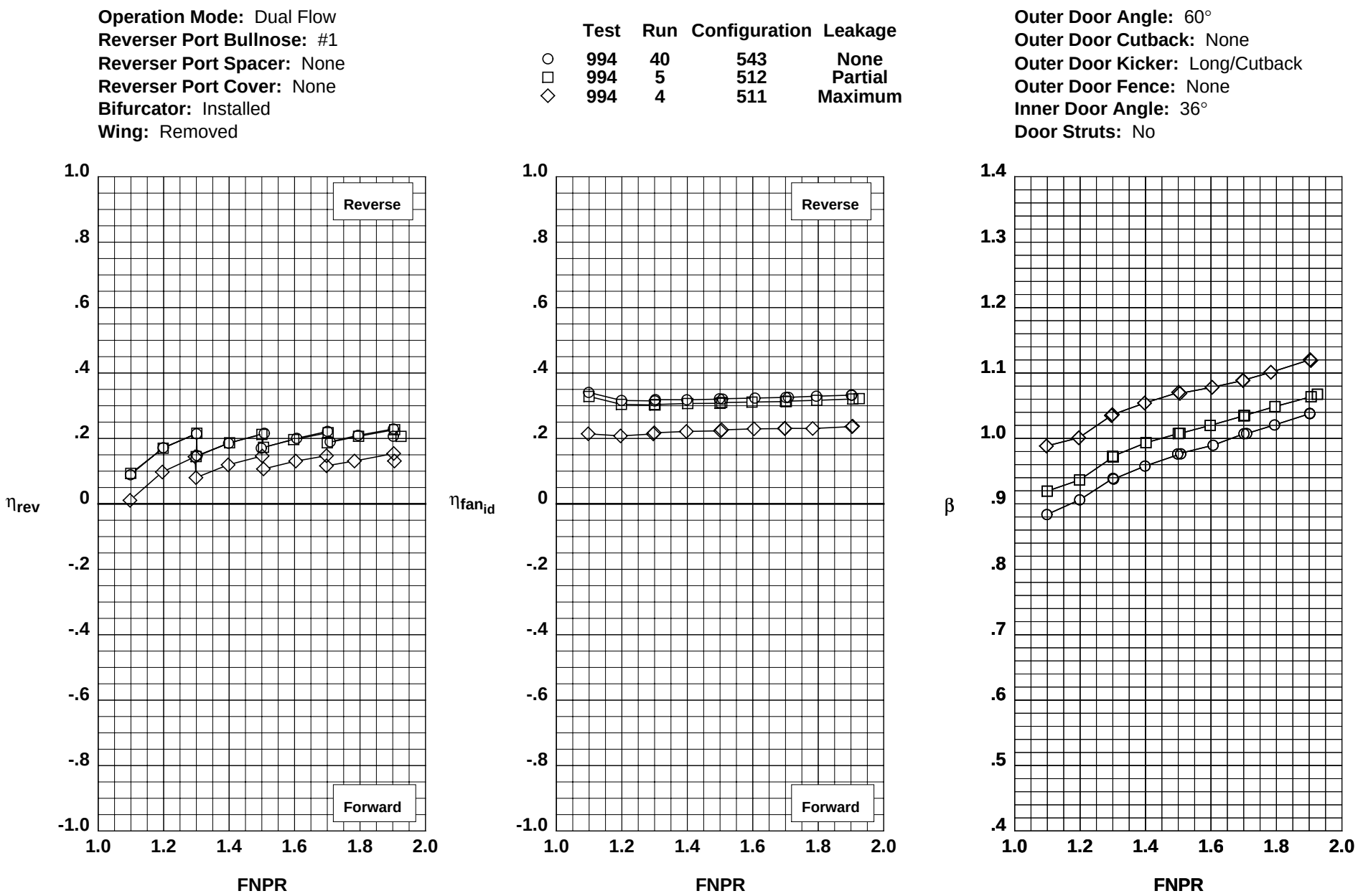

(a) Effects of inner door leakage.

Figure 28. Summary of multi-door crocodile thrust reverser performance characteristics.

Operation Mode: Dual Flow
Reverser Port Spacer: None
Reverser Port Cover: None
Bifurcator: Installed
Wing: Removed

	Test	Run	Configuration	Bullnose
○	994	5	512	#1
□	994	32	536	#2
◇	994	13	519	#3

Outer Door Angle: 60°
Outer Door Cutback: None
Outer Door Kicker: Long/Cutback
Outer Door Fence: None
Inner Door Angle: 36°
Inner Door Fillers All
Door Struts: No
Door Leakage: Partial

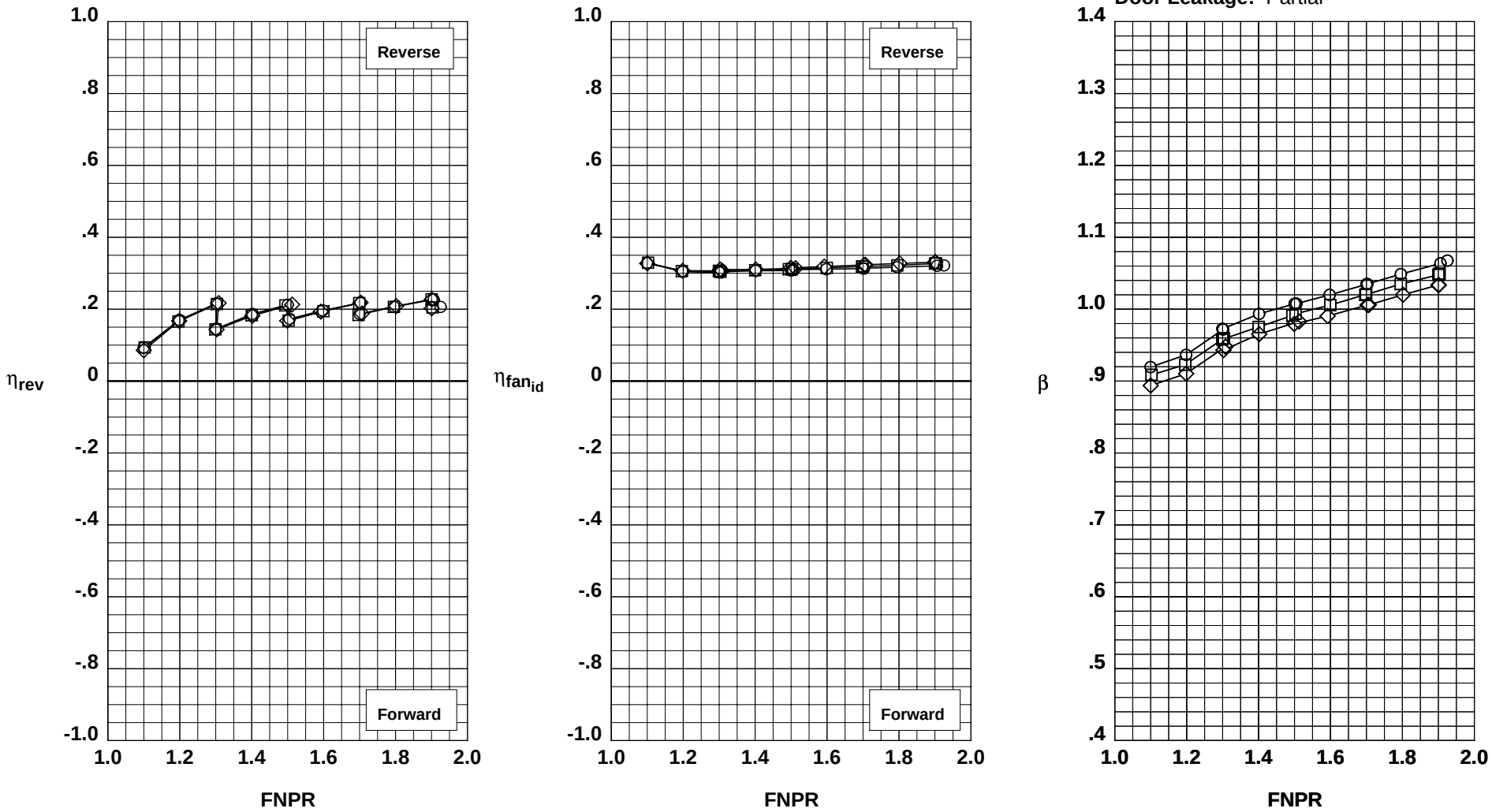

(b) Effects of reverser port bullnose radius.

Figure 28. Continued.

Operation Mode: Dual Flow
Reverser Port Bullnose: #3
Reverser Port Cover: None
Bifurcator: Installed
Wing: Removed

	Test	Run	Configuration	Spacer	AR
○	994	23	519	None	1.598
□	994	30	534	0.20"	1.526
◇	994	24	529	0.40"	1.451

Outer Door Angle: 60°
Outer Door Cutback: None
Outer Door Kicker: Long/Cutback
Outer Door Fence: None
Inner Door Angle: 36°
Inner Door Fillers All
Door Struts: No
Door Leakage: Partial

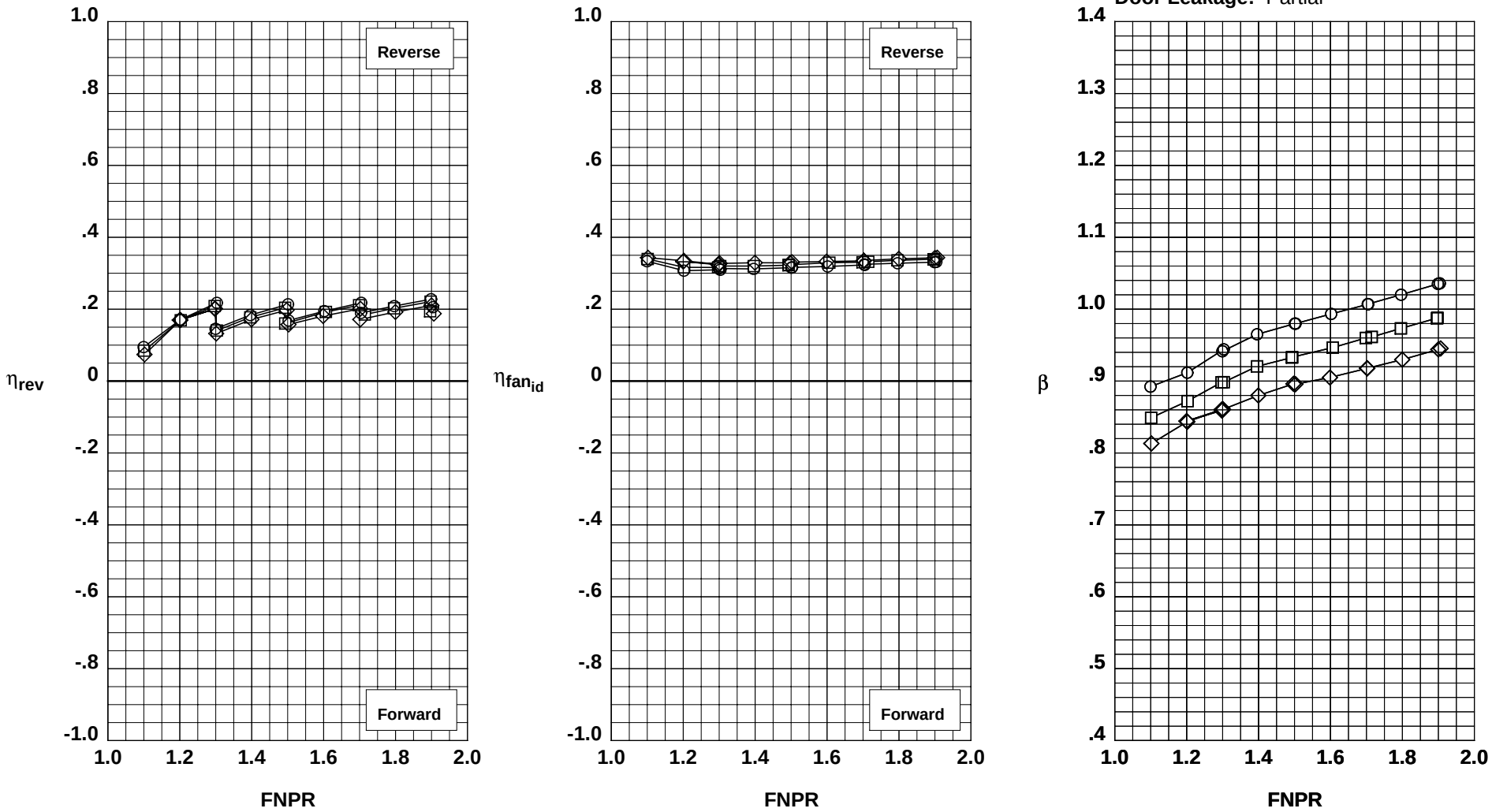

(c) Effects of reverser port area ratio.

Figure 28. Continued.

Operation Mode: Dual Flow
Reverser Port Bullnose: #3
Reverser Port Spacer: None
Reverser Port Cover: None
Bifurcator: Installed
Wing: Removed

	Test	Run	Configuration	Kicker Plate
○	994	12	518	None
□	994	11	517	Long/Cutback
◇	994	10	516	X-Long/Cutback

Outer Door Angle: 50°
Outer Door Cutback: None
Outer Door Fence: None
Inner Door Angle: 36°
Inner Door Fillers All
Door Struts: No
Door Leakage: Partial

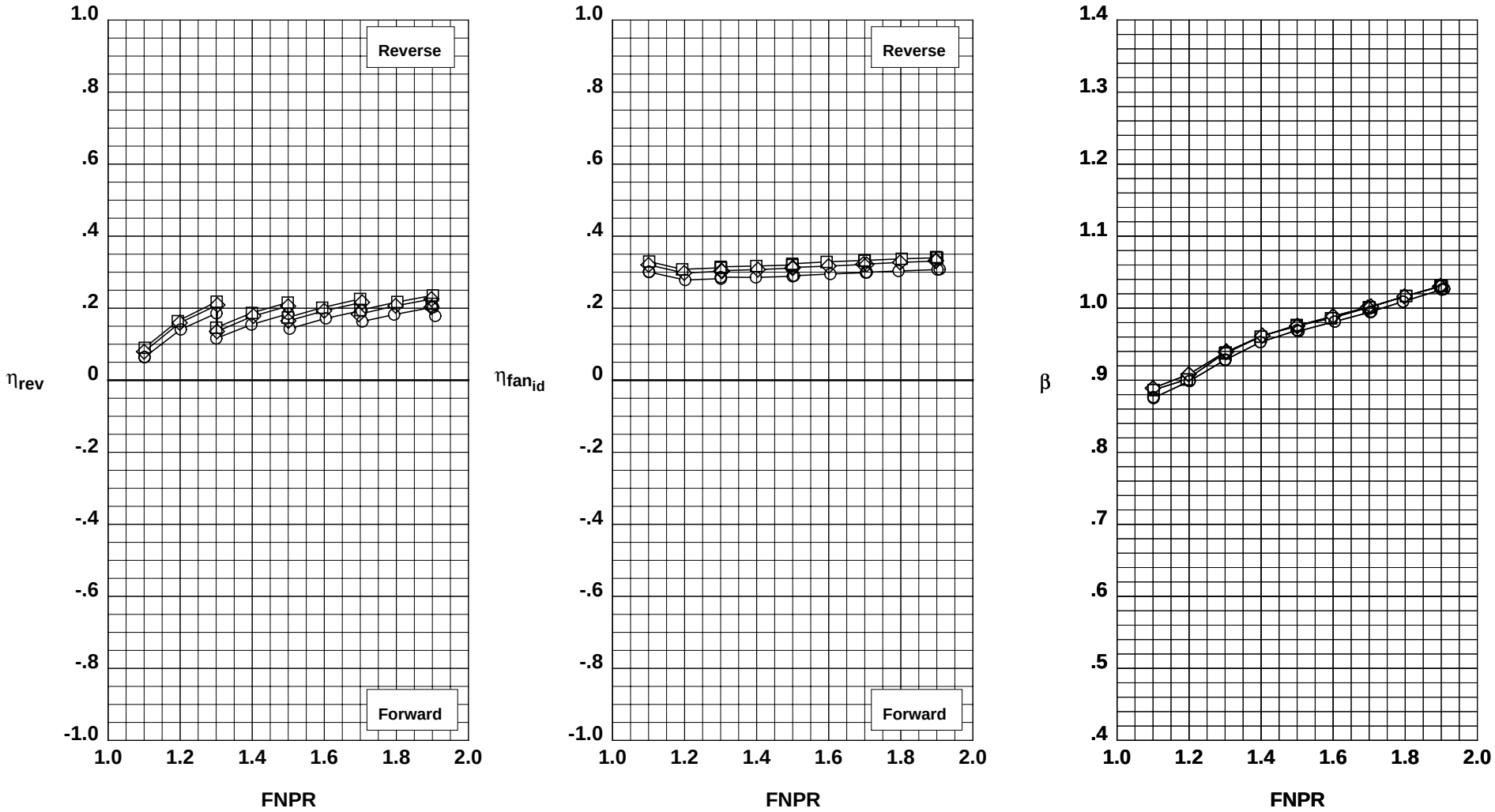

(d) Effects of outer door kicker plate.

Figure 28. Continued.

Operation Mode: Dual Flow
Reverser Port Bullnose: #3
Reverser Port Spacer: None
Bifurcator: Installed
Wing: Removed

	Test	Run	Configuration	Cutback	Cover
○	994	13	519	None	None
□	994	15	521	Partial	Partial
◇	994	16	522	Mixed	Mixed
△	994	17	523	Full	Full

Outer Door Angle: 60°
Outer Door Kicker: Long/Cutback
Outer Door Fence: None
Inner Door Angle: 36°
Inner Door Fillers All
Door Struts: No
Door Leakage: Partial

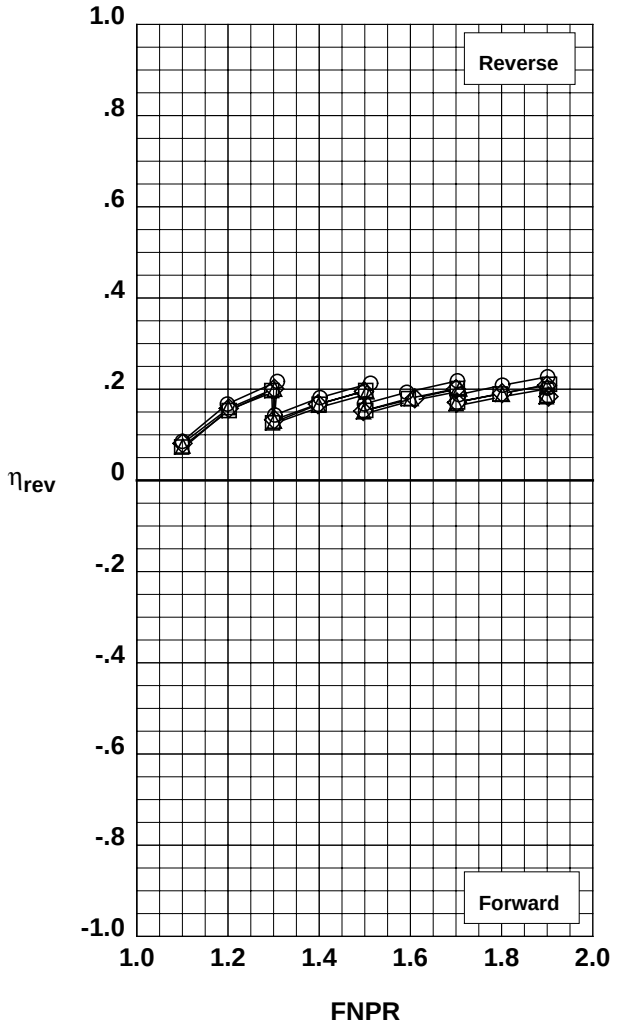

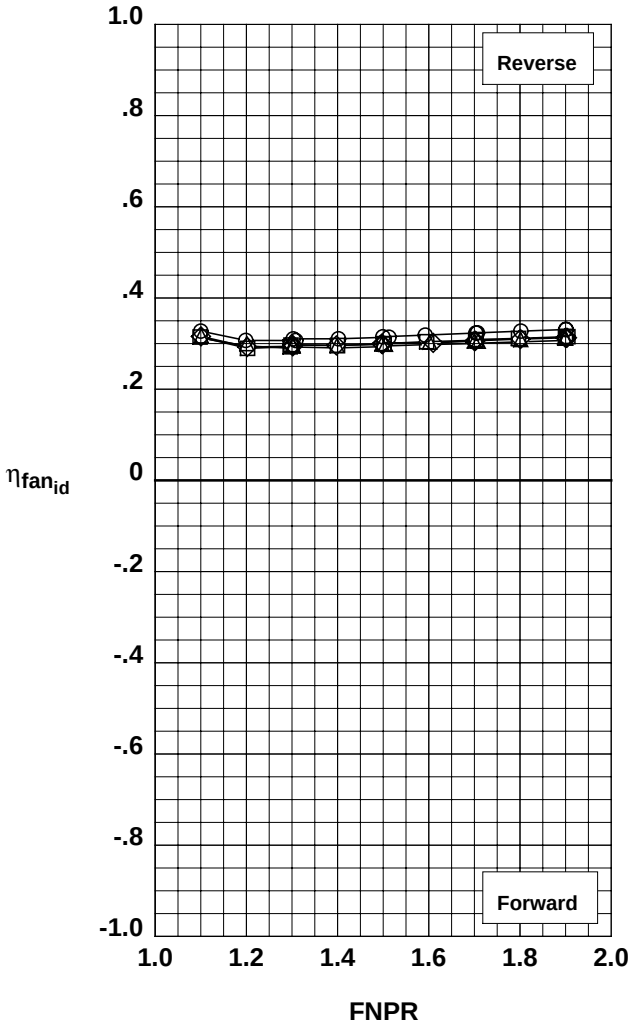

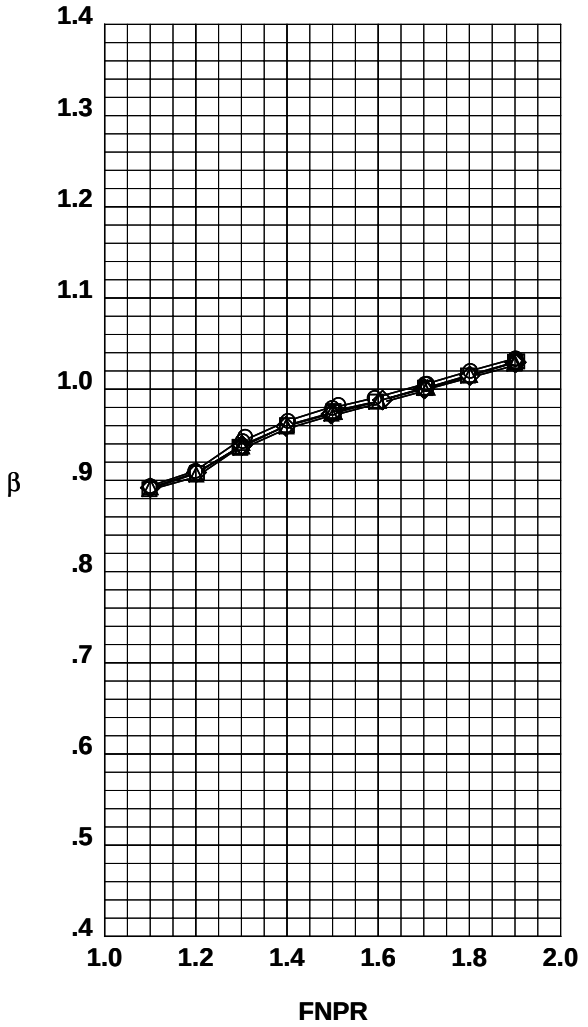

(e) Effects of outer door cutback.

Figure 28. Continued.

Operation Mode: Dual Flow
Reverser Port Bullnose: #3
Reverser Port Spacer: None
Reverser Port Cover: None
Bifurcator: Installed
Wing: Removed

	Test	Run	Configuration	Outer Door Angle, deg
○	1002	24	579	60
□	1002	42	578	50
◇	1002	43	577	40
△	1002	44	576	30
◺	1002	45	575	20
◺	1002	46	574	10

Outer Door Cutback: None
Outer Door Kicker: Long/Cutback
Outer Door Fence: None
Inner Door Angle: 36°
Inner Door Fillers All
Door Struts: No
Door Leakage: Partial

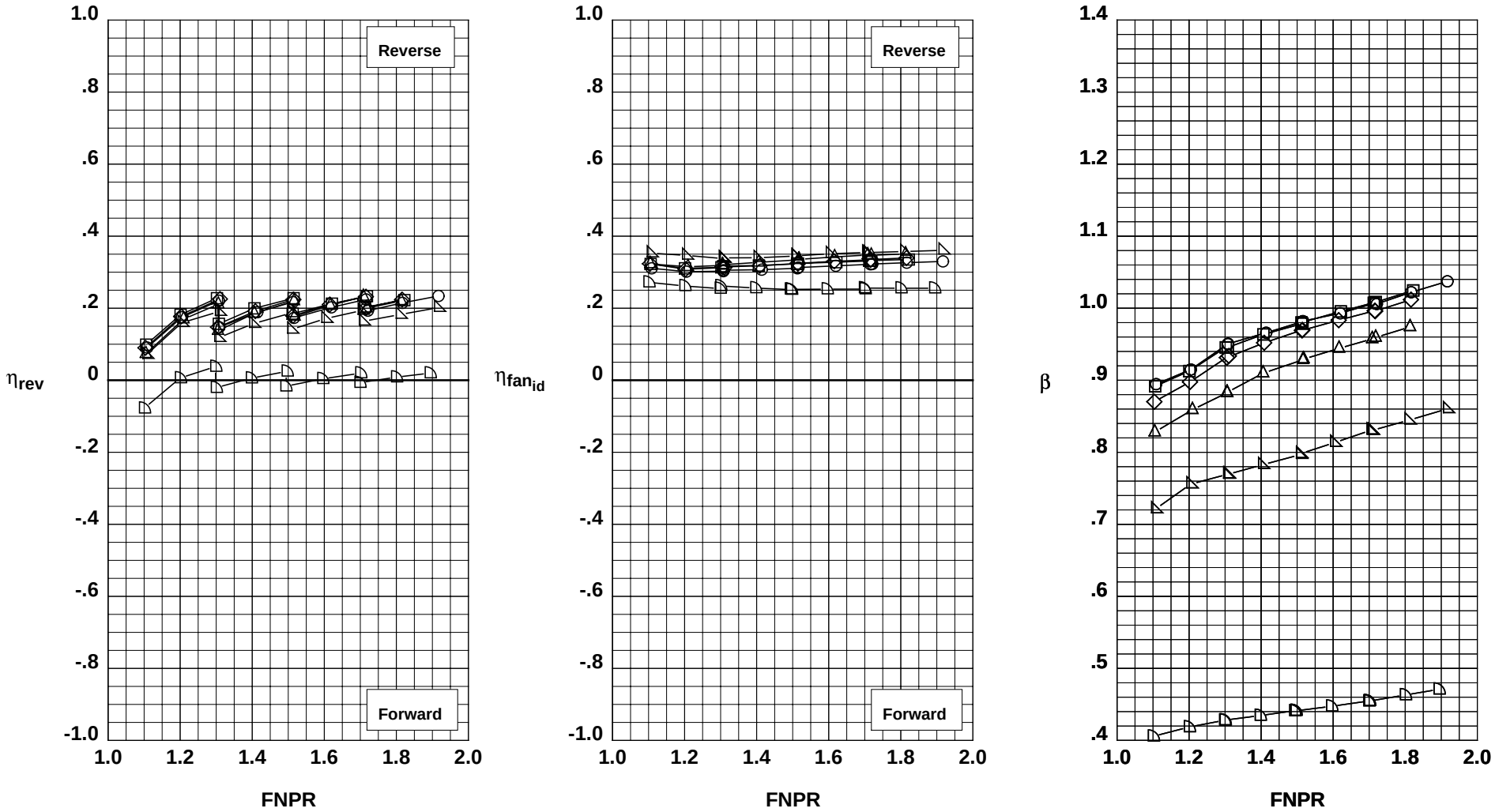

(f) Effects of outer door angle with full size outer doors.

Figure 28. Continued.

Operation Mode: Dual Flow
Reverser Port Bullnose: #3
Reverser Port Spacer: None
Reverser Port Cover: Full
Bifurcator: Installed
Wing: Removed

	Test	Run	Configuration	Outer Door Angle, deg
○	994	17	523	60
□	994	18	524	50
◇	994	22	528	40

Outer Door Cutback: Full
Outer Door Kicker: Long/Cutback
Outer Door Fence: None
Inner Door Angle: 36°
Inner Door Fillers All
Door Struts: No
Door Leakage: Partial

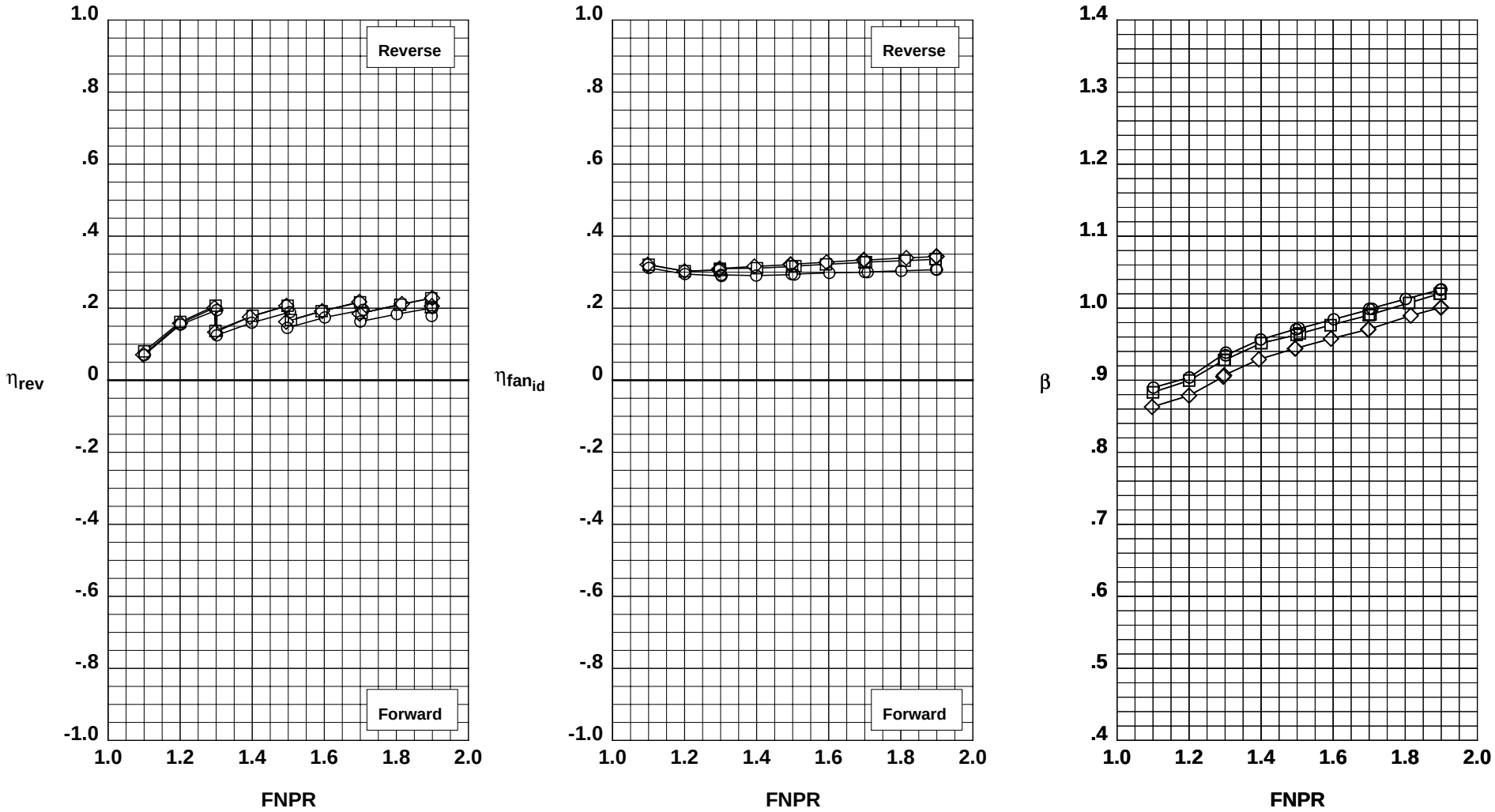

(g) Effects of outer door angle with full cutback outer doors.

Figure 28. Continued.

Operation Mode: Dual Flow
Reverser Port Bullnose: #3
Reverser Port Spacer: None
Reverser Port Cover: Mixed
Bifurcator: Installed
Wing: Removed

	Test	Run	Configuration	Inner/Outer Door Angle, deg
○	994	43	545	6/10
□	994	44	546	12/20
◇	994	36	540	18/30
△	994	35	539	24/40
◺	994	34	538	30/50
◺	994	16	522	36/60

Outer Door Cutback: Mixed
Outer Door Kicker: Long/Cutback
Outer Door Fence: None
Inner Door Fillers All
Door Struts: No
Door Leakage: Partial

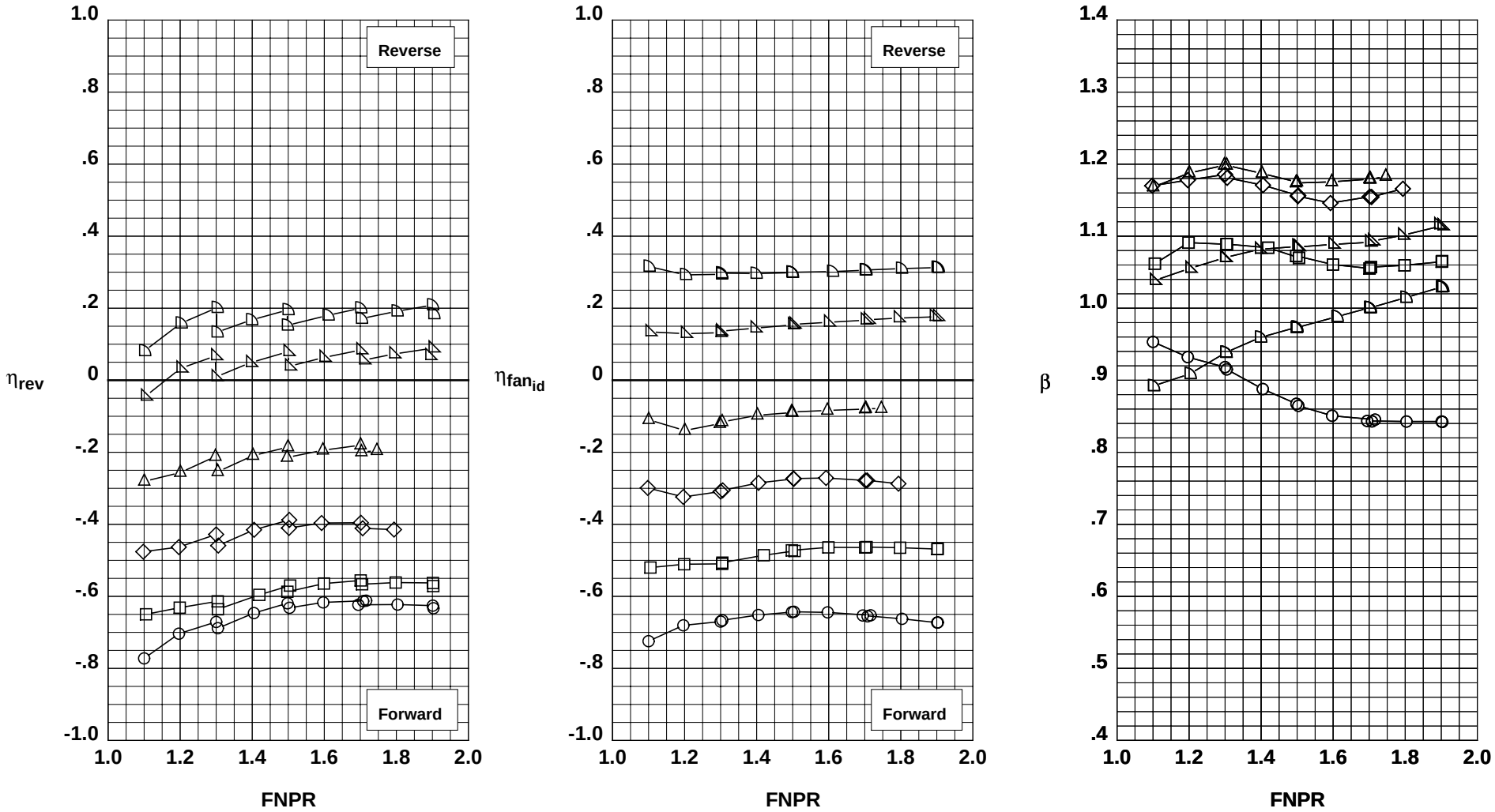

(h) Effects of inner and outer door deployment schedule.

Figure 28. Concluded.

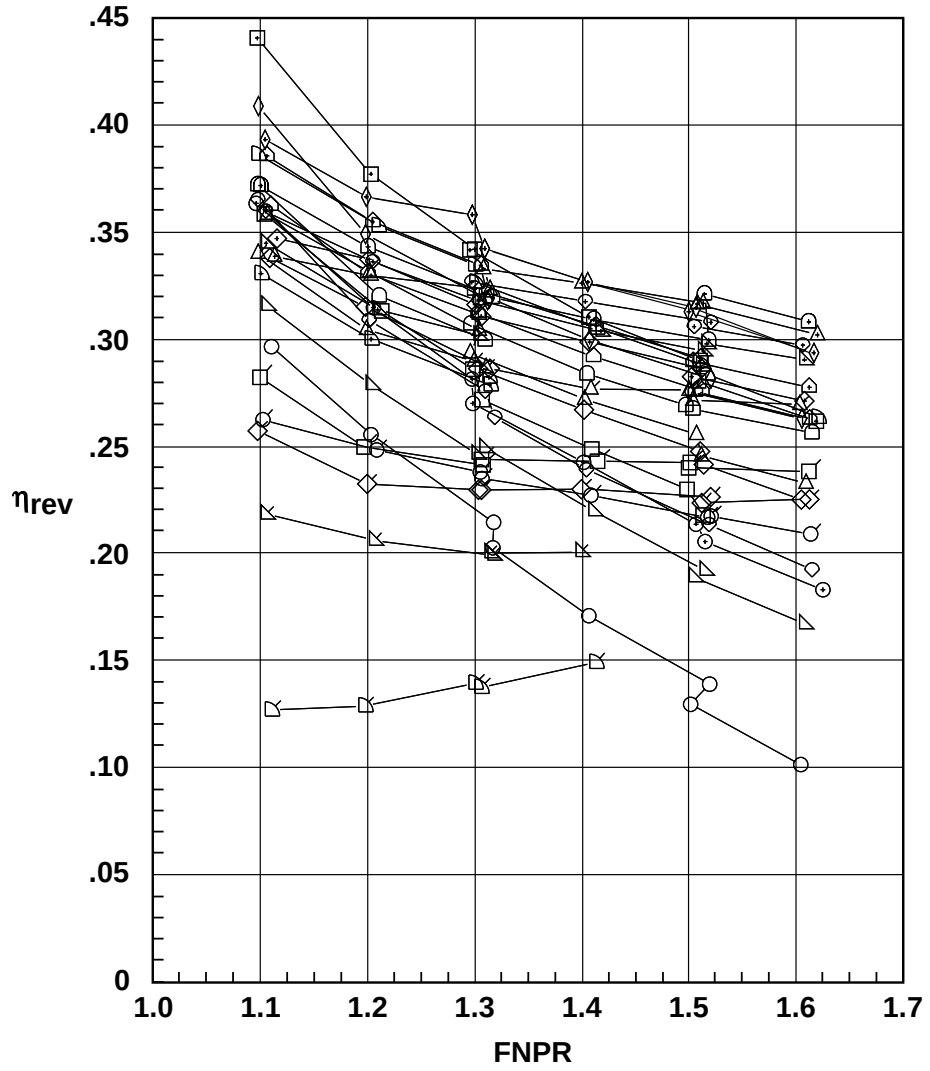

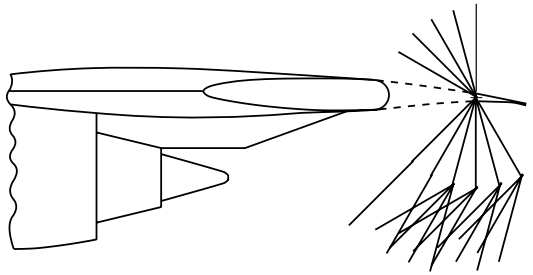

Test	Run	Configuration	ψ_1, deg	ψ_2, deg	ψ_3, deg
1001	47	701	45	-30	15
1001	48	702	45	-30	30
1001	49	703	45	-30	45
1001	50	704	60	-30	45
1001	46	705	30	-15	15
1001	38	706	30	-15	30
1001	45	707	30	-15	45
1001	42	708	45	-15	15
1001	43	709	45	-15	30
1001	44	710	45	-15	45
1001	41	711	60	-15	15
1001	39	712	60	-15	30
1001	40	713	60	-15	45
1001	31	714	30	0	30
1001	32	715	30	0	45
1001	33	716	30	0	60
1001	35	717	45	0	30
1001	34	718	45	0	45
1001	36	719	60	0	30
1001	37	720	60	0	45
1001	28	721	15	15	15
1001	26	722	15	15	30
1001	27	723	15	15	45
1001	25	724	30	15	30
1001	30	729	15	30	30
1001	29	730	15	45	45

Figure 29. Summary of overall reverser effectiveness for wing-mounted thrust reverser configurations with parallel deflector mount angle, long deflector chord length, and deflector edge fences installed.

Operation Mode: Dual Flow
Deflector Mount Position: Parallel
Deflector Chord Lengths: Long/Long/Long
Deflector Fences: Installed
Bifurcator: Removed
Wing: Installed
Ground Plane: Removed

	Test	Run	Configuration	ψ_1, deg	ψ_2, deg	ψ_3, deg
○	1001	38	706	30	-15	30
□	1001	43	709	45	-15	30
◇	1001	39	712	60	-15	30

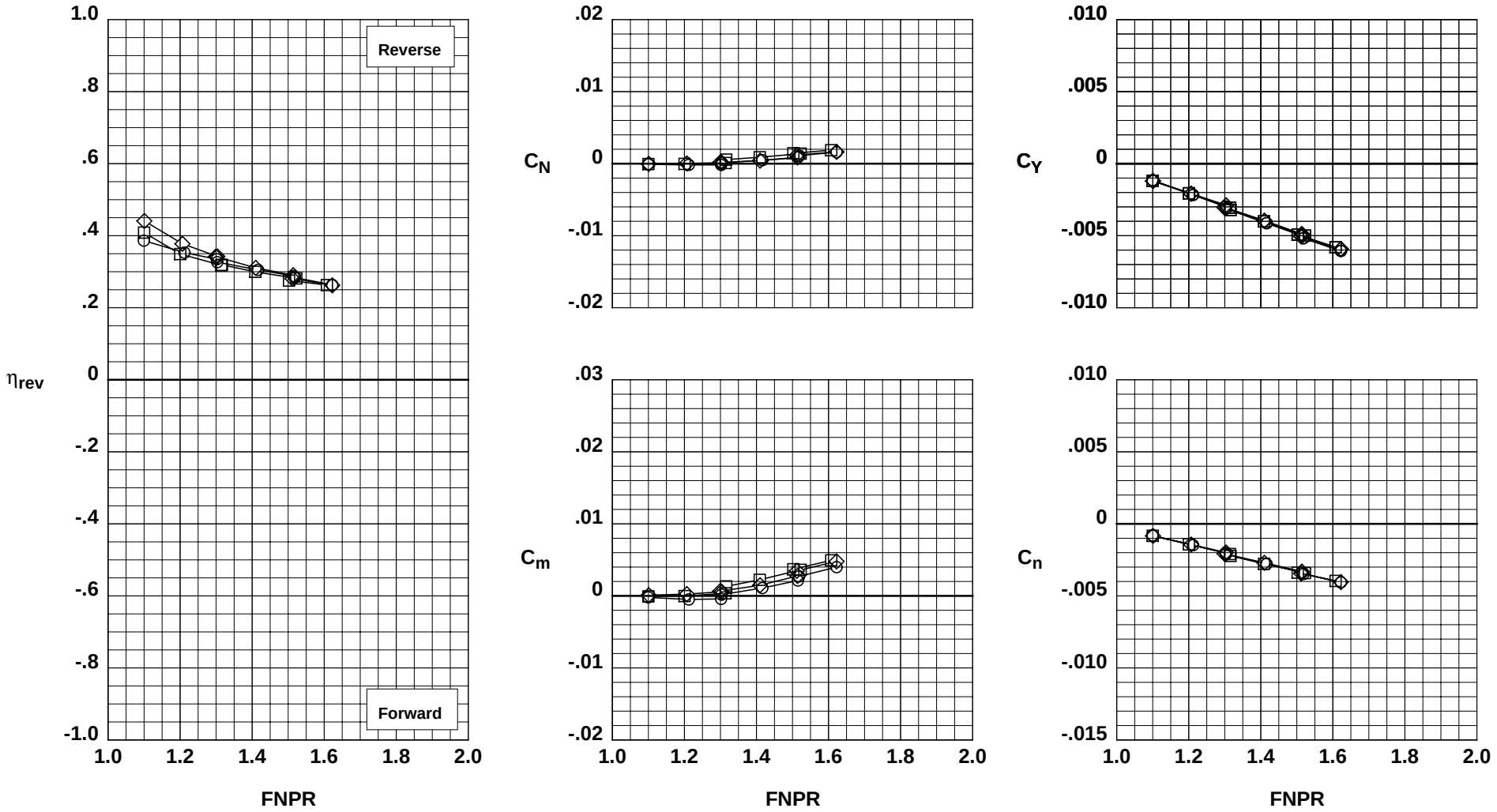

(a) ψ_2 = -15°.

Figure 30. Effects of deflector 1 angle ψ_1 for wing-mounted thrust reverser configurations with parallel deflector mount angle, long deflector chord length, and deflector edge fences installed; ψ_3 = 30°.

Operation Mode: Dual Flow
Deflector Mount Position: Parallel
Deflector Chord Lengths: Long/Long/Long
Deflector Fences: Installed
Bifurcator: Removed
Wing: Installed
Ground Plane: Removed

	Test	Run	Configuration	ψ_1, deg	ψ_2, deg	ψ_3, deg
○	1001	31	714	30	0	30
□	1001	35	717	45	0	30
◇	1001	36	719	60	0	30

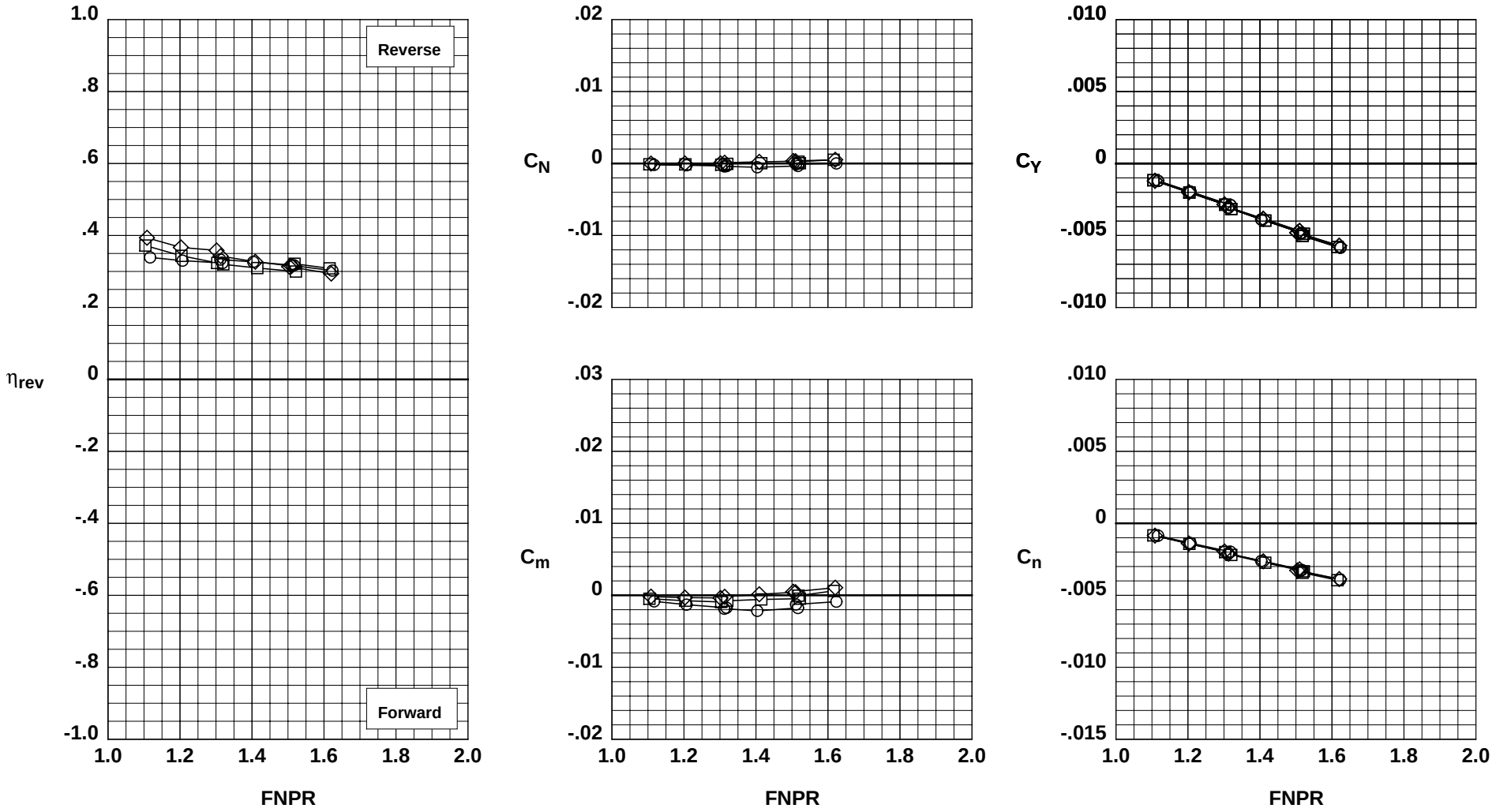

(b) $\psi_2 = 0°$.

Figure 30. Concluded.

Operation Mode: Dual Flow
Deflector Mount Position: Parallel
Deflector Chord Lengths: Long/Long/Long
Deflector Fences: Installed
Bifurcator: Removed
Wing: Installed
Ground Plane: Removed

	Test	Run	Configuration	ψ_1, deg	ψ_2, deg	ψ_3, deg
○	1001	48	702	45	-30	30
□	1001	43	709	45	-15	30
◇	1001	35	717	45	0	30

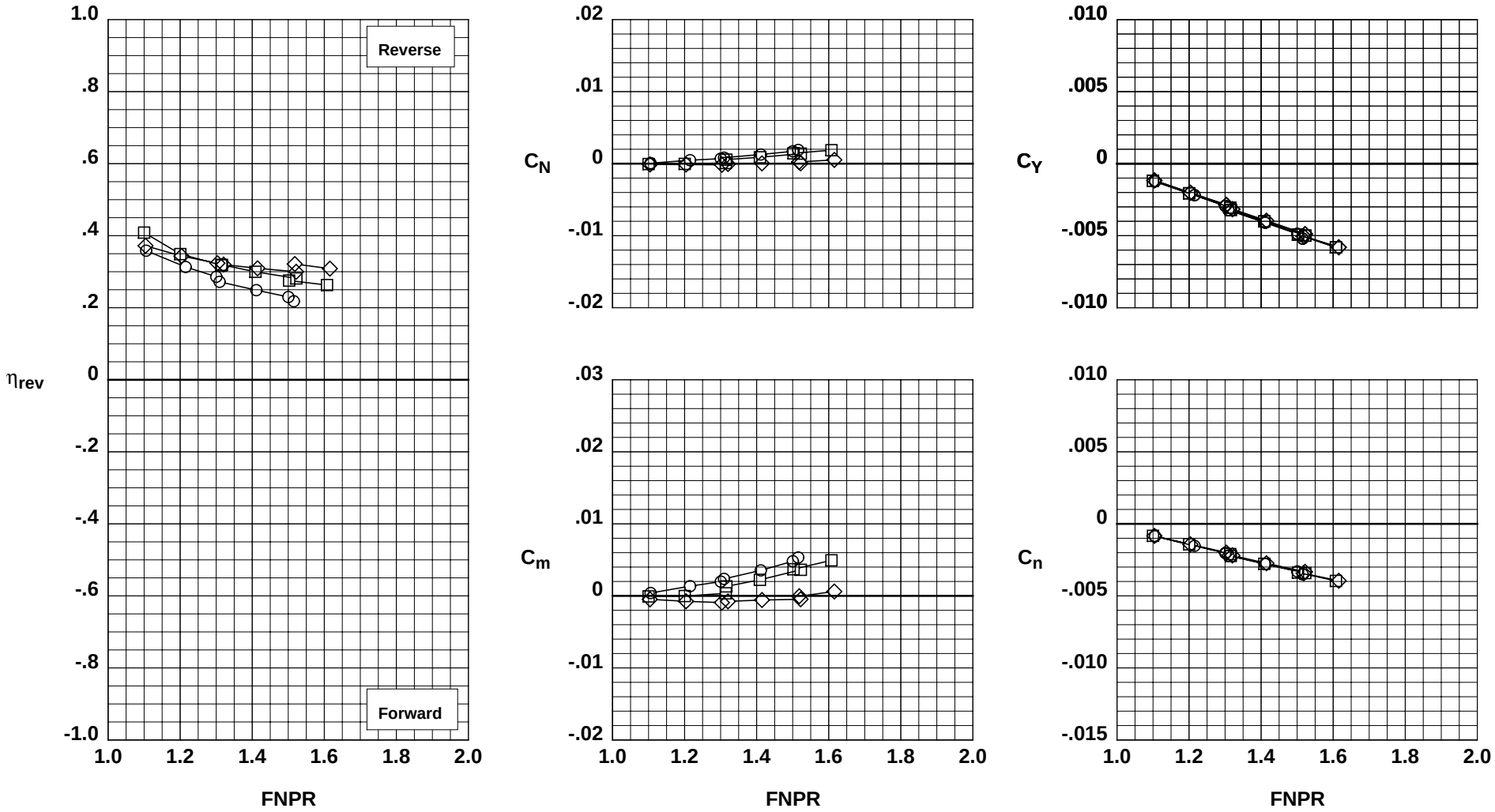

(a) $\psi_3 = 30°$.

Figure 31. Effects of deflector 2 angle ψ_2 for wing-mounted thrust reverser configurations with parallel deflector mount angle, long deflector chord length, and deflector edge fences installed; $\psi_1 = 45°$.

Operation Mode: Dual Flow
Deflector Mount Position: Parallel
Deflector Chord Lengths: Long/Long/Long
Deflector Fences: Installed
Bifurcator: Removed
Wing: Installed
Ground Plane: Removed

	Test	Run	Configuration	ψ_1, deg	ψ_2, deg	ψ_3, deg
○	1001	49	703	45	-30	45
□	1001	44	710	45	-15	45
◇	1001	34	718	45	0	45

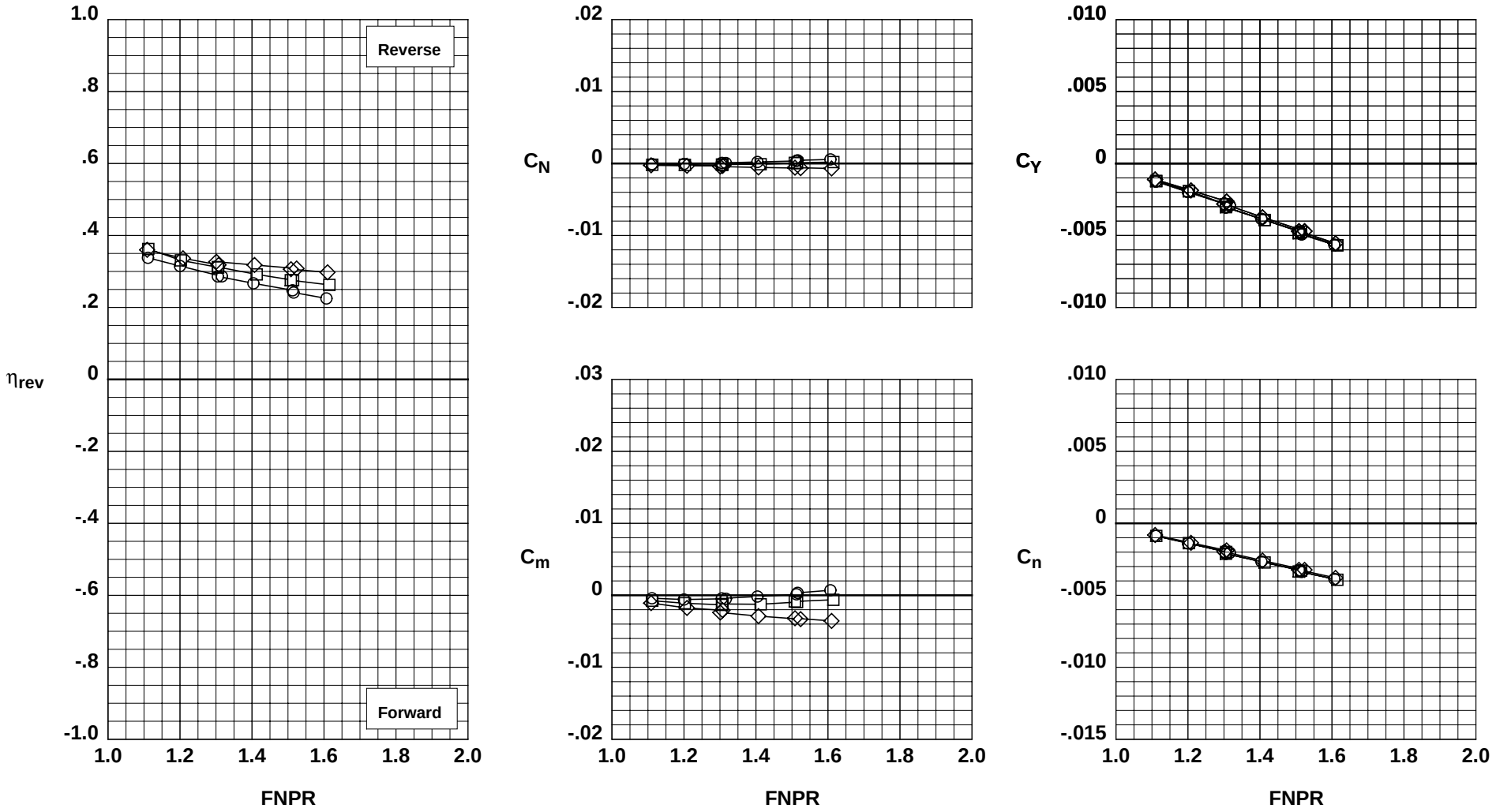

(b) $\psi_3 = 45°$.

Figure 31. Concluded.

Operation Mode: Dual Flow
Deflector Mount Position: Parallel
Deflector Chord Lengths: Long/Long/Long
Deflector Fences: Installed
Bifurcator: Removed
Wing: Installed
Ground Plane: Removed

	Test	Run	Configuration	ψ_1, deg	ψ_2, deg	ψ_3, deg
○	1001	41	711	60	-15	15
□	1001	39	712	60	-15	30
◇	1001	40	713	60	-15	45

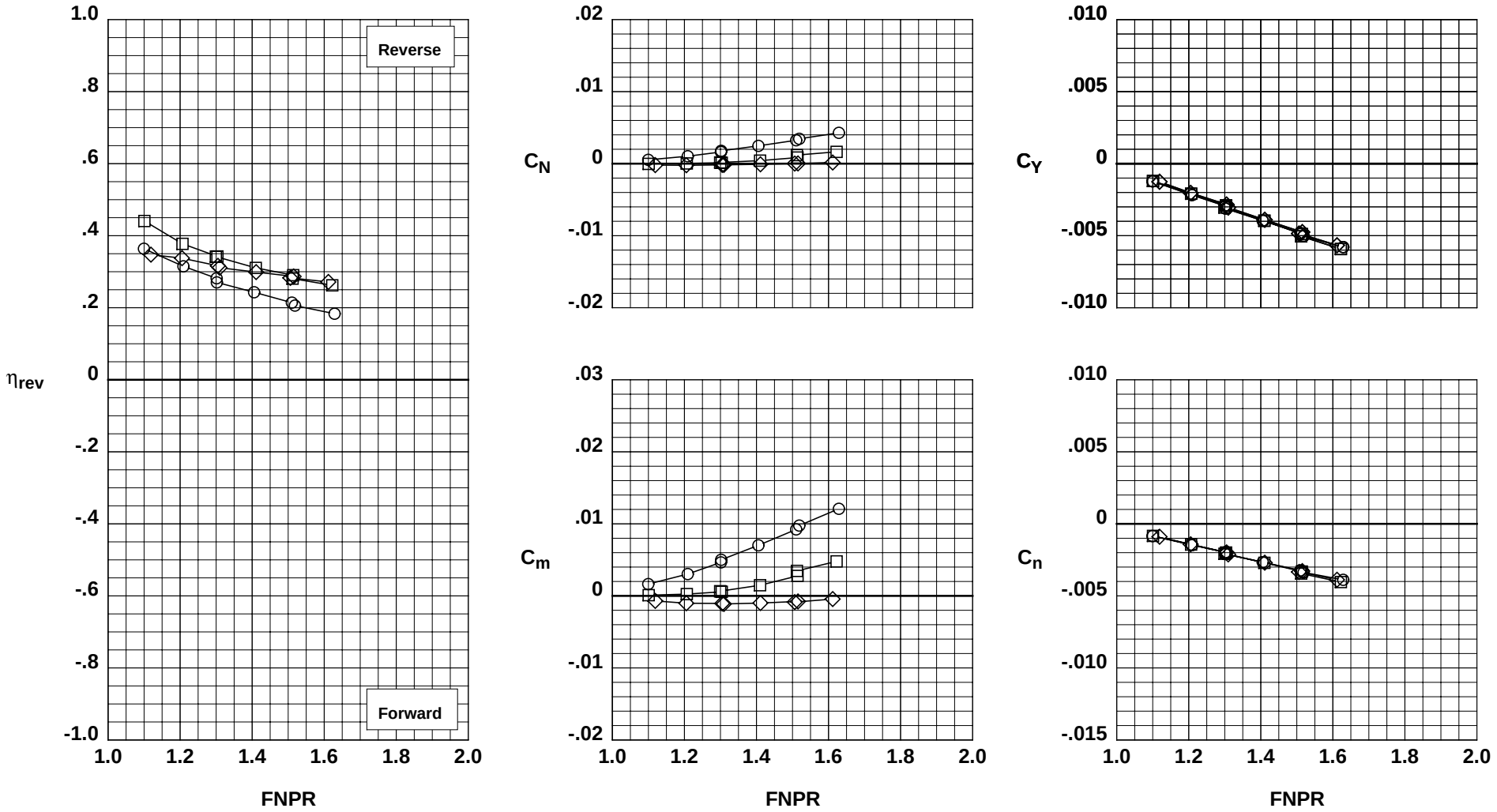

(a) ψ_2 = -15°.

Figure 32. Effects of deflector 3 angle ψ_3 for wing-mounted thrust reverser configurations with parallel deflector mount angle, long deflector chord length, and deflector edge fences installed; ψ_1 = 60°.

Operation Mode: Dual Flow
Deflector Mount Position: Parallel
Deflector Chord Lengths: Long/Long/Long
Deflector Fences: Installed
Bifurcator: Removed
Wing: Installed
Ground Plane: Removed

	Test	Run	Configuration	ψ_1, deg	ψ_2, deg	ψ_3, deg
○	1001	36	719	60	0	30
□	1001	37	720	60	0	45

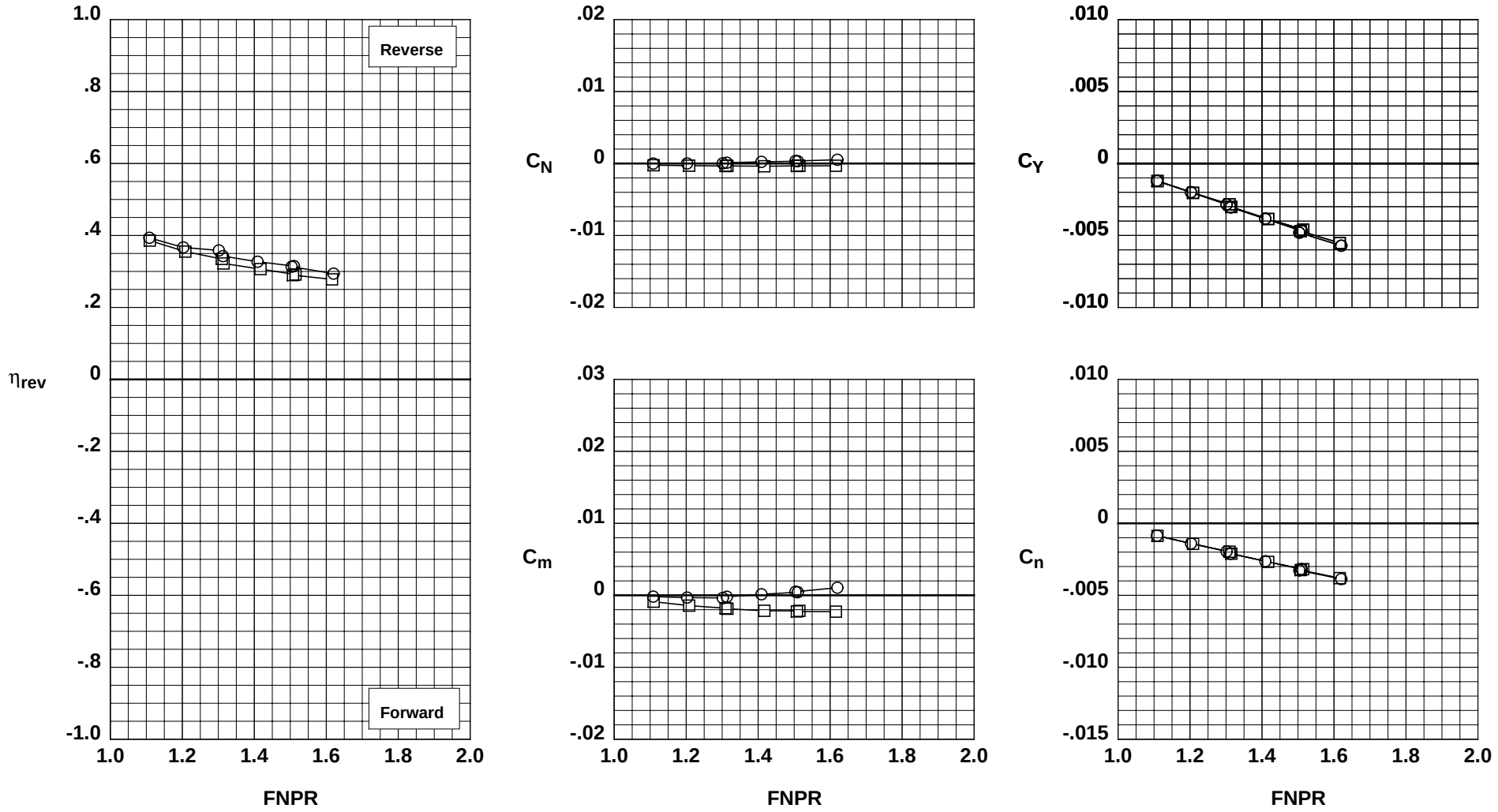

(b) $\psi_2 = 0°$.

Figure 32. Concluded.

Operation Mode: Dual Flow
Deflector Mount Position: Parallel
Deflector Chord Lengths: Long/Long/Long
Bifurcator: Removed
Wing: Installed
Ground Plane: Removed

	Test	Run	Configuration	Fences
○	1001	39	712	Installed
□	1001	58	734	Removed

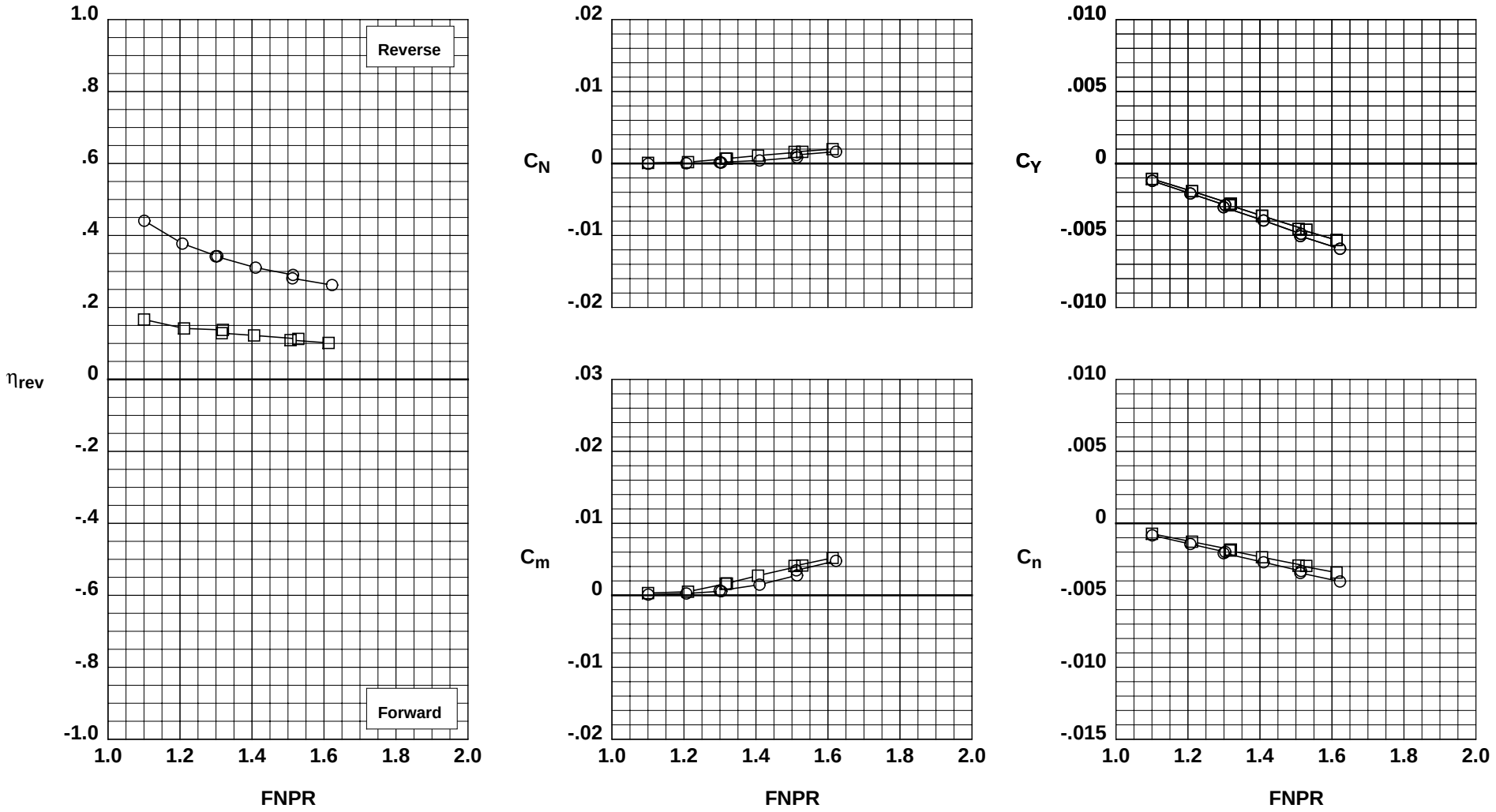

(a) ψ_2 = -15°.

Figure 33. Effects of deflector edge fences for wing-mounted thrust reverser configurations with parallel deflector mount angle and long deflector chord length; ψ_1 = 60° and ψ_3 = 30°.

Operation Mode: Dual Flow
Deflector Mount Position: Parallel
Deflector Chord Lengths: Long/Long/Long
Bifurcator: Removed
Wing: Installed
Ground Plane: Removed

	Test	Run	Configuration	Fences
○	1001	36	719	Installed
□	1001	57	733	Removed

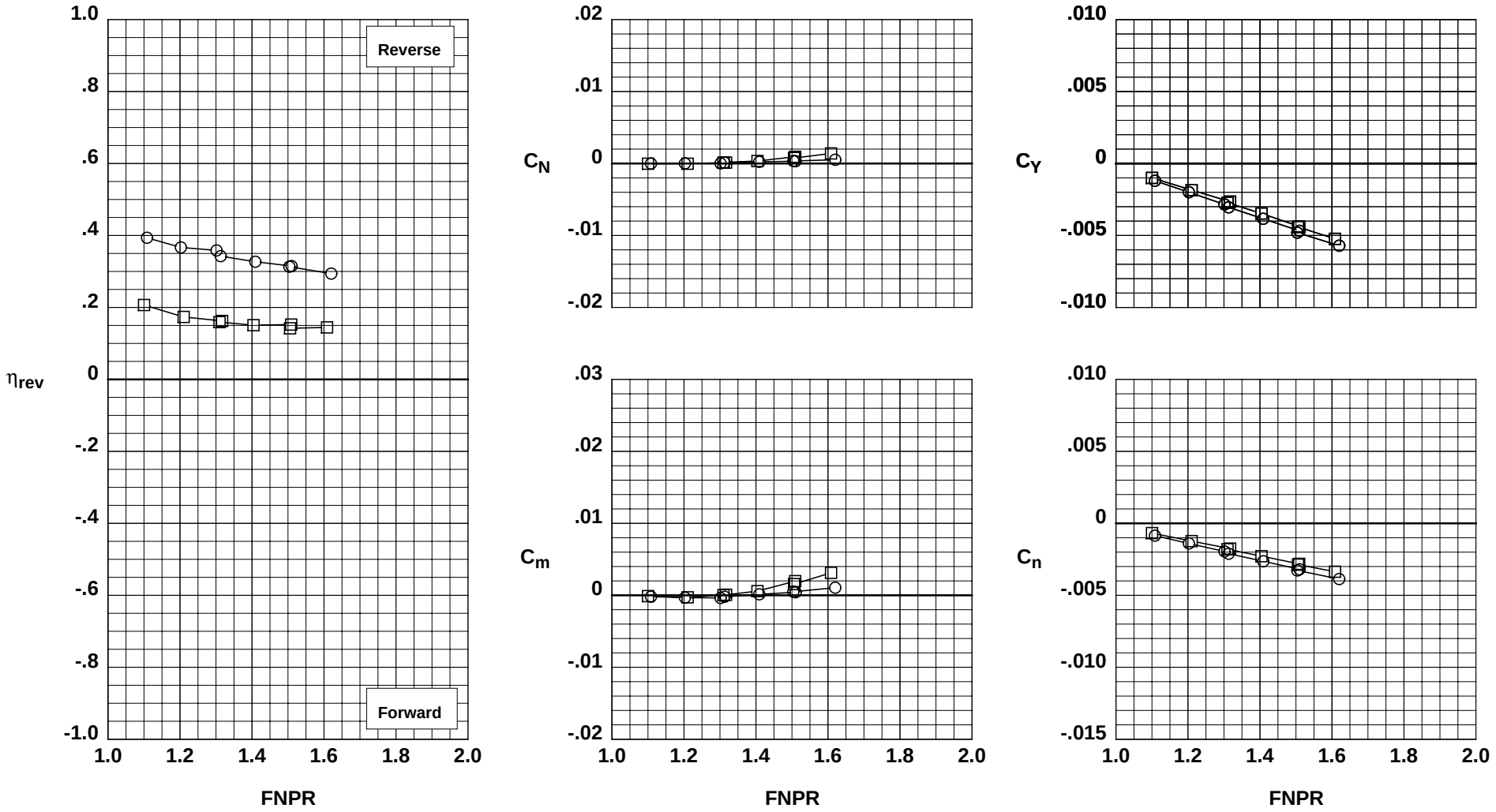

(b) $\psi_2 = 0°$.

Figure 33. Concluded.

Operation Mode: Dual Flow
Deflector Mount Position: Parallel
Deflector Fences: Installed
Bifurcator: Removed
Wing: Installed
Ground Plane: Removed

	Test	Run	Configuration	Chord Length
○	1001	39	712	Long
□	1001	70	741	Short

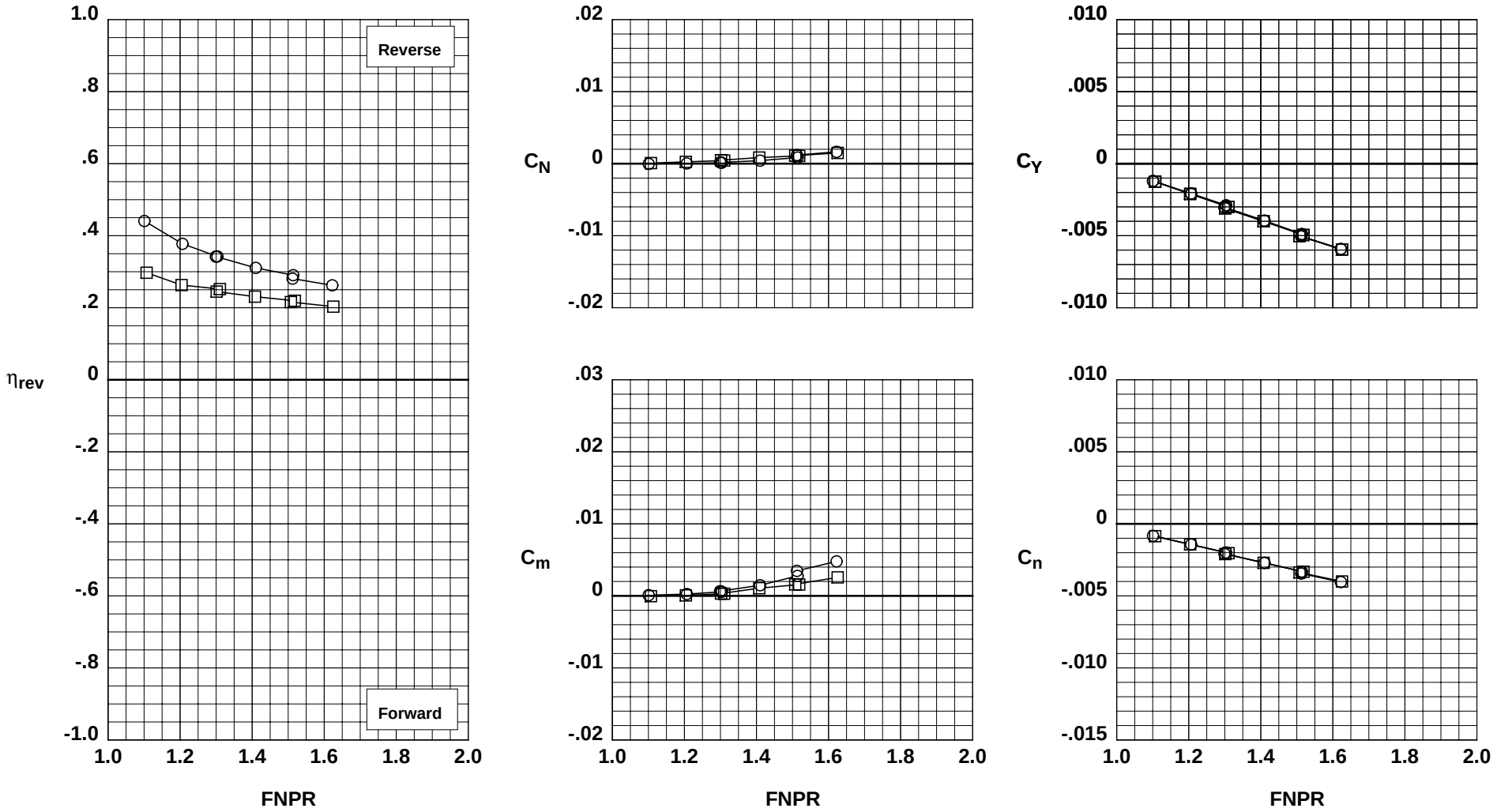

(a) ψ_2 = -15°.

Figure 34. Effects of deflector chord length for wing-mounted thrust reverser configurations with parallel deflector mount angle and deflector edge fences installed; ψ_1 = 60° and ψ_3 = 30°.

Operation Mode: Dual Flow
Deflector Mount Position: Parallel
Deflector Fences: Installed
Bifurcator: Removed
Wing: Installed
Ground Plane: Removed

	Test	Run	Configuration	Chord Length
○	1001	36	719	Long
□	1001	72	743	Short

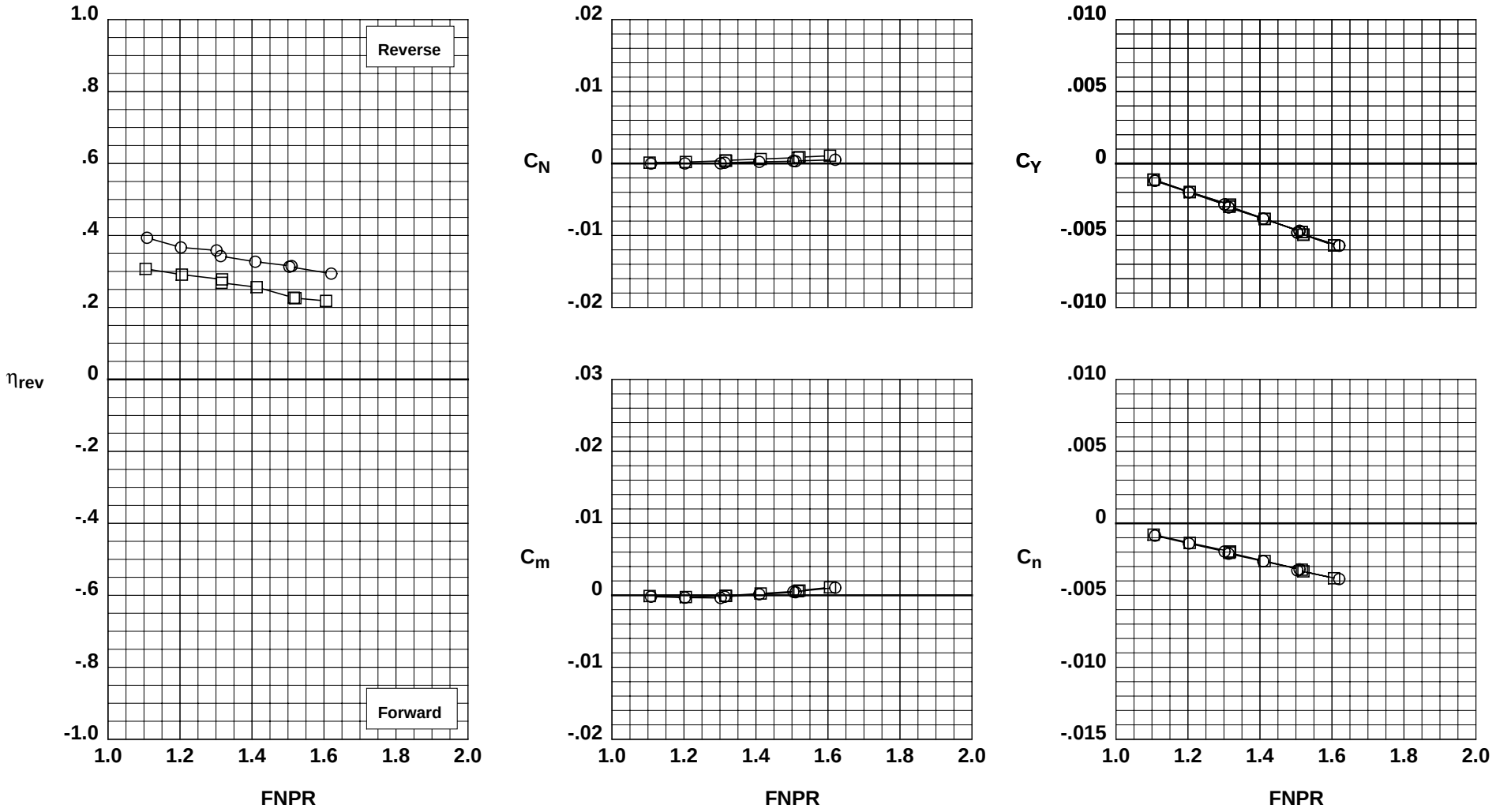

(b) $\psi_2 = 0°$.

Figure 34. Concluded.

Operation Mode: Dual Flow
Deflector Chord Lengths: Long/Long/Long
Deflector Fences: Installed
Bifurcator: Removed
Wing: Installed
Ground Plane: Removed

	Test	Run	Configuration	Mount Angle
○	1001	43	709	Parallel
□	1001	60	740	Normal

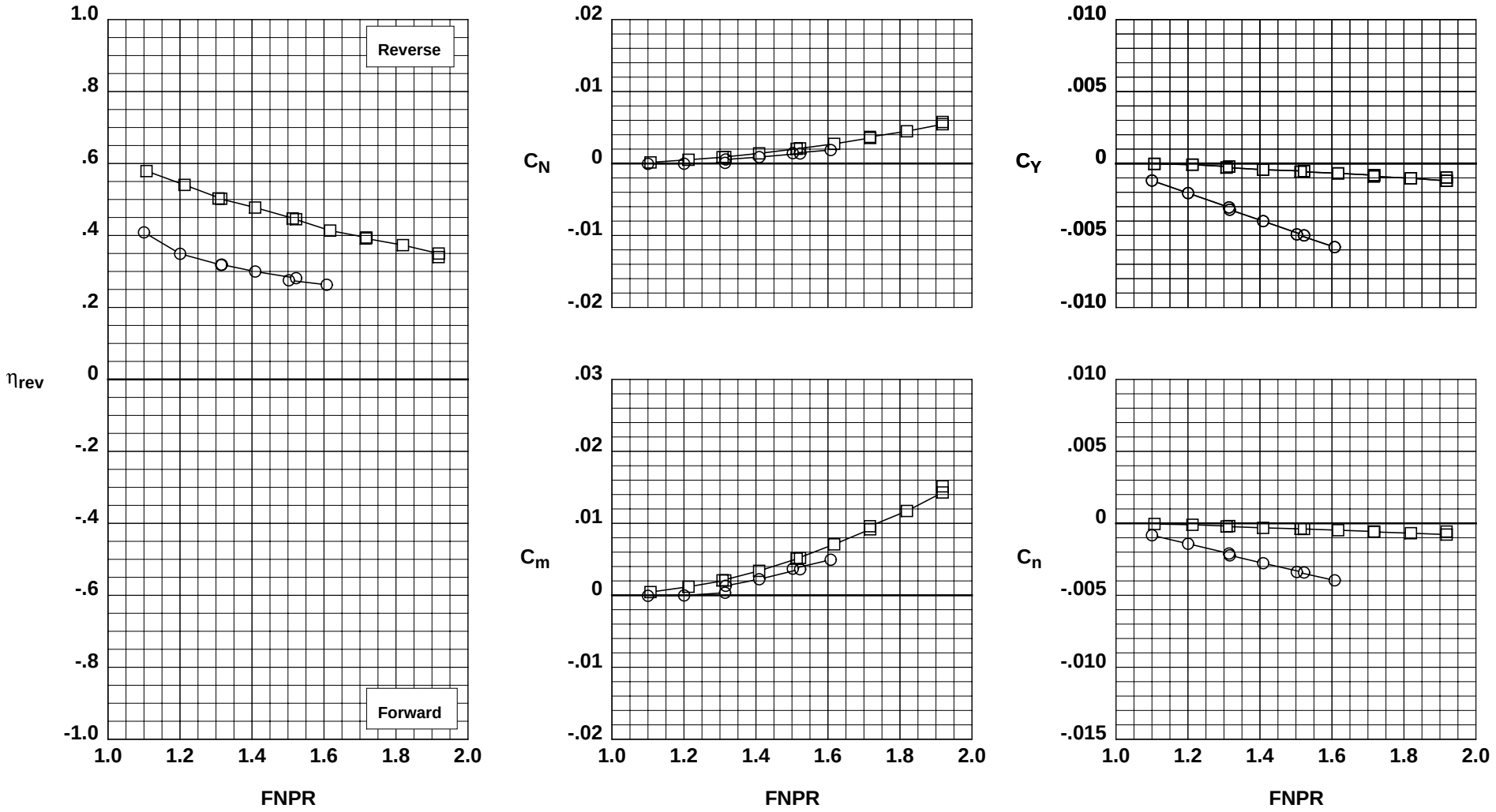

(a) $\psi_1 = 45°$ and $\psi_2 = -15°$.

Figure 35. Effects of deflector mount angle for wing-mounted thrust reverser configurations with long deflector chord lengths and deflector edge fences installed; $\psi_3 = 30°$.

Operation Mode: Dual Flow
Deflector Chord Lengths: Long/Long/Long
Deflector Fences: Installed
Bifurcator: Removed
Wing: Installed
Ground Plane: Removed

	Test	Run	Configuration	Mount Angle
○	1001	36	719	Parallel
□	1001	62	738	Normal

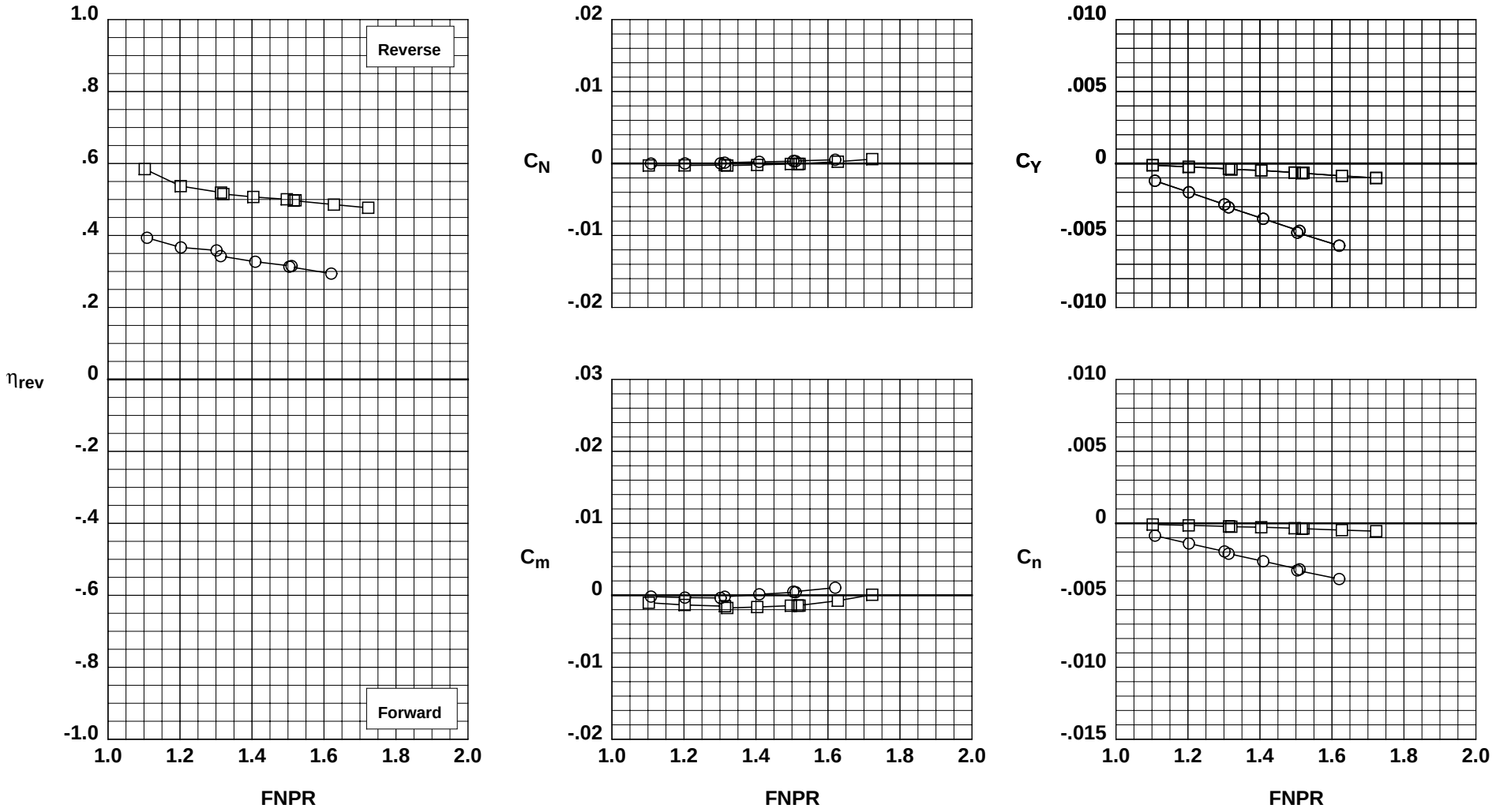

(b) $\psi_1 = 60°$ and $\psi_2 = 0°$.

Figure 35. Concluded.

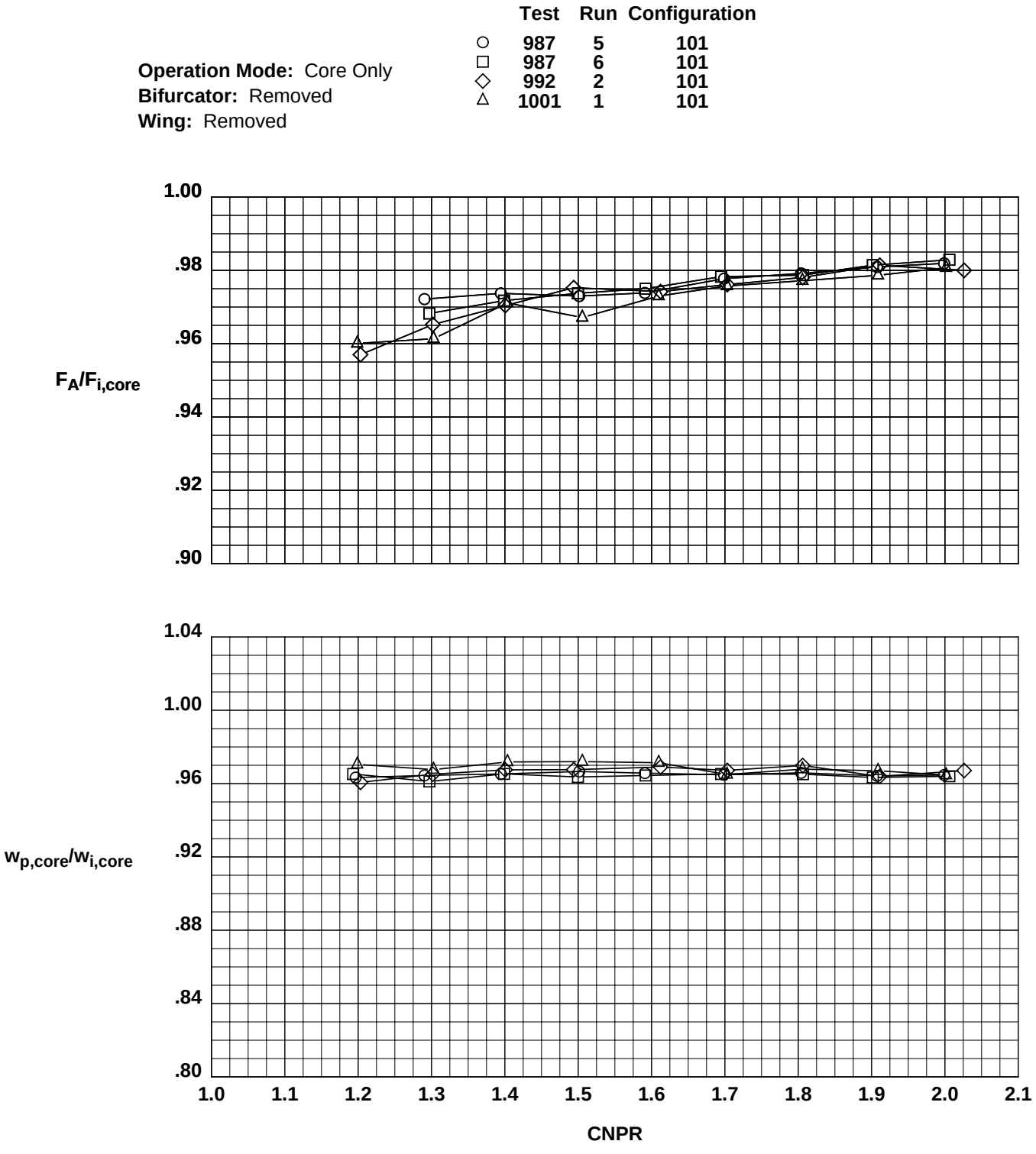

(a) Core only.

Figure A-1. Separate-flow exhaust system performance characteristics for configuration 101.

	Test	Run	Configuration
○	992	3	101
□	1001	2	101

Operation Mode: Fan Only
Bifurcator: Removed
Wing: Removed

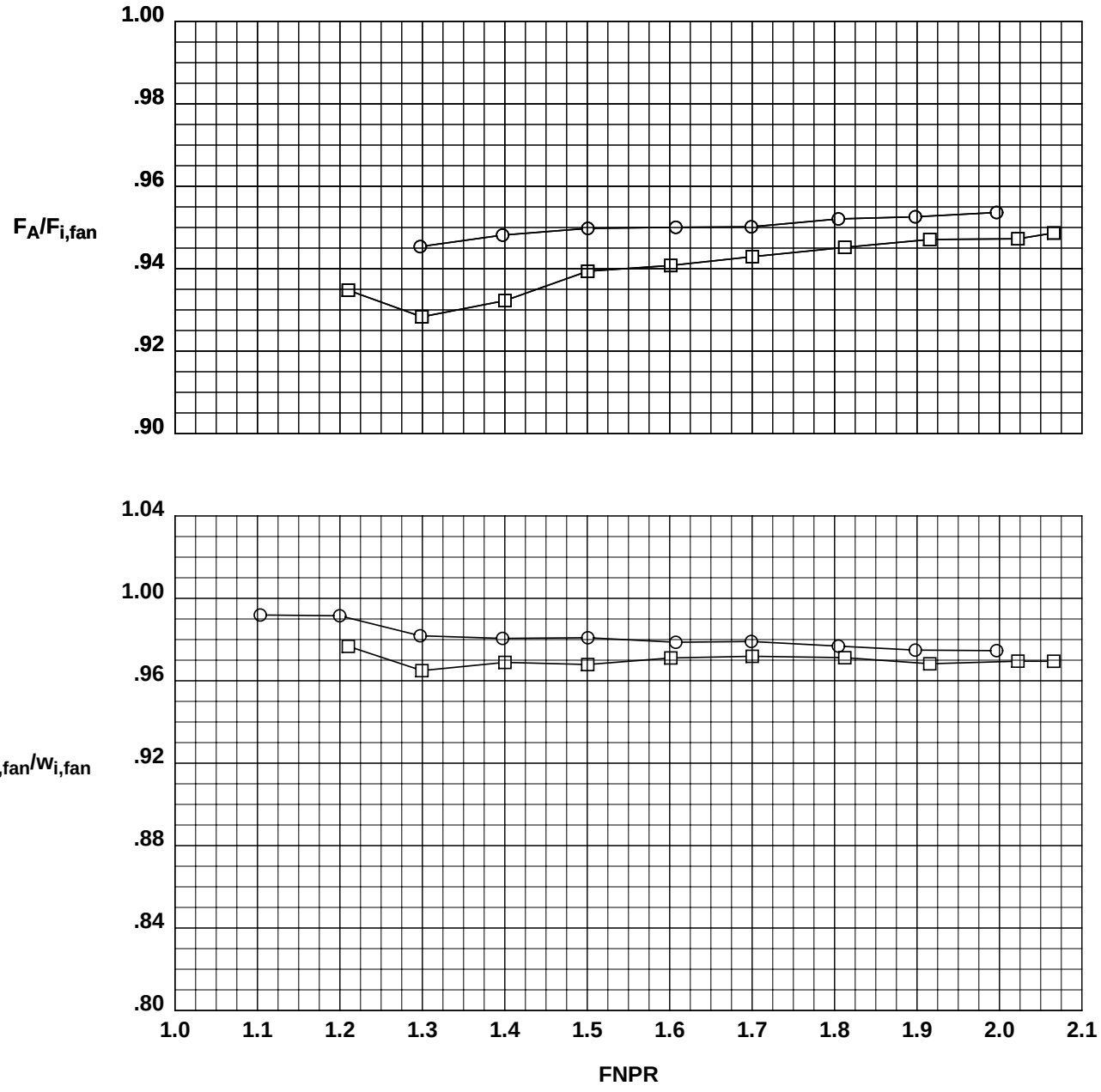

(b) Fan only.

Figure A-1. Continued.

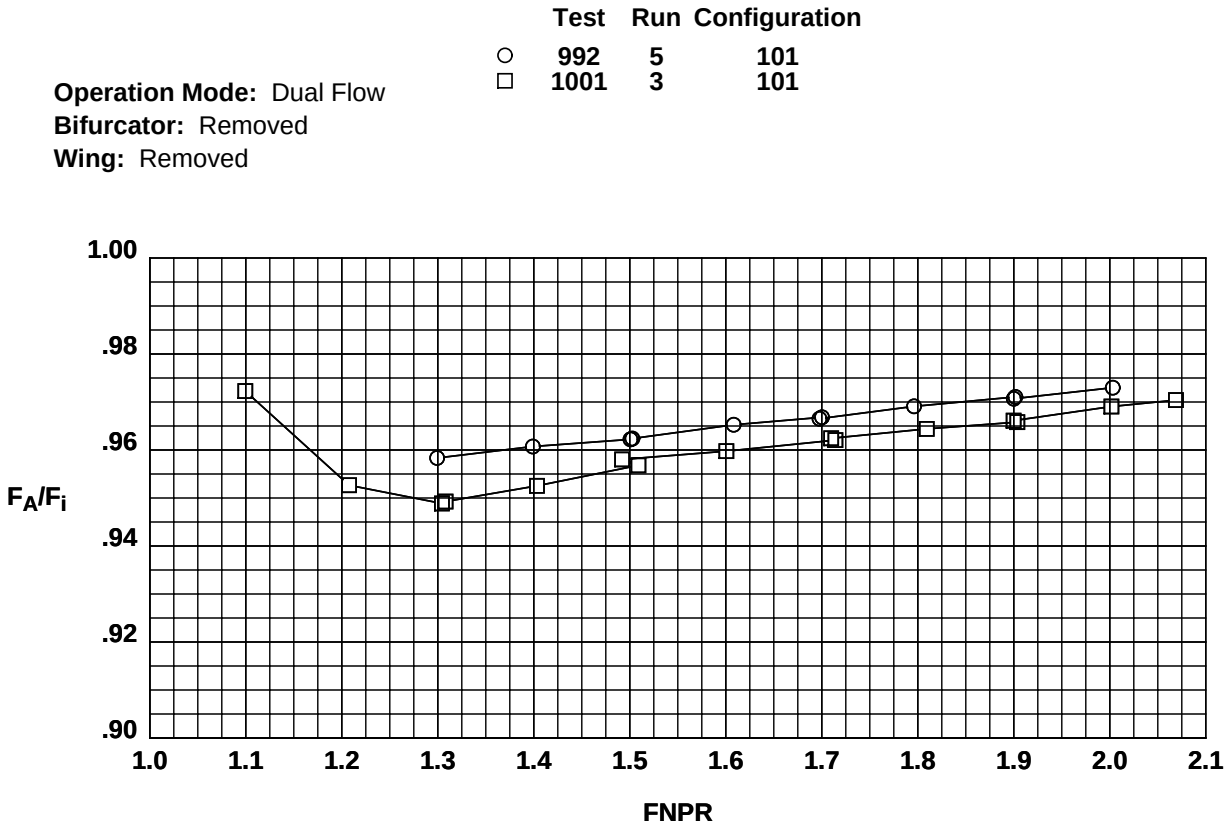

(c) Dual flow.

Figure A-1. Concluded.

	Test	Run	Configuration
○	1001	81	501

Operation Mode: Core Only
Bifurcator: Installed
Wing: Removed

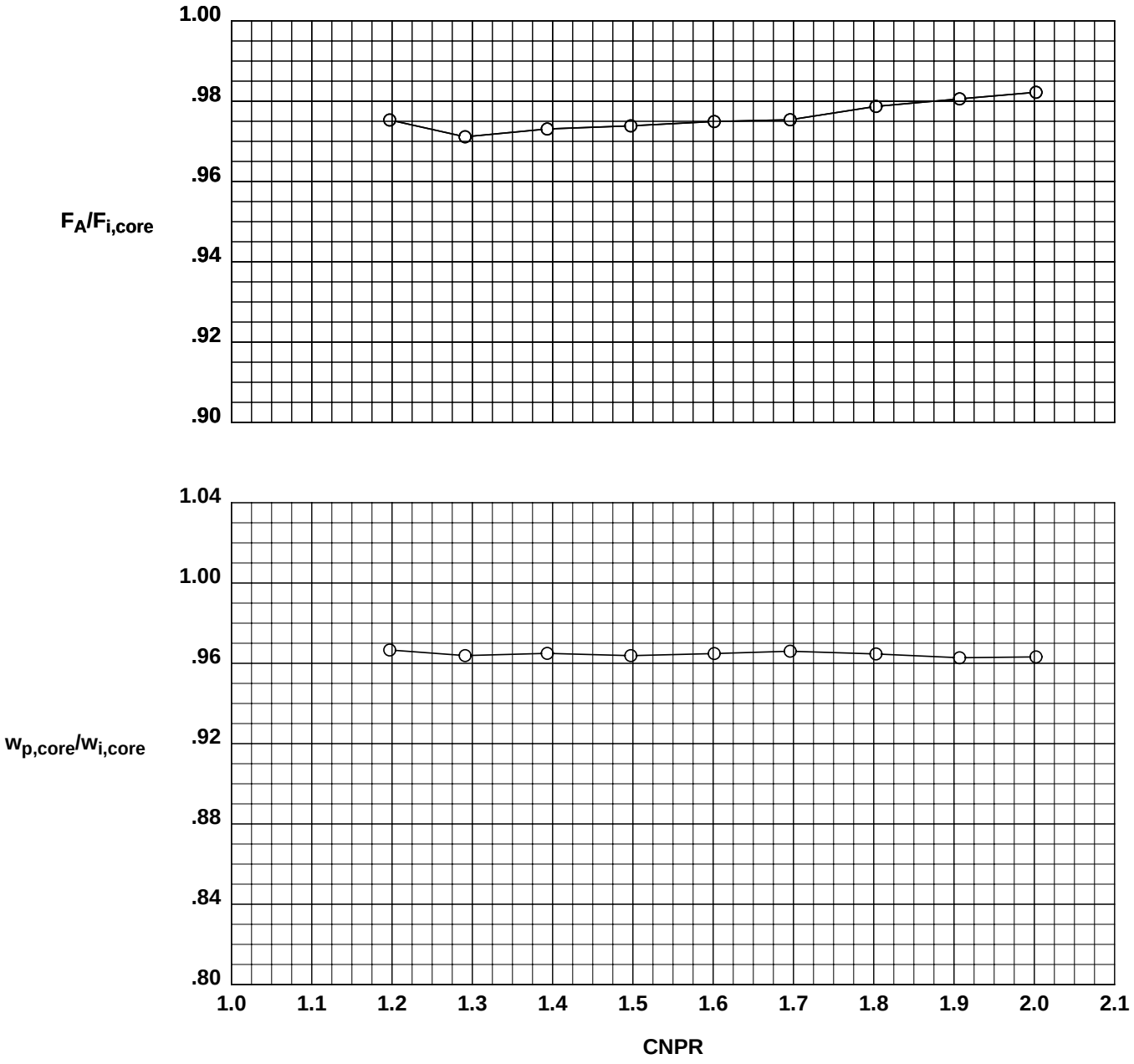

(a) Core only.

Figure A-2. Separate-flow exhaust system performance characteristics for configuration 501.

	Test	Run	Configuration
○	1001	82	501

Operation Mode: Fan Only
Bifurcator: Installed
Wing: Removed

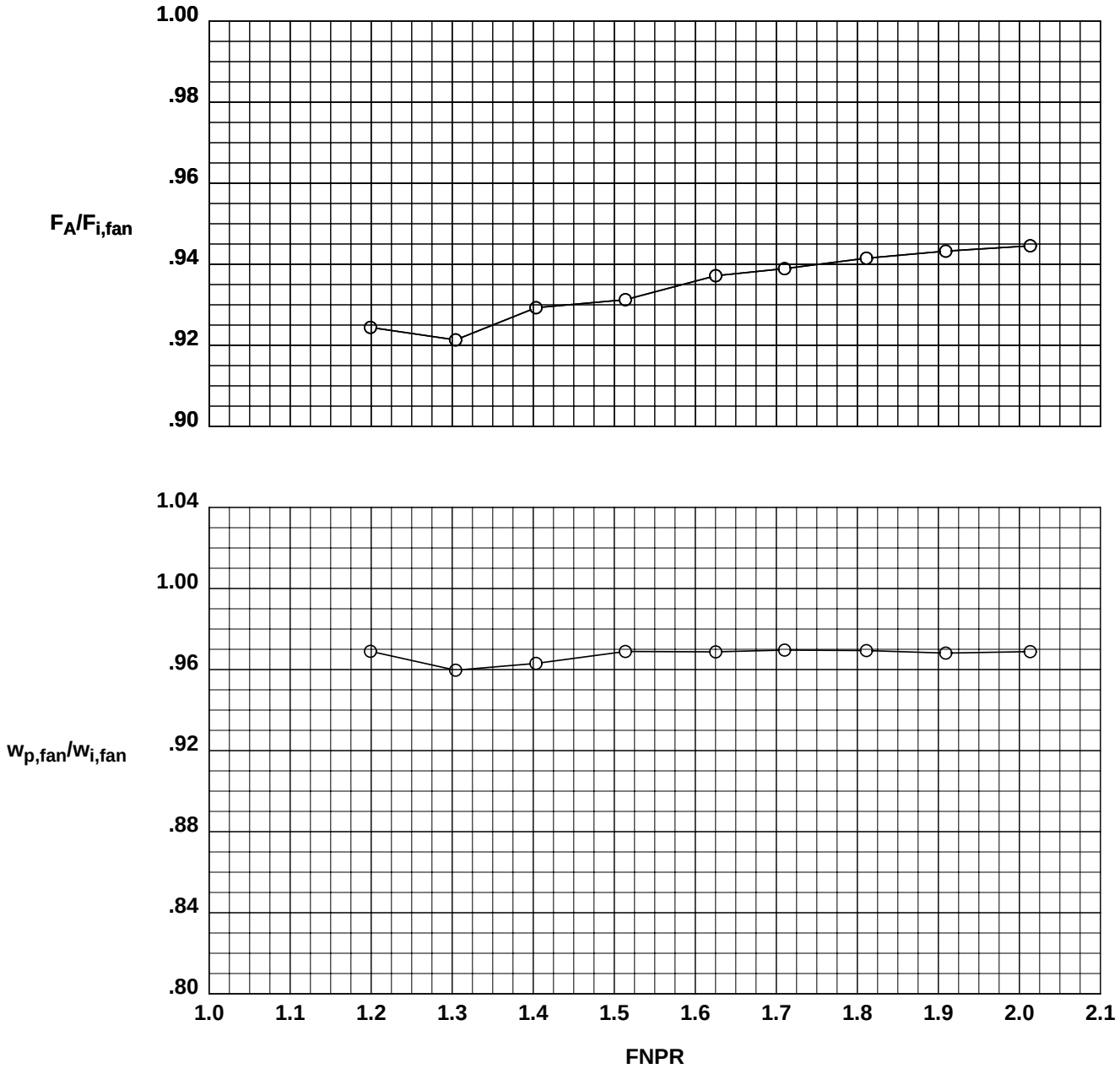

(b) Fan only.

Figure A-2. Continued.

	Test	Run	Configuration
○	994	1	501
□	1001	83	501

Operation Mode: Dual Flow
Bifurcator: Installed
Wing: Removed

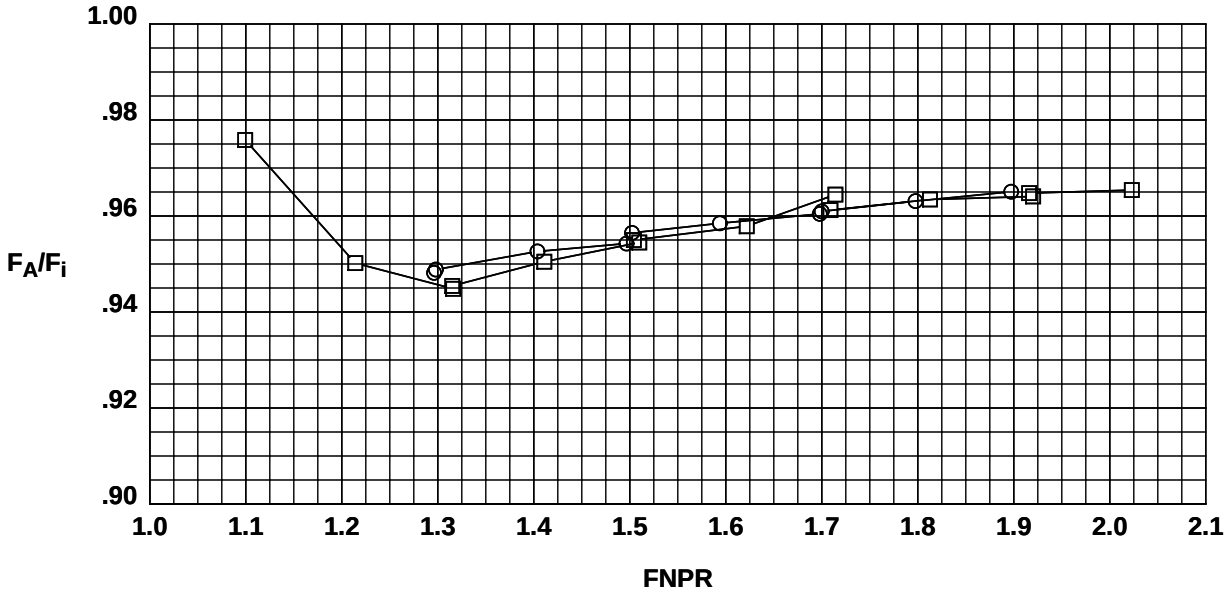

(c) Dual flow.

Figure A-2. Concluded.

	Test	Run	Configuration
○	1001	13	701

Operation Mode: Core Only
Bifurcator: Removed
Wing: Installed

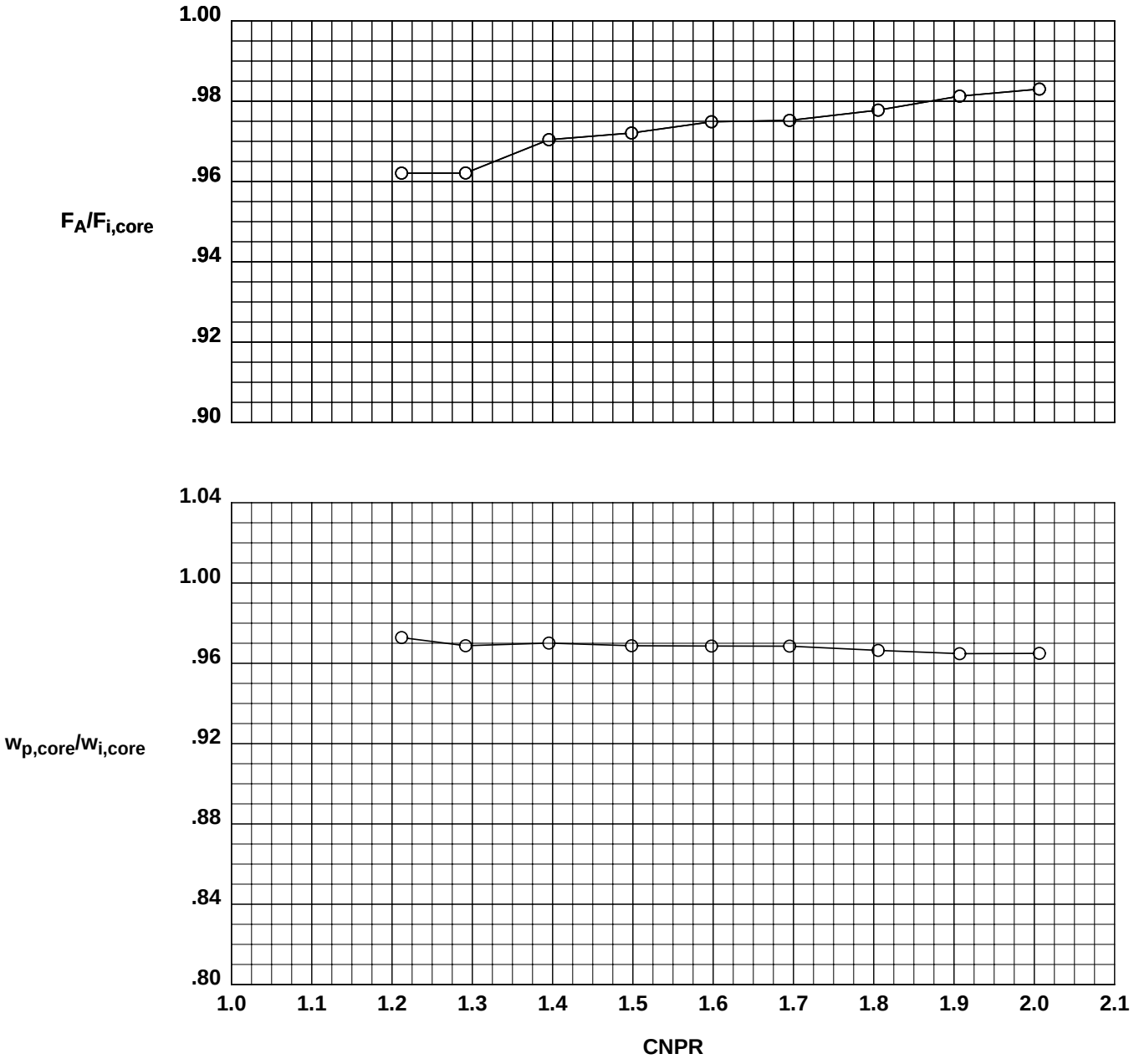

(a) Core only.

Figure A-3. Separate-flow exhaust system performance characteristics for configuration 701.

	Test	Run	Configuration
○	1001	14	701

Operation Mode: Fan Only
Bifurcator: Removed
Wing: Installed

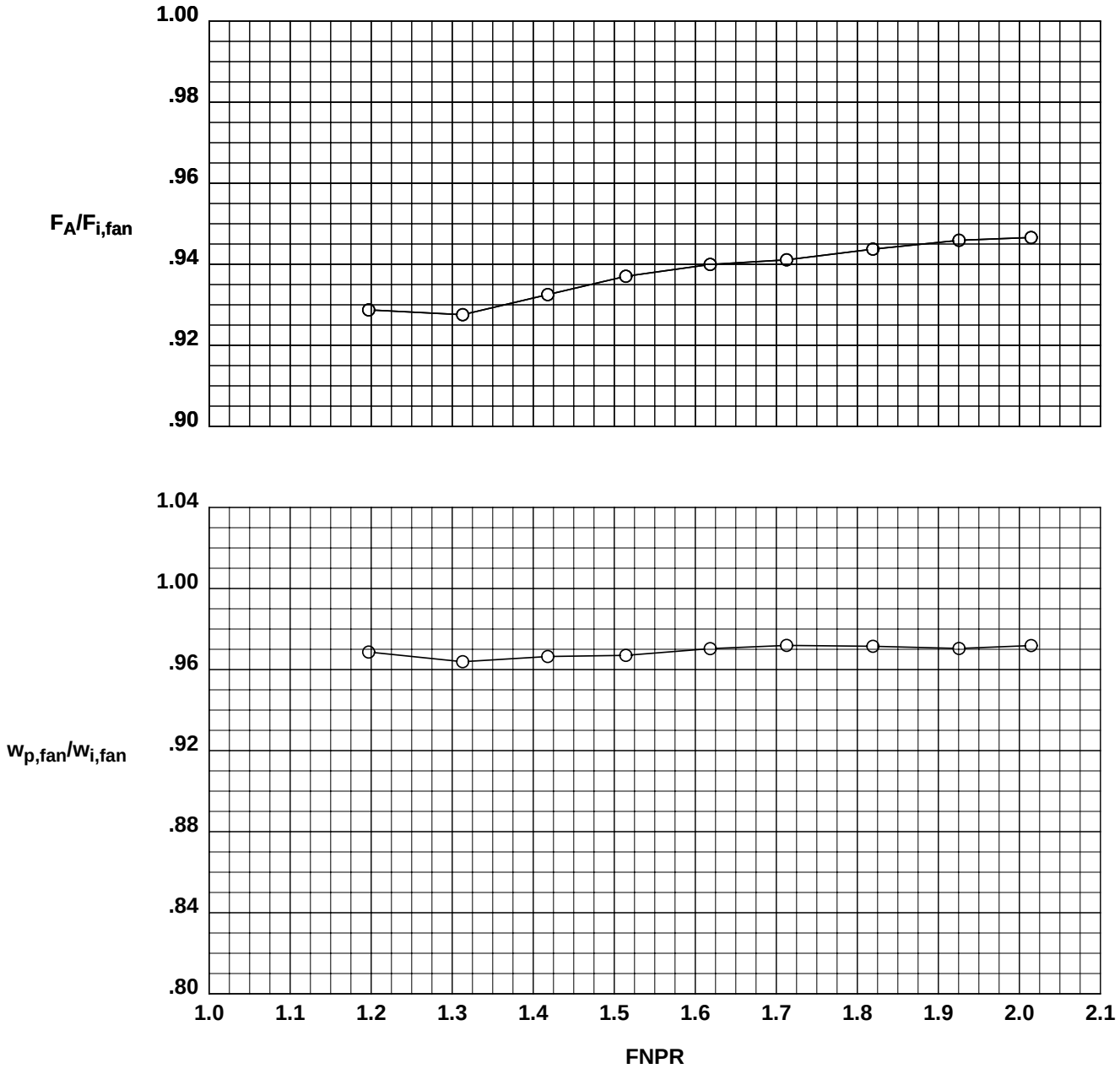

(b) Fan only.

Figure A-3. Continued.

	Test	Run	Configuration
○	1001	15	701

Operation Mode: Dual Flow
Bifurcator: Removed
Wing: Installed

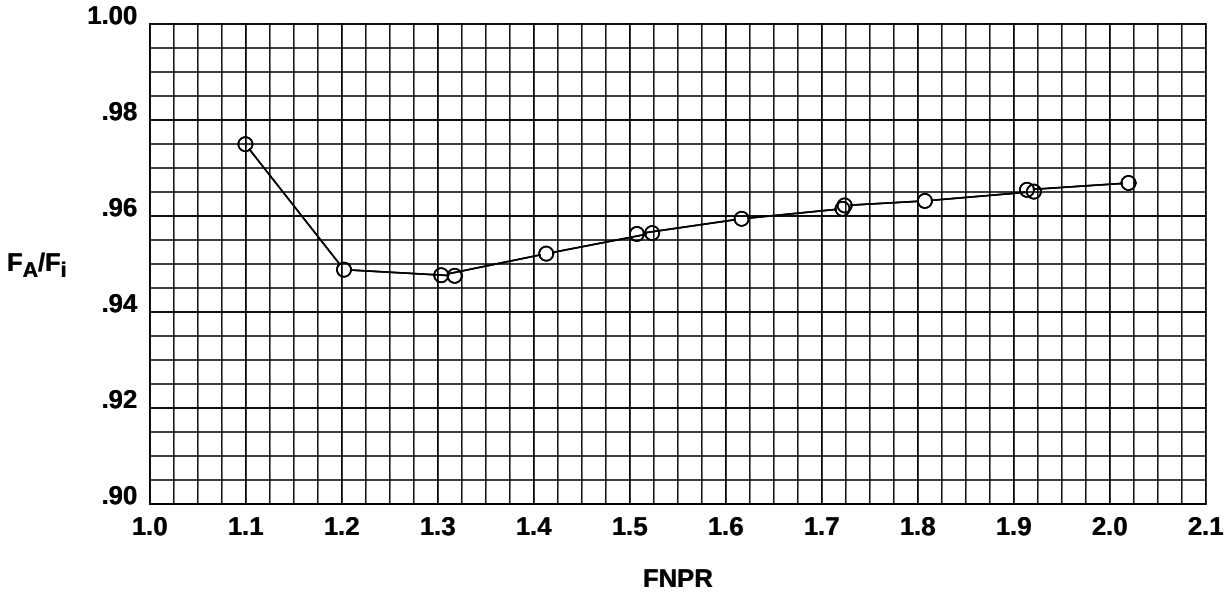

(c) Dual flow.

Figure A-3. Concluded.

Operation Mode: Dual Flow
Cascade Aft Port: Closed
Blocker Porosity: 0%
Bifurcator: Removed
Wing: Removed

	Test	Run	Configuration
○	987	14	201

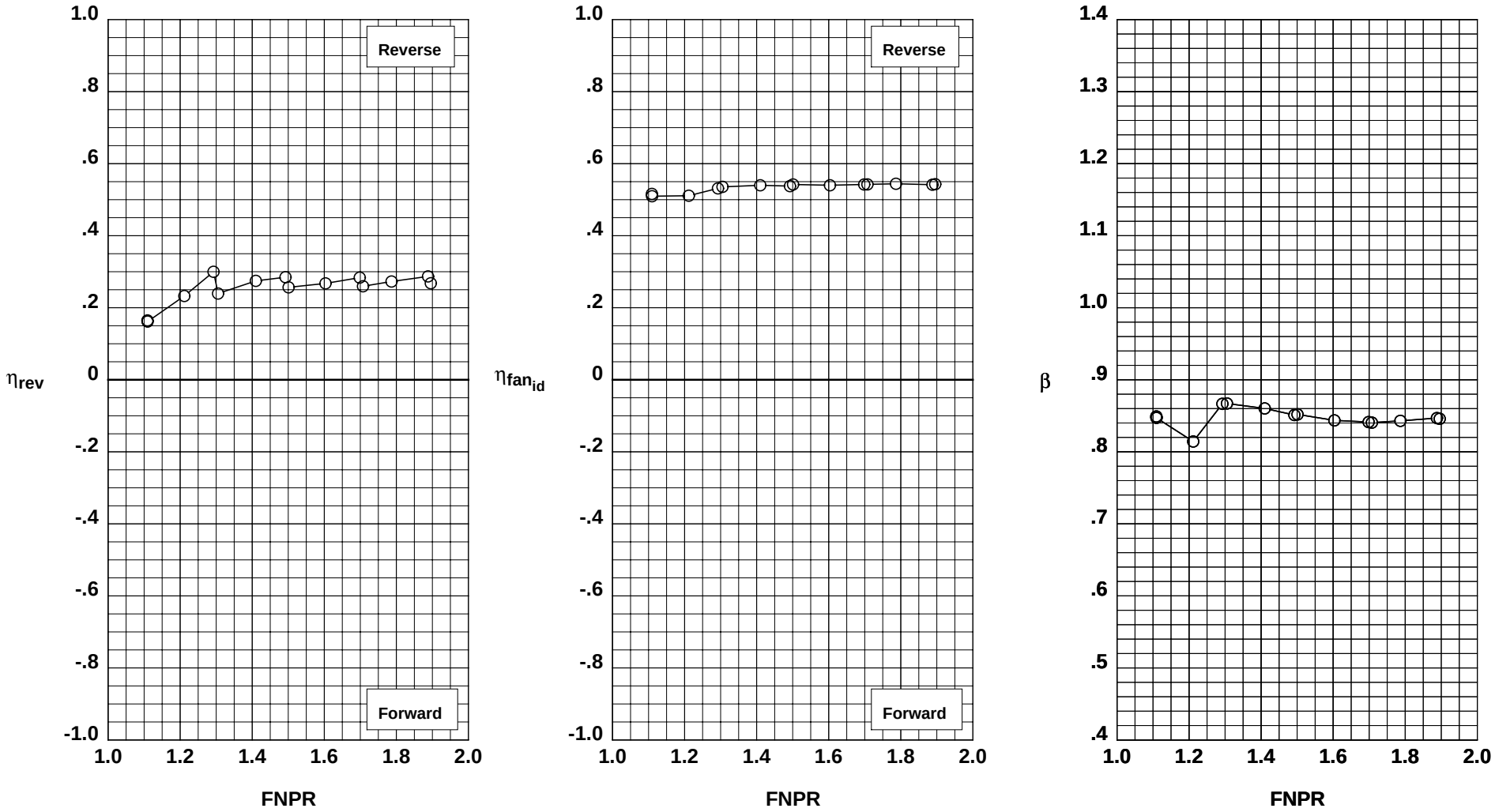

Figure B-1. Conventional cascade thrust reverser performance characteristics for configuration 201.

Operation Mode: Dual Flow
Cascade Aft Port: Closed
Blocker Porosity: 5%
Bifurcator: Removed
Wing: Removed

	Test	Run	Configuration
○	987	17	202

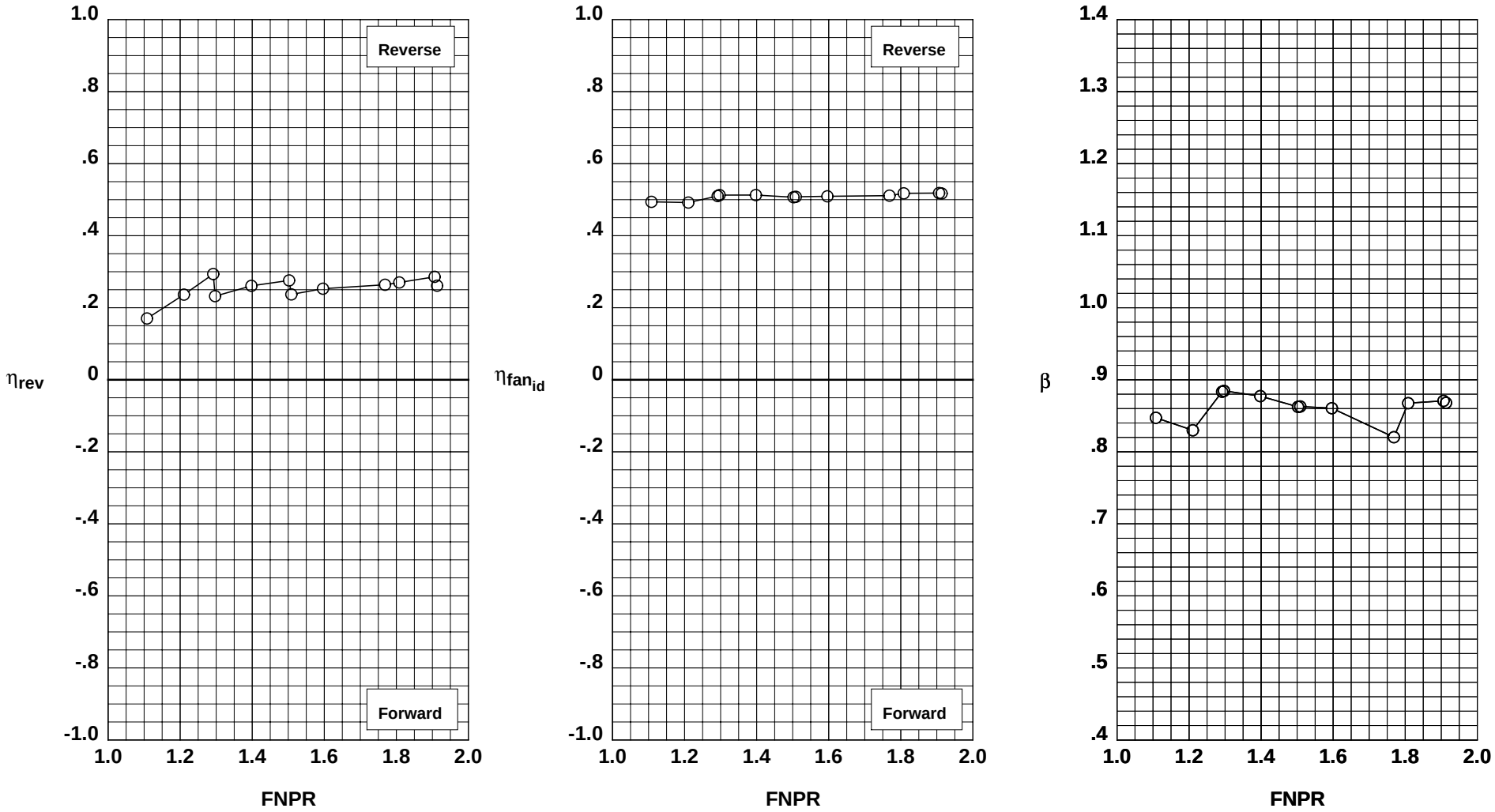

Figure B-2. Conventional cascade thrust reverser performance characteristics for configuration 202.

Operation Mode: Dual Flow
Cascade Aft Port: Open
Blocker Porosity: 0%
Bifurcator: Removed
Wing: Removed

	Test	Run	Configuration
○	987	18	203

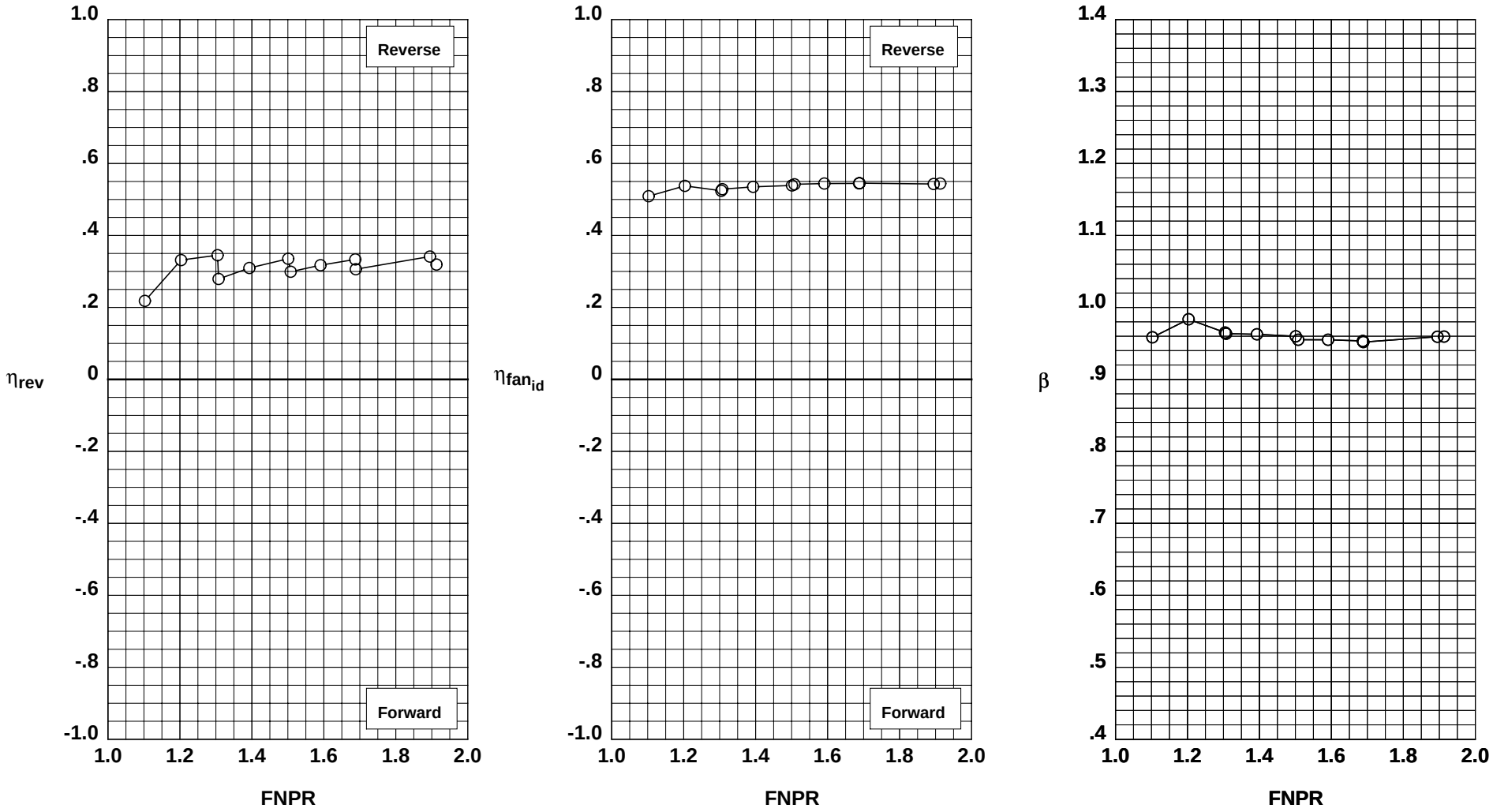

Figure B-3. Conventional cascade thrust reverser performance characteristics for configuration 203.

Operation Mode: Dual Flow
Cascade Aft Port: Open
Blocker Porosity: 5%
Bifurcator: Removed
Wing: Removed

	Test	Run	Configuration
○	987	19	204

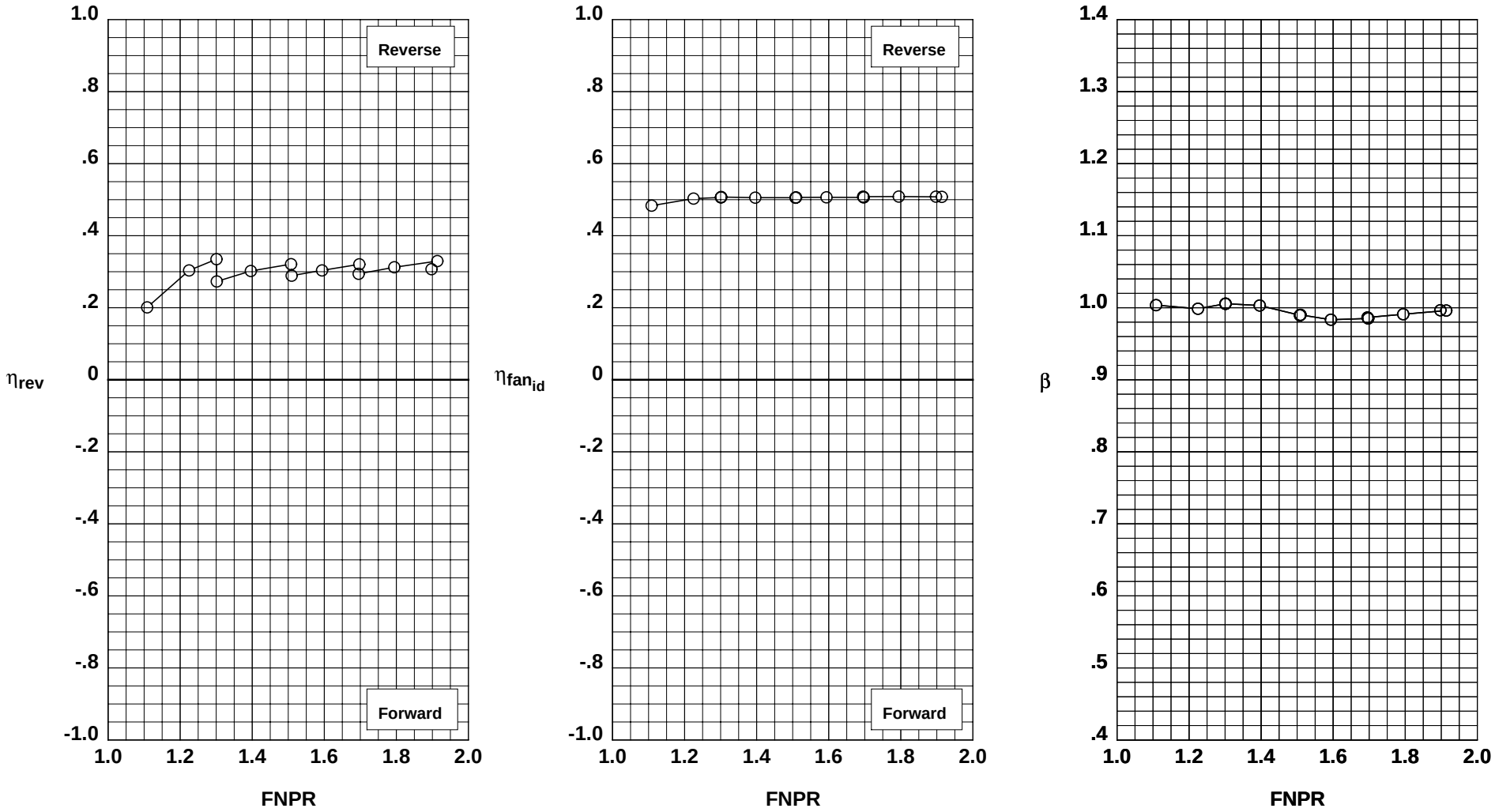

Figure B-4. Conventional cascade thrust reverser performance characteristics for configuration 204.

Operation Mode: Dual Flow
Cascade Aft Port: Open
Blocker Porosity: 12%
Bifurcator: Removed
Wing: Removed

	Test	Run	Configuration
○	987	20	205

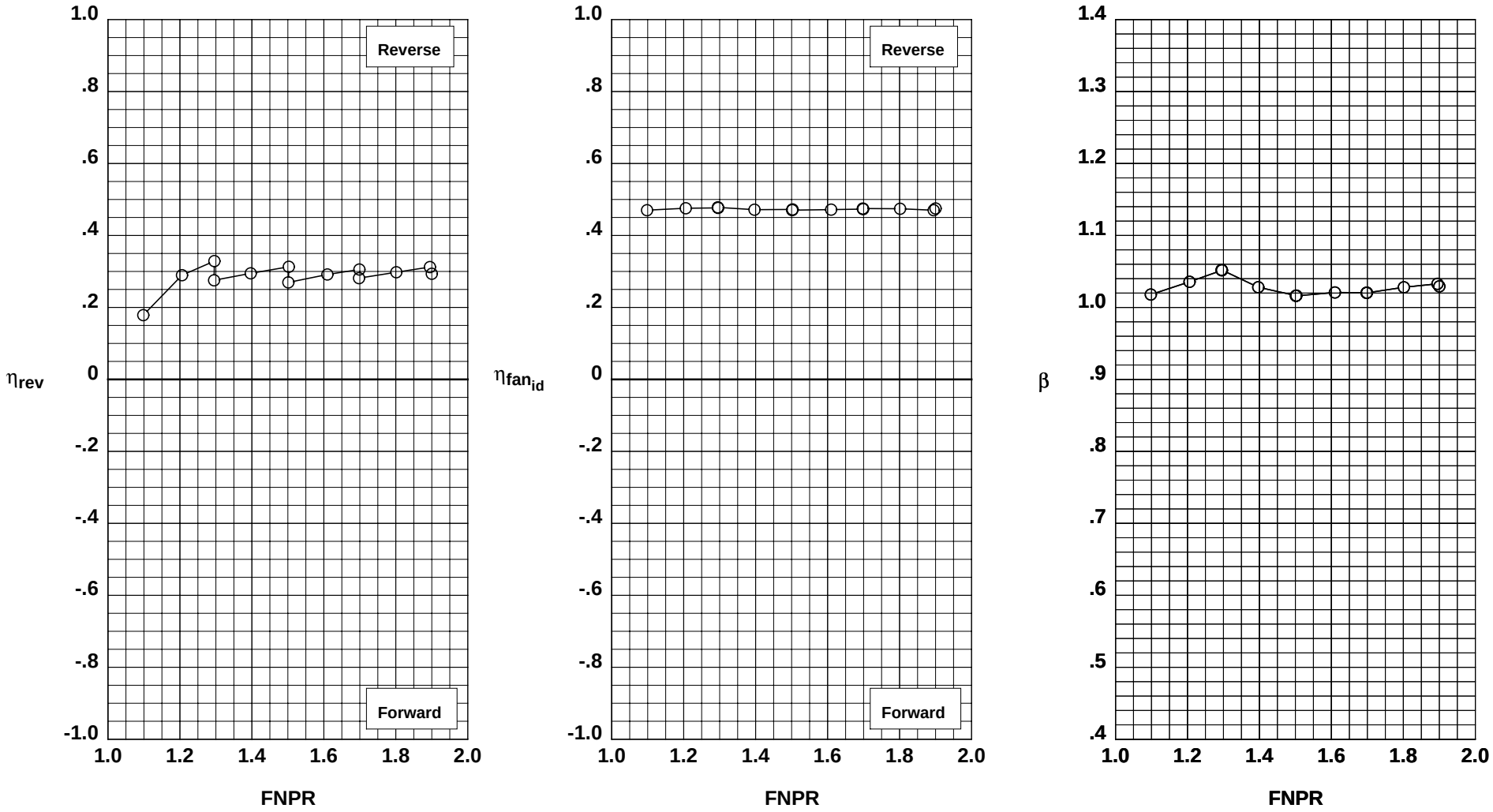

Figure B-5. Conventional cascade thrust reverser performance characteristics for configuration 205.

Operation Mode: Fan Only
Cascade Aft Port: Open
Blocker Porosity: 0%
Bifurcator: Removed
Wing: Removed

	Test	Run	Configuration
○	992	6	206

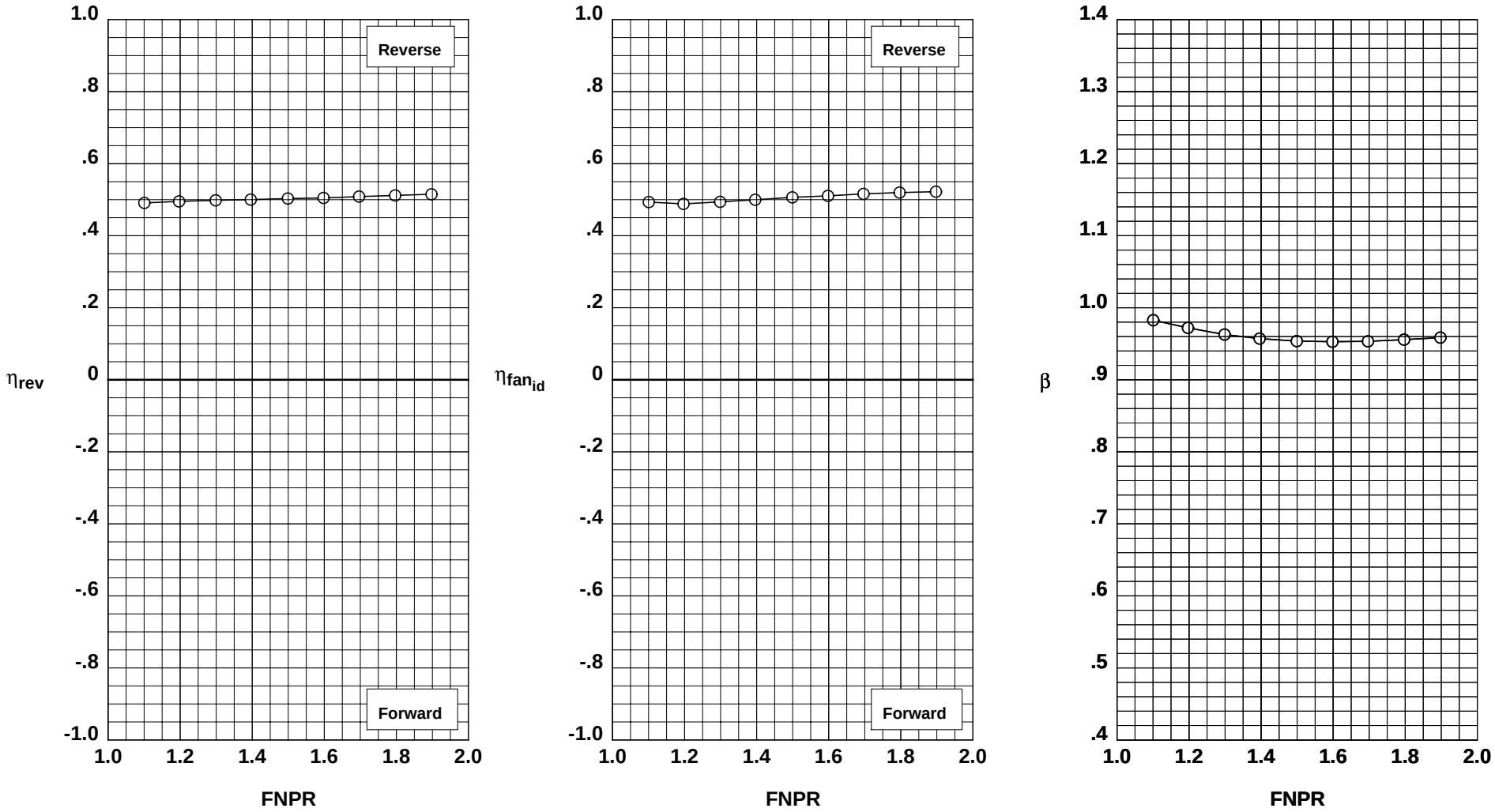

Figure B-6. Conventional cascade thrust reverser performance characteristics for configuration 206.

Operation Mode: Dual Flow
Cascade Aft Port: Open
Blocker Porosity: 50%
Bifurcator: Removed
Wing: Removed

	Test	Run	Configuration
○	987	24	208

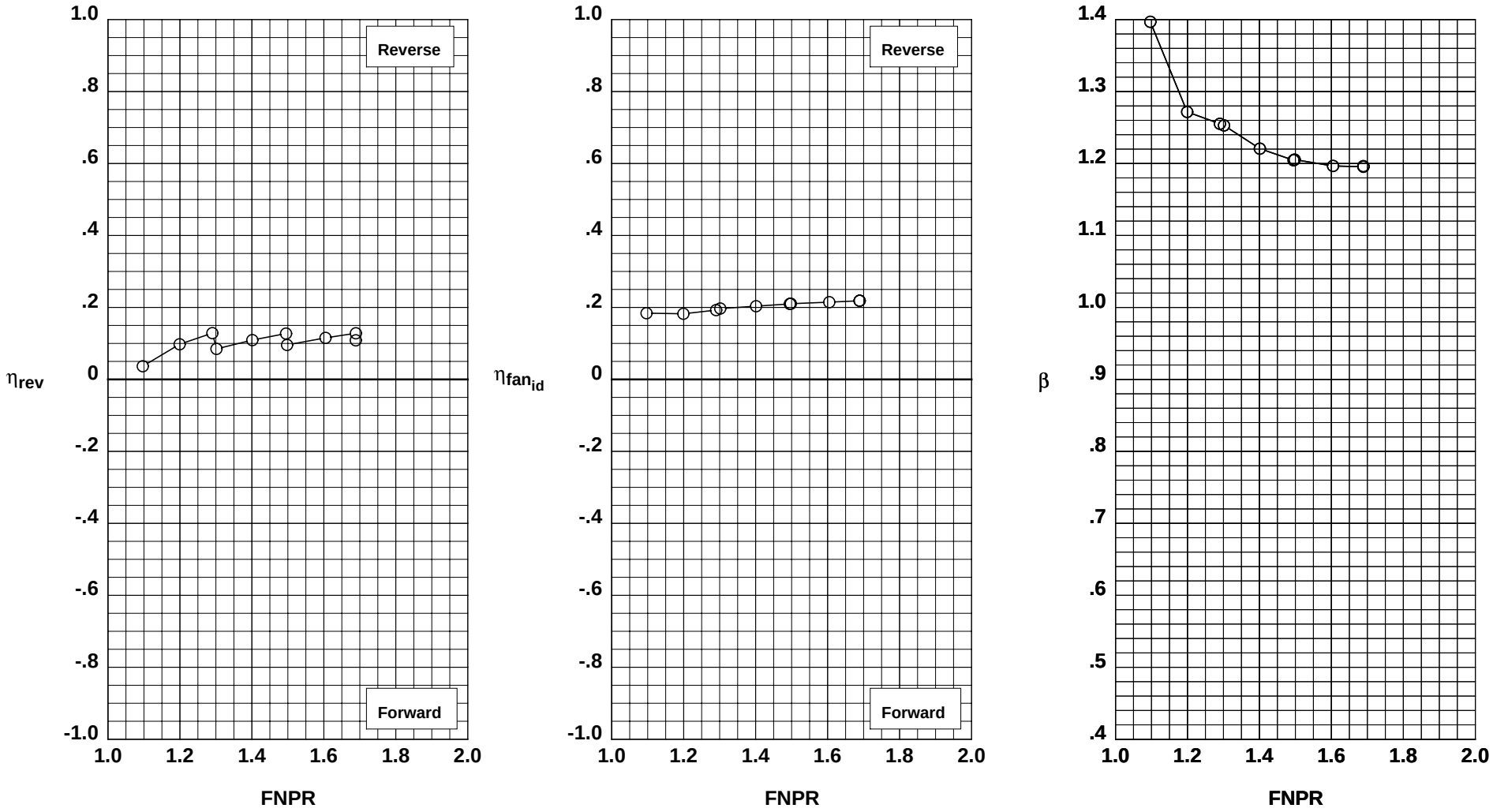

Figure C-1. Cascade thrust reverser with porous blocker performance characteristics for configuration 208.

Operation Mode: Dual Flow
Cascade Aft Port: Open
Blocker Porosity: 25%
Bifurcator: Removed
Wing: Removed

	Test	Run	Configuration
○	987	25	209

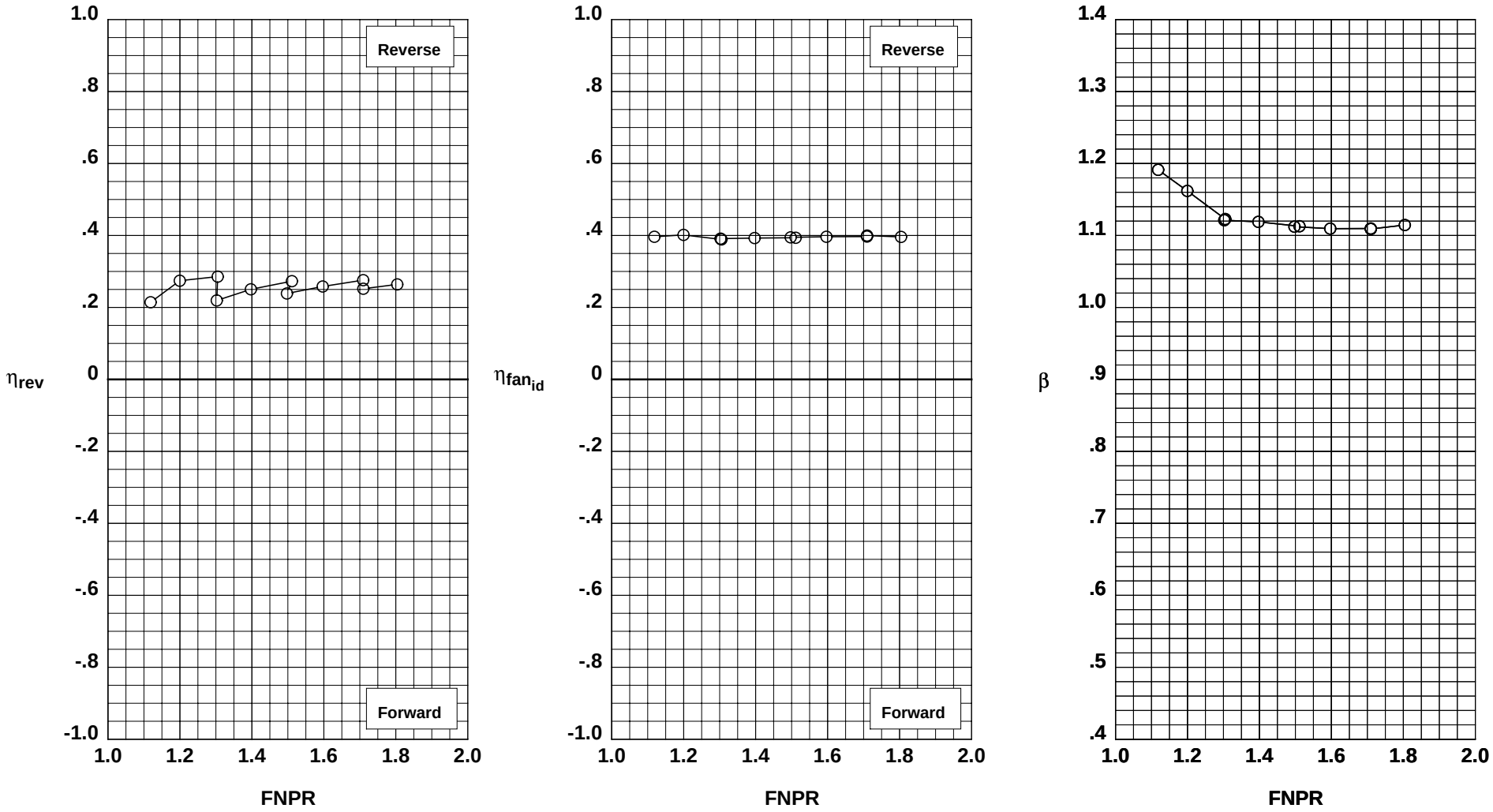

Figure C-2. Cascade thrust reverser with porous blocker performance characteristics for configuration 209.

Fwd Injector: None
Mid Injector: 0.013"@45°
Aft Injector: 0.025" holes
Throat Injector: None

	Test	Run	Configuration	IPR
○	993	3	601	0.00
□	993	2	601	3.99
◇	993	2	601	8.01
△	993	2	601	12.00
◺	993	2	601	16.00

Operation Mode: Fan+Injection
Cascades: Installed
Fwd Bullnose: Bullnose
Port Fairing: #1
Bifurcator: Removed
Wing: Removed

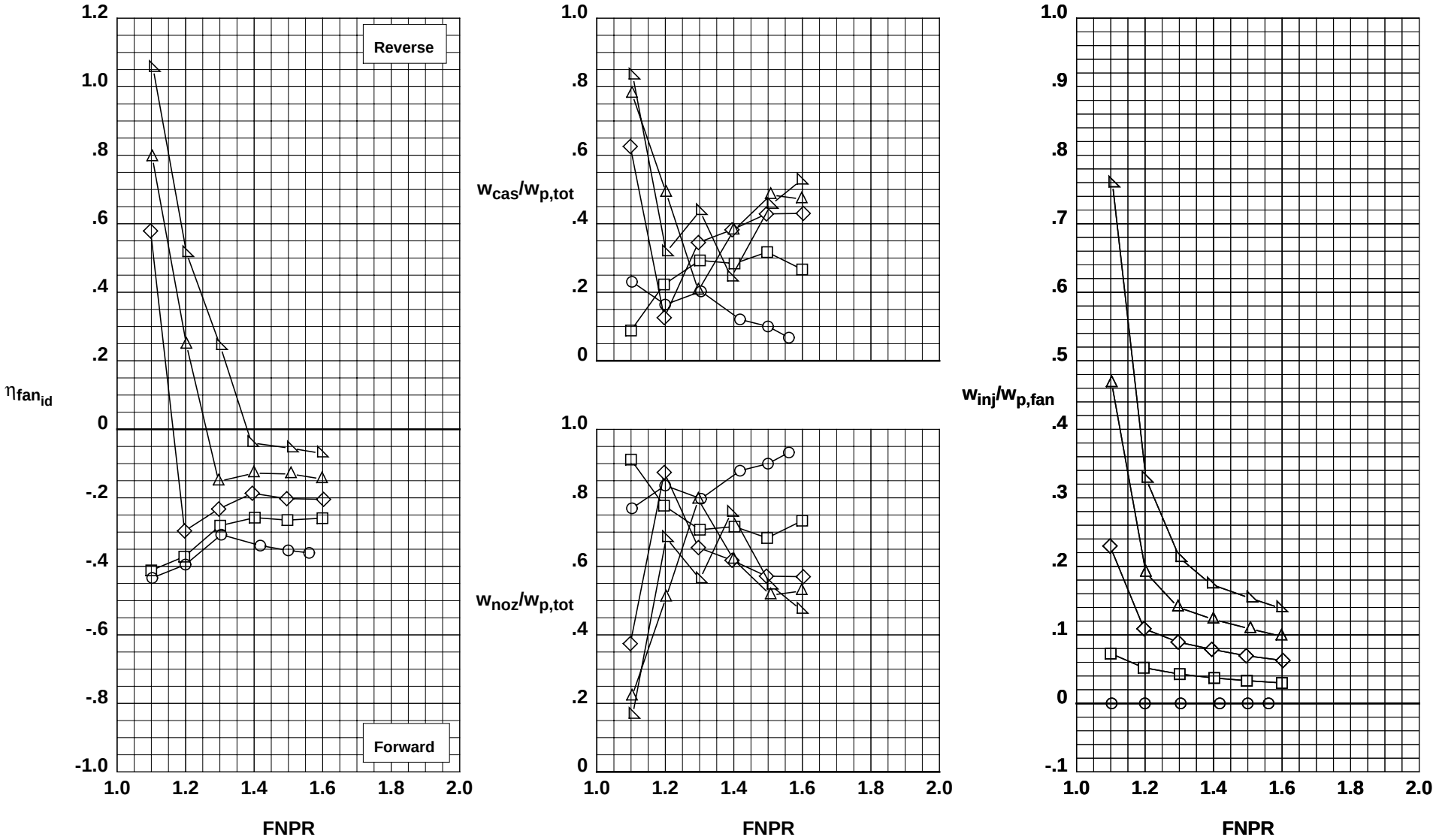

Figure D-1. Blockerless thrust reverser performance characteristics for configuration 601.

Fwd Injector: None
Mid Injector: 0.013"@45°
Aft Injector: 0.025" holes
Throat Injector: None

	Test	Run	Configuration	IPR
○	993	4	602	0.00
□	993	5	602	4.00
◇	993	5	602	8.01
△	993	5	602	12.00
◺	993	5	602	16.01

Operation Mode: Fan+Injection
Cascades: Installed
Fwd Bullnose: Bullnose
Port Fairing: #2
Bifurcator: Removed
Wing: Removed

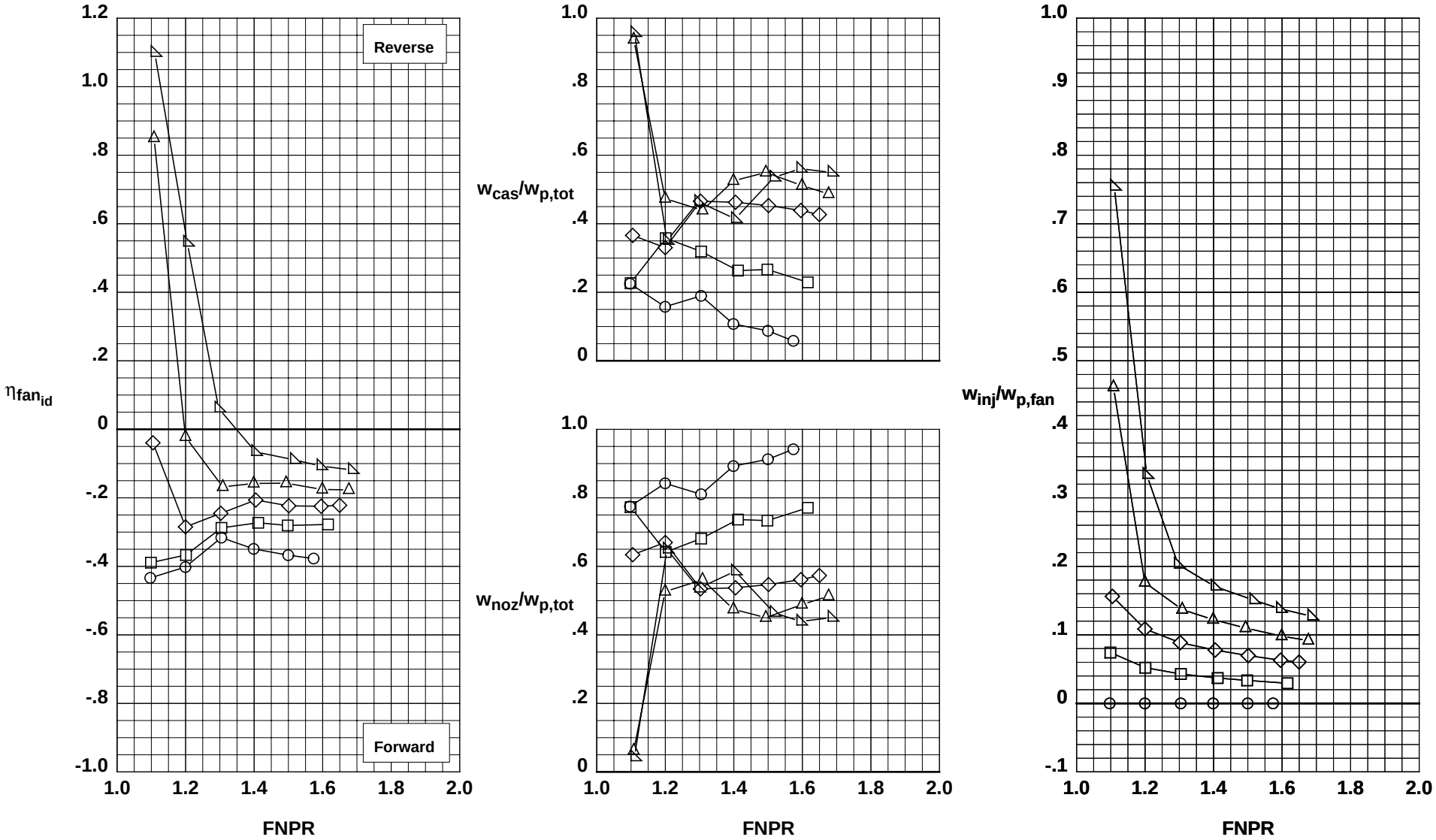

Figure D-2. Blockerless thrust reverser performance characteristics for configuration 602.

Fwd Injector: 0.013"@45°
Mid Injector: 0.013"@45°
Aft Injector: 0.013"@45°
Throat Injector: None

	Test	Run	Configuration	IPR
○	993	6	603	0.00
□	993	7	603	4.00
◇	993	7	603	8.00
△	993	7	603	12.04
◺	993	7	603	16.02

Operation Mode: Fan+Injection
Cascades: Installed
Fwd Bullnose: Bullnose
Port Fairing: #2
Bifurcator: Removed
Wing: Removed

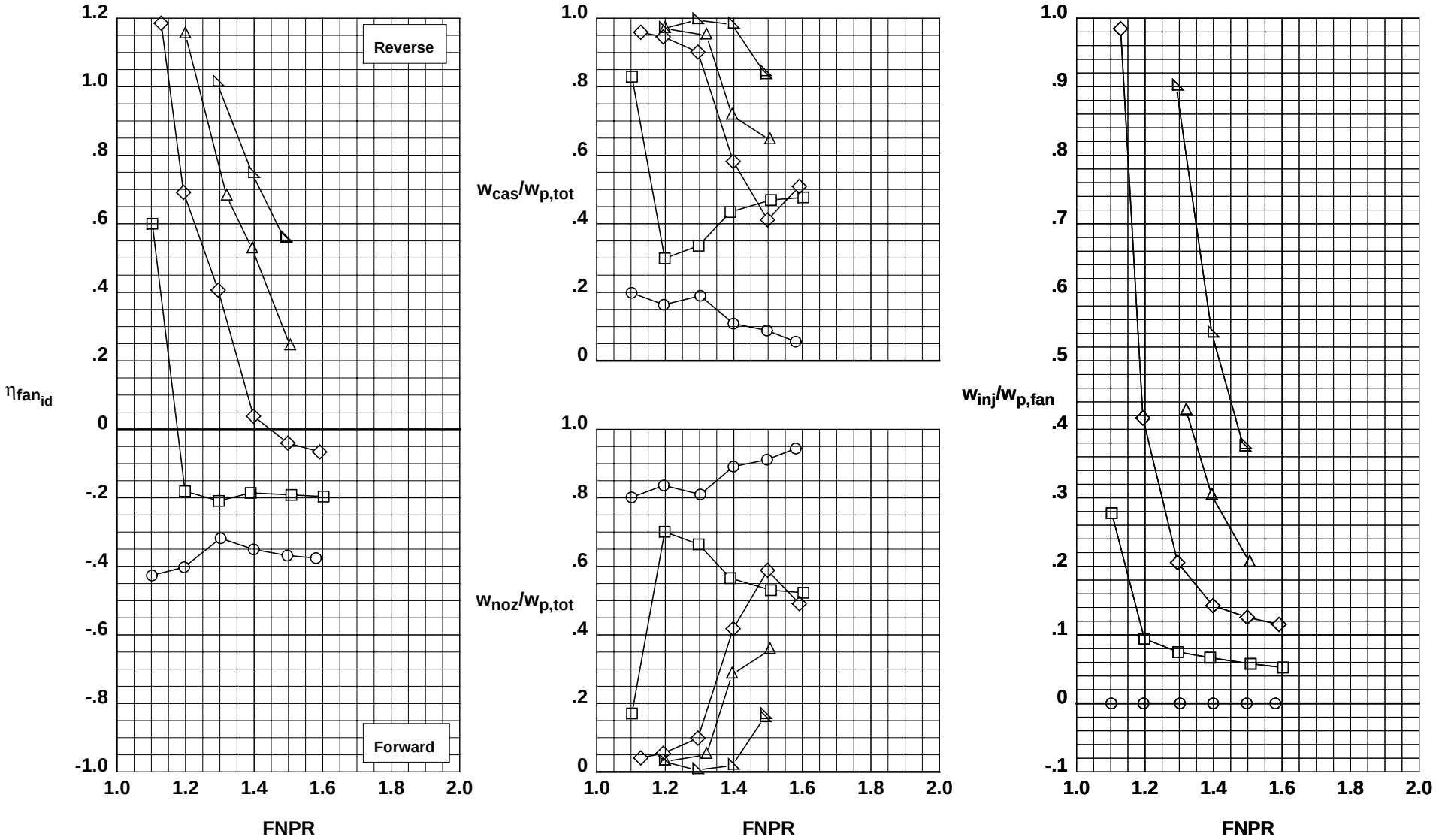

Figure D-3. Blockerless thrust reverser performance characteristics for configuration 603.

Fwd Injector: 0.013"@45°
Mid Injector: None
Aft Injector: 0.013"@45°
Throat Injector: None

	Test	Run	Configuration	IPR
○	993	8	604	0.00
□	993	9	604	4.01
◇	993	9	604	8.05
△	993	9	604	12.08
◺	993	9	604	16.05

Operation Mode: Fan+Injection
Cascades: Installed
Fwd Bullnose: Bullnose
Port Fairing: #2
Bifurcator: Removed
Wing: Removed

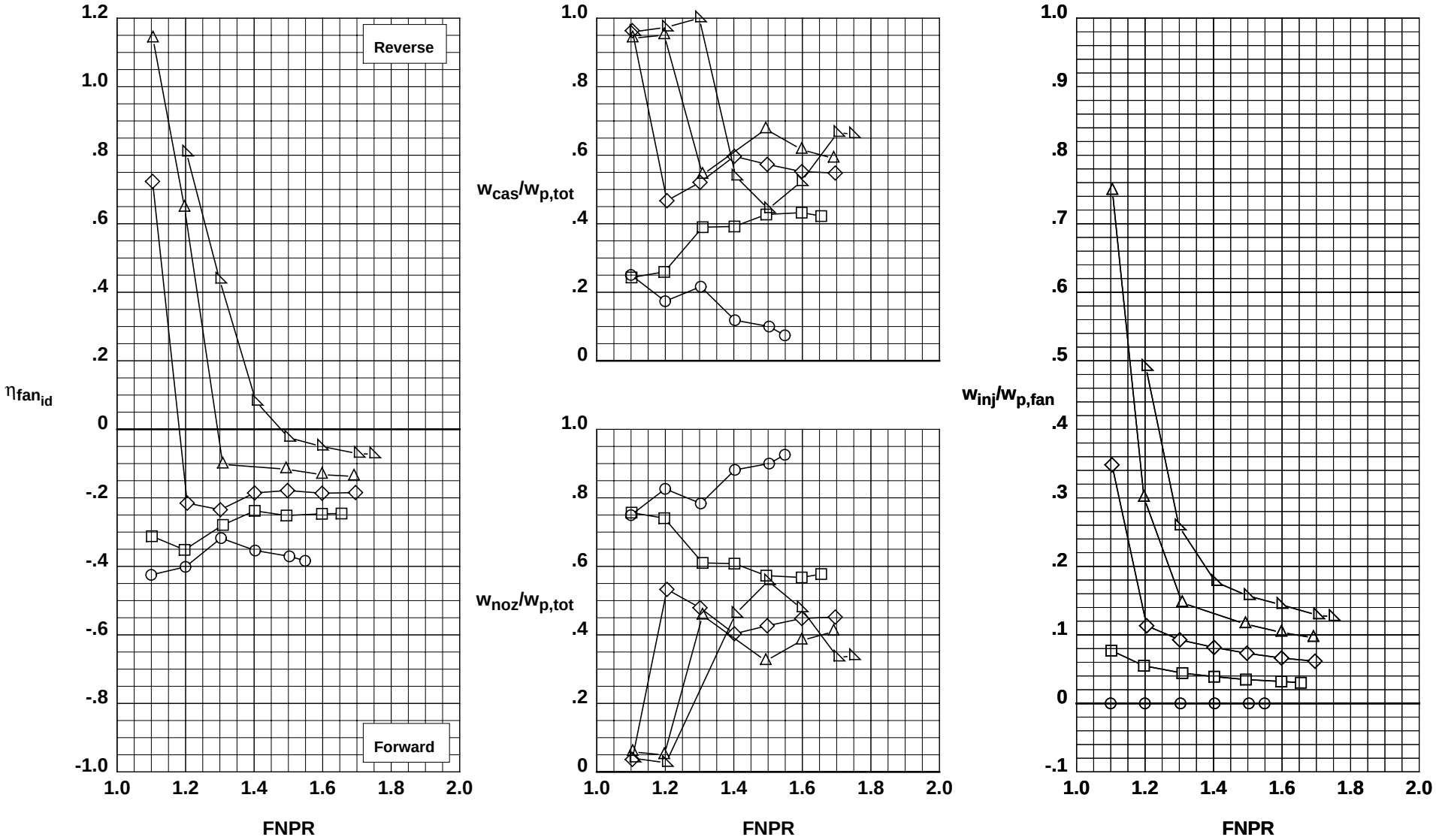

Figure D-4. Blockerless thrust reverser performance characteristics for configuration 604.

Fwd Injector: 0.013"@90°
Mid Injector: None
Aft Injector: 0.013"@90°
Throat Injector: None

	Test	Run	Configuration	IPR
○	993	10	605	0.00
□	993	11	605	4.05
◇	993	11	605	8.08
△	993	11	605	12.02
◺	993	11	605	16.05

Operation Mode: Fan+Injection
Cascades: Installed
Fwd Bullnose: Bullnose
Port Fairing: #2
Bifurcator: Removed
Wing: Removed

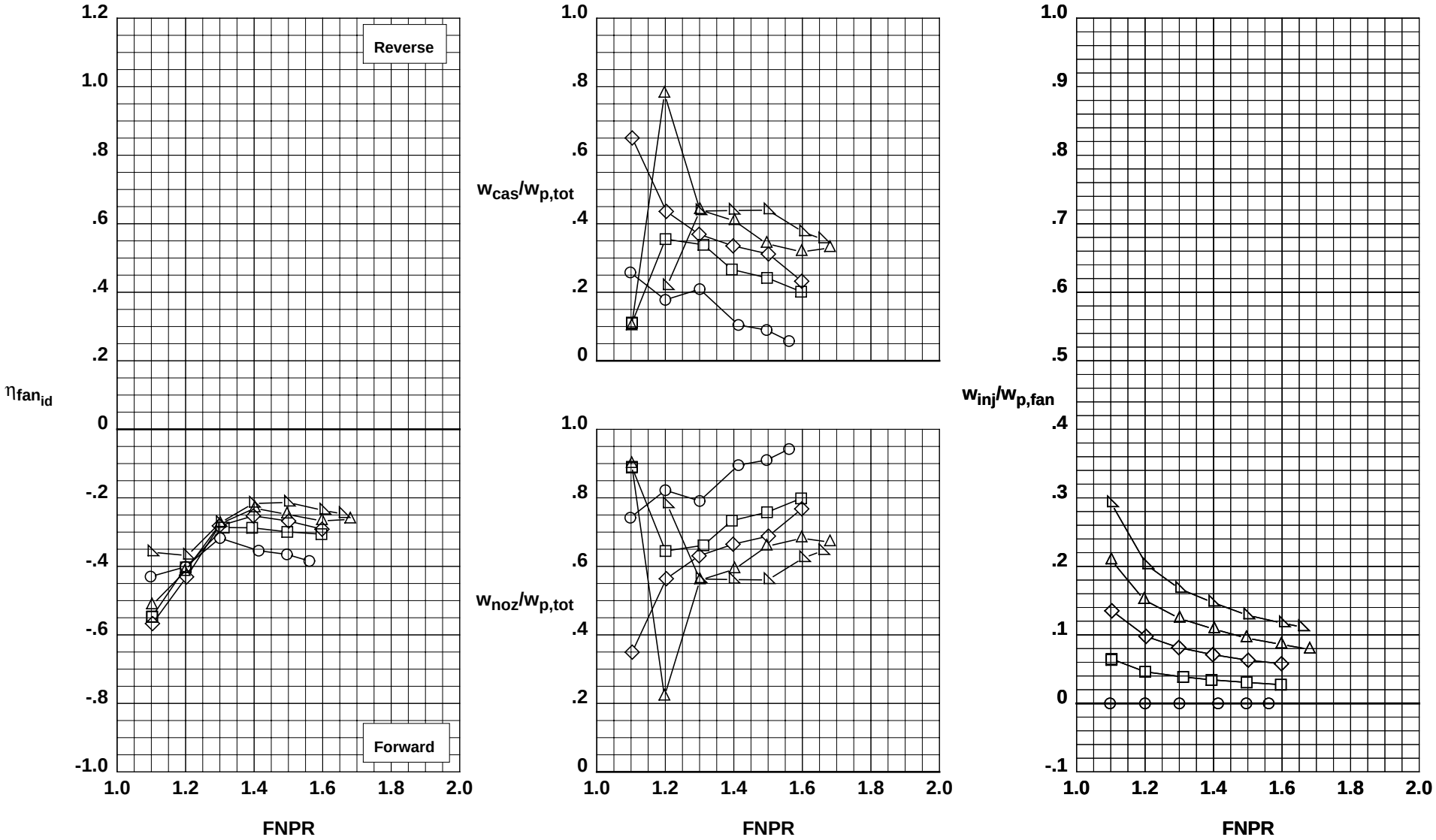

Figure D-5. Blockerless thrust reverser performance characteristics for configuration 605.

Fwd Injector: 0.013"@90°
Mid Injector: 0.013"@90°
Aft Injector: 0.013"@90°
Throat Injector: None

	Test	Run	Configuration	IPR
○	993	12	606	0.00
□	993	13	606	4.00
◇	993	13	606	8.00
△	993	13	606	12.05

Operation Mode: Fan+Injection
Cascades: Installed
Fwd Bullnose: Bullnose
Port Fairing: #2
Bifurcator: Removed
Wing: Removed

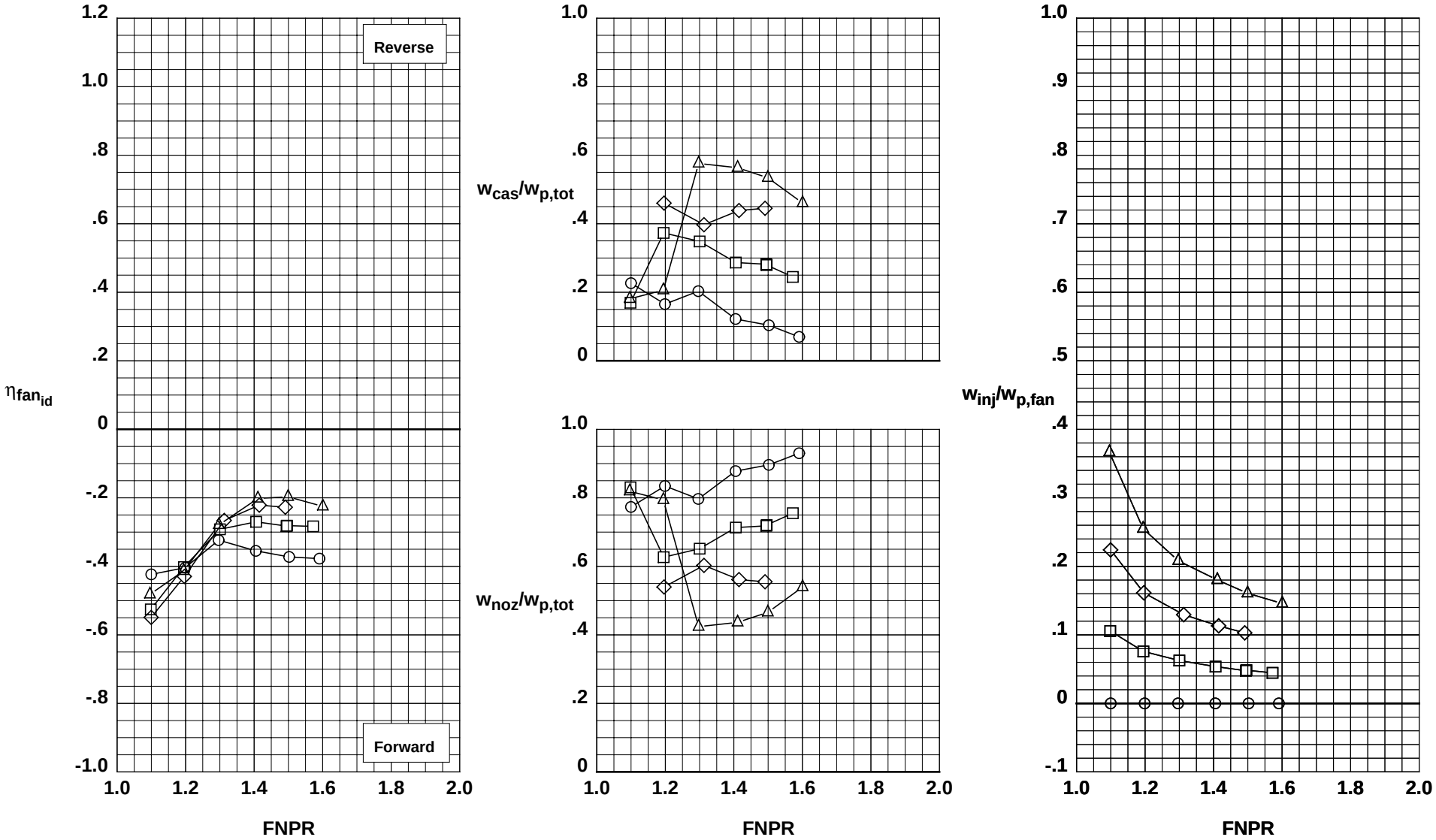

Figure D-6. Blockerless thrust reverser performance characteristics for configuration 606.

Fwd Injector: 0.025"@90°
Mid Injector: None
Aft Injector: None
Throat Injector: None

	Test	Run	Configuration	IPR
○	993	14	607	0.00
□	993	15	607	4.00
◇	993	15	607	8.04
△	993	15	607	12.02
◺	993	15	607	15.97

Operation Mode: Fan+Injection
Cascades: Installed
Fwd Bullnose: Bullnose
Port Fairing: #2
Bifurcator: Removed
Wing: Removed

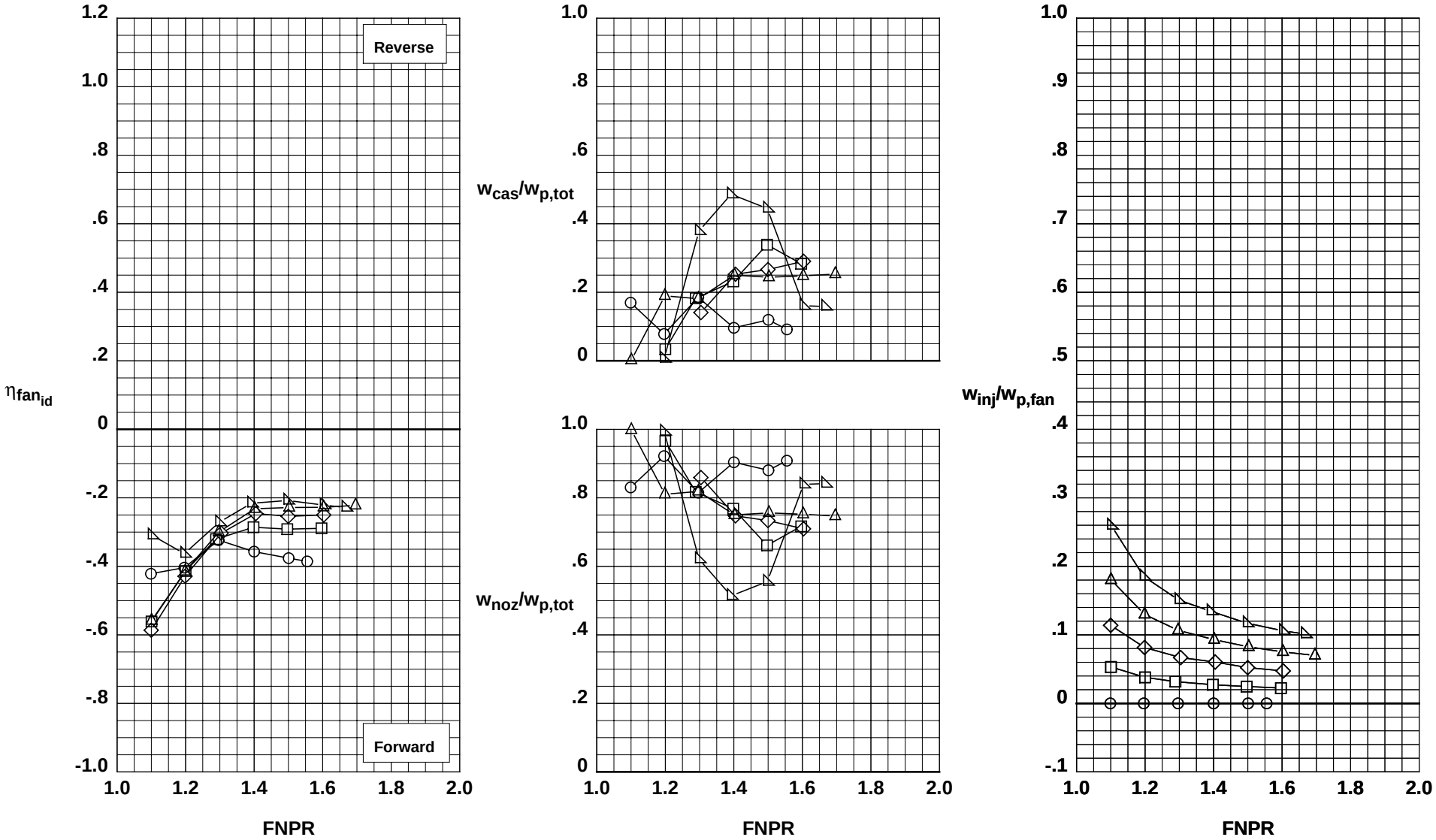

Figure D-7. Blockerless thrust reverser performance characteristics for configuration 607.

Fwd Injector: 0.025"@90°
Mid Injector: None
Aft Injector: None
Throat Injector: None

	Test	Run	Configuration	IPR
○	993	17	608	0.00
□	993	19	608	4.04
◇	993	19	608	8.02
△	993	19	608	12.00
◺	993	19	608	16.01

Operation Mode: Fan+Injection
Cascades: Removed
Fwd Bullnose: Coanda #3
Port Fairing: #2
Bifurcator: Removed
Wing: Removed

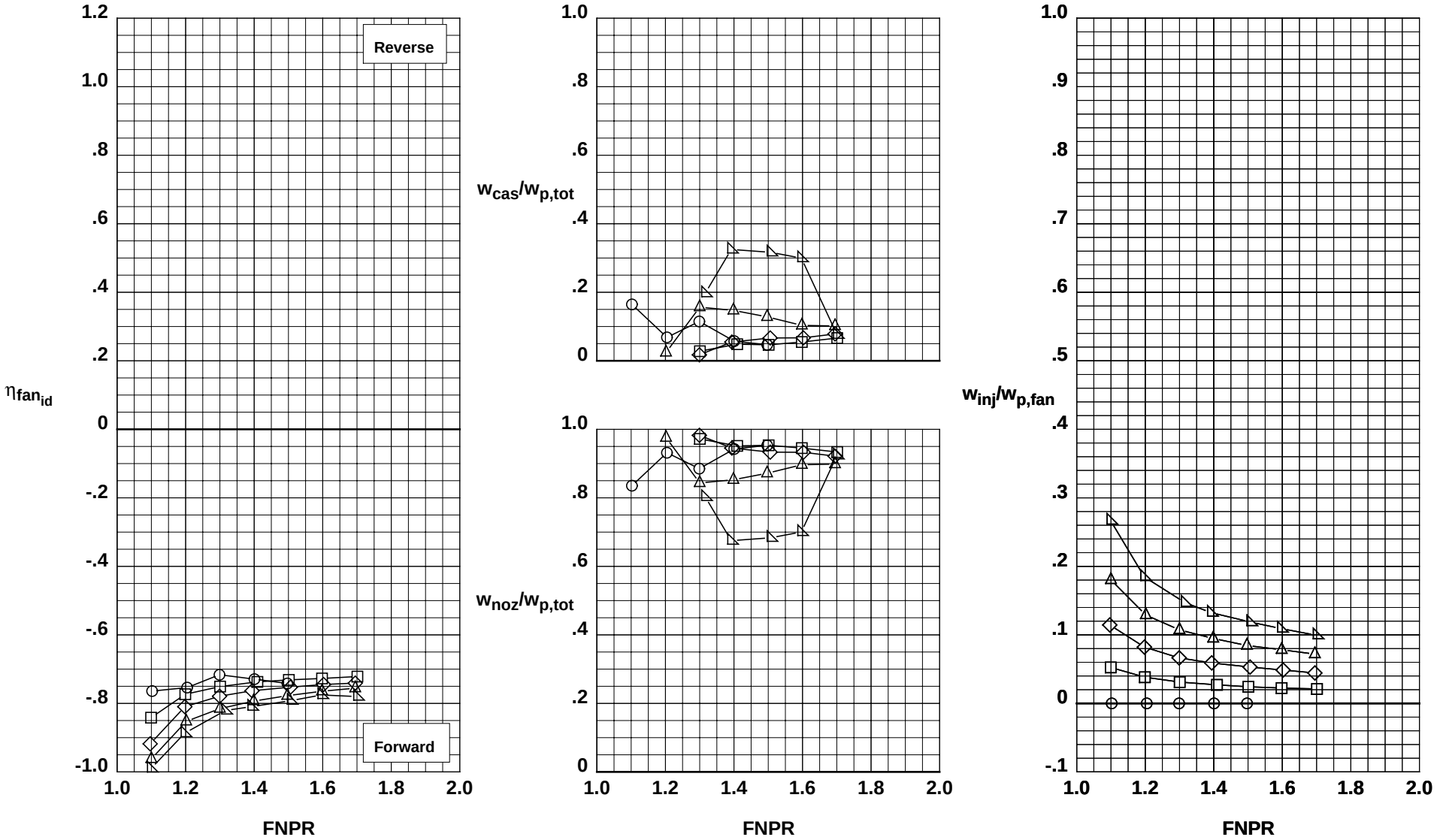

Figure D-8. Blockerless thrust reverser performance characteristics for configuration 608.

Fwd Injector: 0.025"@90°
Mid Injector: None
Aft Injector: None
Throat Injector: None

	Test	Run	Configuration	IPR
○	993	21	609	0.00
□	993	23	609	4.02
◇	993	23	609	8.02

Operation Mode: Fan+Injection
Cascades: Installed
Fwd Bullnose: Coanda #1
Port Fairing: #2
Bifurcator: Removed
Wing: Removed

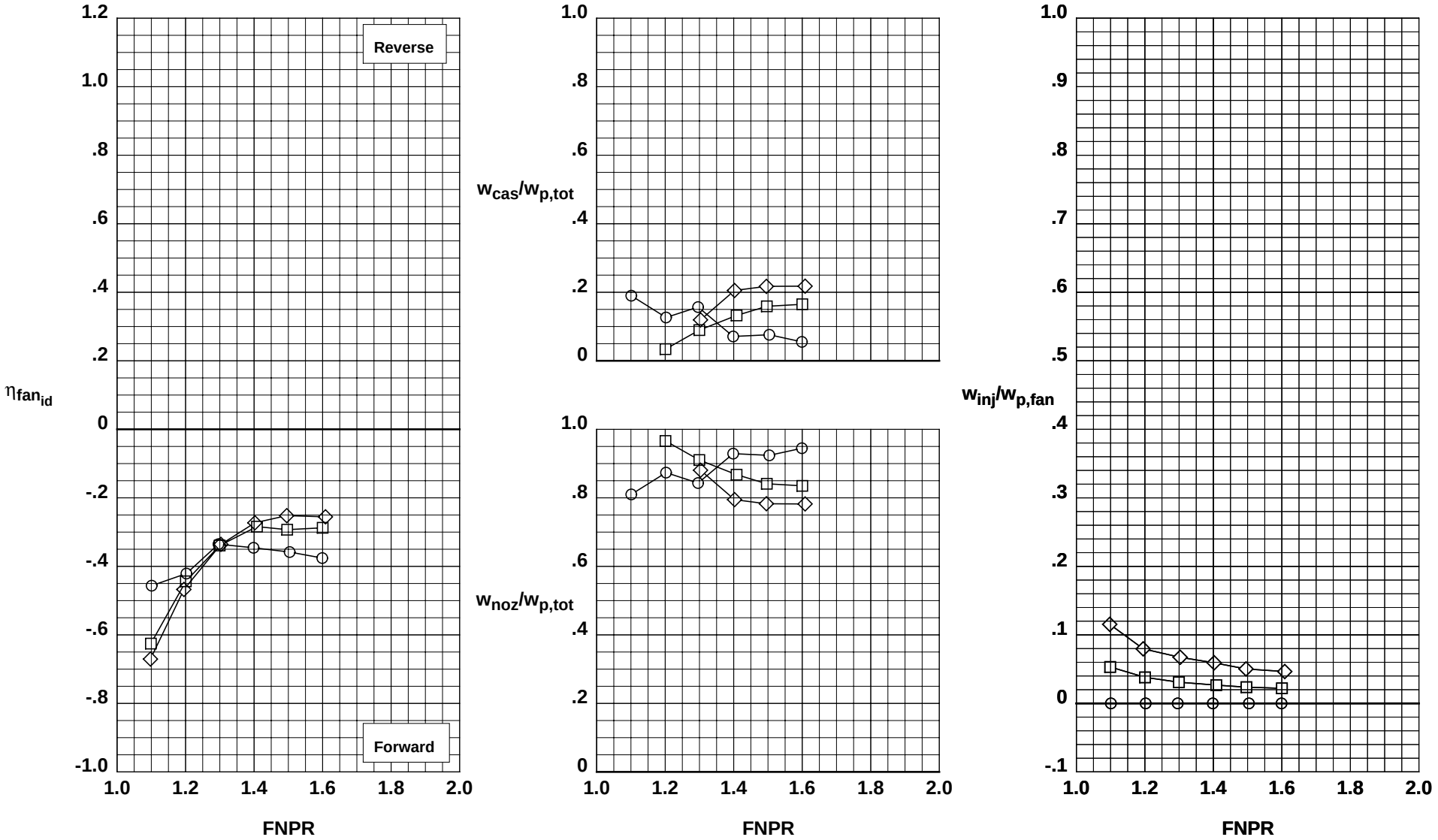

Figure D-9. Blockerless thrust reverser performance characteristics for configuration 609.

Fwd Injector: 0.025"@90°
Mid Injector: None
Aft Injector: None
Throat Injector: None

	Test	Run	Configuration	IPR
○	993	25	610	0.00
□	993	26	610	4.00
◇	993	26	610	8.04
△	993	26	610	12.02
◺	993	26	610	16.01

Operation Mode: Fan+Injection
Cascades: Installed
Fwd Bullnose: Coanda #2
Port Fairing: #2
Bifurcator: Removed
Wing: Removed

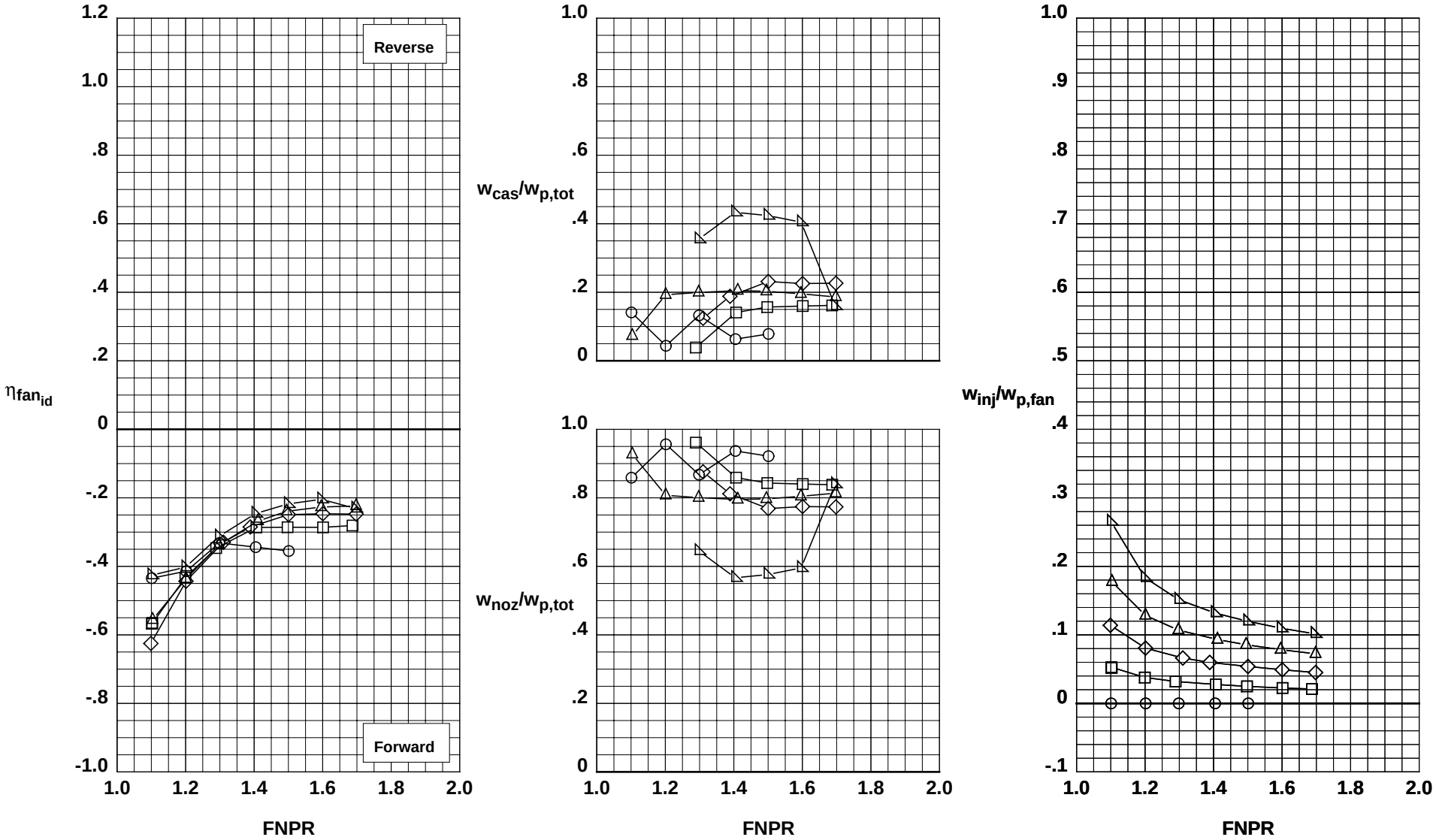

Figure D-10. Blockerless thrust reverser performance characteristics for configuration 610.

Fwd Injector: None
Mid Injector: None
Aft Injector: 0.025" tab3
Throat Injector: None

	Test	Run	Configuration	IPR
○	993	27	611	0.00
□	993	28	611	3.99
◇	993	28	611	8.00
△	993	28	611	12.01
◺	993	28	611	15.99

Operation Mode: Fan+Injection
Cascades: Installed
Fwd Bullnose: Bullnose
Port Fairing: #2
Bifurcator: Removed
Wing: Removed

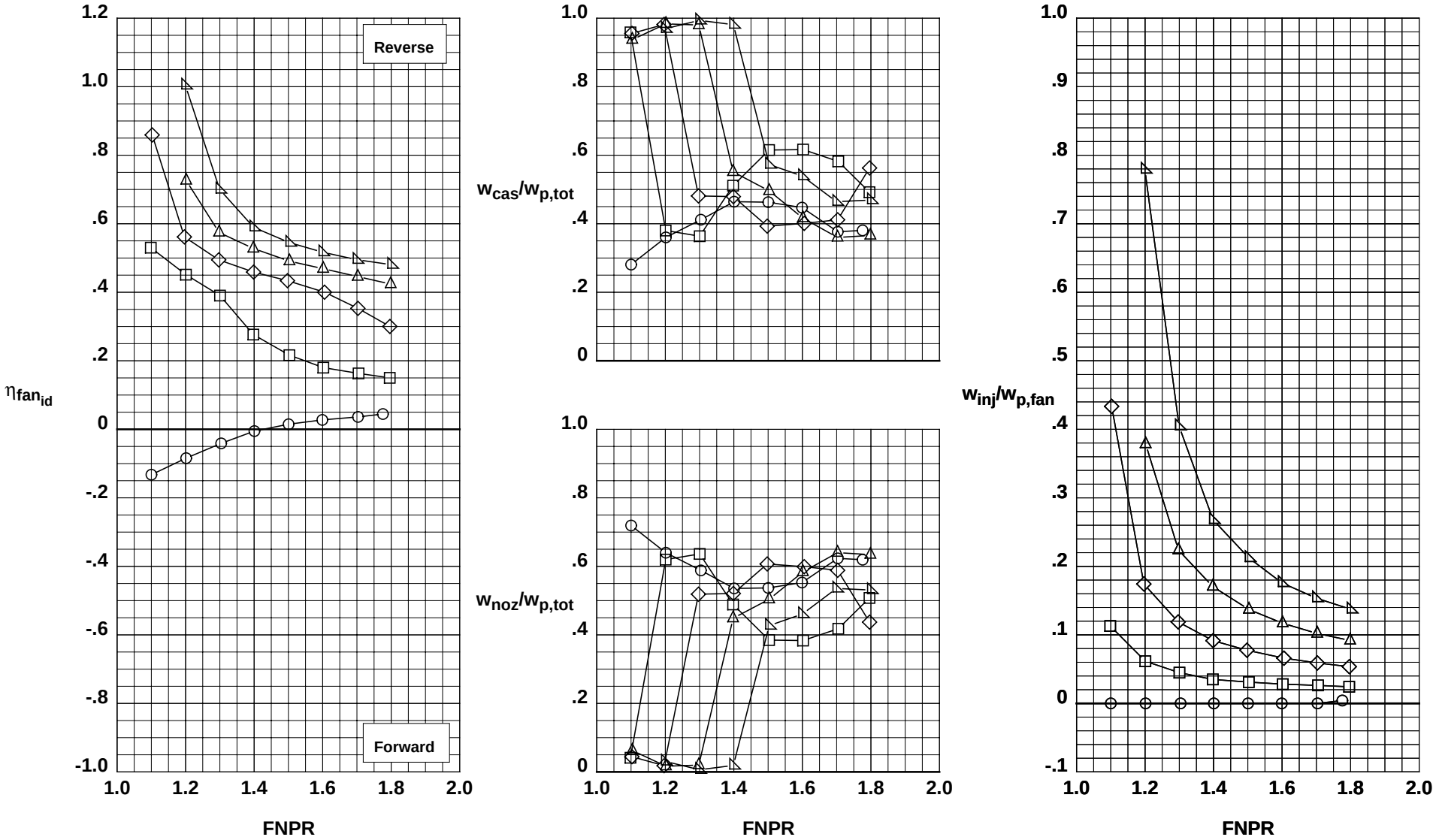

Figure D-11. Blockerless thrust reverser performance characteristics for configuration 611.

Fwd Injector: None
Mid Injector: None
Aft Injector: 0.025" tab1
Throat Injector: None

	Test	Run	Configuration	IPR
○	993	29	612	0.00
□	993	30	612	4.00
◇	993	30	612	8.01
△	993	30	612	11.99
◺	993	30	612	15.99

Operation Mode: Fan+Injection
Cascades: Installed
Fwd Bullnose: Bullnose
Port Fairing: #2
Bifurcator: Removed
Wing: Removed

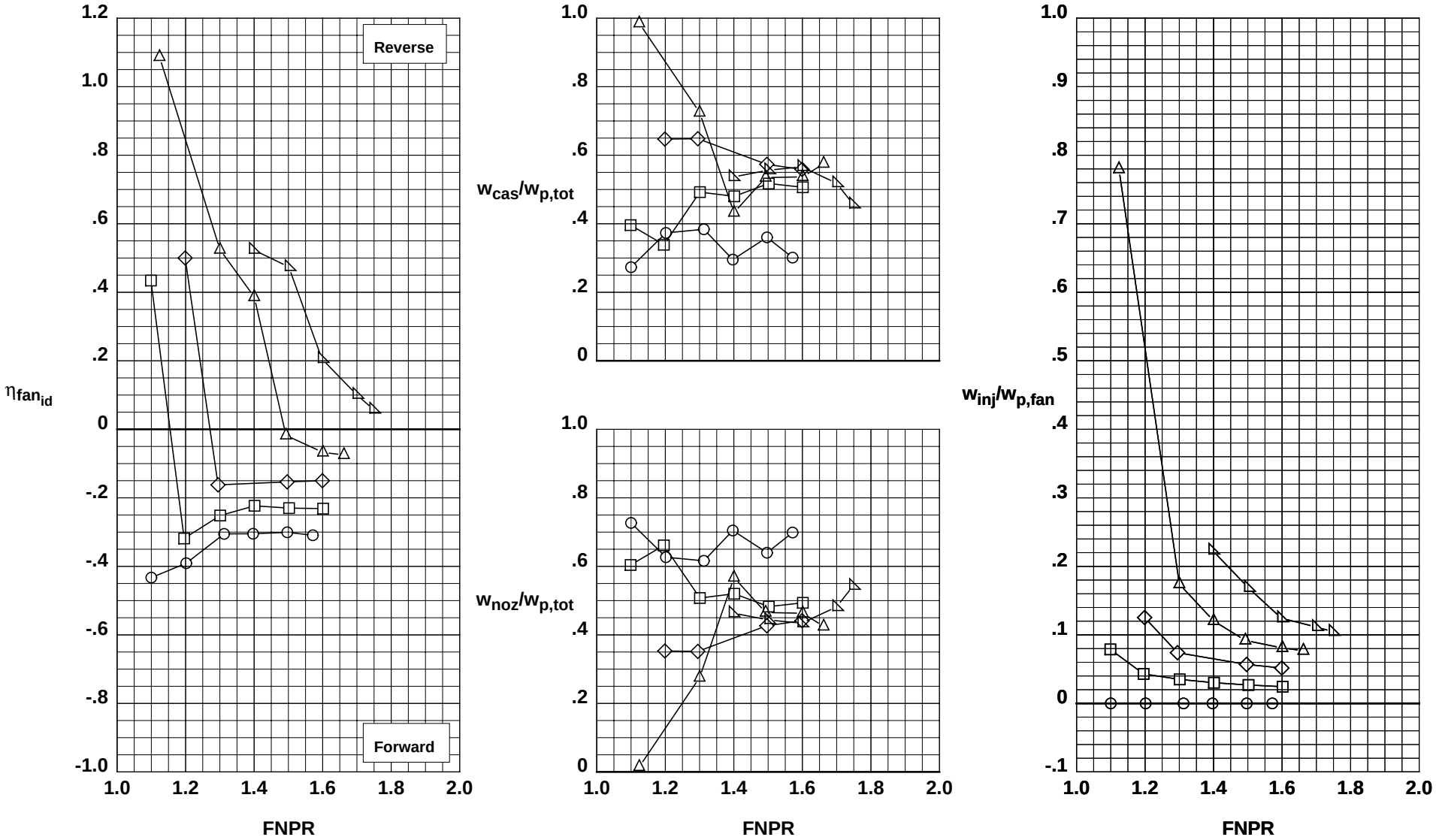

Figure D-12. Blockerless thrust reverser performance characteristics for configuration 612.

Fwd Injector: None
Mid Injector: None
Aft Injector: None
Throat Injector: 0.025@45°

	Test	Run	Configuration	IPR
○	993	31	613	0.00
□	993	32	613	4.02
◇	993	32	613	8.01
△	993	32	613	12.03
◺	993	32	613	16.02

Operation Mode: Fan+Injection
Cascades: Installed
Fwd Bullnose: Bullnose
Port Fairing: #2
Bifurcator: Removed
Wing: Removed

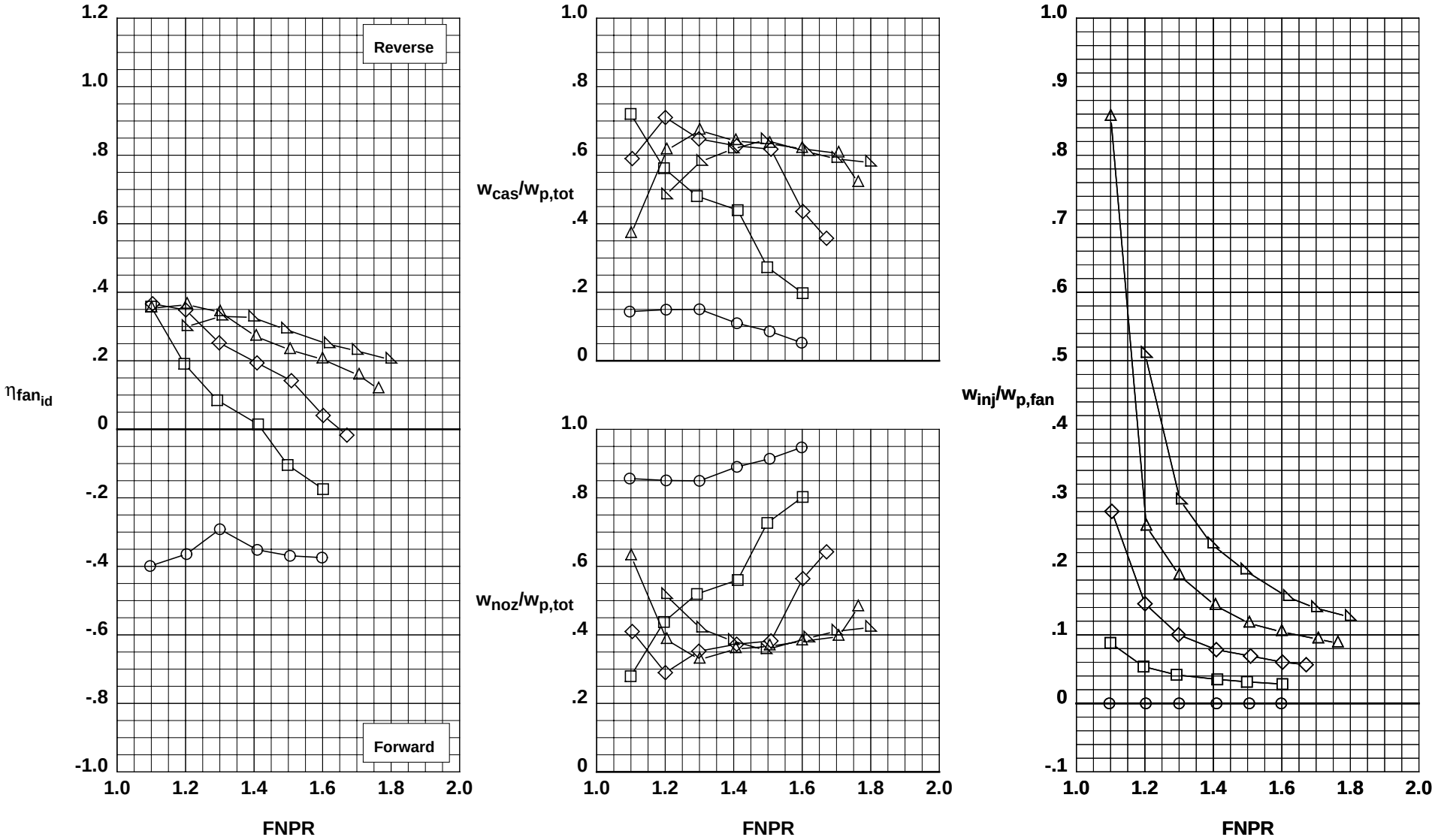

Figure D-13. Blockerless thrust reverser performance characteristics for configuration 613.

Fwd Injector: None
Mid Injector: None
Aft Injector: 0.025@45°
Throat Injector: None

	Test	Run	Configuration	IPR
○	993	33	614	0.00
□	993	34	614	4.00
◇	993	34	614	8.01
△	993	34	614	11.98
◺	993	34	614	16.01

Operation Mode: Fan+Injection
Cascades: Installed
Fwd Bullnose: Bullnose
Port Fairing: #2
Bifurcator: Removed
Wing: Removed

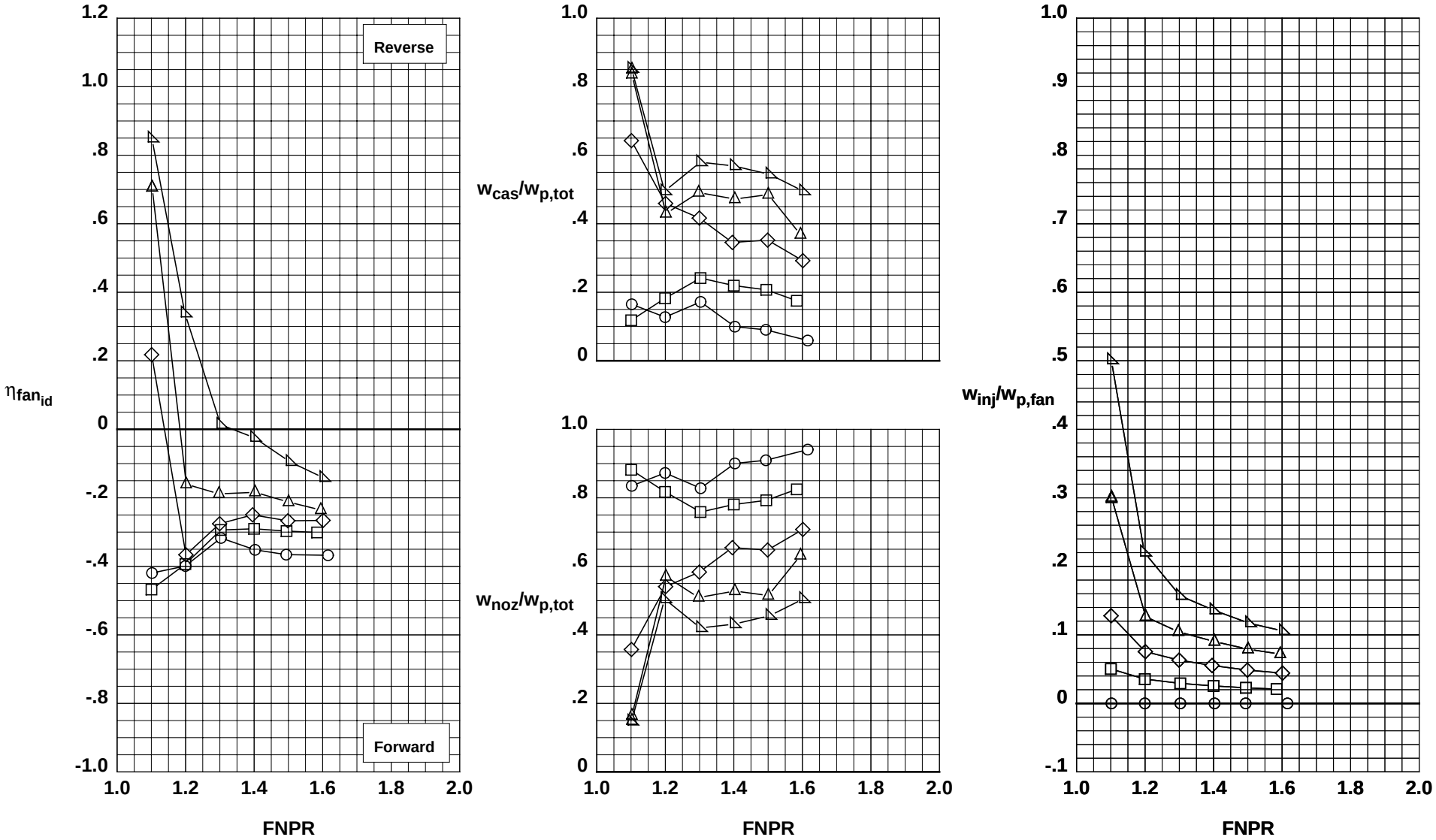

Figure D-14. Blockerless thrust reverser performance characteristics for configuration 614.

Fwd Injector: None
Mid Injector: 0.025"@45°
Aft Injector: None
Throat Injector: None

	Test	Run	Configuration	IPR
○	993	35	615	0.00
□	993	36	615	4.01
◇	993	36	615	8.00
△	993	36	615	12.00
◺	993	36	615	16.00

Operation Mode: Fan+Injection
Cascades: Installed
Fwd Bullnose: Bullnose
Port Fairing: #2
Bifurcator: Removed
Wing: Removed

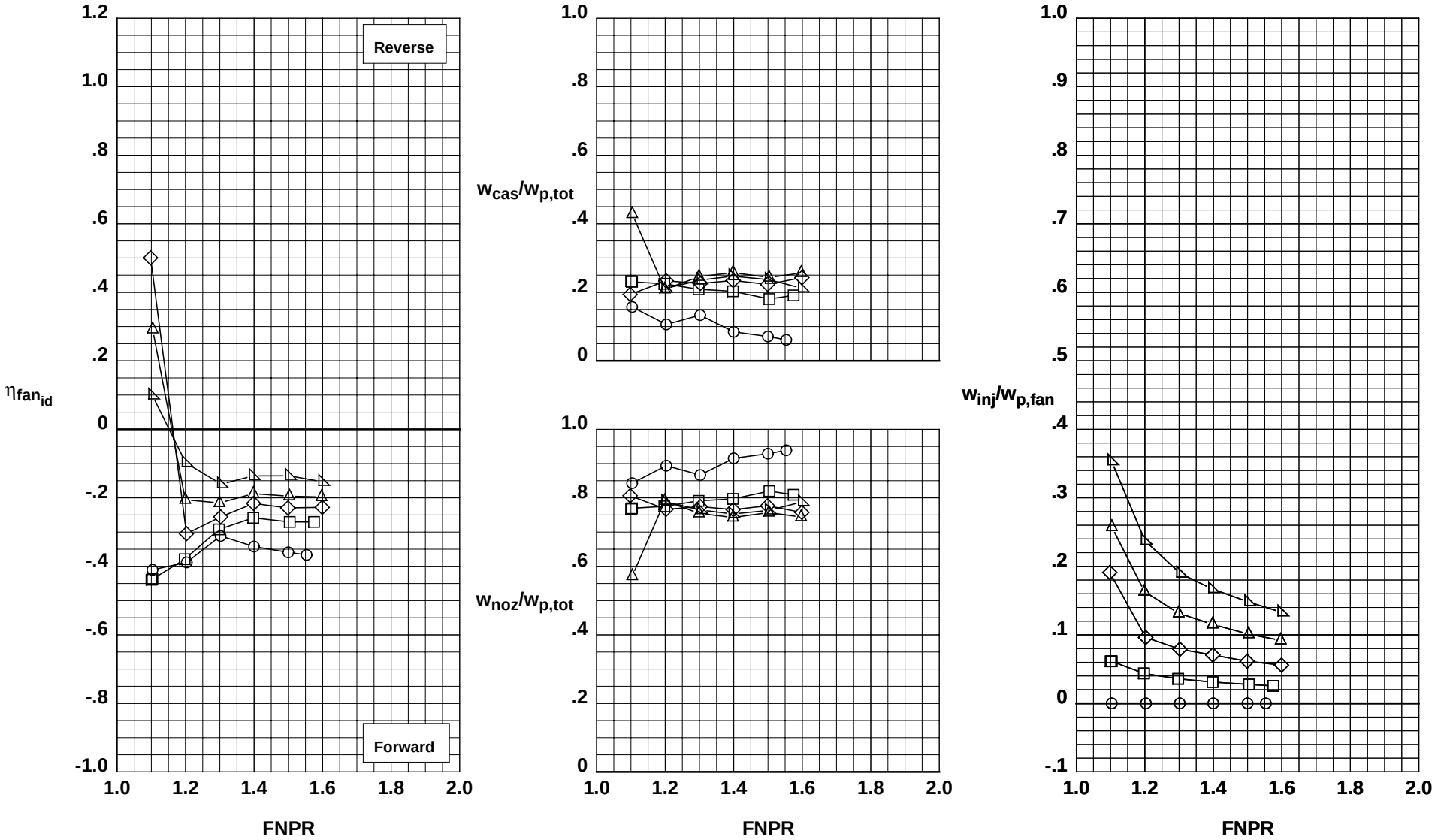

Figure D-15. Blockerless thrust reverser performance characteristics for configuration 615.

Fwd Injector: None
Mid Injector: 0.013"@45°
Aft Injector: 0.013"@45°
Throat Injector: None

	Test	Run	Configuration	IPR
○	993	37	616	0.00
□	993	38	616	4.02
◇	993	38	616	8.02
△	993	38	616	12.00
◺	993	38	616	16.02

Operation Mode: Fan+Injection
Cascades: Installed
Fwd Bullnose: Bullnose
Port Fairing: #2
Bifurcator: Removed
Wing: Removed

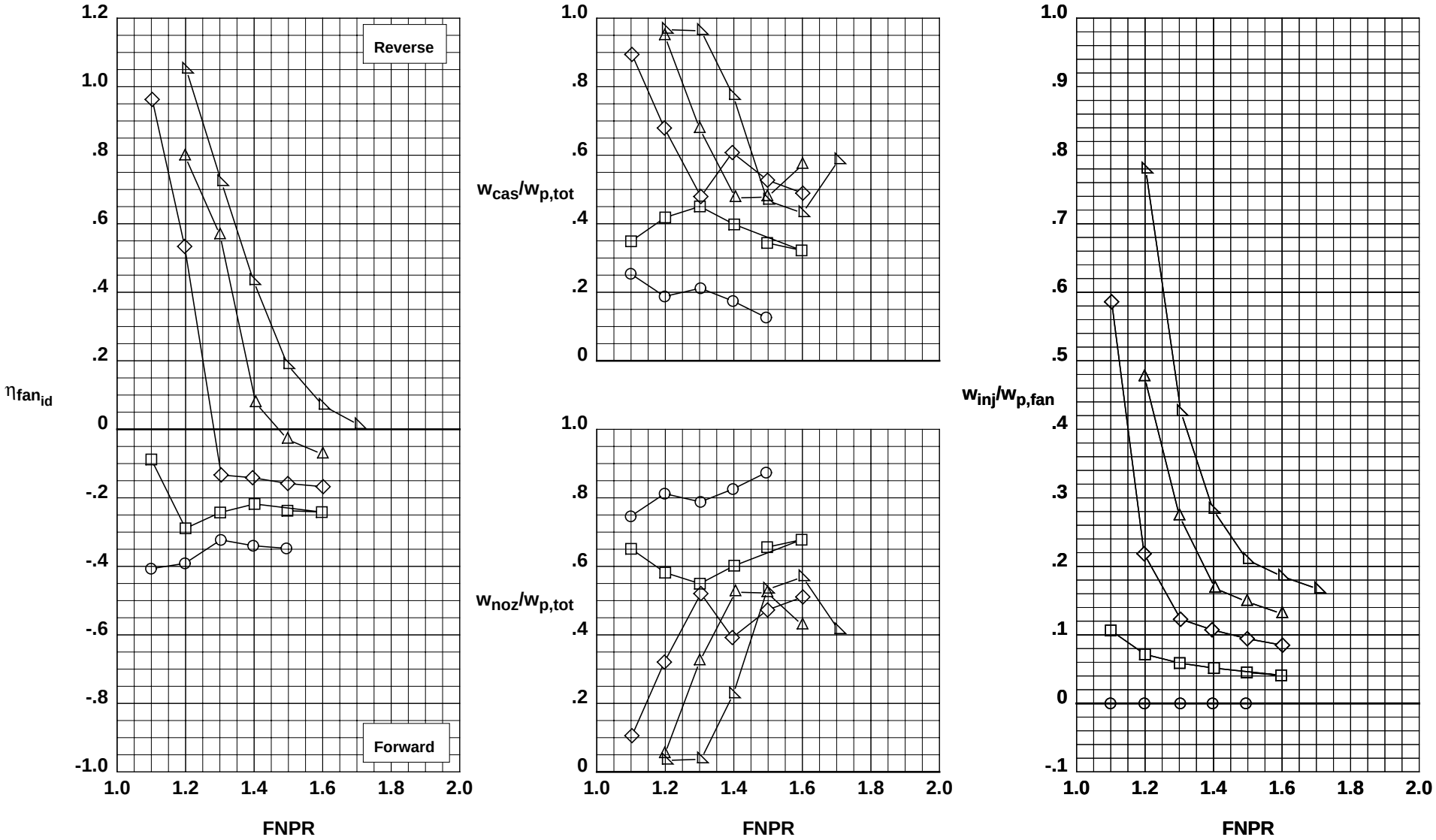

Figure D-16. Blockerless thrust reverser performance characteristics for configuration 616.

Fwd Injector: None
Mid Injector: None
Aft Injector: None
Throat Injector: 0.013@45°

	Test	Run	Configuration	IPR
○	993	39	617	0.00
□	993	40	617	3.99
◇	993	40	617	8.02
△	993	40	617	11.99
◺	993	40	617	16.01

Operation Mode: Fan+Injection
Cascades: Installed
Fwd Bullnose: Bullnose
Port Fairing: #2
Bifurcator: Removed
Wing: Removed

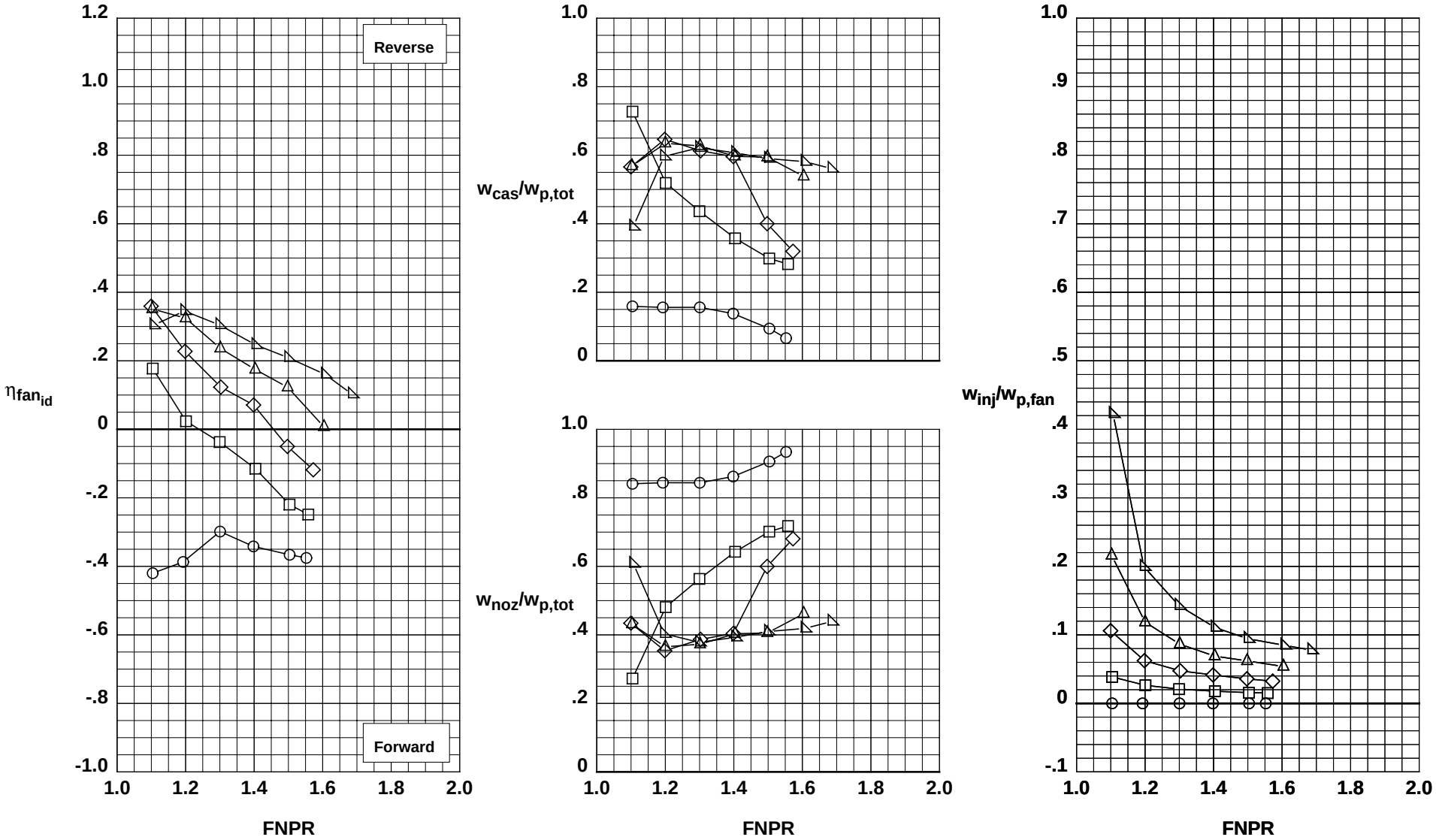

Figure D-17. Blockerless thrust reverser performance characteristics for configuration 617.

Operation Mode: Dual Flow
Target Angle: 20°
Area Ratio: 1.05
Kicker/Extension: None
Bifurcator: Removed
Wing: Removed

	Test	Run	Configuration
○	987	28	301

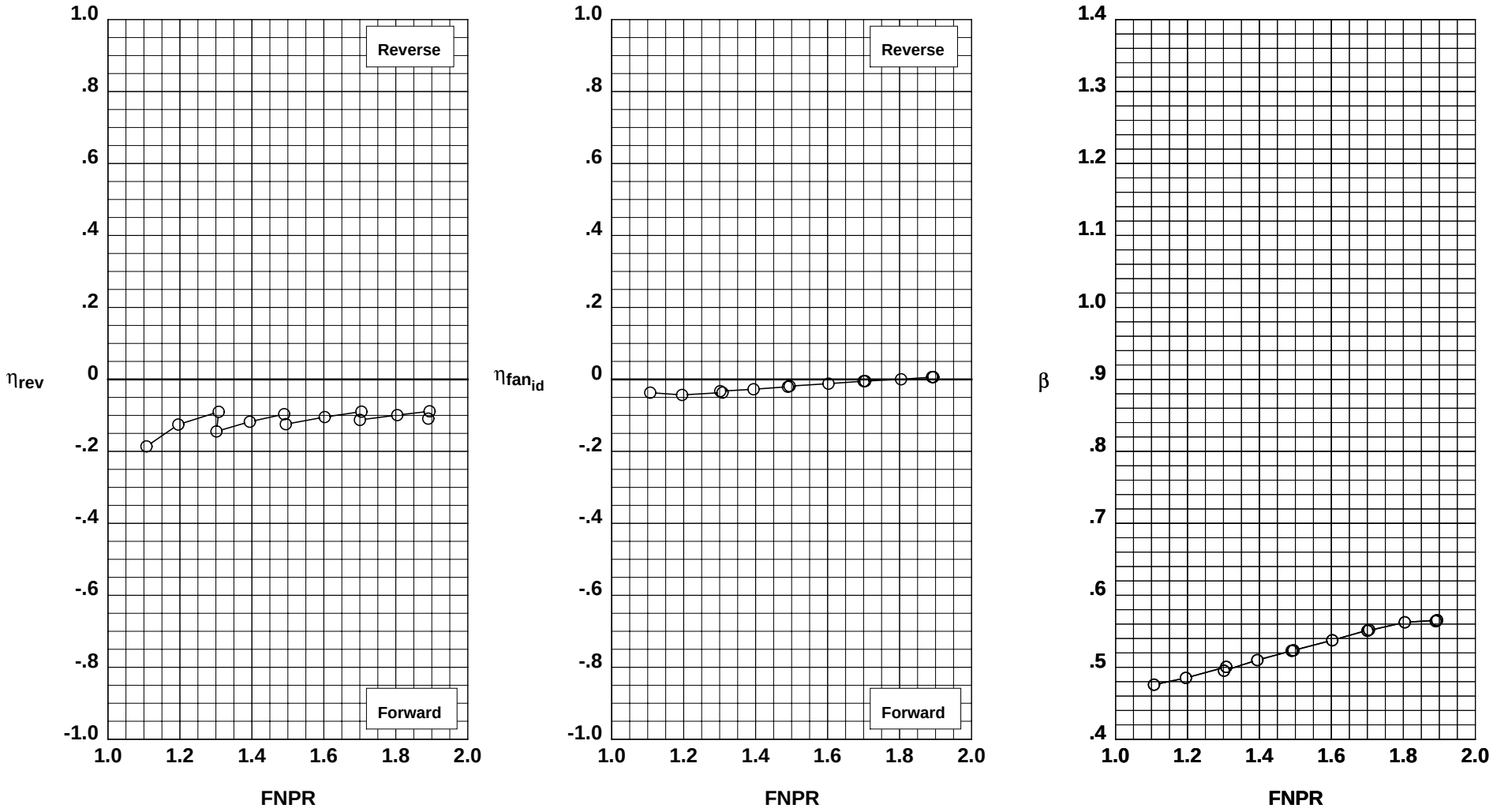

Figure E-1. Annular (metal) target thrust reverser performance characteristics for configuration 301.

Operation Mode: Dual Flow
Target Angle: 20°
Area Ratio: 1.15
Kicker/Extension: None
Bifurcator: Removed
Wing: Removed

	Test	Run	Configuration
○	987	30	302

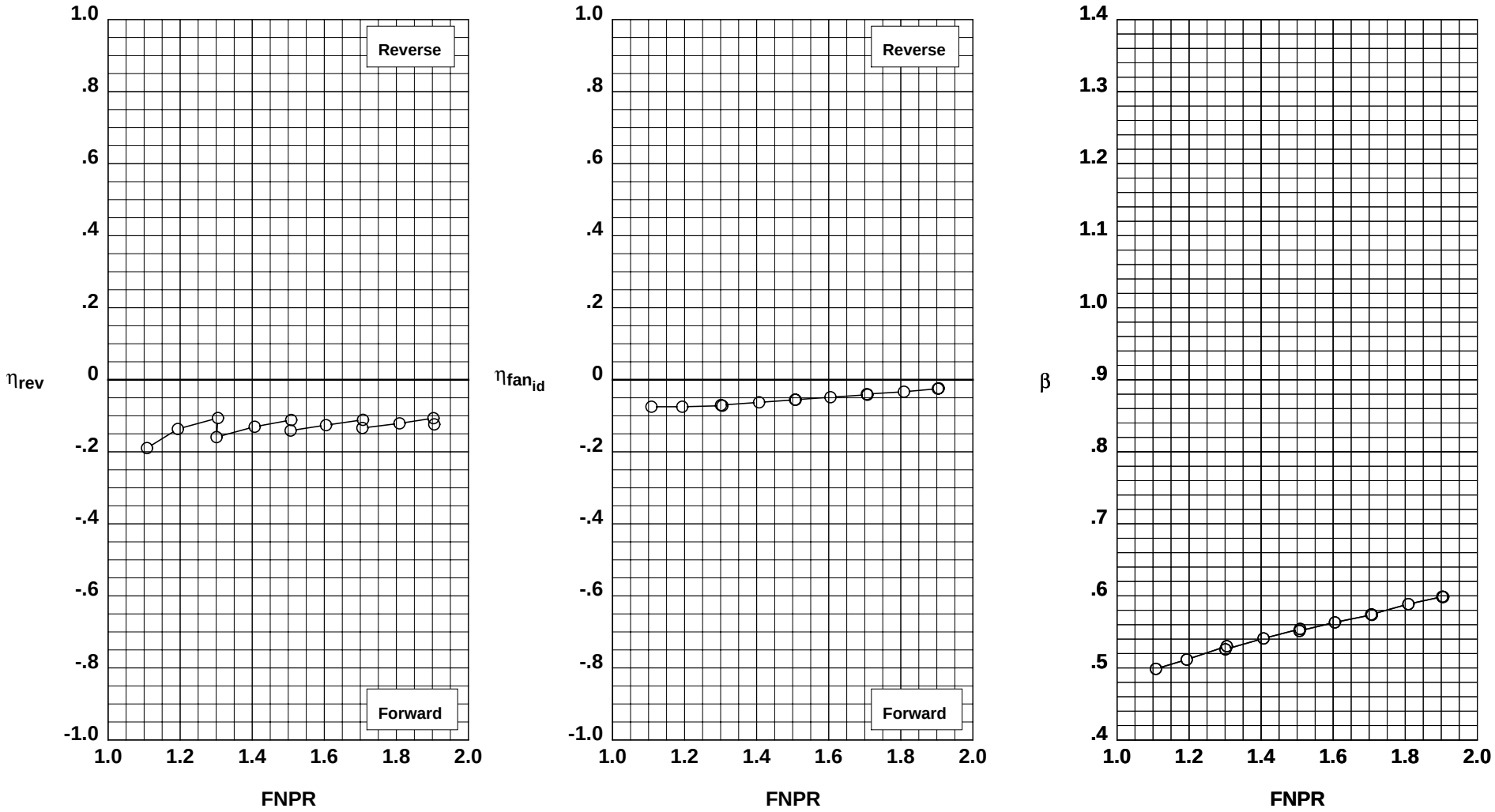

Figure E-2. Annular (metal) target thrust reverser performance characteristics for configuration 302.

Operation Mode: Dual Flow
Target Angle: 20°
Area Ratio: 1.25
Kicker/Extension: None
Bifurcator: Removed
Wing: Removed

	Test	Run	Configuration
○	987	31	303

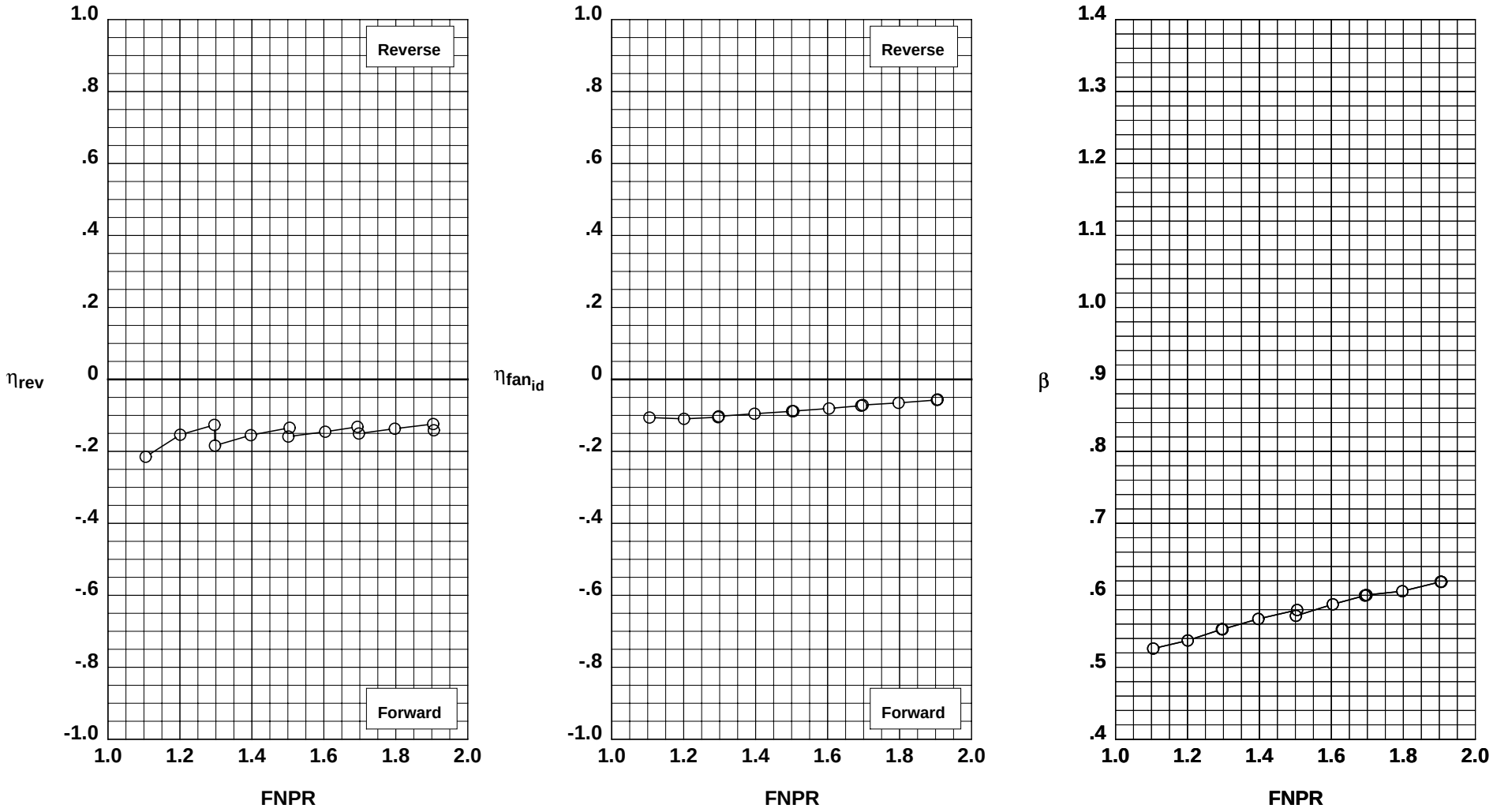

Figure E-3. Annular (metal) target thrust reverser performance characteristics for configuration 303.

Operation Mode: Dual Flow
Target Angle: 20°
Area Ratio: 1.25
Kicker/Extension: Kicker
Bifurcator: Removed
Wing: Removed

	Test	Run	Configuration
○	987	32	304

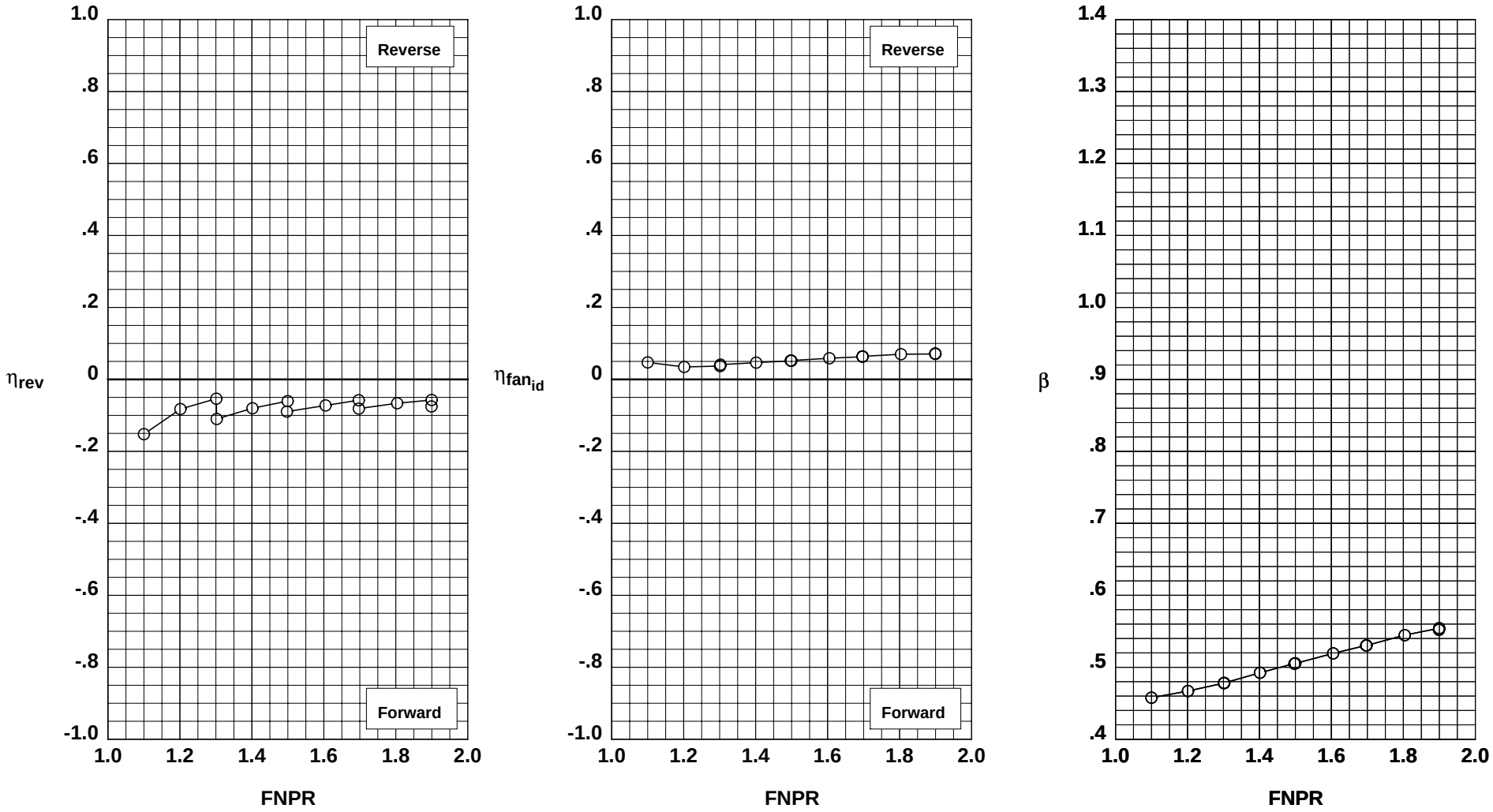

Figure E-4. Annular (metal) target thrust reverser performance characteristics for configuration 304.

Operation Mode: Dual Flow
Target Angle: 40°
Area Ratio: 1.05
Kicker/Extension: None
Bifurcator: Removed
Wing: Removed

	Test	Run	Configuration
○	987	33	305

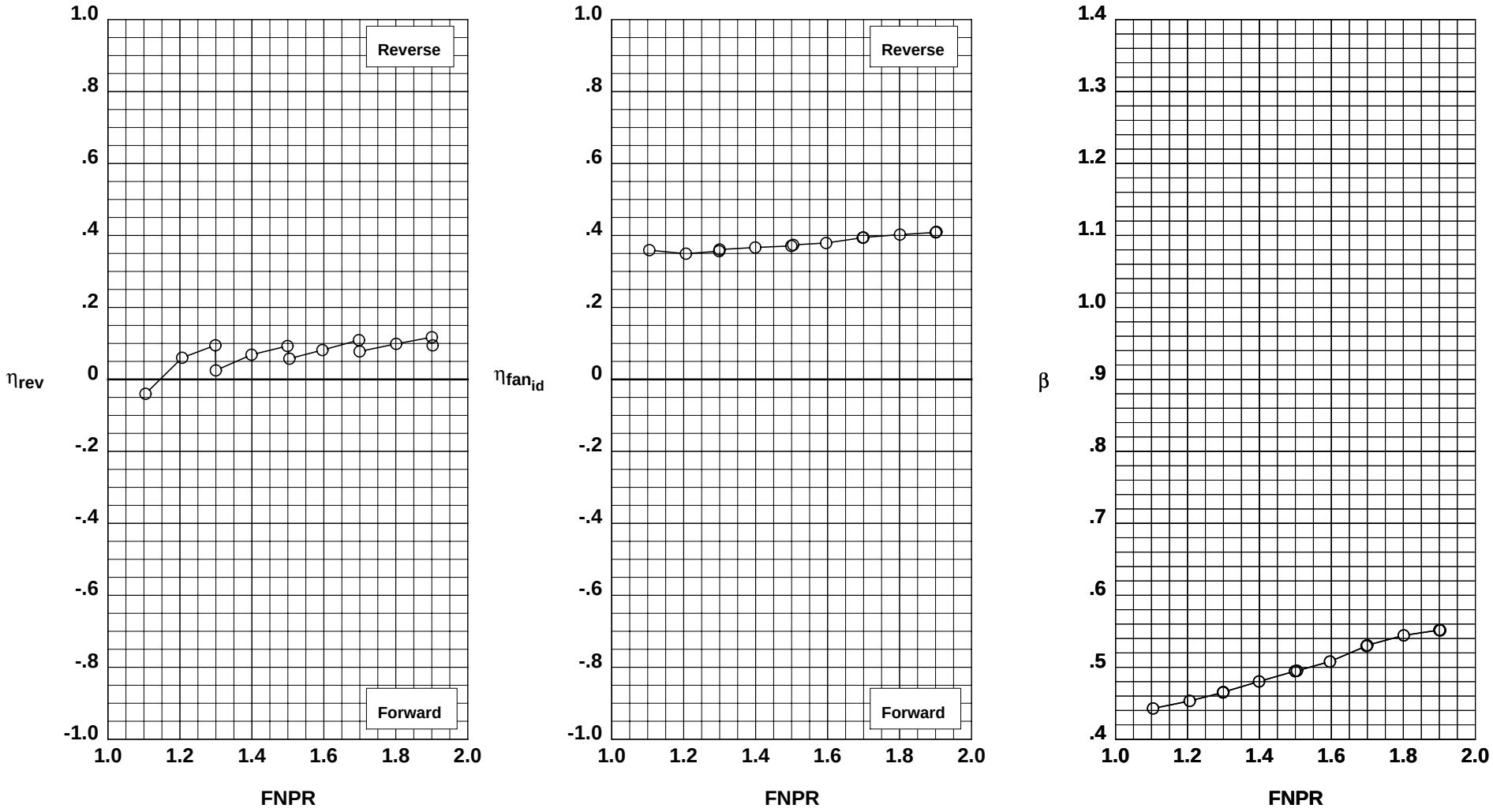

Figure E-5. Annular (metal) target thrust reverser performance characteristics for configuration 305.

Operation Mode: Dual Flow
Target Angle: 40°
Area Ratio: 1.15
Kicker/Extension: None
Bifurcator: Removed
Wing: Removed

	Test	Run	Configuration
○	987	34	306

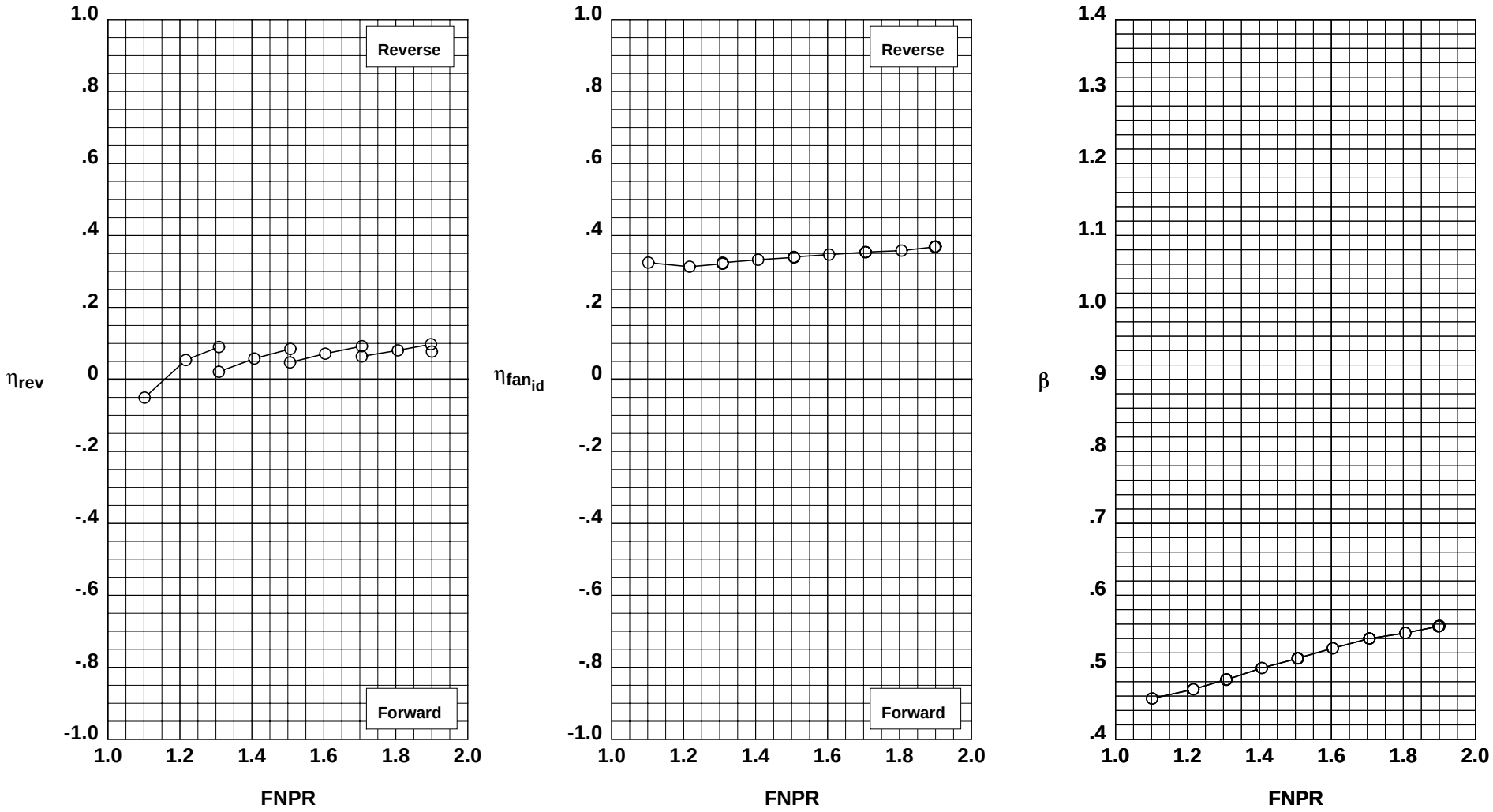

Figure E-6. Annular (metal) target thrust reverser performance characteristics for configuration 306.

Operation Mode: Dual Flow
Target Angle: 40°
Area Ratio: 1.25
Kicker/Extension: None
Bifurcator: Removed
Wing: Removed

	Test	Run	Configuration
○	987	35	307

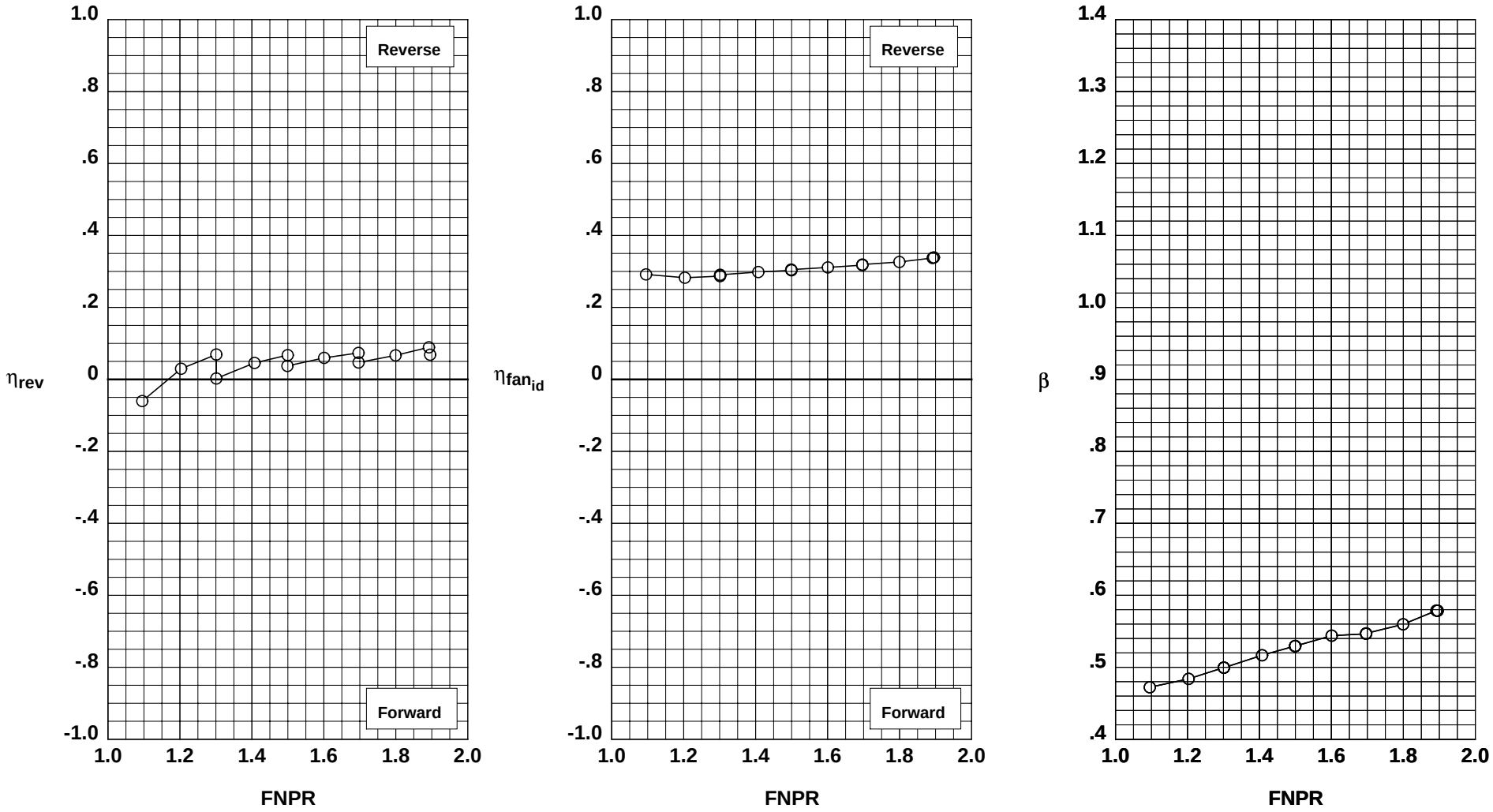

Figure E-7. Annular (metal) target thrust reverser performance characteristics for configuration 307.

Operation Mode: Dual Flow
Target Angle: 40°
Area Ratio: 1.25
Kicker/Extension: Extension
Bifurcator: Removed
Wing: Removed

	Test	Run	Configuration
○	987	36	308

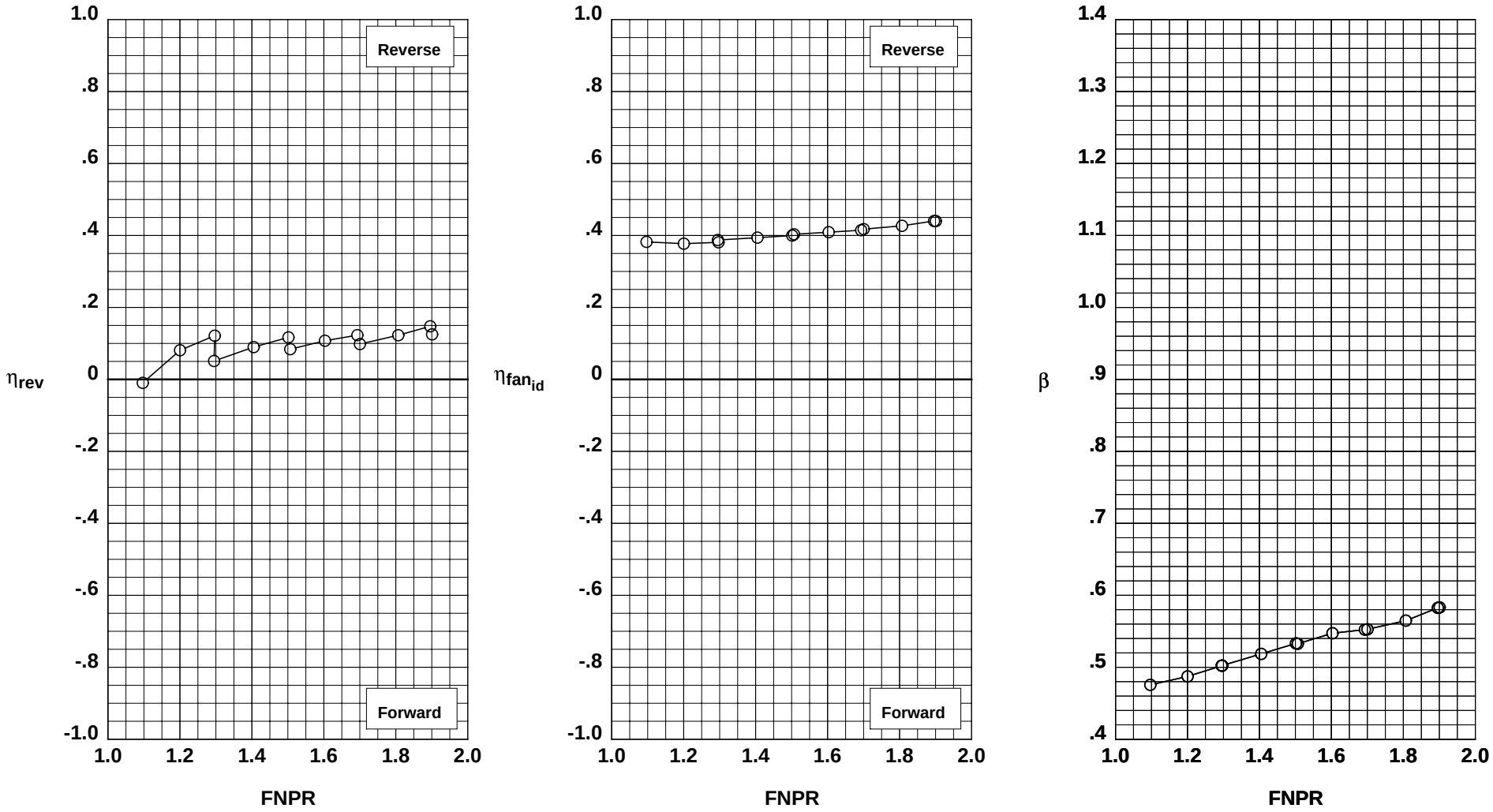

Figure E-8. Annular (metal) target thrust reverser performance characteristics for configuration 308.

Operation Mode: Dual Flow
Target Angle: 20°
Area Ratio: 1.15
Fabric: Short
Bifurcator: Removed
Wing: Removed

	Test	Run	Configuration
○	987	37	401

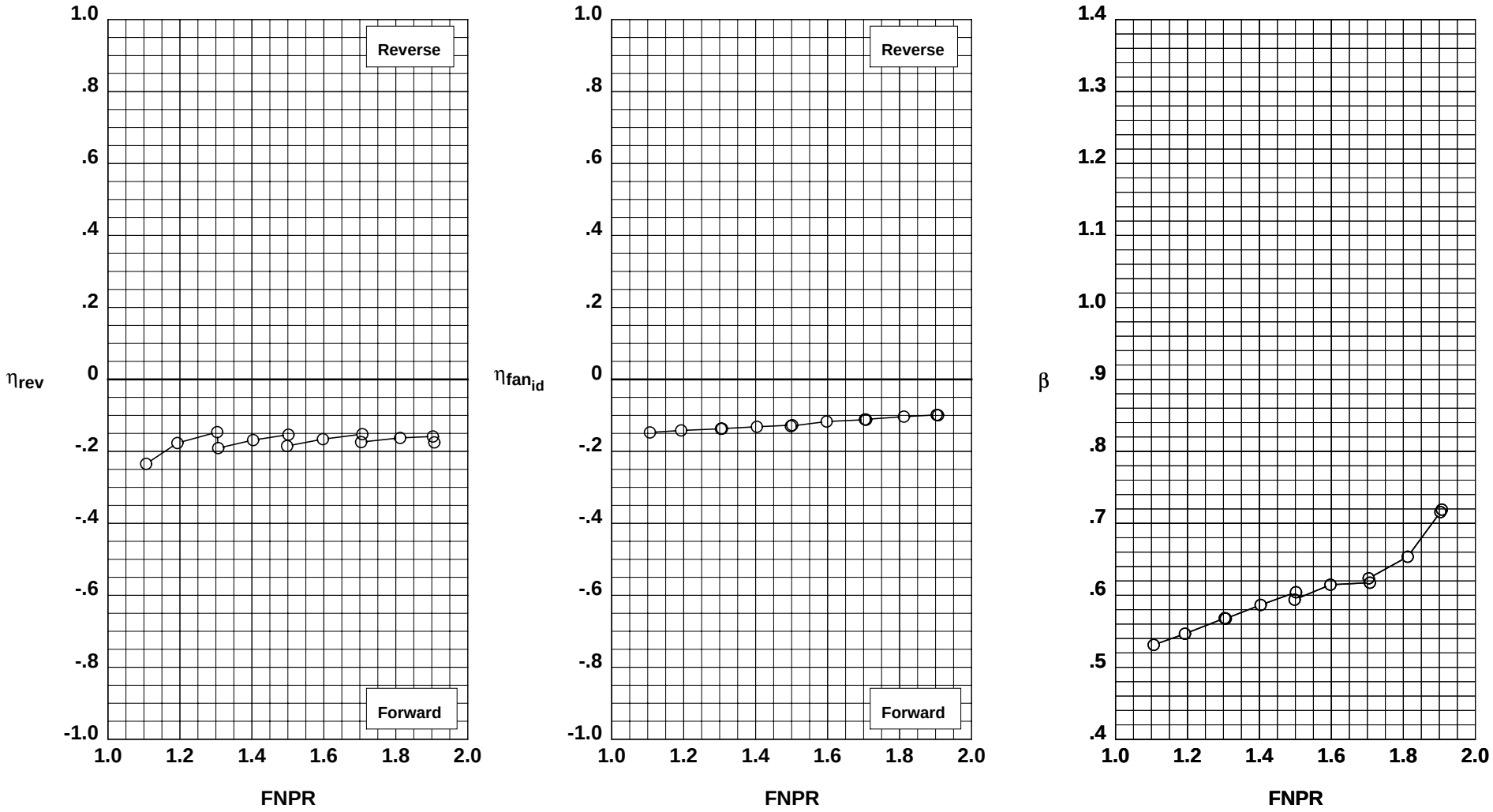

Figure F-1. Fabric target thrust reverser performance characteristics for configuration 401.

Operation Mode: Dual Flow
Target Angle: 40°
Area Ratio: 1.15
Fabric: Short
Bifurcator: Removed
Wing: Removed

	Test	Run	Configuration
○	987	38	402

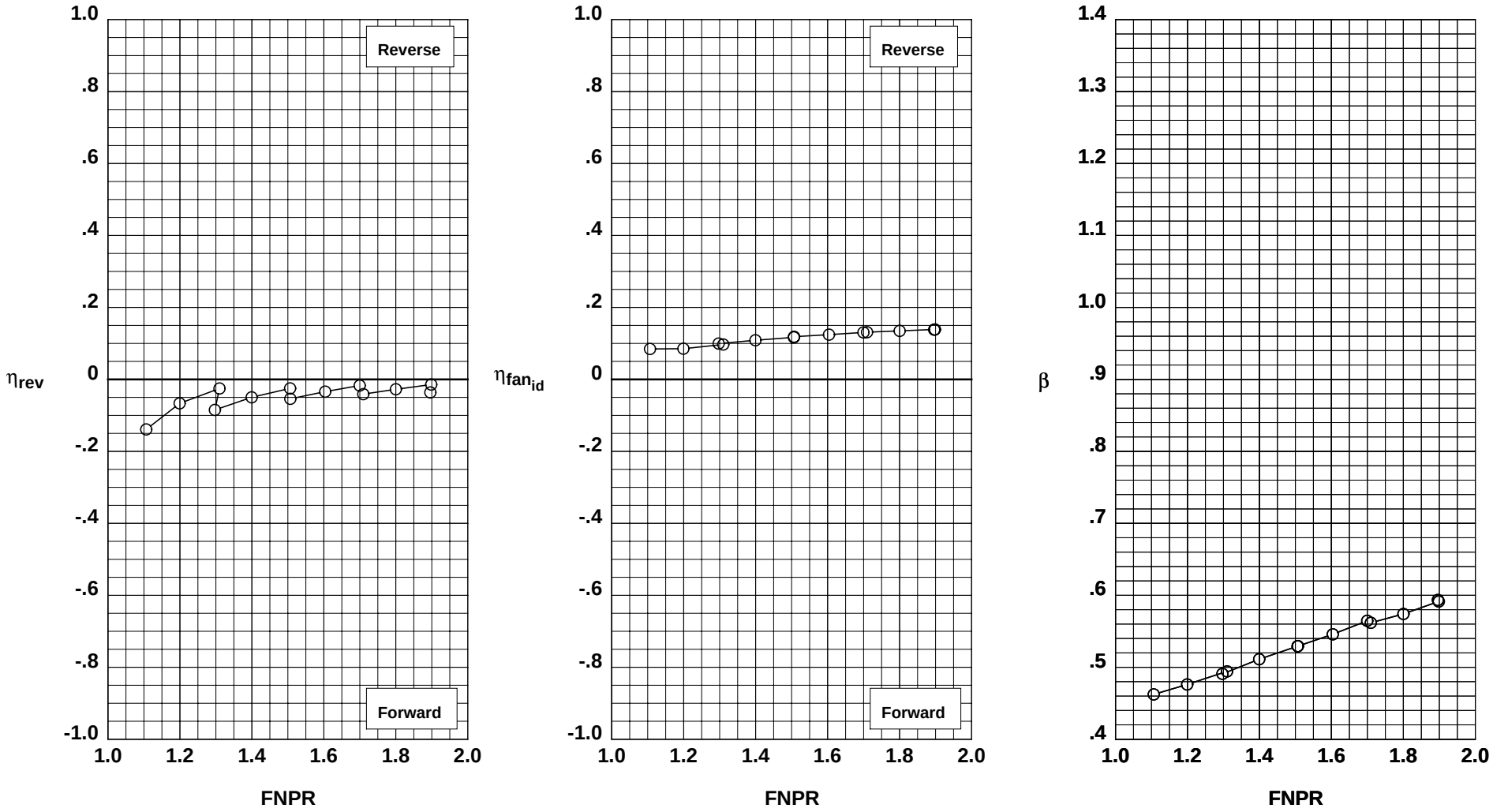

Figure F-2. Fabric target thrust reverser performance characteristics for configuration 402.

Operation Mode: Dual Flow
Target Angle: 40°
Area Ratio: 1.15
Fabric: Long
Bifurcator: Removed
Wing: Removed

	Test	Run	Configuration
○	987	39	403

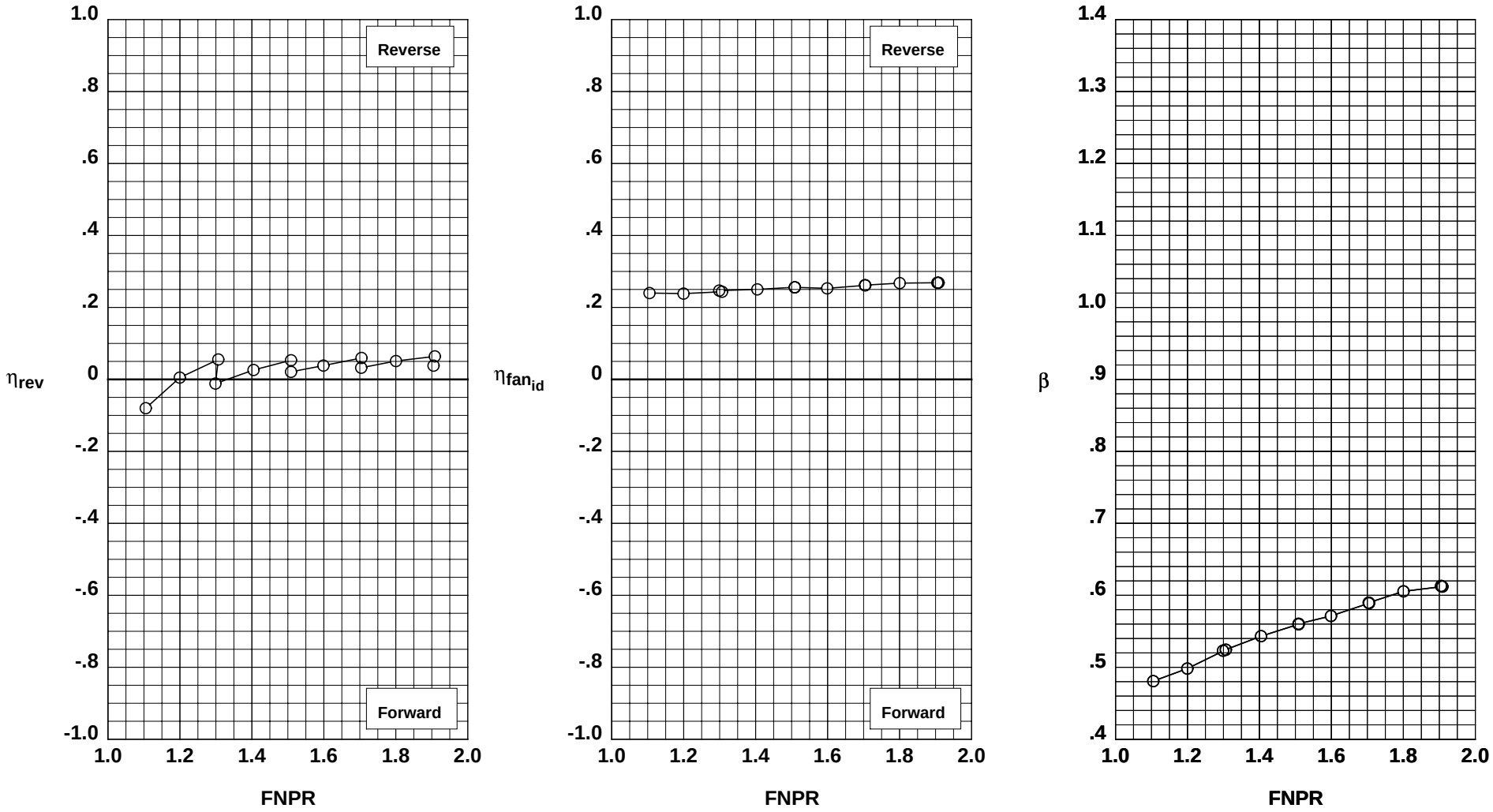

Figure F-3. Fabric target thrust reverser performance characteristics for configuration 403.

Operation Mode: Dual Flow
Target Angle: 20°
Area Ratio: 1.15
Fabric: Long
Bifurcator: Removed
Wing: Removed

	Test	Run	Configuration
○	987	40	404

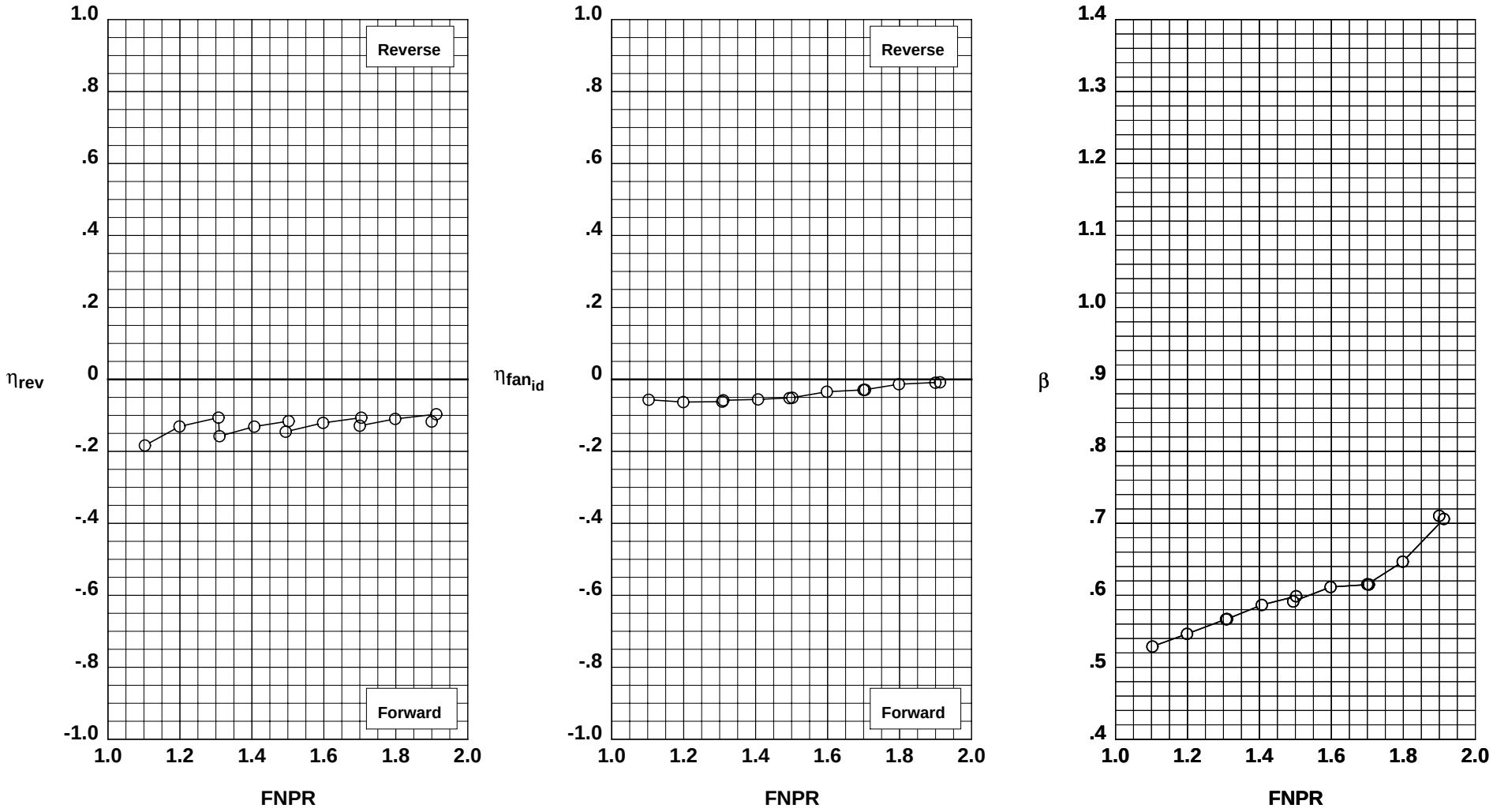

Figure F-4. Fabric target thrust reverser performance characteristics for configuration 404.

Operation Mode: Dual Flow
Reverser Port Bullnose: #1
Reverser Port Spacer: None
Reverser Port Cover: None
Bifurcator: Installed
Wing: Removed

	Test	Run	Configuration
○	988	1	502

Outer Door Angle: 60°
Outer Door Cutback: None
Outer Door Kicker: Long/Cutback
Outer Door Fence: None
Inner Door Angle: 36°
Inner Door Fillers: None
Door Struts: Yes
Door Leakage: Maximum

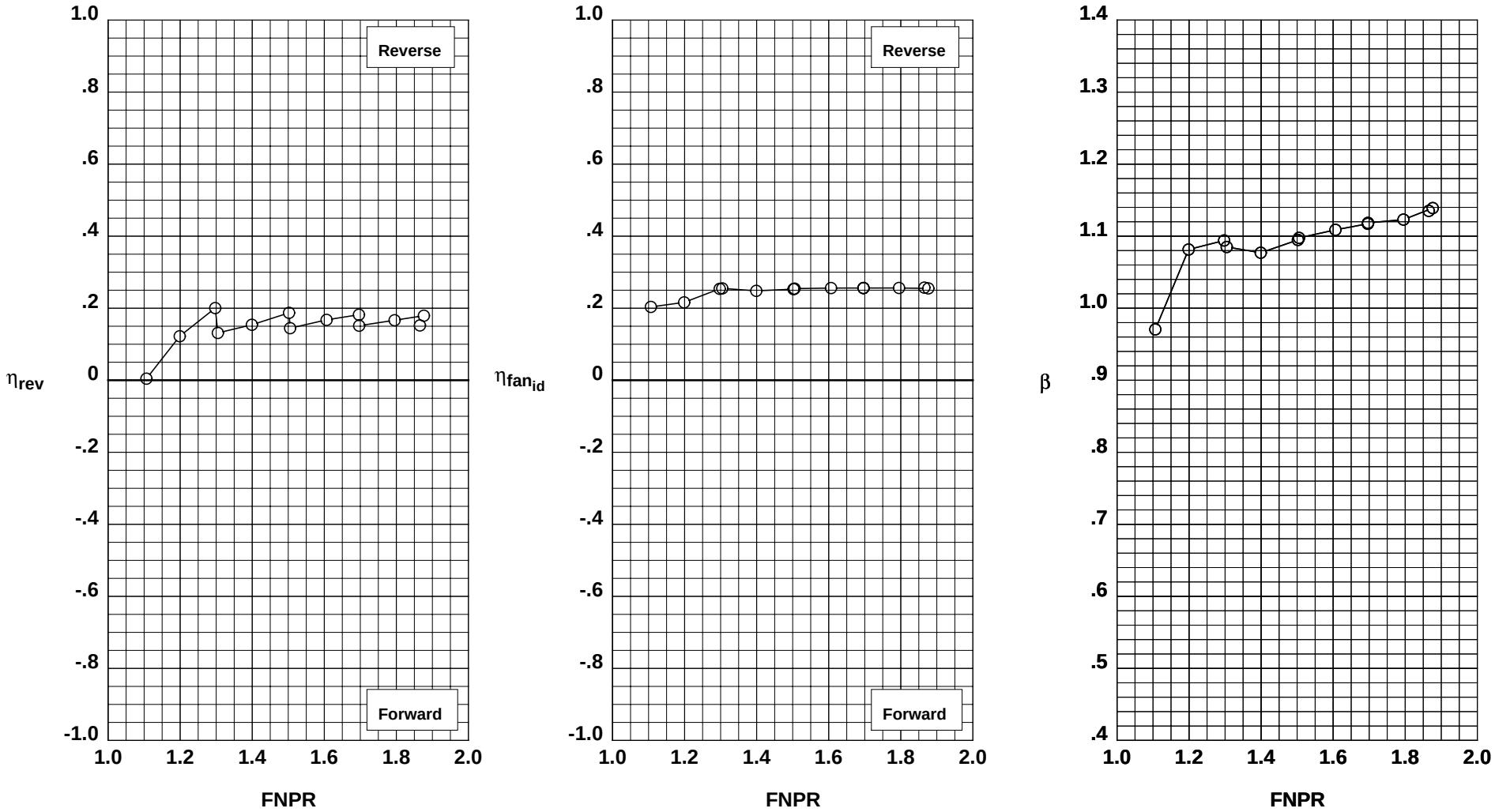

Figure G-1. Multi-door crocodile thrust reverser performance characteristics for configuration 502.

Operation Mode: Fan Only
Reverser Port Bullnose: #1
Reverser Port Spacer: None
Reverser Port Cover: None
Bifurcator: Installed
Wing: Removed

	Test	Run	Configuration
○	988	2	503

Outer Door Angle: 60°
Outer Door Cutback: None
Outer Door Kicker: None
Outer Door Fence: None
Inner Door Angle: 36°
Inner Door Fillers: None
Door Struts: Yes
Door Leakage: Maximum

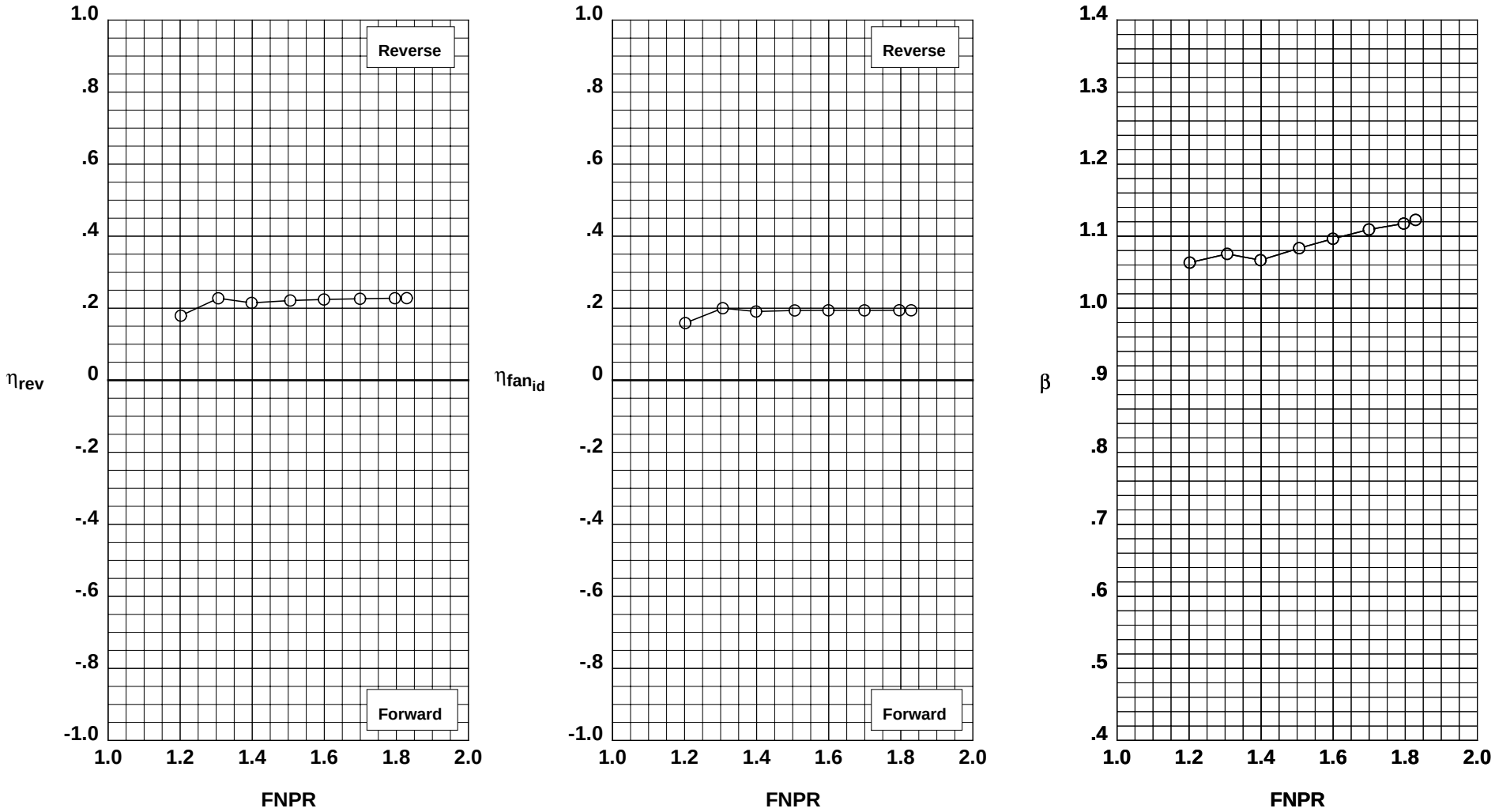

Figure G-2. Multi-door crocodile thrust reverser performance characteristics for configuration 503.

Operation Mode: Fan Only
Reverser Port Bullnose: #1
Reverser Port Spacer: 0.20"
Reverser Port Cover: None
Bifurcator: Installed
Wing: Removed

	Test	Run	Configuration
○	988	3	504

Outer Door Angle: 60°
Outer Door Cutback: None
Outer Door Kicker: Long/Cutback
Outer Door Fence: None
Inner Door Angle: 36°
Inner Door Fillers: None
Door Struts: Yes
Door Leakage: Maximum

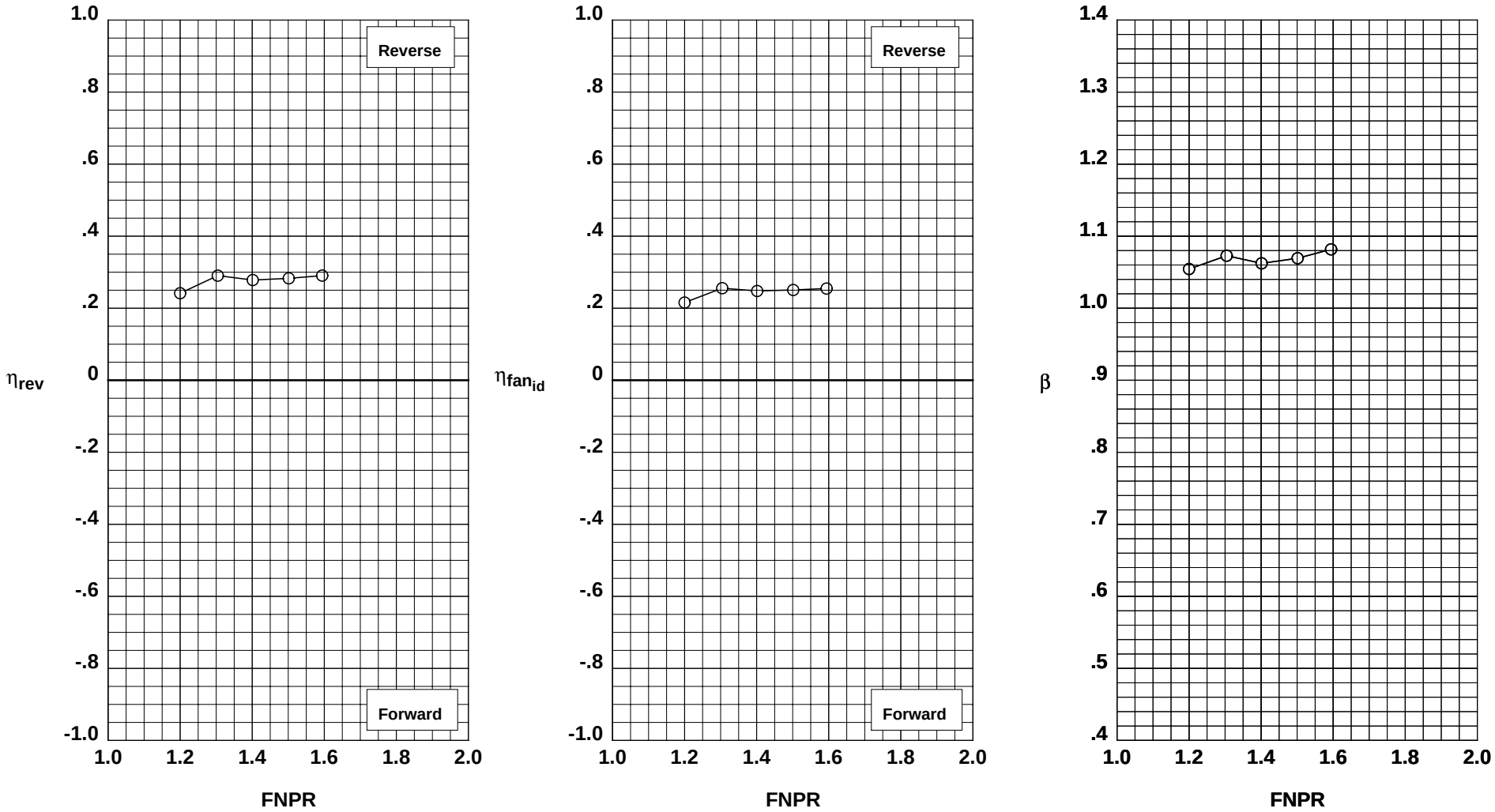

Figure G-3. Multi-door crocodile thrust reverser performance characteristics for configuration 504.

Operation Mode: Fan Only
Reverser Port Bullnose: #1
Reverser Port Spacer: 0.40"
Reverser Port Cover: None
Bifurcator: Installed
Wing: Removed

	Test	Run	Configuration
○	988	4	505

Outer Door Angle: 60°
Outer Door Cutback: None
Outer Door Kicker: Long/Cutback
Outer Door Fence: None
Inner Door Angle: 36°
Inner Door Fillers: None
Door Struts: Yes
Door Leakage: Maximum

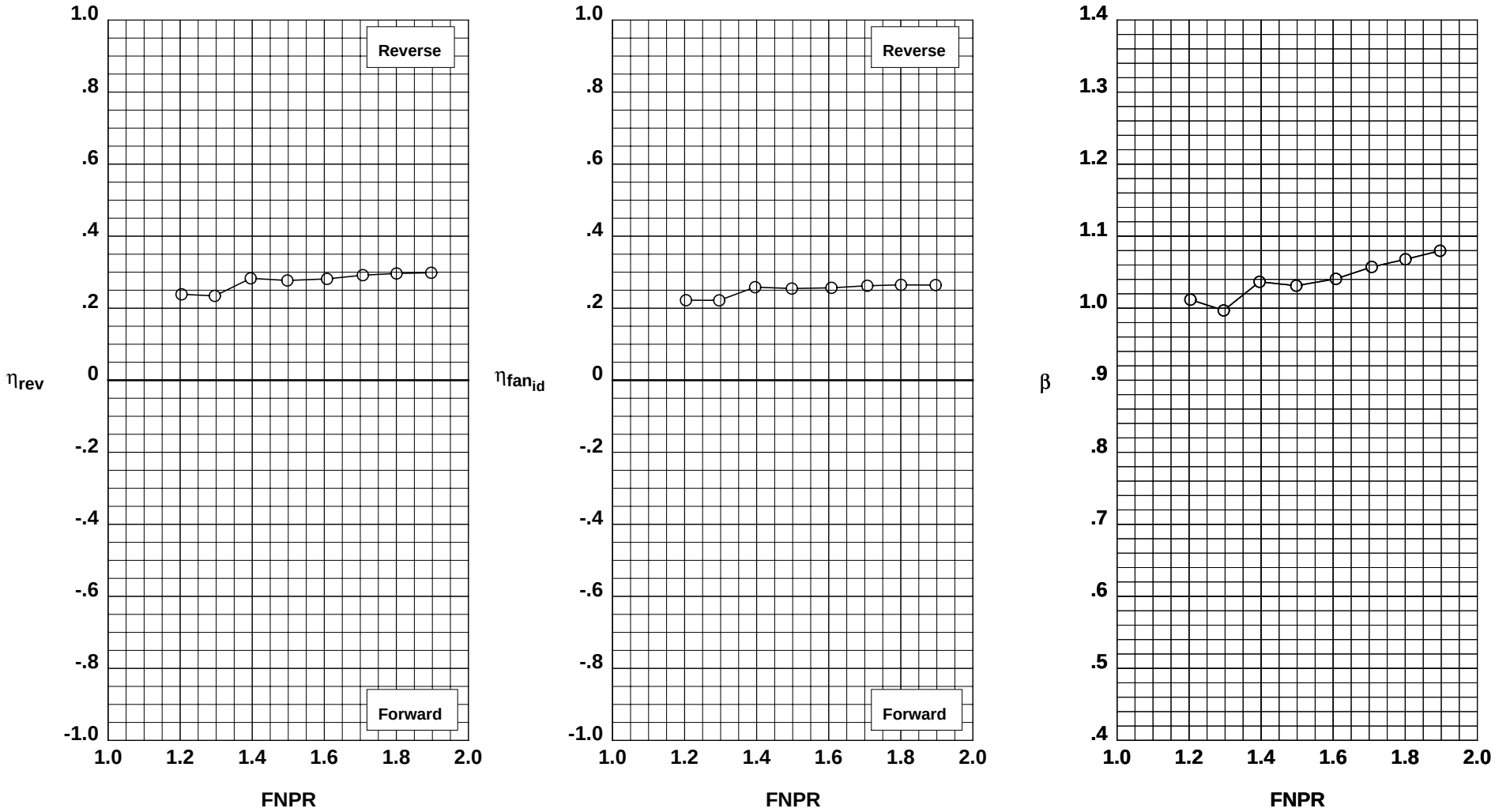

Figure G-4. Multi-door crocodile thrust reverser performance characteristics for configuration 505.

Operation Mode: Fan Only
Reverser Port Bullnose: #2
Reverser Port Spacer: 0.40"
Reverser Port Cover: None
Bifurcator: Installed
Wing: Removed

	Test	Run	Configuration
○	988	5	506

Outer Door Angle: 60°
Outer Door Cutback: None
Outer Door Kicker: Long/Cutback
Outer Door Fence: None
Inner Door Angle: 36°
Inner Door Fillers: None
Door Struts: Yes
Door Leakage: Maximum

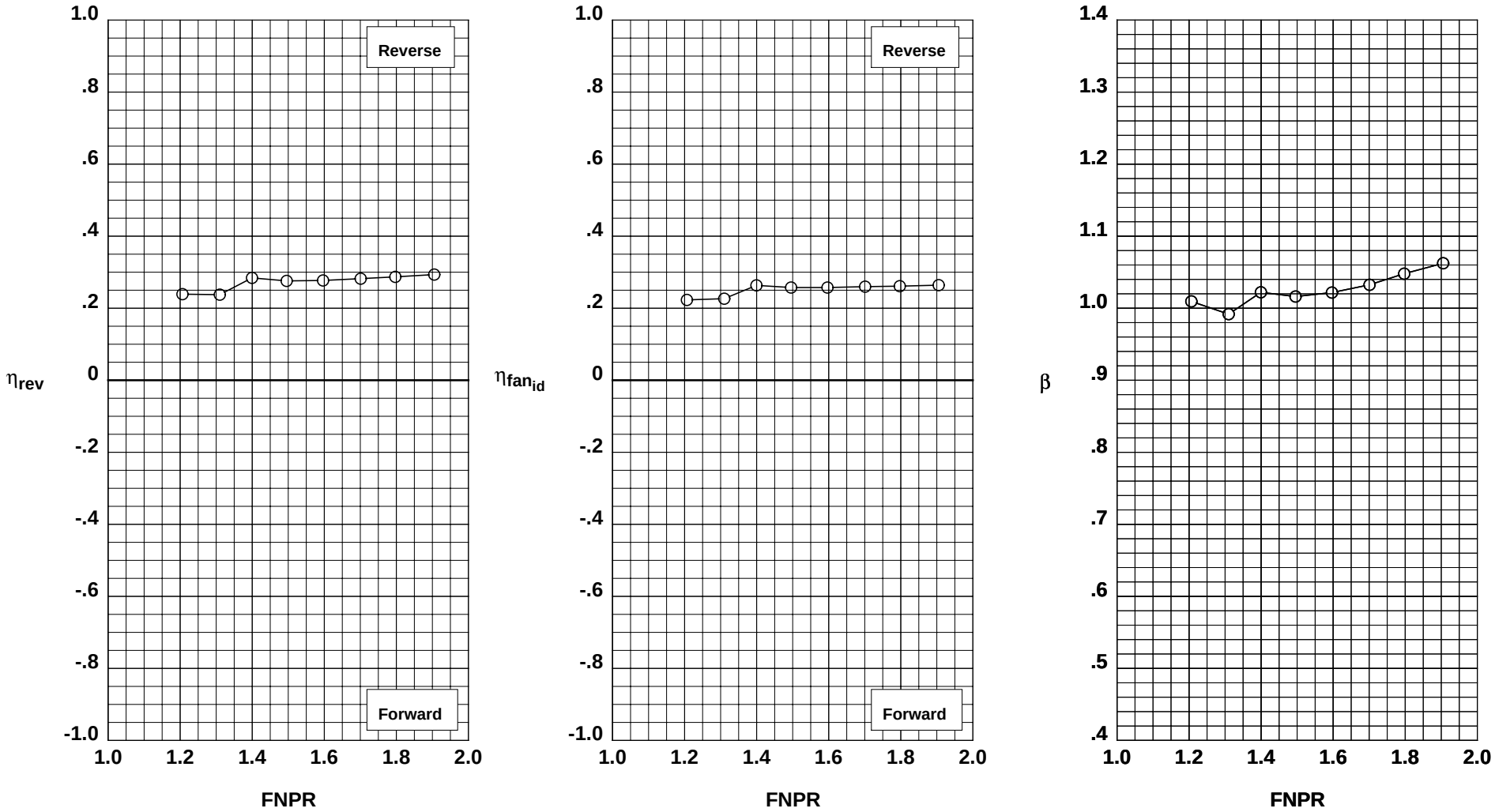

Figure G-5. Multi-door crocodile thrust reverser performance characteristics for configuration 506.

Operation Mode: Fan Only
Reverser Port Bullnose: #3
Reverser Port Spacer: 0.40"
Reverser Port Cover: None
Bifurcator: Installed
Wing: Removed

	Test	Run	Configuration
○	988	6	507

Outer Door Angle: 60°
Outer Door Cutback: None
Outer Door Kicker: Long/Cutback
Outer Door Fence: None
Inner Door Angle: 36°
Inner Door Fillers: None
Door Struts: Yes
Door Leakage: Maximum

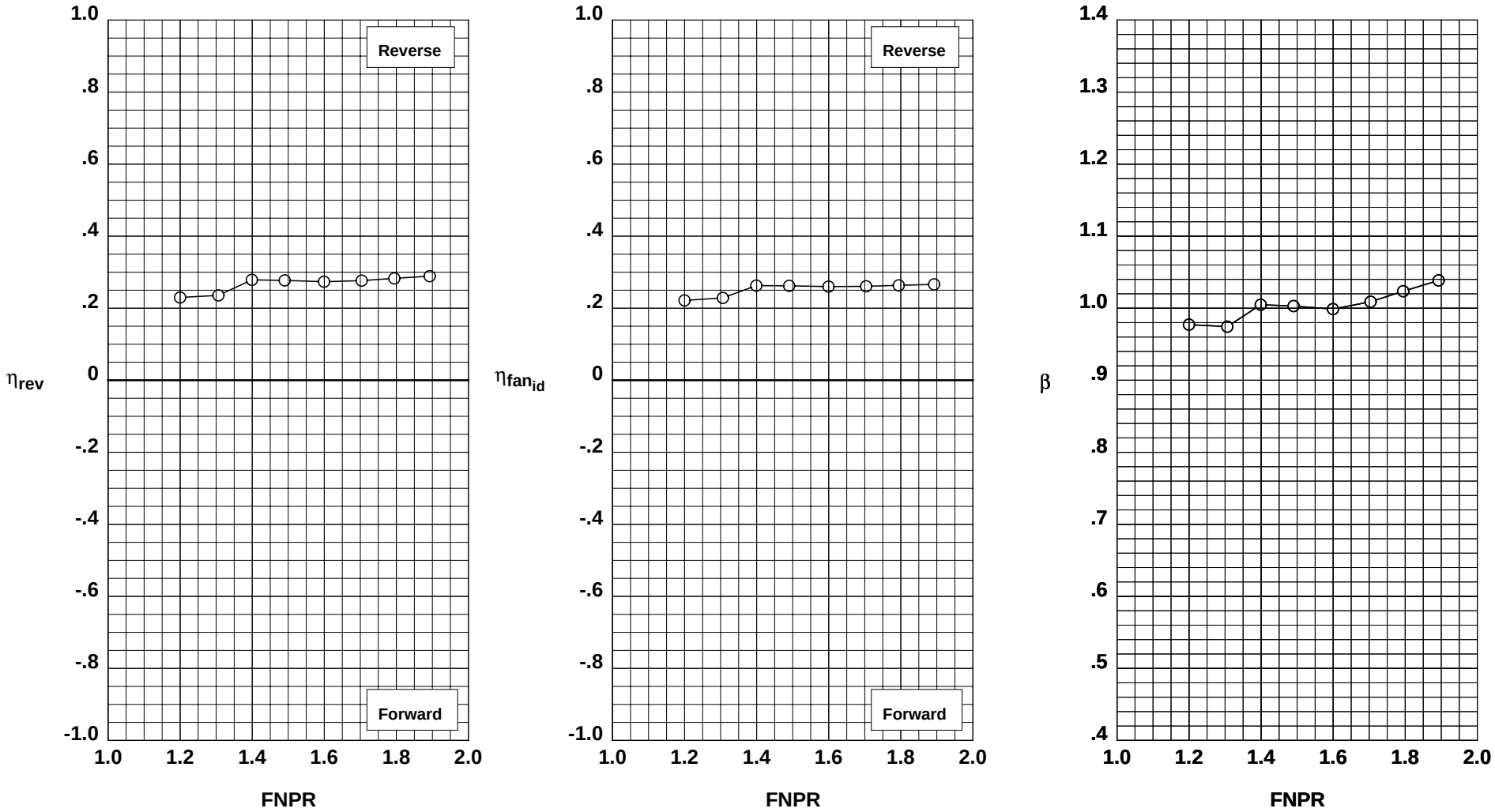

Figure G-6. Multi-door crocodile thrust reverser performance characteristics for configuration 507.

Operation Mode: Fan Only
Reverser Port Bullnose: #1
Reverser Port Spacer: None
Reverser Port Cover: None
Bifurcator: Installed
Wing: Removed

	Test	Run	Configuration
○	988	7	508

Outer Door Angle: 60°
Outer Door Cutback: None
Outer Door Kicker: Long/Cutback
Outer Door Fence: None
Inner Door Angle: 36°
Inner Door Fillers: All
Door Struts: Yes
Door Leakage: Partial

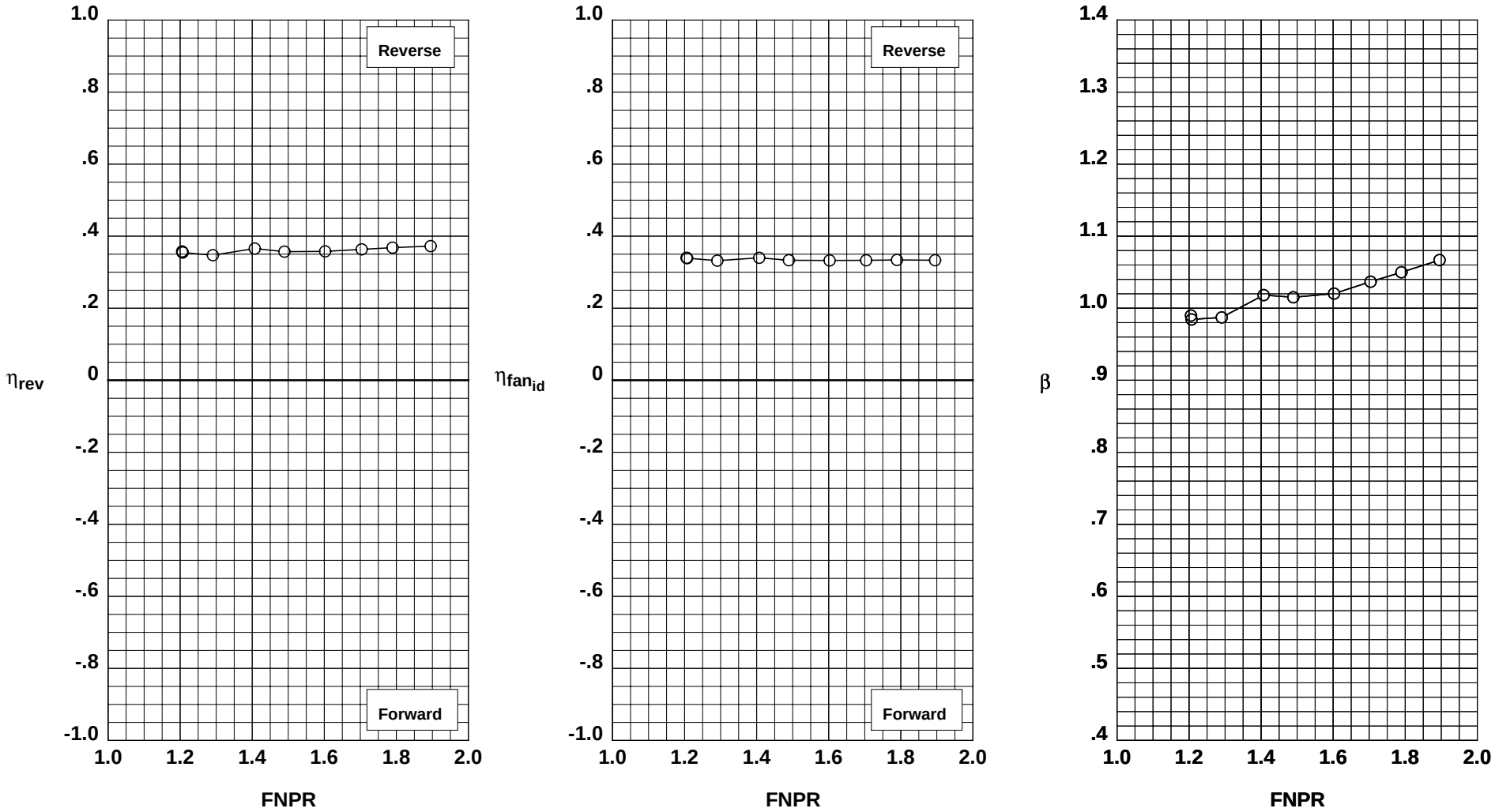

Figure G-7. Multi-door crocodile thrust reverser performance characteristics for configuration 508.

Operation Mode: Fan Only
Reverser Port Bullnose: #1
Reverser Port Spacer: None
Reverser Port Cover: None
Bifurcator: Installed
Wing: Removed

	Test	Run	Configuration
○	988	8	509

Outer Door Angle: 60°
Outer Door Cutback: None
Outer Door Kicker: Long/Cutback
Outer Door Fence: None
Inner Door Angle: 36°
Inner Door Fillers: Upper
Door Struts: Yes
Door Leakage: Partial

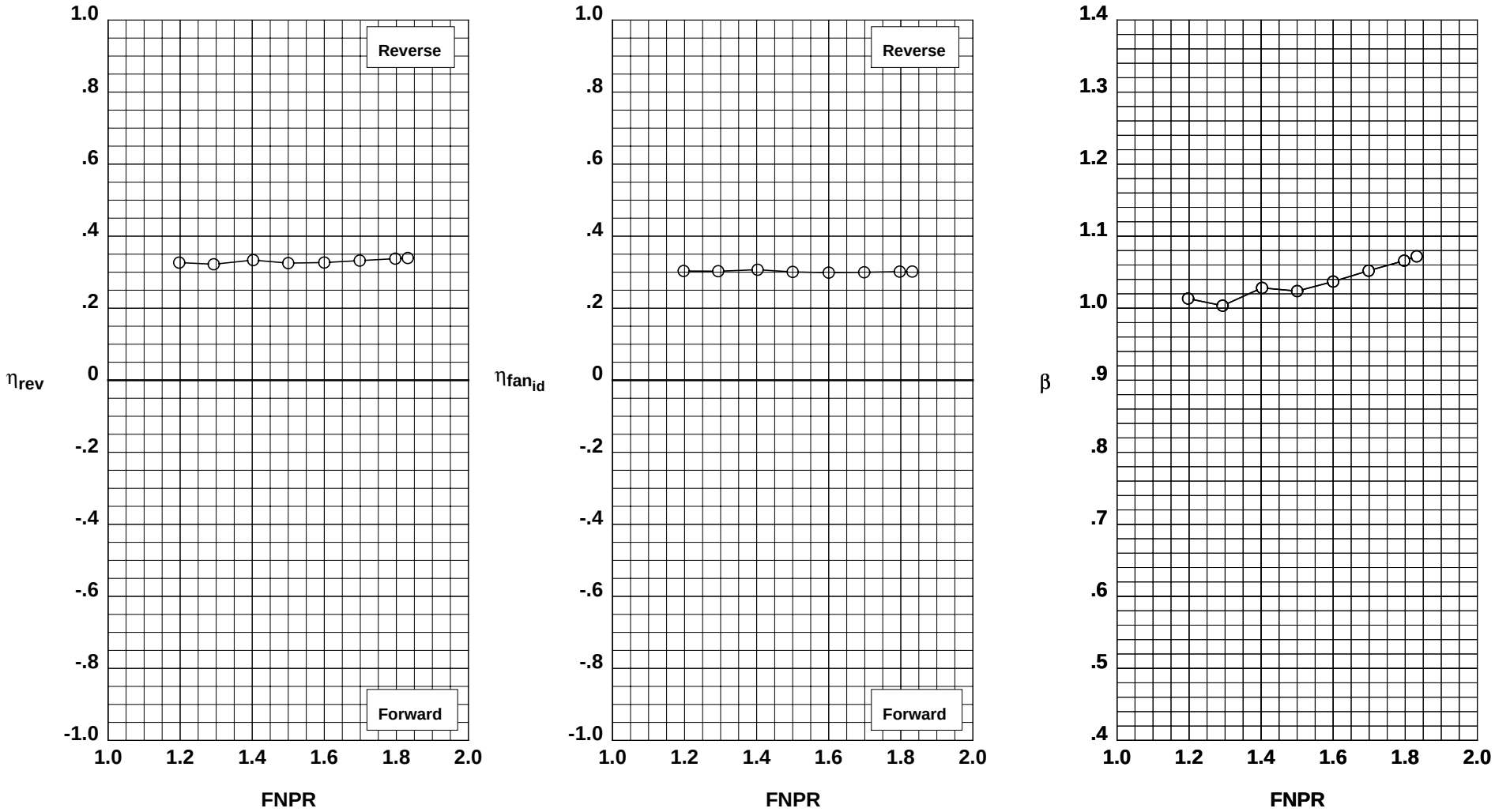

Figure G-8. Multi-door crocodile thrust reverser performance characteristics for configuration 509.

Operation Mode: Dual Flow
Reverser Port Bullnose: #1
Reverser Port Spacer: None
Reverser Port Cover: Full
Bifurcator: Installed
Wing: Removed

	Test	Run	Configuration
○	988	9	510

Outer Door Angle: 60°
Outer Door Cutback: Full
Outer Door Kicker: None
Outer Door Fence: None
Inner Door Angle: 36°
Inner Door Fillers: Upper
Door Struts: Yes
Door Leakage: Partial

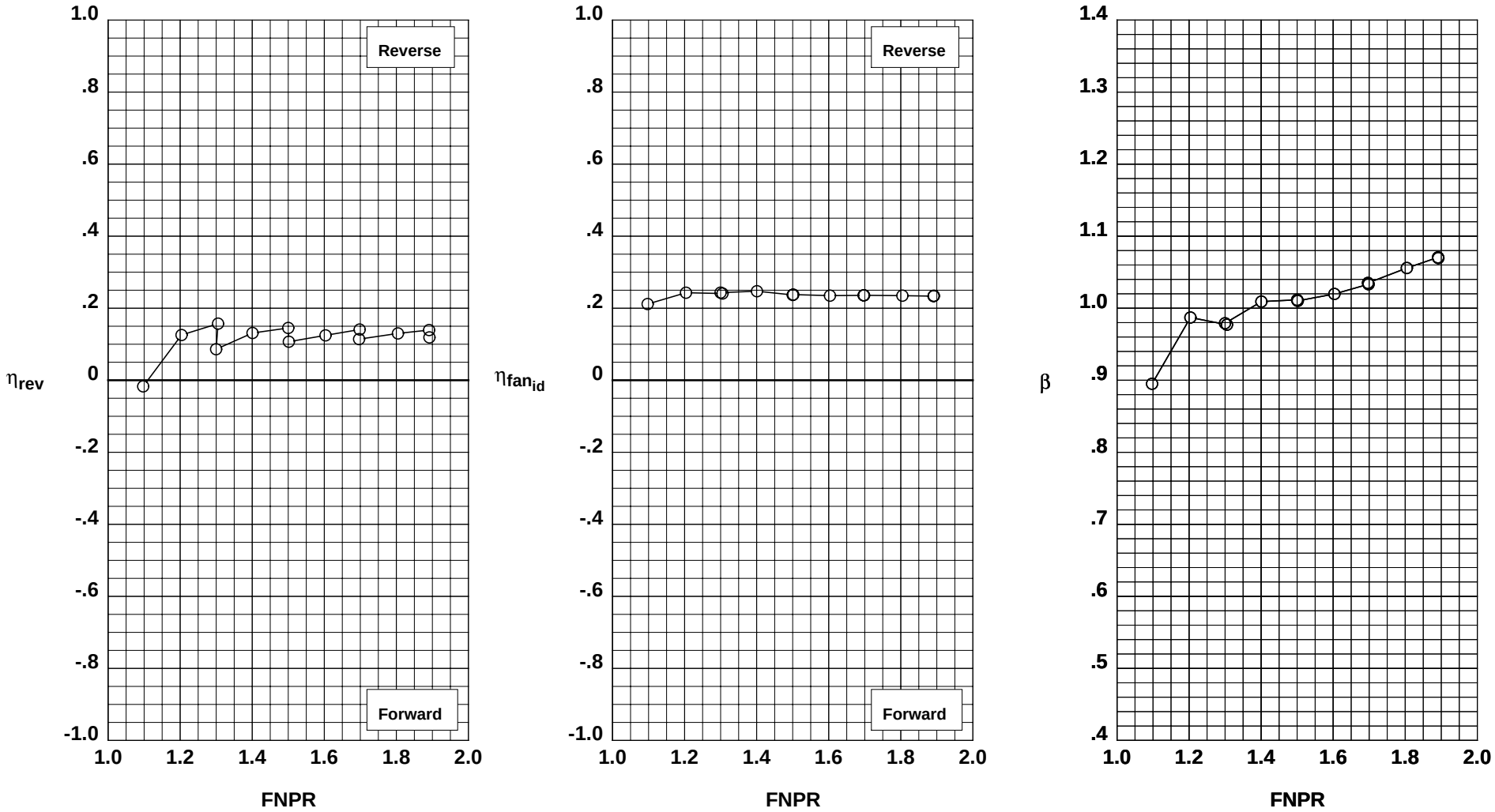

Figure G-9. Multi-door crocodile thrust reverser performance characteristics for configuration 510.

Operation Mode: Fan Only
Reverser Port Bullnose: #1
Reverser Port Spacer: None
Reverser Port Cover: None
Bifurcator: Installed
Wing: Removed

	Test	Run	Configuration
○	994	2	511

Outer Door Angle: 60°
Outer Door Cutback: None
Outer Door Kicker: Long/Cutback
Outer Door Fence: None
Inner Door Angle: 36°
Inner Door Fillers: None
Door Struts: No
Door Leakage: Maximum

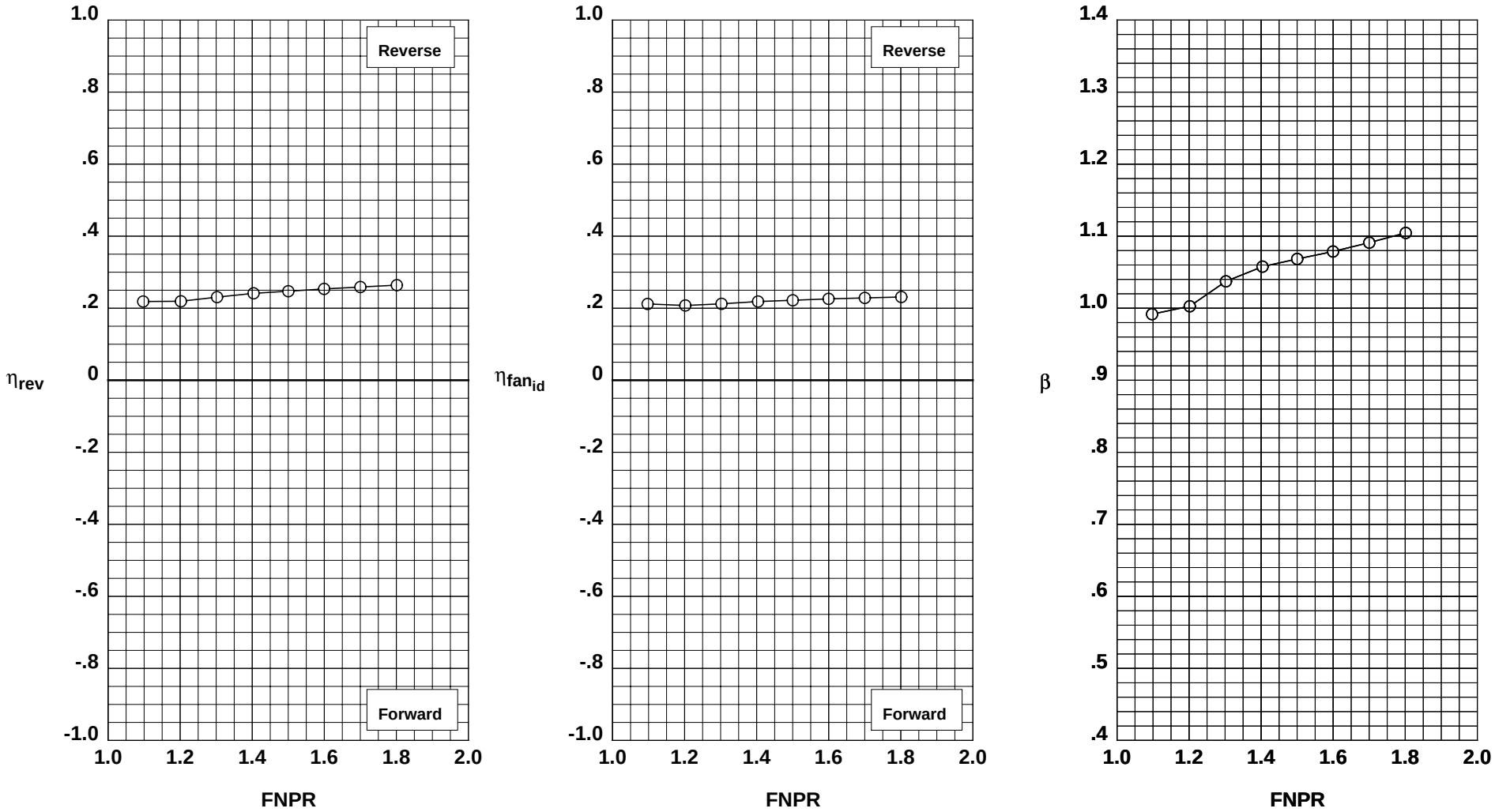

Figure G-10. Multi-door crocodile thrust reverser performance characteristics for configuration 511.

Operation Mode: Dual Flow
Reverser Port Bullnose: #1
Reverser Port Spacer: None
Reverser Port Cover: None
Bifurcator: Installed
Wing: Removed

	Test	Run	Configuration
○	994	4	511

Outer Door Angle: 60°
Outer Door Cutback: None
Outer Door Kicker: Long/Cutback
Outer Door Fence: None
Inner Door Angle: 36°
Inner Door Fillers: None
Door Struts: No
Door Leakage: Maximum

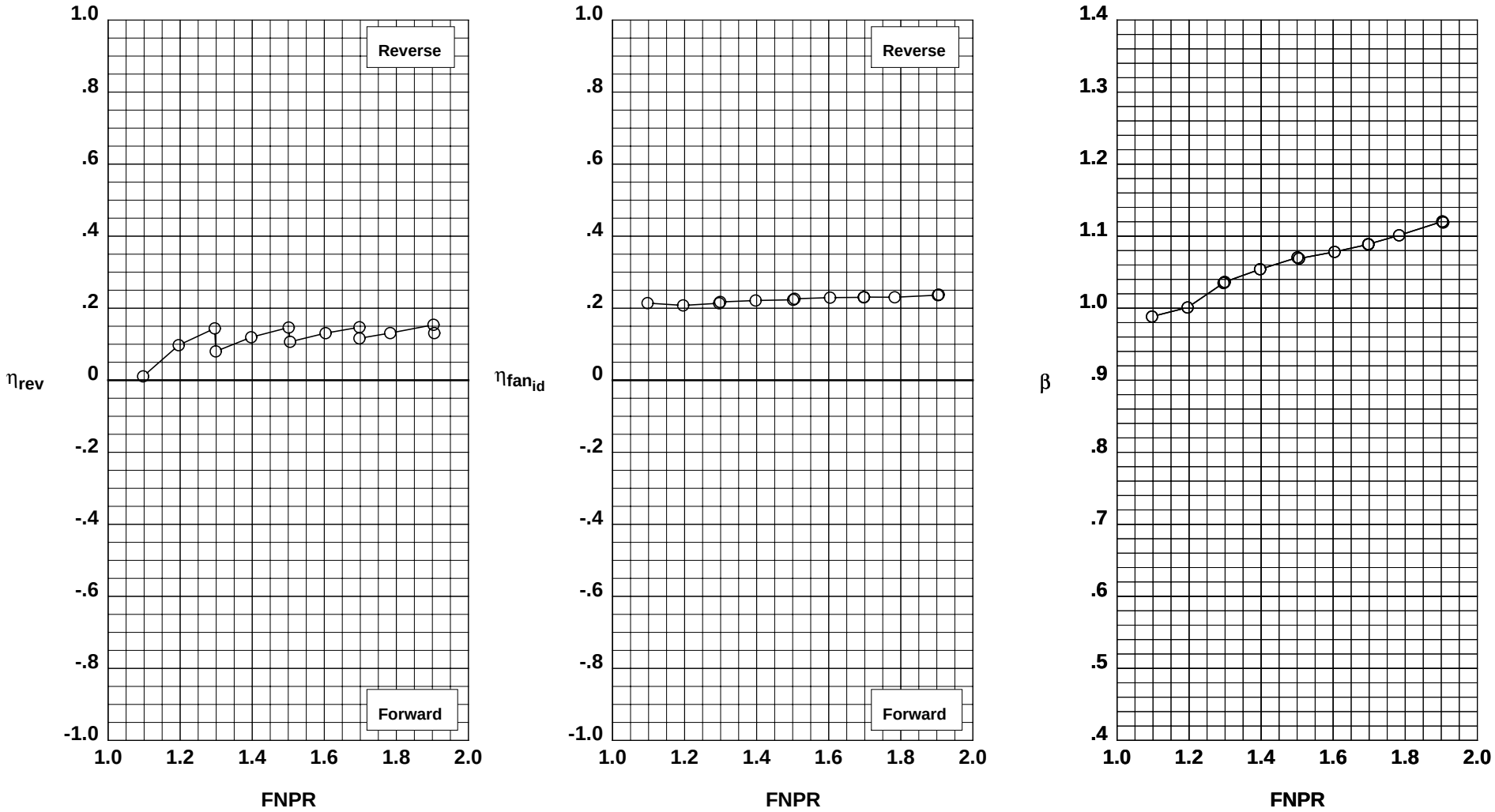

Figure G-11. Multi-door crocodile thrust reverser performance characteristics for configuration 511.

Operation Mode: Dual Flow
Reverser Port Bullnose: #1
Reverser Port Spacer: None
Reverser Port Cover: None
Bifurcator: Installed
Wing: Removed

	Test	Run	Configuration
○	994	5	512

Outer Door Angle: 60°
Outer Door Cutback: None
Outer Door Kicker: Long/Cutback
Outer Door Fence: None
Inner Door Angle: 36°
Inner Door Fillers: All
Door Struts: No
Door Leakage: Partial

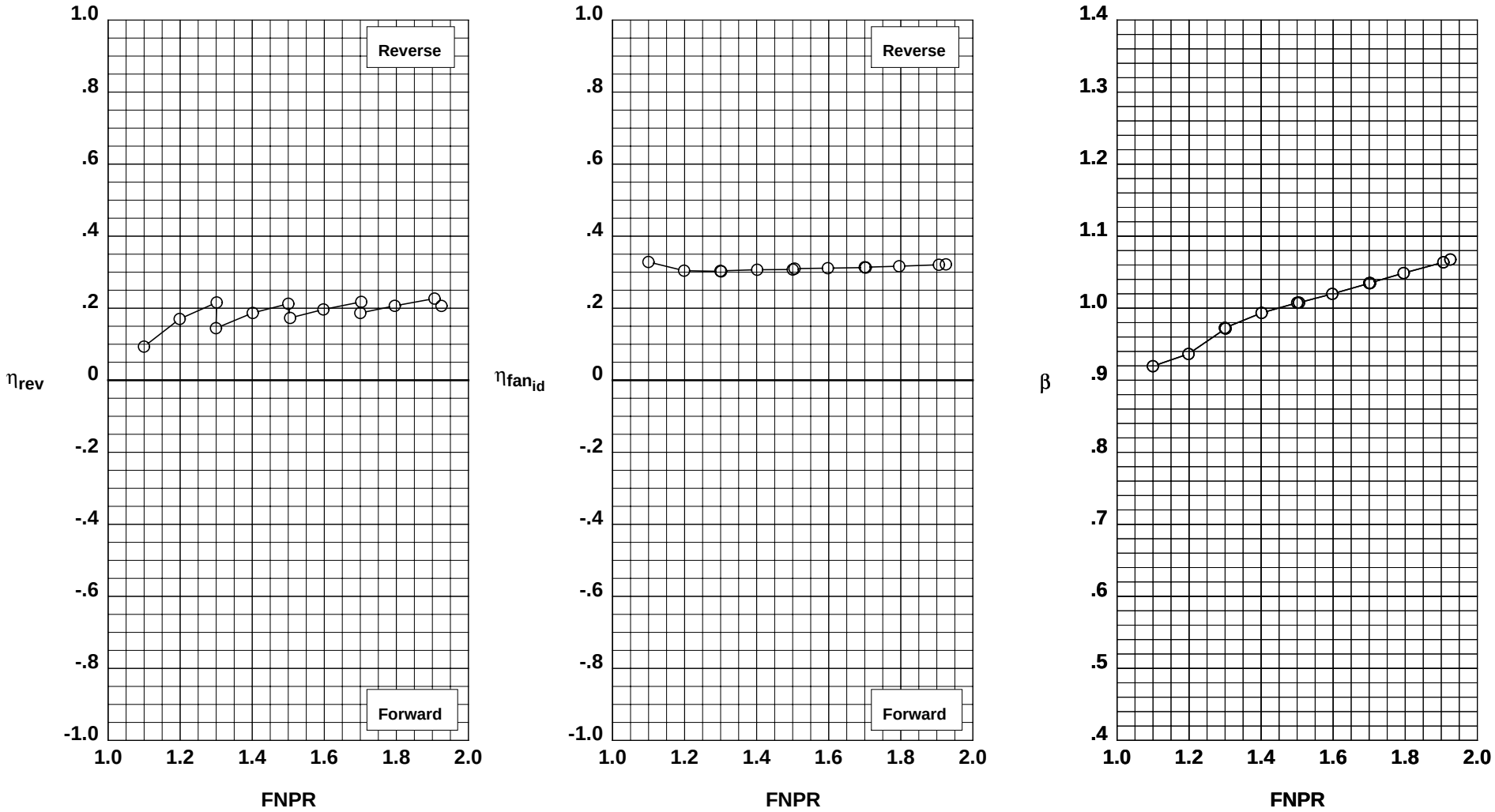

Figure G-12. Multi-door crocodile thrust reverser performance characteristics for configuration 512.

Operation Mode: Dual Flow
Reverser Port Bullnose: #1
Reverser Port Spacer: None
Reverser Port Cover: None
Bifurcator: Installed
Wing: Removed

	Test	Run	Configuration
○	994	6	513

Outer Door Angle: 40°
Outer Door Cutback: None
Outer Door Kicker: Long/Cutback
Outer Door Fence: None
Inner Door Angle: 36°
Inner Door Fillers: All
Door Struts: No
Door Leakage: Partial

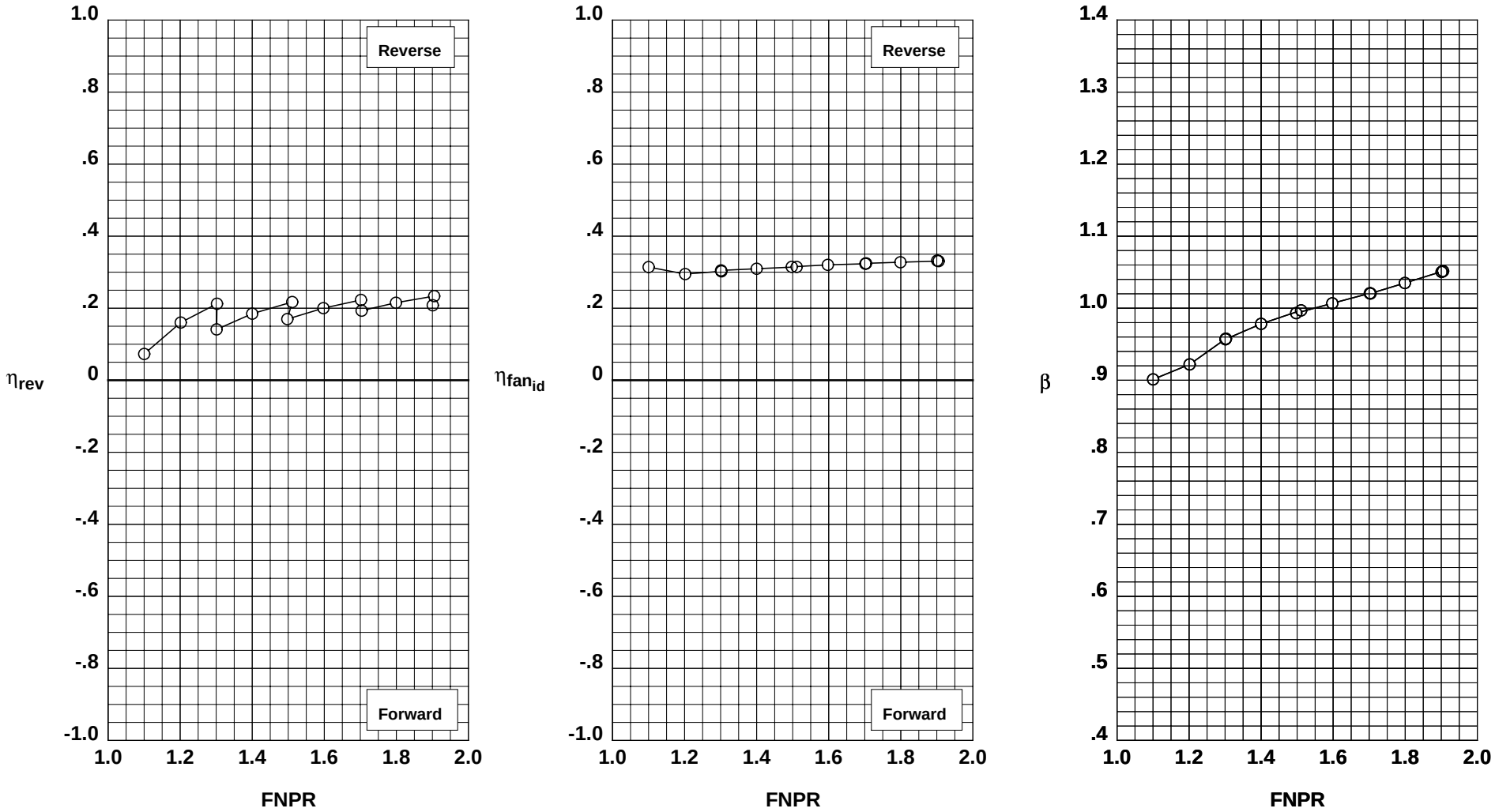

Figure G-13. Multi-door crocodile thrust reverser performance characteristics for configuration 513.

Operation Mode: Dual Flow
Reverser Port Bullnose: #3
Reverser Port Spacer: None
Reverser Port Cover: None
Bifurcator: Installed
Wing: Removed

	Test	Run	Configuration
○	994	7	514

Outer Door Angle: 40°
Outer Door Cutback: None
Outer Door Kicker: Long/Cutback
Outer Door Fence: None
Inner Door Angle: 36°
Inner Door Fillers: All
Door Struts: No
Door Leakage: Partial

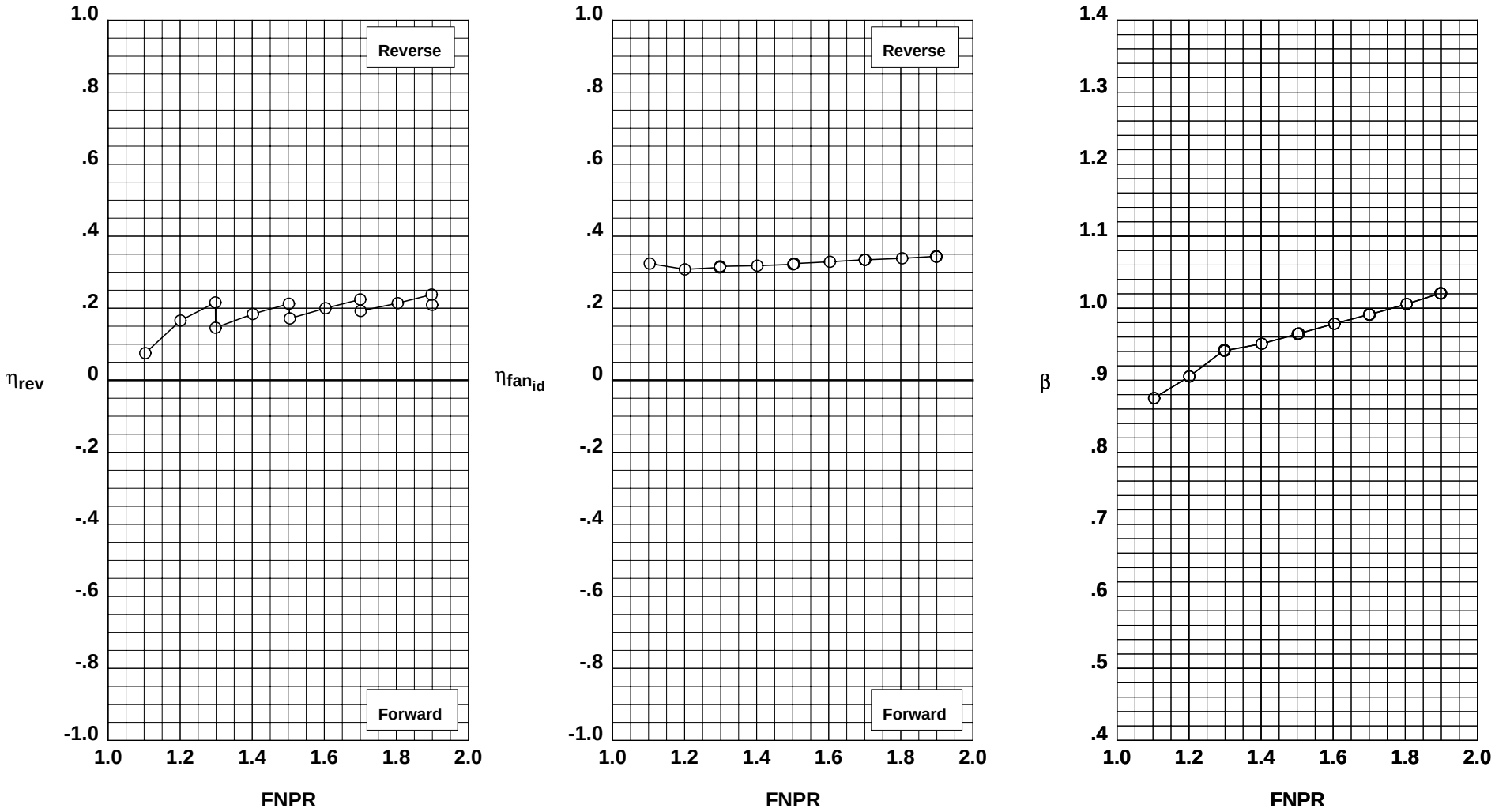

Figure G-14. Multi-door crocodile thrust reverser performance characteristics for configuration 514.

Operation Mode: Dual Flow
Reverser Port Bullnose: #3
Reverser Port Spacer: None
Reverser Port Cover: None
Bifurcator: Installed
Wing: Removed

	Test	Run	Configuration
○	994	8	515

Outer Door Angle: 40°
Outer Door Cutback: None
Outer Door Kicker: X-Long/Cutback
Outer Door Fence: None
Inner Door Angle: 36°
Inner Door Fillers: All
Door Struts: No
Door Leakage: Partial

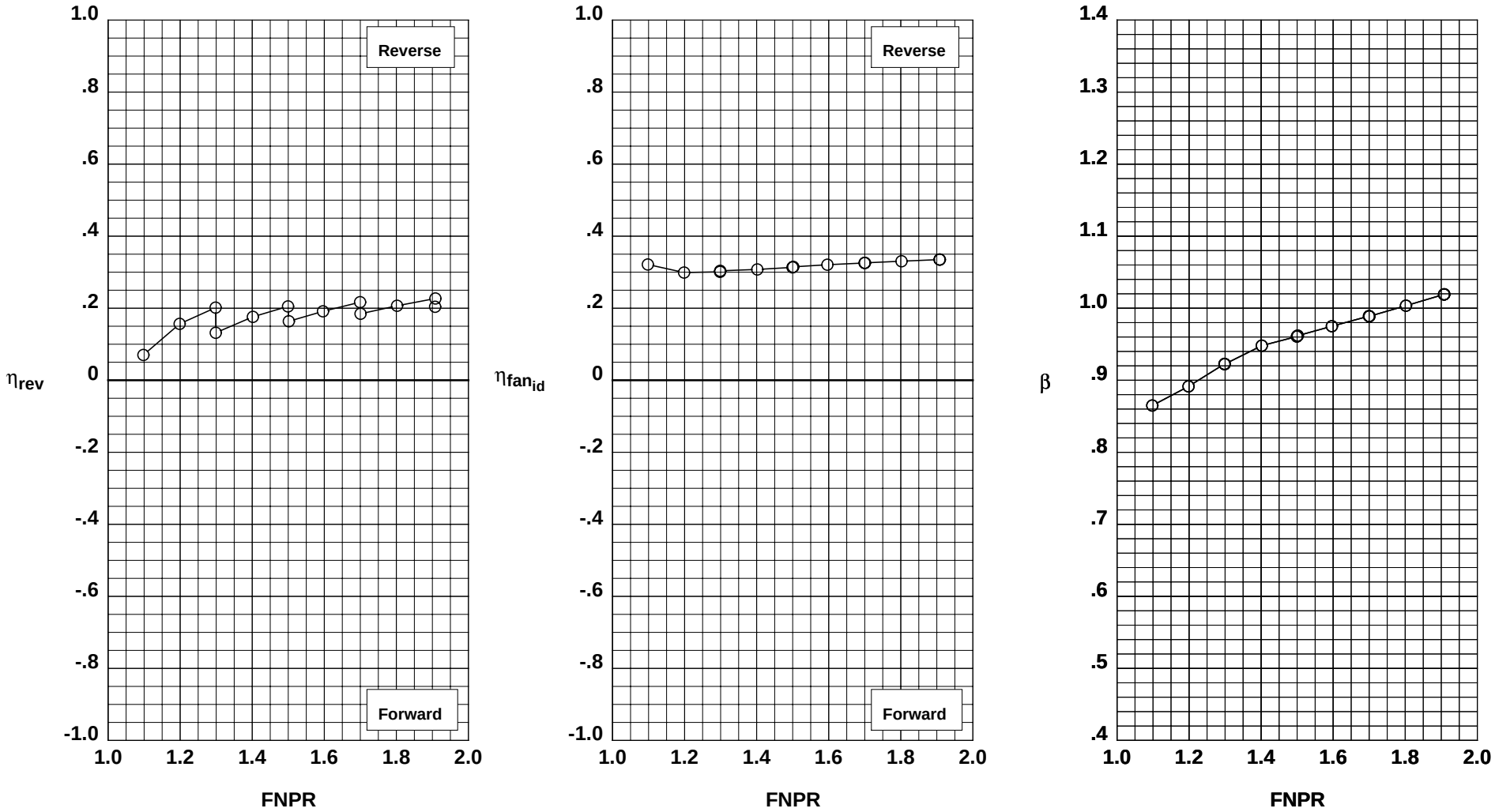

Figure G-15. Multi-door crocodile thrust reverser performance characteristics for configuration 515.

Operation Mode: Dual Flow
Reverser Port Bullnose: #3
Reverser Port Spacer: None
Reverser Port Cover: None
Bifurcator: Installed
Wing: Removed

	Test	Run	Configuration
○	994	10	516

Outer Door Angle: 50°
Outer Door Cutback: None
Outer Door Kicker: X-Long/Cutback
Outer Door Fence: None
Inner Door Angle: 36°
Inner Door Fillers: All
Door Struts: No
Door Leakage: Partial

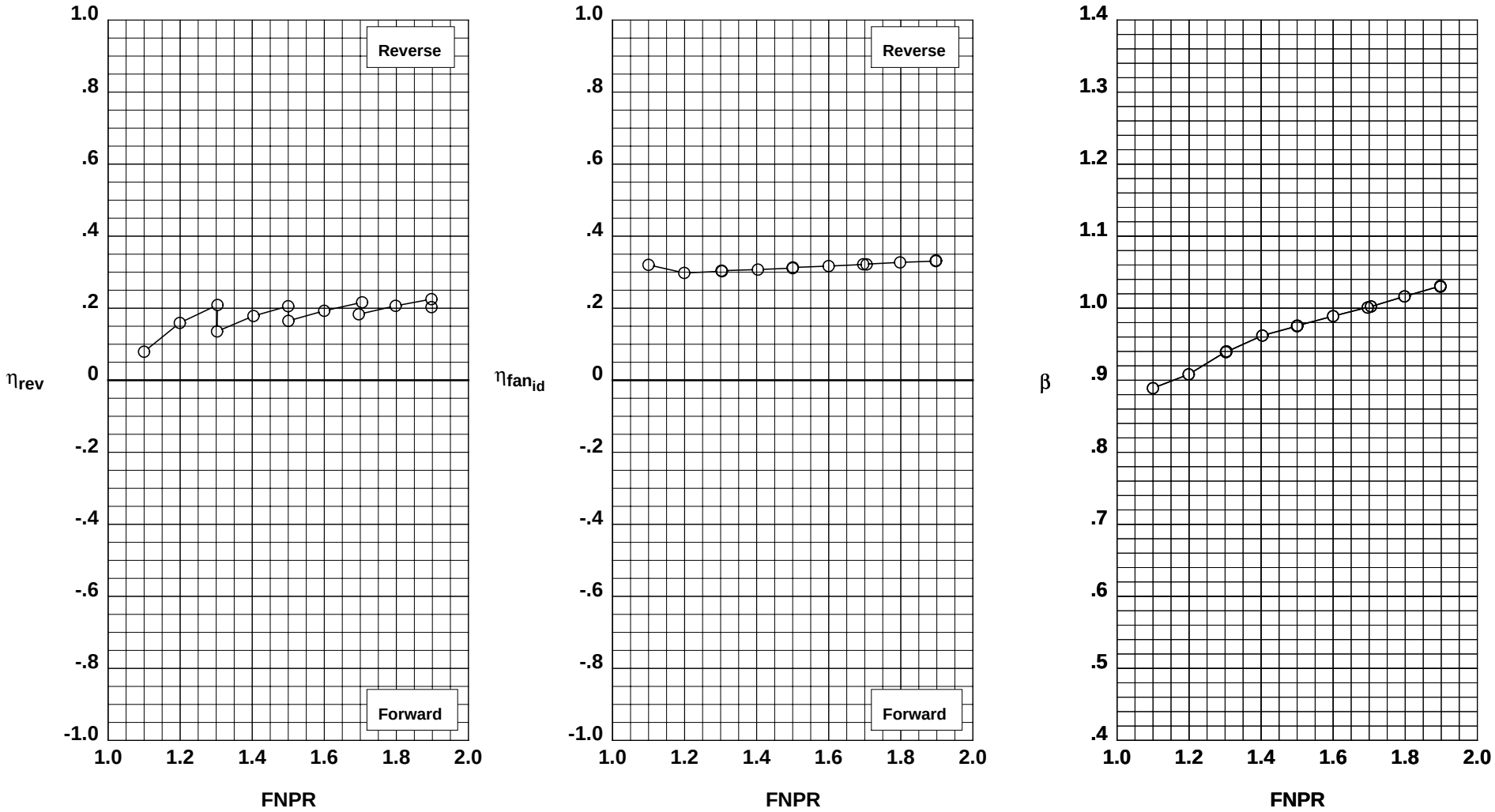

Figure G-16. Multi-door crocodile thrust reverser performance characteristics for configuration 516.

Operation Mode: Dual Flow
Reverser Port Bullnose: #3
Reverser Port Spacer: None
Reverser Port Cover: None
Bifurcator: Installed
Wing: Removed

	Test	Run	Configuration
○	994	11	517

Outer Door Angle: 50°
Outer Door Cutback: None
Outer Door Kicker: Long/Cutback
Outer Door Fence: None
Inner Door Angle: 36°
Inner Door Fillers: All
Door Struts: No
Door Leakage: Partial

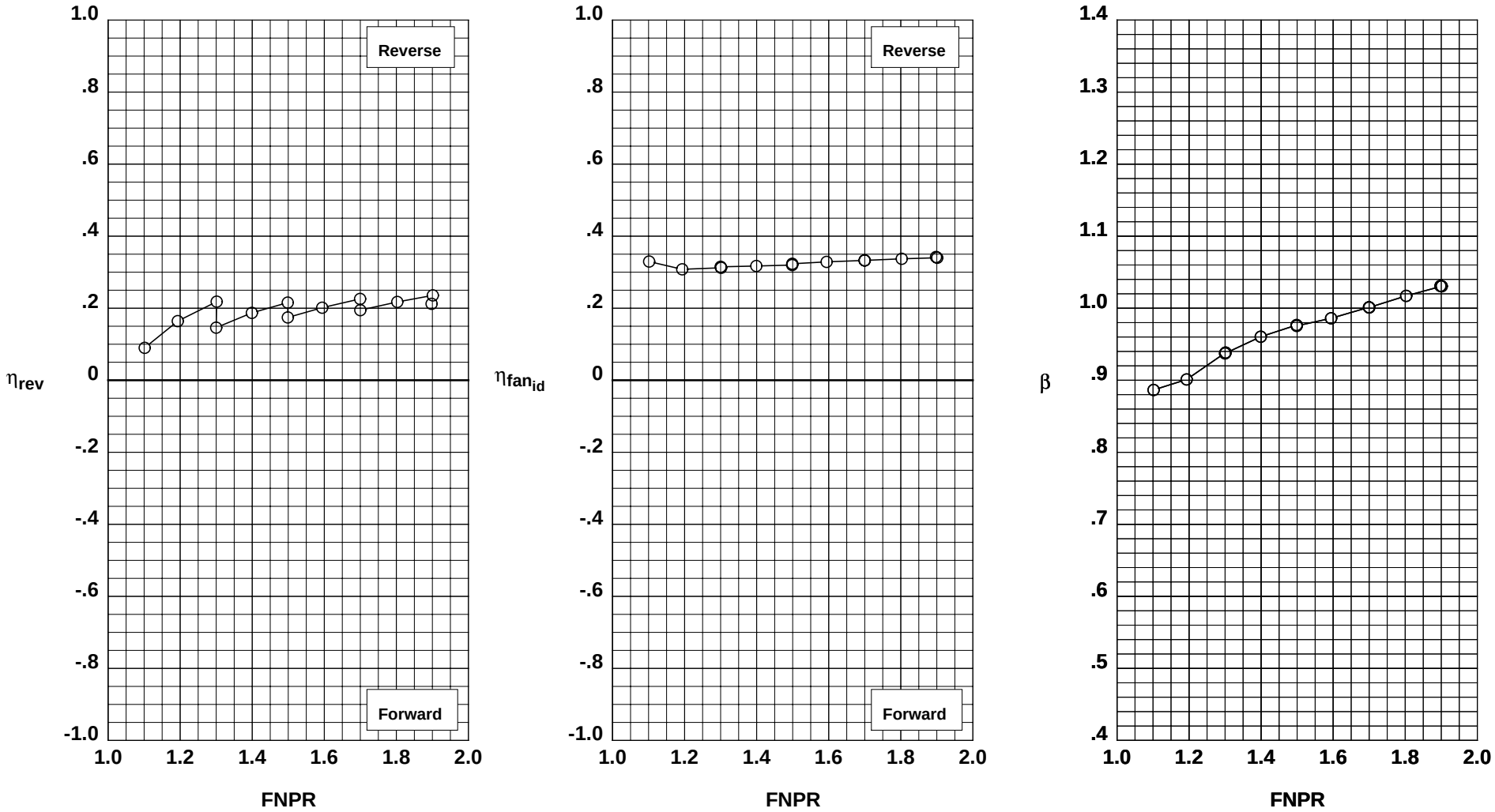

Figure G-17. Multi-door crocodile thrust reverser performance characteristics for configuration 517.

Operation Mode: Dual Flow
Reverser Port Bullnose: #3
Reverser Port Spacer: None
Reverser Port Cover: None
Bifurcator: Installed
Wing: Removed

	Test	Run	Configuration
○	994	12	518

Outer Door Angle: 50°
Outer Door Cutback: None
Outer Door Kicker: None
Outer Door Fence: None
Inner Door Angle: 36°
Inner Door Fillers: All
Door Struts: No
Door Leakage: Partial

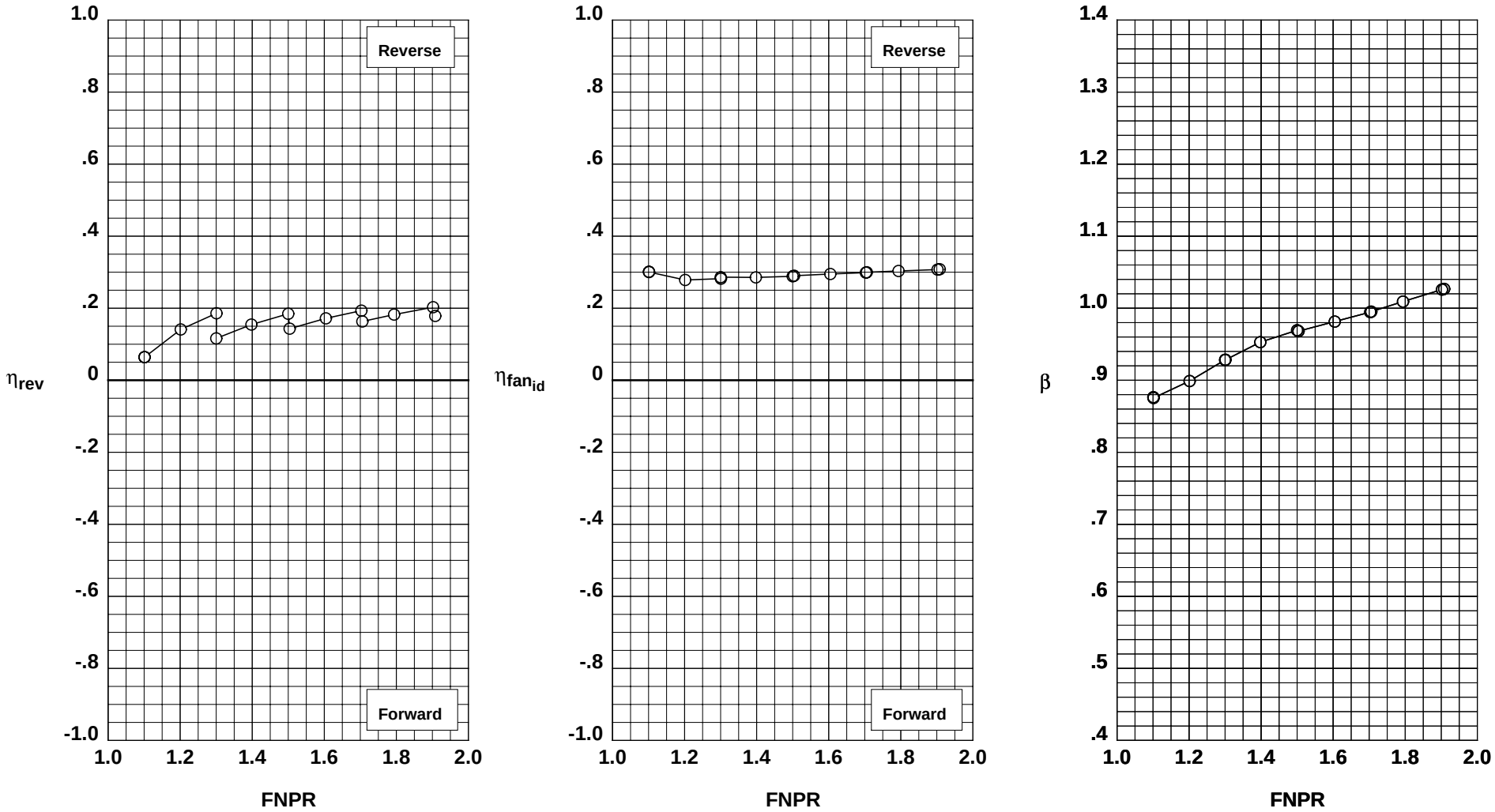

Figure G-18. Multi-door crocodile thrust reverser performance characteristics for configuration 518.

Operation Mode: Dual Flow
Reverser Port Bullnose: #3
Reverser Port Spacer: None
Reverser Port Cover: None
Bifurcator: Installed
Wing: Removed

	Test	Run	Configuration
○	994	13	519

Outer Door Angle: 60°
Outer Door Cutback: None
Outer Door Kicker: Long/Cutback
Outer Door Fence: None
Inner Door Angle: 36°
Inner Door Fillers: All
Door Struts: No
Door Leakage: Partial

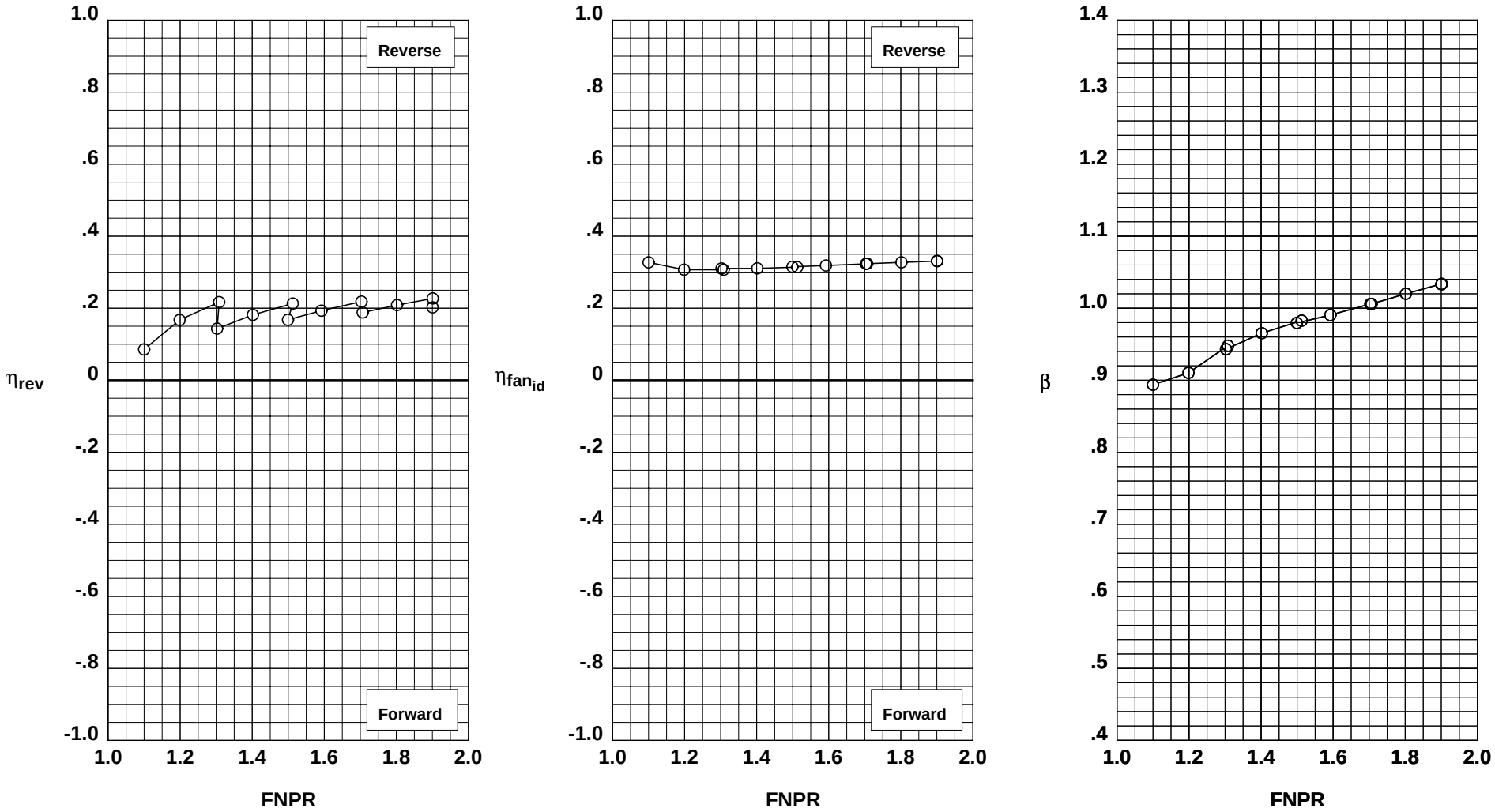

Figure G-19. Multi-door crocodile thrust reverser performance characteristics for configuration 519.

Operation Mode: Dual Flow
Reverser Port Bullnose: #3
Reverser Port Spacer: None
Reverser Port Cover: None
Bifurcator: Installed
Wing: Removed

	Test	Run	Configuration
○	994	14	520

Outer Door Angle: 60°
Outer Door Cutback: None
Outer Door Kicker: X-Long/Cutback
Outer Door Fence: None
Inner Door Angle: 36°
Inner Door Fillers: All
Door Struts: No
Door Leakage: Partial

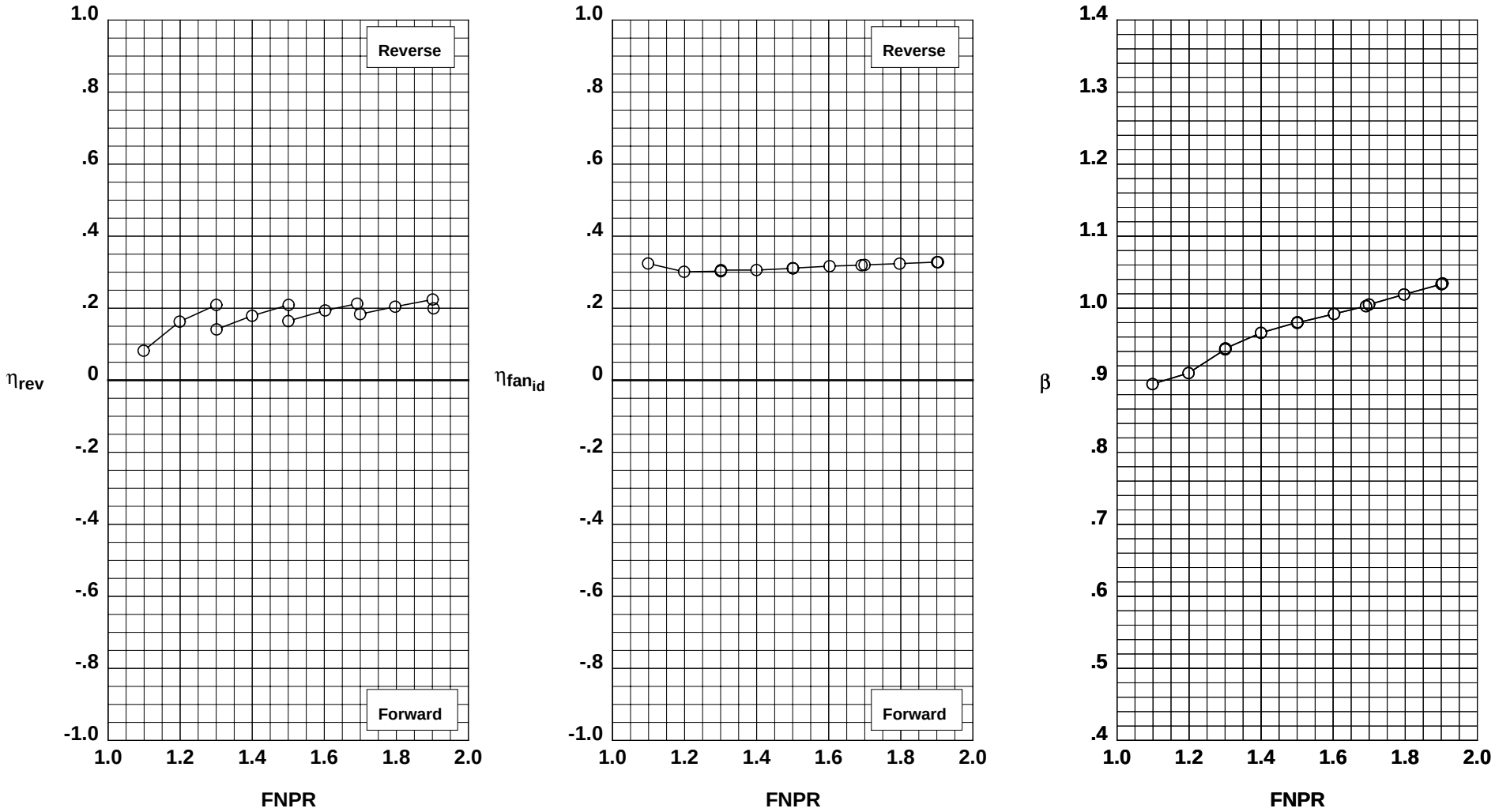

Figure G-20. Multi-door crocodile thrust reverser performance characteristics for configuration 520.

Operation Mode: Dual Flow
Reverser Port Bullnose: #3
Reverser Port Spacer: None
Reverser Port Cover: Partial
Bifurcator: Installed
Wing: Removed

	Test	Run	Configuration
○	994	15	521

Outer Door Angle: 60°
Outer Door Cutback: Partial
Outer Door Kicker: Long/Cutback
Outer Door Fence: None
Inner Door Angle: 36°
Inner Door Fillers: All
Door Struts: No
Door Leakage: Partial

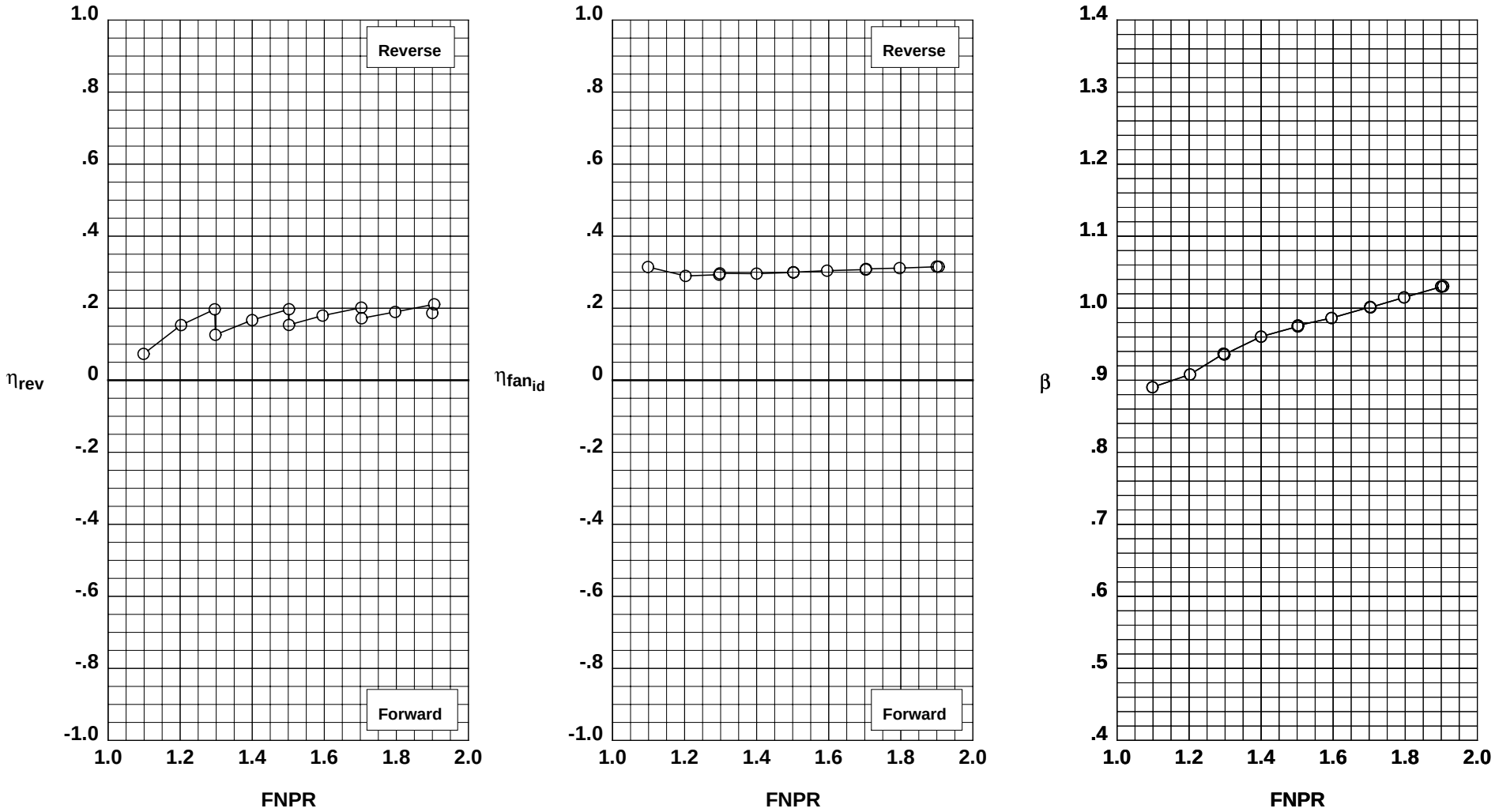

Figure G-21. Multi-door crocodile thrust reverser performance characteristics for configuration 521.

Operation Mode: Dual Flow
Reverser Port Bullnose: #3
Reverser Port Spacer: None
Reverser Port Cover: Mixed
Bifurcator: Installed
Wing: Removed

	Test	Run	Configuration
○	994	16	522

Outer Door Angle: 60°
Outer Door Cutback: Mixed
Outer Door Kicker: Long/Cutback
Outer Door Fence: None
Inner Door Angle: 36°
Inner Door Fillers: All
Door Struts: No
Door Leakage: Partial

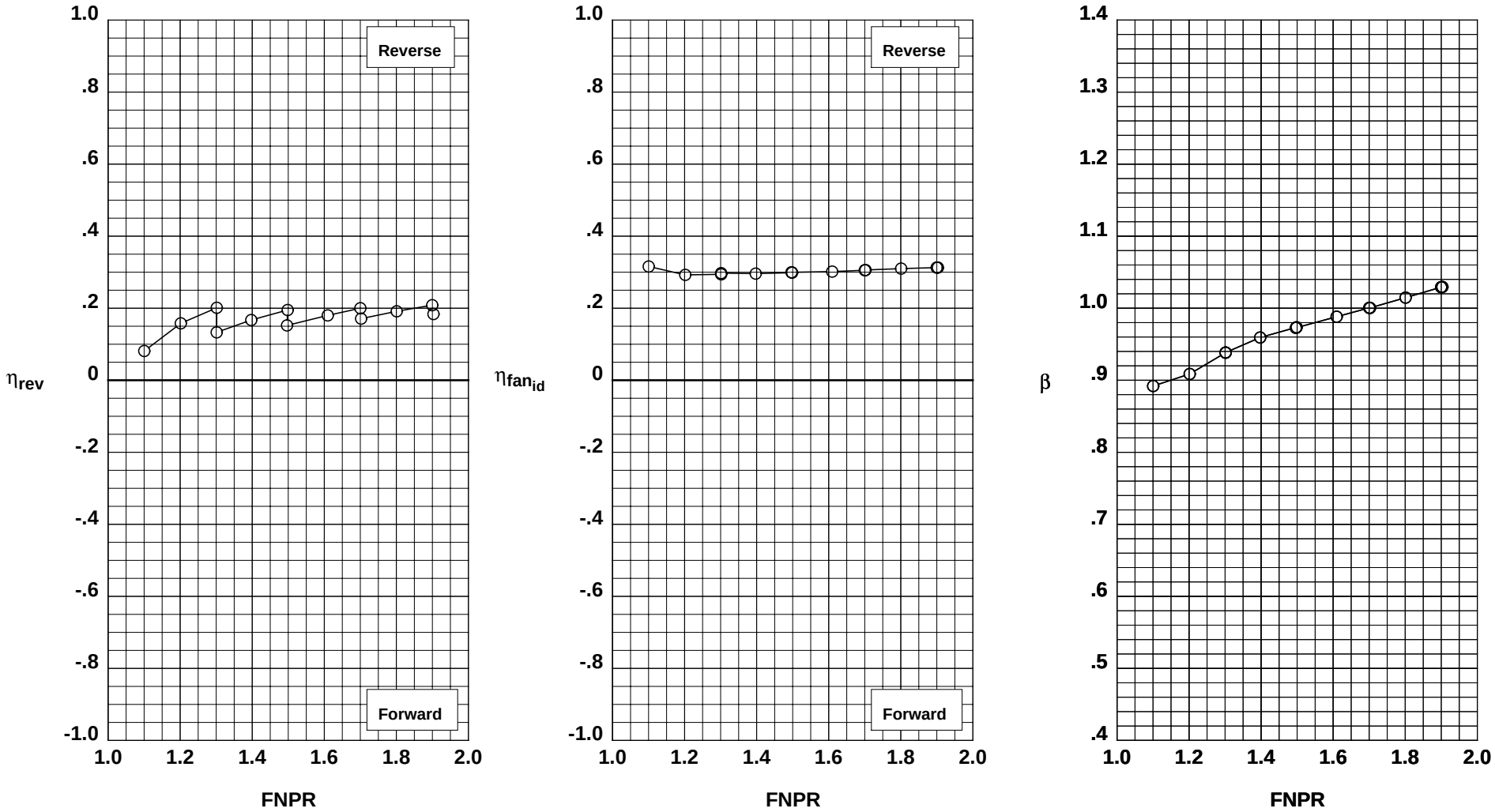

Figure G-22. Multi-door crocodile thrust reverser performance characteristics for configuration 522.

Operation Mode: Dual Flow
Reverser Port Bullnose: #3
Reverser Port Spacer: None
Reverser Port Cover: Full
Bifurcator: Installed
Wing: Removed

	Test	Run	Configuration
○	994	17	523

Outer Door Angle: 60°
Outer Door Cutback: Full
Outer Door Kicker: Long/Cutback
Outer Door Fence: None
Inner Door Angle: 36°
Inner Door Fillers: All
Door Struts: No
Door Leakage: Partial

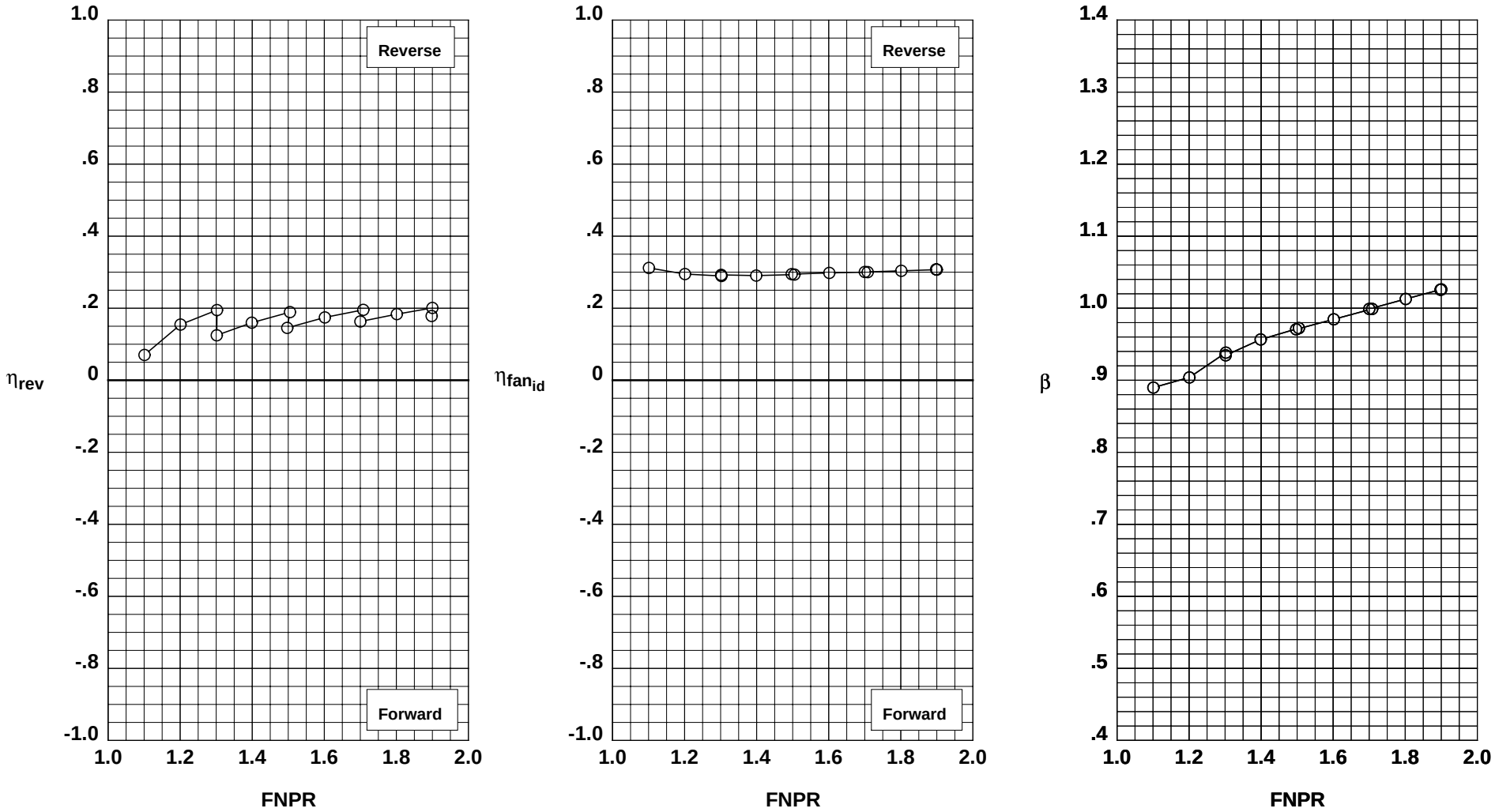

Figure G-23. Multi-door crocodile thrust reverser performance characteristics for configuration 523.

Operation Mode: Dual Flow
Reverser Port Bullnose: #3
Reverser Port Spacer: None
Reverser Port Cover: Full
Bifurcator: Installed
Wing: Removed

	Test	Run	Configuration
○	994	18	524

Outer Door Angle: 50°
Outer Door Cutback: Full
Outer Door Kicker: Long/Cutback
Outer Door Fence: None
Inner Door Angle: 36°
Inner Door Fillers: All
Door Struts: No
Door Leakage: Partial

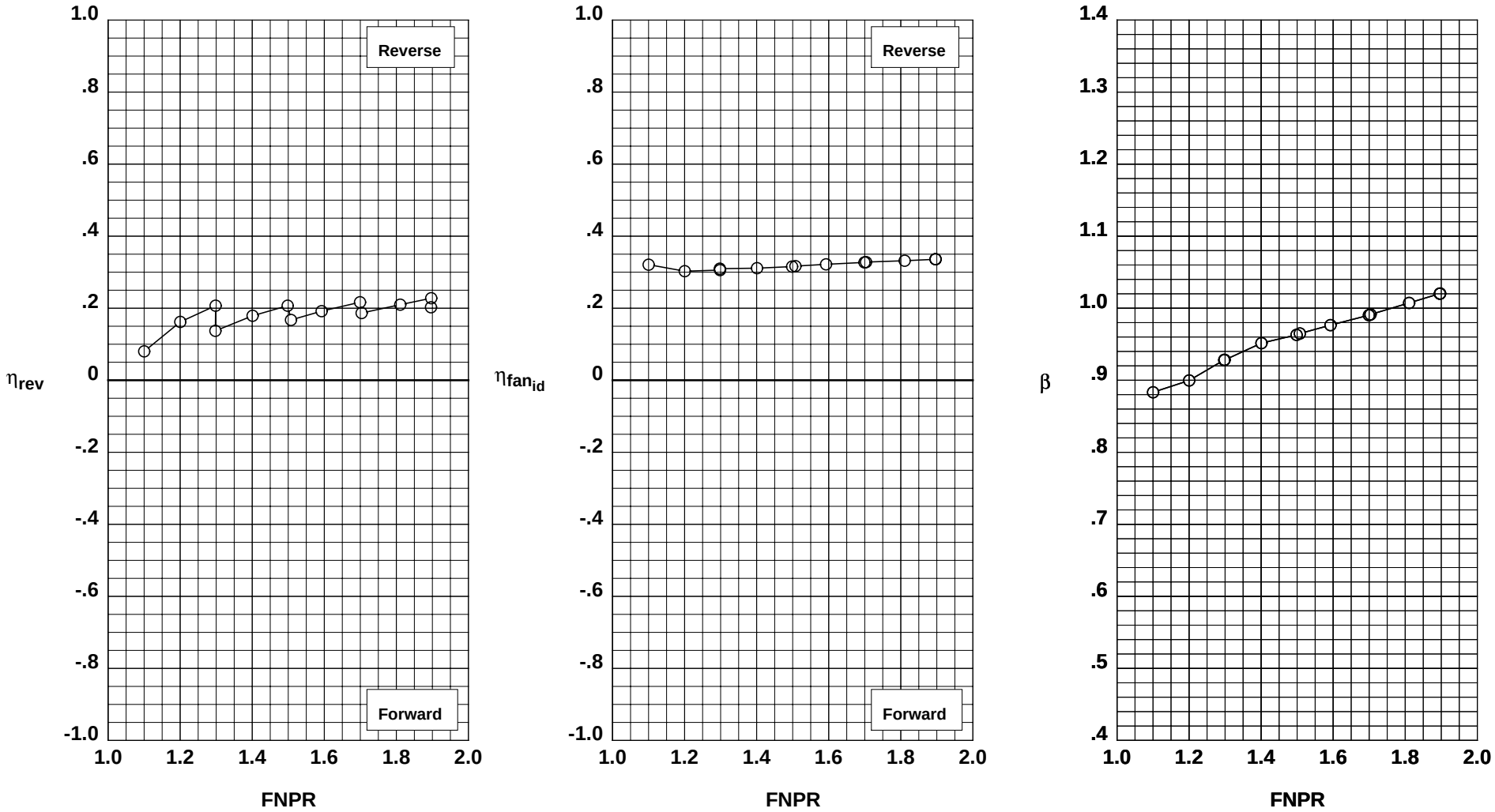

Figure G-24. Multi-door crocodile thrust reverser performance characteristics for configuration 524.

Operation Mode: Dual Flow
Reverser Port Bullnose: #3
Reverser Port Spacer: None
Reverser Port Cover: Mixed
Bifurcator: Installed
Wing: Removed

	Test	Run	Configuration
○	994	19	525

Outer Door Angle: 50°
Outer Door Cutback: Mixed
Outer Door Kicker: Long/Cutback
Outer Door Fence: None
Inner Door Angle: 36°
Inner Door Fillers: All
Door Struts: No
Door Leakage: Partial

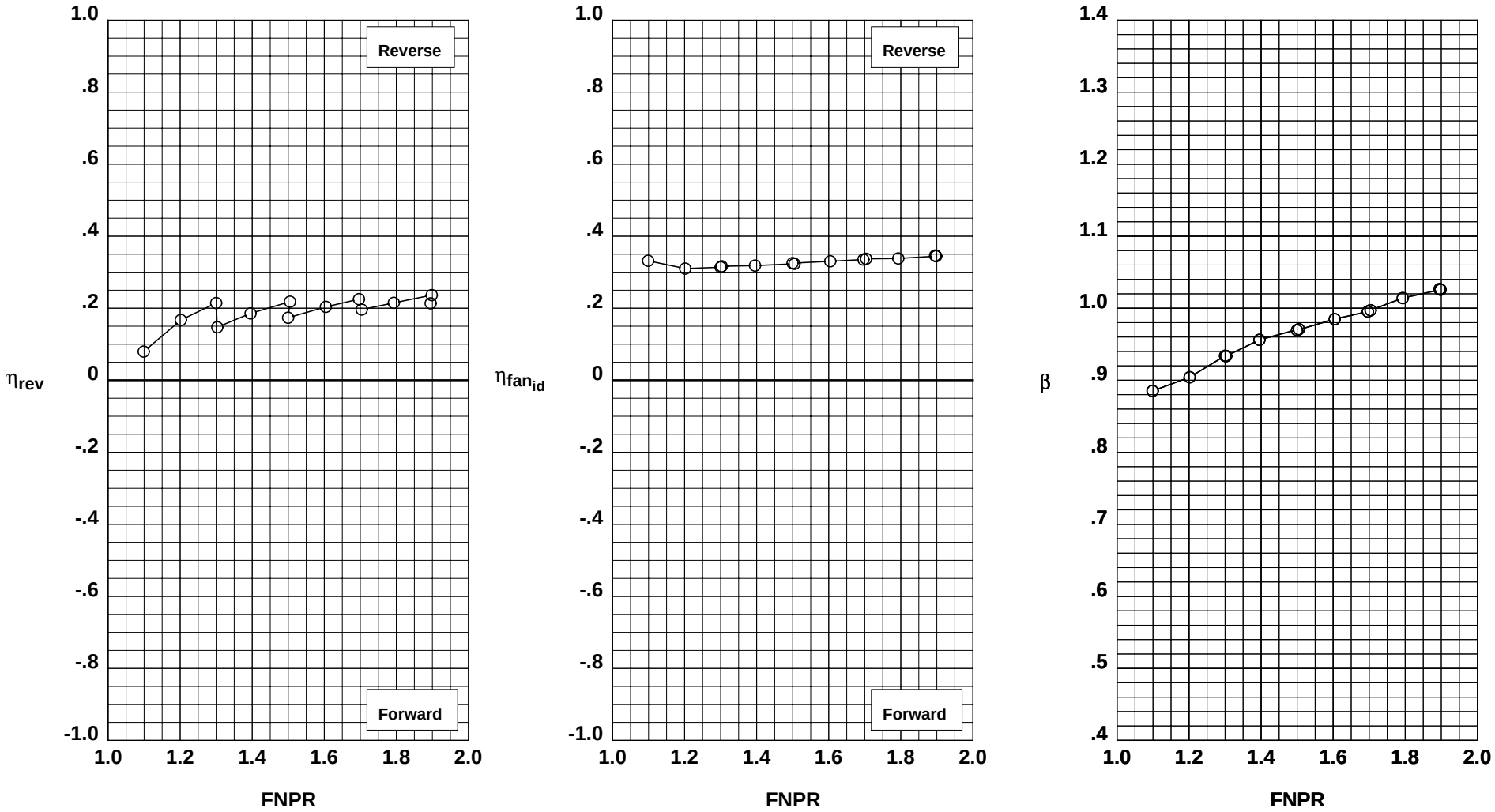

Figure G-25. Multi-door crocodile thrust reverser performance characteristics for configuration 525.

Operation Mode: Dual Flow
Reverser Port Bullnose: #3
Reverser Port Spacer: None
Reverser Port Cover: Partial
Bifurcator: Installed
Wing: Removed

	Test	Run	Configuration
○	994	20	526

Outer Door Angle: 50°
Outer Door Cutback: Partial
Outer Door Kicker: Long/Cutback
Outer Door Fence: None
Inner Door Angle: 36°
Inner Door Fillers: All
Door Struts: No
Door Leakage: Partial

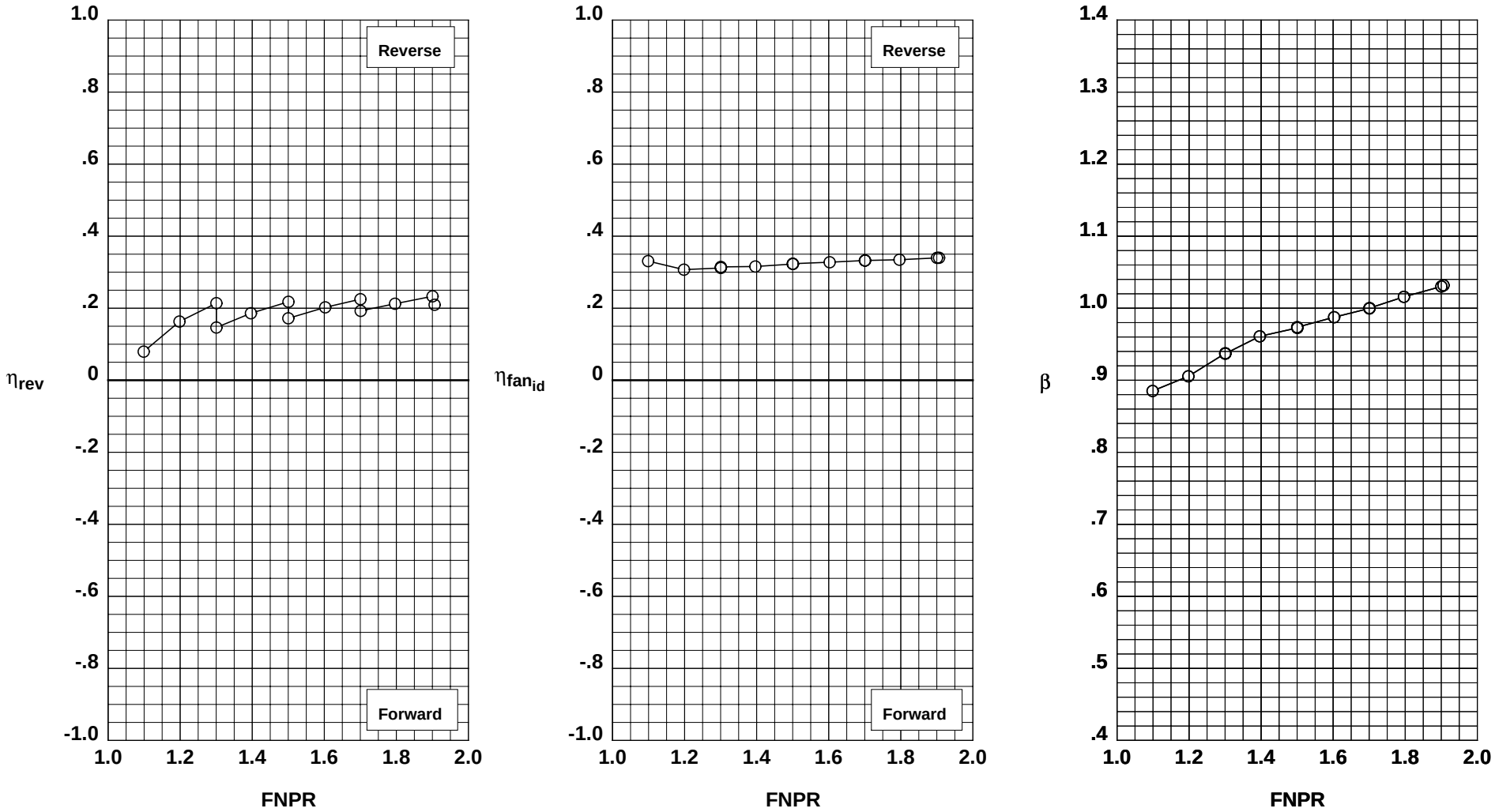

Figure G-26. Multi-door crocodile thrust reverser performance characteristics for configuration 526.

Operation Mode: Dual Flow
Reverser Port Bullnose: #3
Reverser Port Spacer: None
Reverser Port Cover: Partial
Bifurcator: Installed
Wing: Removed

	Test	Run	Configuration
○	994	21	527

Outer Door Angle: 40°
Outer Door Cutback: Partial
Outer Door Kicker: Long/Cutback
Outer Door Fence: None
Inner Door Angle: 36°
Inner Door Fillers: All
Door Struts: No
Door Leakage: Partial

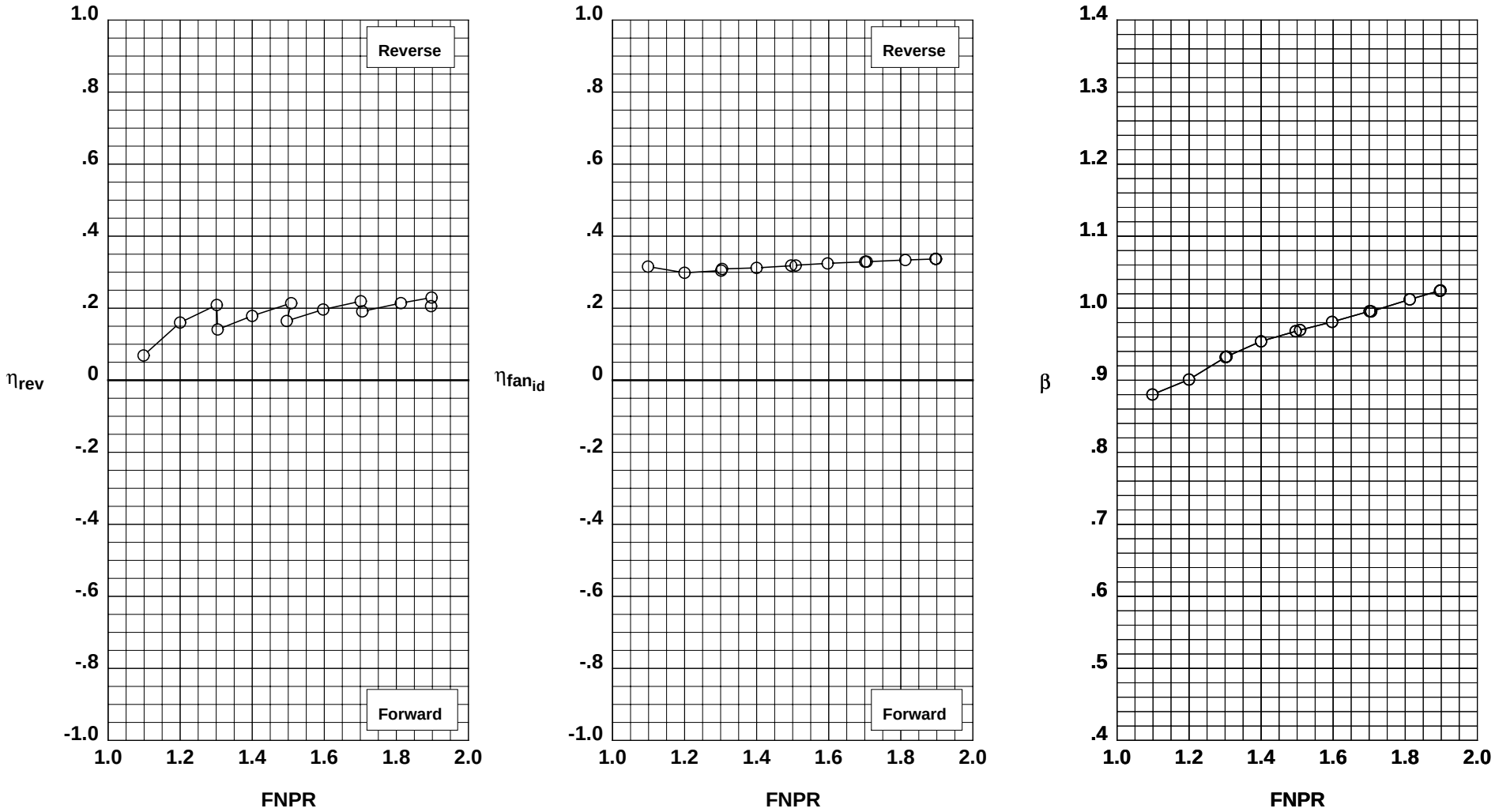

Figure G-27. Multi-door crocodile thrust reverser performance characteristics for configuration 527.

Operation Mode: Dual Flow
Reverser Port Bullnose: #3
Reverser Port Spacer: None
Reverser Port Cover: Full
Bifurcator: Installed
Wing: Removed

	Test	Run	Configuration
○	994	22	528

Outer Door Angle: 40°
Outer Door Cutback: Full
Outer Door Kicker: Long/Cutback
Outer Door Fence: None
Inner Door Angle: 36°
Inner Door Fillers: All
Door Struts: No
Door Leakage: Partial

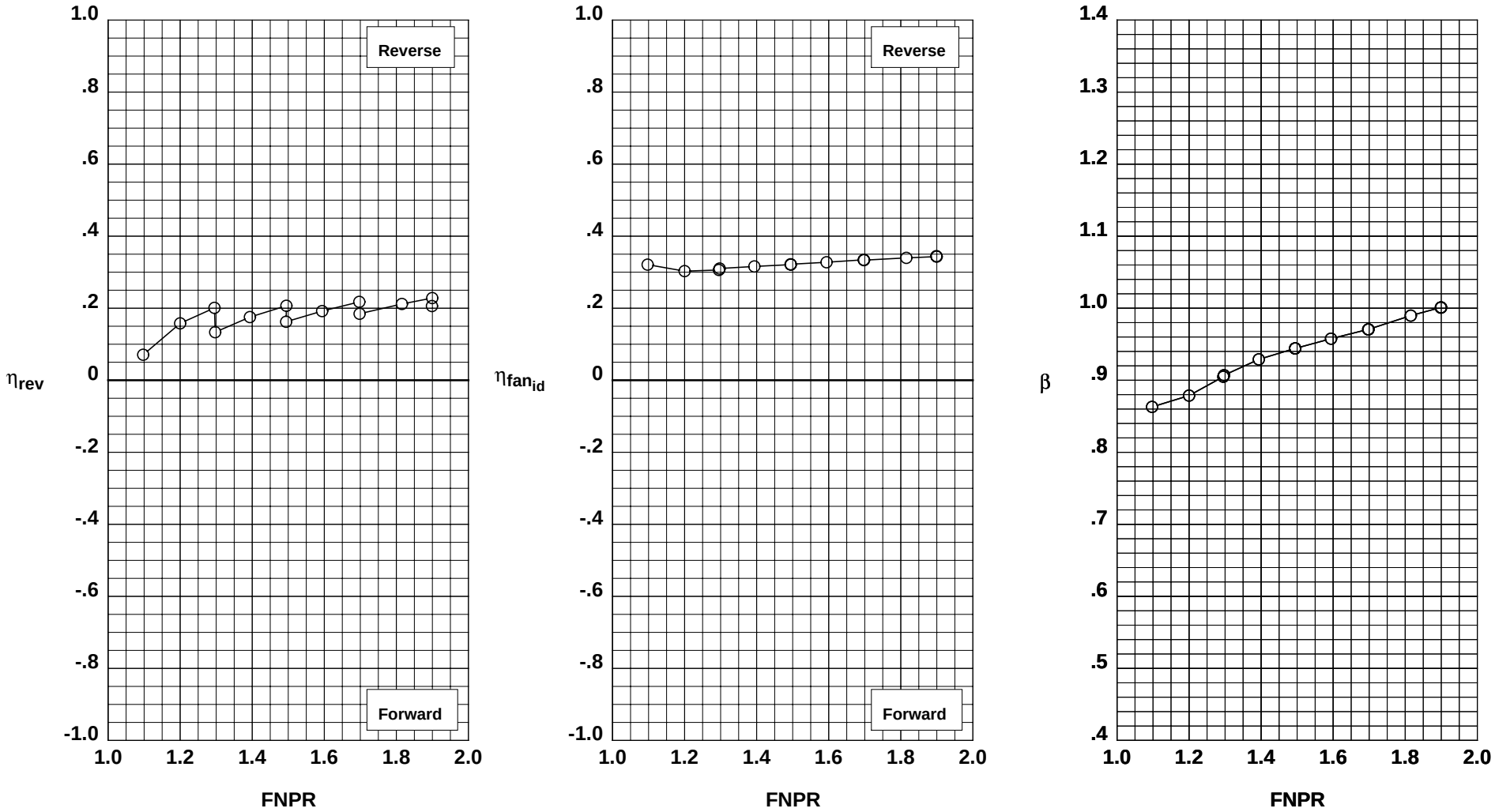

Figure G-28. Multi-door crocodile thrust reverser performance characteristics for configuration 528.

Operation Mode: Dual Flow
Reverser Port Bullnose: #3
Reverser Port Spacer: None
Reverser Port Cover: None
Bifurcator: Installed
Wing: Removed

	Test	Run	Configuration
○	994	23	519

Outer Door Angle: 60°
Outer Door Cutback: None
Outer Door Kicker: Long/Cutback
Outer Door Fence: None
Inner Door Angle: 36°
Inner Door Fillers: All
Door Struts: No
Door Leakage: Partial

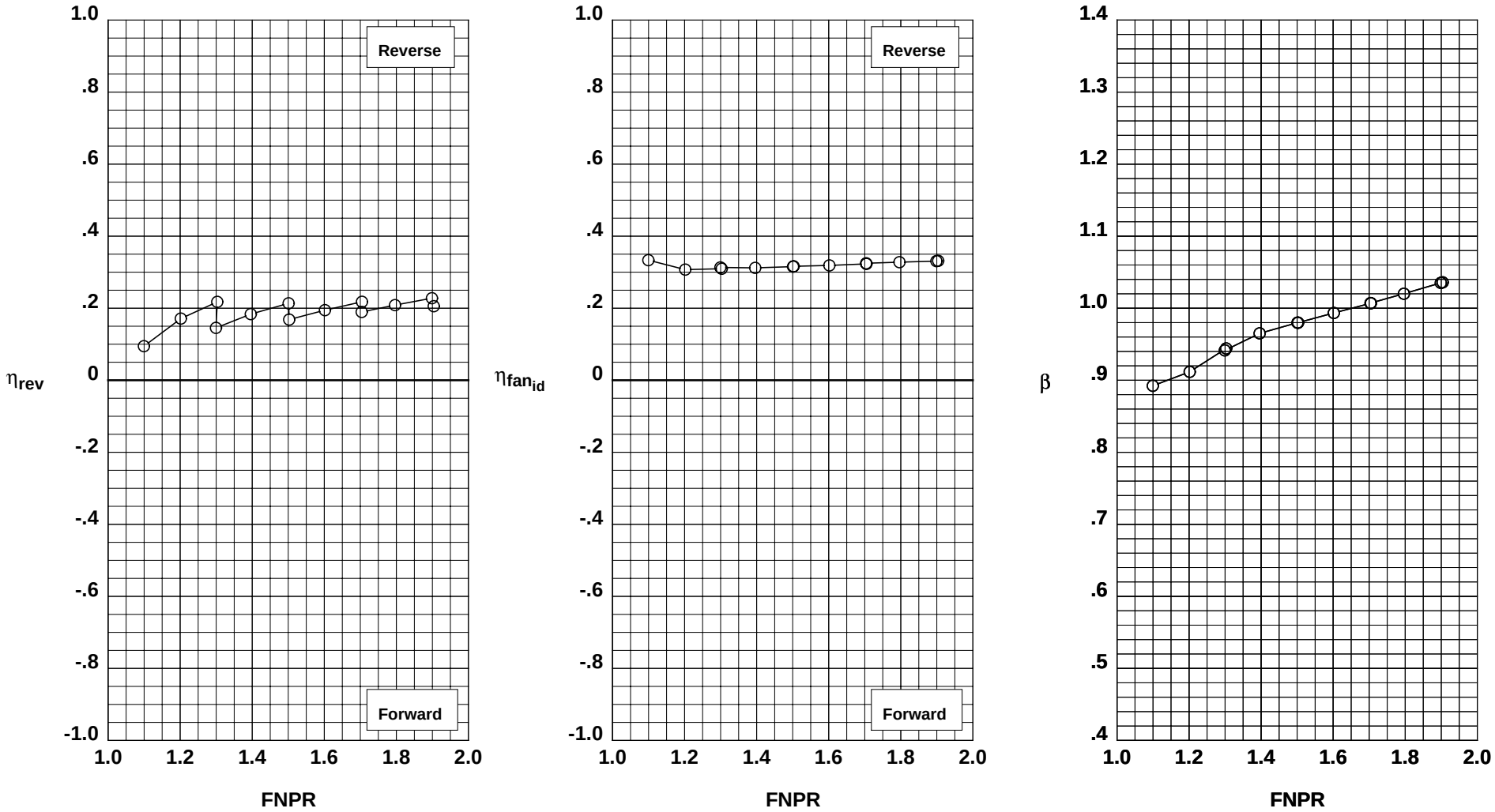

Figure G-29. Multi-door crocodile thrust reverser performance characteristics for configuration 519.

Operation Mode: Dual Flow
Reverser Port Bullnose: #3
Reverser Port Spacer: 0.40"
Reverser Port Cover: None
Bifurcator: Installed
Wing: Removed

	Test	Run	Configuration
○	994	24	529

Outer Door Angle: 60°
Outer Door Cutback: None
Outer Door Kicker: Long/Cutback
Outer Door Fence: None
Inner Door Angle: 36°
Inner Door Fillers: All
Door Struts: No
Door Leakage: Partial

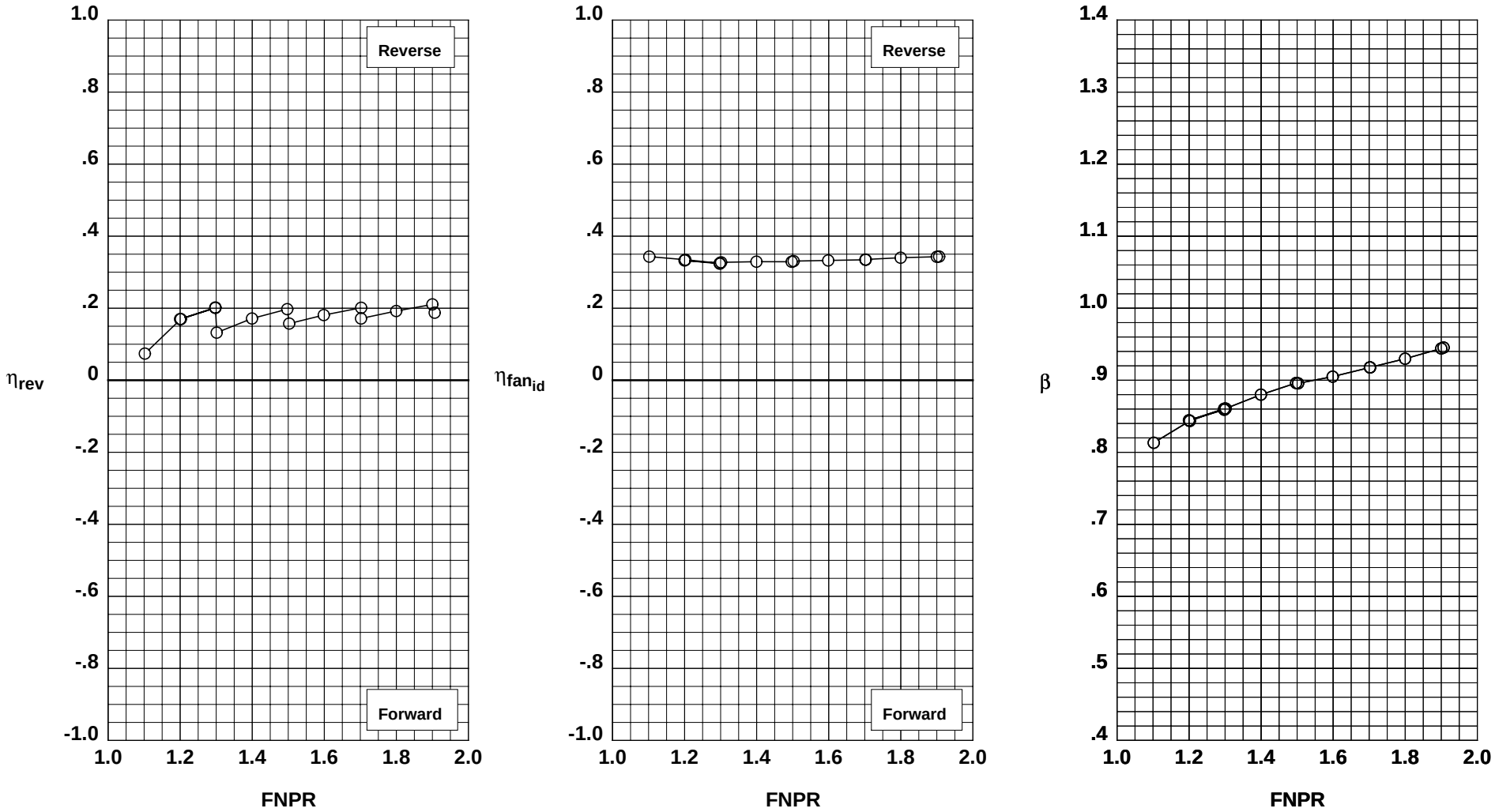

Figure G-30. Multi-door crocodile thrust reverser performance characteristics for configuration 529.

Operation Mode: Dual Flow
Reverser Port Bullnose: #3
Reverser Port Spacer: 0.40"
Reverser Port Cover: None
Bifurcator: Installed
Wing: Removed

	Test	Run	Configuration
○	994	25	530

Outer Door Angle: 50°
Outer Door Cutback: None
Outer Door Kicker: Long/Cutback
Outer Door Fence: None
Inner Door Angle: 36°
Inner Door Fillers: All
Door Struts: No
Door Leakage: Partial

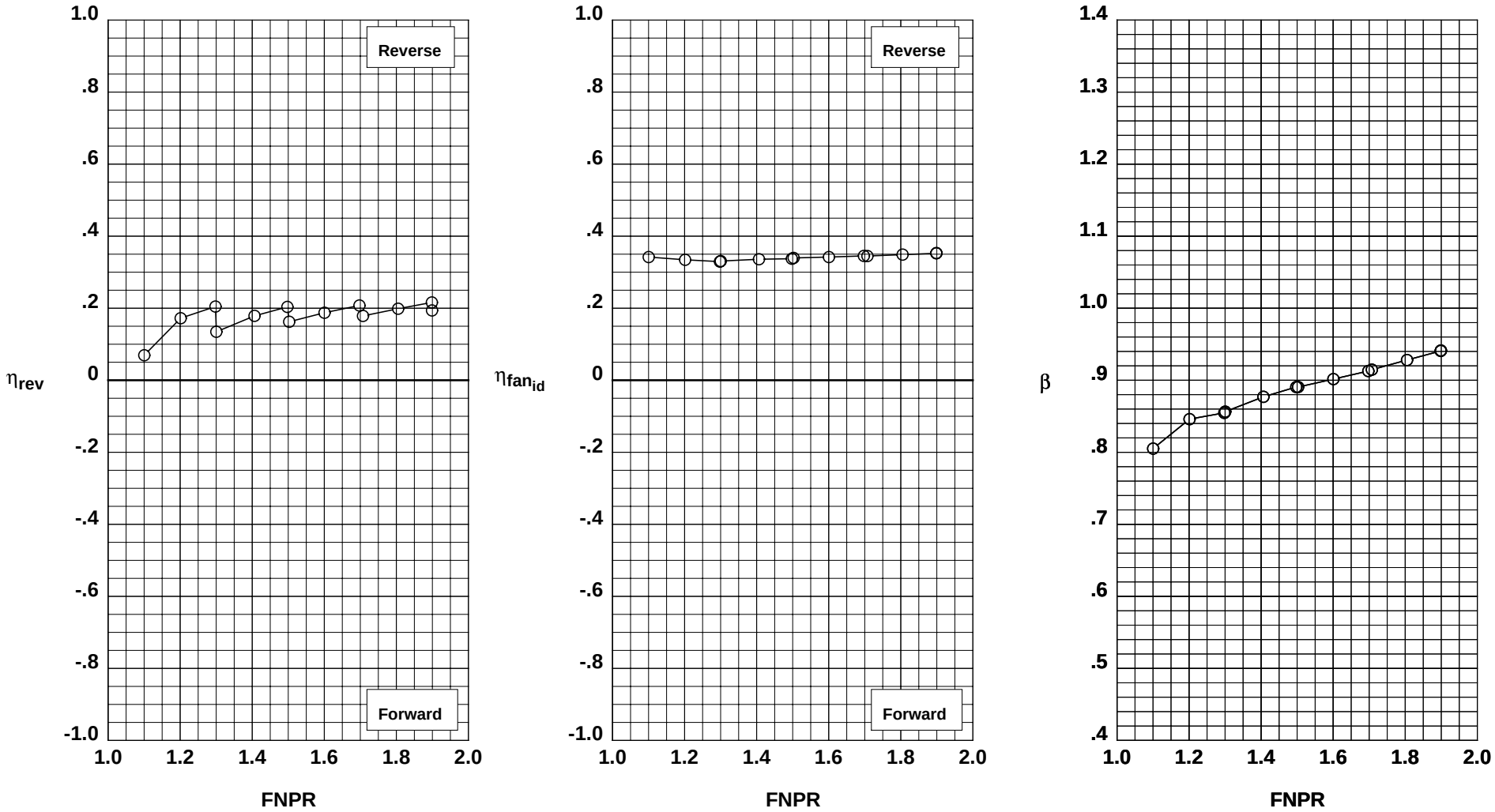

Figure G-31. Multi-door crocodile thrust reverser performance characteristics for configuration 530.

Operation Mode: Dual Flow
Reverser Port Bullnose: #3
Reverser Port Spacer: 0.40"
Reverser Port Cover: None
Bifurcator: Installed
Wing: Removed

	Test	Run	Configuration
○	994	26	531

Outer Door Angle: 40°
Outer Door Cutback: None
Outer Door Kicker: Long/Cutback
Outer Door Fence: None
Inner Door Angle: 36°
Inner Door Fillers: All
Door Struts: No
Door Leakage: Partial

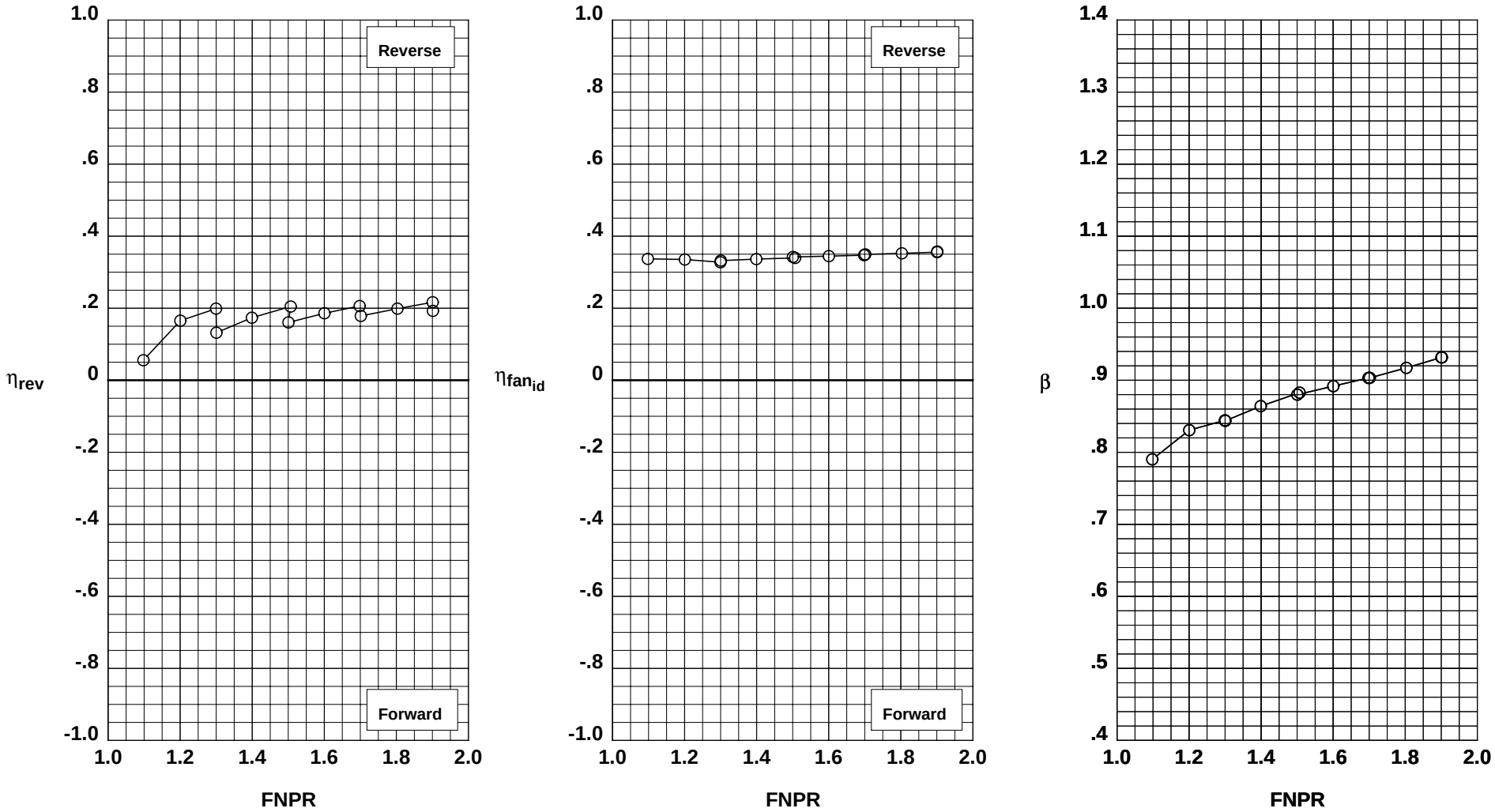

Figure G-32. Multi-door crocodile thrust reverser performance characteristics for configuration 531.

Operation Mode: Dual Flow
Reverser Port Bullnose: #3
Reverser Port Spacer: 0.20"
Reverser Port Cover: None
Bifurcator: Installed
Wing: Removed

	Test	Run	Configuration
○	994	27	532

Outer Door Angle: 40°
Outer Door Cutback: None
Outer Door Kicker: Long/Cutback
Outer Door Fence: None
Inner Door Angle: 36°
Inner Door Fillers: All
Door Struts: No
Door Leakage: Partial

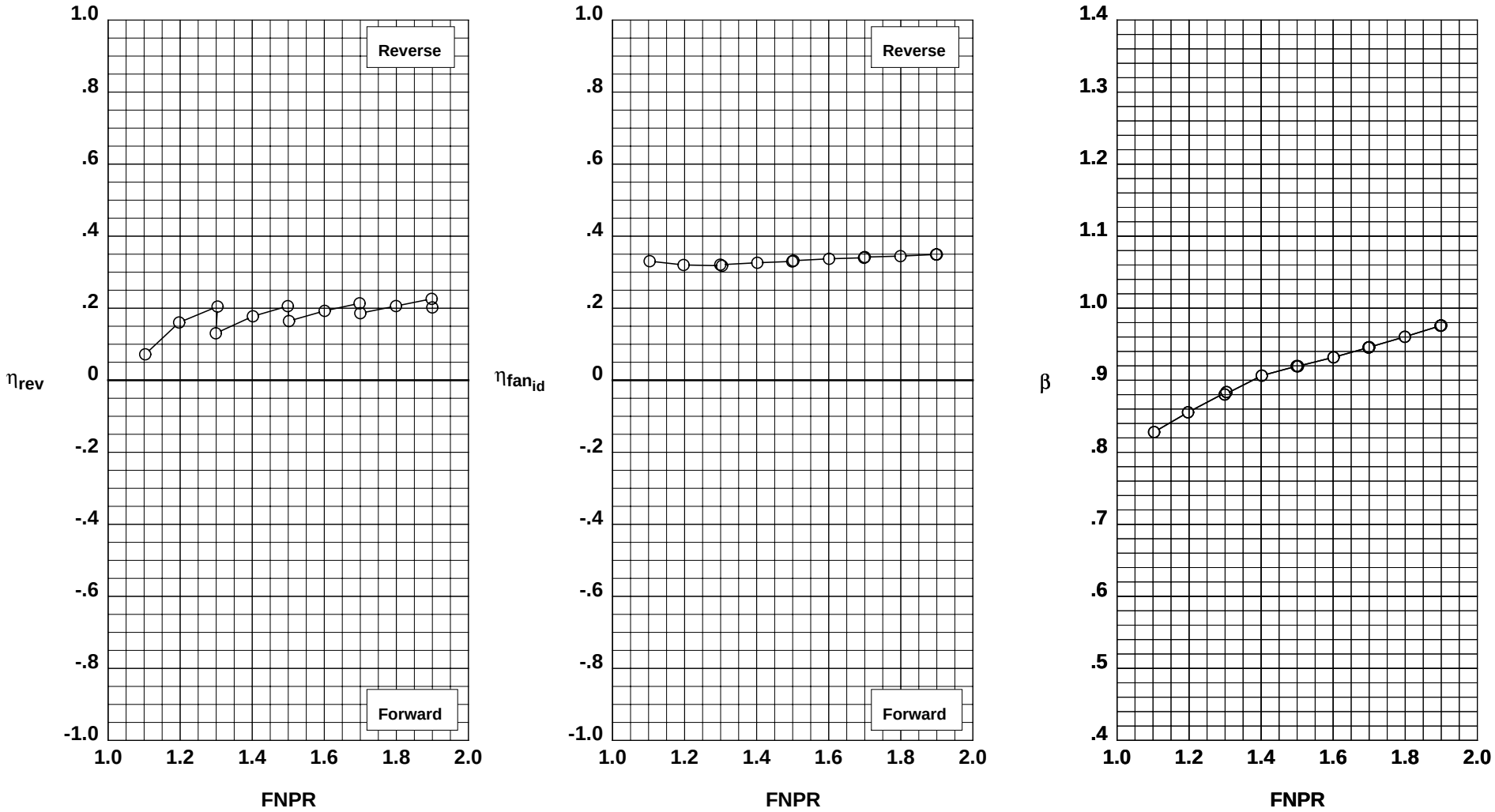

Figure G-33. Multi-door crocodile thrust reverser performance characteristics for configuration 532.

Operation Mode: Dual Flow
Reverser Port Bullnose: #3
Reverser Port Spacer: 0.20"
Reverser Port Cover: None
Bifurcator: Installed
Wing: Removed

	Test	Run	Configuration
○	994	29	533

Outer Door Angle: 50°
Outer Door Cutback: None
Outer Door Kicker: Long/Cutback
Outer Door Fence: None
Inner Door Angle: 36°
Inner Door Fillers: All
Door Struts: No
Door Leakage: Partial

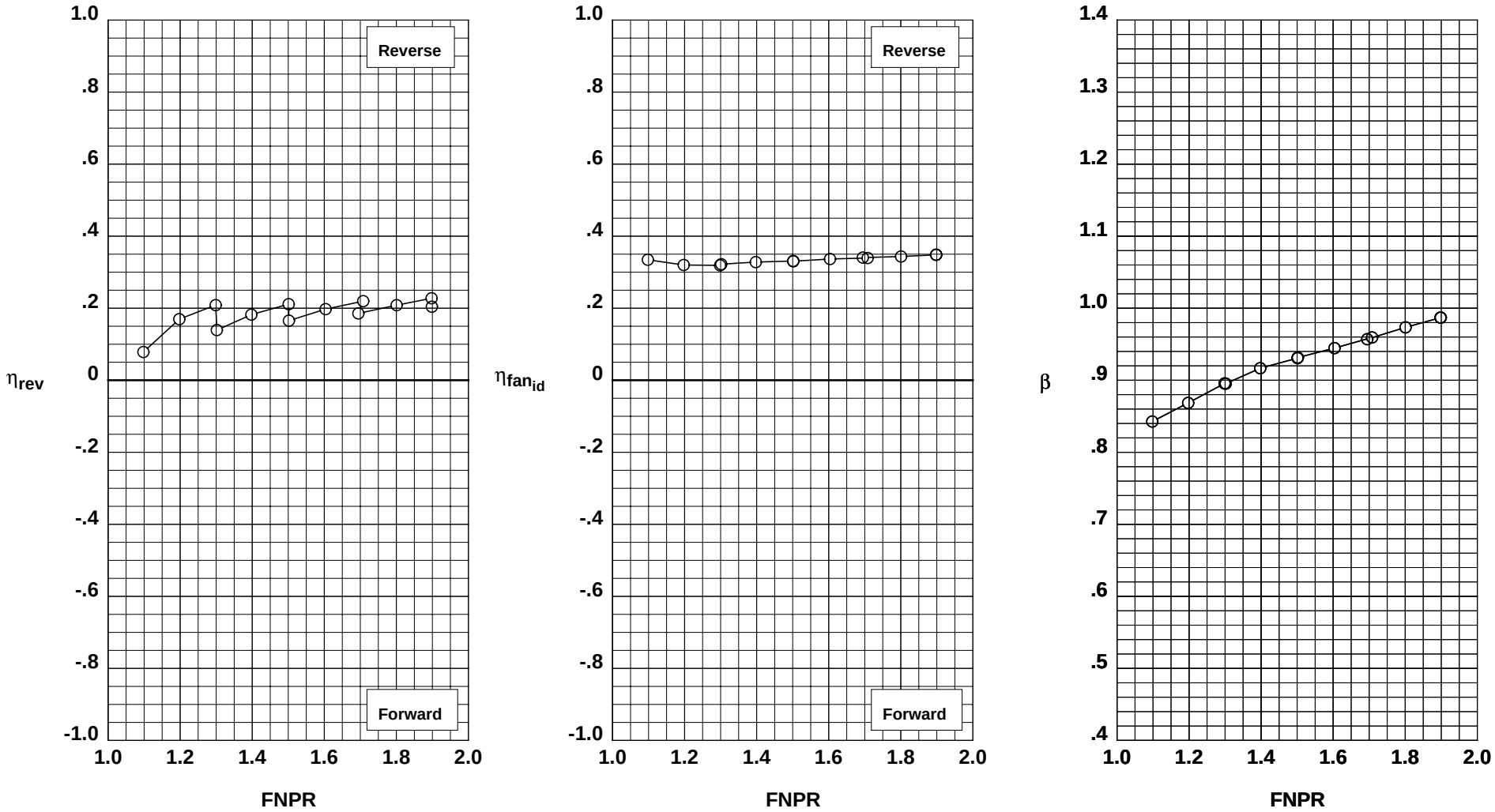

Figure G-34. Multi-door crocodile thrust reverser performance characteristics for configuration 533.

Operation Mode: Dual Flow
Reverser Port Bullnose: #3
Reverser Port Spacer: 0.20"
Reverser Port Cover: None
Bifurcator: Installed
Wing: Removed

	Test	Run	Configuration
○	994	30	534

Outer Door Angle: 60°
Outer Door Cutback: None
Outer Door Kicker: Long/Cutback
Outer Door Fence: None
Inner Door Angle: 36°
Inner Door Fillers: All
Door Struts: No
Door Leakage: Partial

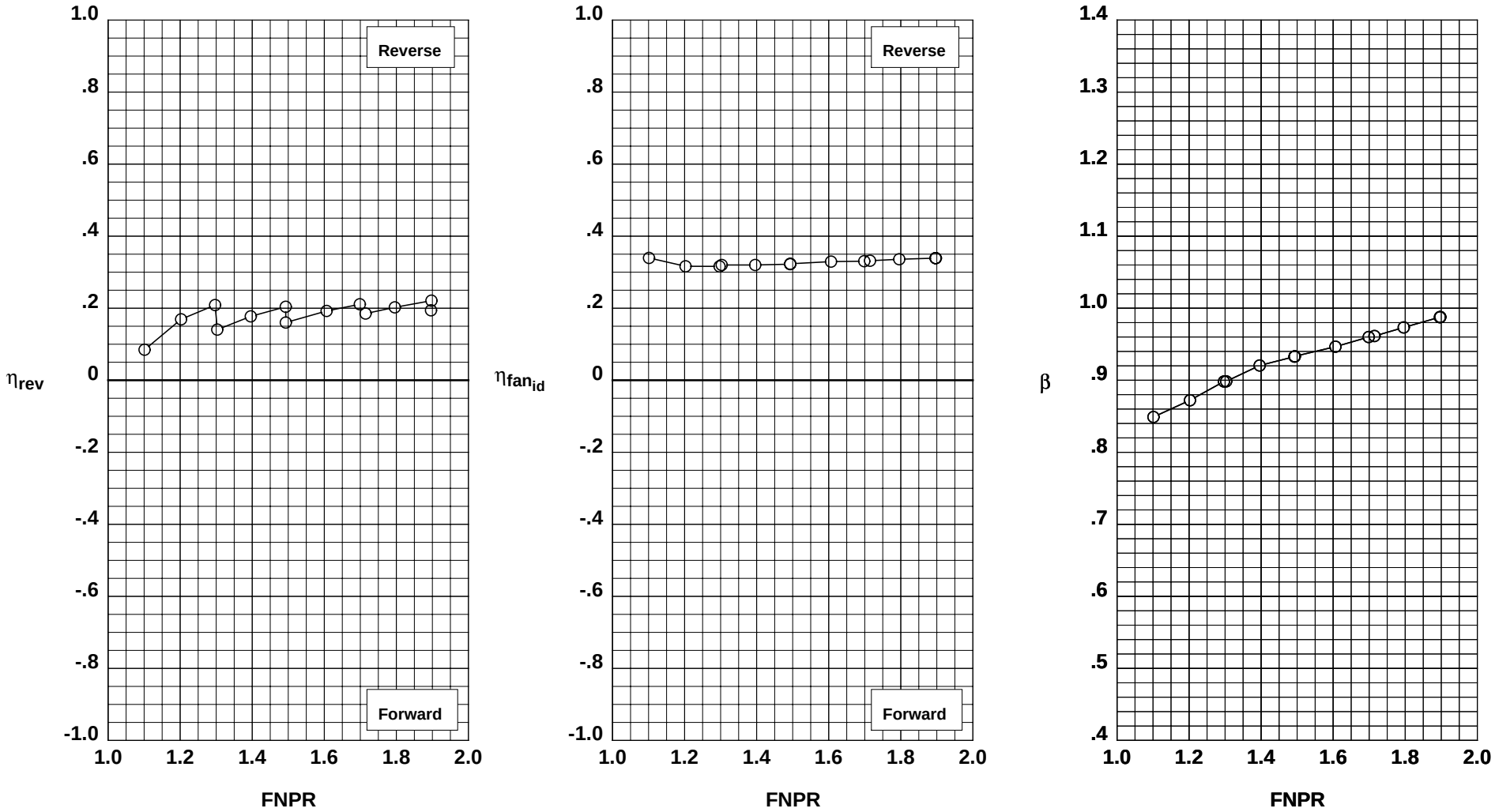

Figure G-35. Multi-door crocodile thrust reverser performance characteristics for configuration 534.

Operation Mode: Dual Flow
Reverser Port Bullnose: #1
Reverser Port Spacer: 0.40"
Reverser Port Cover: None
Bifurcator: Installed
Wing: Removed

	Test	Run	Configuration
○	994	31	535

Outer Door Angle: 60°
Outer Door Cutback: None
Outer Door Kicker: Long/Cutback
Outer Door Fence: None
Inner Door Angle: 36°
Inner Door Fillers: All
Door Struts: No
Door Leakage: Partial

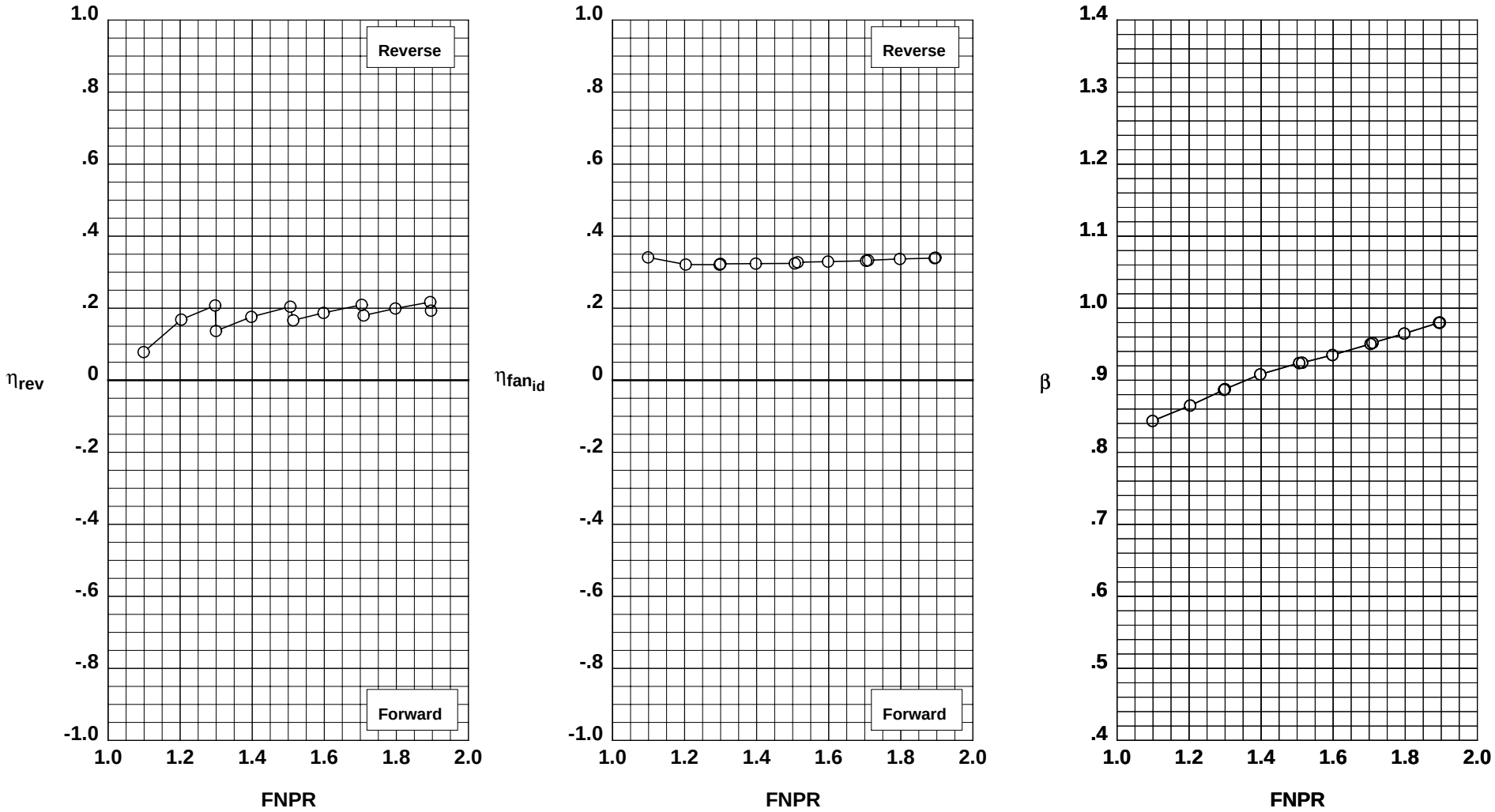

Figure G-36. Multi-door crocodile thrust reverser performance characteristics for configuration 535.

Operation Mode: Dual Flow
Reverser Port Bullnose: #2
Reverser Port Spacer: None
Reverser Port Cover: None
Bifurcator: Installed
Wing: Removed

	Test	Run	Configuration
○	994	32	536

Outer Door Angle: 60°
Outer Door Cutback: None
Outer Door Kicker: Long/Cutback
Outer Door Fence: None
Inner Door Angle: 36°
Inner Door Fillers: All
Door Struts: No
Door Leakage: Partial

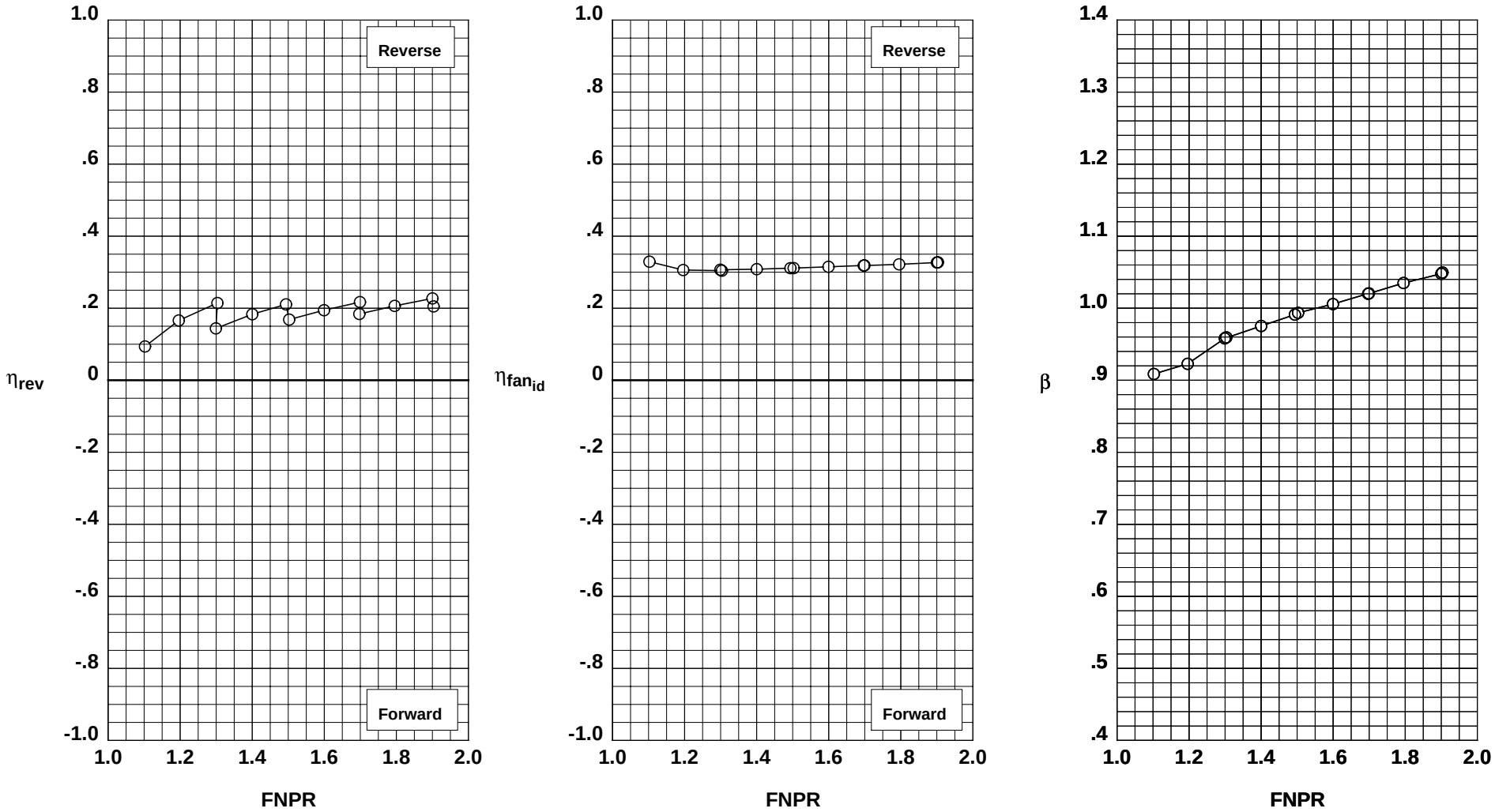

Figure G-37. Multi-door crocodile thrust reverser performance characteristics for configuration 536.

Operation Mode: Dual Flow
Reverser Port Bullnose: #2
Reverser Port Spacer: None
Reverser Port Cover: None
Bifurcator: Installed
Wing: Removed

	Test	Run	Configuration
○	994	33	537

Outer Door Angle: 50°
Outer Door Cutback: None
Outer Door Kicker: Long/Cutback
Outer Door Fence: None
Inner Door Angle: 36°
Inner Door Fillers: All
Door Struts: No
Door Leakage: Partial

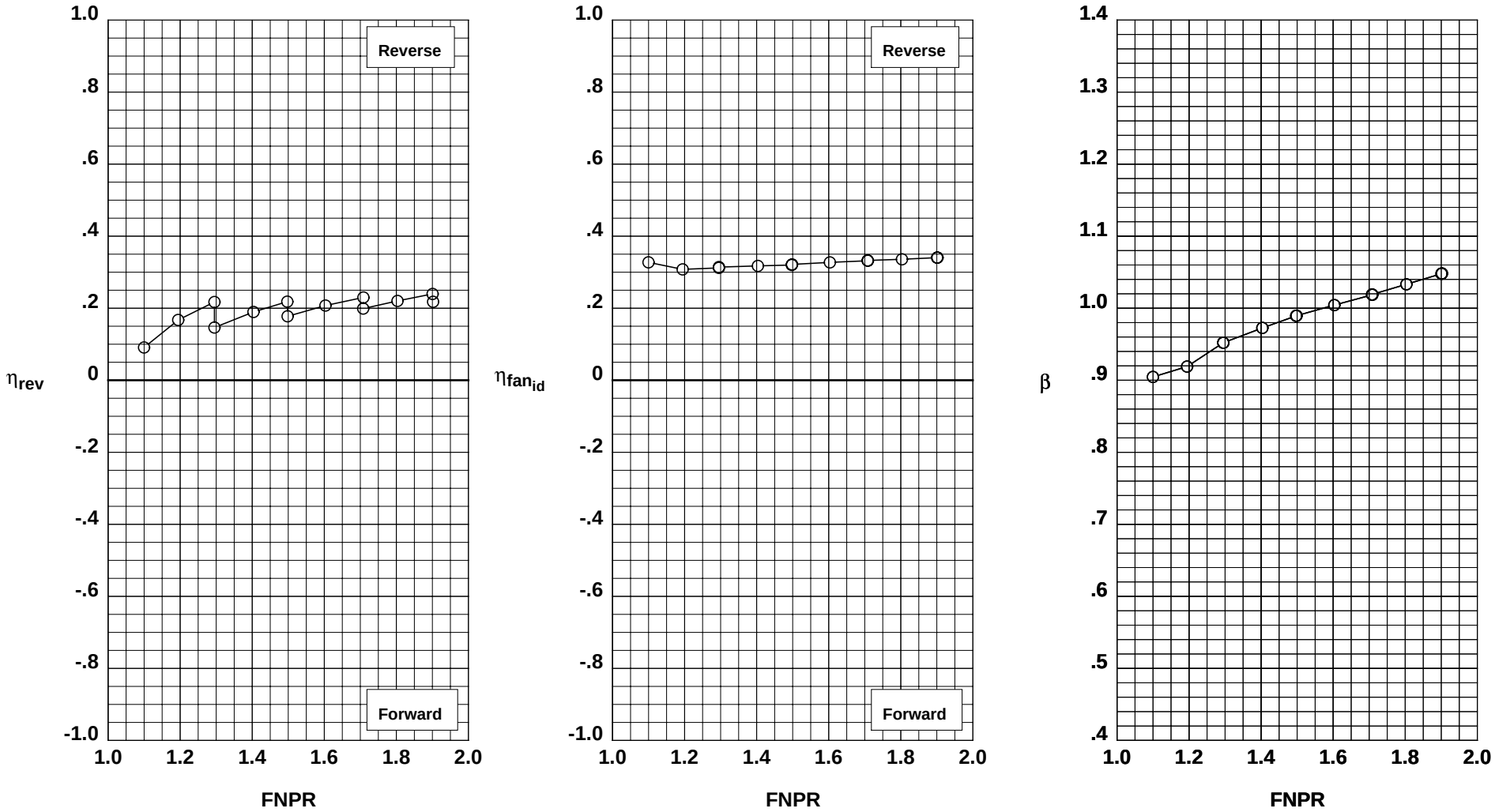

Figure G-38. Multi-door crocodile thrust reverser performance characteristics for configuration 537.

Operation Mode: Dual Flow
Reverser Port Bullnose: #3
Reverser Port Spacer: None
Reverser Port Cover: Mixed
Bifurcator: Installed
Wing: Removed

	Test	Run	Configuration
○	994	34	538

Outer Door Angle: 50°
Outer Door Cutback: Mixed
Outer Door Kicker: Long/Cutback
Outer Door Fence: None
Inner Door Angle: 30°
Inner Door Fillers: All
Door Struts: No
Door Leakage: Partial

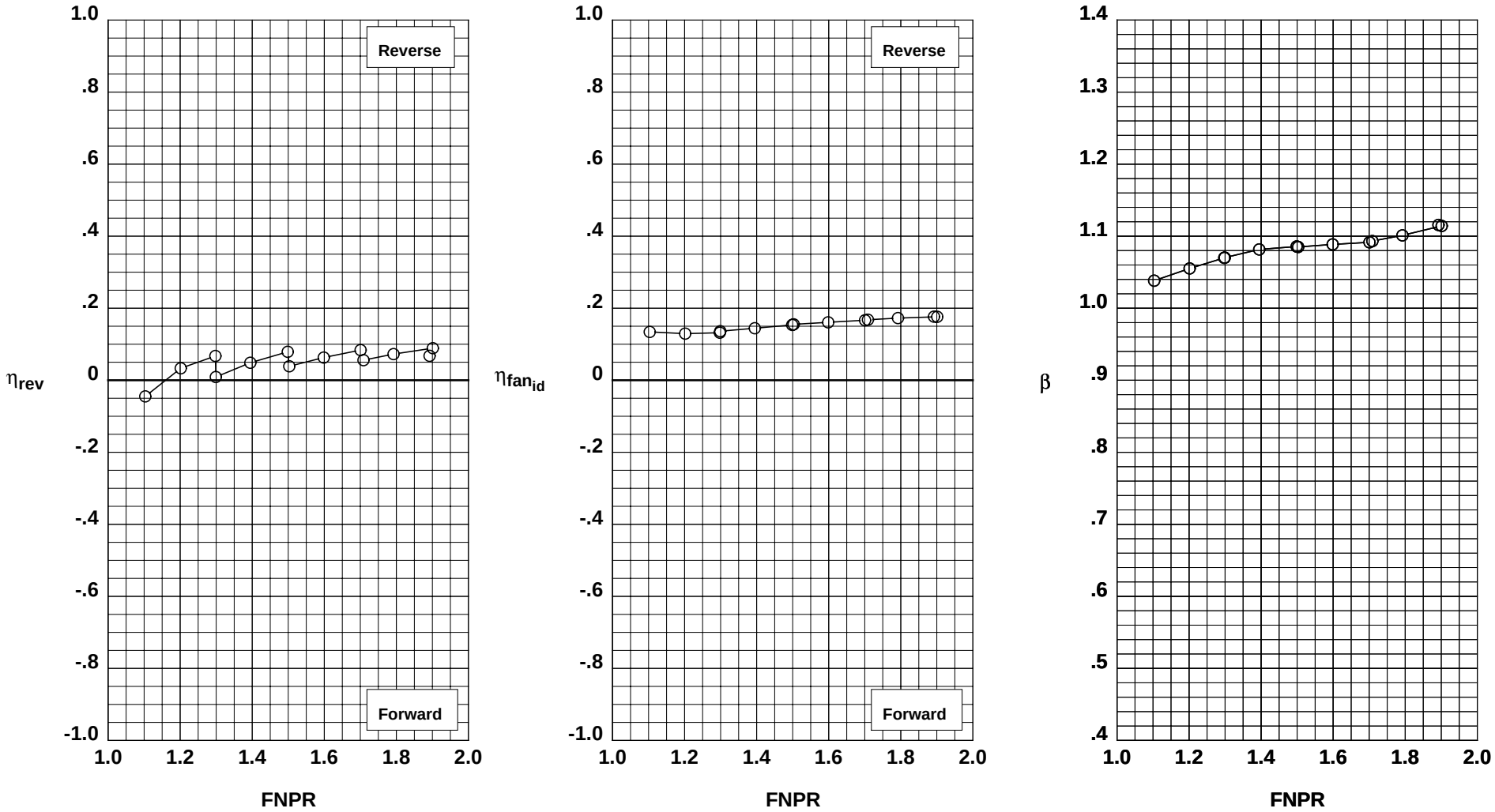

Figure G-39. Multi-door crocodile thrust reverser performance characteristics for configuration 538.

Operation Mode: Dual Flow
Reverser Port Bullnose: #3
Reverser Port Spacer: None
Reverser Port Cover: Mixed
Bifurcator: Installed
Wing: Removed

	Test	Run	Configuration
○	994	35	539

Outer Door Angle: 40°
Outer Door Cutback: Mixed
Outer Door Kicker: Long/Cutback
Outer Door Fence: None
Inner Door Angle: 24°
Inner Door Fillers: All
Door Struts: No
Door Leakage: Partial

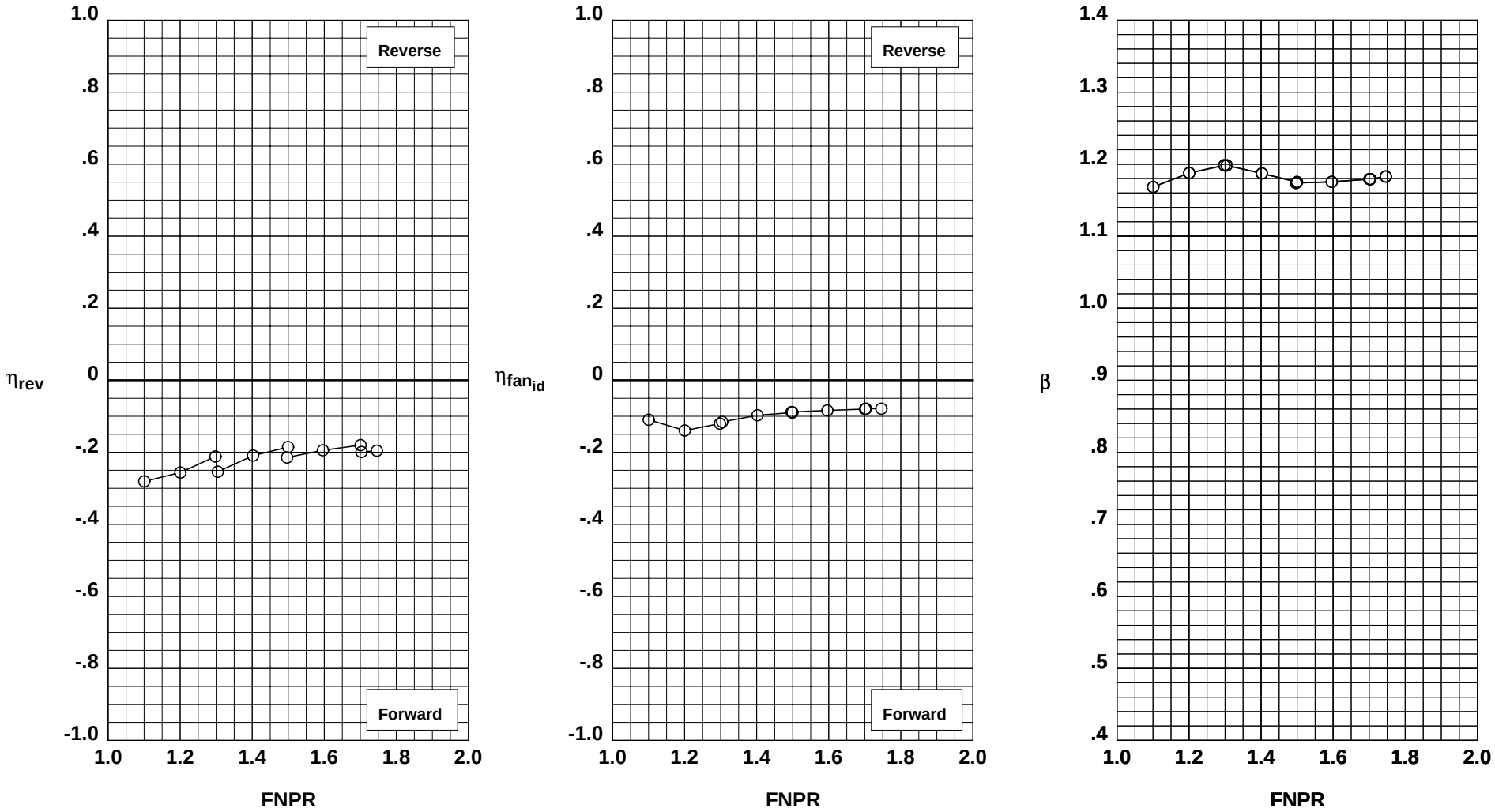

Figure G-40. Multi-door crocodile thrust reverser performance characteristics for configuration 539.

Operation Mode: Dual Flow
Reverser Port Bullnose: #3
Reverser Port Spacer: None
Reverser Port Cover: Mixed
Bifurcator: Installed
Wing: Removed

	Test	Run	Configuration
○	994	36	540

Outer Door Angle: 30°
Outer Door Cutback: Mixed
Outer Door Kicker: Long/Cutback
Outer Door Fence: None
Inner Door Angle: 18°
Inner Door Fillers: All
Door Struts: No
Door Leakage: Partial

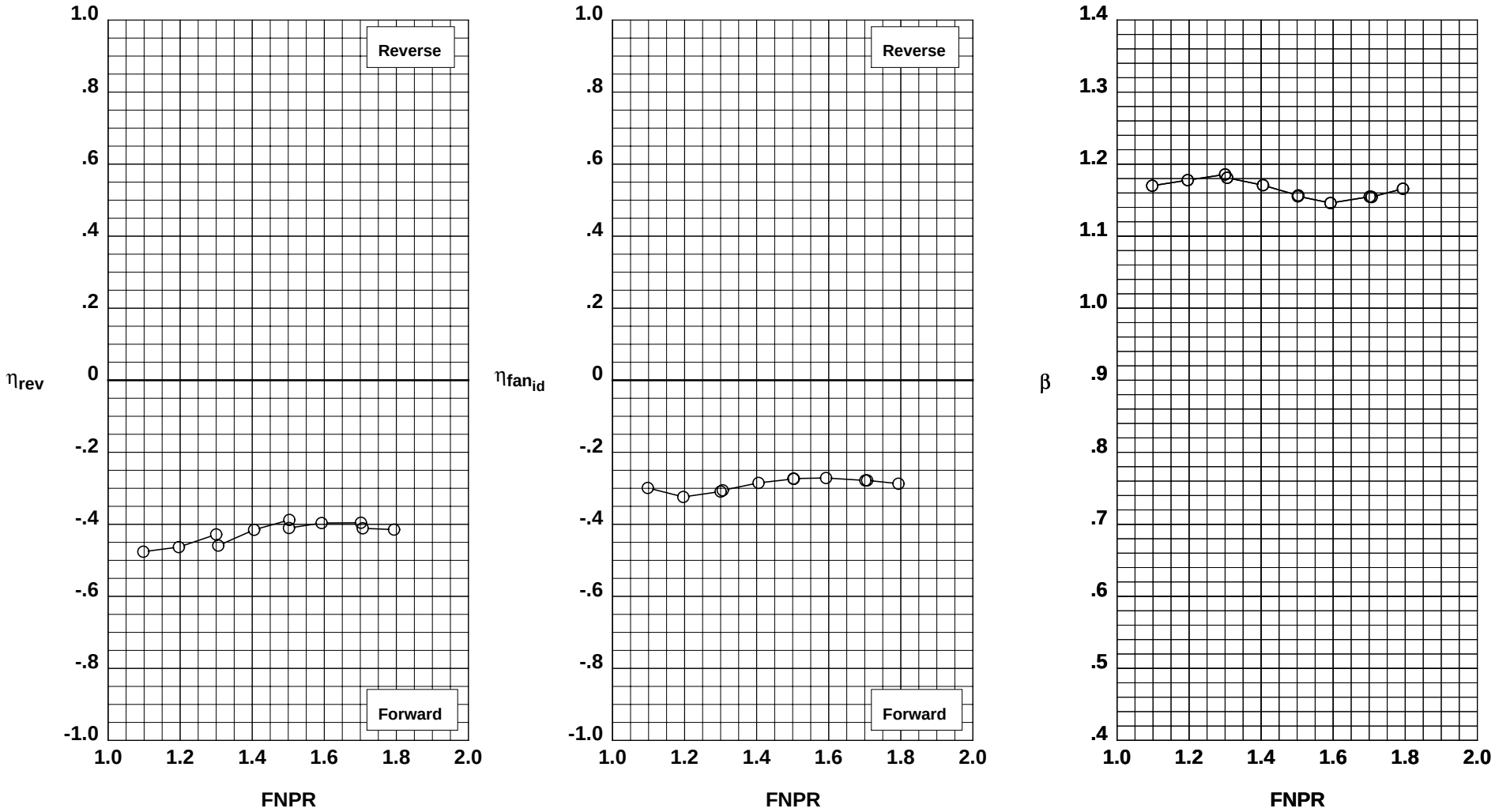

Figure G-41. Multi-door crocodile thrust reverser performance characteristics for configuration 540.

Operation Mode: Dual Flow
Reverser Port Bullnose: #3
Reverser Port Spacer: None
Reverser Port Cover: None
Bifurcator: Installed
Wing: Removed

	Test	Run	Configuration
○	994	37	519

Outer Door Angle: 60°
Outer Door Cutback: None
Outer Door Kicker: Long/Cutback
Outer Door Fence: None
Inner Door Angle: 36°
Inner Door Fillers: All
Door Struts: No
Door Leakage: Partial

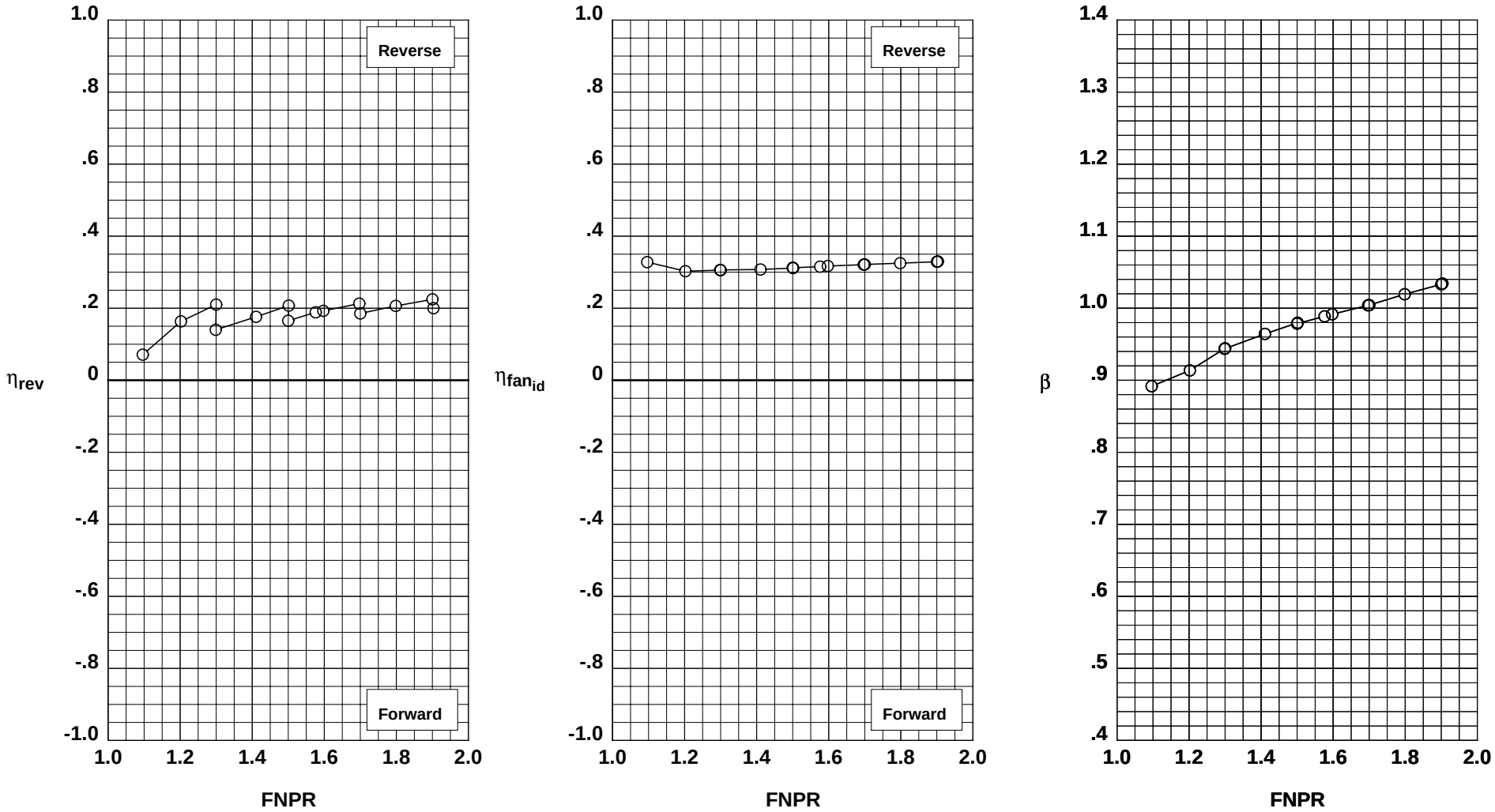

Figure G-42. Multi-door crocodile thrust reverser performance characteristics for configuration 519.

Operation Mode: Dual Flow
Reverser Port Bullnose: #1
Reverser Port Spacer: 0.20"
Reverser Port Cover: None
Bifurcator: Installed
Wing: Removed

	Test	Run	Configuration
○	994	38	541

Outer Door Angle: 60°
Outer Door Cutback: None
Outer Door Kicker: Long/Cutback
Outer Door Fence: None
Inner Door Angle: 36°
Inner Door Fillers: All
Door Struts: No
Door Leakage: Partial

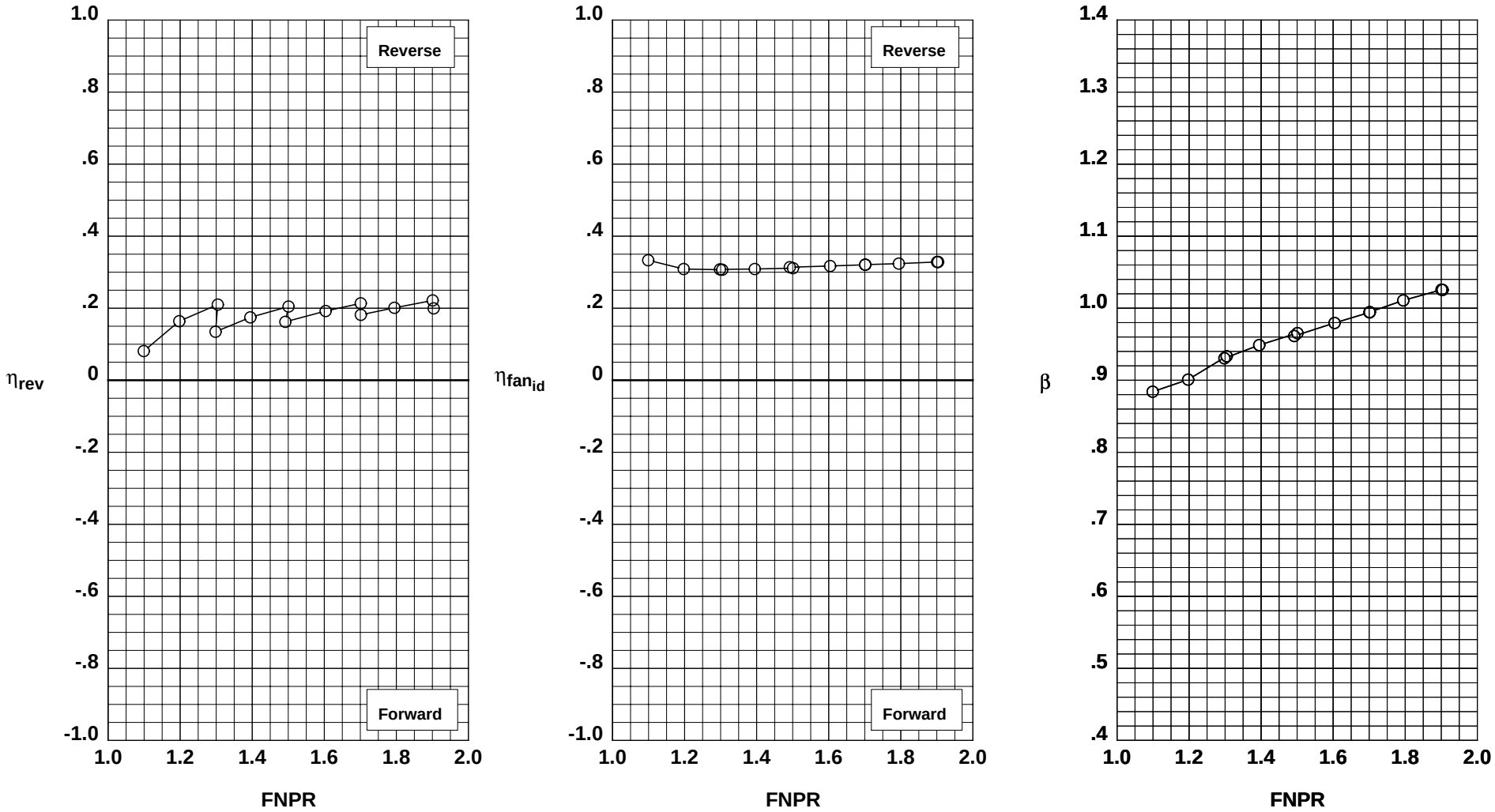

Figure G-43. Multi-door crocodile thrust reverser performance characteristics for configuration 541.

Operation Mode: Dual Flow
Reverser Port Bullnose: #2
Reverser Port Spacer: 0.20"
Reverser Port Cover: None
Bifurcator: Installed
Wing: Removed

	Test	Run	Configuration
○	994	39	542

Outer Door Angle: 50°
Outer Door Cutback: None
Outer Door Kicker: Long/Cutback
Outer Door Fence: None
Inner Door Angle: 36°
Inner Door Fillers: All
Door Struts: No
Door Leakage: Partial

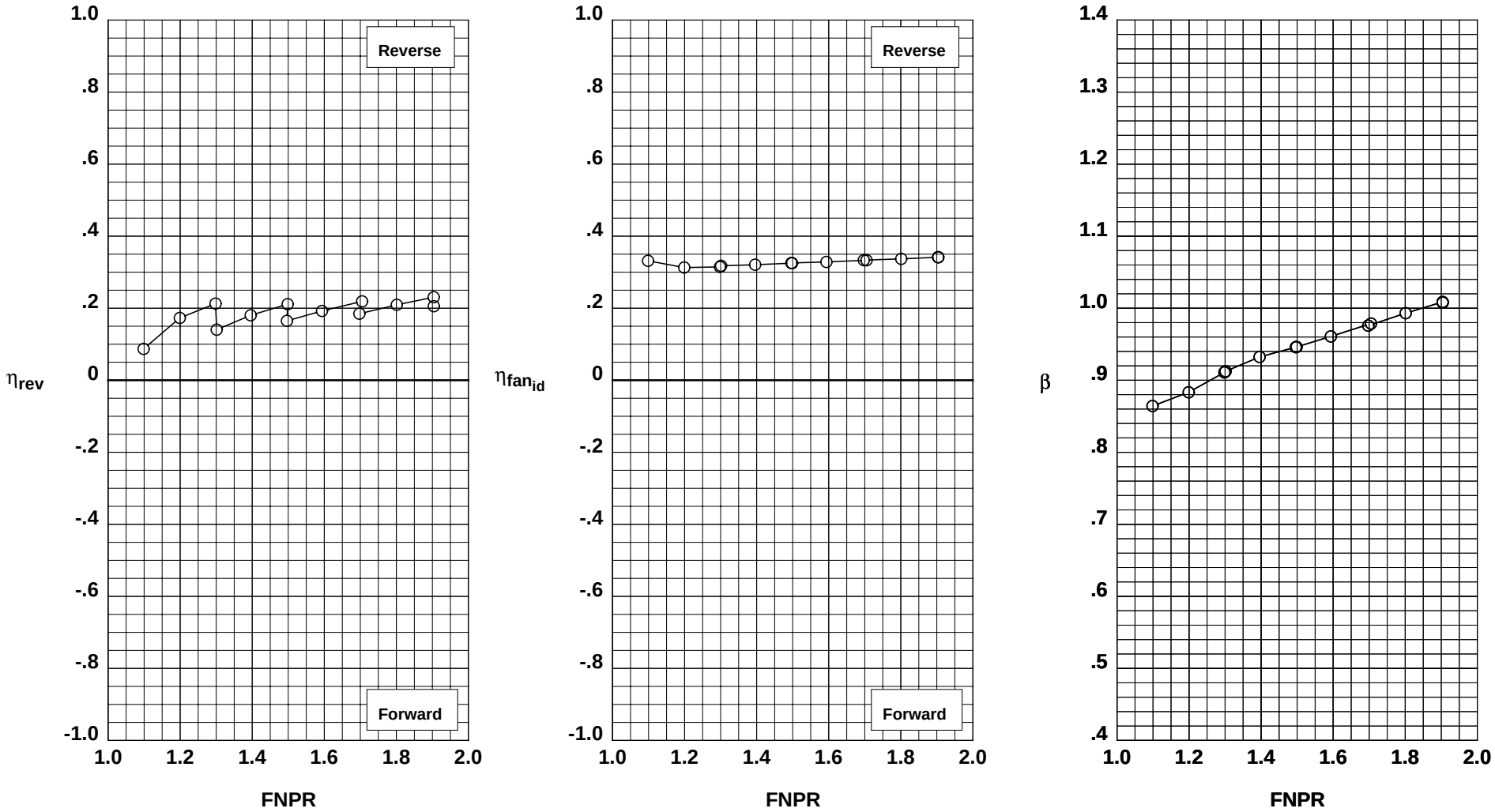

Figure G-44. Multi-door crocodile thrust reverser performance characteristics for configuration 542.

Operation Mode: Dual Flow
Reverser Port Bullnose: #1
Reverser Port Spacer: None
Reverser Port Cover: None
Bifurcator: Installed
Wing: Removed

	Test	Run	Configuration
○	994	40	543

Outer Door Angle: 60°
Outer Door Cutback: None
Outer Door Kicker: Long/Cutback
Outer Door Fence: None
Inner Door Angle: 36°
Inner Door Fillers: All+Tape
Door Struts: No
Door Leakage: None

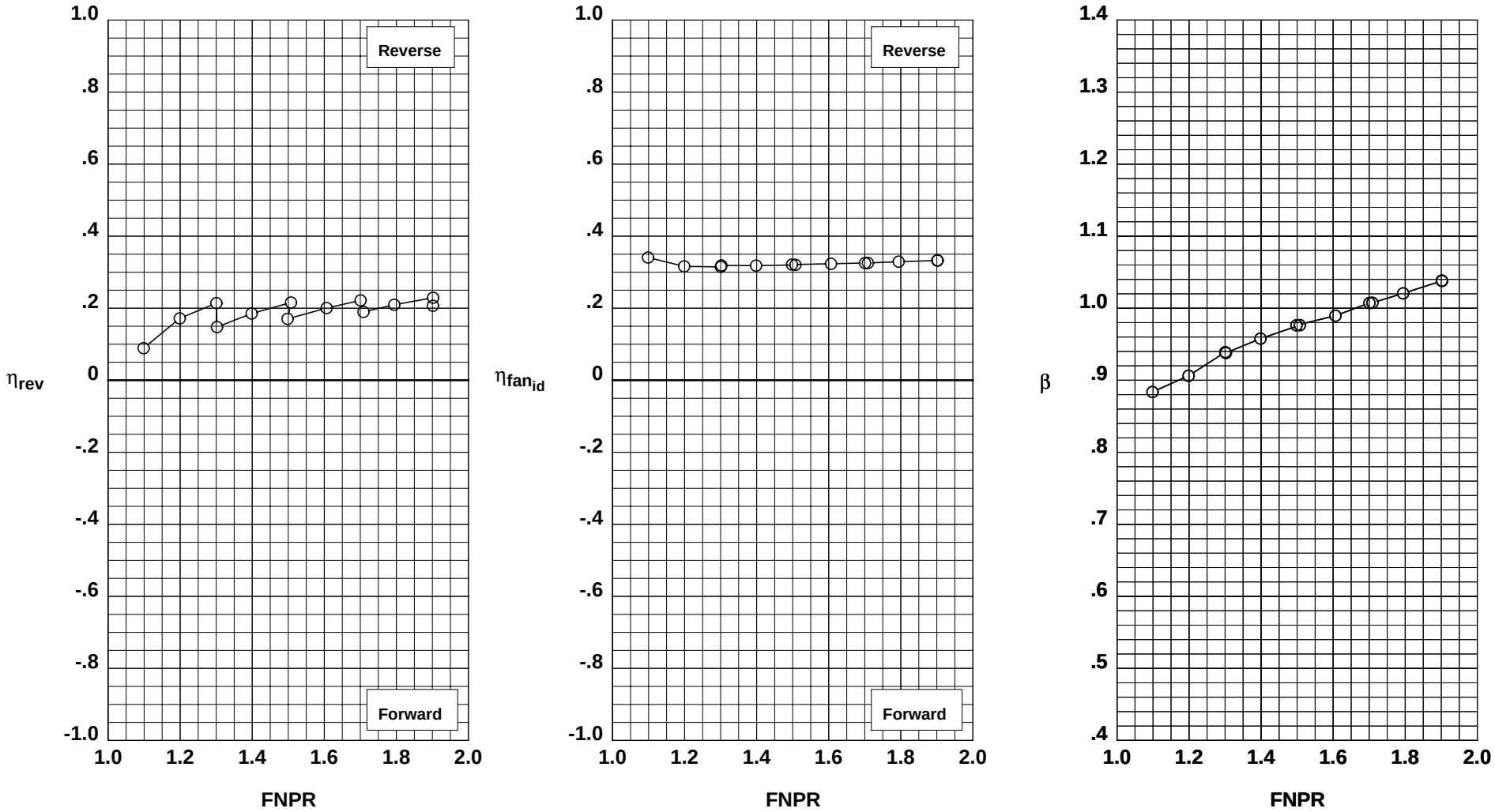

Figure G-45. Multi-door crocodile thrust reverser performance characteristics for configuration 543.

Operation Mode: Dual Flow
Reverser Port Bullnose: #3
Reverser Port Spacer: None
Reverser Port Cover: None
Bifurcator: Installed
Wing: Removed

	Test	Run	Configuration
○	994	41	544

Outer Door Angle: 60°
Outer Door Cutback: None
Outer Door Kicker: Long/Cutback
Outer Door Fence: None
Inner Door Angle: 36°
Inner Door Fillers: All+Tape
Door Struts: No
Door Leakage: None

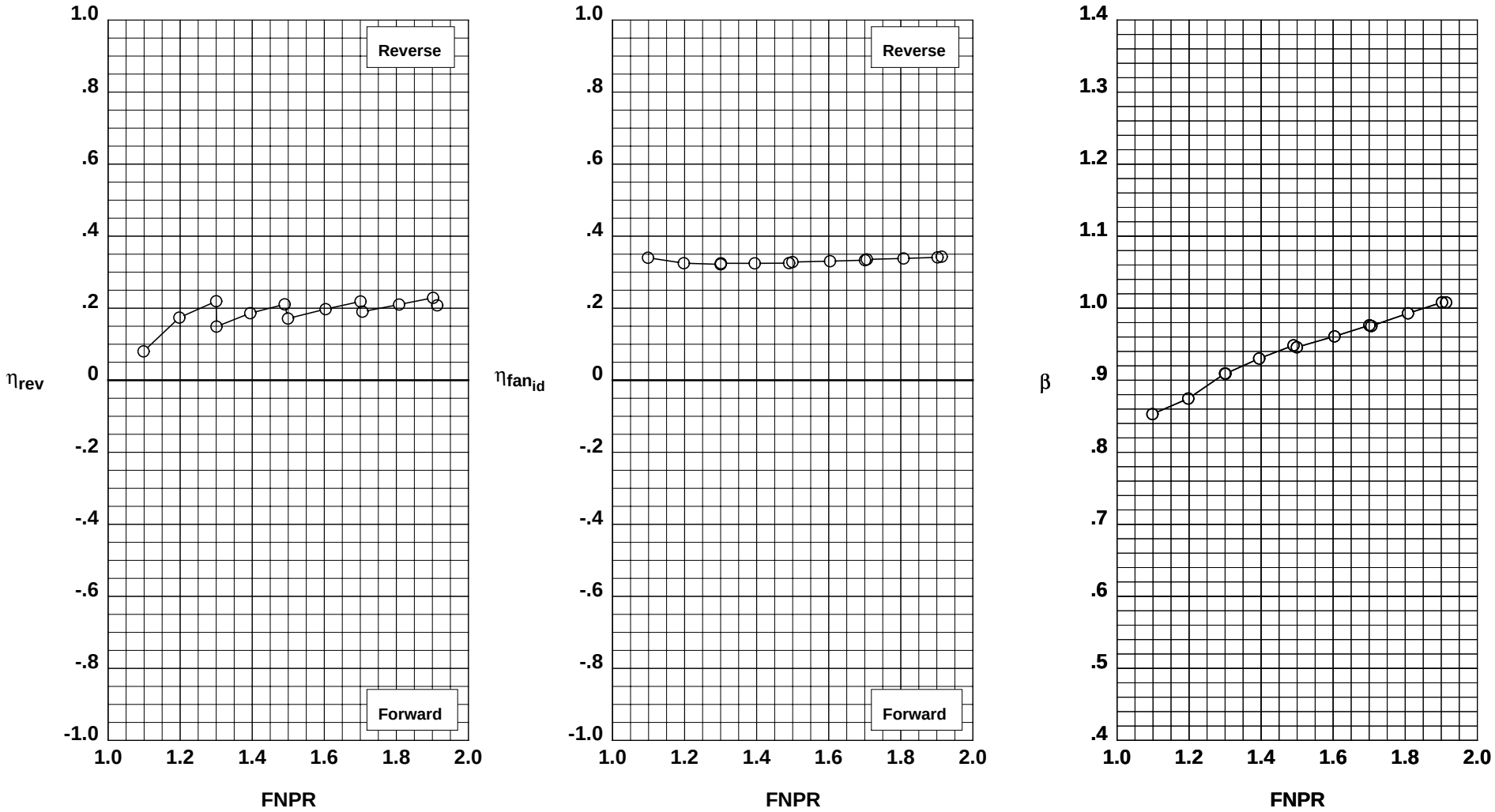

Figure G-46. Multi-door crocodile thrust reverser performance characteristics for configuration 544.

Operation Mode: Dual Flow
Reverser Port Bullnose: #3
Reverser Port Spacer: None
Reverser Port Cover: Mixed
Bifurcator: Installed
Wing: Removed

	Test	Run	Configuration
○	994	43	545

Outer Door Angle: 10°
Outer Door Cutback: Mixed
Outer Door Kicker: Long/Cutback
Outer Door Fence: None
Inner Door Angle: 6°
Inner Door Fillers: All
Door Struts: No
Door Leakage: Partial

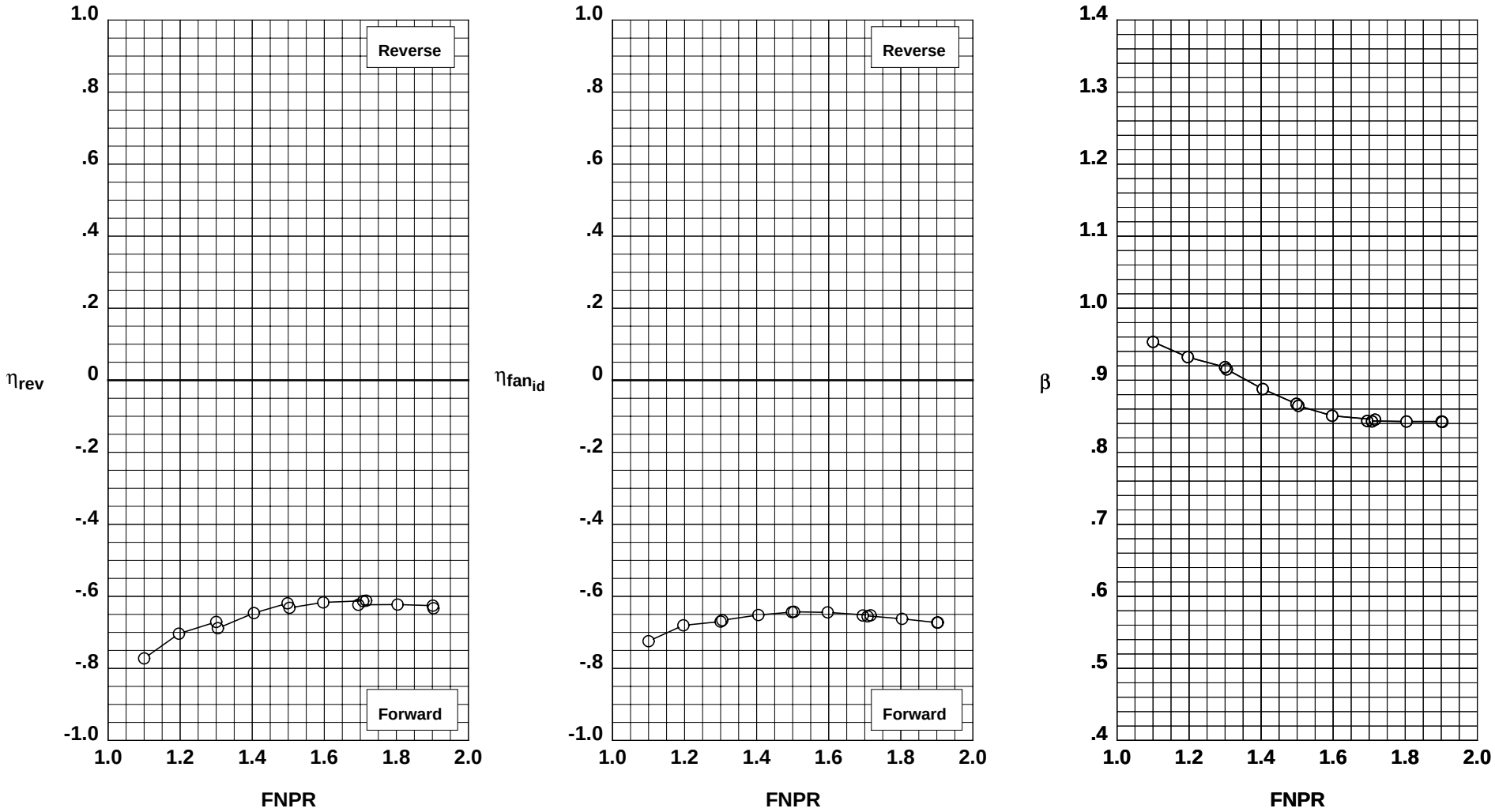

Figure G-47. Multi-door crocodile thrust reverser performance characteristics for configuration 545.

Operation Mode: Dual Flow
Reverser Port Bullnose: #3
Reverser Port Spacer: None
Reverser Port Cover: Mixed
Bifurcator: Installed
Wing: Removed

	Test	Run	Configuration
○	994	44	546

Outer Door Angle: 20°
Outer Door Cutback: Mixed
Outer Door Kicker: Long/Cutback
Outer Door Fence: None
Inner Door Angle: 12°
Inner Door Fillers: All
Door Struts: No
Door Leakage: Partial

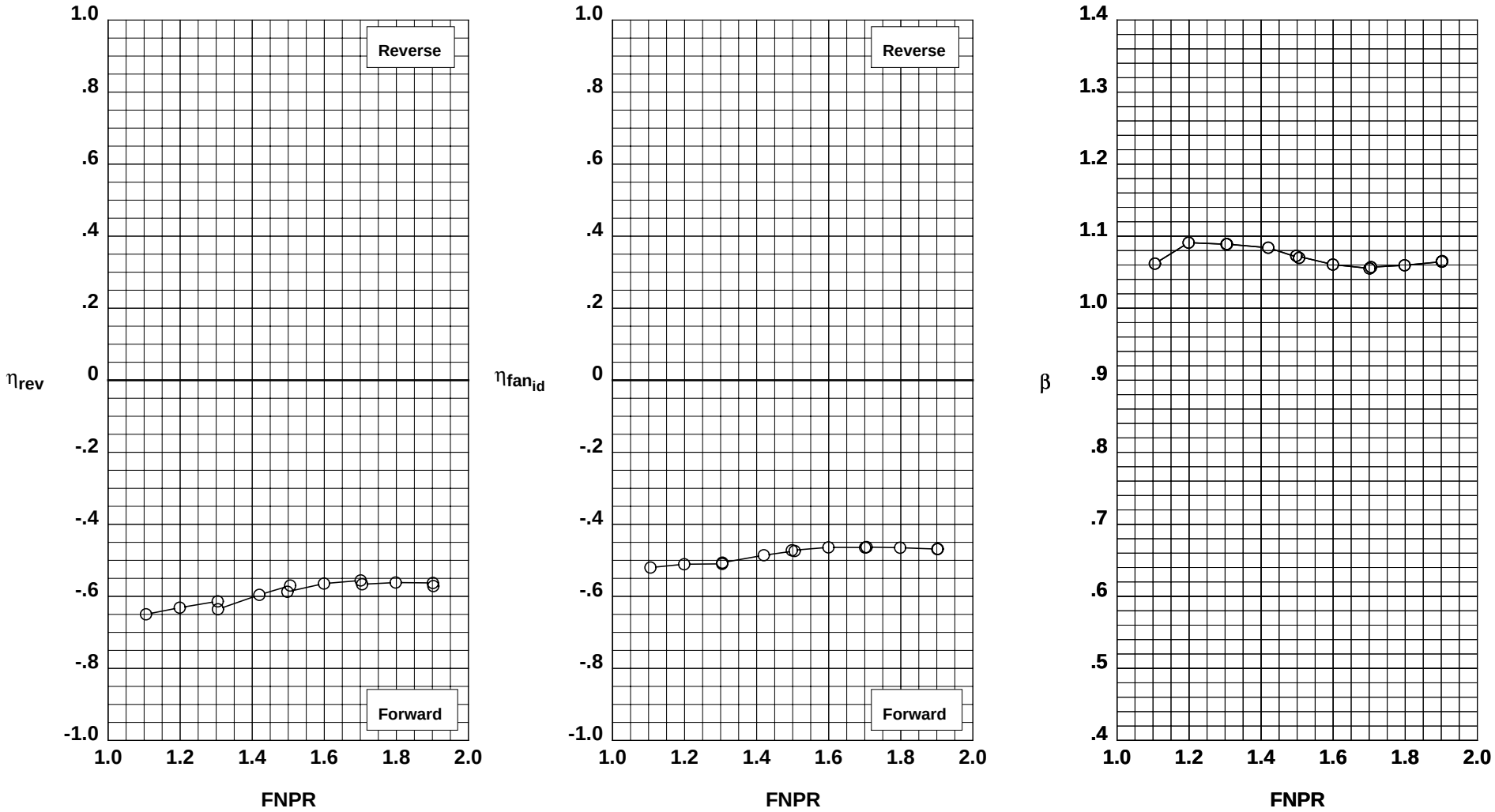

Figure G-48. Multi-door crocodile thrust reverser performance characteristics for configuration 546.

Operation Mode: Fan Only
Reverser Port Bullnose: #1
Reverser Port Spacer: None
Reverser Port Cover: None
Bifurcator: Installed
Wing: Removed

	Test	Run	Configuration
○	1002	48	547

Outer Door Angle: 60°
Outer Door Cutback: None
Outer Door Kicker: Long/Cutback
Outer Door Fence: None
Inner Door Angle: 36°
Inner Door Fillers: All
Door Struts: No
Door Leakage: Partial

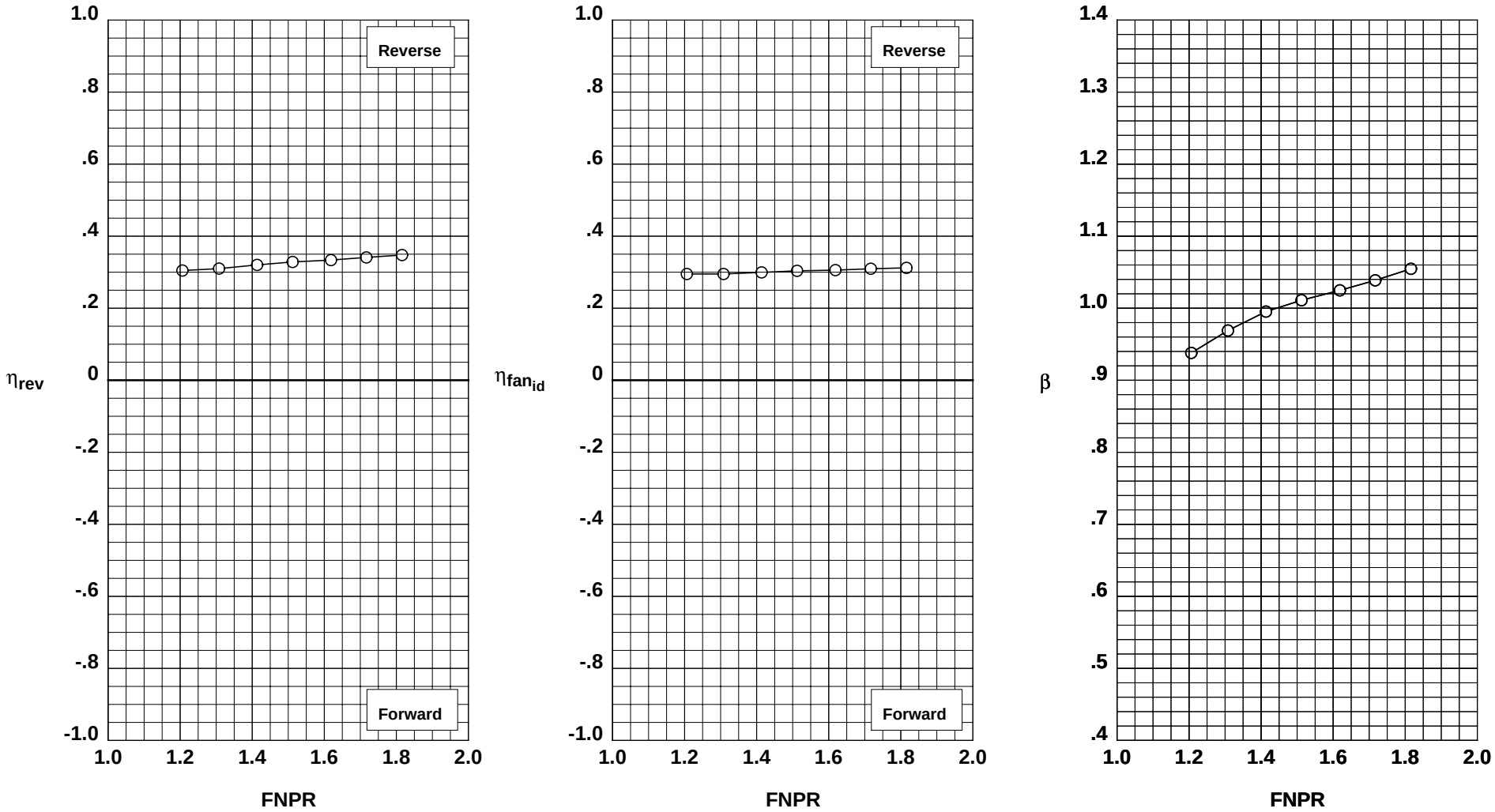

Figure G-49. Multi-door crocodile thrust reverser performance characteristics for configuration 547.

Operation Mode: Dual Flow
Reverser Port Bullnose: #1
Reverser Port Spacer: None
Reverser Port Cover: None
Bifurcator: Installed
Wing: Removed

	Test	Run	Configuration
○	1002	49	547

Outer Door Angle: 60°
Outer Door Cutback: None
Outer Door Kicker: Long/Cutback
Outer Door Fence: None
Inner Door Angle: 36°
Inner Door Fillers: All
Door Struts: No
Door Leakage: Partial

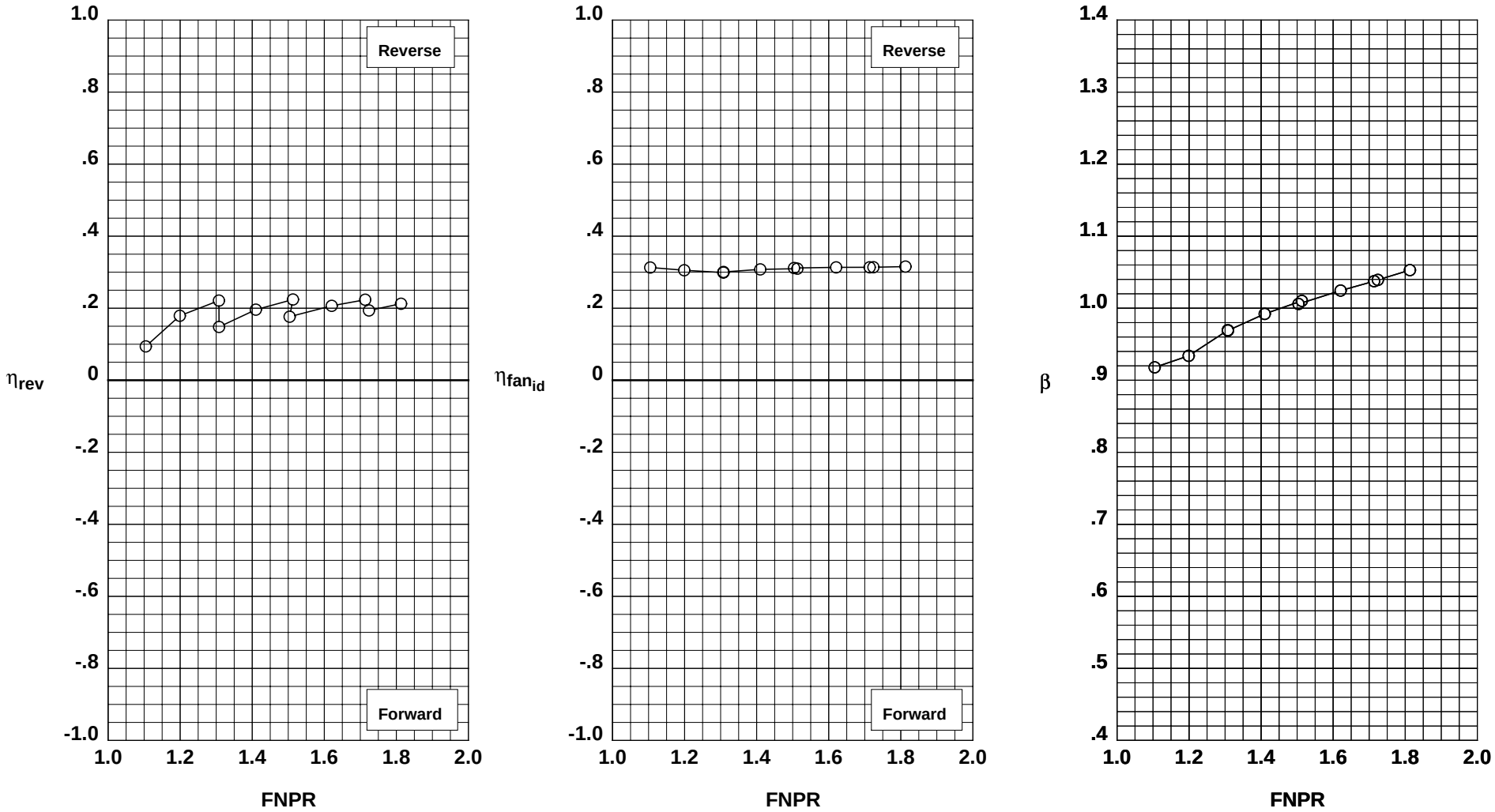

Figure G-50. Multi-door crocodile thrust reverser performance characteristics for configuration 547.

Operation Mode: Dual Flow
Reverser Port Bullnose: #1
Reverser Port Spacer: None
Reverser Port Cover: None
Bifurcator: Installed
Wing: Removed

	Test	Run	Configuration
○	1002	20	543

Outer Door Angle: 60°
Outer Door Cutback: None
Outer Door Kicker: Long/Cutback
Outer Door Fence: None
Inner Door Angle: 36°
Inner Door Fillers: All+Tape
Door Struts: No
Door Leakage: None

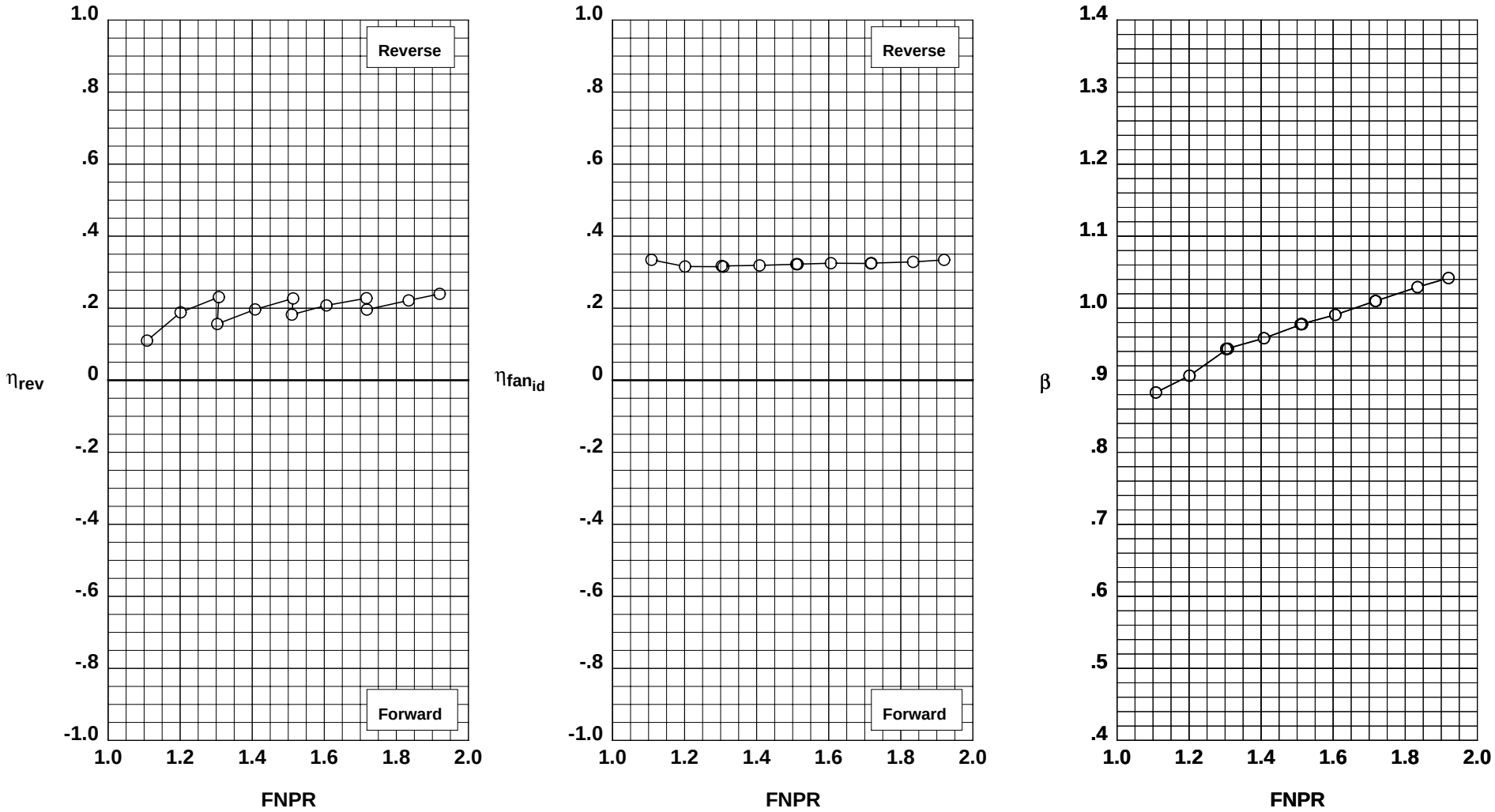

Figure G-51. Multi-door crocodile thrust reverser performance characteristics for configuration 543.

Operation Mode: Dual Flow
Reverser Port Bullnose: #1
Reverser Port Spacer: None
Reverser Port Cover: None
Bifurcator: Installed
Wing: Removed

	Test	Run	Configuration
○	1002	21	548

Outer Door Angle: 60°
Outer Door Cutback: None
Outer Door Kicker: Long
Outer Door Fence: Yes
Inner Door Angle: 36°
Inner Door Fillers: All+Tape
Door Struts: No
Door Leakage: None

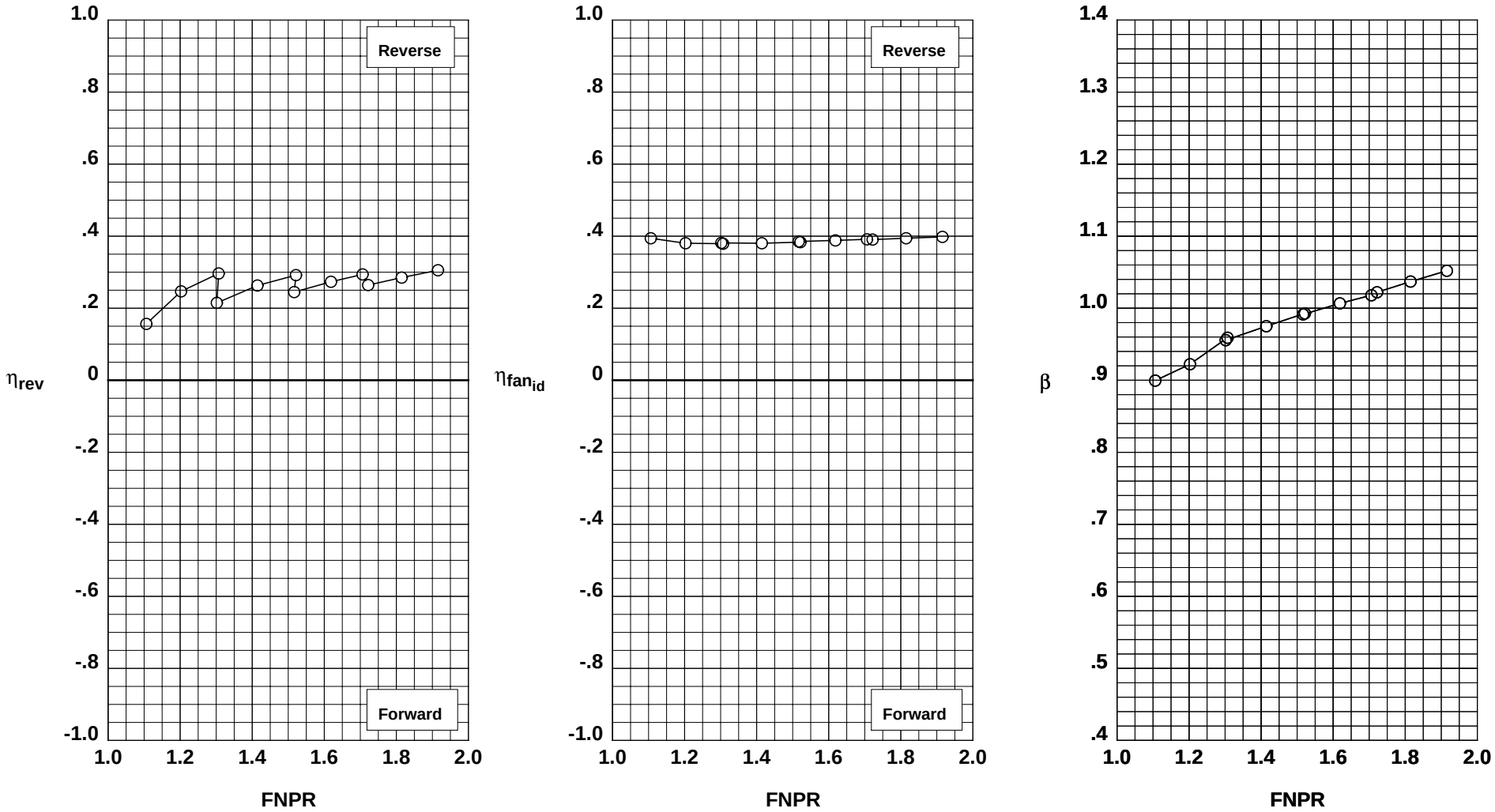

Figure G-52. Multi-door crocodile thrust reverser performance characteristics for configuration 548.

Operation Mode: Dual Flow
Reverser Port Bullnose: #3
Reverser Port Spacer: None
Reverser Port Cover: None
Bifurcator: Installed
Wing: Removed

	Test	Run	Configuration
○	1002	22	549

Outer Door Angle: 60°
Outer Door Cutback: None
Outer Door Kicker: Long
Outer Door Fence: Yes
Inner Door Angle: 36°
Inner Door Fillers: All+Tape
Door Struts: No
Door Leakage: None

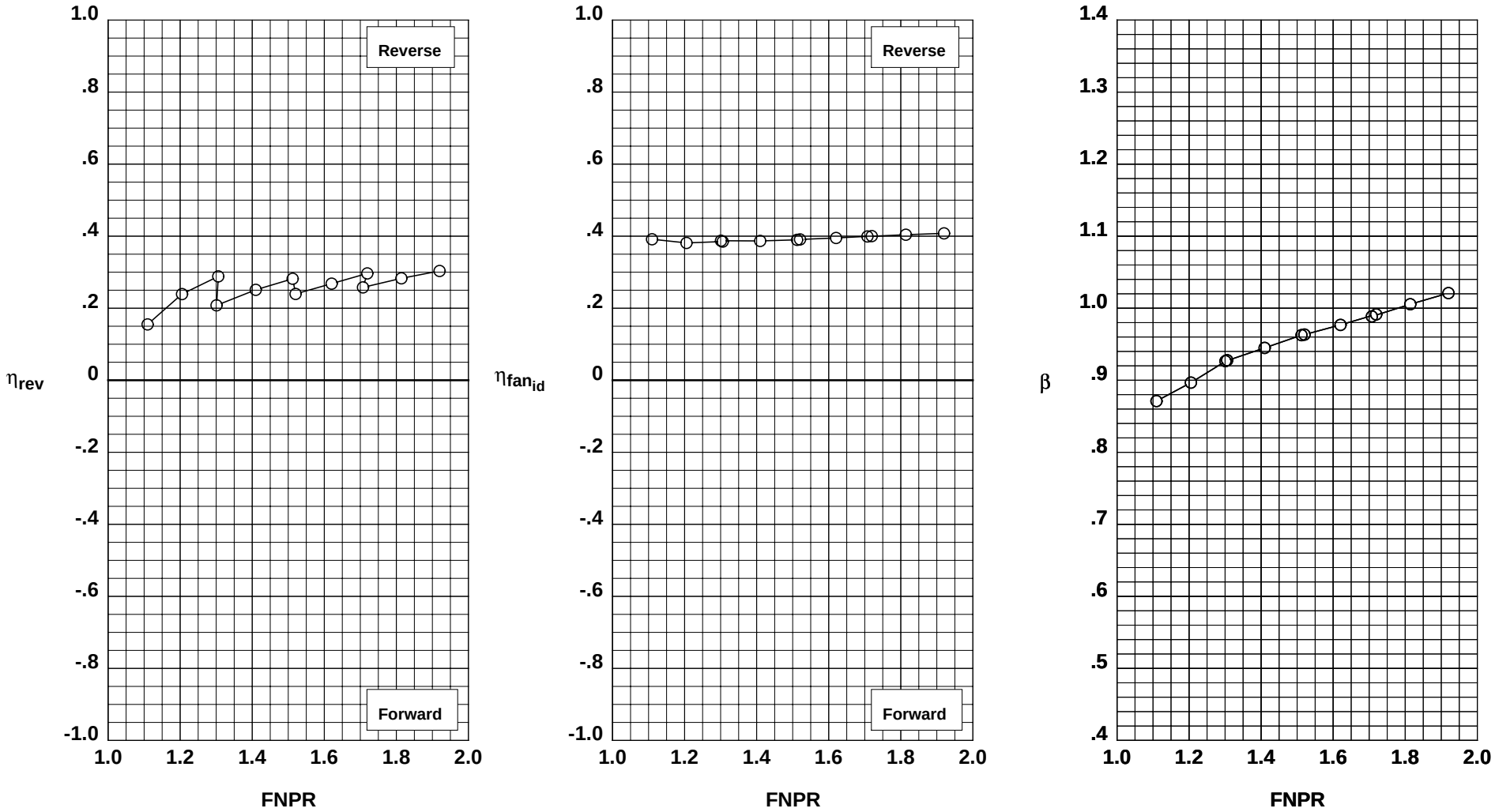

Figure G-53. Multi-door crocodile thrust reverser performance characteristics for configuration 549.

Operation Mode: Dual Flow
Reverser Port Bullnose: #3
Reverser Port Spacer: None
Reverser Port Cover: None
Bifurcator: Installed
Wing: Removed

	Test	Run	Configuration
○	1002	23	544

Outer Door Angle: 60°
Outer Door Cutback: None
Outer Door Kicker: Long/Cutback
Outer Door Fence: None
Inner Door Angle: 36°
Inner Door Fillers: All+Tape
Door Struts: No
Door Leakage: None

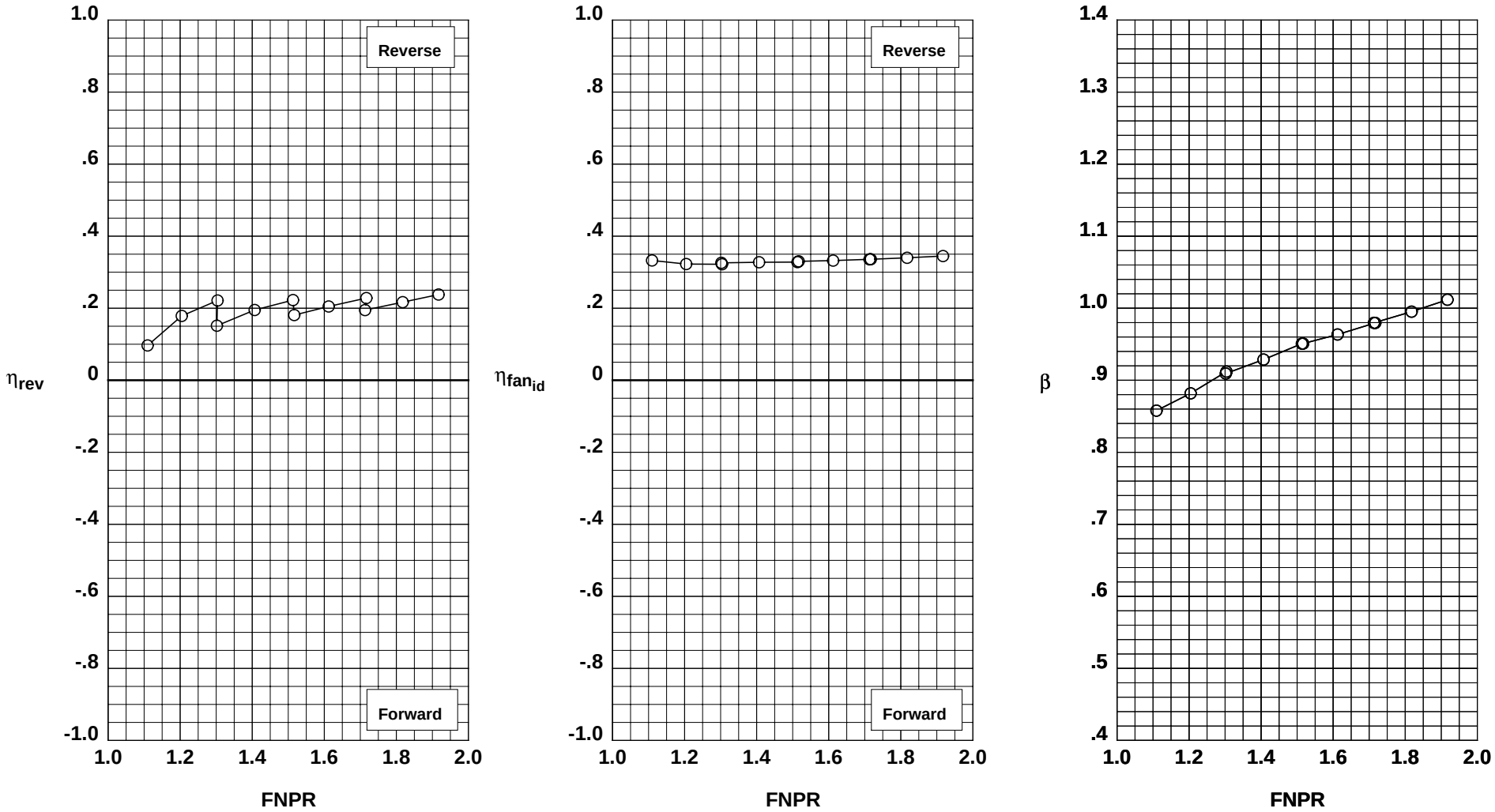

Figure G-54. Multi-door crocodile thrust reverser performance characteristics for configuration 544.

Operation Mode: Dual Flow
Reverser Port Bullnose: #3
Reverser Port Spacer: None
Reverser Port Cover: None
Bifurcator: Installed
Wing: Removed

	Test	Run	Configuration
○	1002	4	544

Outer Door Angle: 60°
Outer Door Cutback: None
Outer Door Kicker: Long/Cutback
Outer Door Fence: None
Inner Door Angle: 36°
Inner Door Fillers: All+Tape
Door Struts: No
Door Leakage: None

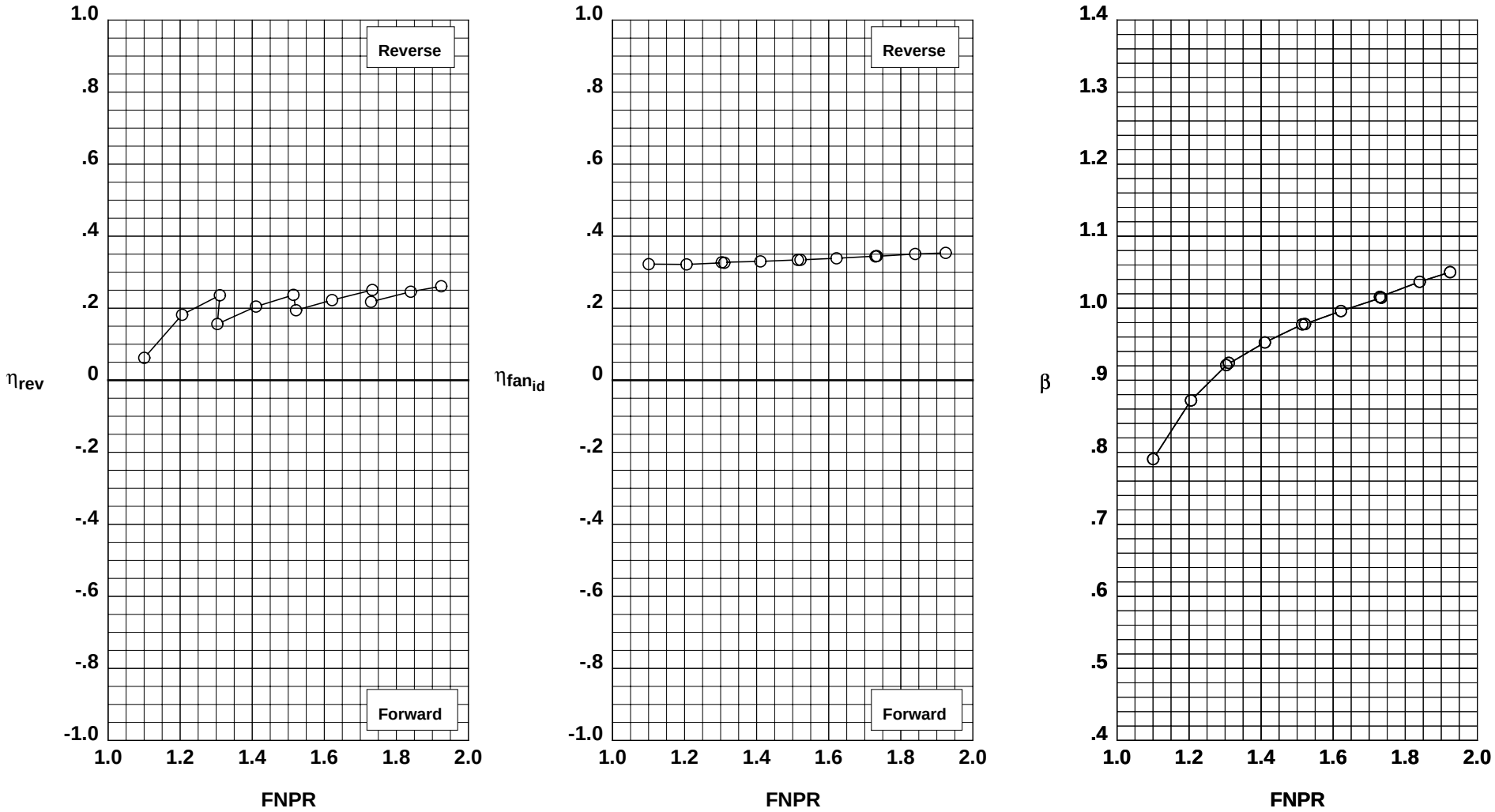

Figure G-55. Multi-door crocodile thrust reverser performance characteristics for configuration 544.

Operation Mode: Dual Flow
Reverser Port Bullnose: #2
Reverser Port Spacer: None
Reverser Port Cover: None
Bifurcator: Installed
Wing: Removed

	Test	Run	Configuration
○	1002	9	550

Outer Door Angle: 60°
Outer Door Cutback: None
Outer Door Kicker: Long/Cutback
Outer Door Fence: None
Inner Door Angle: 36°
Inner Door Fillers: All+Tape
Door Struts: No
Door Leakage: None

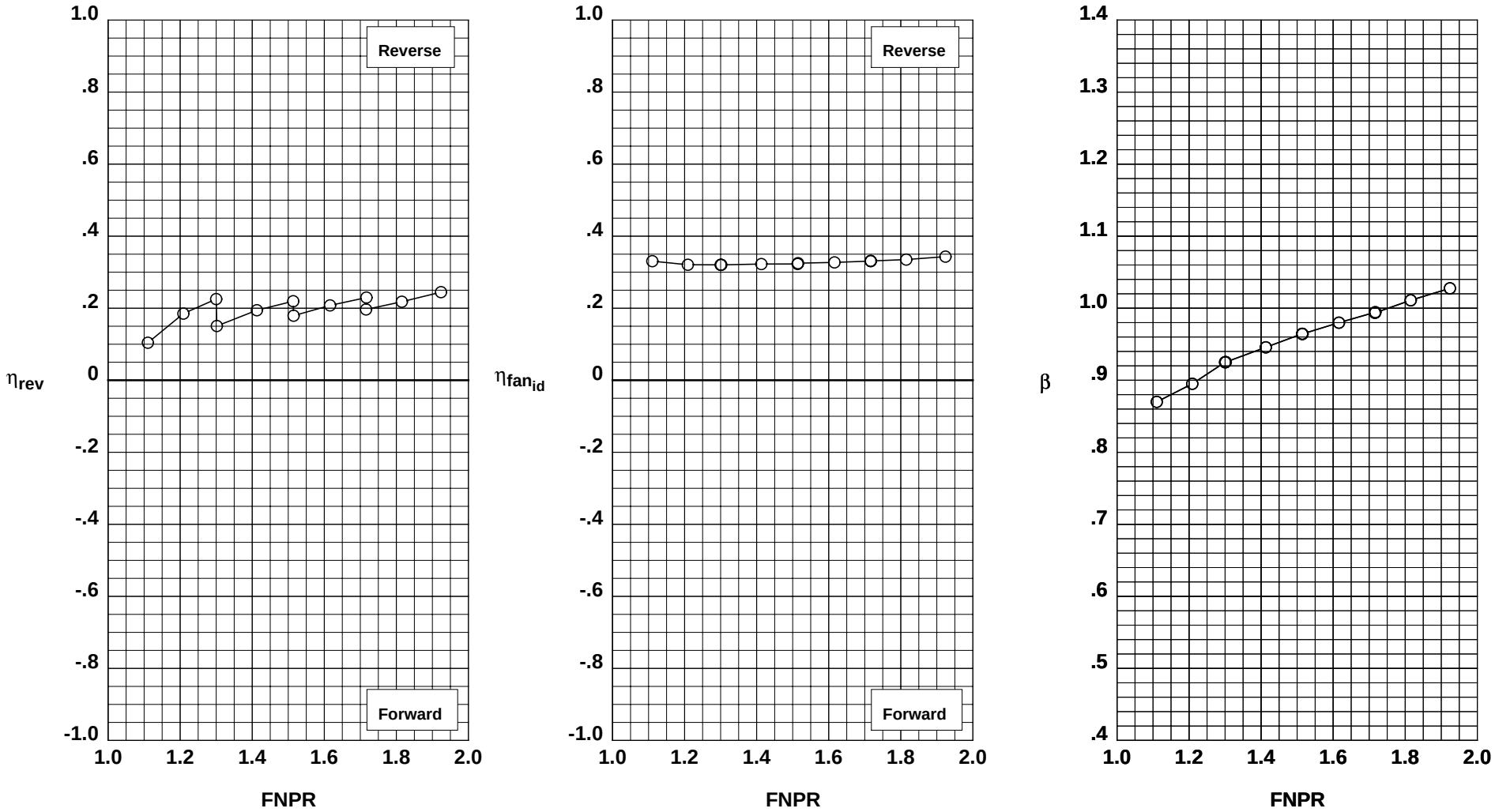

Figure G-56. Multi-door crocodile thrust reverser performance characteristics for configuration 550.

Operation Mode: Dual Flow
Reverser Port Bullnose: #1
Reverser Port Spacer: None
Reverser Port Cover: None
Bifurcator: Installed
Wing: Removed

	Test	Run	Configuration
○	1002	10	543

Outer Door Angle: 60°
Outer Door Cutback: None
Outer Door Kicker: Long/Cutback
Outer Door Fence: None
Inner Door Angle: 36°
Inner Door Fillers: All+Tape
Door Struts: No
Door Leakage: None

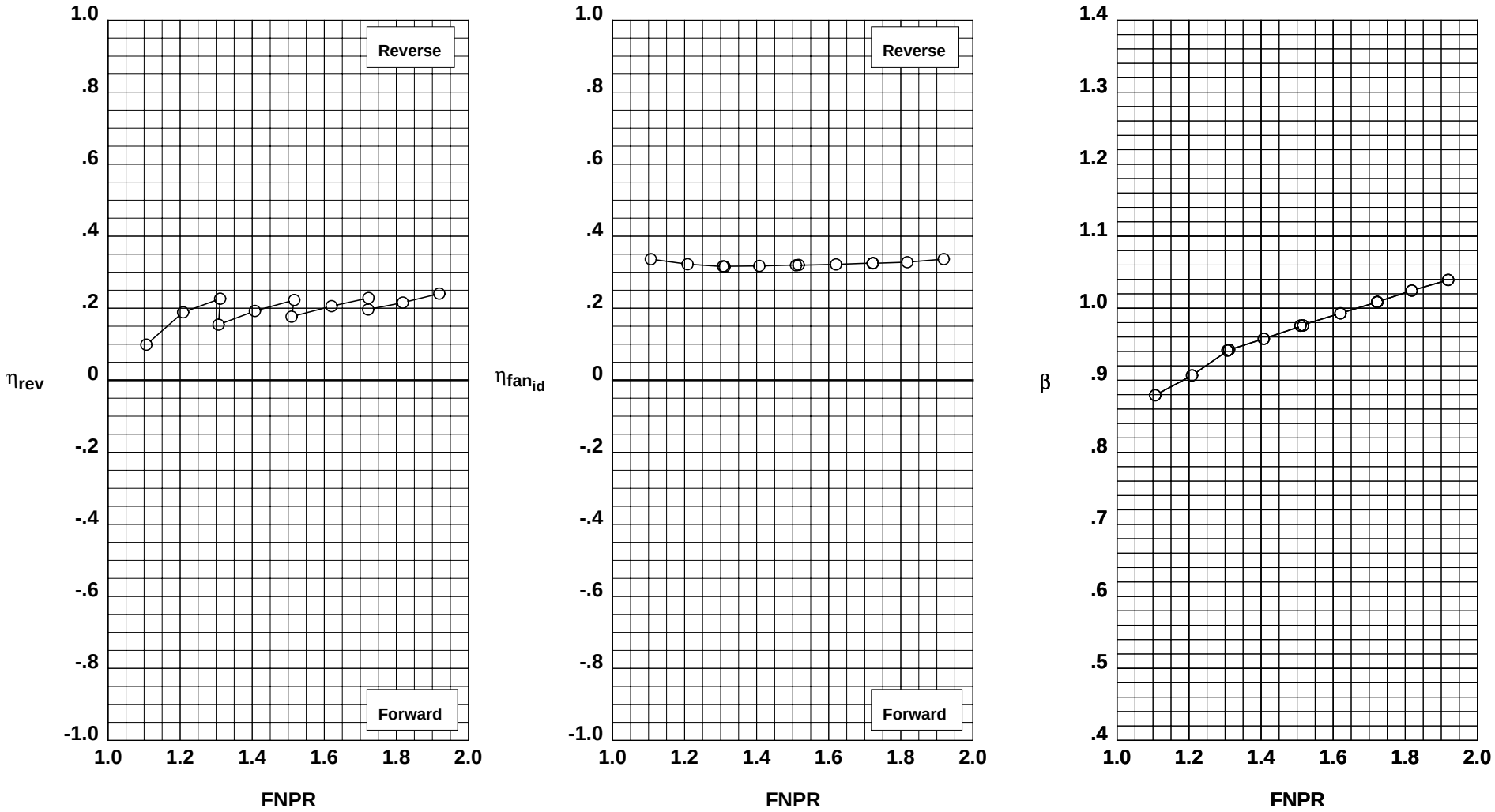

Figure G-57. Multi-door crocodile thrust reverser performance characteristics for configuration 543.

Operation Mode: Dual Flow
Reverser Port Bullnose: None
Reverser Port Spacer: None
Reverser Port Cover: None
Bifurcator: Installed
Wing: Removed

	Test	Run	Configuration
○	1002	11	551

Outer Door Angle: 60°
Outer Door Cutback: None
Outer Door Kicker: Long/Cutback
Outer Door Fence: None
Inner Door Angle: 36°
Inner Door Fillers: All+Tape
Door Struts: No
Door Leakage: None

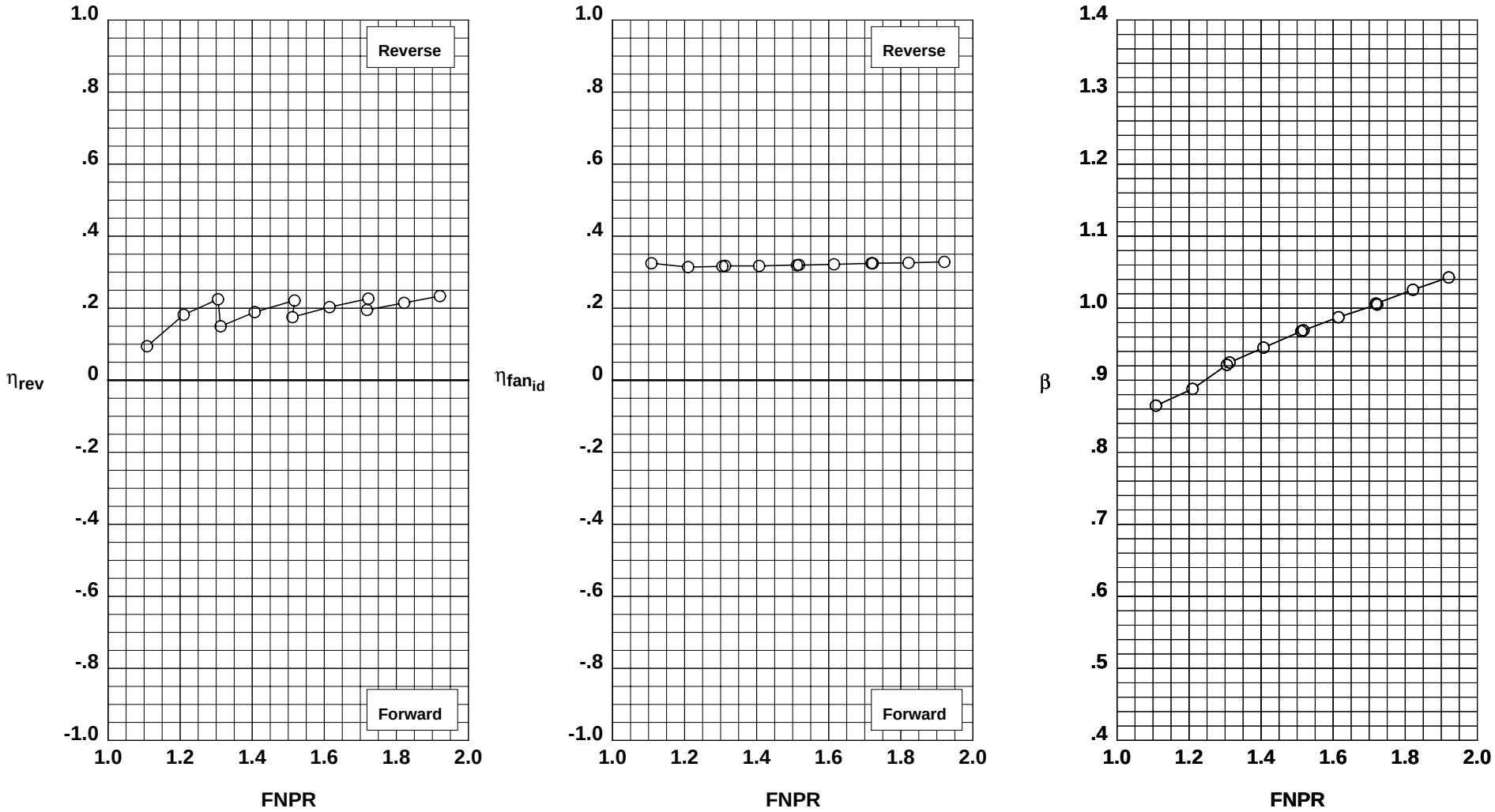

Figure G-58. Multi-door crocodile thrust reverser performance characteristics for configuration 551.

Operation Mode: Dual Flow
Reverser Port Bullnose: None
Reverser Port Spacer: 0.20"
Reverser Port Cover: None
Bifurcator: Installed
Wing: Removed

	Test	Run	Configuration
○	1002	12	552

Outer Door Angle: 60°
Outer Door Cutback: None
Outer Door Kicker: Long/Cutback
Outer Door Fence: None
Inner Door Angle: 36°
Inner Door Fillers: All+Tape
Door Struts: No
Door Leakage: None

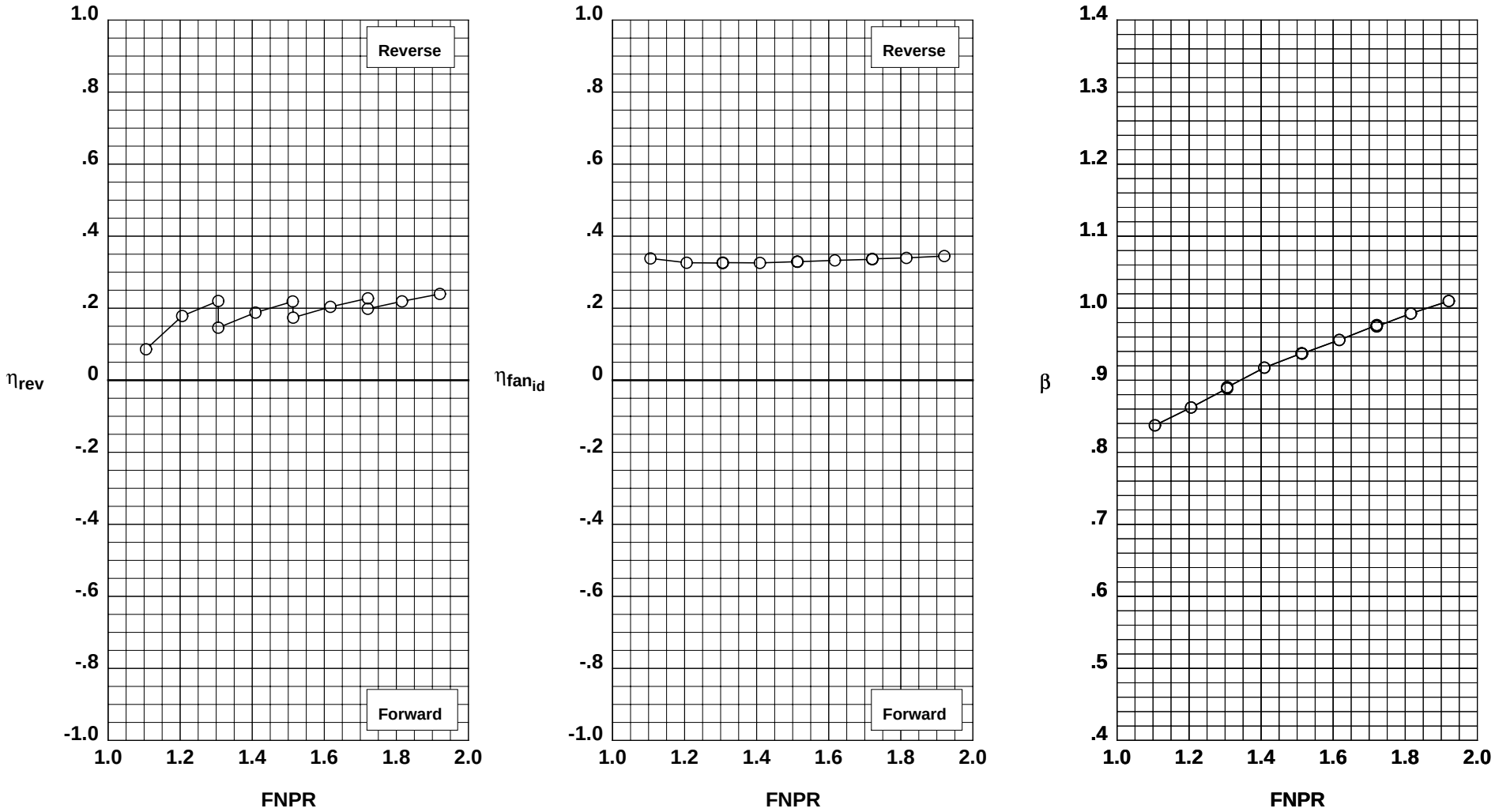

Figure G-59. Multi-door crocodile thrust reverser performance characteristics for configuration 552.

Operation Mode: Dual Flow
Reverser Port Bullnose: #1
Reverser Port Spacer: 0.20"
Reverser Port Cover: None
Bifurcator: Installed
Wing: Removed

	Test	Run	Configuration
○	1002	13	553

Outer Door Angle: 60°
Outer Door Cutback: None
Outer Door Kicker: Long/Cutback
Outer Door Fence: None
Inner Door Angle: 36°
Inner Door Fillers: All+Tape
Door Struts: No
Door Leakage: None

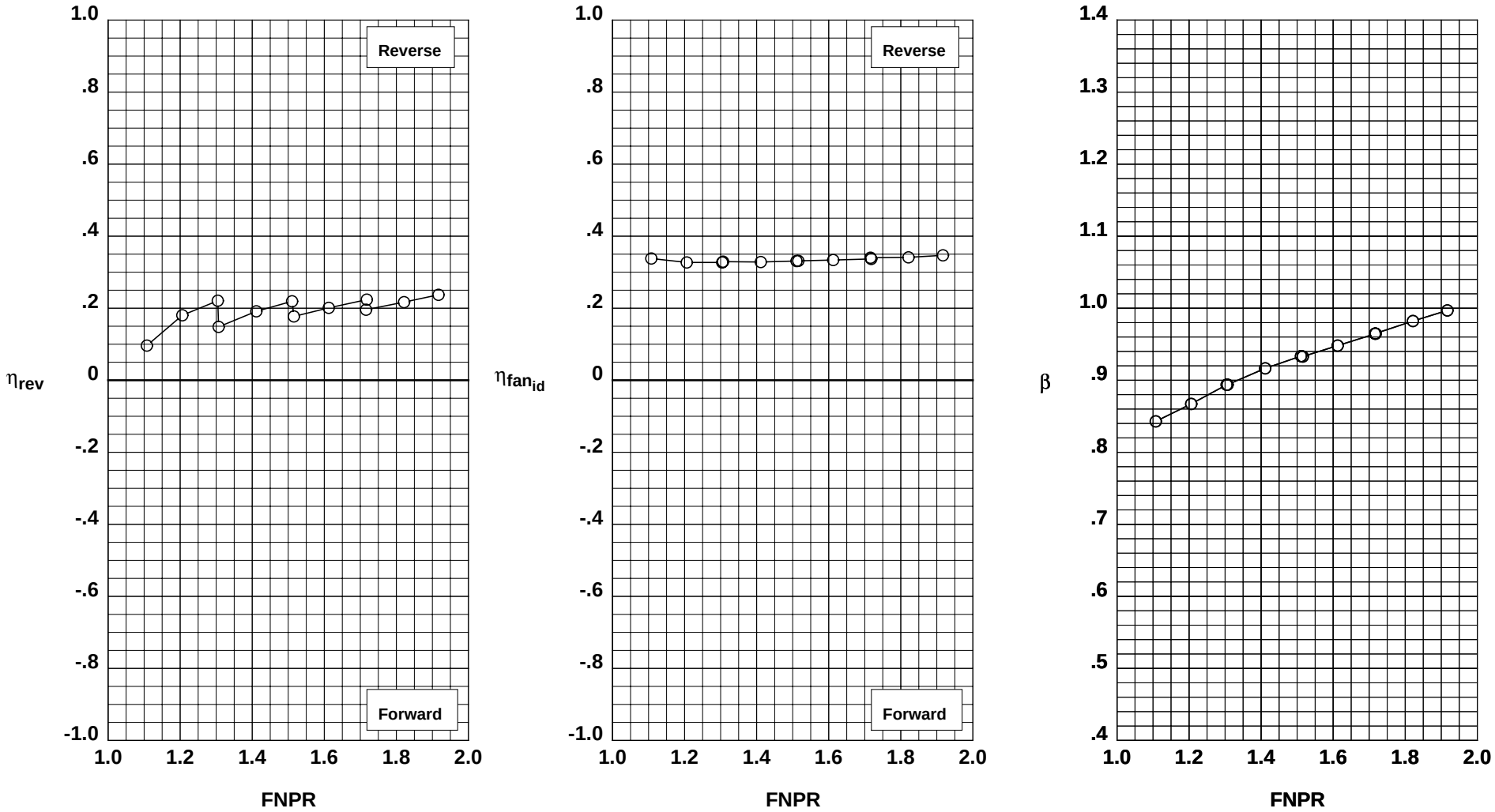

Figure G-60. Multi-door crocodile thrust reverser performance characteristics for configuration 553.

Operation Mode: Dual Flow
Reverser Port Bullnose: #2
Reverser Port Spacer: 0.20"
Reverser Port Cover: None
Bifurcator: Installed
Wing: Removed

	Test	Run	Configuration
○	1002	14	554

Outer Door Angle: 60°
Outer Door Cutback: None
Outer Door Kicker: Long/Cutback
Outer Door Fence: None
Inner Door Angle: 36°
Inner Door Fillers: All+Tape
Door Struts: No
Door Leakage: None

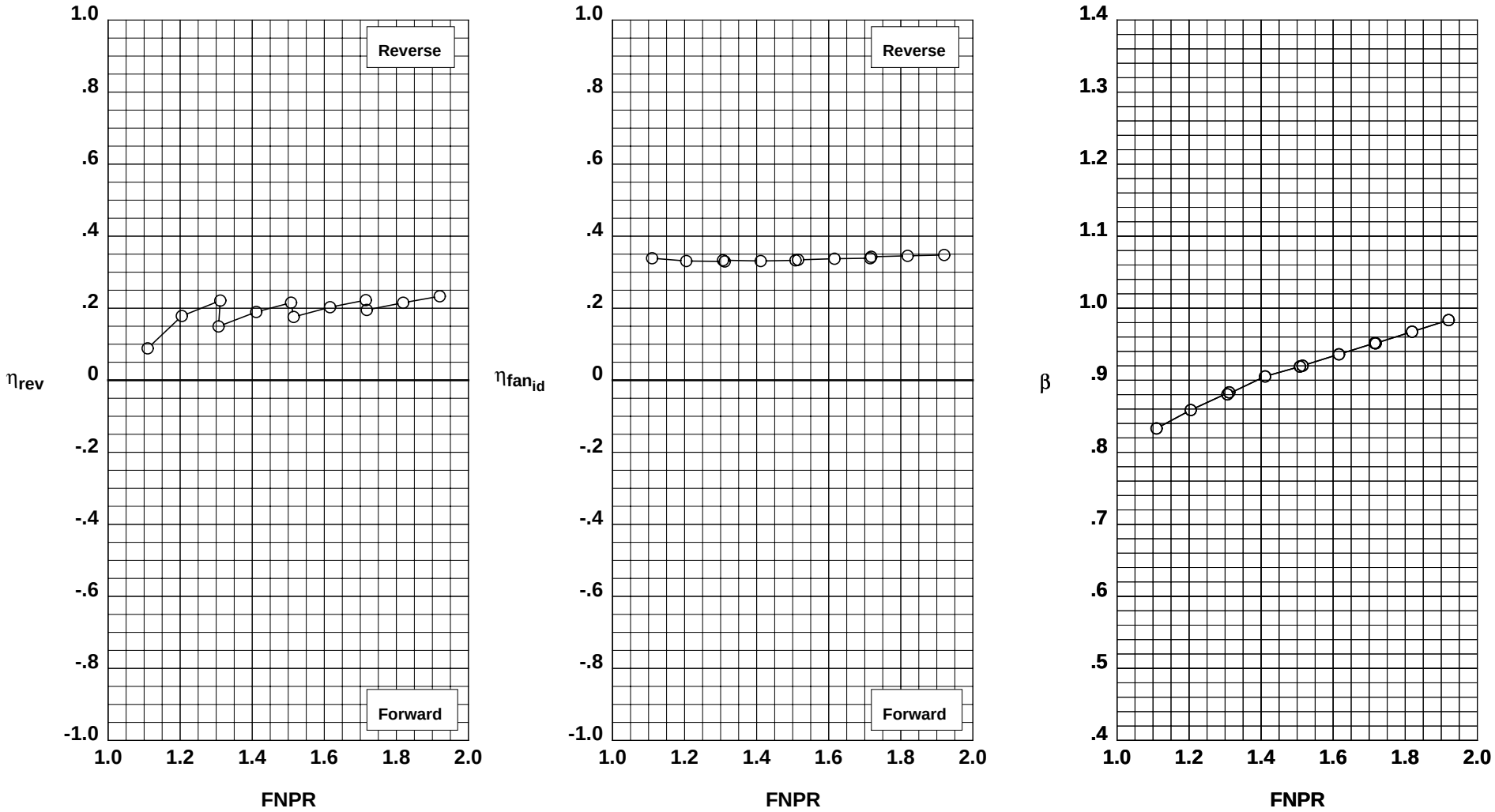

Figure G-61. Multi-door crocodile thrust reverser performance characteristics for configuration 554.

Operation Mode: Dual Flow
Reverser Port Bullnose: #3
Reverser Port Spacer: 0.20"
Reverser Port Cover: None
Bifurcator: Installed
Wing: Removed

	Test	Run	Configuration
○	1002	15	555

Outer Door Angle: 60°
Outer Door Cutback: None
Outer Door Kicker: Long/Cutback
Outer Door Fence: None
Inner Door Angle: 36°
Inner Door Fillers: All+Tape
Door Struts: No
Door Leakage: None

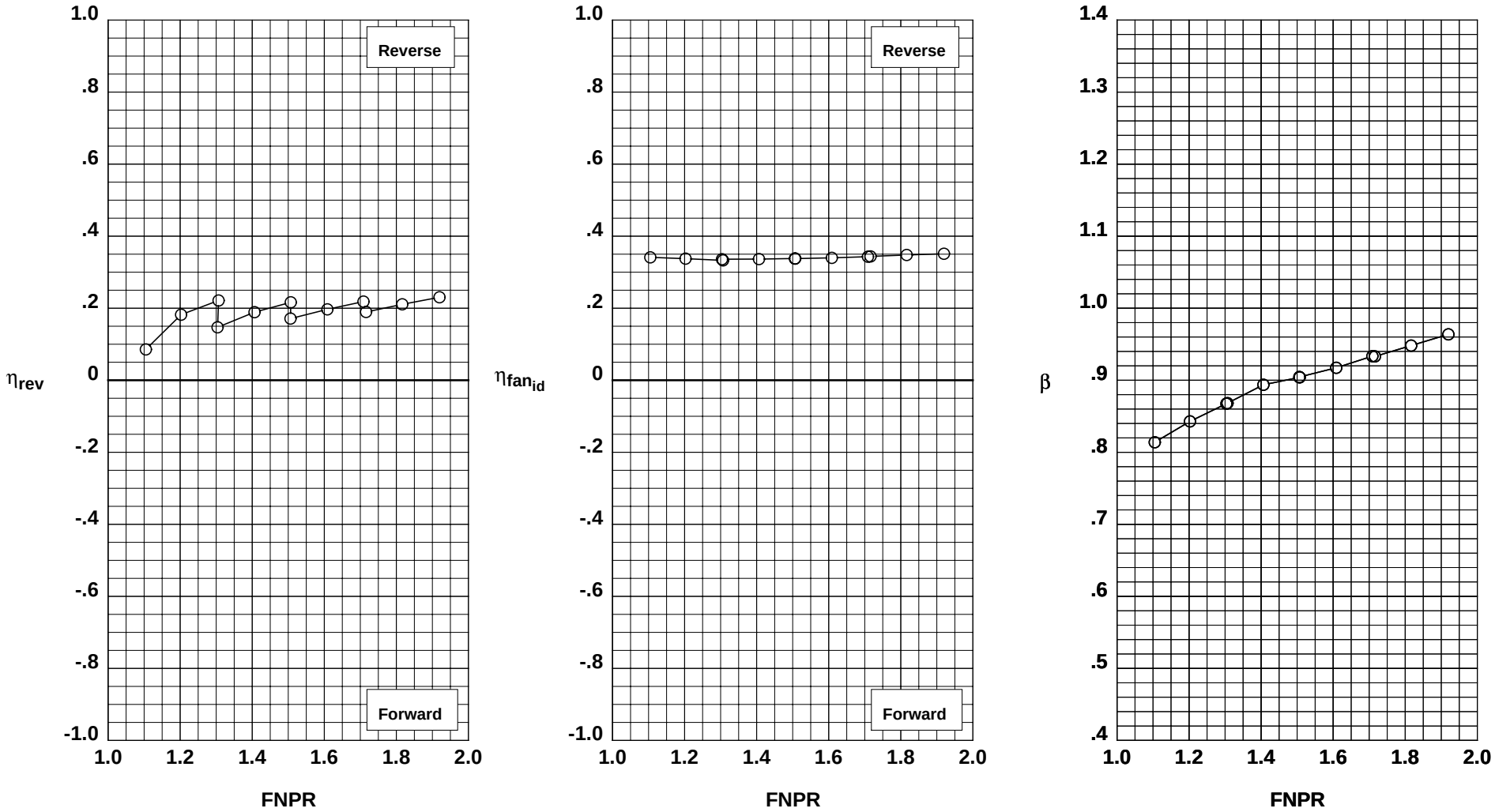

Figure G-62. Multi-door crocodile thrust reverser performance characteristics for configuration 555.

Operation Mode: Dual Flow
Reverser Port Bullnose: None
Reverser Port Spacer: 0.40"
Reverser Port Cover: None
Bifurcator: Installed
Wing: Removed

	Test	Run	Configuration
○	1002	16	556

Outer Door Angle: 60°
Outer Door Cutback: None
Outer Door Kicker: Long/Cutback
Outer Door Fence: None
Inner Door Angle: 36°
Inner Door Fillers: All+Tape
Door Struts: No
Door Leakage: None

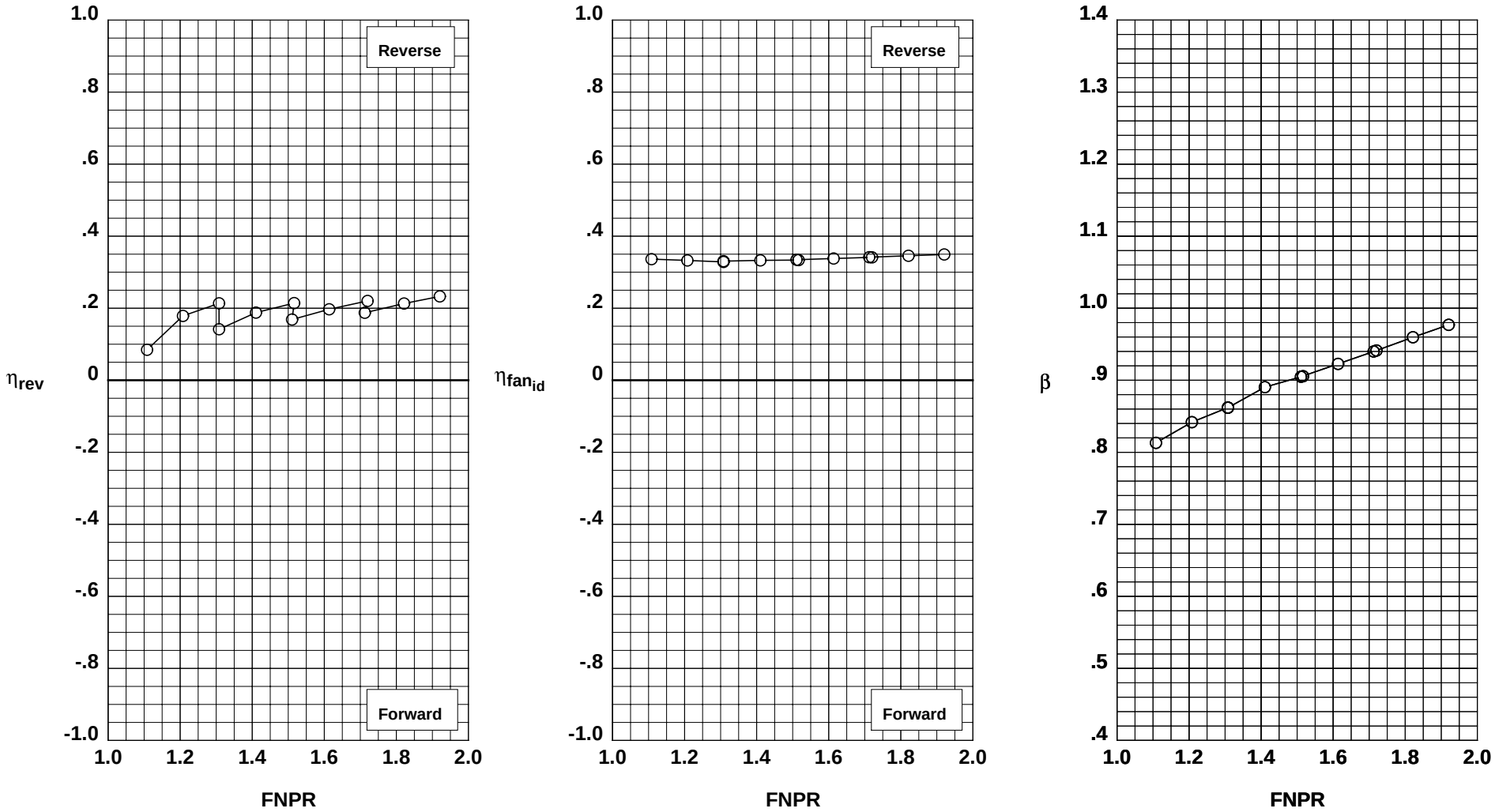

Figure G-63. Multi-door crocodile thrust reverser performance characteristics for configuration 556.

Operation Mode: Dual Flow
Reverser Port Bullnose: #1
Reverser Port Spacer: 0.40"
Reverser Port Cover: None
Bifurcator: Installed
Wing: Removed

	Test	Run	Configuration
○	1002	17	557

Outer Door Angle: 60°
Outer Door Cutback: None
Outer Door Kicker: Long/Cutback
Outer Door Fence: None
Inner Door Angle: 36°
Inner Door Fillers: All+Tape
Door Struts: No
Door Leakage: None

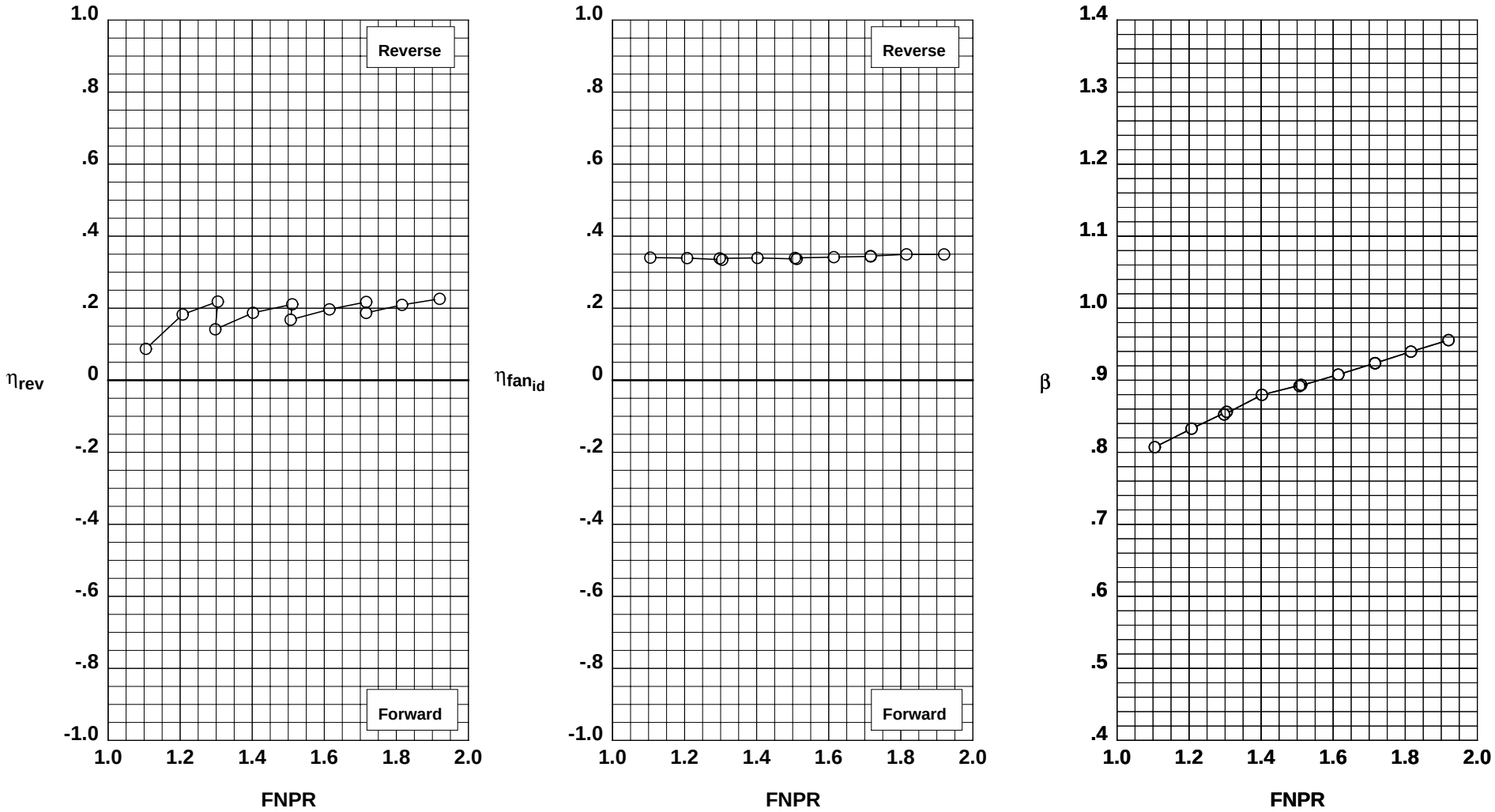

Figure G-64. Multi-door crocodile thrust reverser performance characteristics for configuration 557.

Operation Mode: Dual Flow
Reverser Port Bullnose: #2
Reverser Port Spacer: 0.40"
Reverser Port Cover: None
Bifurcator: Installed
Wing: Removed

	Test	Run	Configuration
○	1002	18	558

Outer Door Angle: 60°
Outer Door Cutback: None
Outer Door Kicker: Long/Cutback
Outer Door Fence: None
Inner Door Angle: 36°
Inner Door Fillers: All+Tape
Door Struts: No
Door Leakage: None

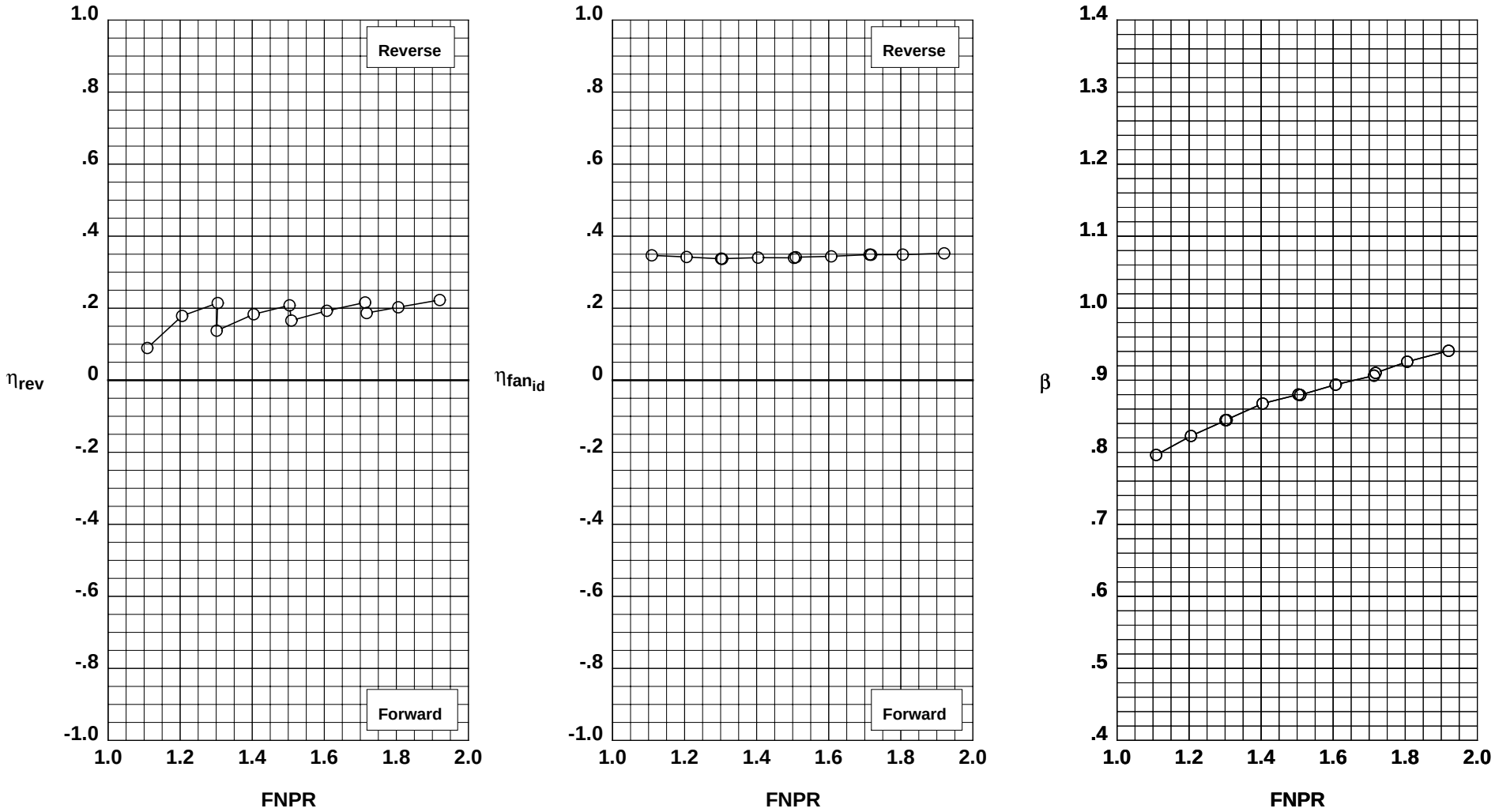

Figure G-65. Multi-door crocodile thrust reverser performance characteristics for configuration 558.

Operation Mode: Dual Flow
Reverser Port Bullnose: #3
Reverser Port Spacer: 0.40"
Reverser Port Cover: None
Bifurcator: Installed
Wing: Removed

	Test	Run	Configuration
○	1002	19	559

Outer Door Angle: 60°
Outer Door Cutback: None
Outer Door Kicker: Long/Cutback
Outer Door Fence: None
Inner Door Angle: 36°
Inner Door Fillers: All+Tape
Door Struts: No
Door Leakage: None

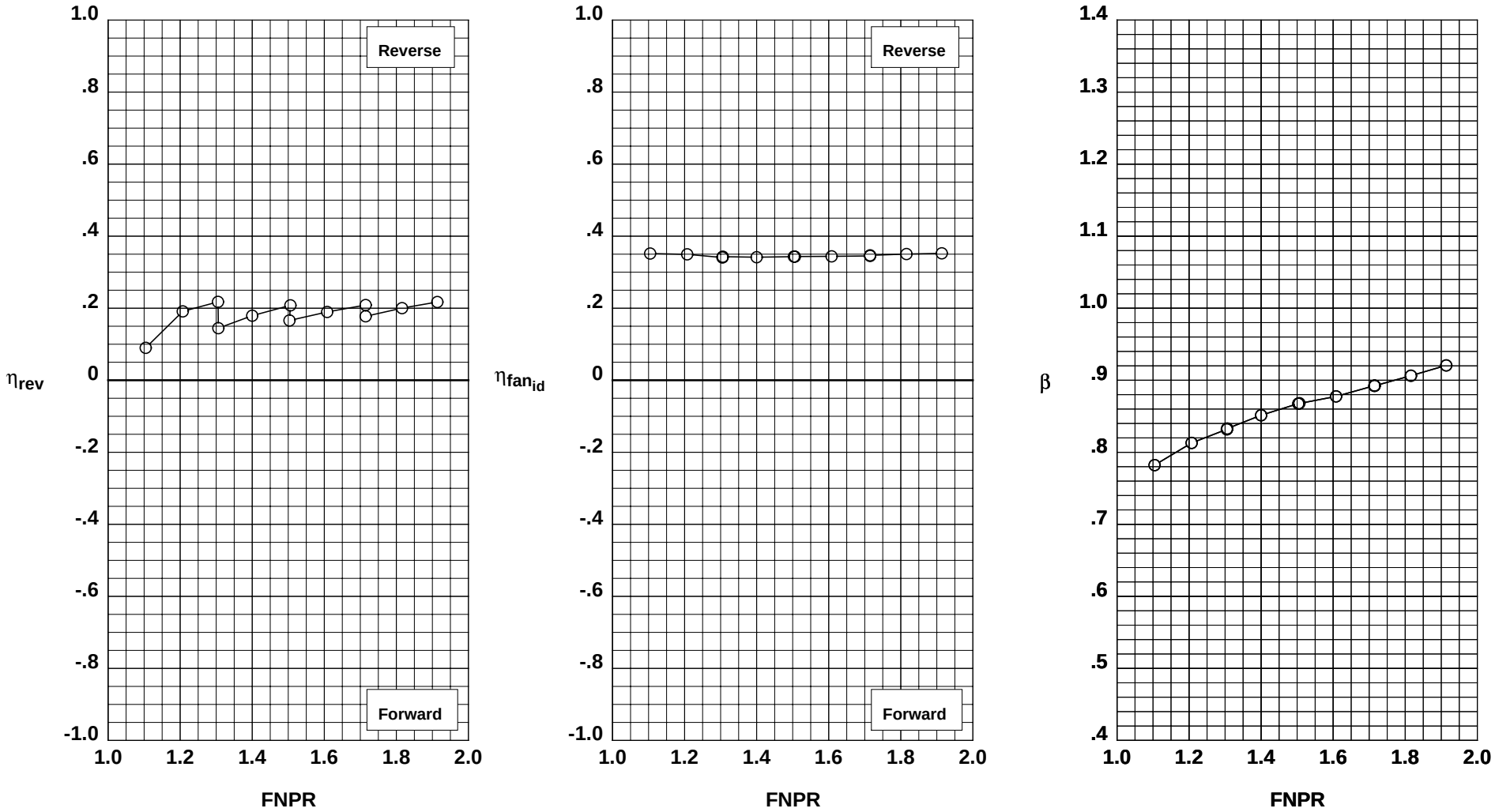

Figure G-66. Multi-door crocodile thrust reverser performance characteristics for configuration 559.

Operation Mode: Dual Flow
Reverser Port Bullnose: #3
Reverser Port Spacer: None
Reverser Port Cover: None
Bifurcator: Installed
Wing: Removed

	Test	Run	Configuration
○	1002	8	544

Outer Door Angle: 60°
Outer Door Cutback: None
Outer Door Kicker: Long/Cutback
Outer Door Fence: None
Inner Door Angle: 36°
Inner Door Fillers: All+Tape
Door Struts: No
Door Leakage: None

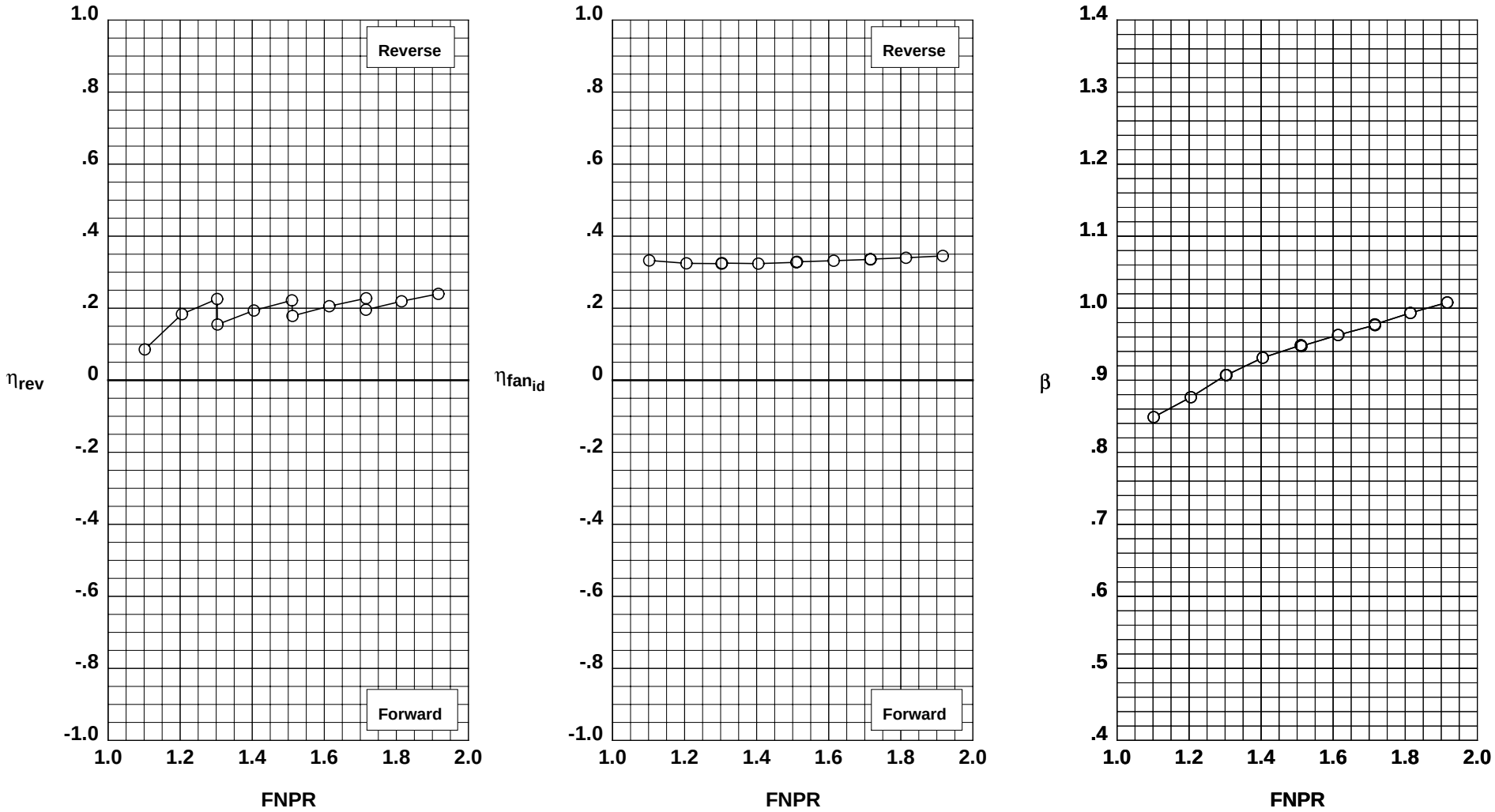

Figure G-67. Multi-door crocodile thrust reverser performance characteristics for configuration 544.

Operation Mode: Dual Flow
Reverser Port Bullnose: #3
Reverser Port Spacer: None
Reverser Port Cover: None
Bifurcator: Installed
Wing: Removed

	Test	Run	Configuration
○	1002	5	560

Outer Door Angle: 60°
Outer Door Cutback: None
Outer Door Kicker: X-Long
Outer Door Fence: Yes
Inner Door Angle: 36°
Inner Door Fillers: All+Tape
Door Struts: No
Door Leakage: None

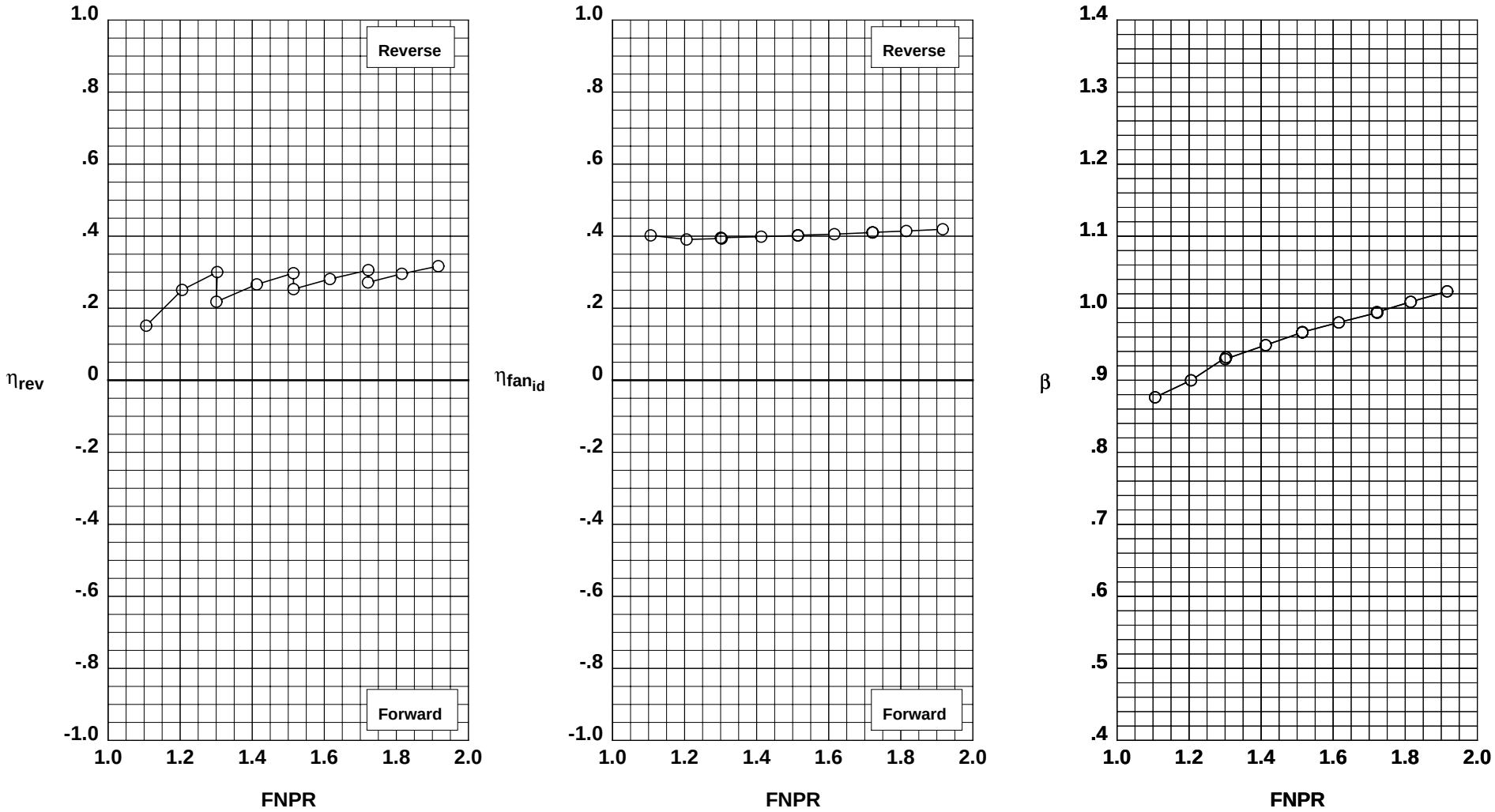

Figure G-68. Multi-door crocodile thrust reverser performance characteristics for configuration 560.

Operation Mode: Dual Flow
Reverser Port Bullnose: #3
Reverser Port Spacer: None
Reverser Port Cover: None
Bifurcator: Installed
Wing: Removed

	Test	Run	Configuration
○	1002	7	561

Outer Door Angle: 60°
Outer Door Cutback: None
Outer Door Kicker: X-Long/Cutback
Outer Door Fence: None
Inner Door Angle: 36°
Inner Door Fillers: All+Tape
Door Struts: No
Door Leakage: None

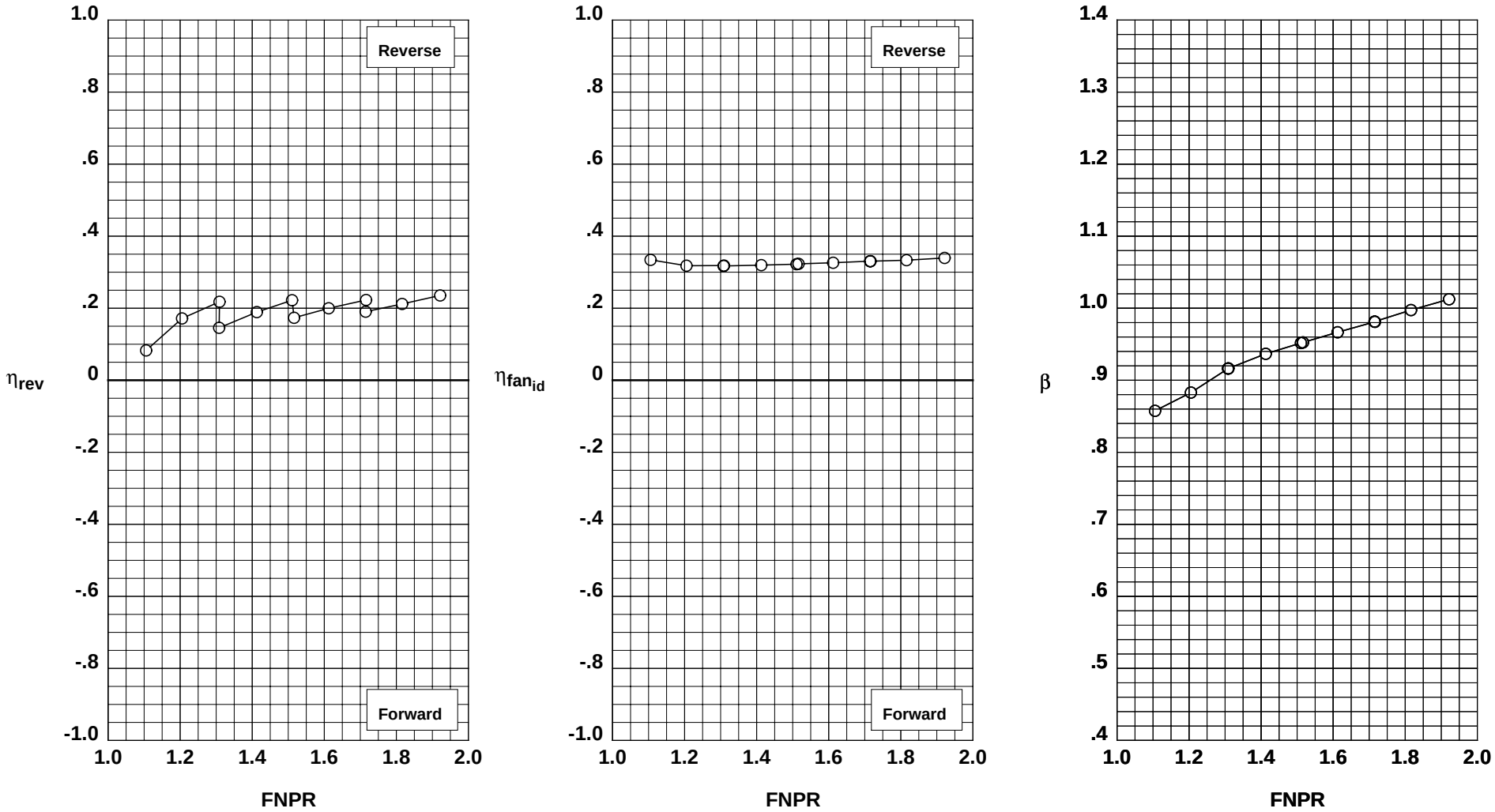

Figure G-69. Multi-door crocodile thrust reverser performance characteristics for configuration 561.

Operation Mode: Dual Flow
Reverser Port Bullnose: #3
Reverser Port Spacer: None
Reverser Port Cover: None
Bifurcator: Installed
Wing: Removed

	Test	Run	Configuration
○	1002	33	562

Outer Door Angle: 10°
Outer Door Cutback: None
Outer Door Kicker: Long/Cutback
Outer Door Fence: None
Inner Door Angle: 12°
Inner Door Fillers: All
Door Struts: No
Door Leakage: Partial

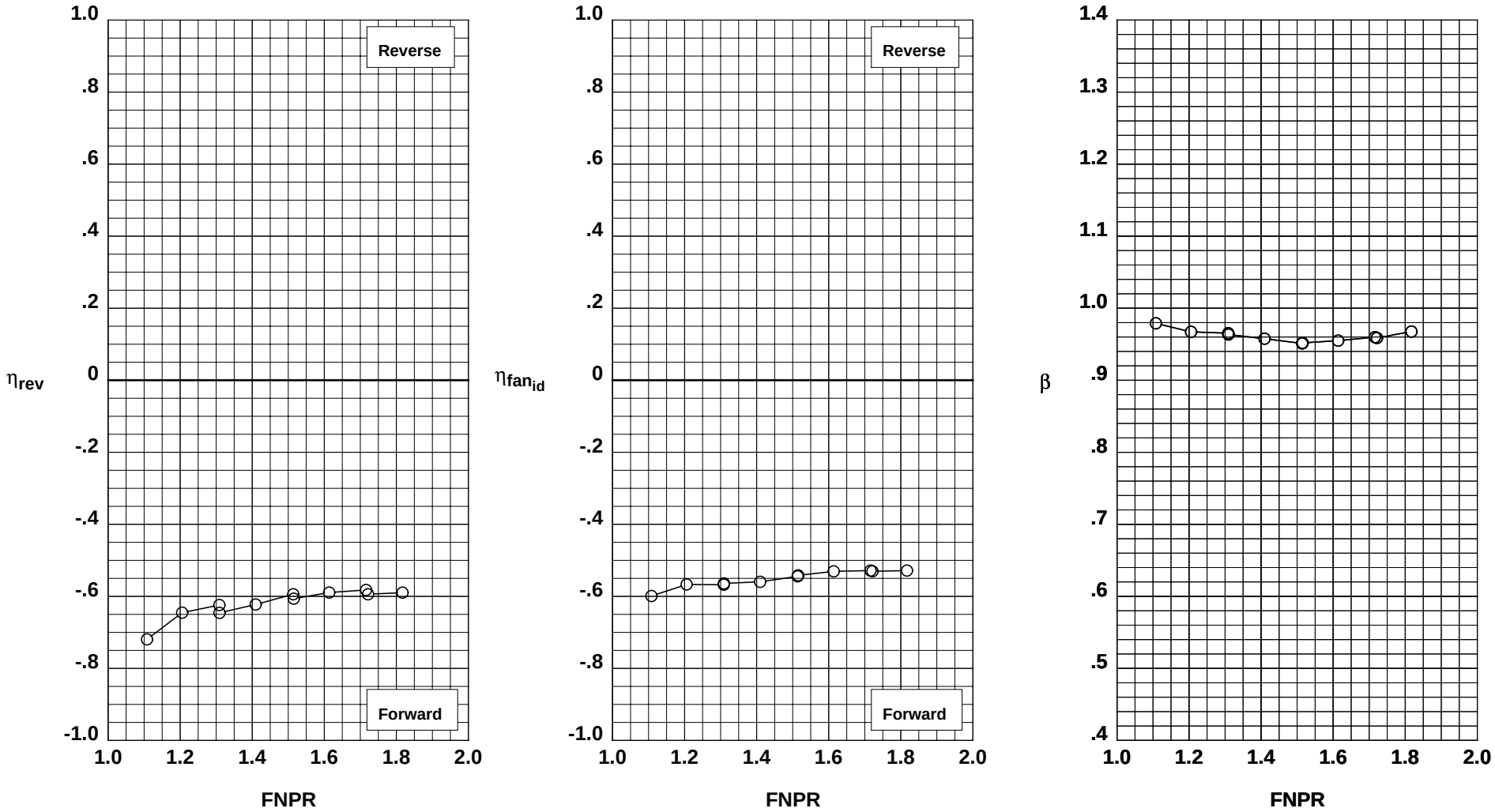

Figure G-70. Multi-door crocodile thrust reverser performance characteristics for configuration 562.

Operation Mode: Dual Flow
Reverser Port Bullnose: #3
Reverser Port Spacer: None
Reverser Port Cover: None
Bifurcator: Installed
Wing: Removed

	Test	Run	Configuration
○	1002	34	563

Outer Door Angle: 20°
Outer Door Cutback: None
Outer Door Kicker: Long/Cutback
Outer Door Fence: None
Inner Door Angle: 12°
Inner Door Fillers: All
Door Struts: No
Door Leakage: Partial

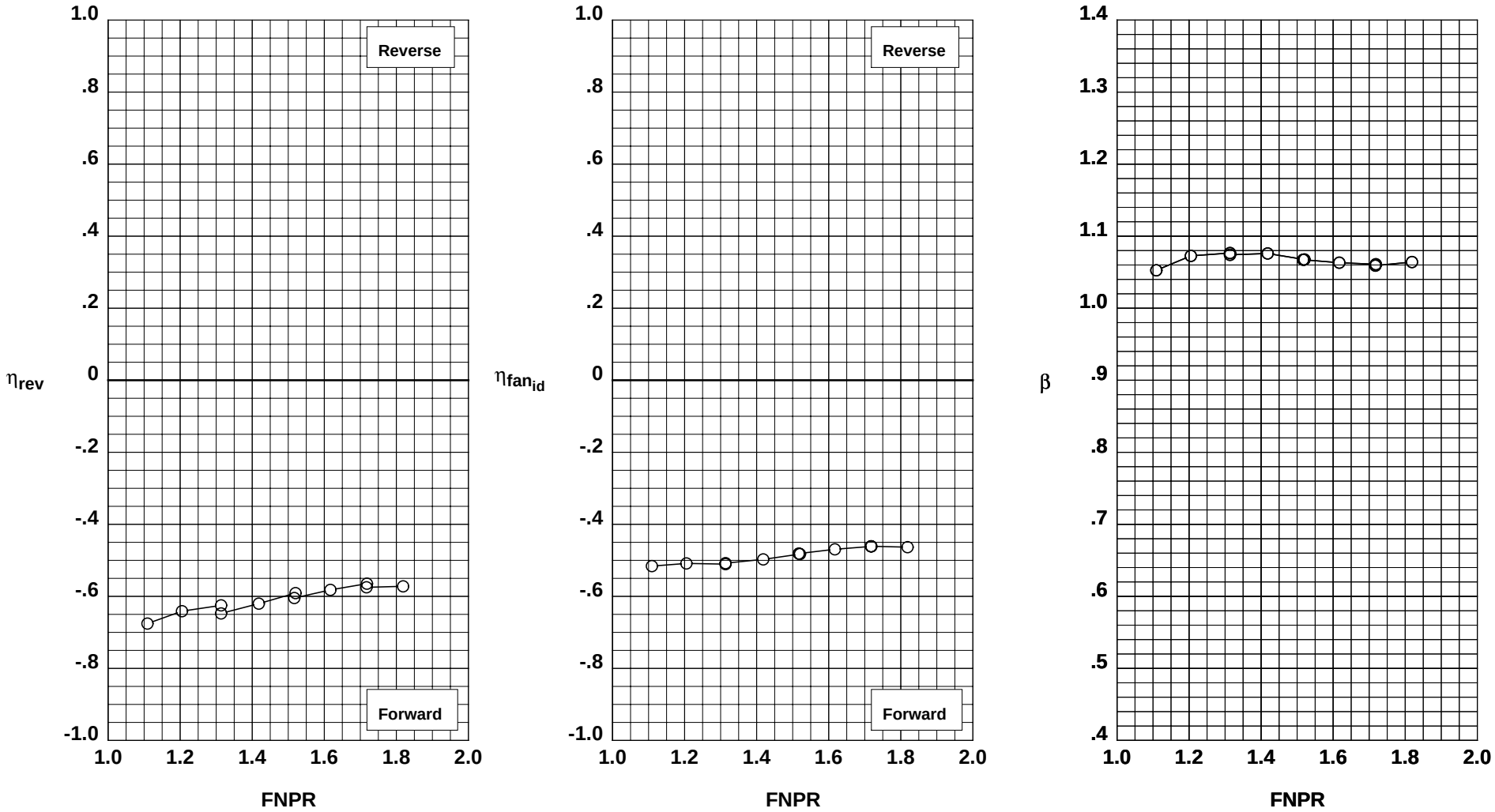

Figure G-71. Multi-door crocodile thrust reverser performance characteristics for configuration 563.

Operation Mode: Dual Flow
Reverser Port Bullnose: #3
Reverser Port Spacer: None
Reverser Port Cover: None
Bifurcator: Installed
Wing: Removed

	Test	Run	Configuration
○	1002	35	564

Outer Door Angle: 30°
Outer Door Cutback: None
Outer Door Kicker: Long/Cutback
Outer Door Fence: None
Inner Door Angle: 12°
Inner Door Fillers: All
Door Struts: No
Door Leakage: Partial

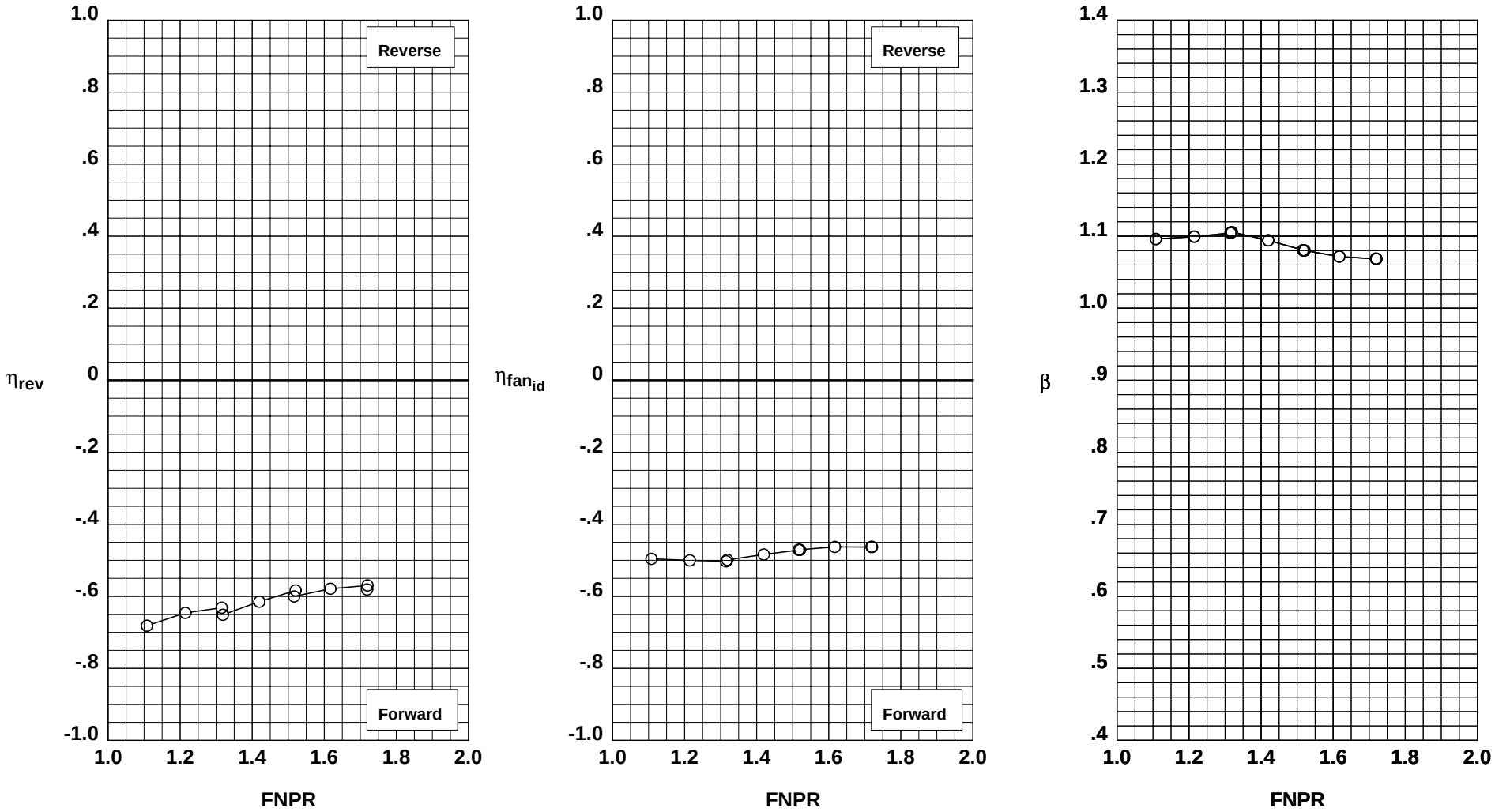

Figure G-72. Multi-door crocodile thrust reverser performance characteristics for configuration 564.

Operation Mode: Dual Flow
Reverser Port Bullnose: #3
Reverser Port Spacer: None
Reverser Port Cover: None
Bifurcator: Installed
Wing: Removed

	Test	Run	Configuration
○	1002	36	565

Outer Door Angle: 40°
Outer Door Cutback: None
Outer Door Kicker: Long/Cutback
Outer Door Fence: None
Inner Door Angle: 12°
Inner Door Fillers: All
Door Struts: No
Door Leakage: Partial

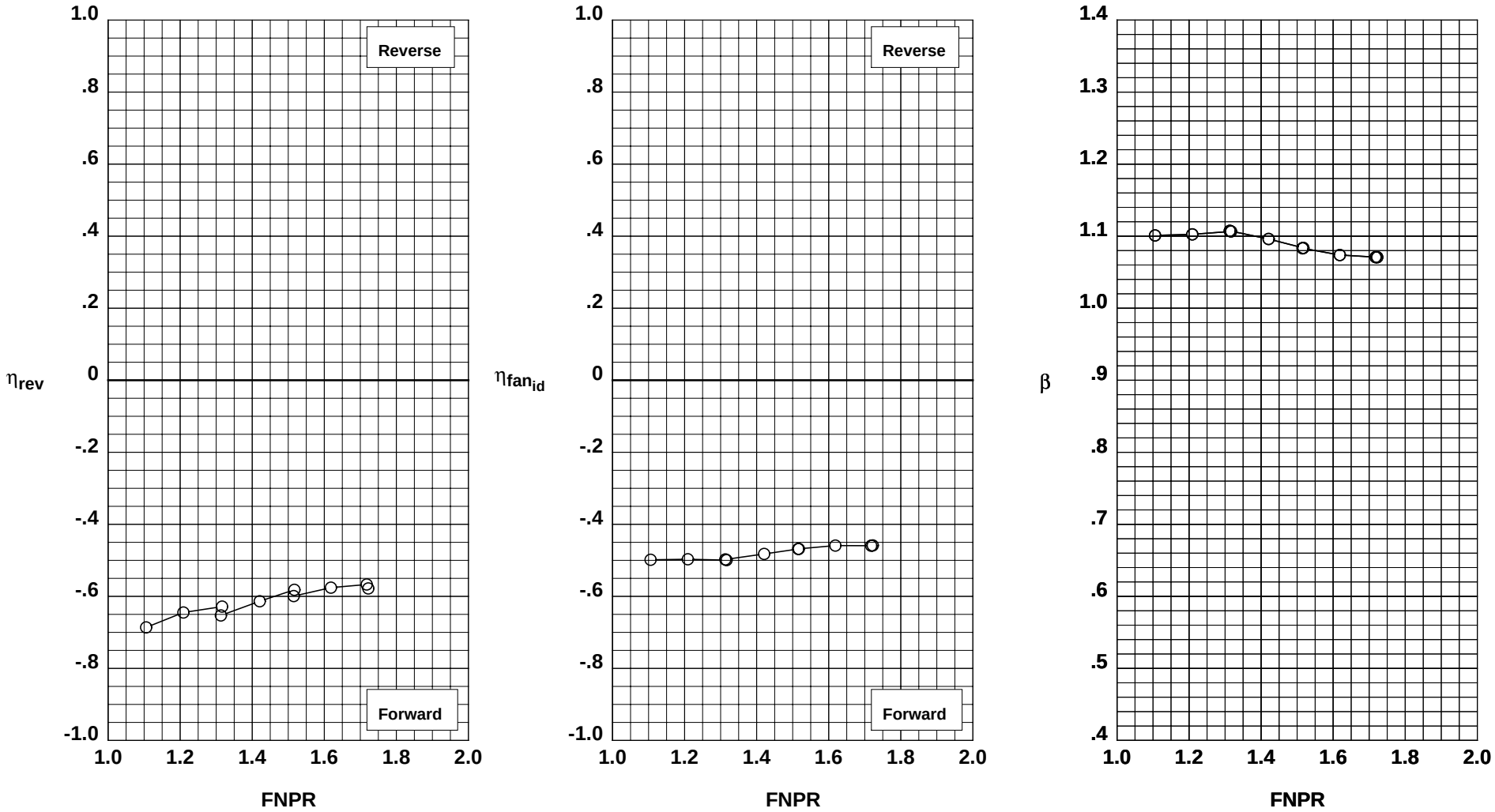

Figure G-73. Multi-door crocodile thrust reverser performance characteristics for configuration 565.

Operation Mode: Dual Flow
Reverser Port Bullnose: #3
Reverser Port Spacer: None
Reverser Port Cover: None
Bifurcator: Installed
Wing: Removed

	Test	Run	Configuration
○	1002	37	566

Outer Door Angle: 50°
Outer Door Cutback: None
Outer Door Kicker: Long/Cutback
Outer Door Fence: None
Inner Door Angle: 12°
Inner Door Fillers: All
Door Struts: No
Door Leakage: Partial

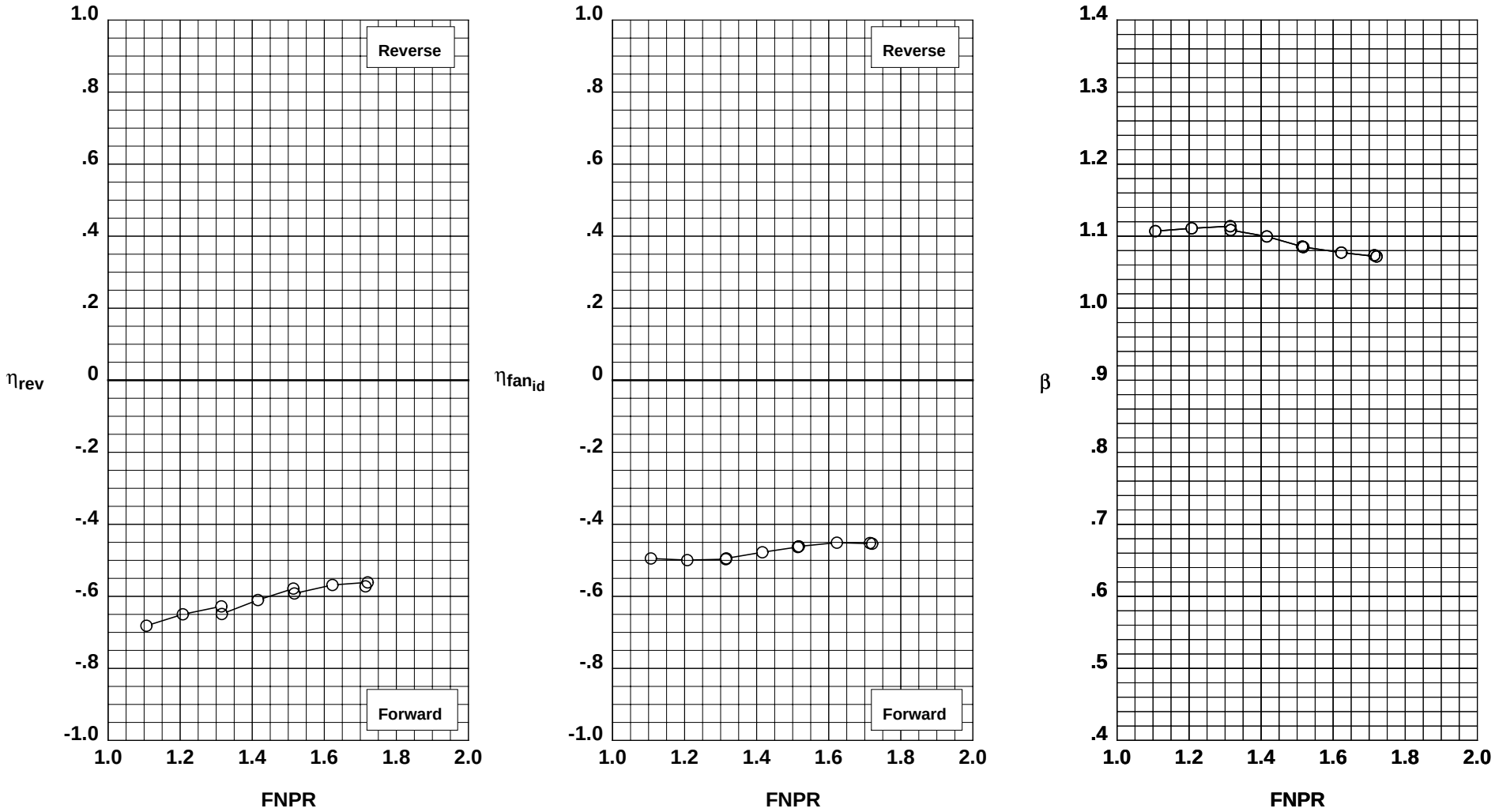

Figure G-74. Multi-door crocodile thrust reverser performance characteristics for configuration 566.

Operation Mode: Dual Flow
Reverser Port Bullnose: #3
Reverser Port Spacer: None
Reverser Port Cover: None
Bifurcator: Installed
Wing: Removed

	Test	Run	Configuration
○	1002	38	567

Outer Door Angle: 60°
Outer Door Cutback: None
Outer Door Kicker: Long/Cutback
Outer Door Fence: None
Inner Door Angle: 12°
Inner Door Fillers: All
Door Struts: No
Door Leakage: Partial

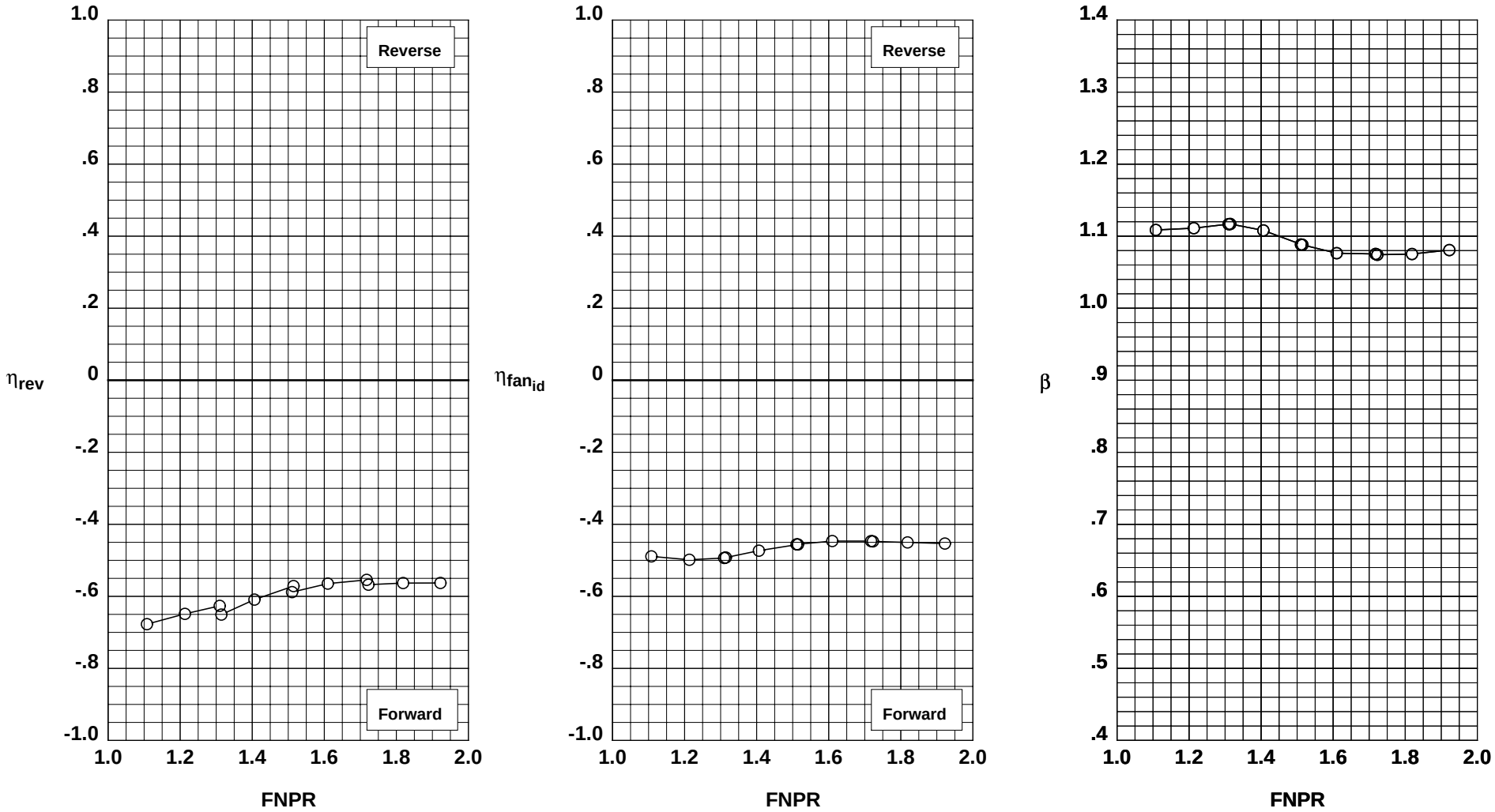

Figure G-75. Multi-door crocodile thrust reverser performance characteristics for configuration 567.

Operation Mode: Dual Flow
Reverser Port Bullnose: #3
Reverser Port Spacer: None
Reverser Port Cover: None
Bifurcator: Installed
Wing: Removed

	Test	Run	Configuration
○	1002	32	568

Outer Door Angle: 10°
Outer Door Cutback: None
Outer Door Kicker: Long/Cutback
Outer Door Fence: None
Inner Door Angle: 24°
Inner Door Fillers: All
Door Struts: No
Door Leakage: Partial

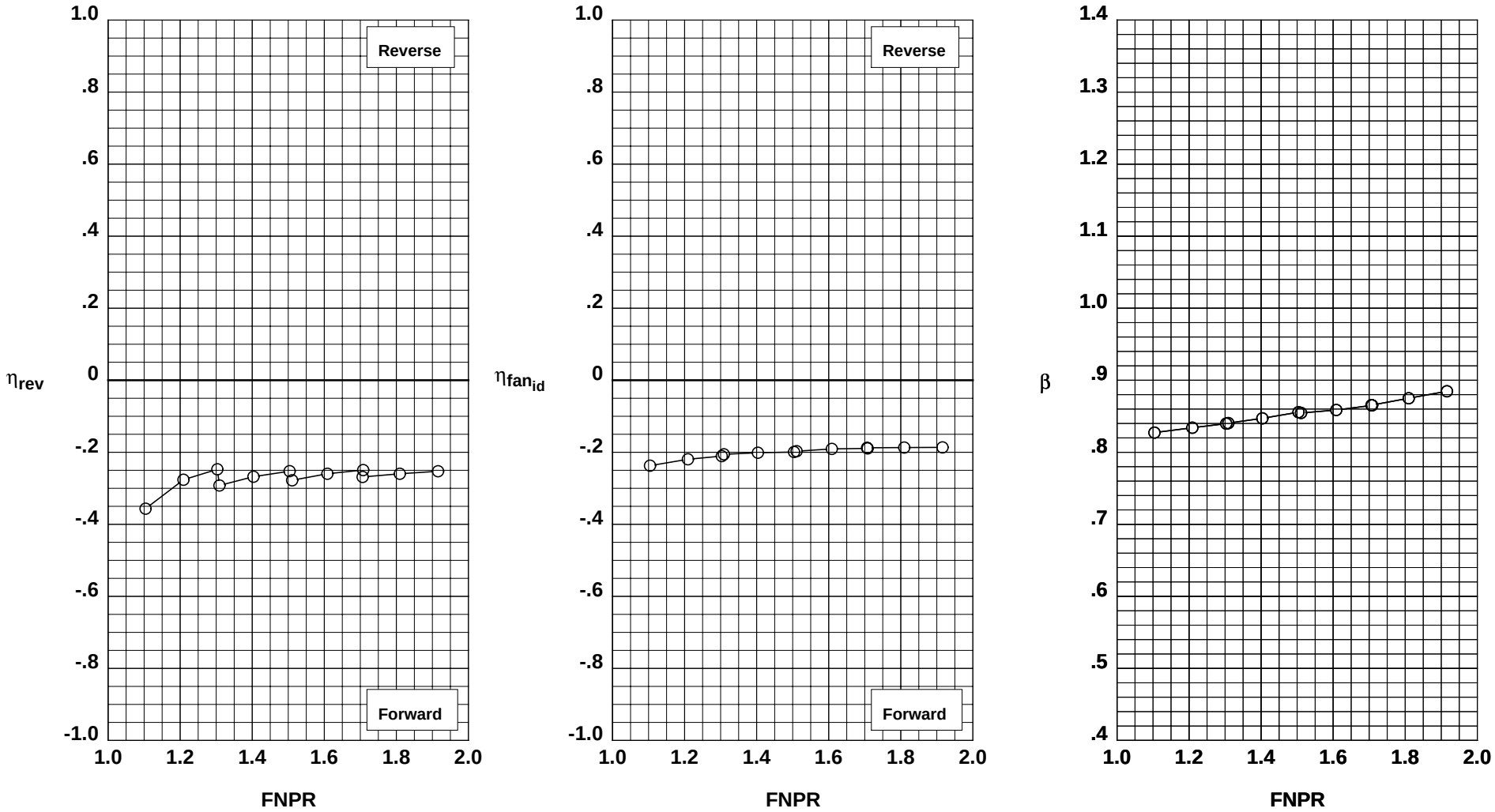

Figure G-76. Multi-door crocodile thrust reverser performance characteristics for configuration 568.

Operation Mode: Dual Flow
Reverser Port Bullnose: #3
Reverser Port Spacer: None
Reverser Port Cover: None
Bifurcator: Installed
Wing: Removed

	Test	Run	Configuration
○	1002	31	569

Outer Door Angle: 20°
Outer Door Cutback: None
Outer Door Kicker: Long/Cutback
Outer Door Fence: None
Inner Door Angle: 24°
Inner Door Fillers: All
Door Struts: No
Door Leakage: Partial

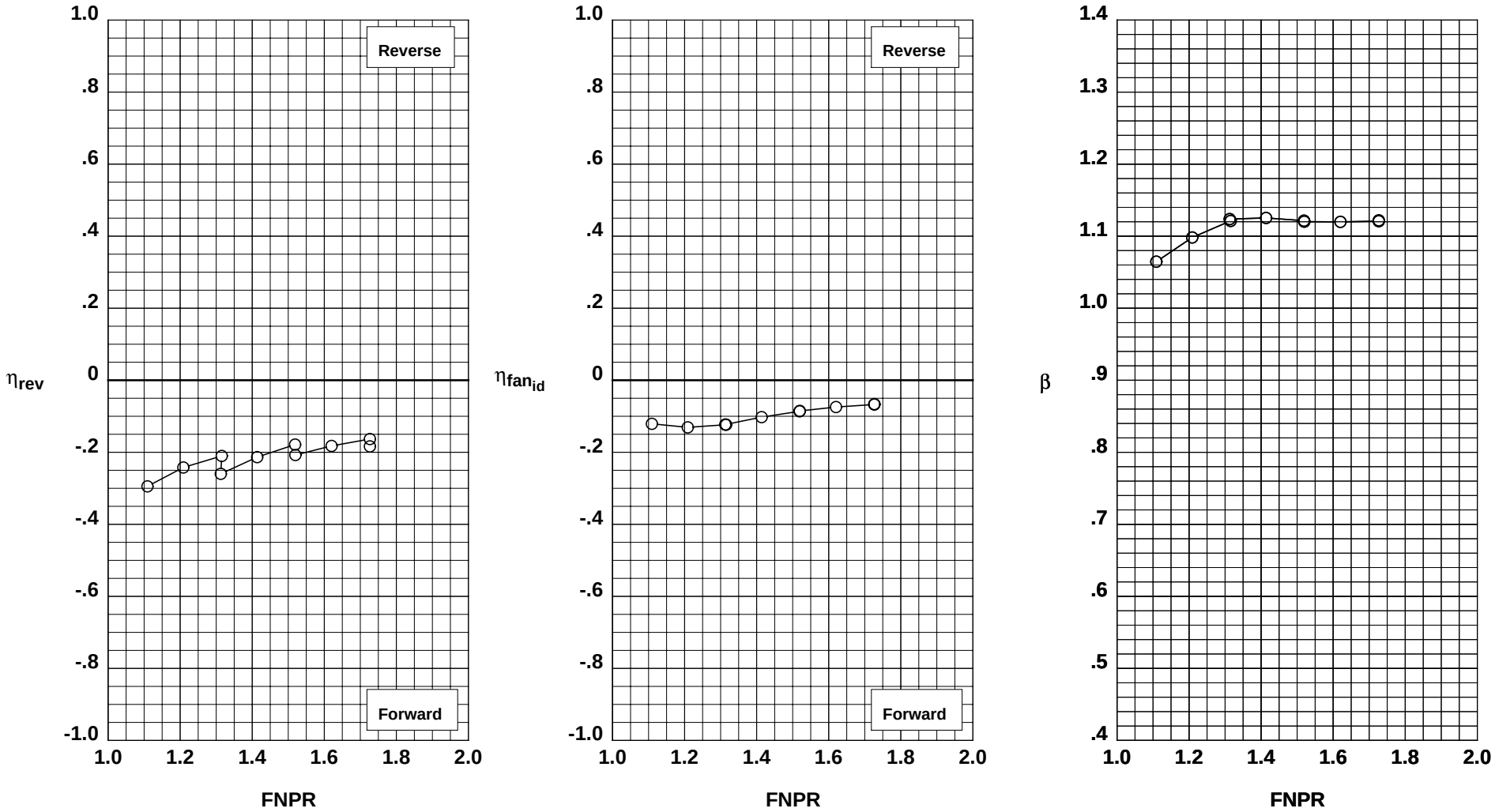

Figure G-77. Multi-door crocodile thrust reverser performance characteristics for configuration 569.

Operation Mode: Dual Flow
Reverser Port Bullnose: #3
Reverser Port Spacer: None
Reverser Port Cover: None
Bifurcator: Installed
Wing: Removed

	Test	Run	Configuration
○	1002	30	570

Outer Door Angle: 30°
Outer Door Cutback: None
Outer Door Kicker: Long/Cutback
Outer Door Fence: None
Inner Door Angle: 24°
Inner Door Fillers: All
Door Struts: No
Door Leakage: Partial

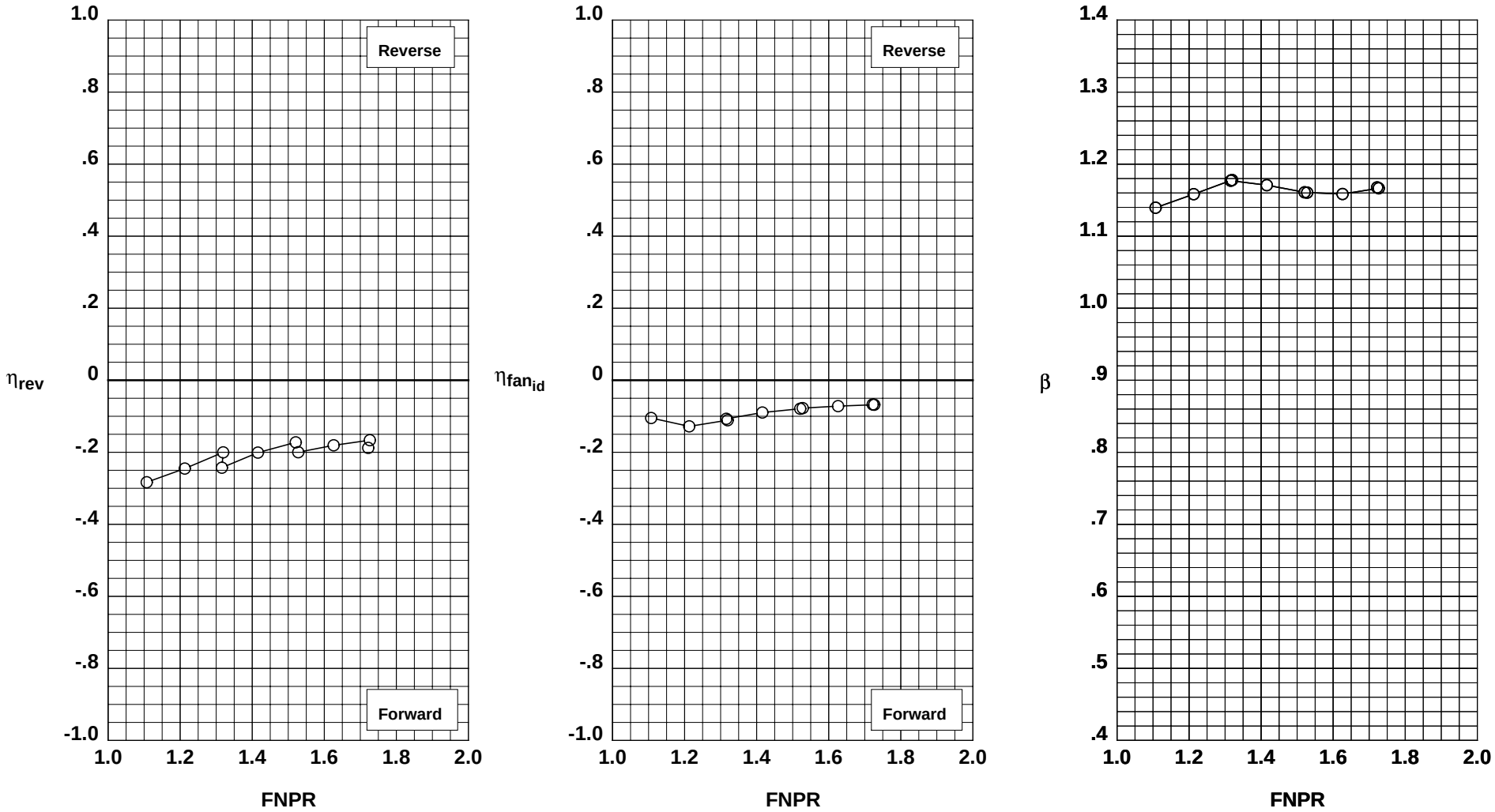

Figure G-78. Multi-door crocodile thrust reverser performance characteristics for configuration 570.

Operation Mode: Dual Flow
Reverser Port Bullnose: #3
Reverser Port Spacer: None
Reverser Port Cover: None
Bifurcator: Installed
Wing: Removed

	Test	Run	Configuration
○	1002	29	571

Outer Door Angle: 40°
Outer Door Cutback: None
Outer Door Kicker: Long/Cutback
Outer Door Fence: None
Inner Door Angle: 24°
Inner Door Fillers: All
Door Struts: No
Door Leakage: Partial

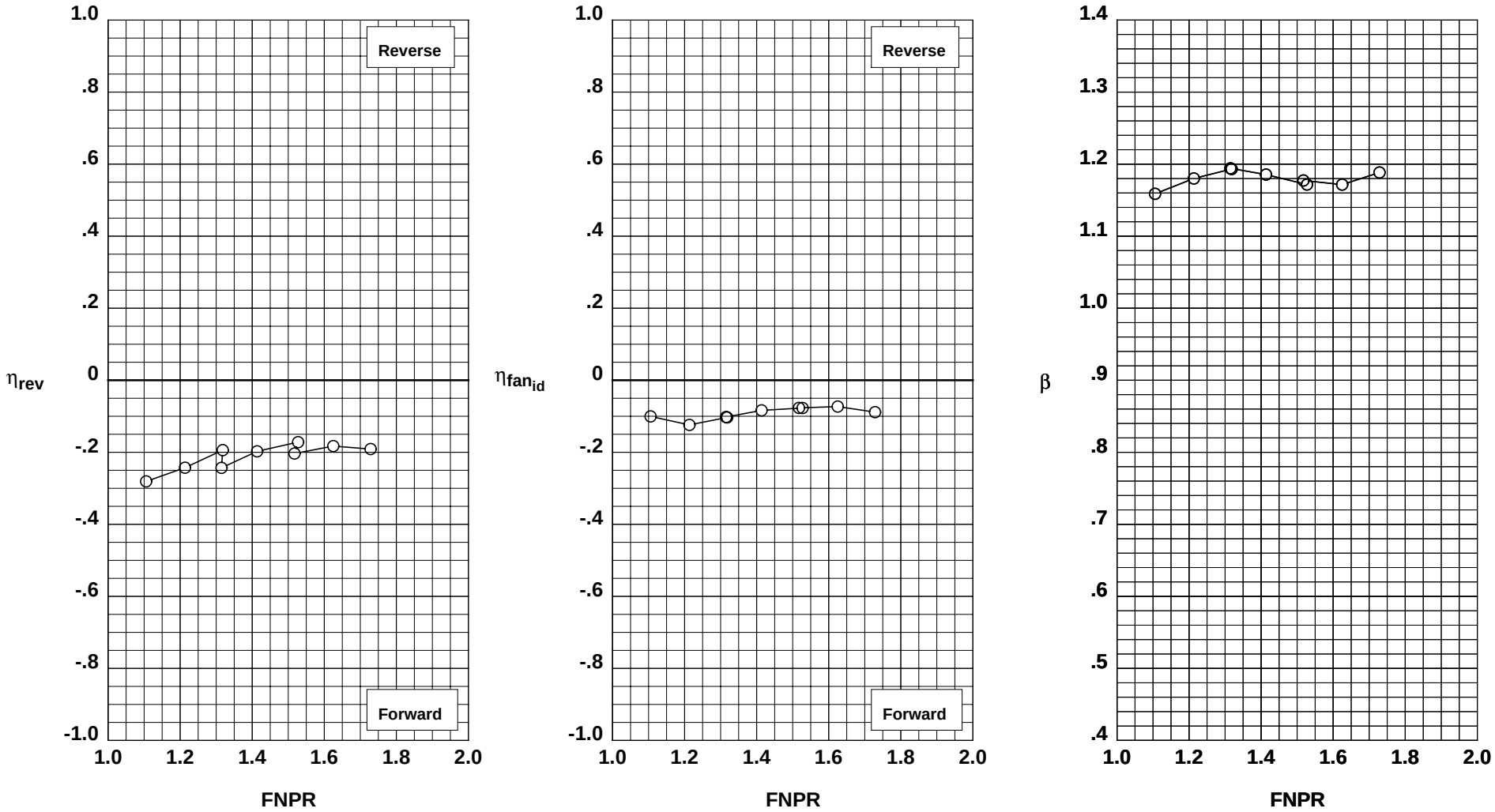

Figure G-79. Multi-door crocodile thrust reverser performance characteristics for configuration 571.

Operation Mode: Dual Flow
Reverser Port Bullnose: #3
Reverser Port Spacer: None
Reverser Port Cover: None
Bifurcator: Installed
Wing: Removed

	Test	Run	Configuration
○	1002	28	572

Outer Door Angle: 50°
Outer Door Cutback: None
Outer Door Kicker: Long/Cutback
Outer Door Fence: None
Inner Door Angle: 24°
Inner Door Fillers: All
Door Struts: No
Door Leakage: Partial

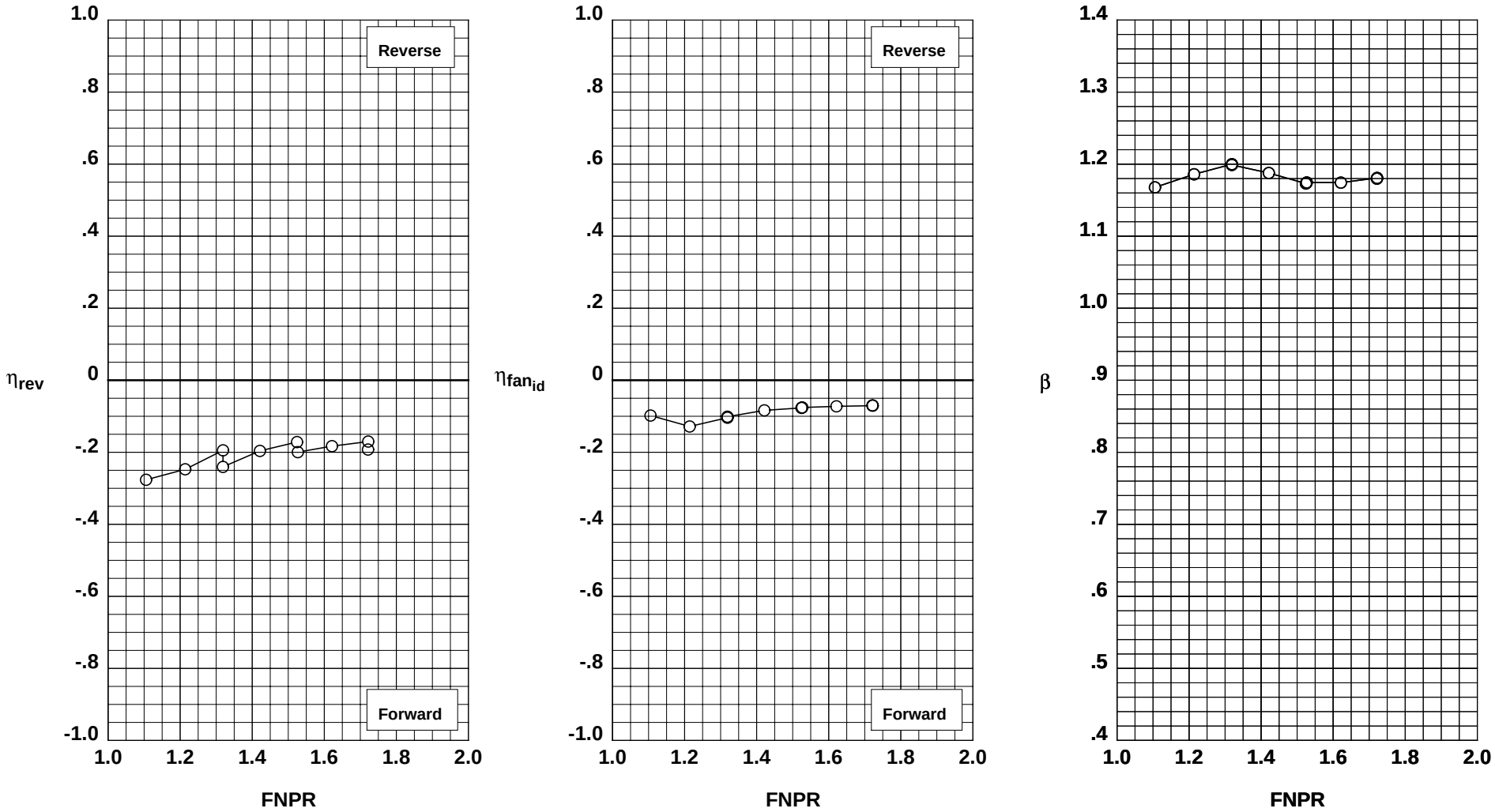

Figure G-80. Multi-door crocodile thrust reverser performance characteristics for configuration 572.

Operation Mode: Dual Flow
Reverser Port Bullnose: #3
Reverser Port Spacer: None
Reverser Port Cover: None
Bifurcator: Installed
Wing: Removed

	Test	Run	Configuration
○	1002	27	573

Outer Door Angle: 60°
Outer Door Cutback: None
Outer Door Kicker: Long/Cutback
Outer Door Fence: None
Inner Door Angle: 24°
Inner Door Fillers: All
Door Struts: No
Door Leakage: Partial

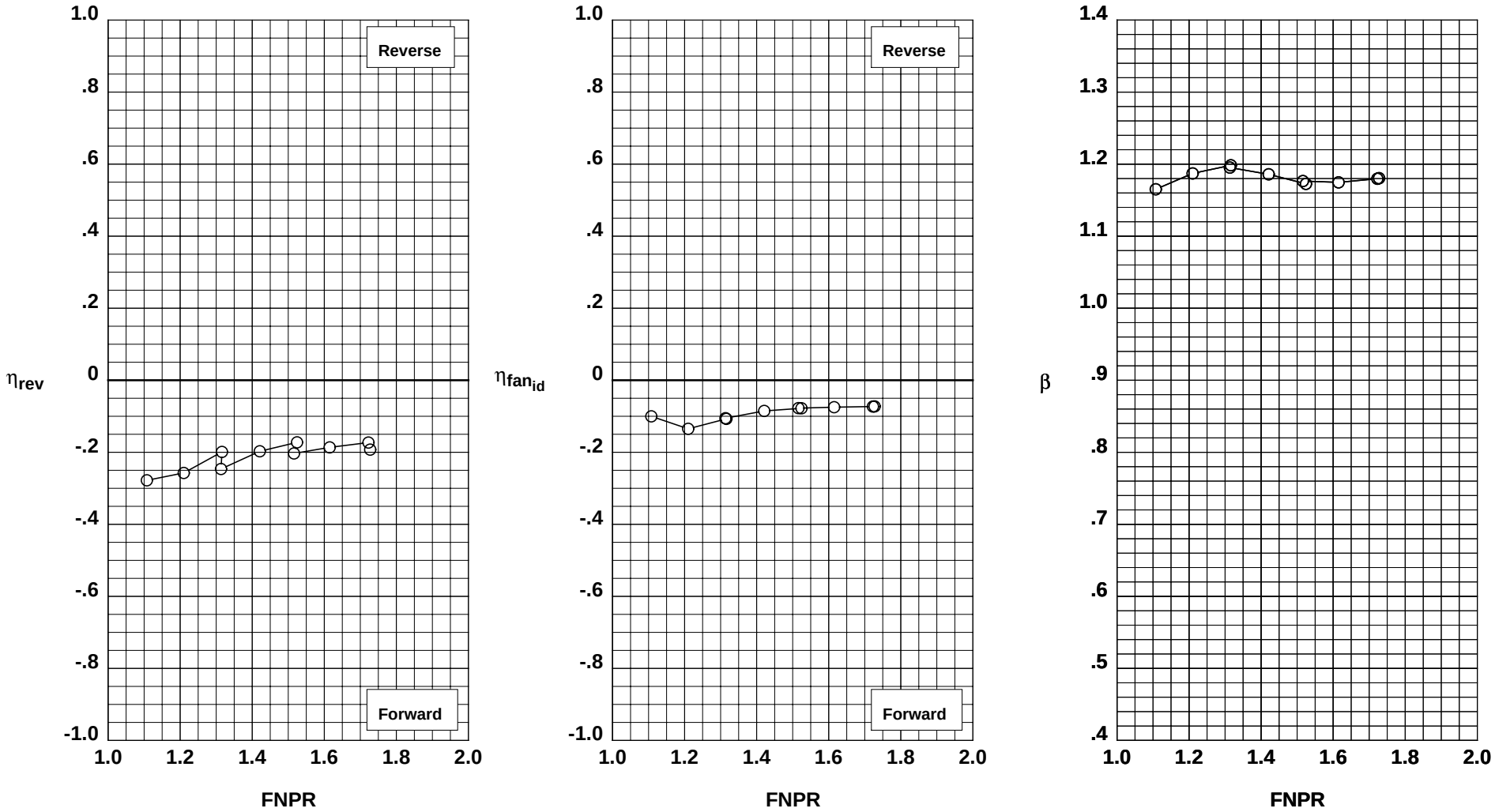

Figure G-81. Multi-door crocodile thrust reverser performance characteristics for configuration 573.

Operation Mode: Dual Flow
Reverser Port Bullnose: #3
Reverser Port Spacer: None
Reverser Port Cover: None
Bifurcator: Installed
Wing: Removed

	Test	Run	Configuration
○	1002	46	574

Outer Door Angle: 10°
Outer Door Cutback: None
Outer Door Kicker: Long/Cutback
Outer Door Fence: None
Inner Door Angle: 36°
Inner Door Fillers: All
Door Struts: No
Door Leakage: Partial

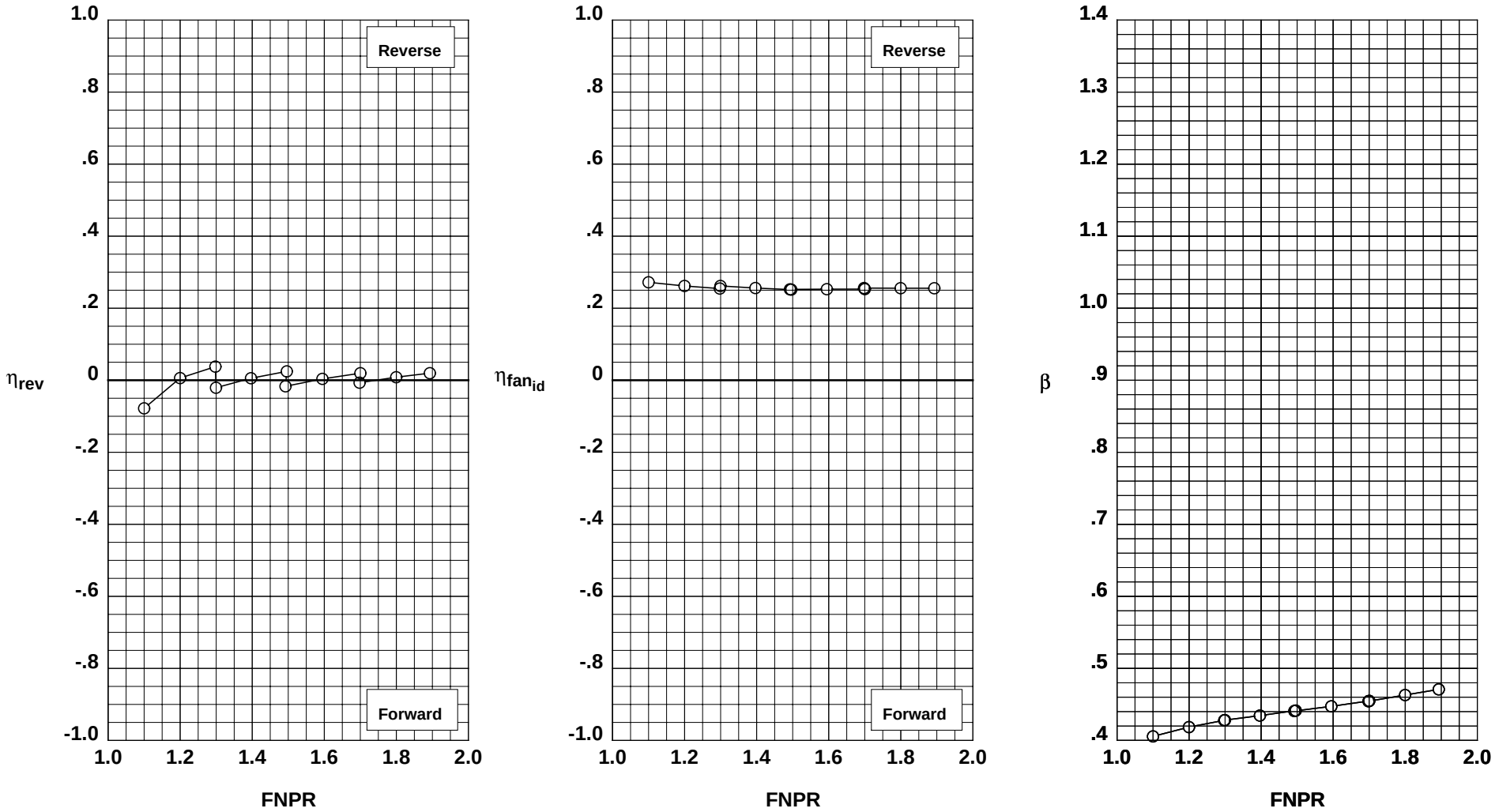

Figure G-82. Multi-door crocodile thrust reverser performance characteristics for configuration 574.

Operation Mode: Dual Flow
Reverser Port Bullnose: #3
Reverser Port Spacer: None
Reverser Port Cover: None
Bifurcator: Installed
Wing: Removed

	Test	Run	Configuration
○	1002	45	575

Outer Door Angle: 20°
Outer Door Cutback: None
Outer Door Kicker: Long/Cutback
Outer Door Fence: None
Inner Door Angle: 36°
Inner Door Fillers: All
Door Struts: No
Door Leakage: Partial

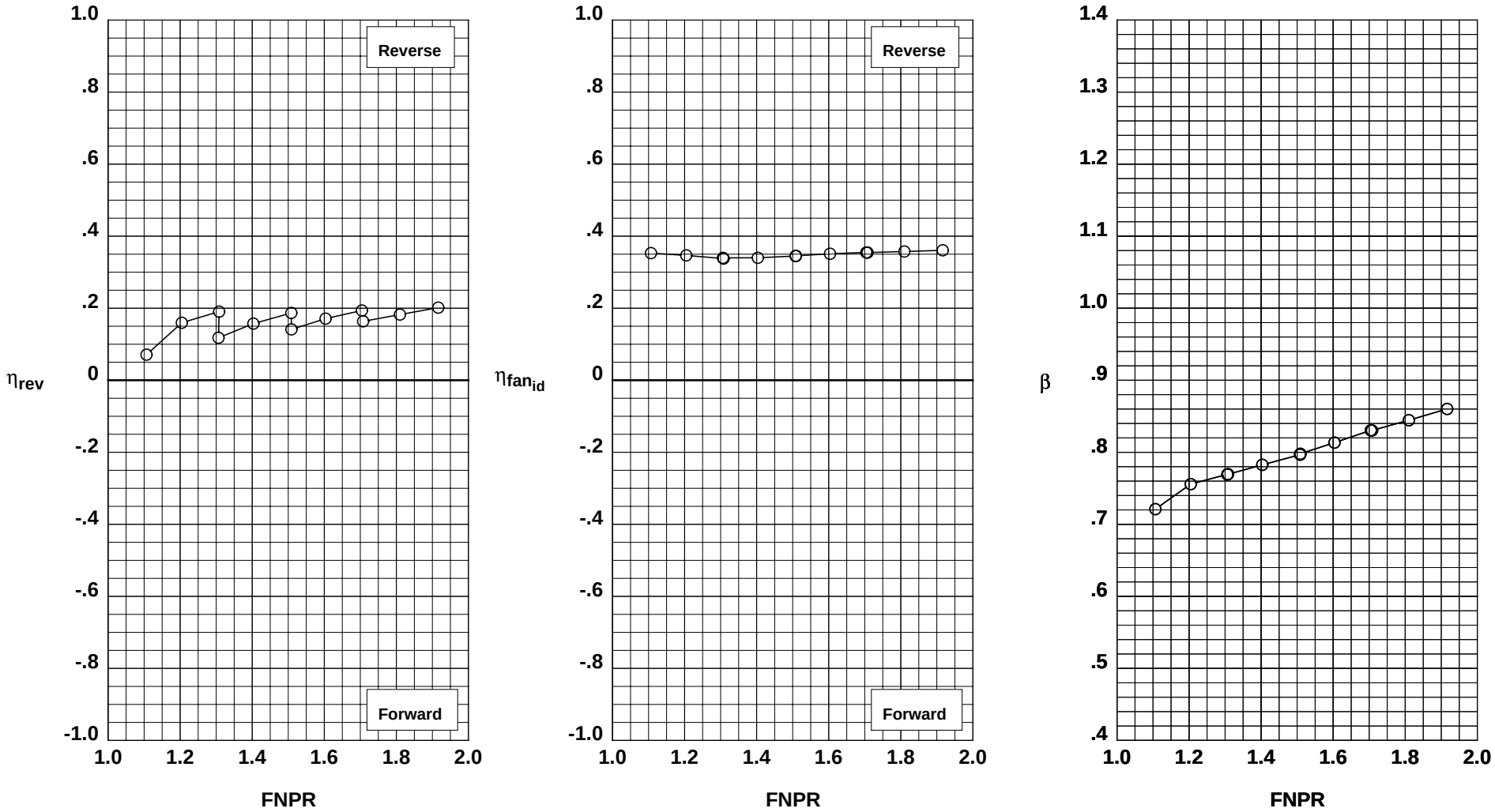

Figure G-83. Multi-door crocodile thrust reverser performance characteristics for configuration 575.

Operation Mode: Dual Flow
Reverser Port Bullnose: #3
Reverser Port Spacer: None
Reverser Port Cover: None
Bifurcator: Installed
Wing: Removed

	Test	Run	Configuration
○	1002	44	576

Outer Door Angle: 30°
Outer Door Cutback: None
Outer Door Kicker: Long/Cutback
Outer Door Fence: None
Inner Door Angle: 36°
Inner Door Fillers: All
Door Struts: No
Door Leakage: Partial

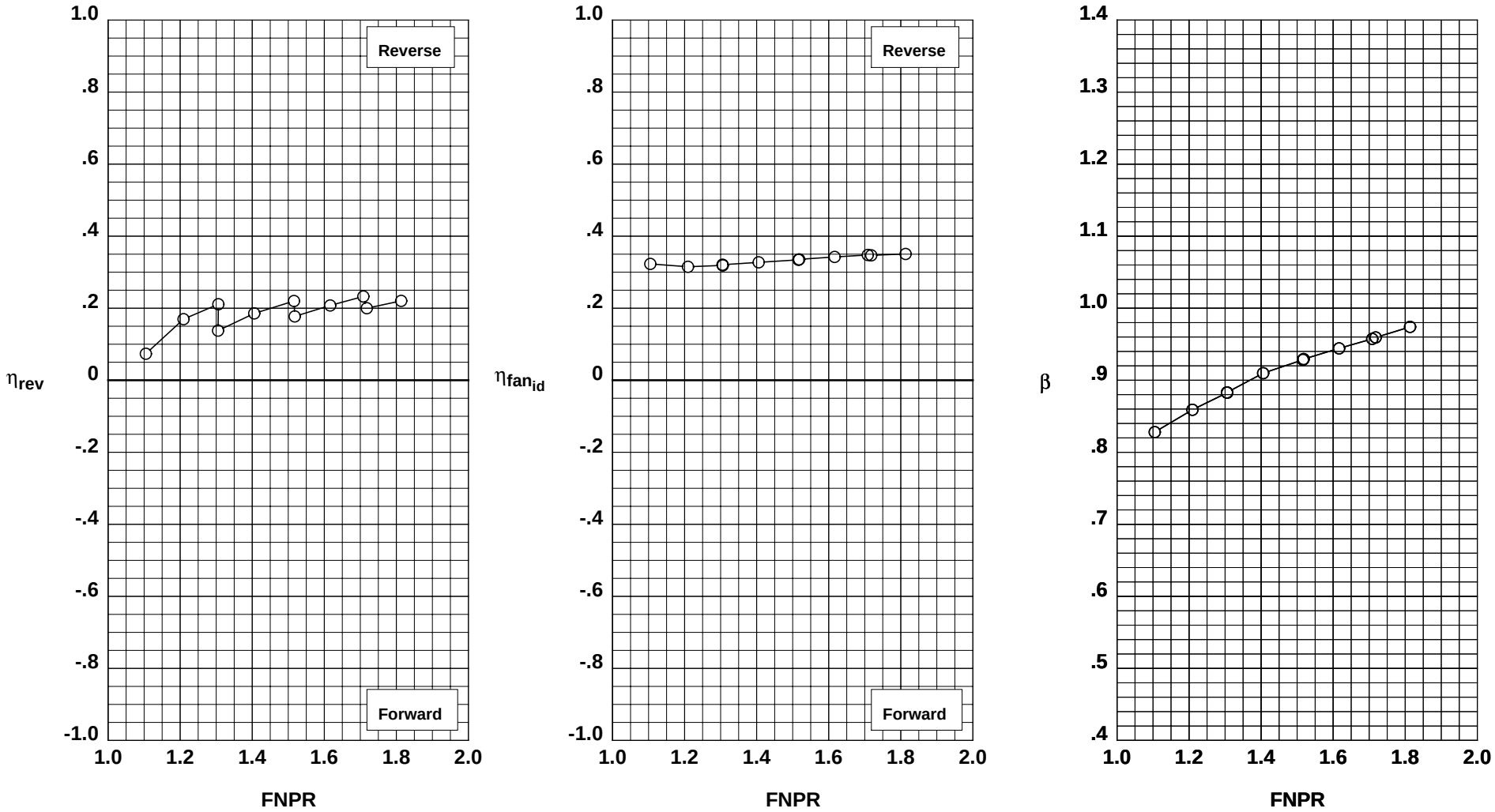

Figure G-84. Multi-door crocodile thrust reverser performance characteristics for configuration 576.

Operation Mode: Dual Flow
Reverser Port Bullnose: #3
Reverser Port Spacer: None
Reverser Port Cover: None
Bifurcator: Installed
Wing: Removed

	Test	Run	Configuration
○	1002	43	577

Outer Door Angle: 40°
Outer Door Cutback: None
Outer Door Kicker: Long/Cutback
Outer Door Fence: None
Inner Door Angle: 36°
Inner Door Fillers: All
Door Struts: No
Door Leakage: Partial

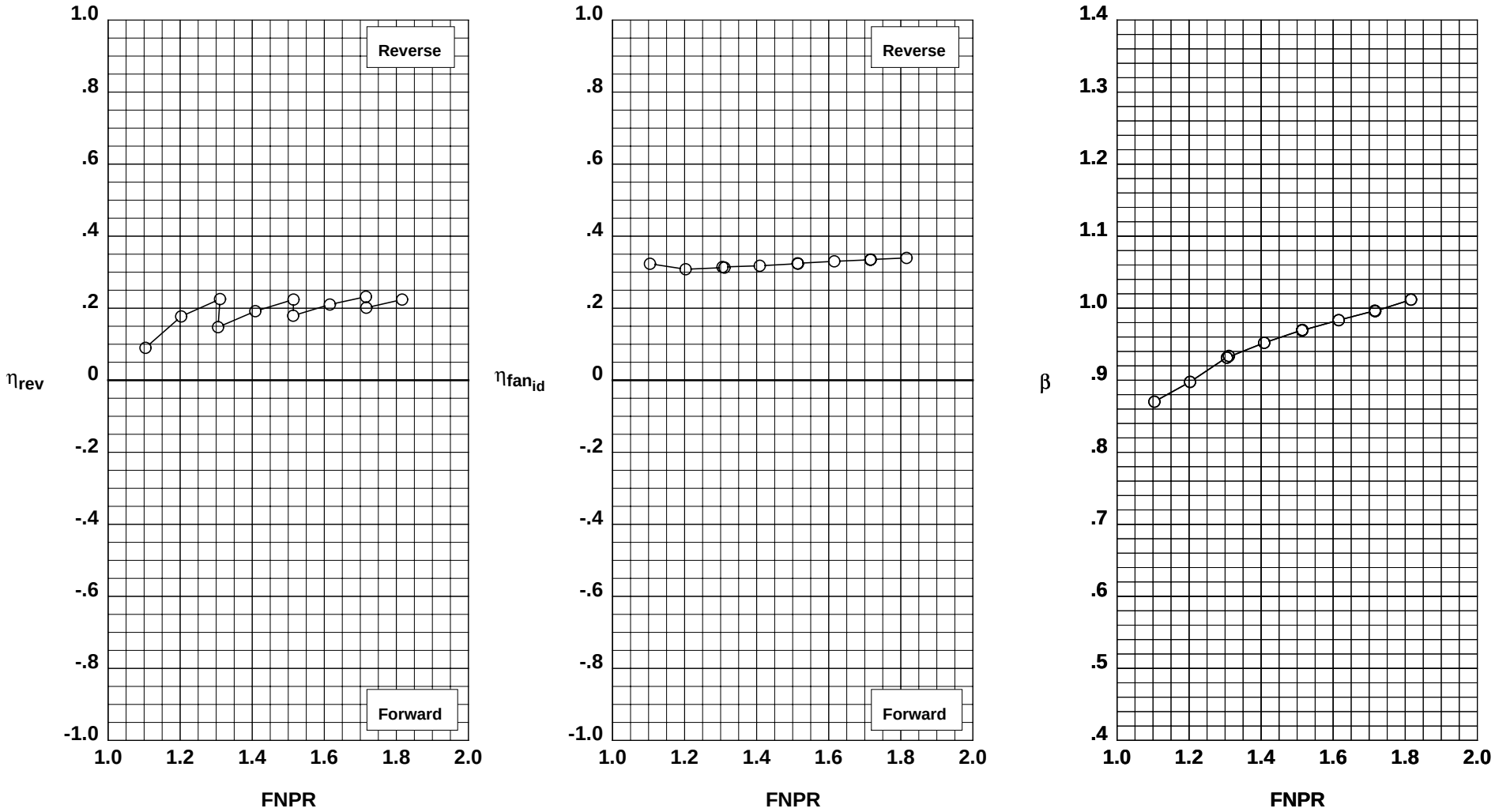

Figure G-85. Multi-door crocodile thrust reverser performance characteristics for configuration 577.

Operation Mode: Dual Flow
Reverser Port Bullnose: #3
Reverser Port Spacer: None
Reverser Port Cover: None
Bifurcator: Installed
Wing: Removed

	Test	Run	Configuration
○	1002	42	578

Outer Door Angle: 50°
Outer Door Cutback: None
Outer Door Kicker: Long/Cutback
Outer Door Fence: None
Inner Door Angle: 36°
Inner Door Fillers: All
Door Struts: No
Door Leakage: Partial

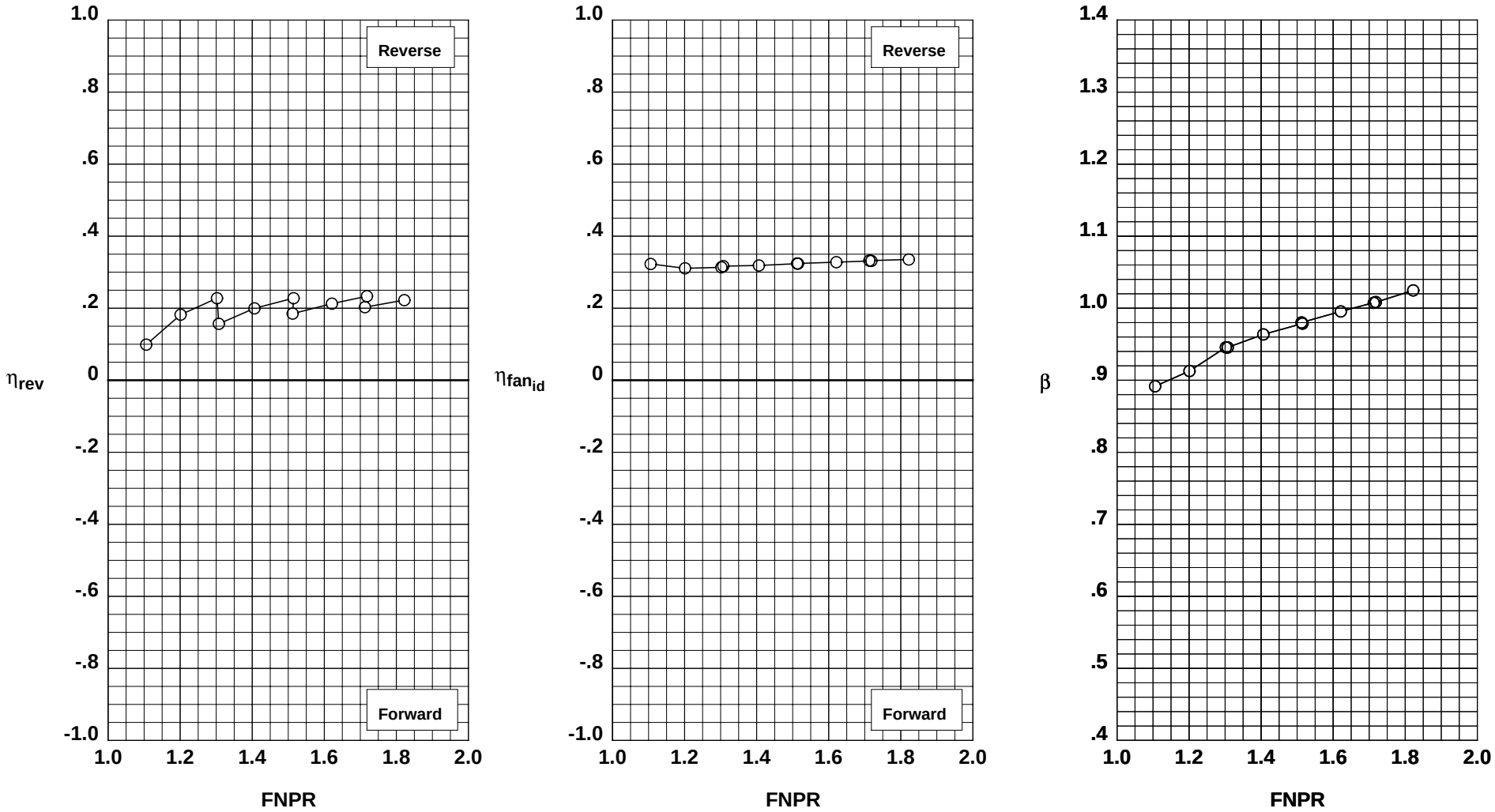

Figure G-86. Multi-door crocodile thrust reverser performance characteristics for configuration 578.

Operation Mode: Dual Flow
Reverser Port Bullnose: #3
Reverser Port Spacer: None
Reverser Port Cover: None
Bifurcator: Installed
Wing: Removed

	Test	Run	Configuration
○	1002	24	579

Outer Door Angle: 60°
Outer Door Cutback: None
Outer Door Kicker: Long/Cutback
Outer Door Fence: None
Inner Door Angle: 36°
Inner Door Fillers: All
Door Struts: No
Door Leakage: Partial

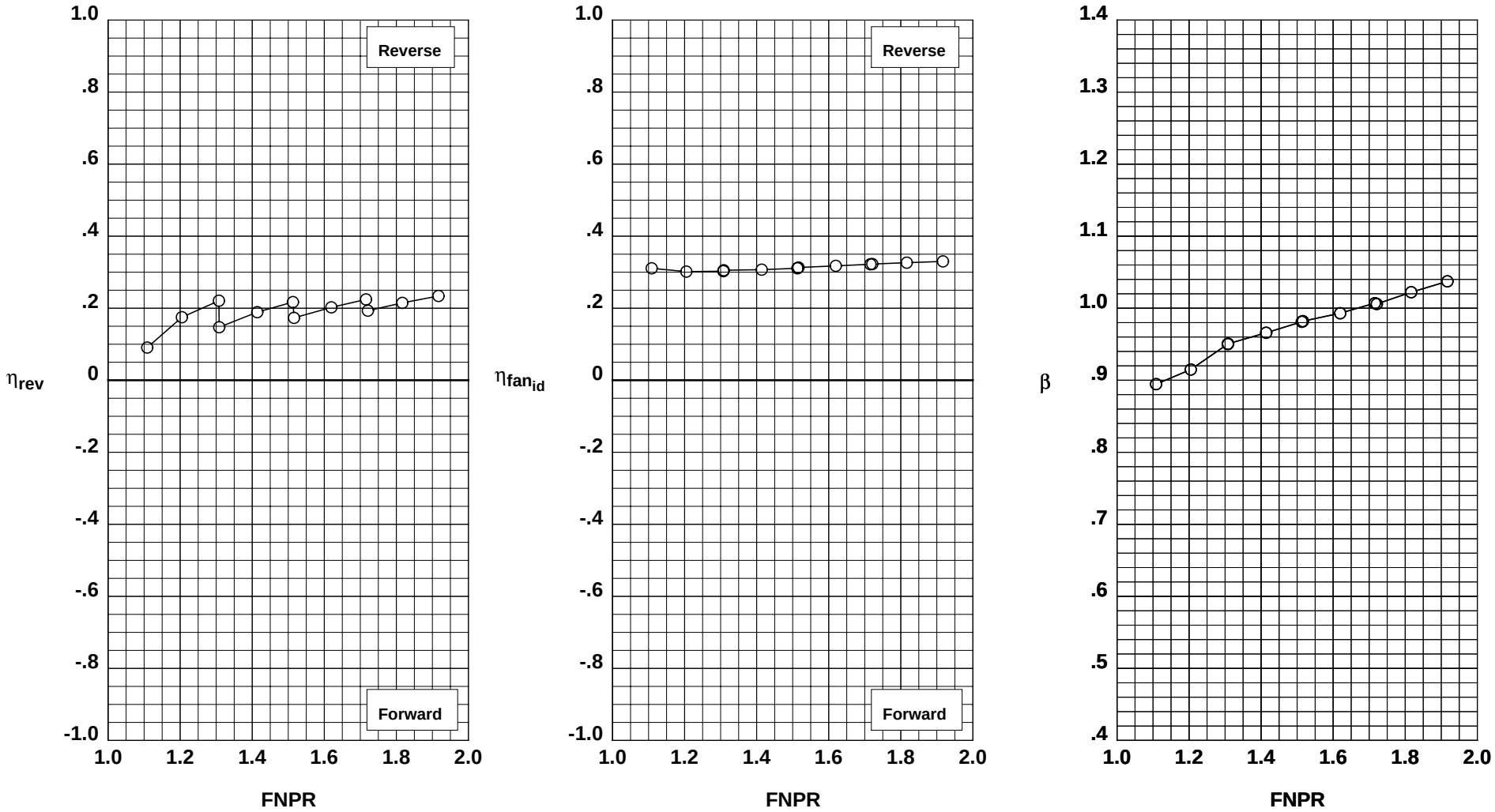

Figure G-87. Multi-door crocodile thrust reverser performance characteristics for configuration 579.

Operation Mode: Dual Flow
Reverser Port Bullnose: #3
Reverser Port Spacer: None
Reverser Port Cover: None
Bifurcator: Installed
Wing: Removed

	Test	Run	Configuration
○	1002	41	580

Outer Door Angle: 60°
Outer Door Cutback: None
Outer Door Kicker: Long/Cutback
Outer Door Fence: None
Inner Door Angle: 6°
Inner Door Fillers: All
Door Struts: No
Door Leakage: Partial

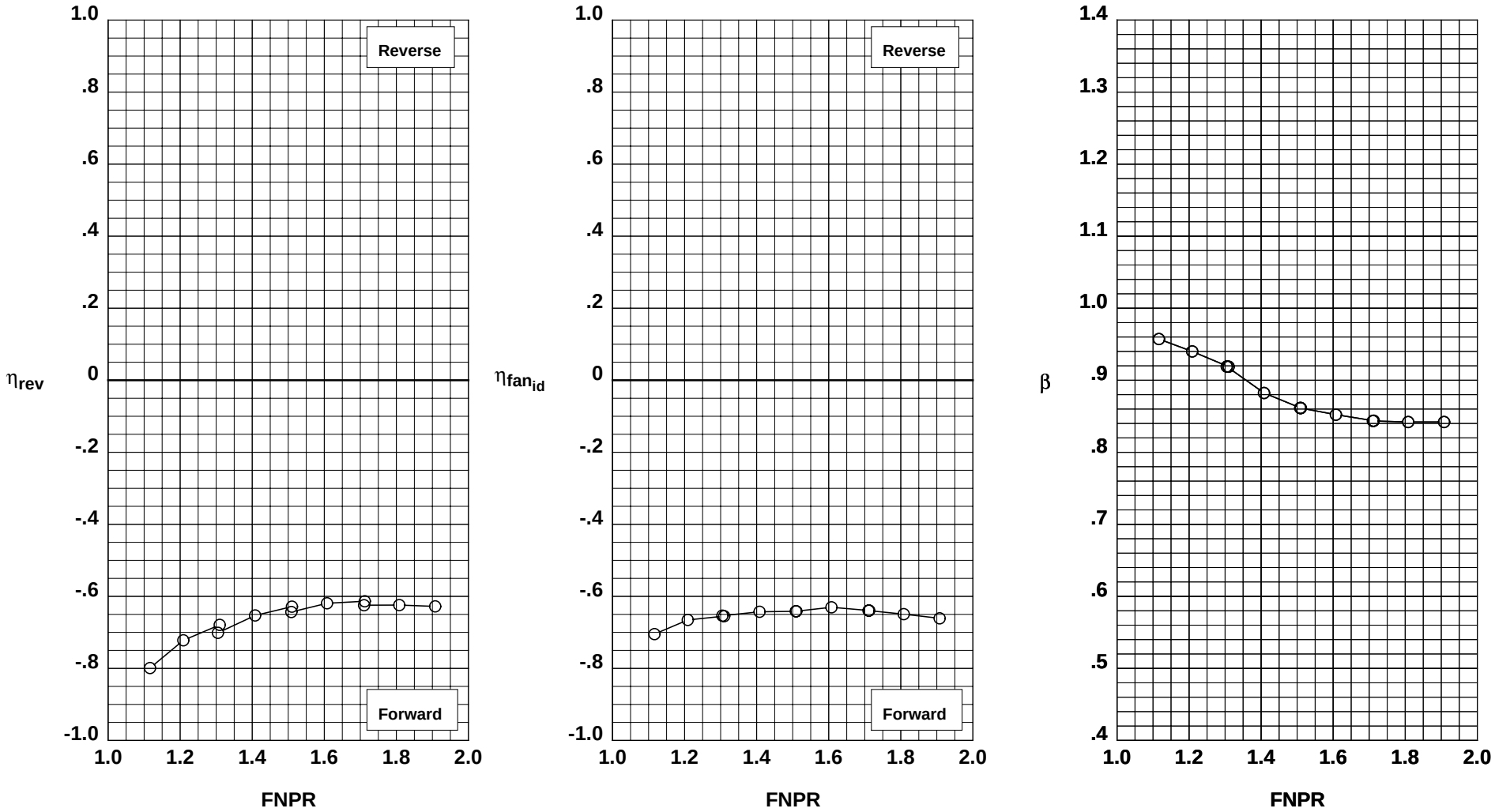

Figure G-88. Multi-door crocodile thrust reverser performance characteristics for configuration 580.

Operation Mode: Dual Flow
Reverser Port Bullnose: #3
Reverser Port Spacer: None
Reverser Port Cover: None
Bifurcator: Installed
Wing: Removed

	Test	Run	Configuration
○	1002	40	581

Outer Door Angle: 60°
Outer Door Cutback: None
Outer Door Kicker: Long/Cutback
Outer Door Fence: None
Inner Door Angle: 18°
Inner Door Fillers: All
Door Struts: No
Door Leakage: Partial

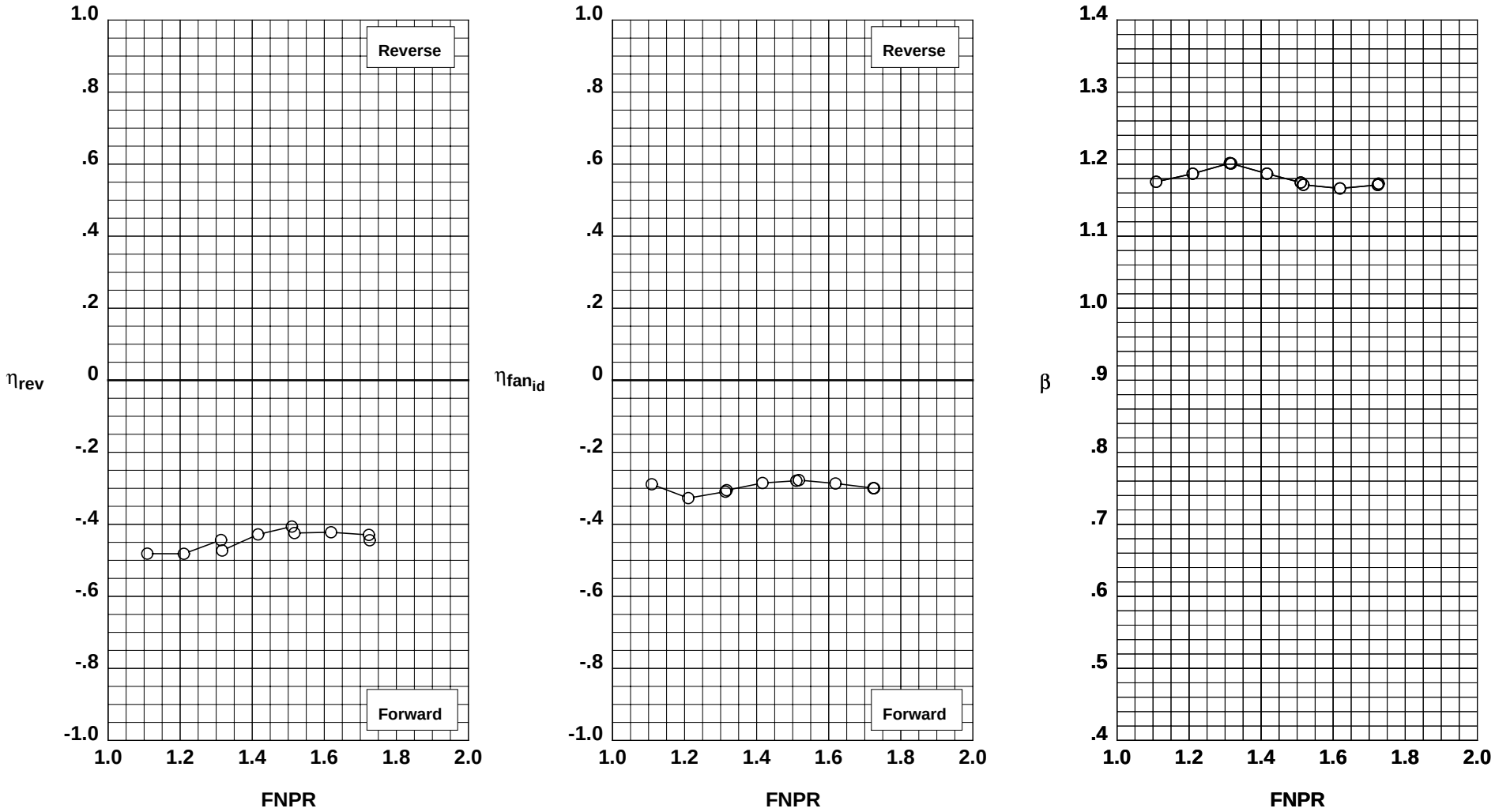

Figure G-89. Multi-door crocodile thrust reverser performance characteristics for configuration 581.

Operation Mode: Dual Flow
Reverser Port Bullnose: #3
Reverser Port Spacer: None
Reverser Port Cover: None
Bifurcator: Installed
Wing: Removed

	Test	Run	Configuration
○	1002	25	581

Outer Door Angle: 60°
Outer Door Cutback: None
Outer Door Kicker: Long/Cutback
Outer Door Fence: None
Inner Door Angle: 30°
Inner Door Fillers: All
Door Struts: No
Door Leakage: Partial

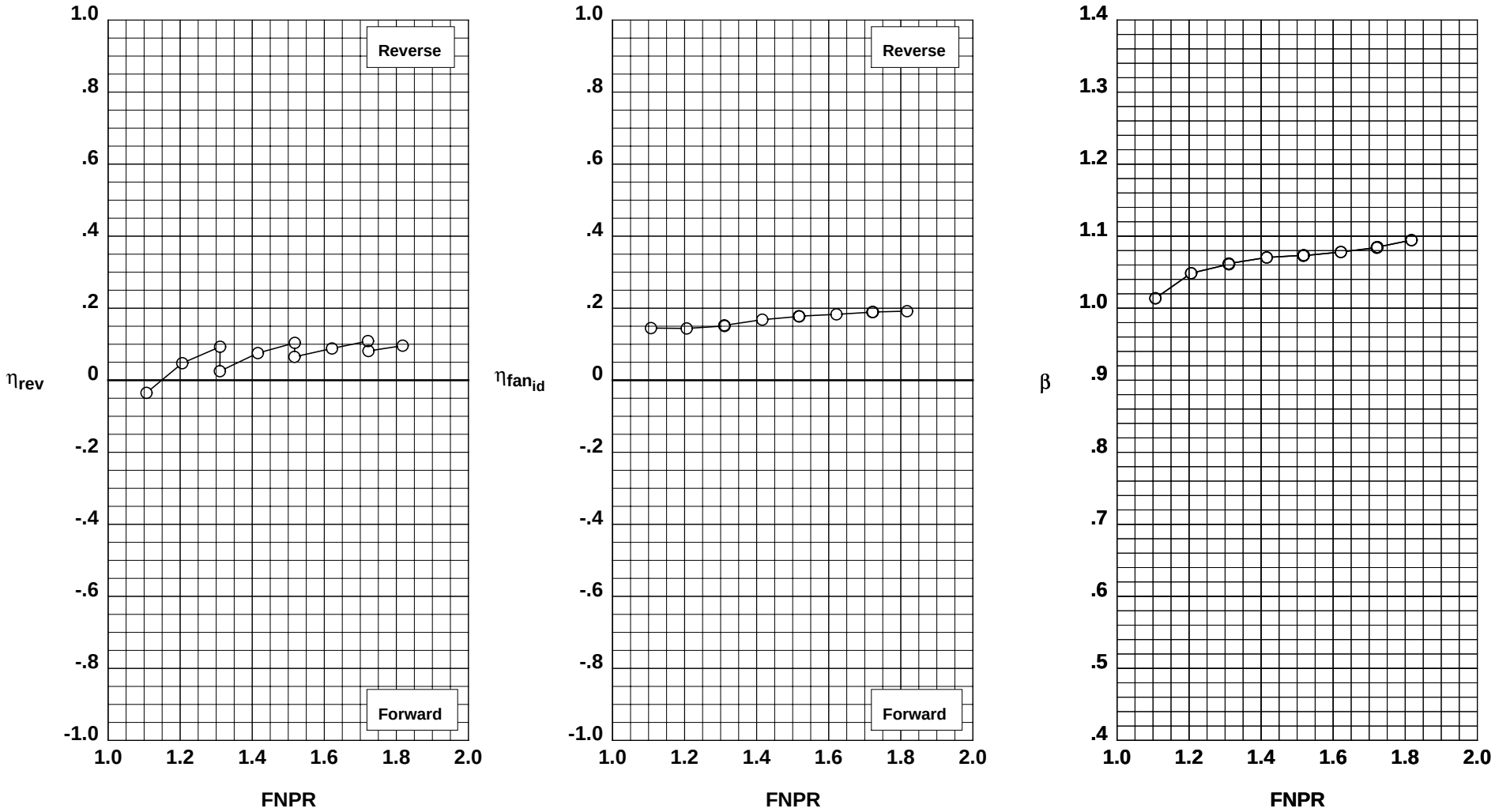

Figure G-90. Multi-door crocodile thrust reverser performance characteristics for configuration 581.

Operation Mode: Dual Flow
Deflector Mount Position: Parallel
Deflector Chord Lengths: Long/Long/Long
Deflector Angles: 45°/-30°/15°
Deflector Fences: Installed
Ground Plane: Removed

	Test	Run	Configuration
○	1001	47	701

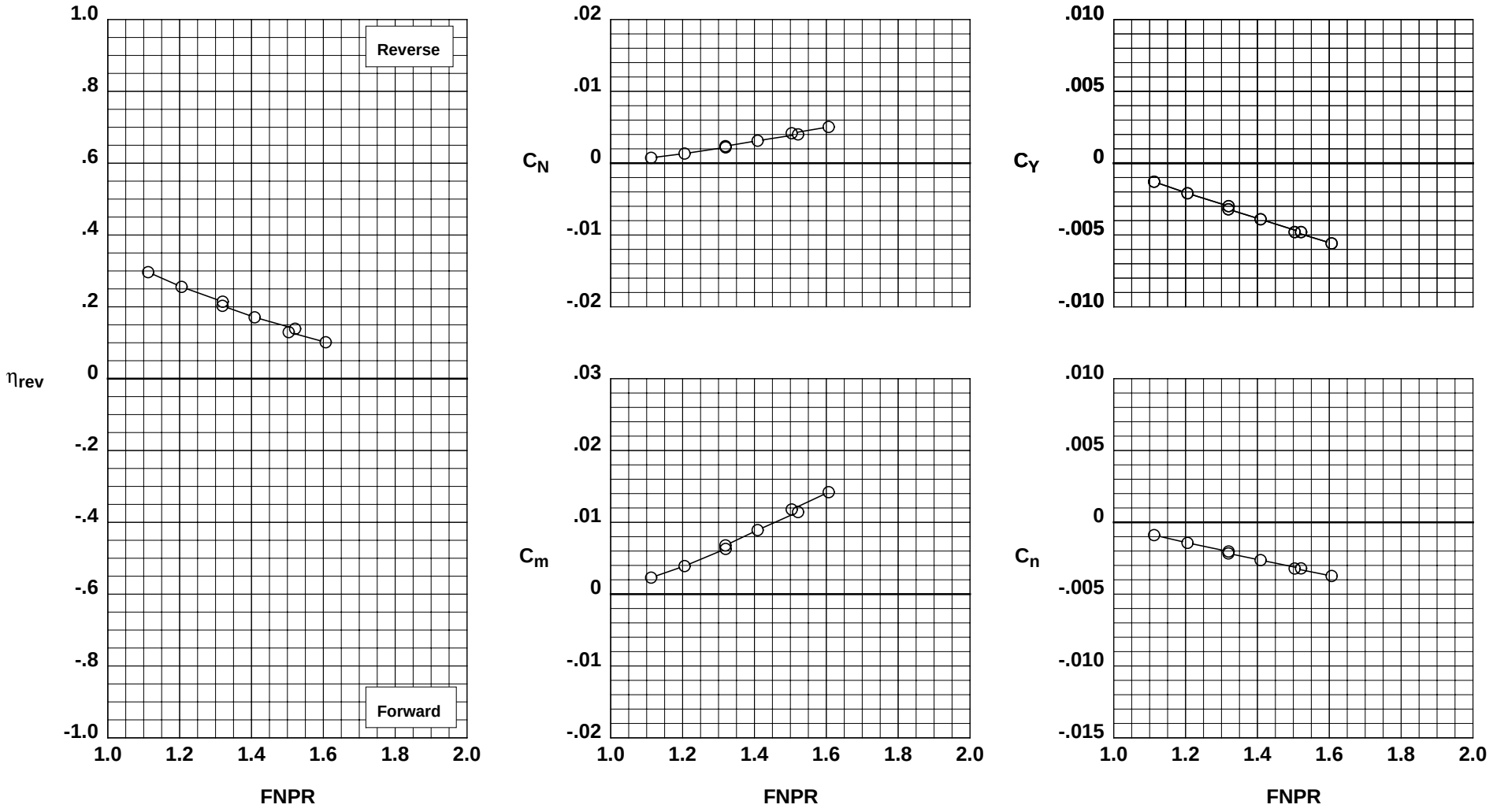

Figure H-1. Wing-mounted thrust reverser performance characteristics for configuration 701.

Operation Mode: Dual Flow
Deflector Mount Position: Parallel
Deflector Chord Lengths: Long/Long/Long
Deflector Angles: 45°/-30°/30°
Deflector Fences: Installed
Ground Plane: Removed

	Test	Run	Configuration
○	1001	48	702

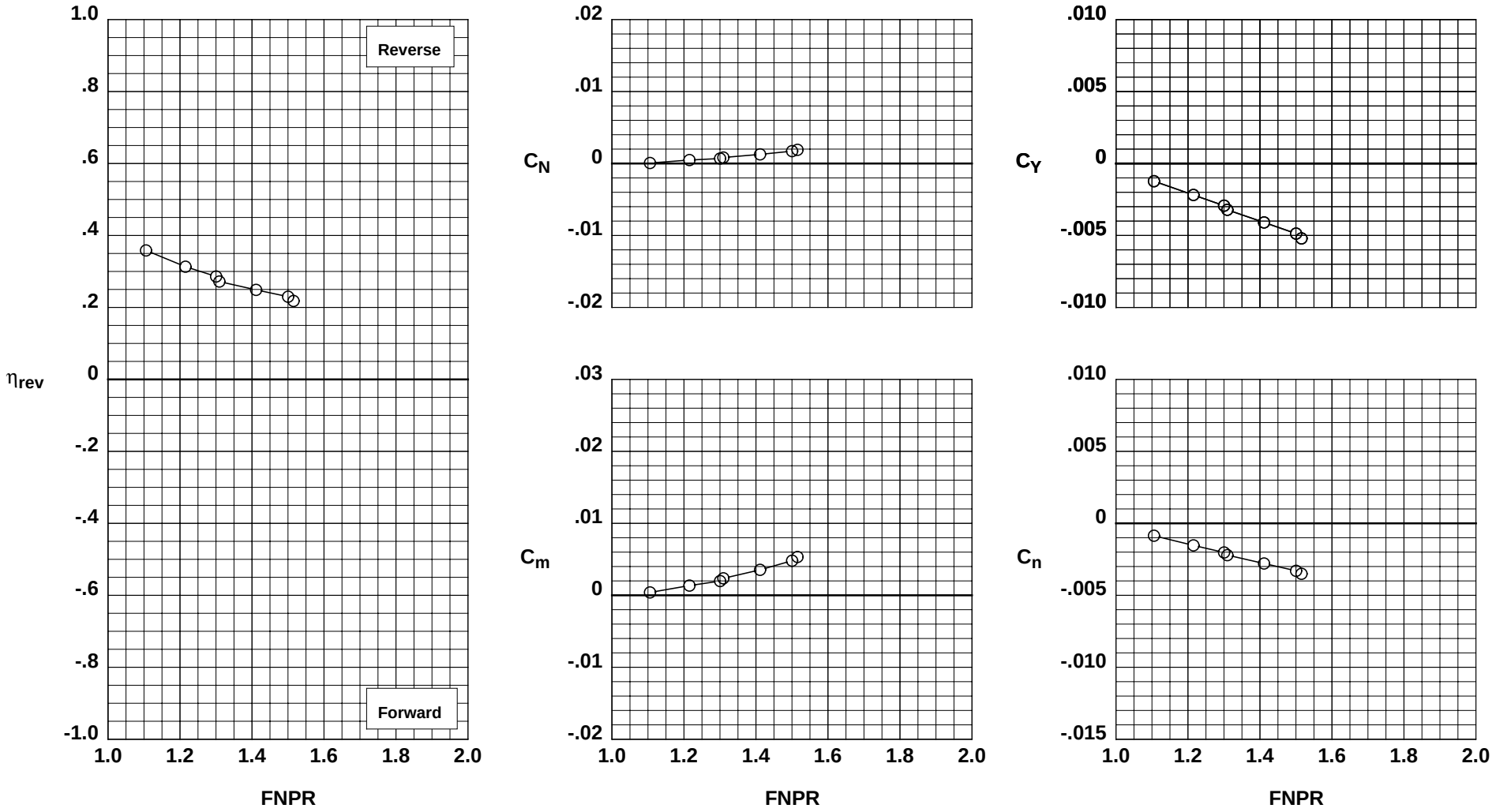

Figure H-2. Wing-mounted thrust reverser performance characteristics for configuration 702.

Operation Mode: Dual Flow
Deflector Mount Position: Parallel
Deflector Chord Lengths: Long/Long/Long
Deflector Angles: 45°/-30°/45°
Deflector Fences: Installed
Ground Plane: Removed

	Test	Run	Configuration
○	1001	49	703

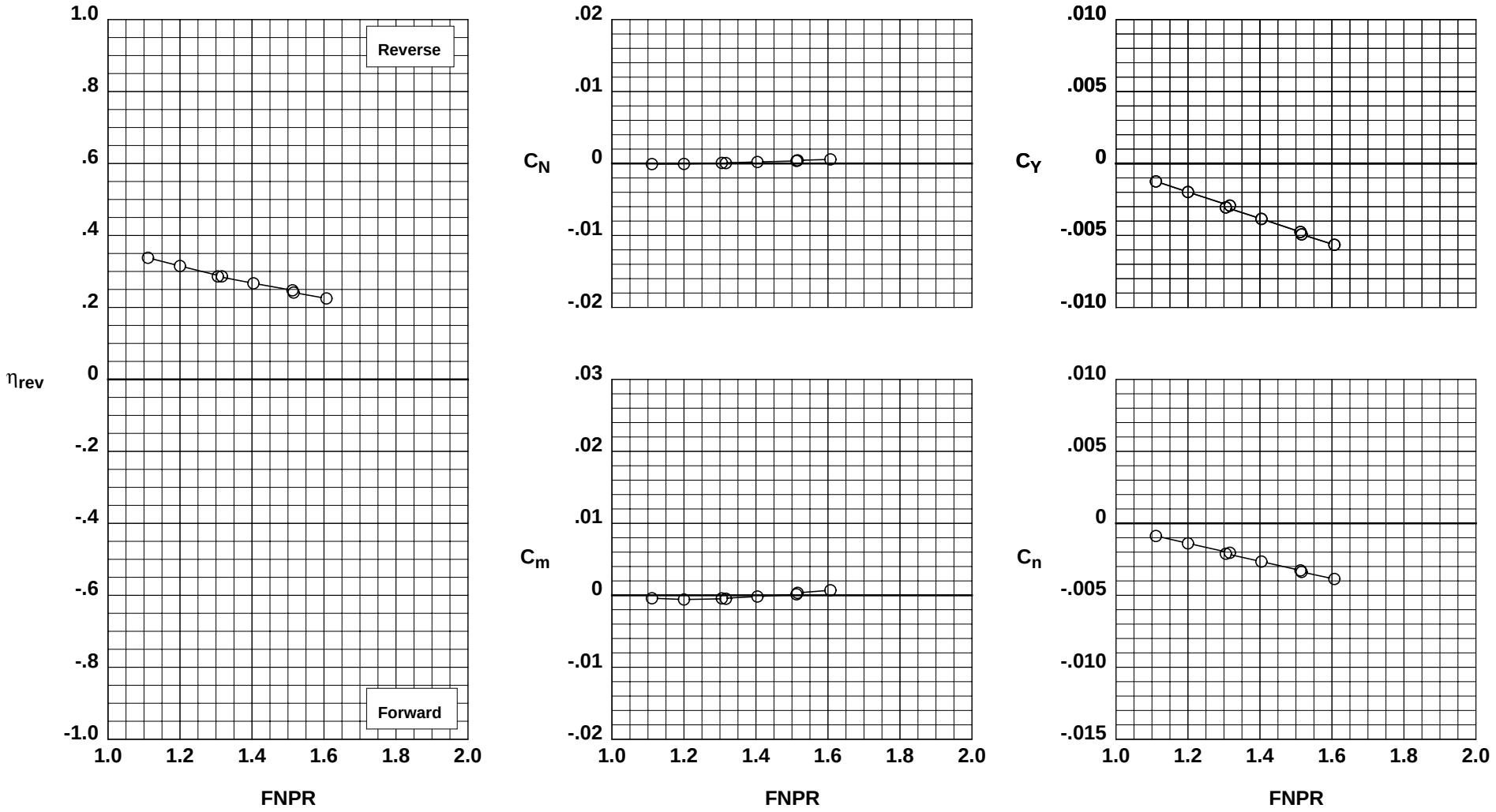

Figure H-3. Wing-mounted thrust reverser performance characteristics for configuration 703.

Operation Mode: Dual Flow
Deflector Mount Position: Parallel
Deflector Chord Lengths: Long/Long/Long
Deflector Angles: 60°/-30°/45°
Deflector Fences: Installed
Ground Plane: Removed

	Test	Run	Configuration
○	1001	50	704

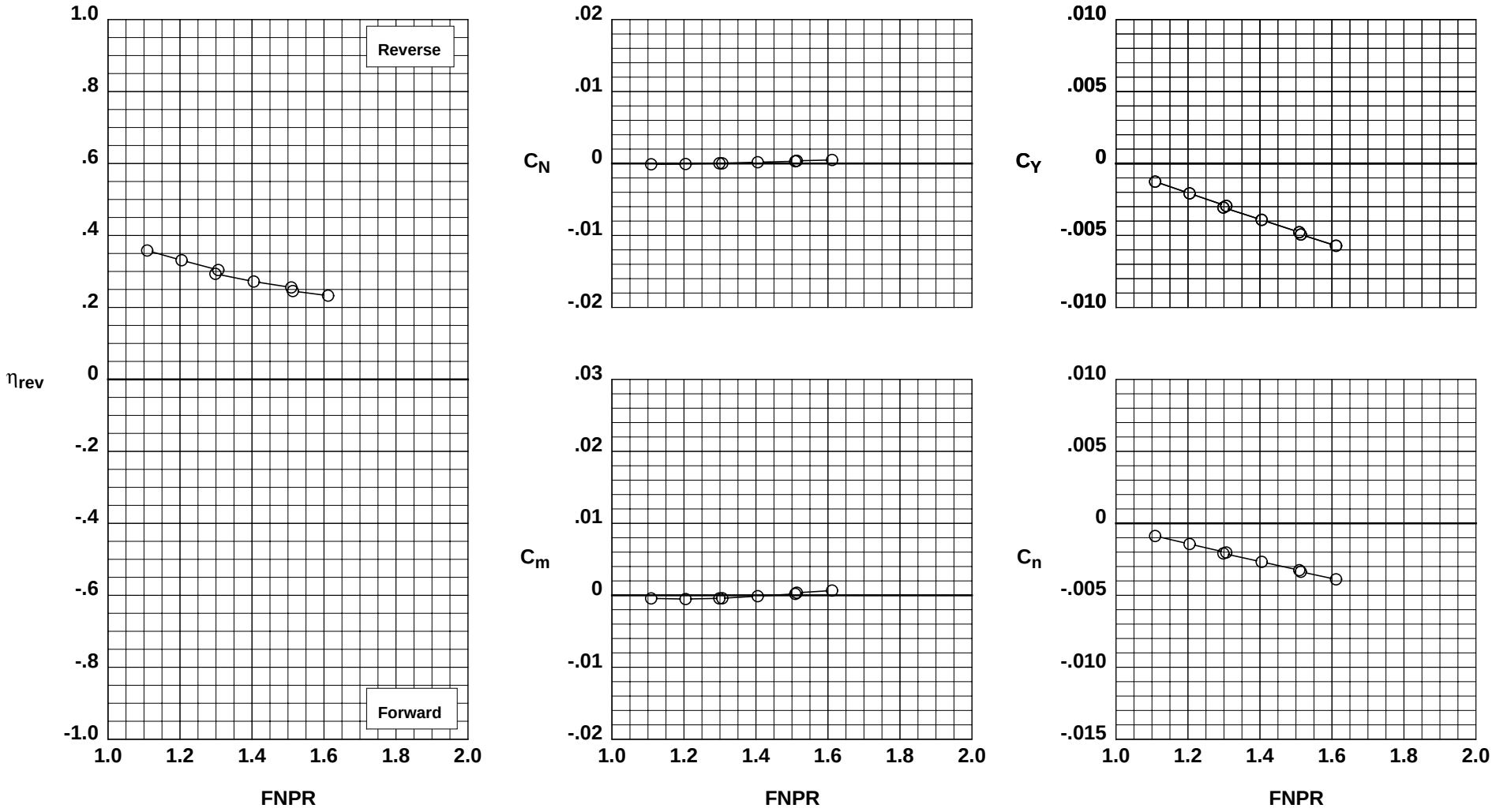

Figure H-4. Wing-mounted thrust reverser performance characteristics for configuration 704.

Operation Mode: Dual Flow
Deflector Mount Position: Parallel
Deflector Chord Lengths: Long/Long/Long
Deflector Angles: 30°/-15°/15°
Deflector Fences: Installed
Ground Plane: Removed

	Test	Run	Configuration
○	1001	46	705

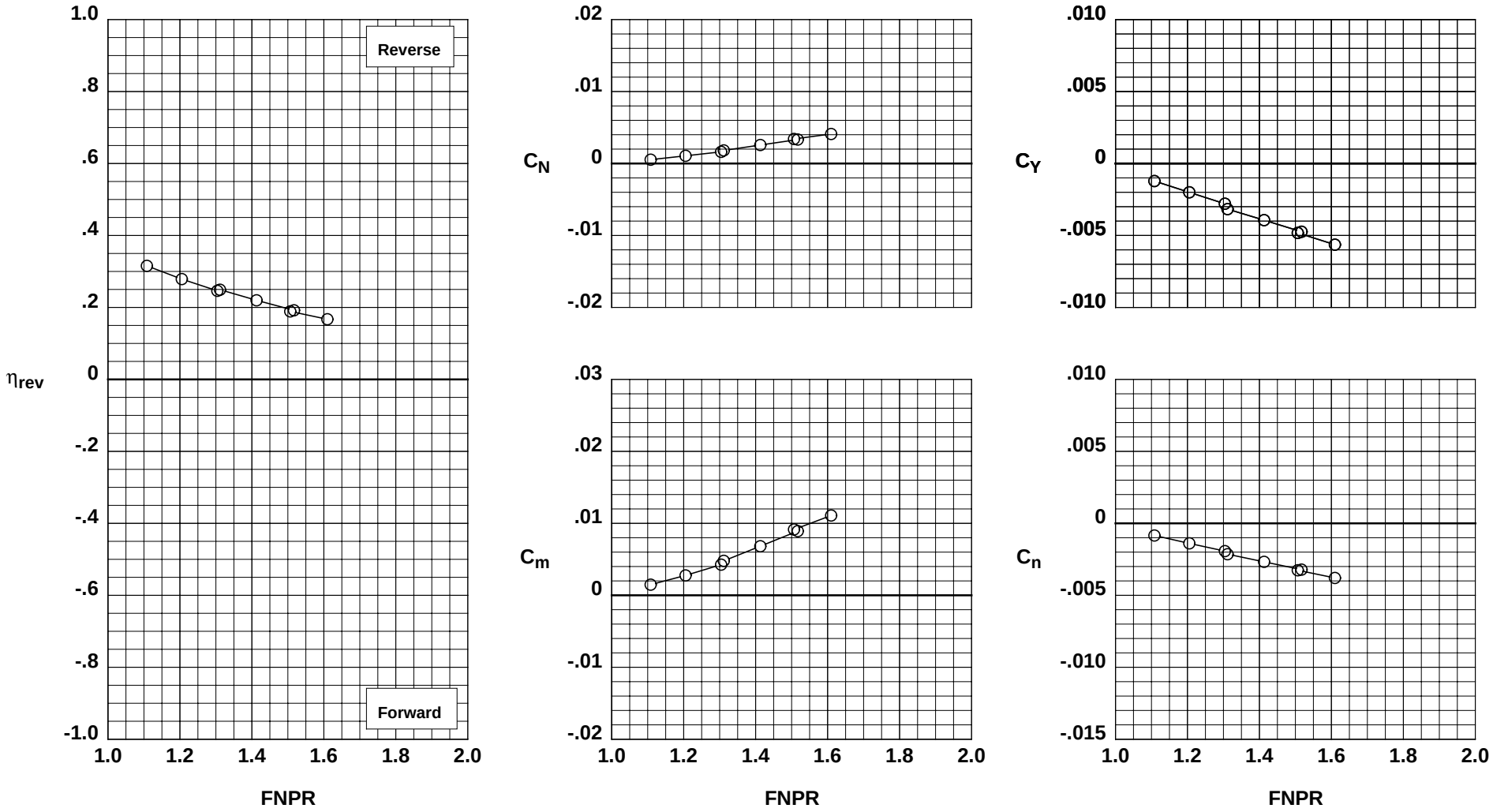

Figure H-5. Wing-mounted thrust reverser performance characteristics for configuration 705.

Operation Mode: Dual Flow
Deflector Mount Position: Parallel
Deflector Chord Lengths: Long/Long/Long
Deflector Angles: 30°/-15°/30°
Deflector Fences: Installed
Ground Plane: Removed

	Test	Run	Configuration
○	1001	38	706

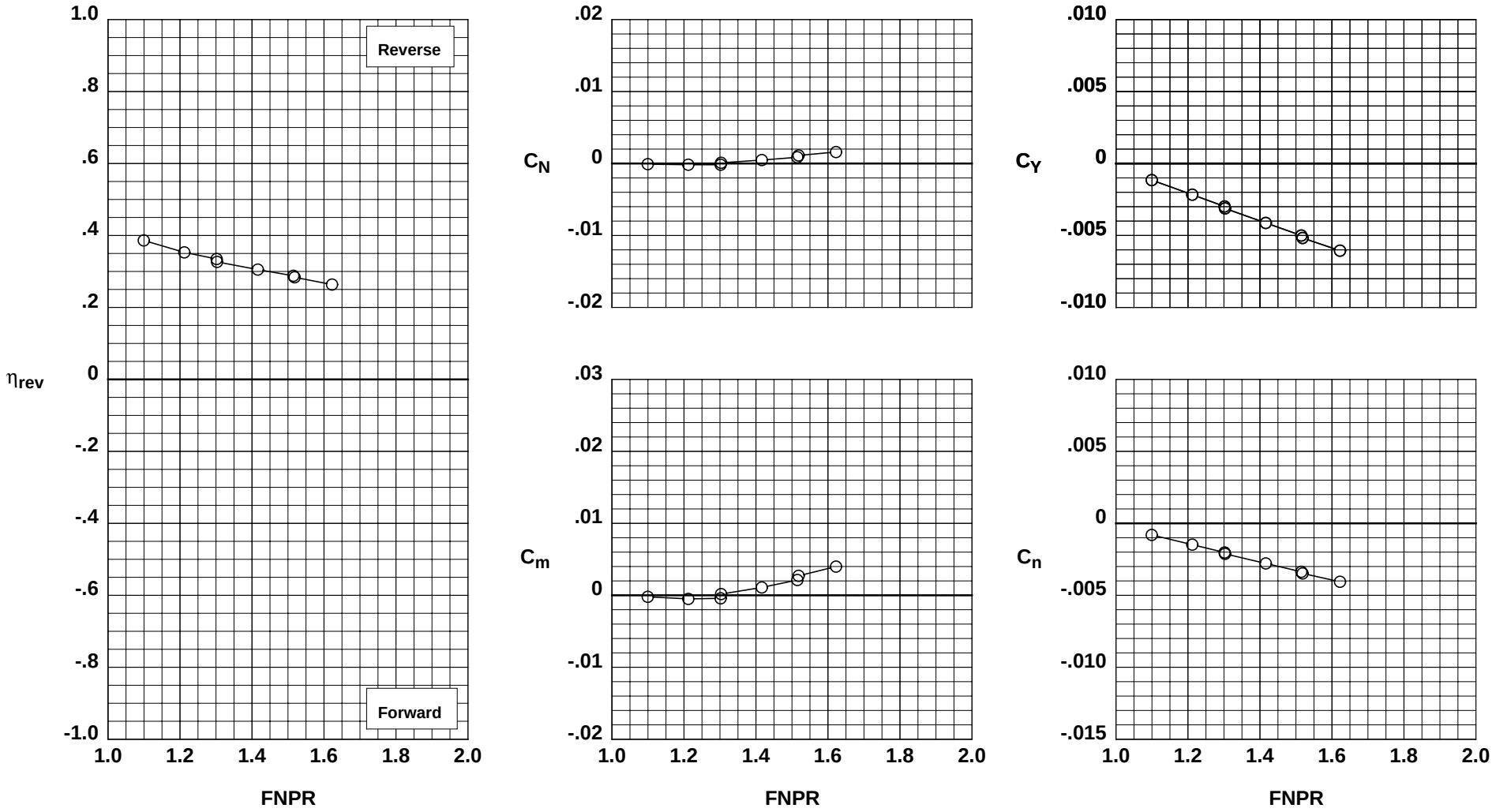

Figure H-6. Wing-mounted thrust reverser performance characteristics for configuration 706.

Operation Mode: Dual Flow
Deflector Mount Position: Parallel
Deflector Chord Lengths: Long/Long/Long
Deflector Angles: 30°/-15°/45°
Deflector Fences: Installed
Ground Plane: Removed

	Test	Run	Configuration
○	1001	45	707

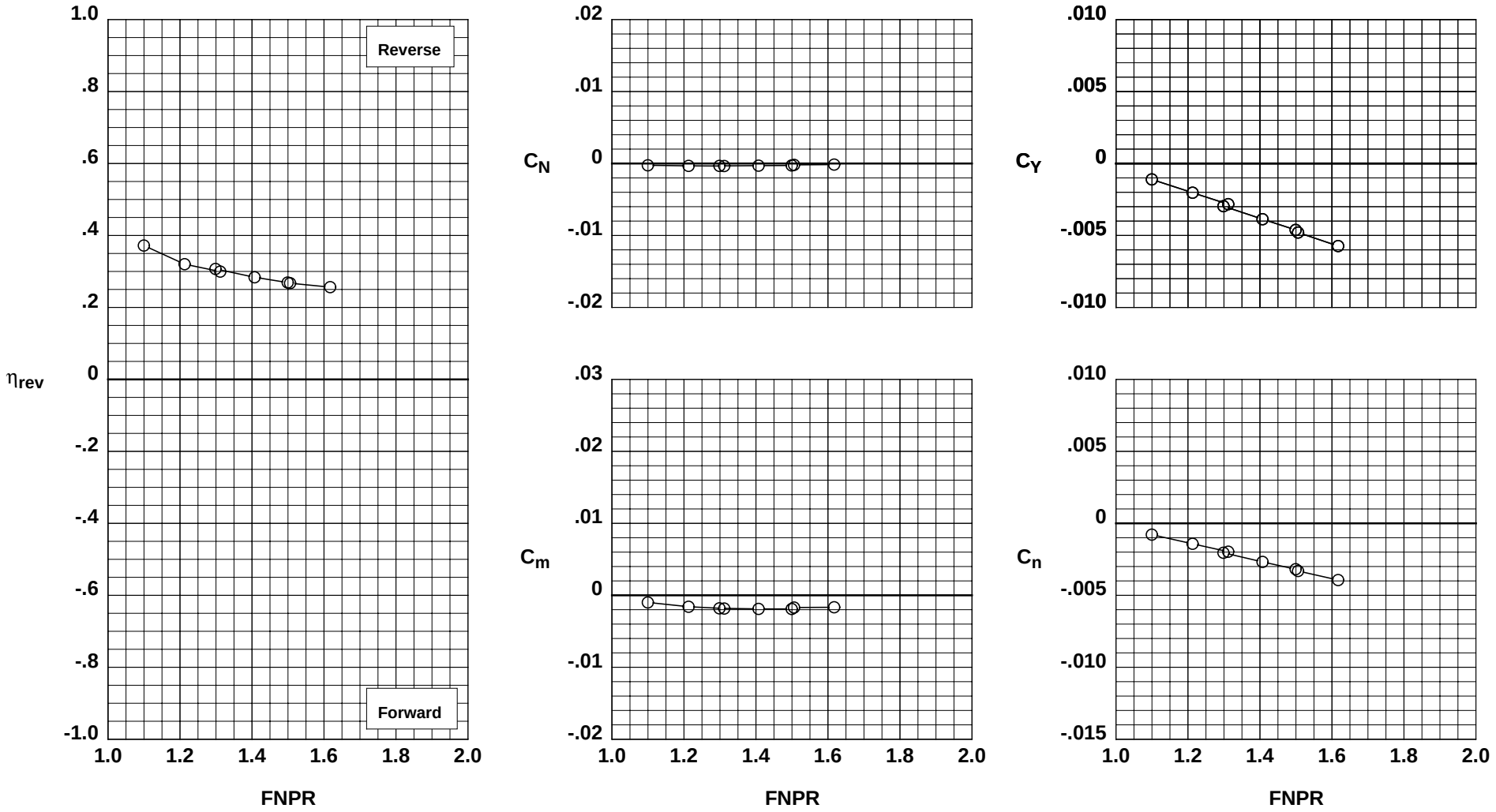

Figure H-7. Wing-mounted thrust reverser performance characteristics for configuration 707.

Operation Mode: Dual Flow
Deflector Mount Position: Parallel
Deflector Chord Lengths: Long/Long/Long
Deflector Angles: 45°/-15°/15°
Deflector Fences: Installed
Ground Plane: Removed

	Test	Run	Configuration
○	1001	42	708

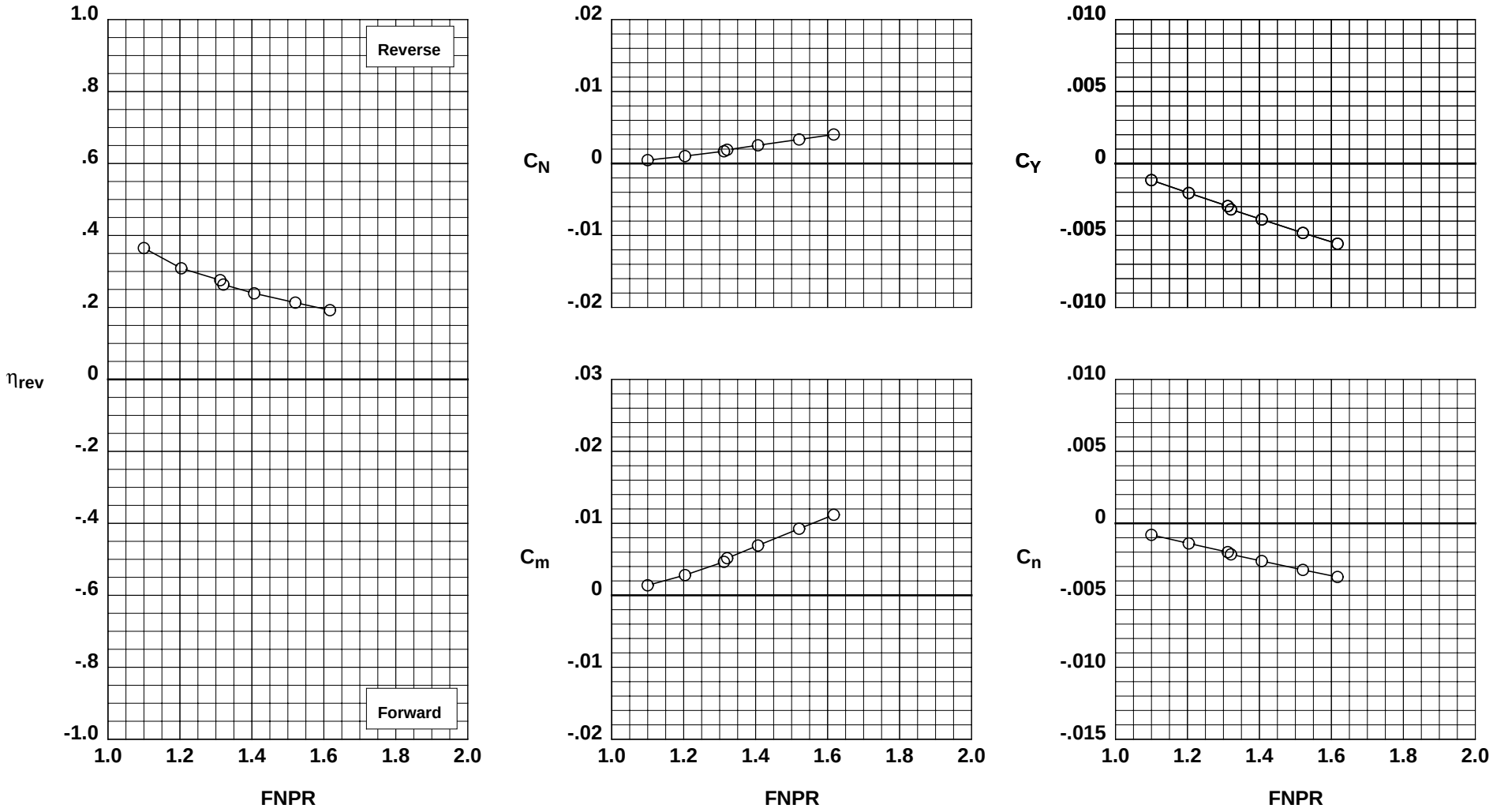

Figure H-8. Wing-mounted thrust reverser performance characteristics for configuration 708.

Operation Mode: Dual Flow
Deflector Mount Position: Parallel
Deflector Chord Lengths: Long/Long/Long
Deflector Angles: 45°/-15°/30°
Deflector Fences: Installed
Ground Plane: Removed

	Test	Run	Configuration
○	1001	43	709

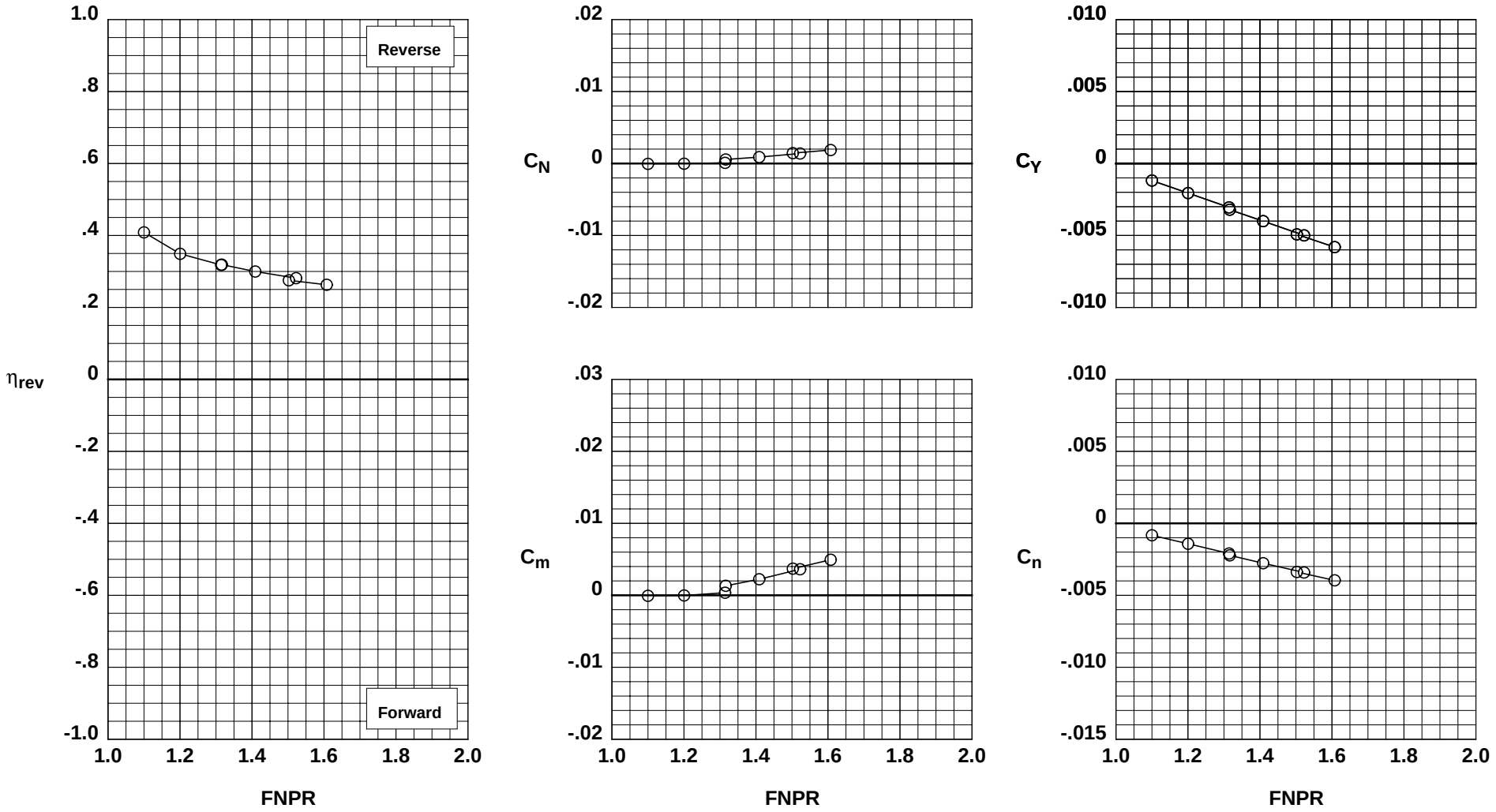

Figure H-9. Wing-mounted thrust reverser performance characteristics for configuration 709.

Operation Mode: Dual Flow
Deflector Mount Position: Parallel
Deflector Chord Lengths: Long/Long/Long
Deflector Angles: 45°/-15°/45°
Deflector Fences: Installed
Ground Plane: Removed

	Test	Run	Configuration
○	1001	44	710

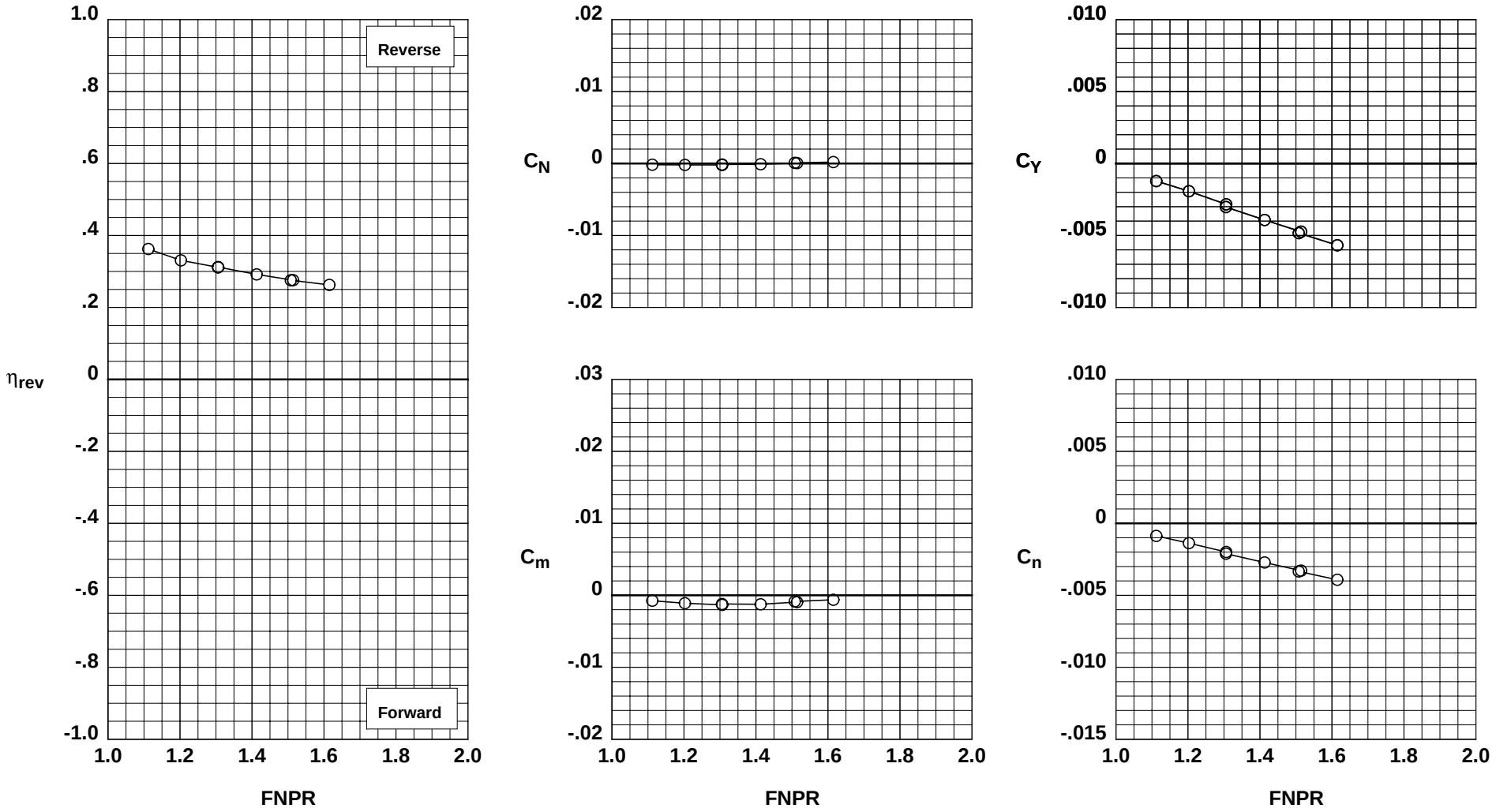

Figure H-10. Wing-mounted thrust reverser performance characteristics for configuration 710.

Operation Mode: Dual Flow
Deflector Mount Position: Parallel
Deflector Chord Lengths: Long/Long/Long
Deflector Angles: 60°/-15°/15°
Deflector Fences: Installed
Ground Plane: Removed

	Test	Run	Configuration
○	1001	41	711

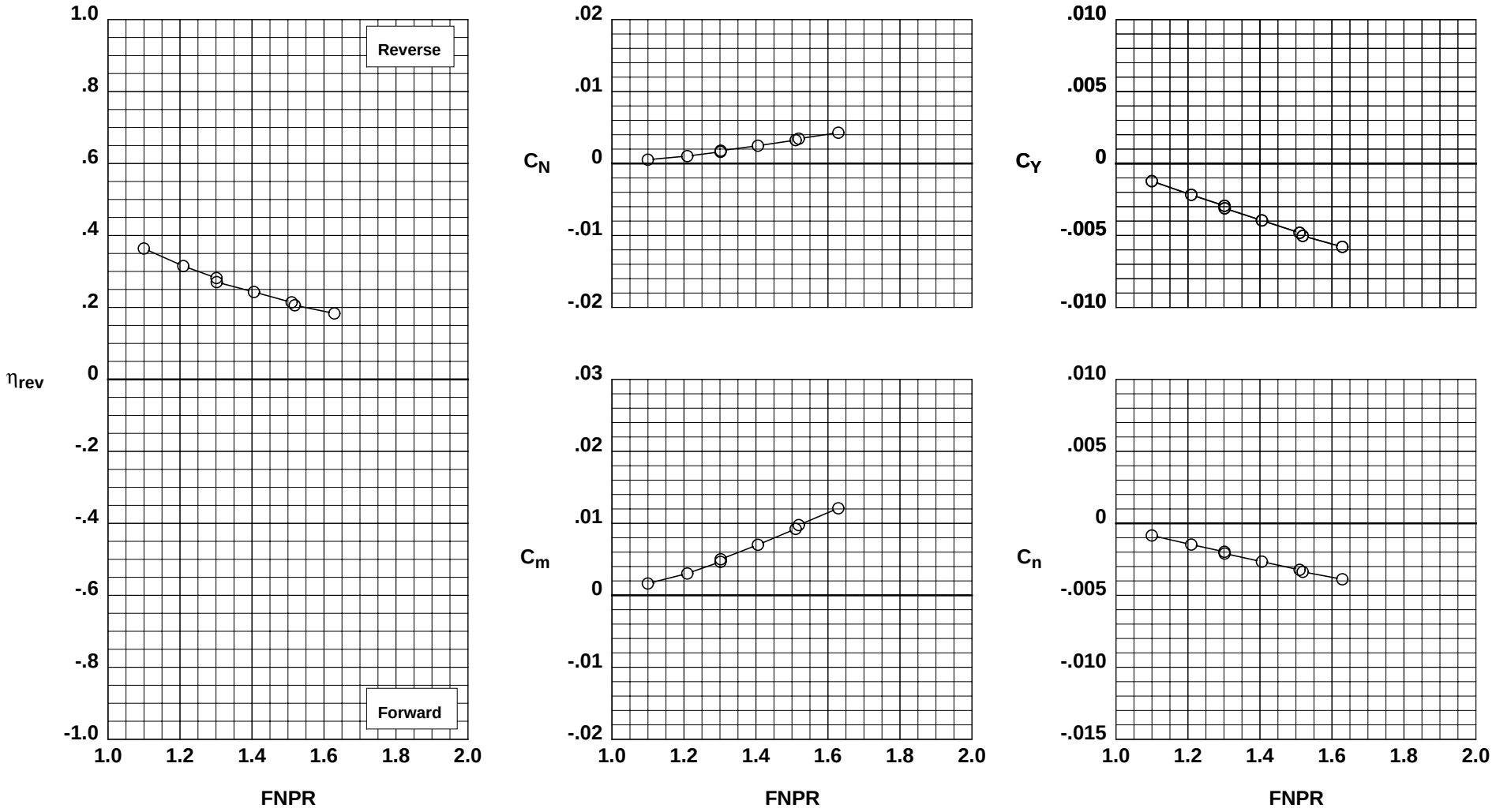

Figure H-11. Wing-mounted thrust reverser performance characteristics for configuration 711.

Operation Mode: Dual Flow
Deflector Mount Position: Parallel
Deflector Chord Lengths: Long/Long/Long
Deflector Angles: 60°/-15°/30°
Deflector Fences: Installed
Ground Plane: Removed

	Test	Run	Configuration
○	1001	39	712

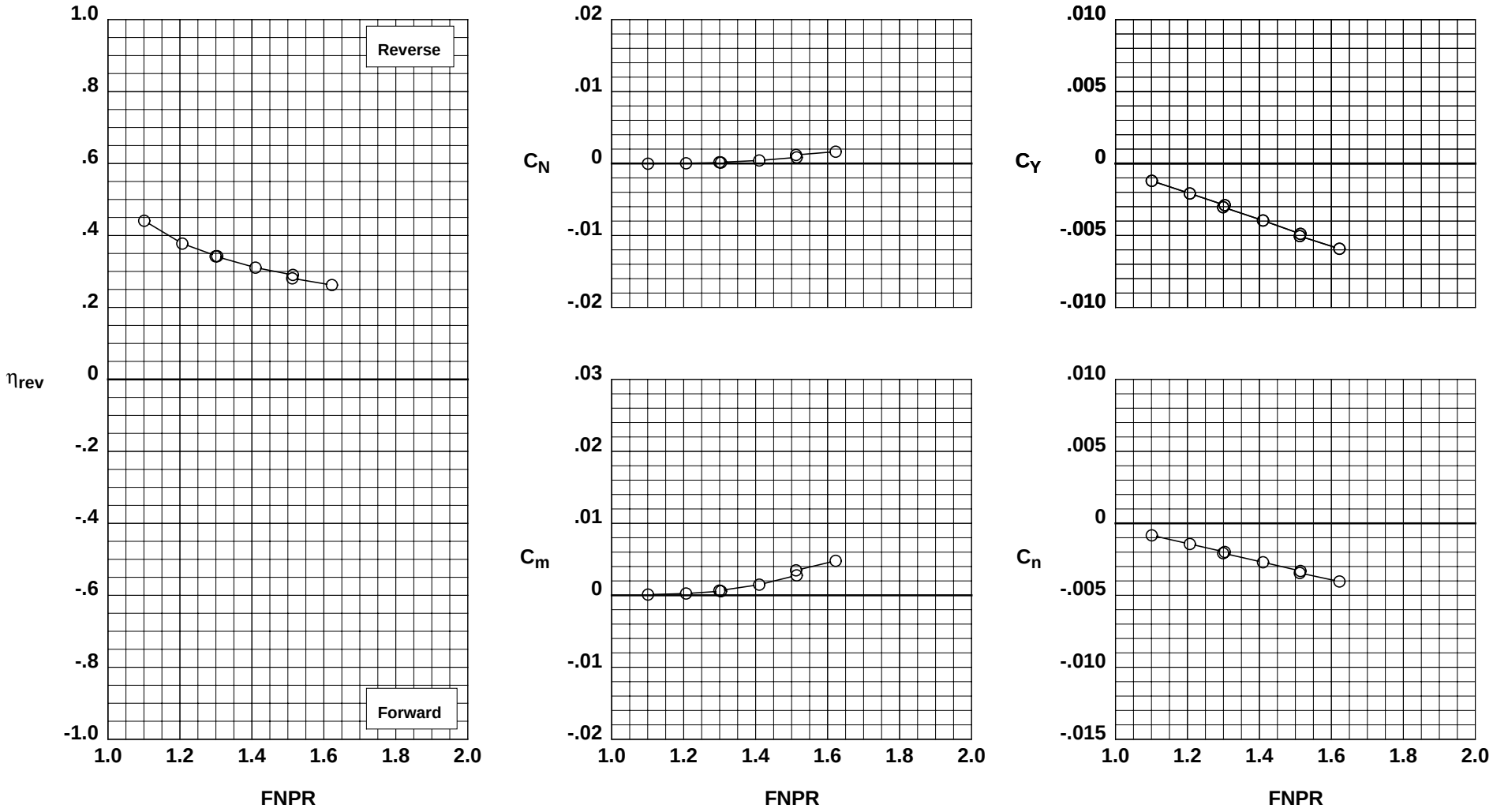

Figure H-12. Wing-mounted thrust reverser performance characteristics for configuration 712.

Operation Mode: Dual Flow
Deflector Mount Position: Parallel
Deflector Chord Lengths: Long/Long/Long
Deflector Angles: 60°/-15°/45°
Deflector Fences: Installed
Ground Plane: Removed

	Test	Run	Configuration
○	1001	40	713

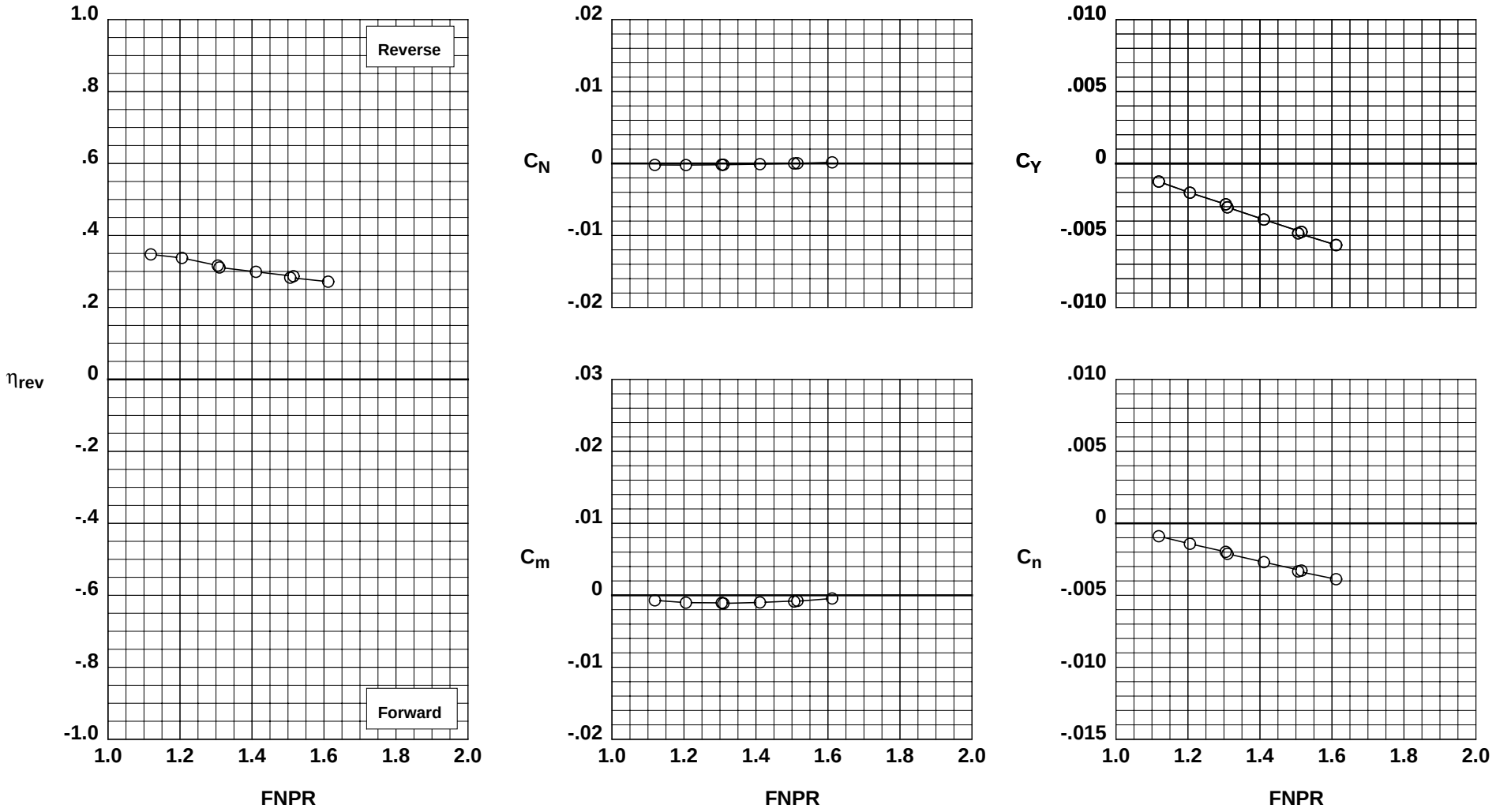

Figure H-13. Wing-mounted thrust reverser performance characteristics for configuration 713.

Operation Mode: Dual Flow
Deflector Mount Position: Parallel
Deflector Chord Lengths: Long/Long/Long
Deflector Angles: 30°/ 0°/30°
Deflector Fences: Installed
Ground Plane: Removed

	Test	Run	Configuration
○	1001	31	714

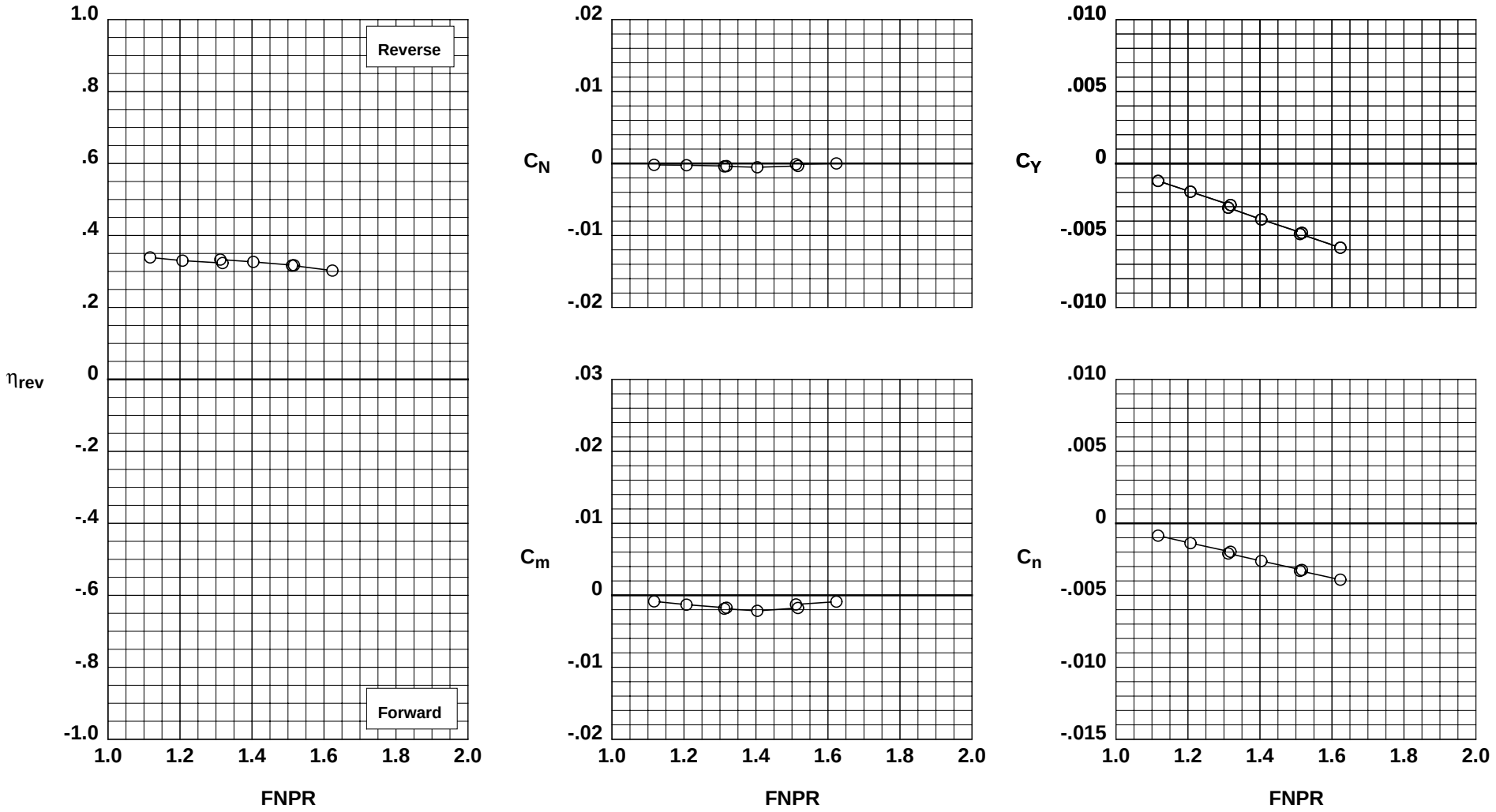

Figure H-14. Wing-mounted thrust reverser performance characteristics for configuration 714.

Operation Mode: Dual Flow
Deflector Mount Position: Parallel
Deflector Chord Lengths: Long/Long/Long
Deflector Angles: 30°/ 0°/45°
Deflector Fences: Installed
Ground Plane: Removed

	Test	Run	Configuration
○	1001	32	715

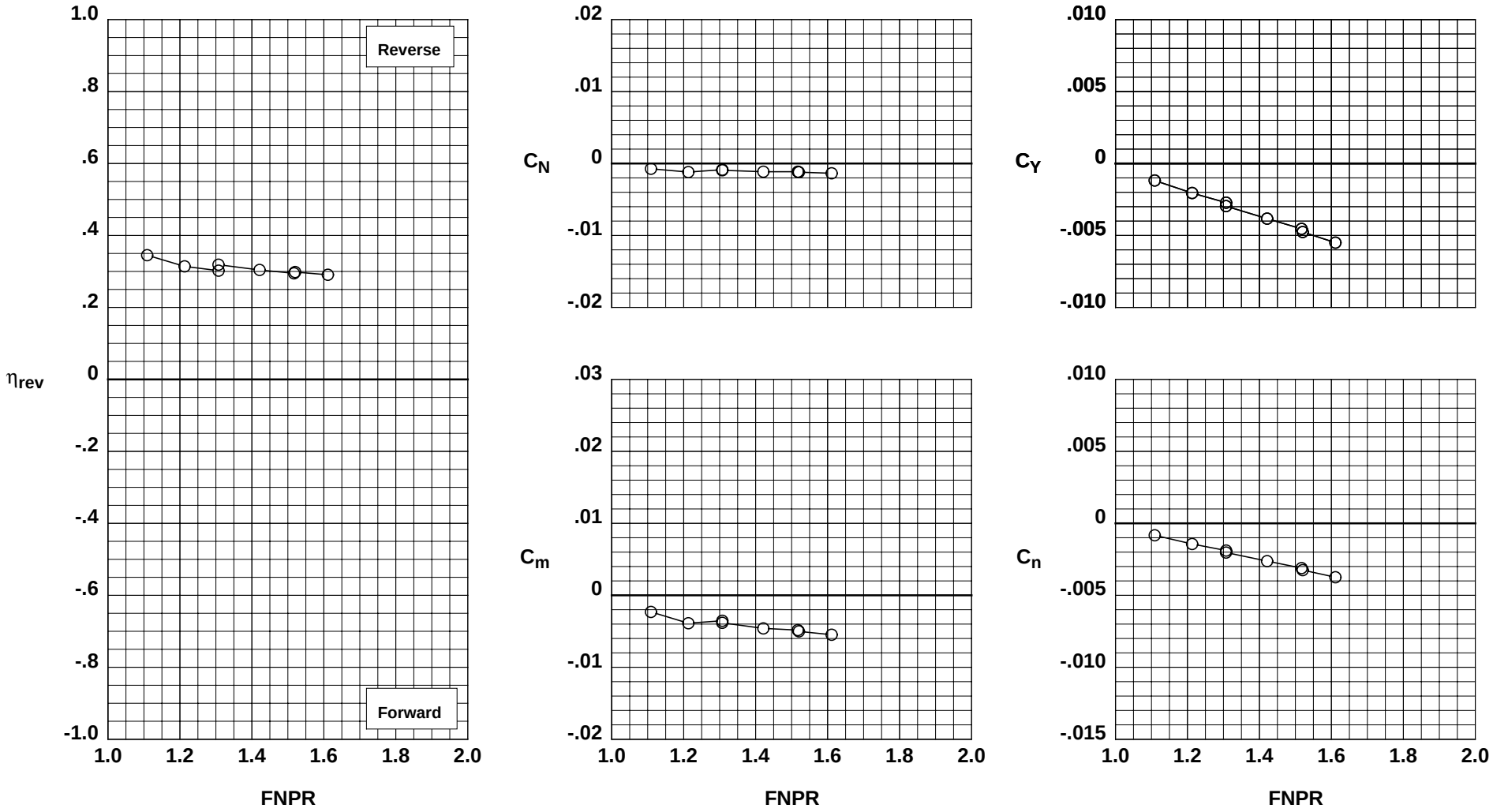

Figure H-15. Wing-mounted thrust reverser performance characteristics for configuration 715.

Operation Mode: Dual Flow
Deflector Mount Position: Parallel
Deflector Chord Lengths: Long/Long/Long
Deflector Angles: 30°/ 0°/60°
Deflector Fences: Installed
Ground Plane: Removed

	Test	Run	Configuration
○	1001	33	716

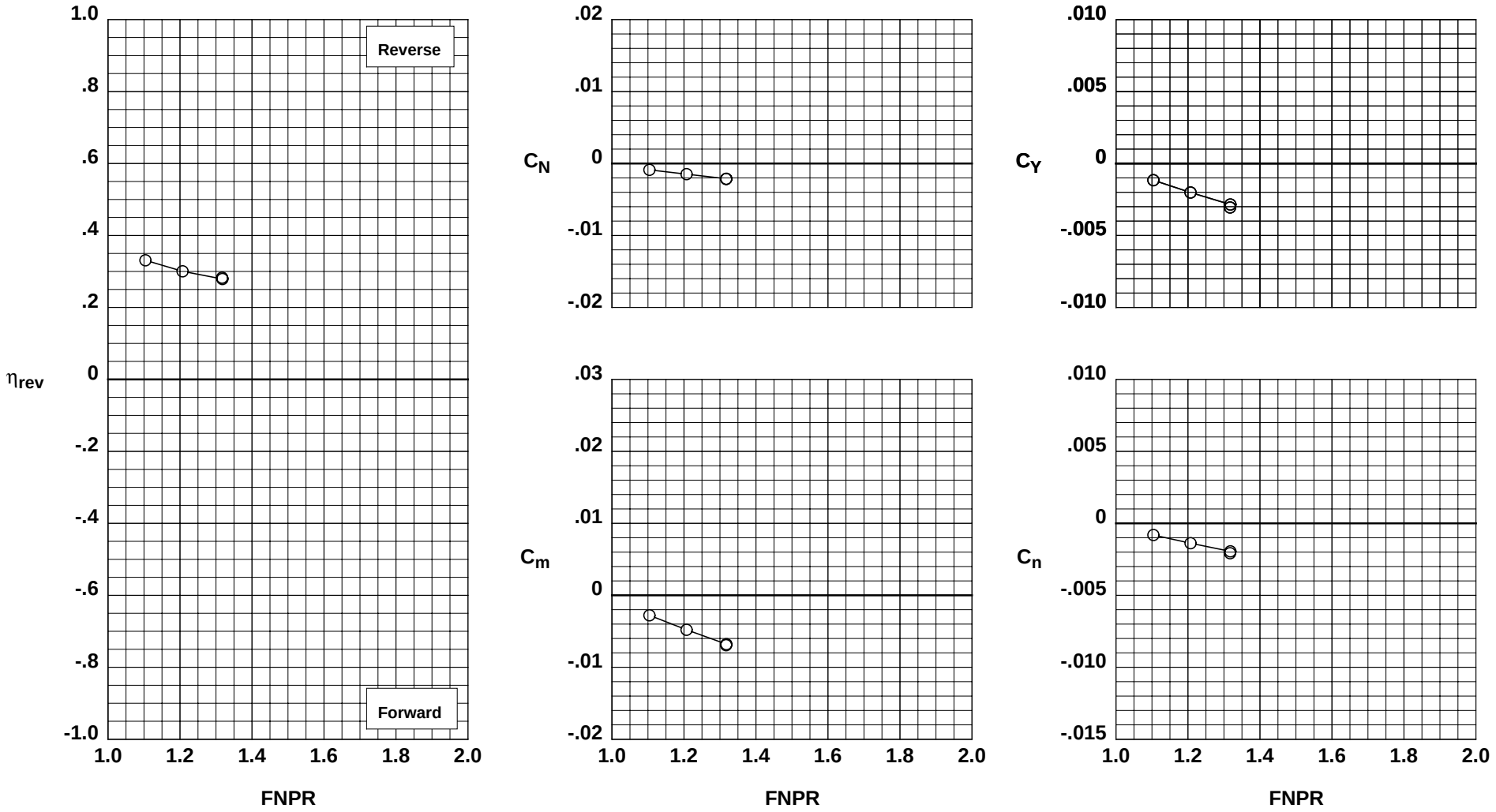

Figure H-16. Wing-mounted thrust reverser performance characteristics for configuration 716.

Operation Mode: Dual Flow
Deflector Mount Position: Parallel
Deflector Chord Lengths: Long/Long/Long
Deflector Angles: 45°/ 0°/30°
Deflector Fences: Installed
Ground Plane: Removed

	Test	Run	Configuration
○	1001	35	717

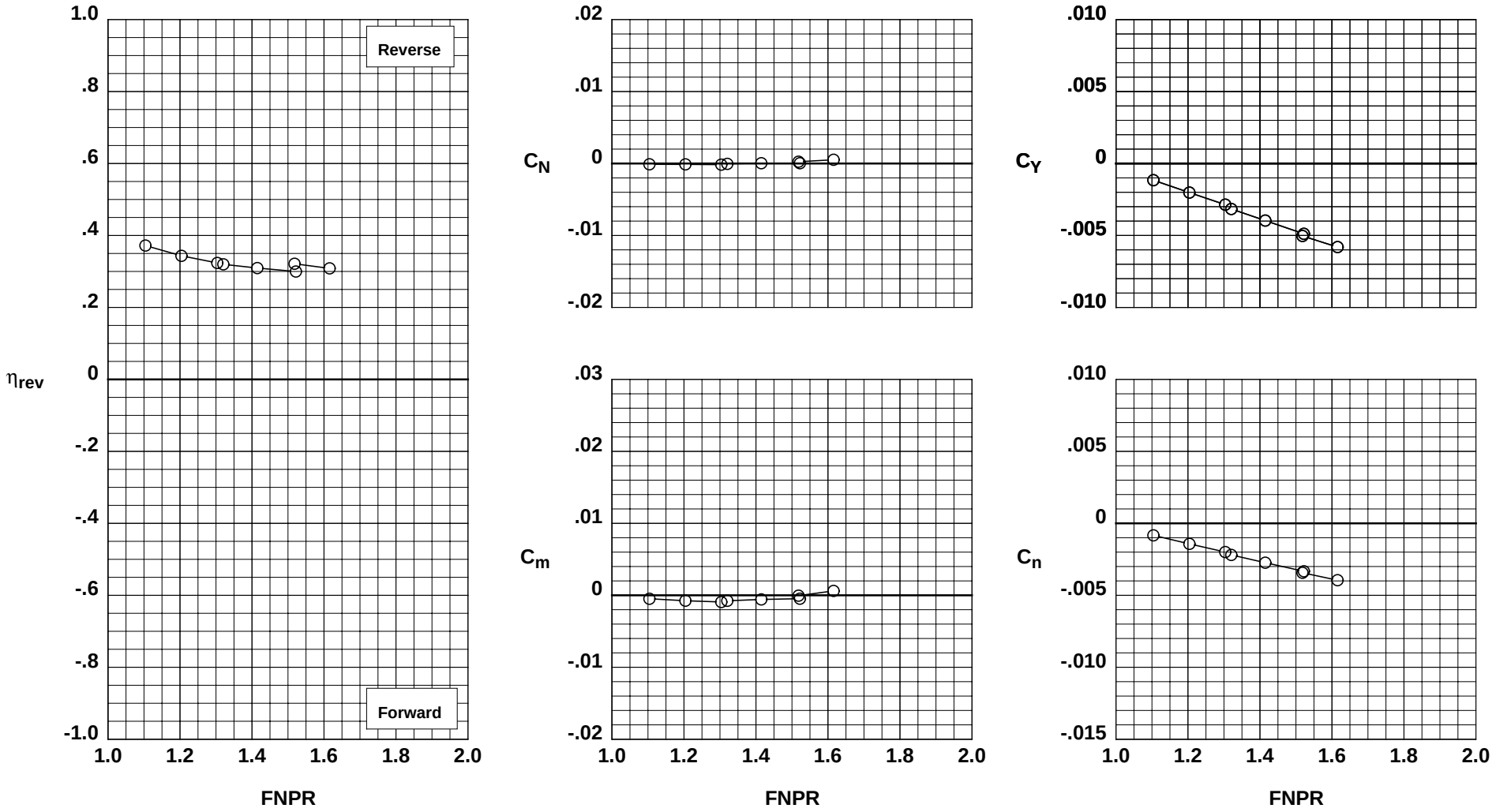

Figure H-17. Wing-mounted thrust reverser performance characteristics for configuration 717.

Operation Mode: Dual Flow
Deflector Mount Position: Parallel
Deflector Chord Lengths: Long/Long/Long
Deflector Angles: 45°/ 0°/45°
Deflector Fences: Installed
Ground Plane: Removed

	Test	Run	Configuration
○	1001	34	718

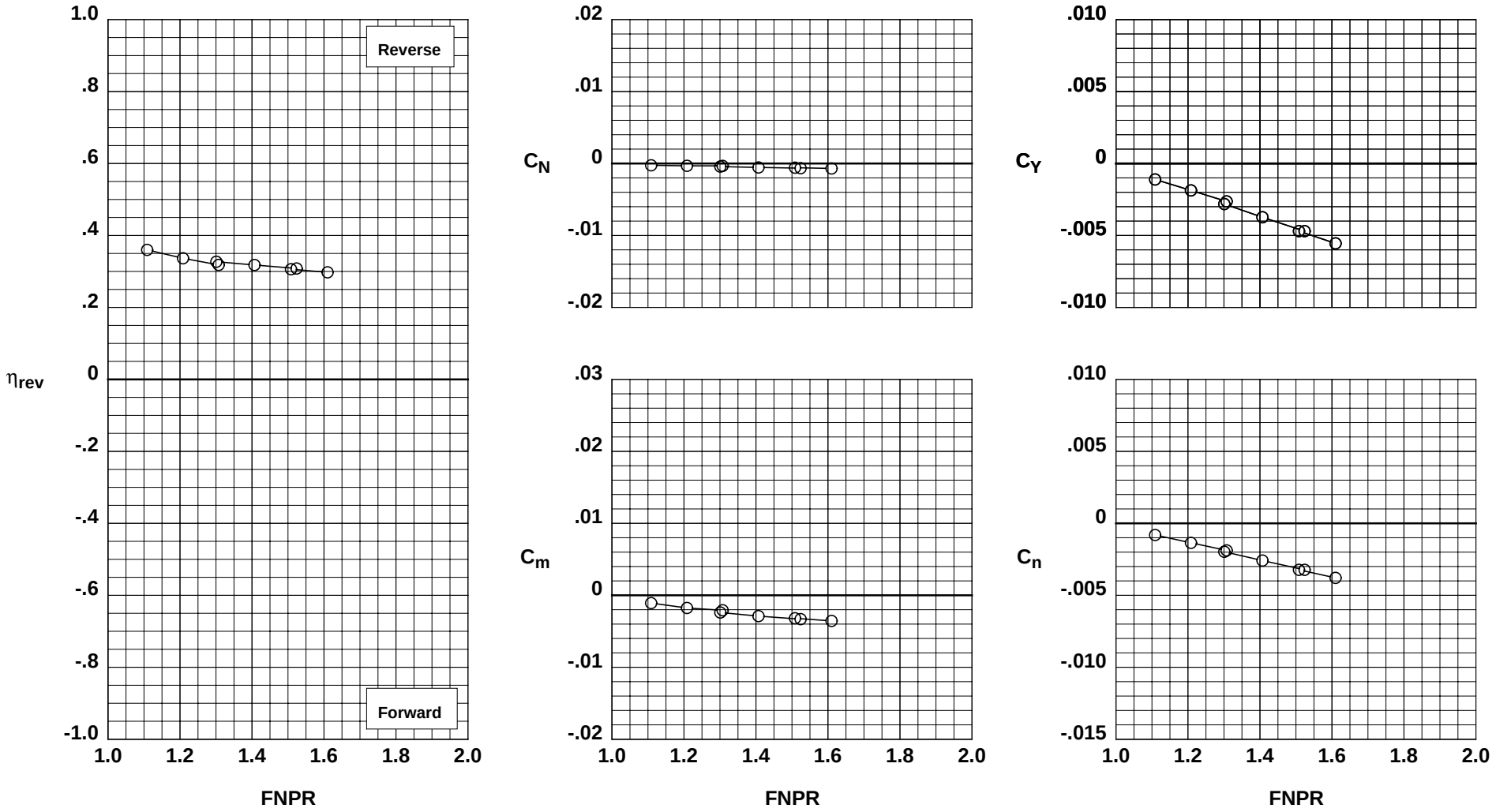

Figure H-18. Wing-mounted thrust reverser performance characteristics for configuration 718.

Operation Mode: Dual Flow
Deflector Mount Position: Parallel
Deflector Chord Lengths: Long/Long/Long
Deflector Angles: 60°/ 0°/30°
Deflector Fences: Installed
Ground Plane: Removed

	Test	Run	Configuration
○	1001	36	719

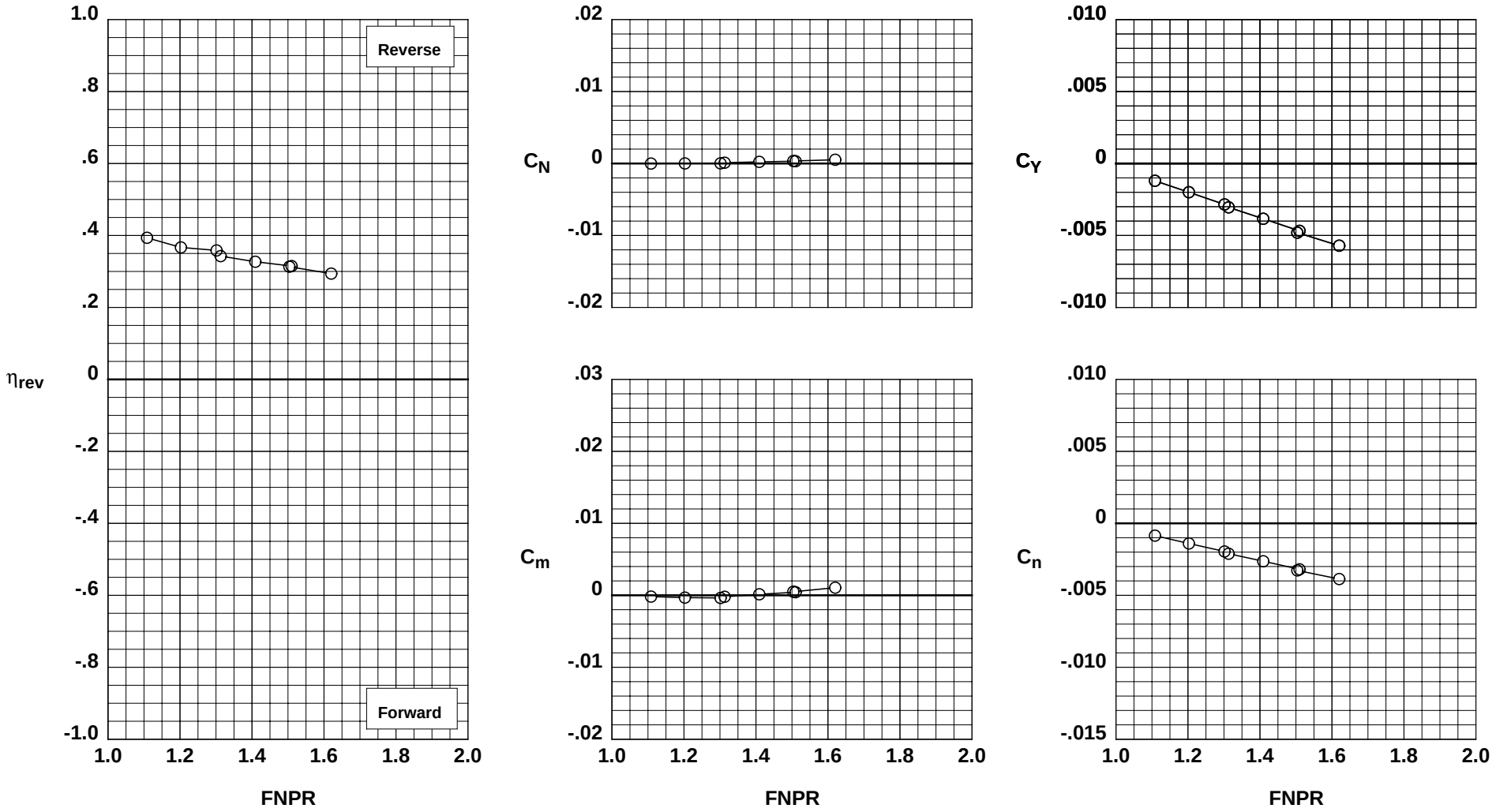

Figure H-19. Wing-mounted thrust reverser performance characteristics for configuration 719.

Operation Mode: Dual Flow
Deflector Mount Position: Parallel
Deflector Chord Lengths: Long/Long/Long
Deflector Angles: 60°/ 0°/45°
Deflector Fences: Installed
Ground Plane: Removed

	Test	Run	Configuration
○	1001	37	720

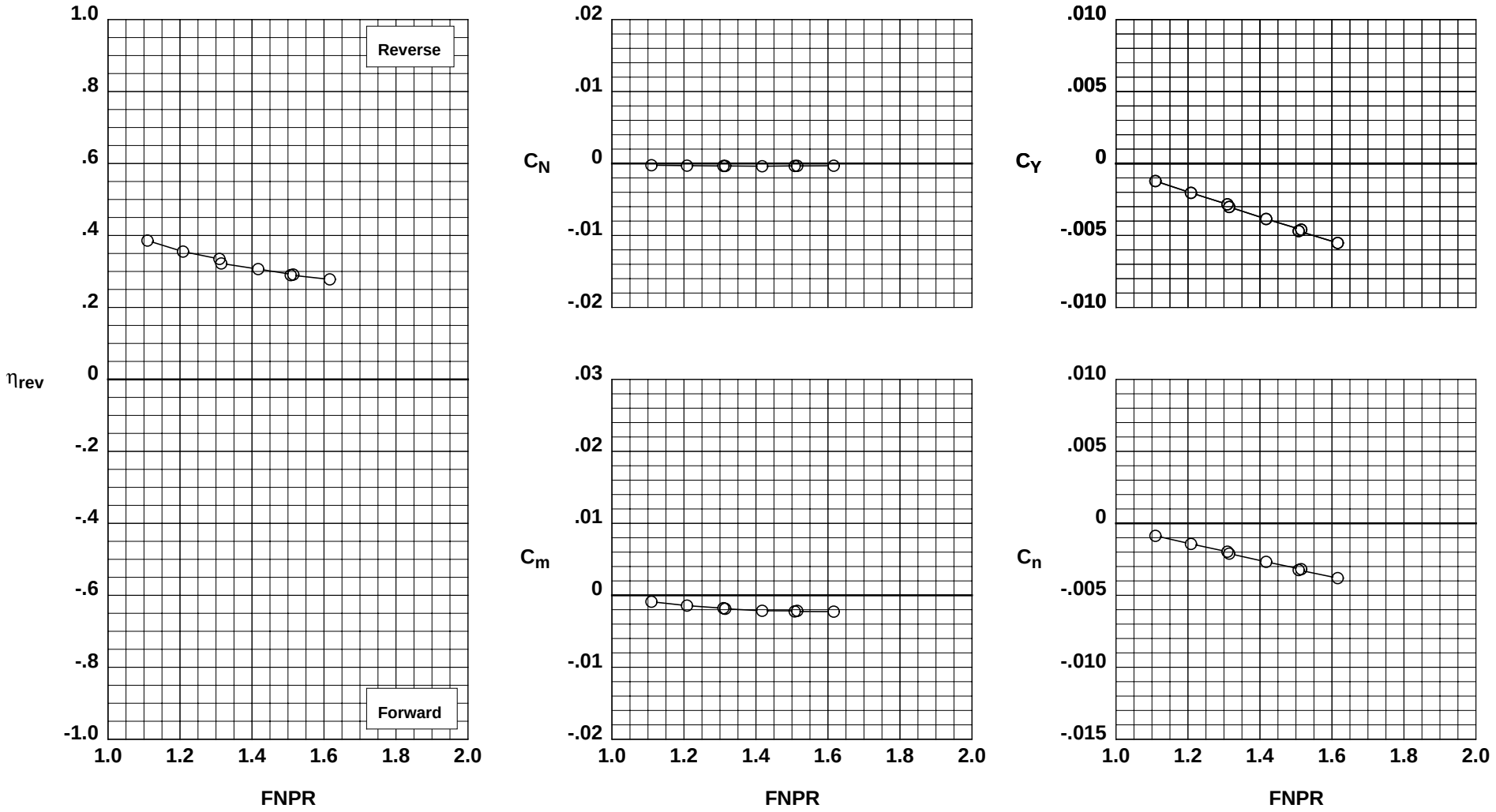

Figure H-20. Wing-mounted thrust reverser performance characteristics for configuration 720.

Operation Mode: Dual Flow
Deflector Mount Position: Parallel
Deflector Chord Lengths: Long/Long/Long
Deflector Angles: 15°/ 15°/15°
Deflector Fences: Installed
Ground Plane: Removed

	Test	Run	Configuration
○	1001	28	721

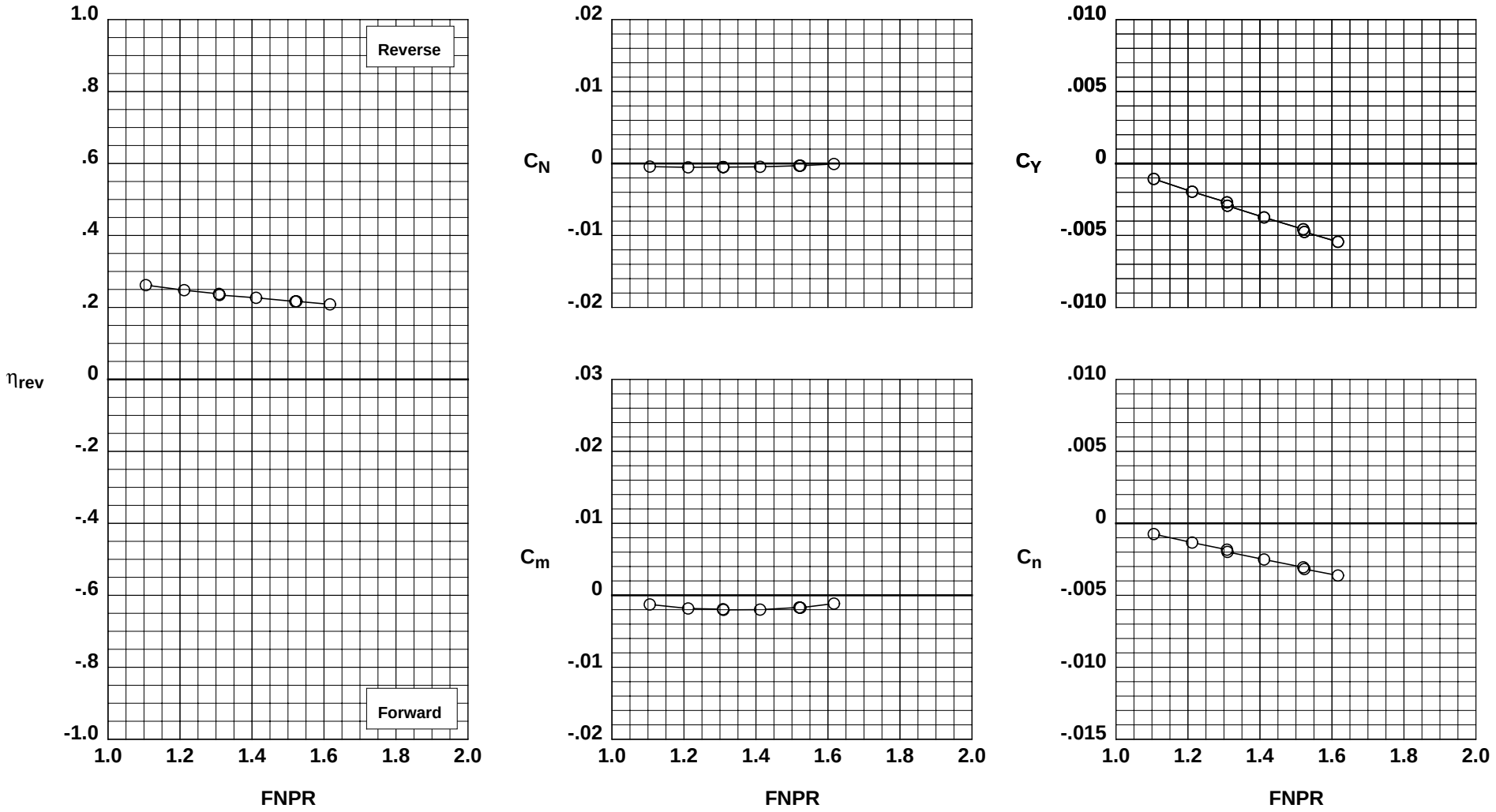

Figure H-21. Wing-mounted thrust reverser performance characteristics for configuration 721.

Operation Mode: Dual Flow
Deflector Mount Position: Parallel
Deflector Chord Lengths: Long/Long/Long
Deflector Angles: 15°/ 15°/30°
Deflector Fences: Installed
Ground Plane: Removed

	Test	Run	Configuration
○	1001	26	722

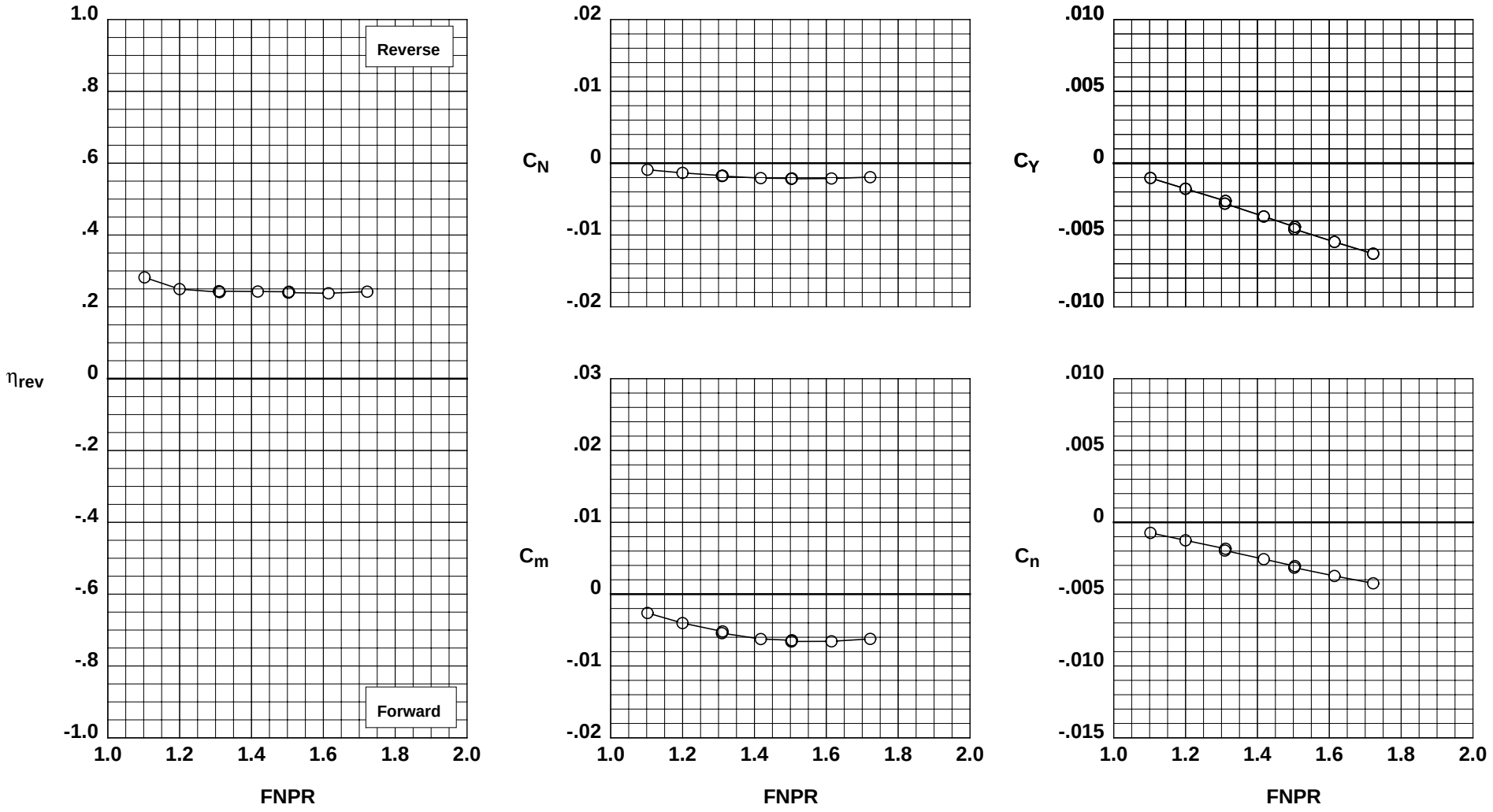

Figure H-22. Wing-mounted thrust reverser performance characteristics for configuration 722.

Operation Mode: Dual Flow
Deflector Mount Position: Parallel
Deflector Chord Lengths: Long/Long/Long
Deflector Angles: 15°/ 15°/45°
Deflector Fences: Installed
Ground Plane: Removed

	Test	Run	Configuration
○	1001	27	723

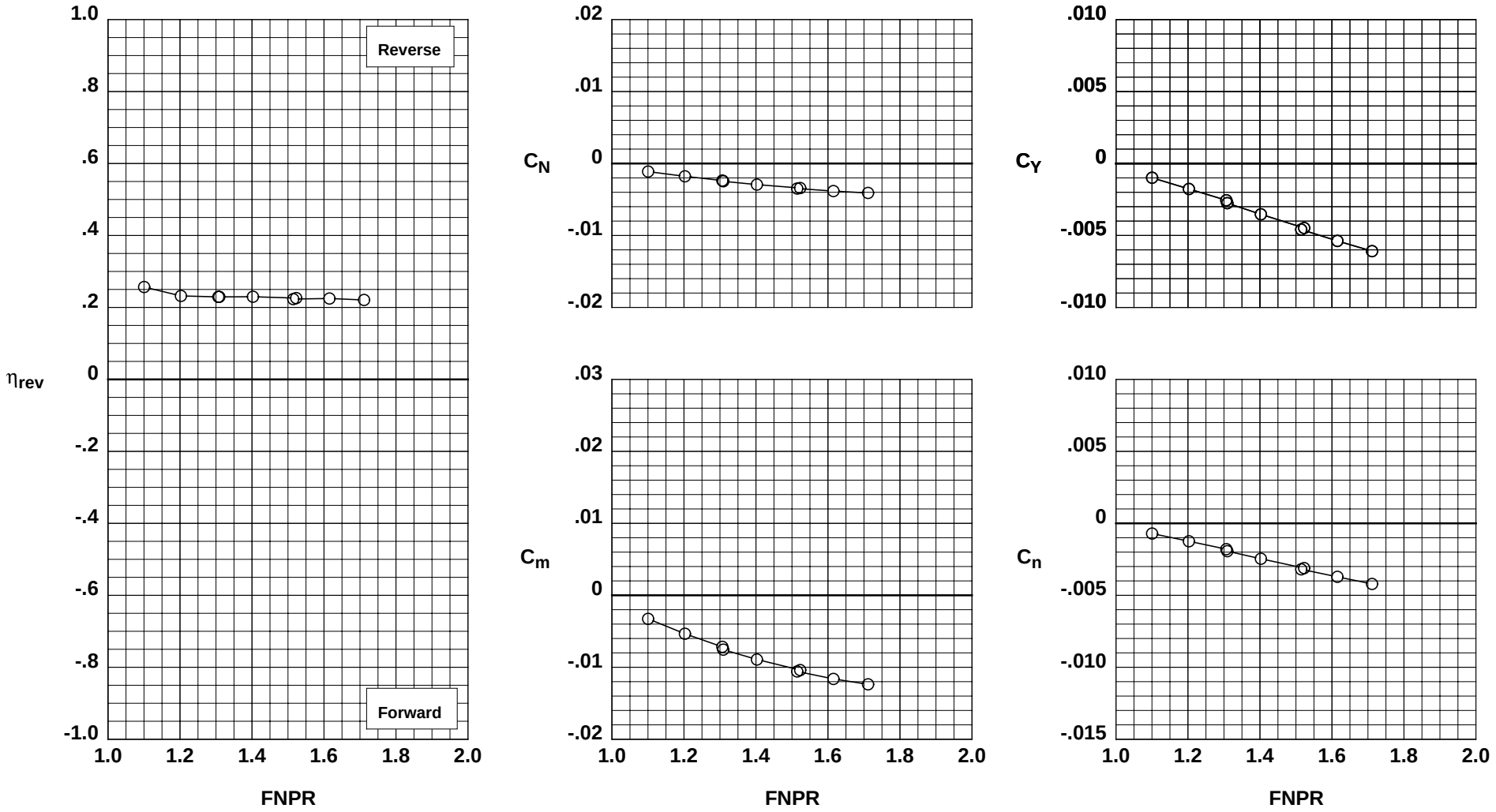

Figure H-23. Wing-mounted thrust reverser performance characteristics for configuration 723.

Operation Mode: Dual Flow
Deflector Mount Position: Parallel
Deflector Chord Lengths: Long/Long/Long
Deflector Angles: 30°/ 15°/30°
Deflector Fences: Installed
Ground Plane: Removed

	Test	Run	Configuration
○	1001	25	724

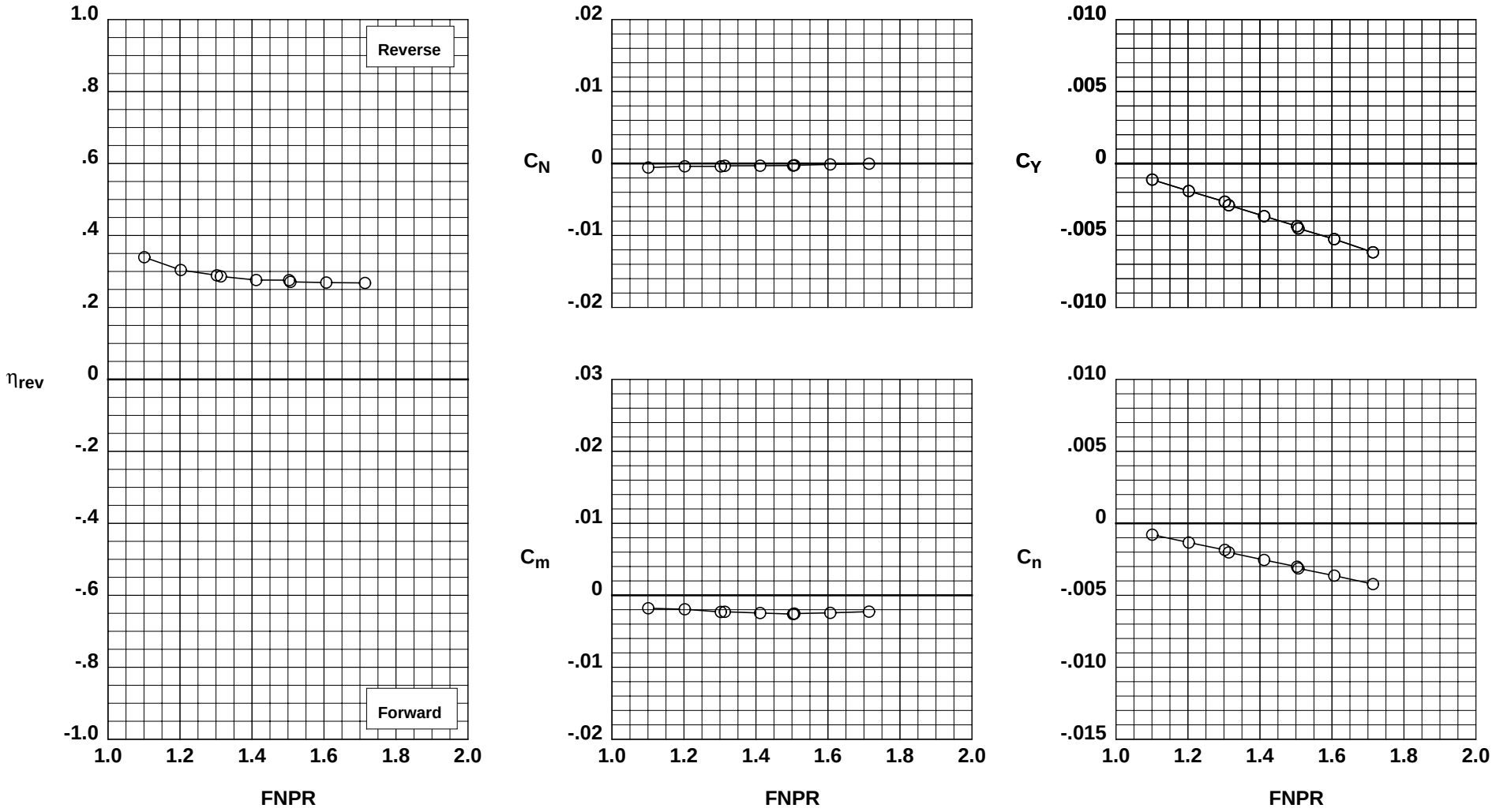

Figure H-24. Wing-mounted thrust reverser performance characteristics for configuration 724.

Operation Mode: Dual Flow
Deflector Mount Position: Parallel
Deflector Chord Lengths: Long/Long/Long
Deflector Angles: 45°/ 15°/15°
Deflector Fences: Installed
Ground Plane: Removed

	Test	Run	Configuration
○	1001	51	725

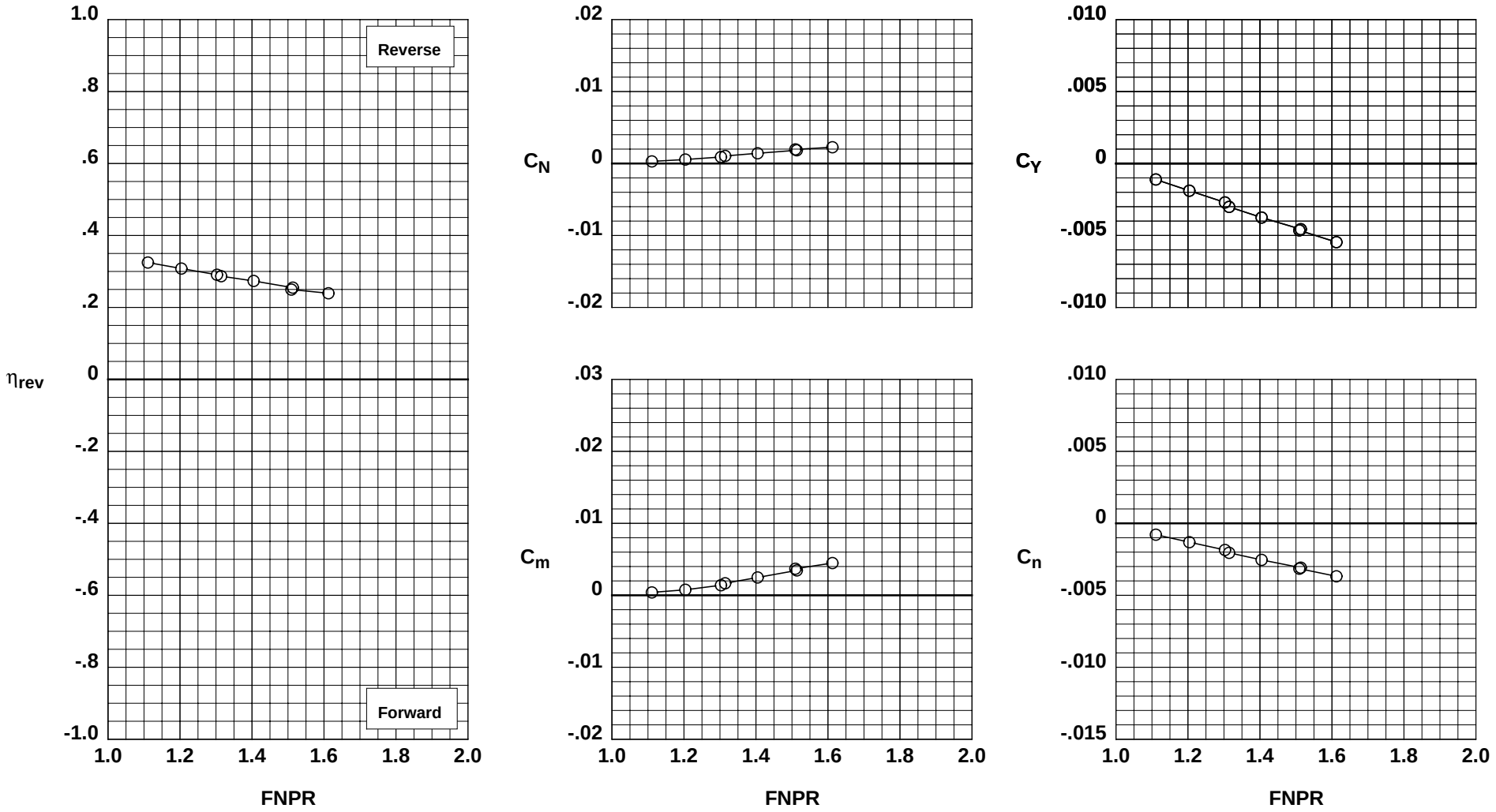

Figure H-25. Wing-mounted thrust reverser performance characteristics for configuration 725.

Operation Mode: Dual Flow
Deflector Mount Position: Parallel
Deflector Chord Lengths: Long/Long/Long
Deflector Angles: 45°/ 15°/30°
Deflector Fences: Installed
Ground Plane: Removed

	Test	Run	Configuration
○	1001	52	726

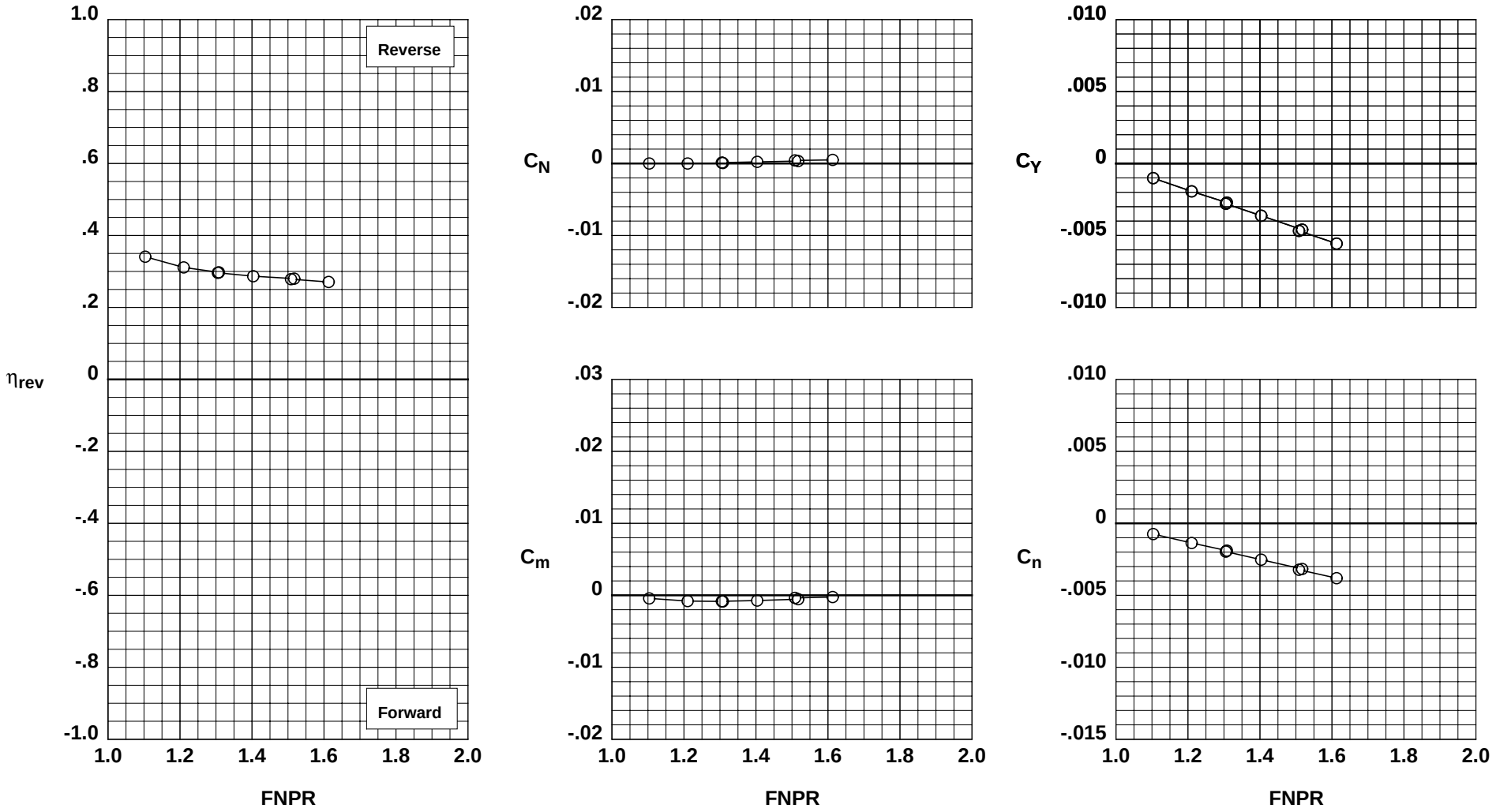

Figure H-26. Wing-mounted thrust reverser performance characteristics for configuration 726.

Operation Mode: Dual Flow
Deflector Mount Position: Parallel
Deflector Chord Lengths: Long/Long/Long
Deflector Angles: 45°/ 15°/45°
Deflector Fences: Installed
Ground Plane: Removed

	Test	Run	Configuration
○	1001	53	727

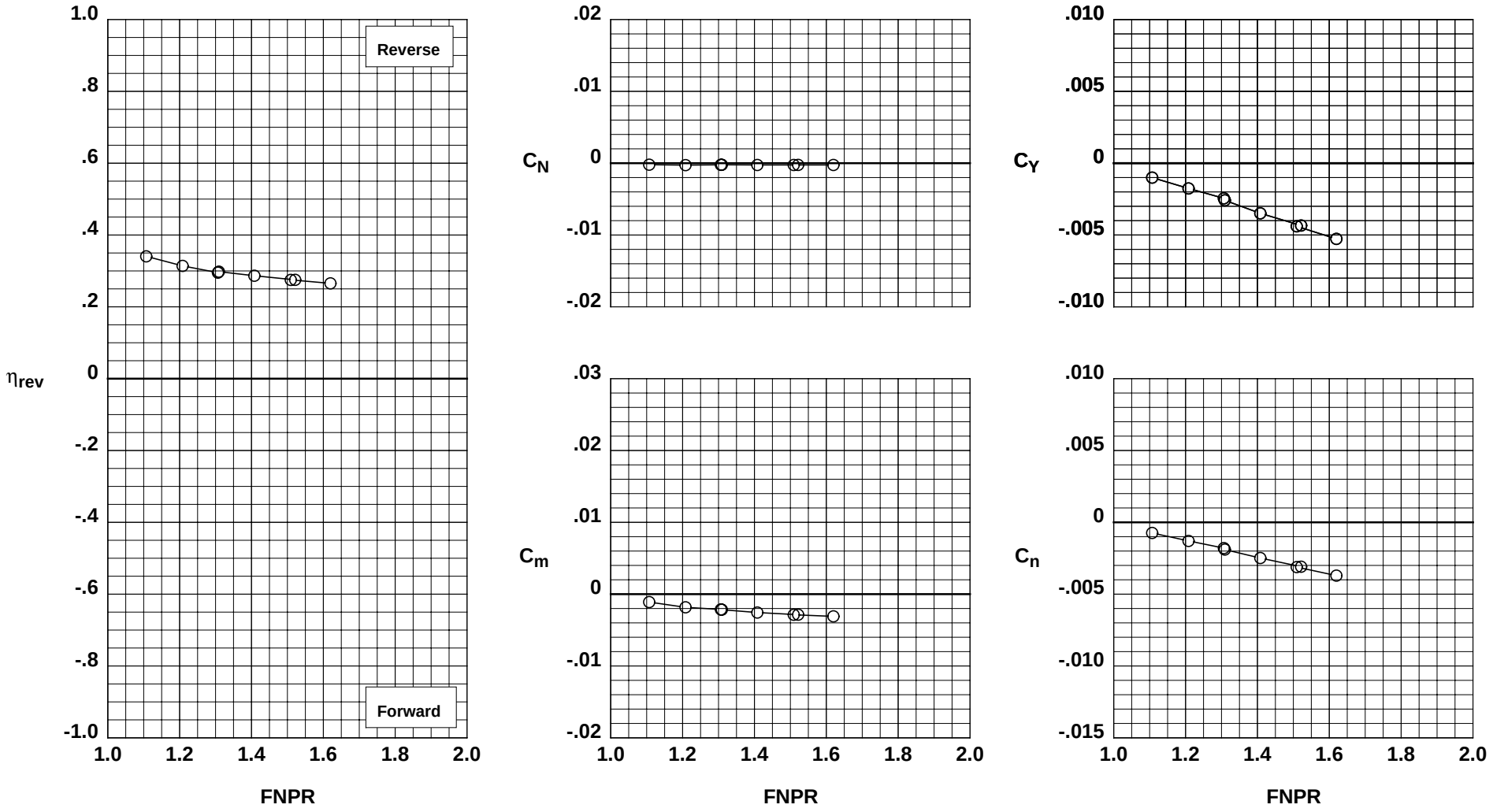

Figure H-27. Wing-mounted thrust reverser performance characteristics for configuration 727.

Operation Mode: Dual Flow
Deflector Mount Position: Parallel
Deflector Chord Lengths: Long/Long/Long
Deflector Angles: 30°/ 15°/60°
Deflector Fences: Installed
Ground Plane: Removed

	Test	Run	Configuration
○	1001	54	728

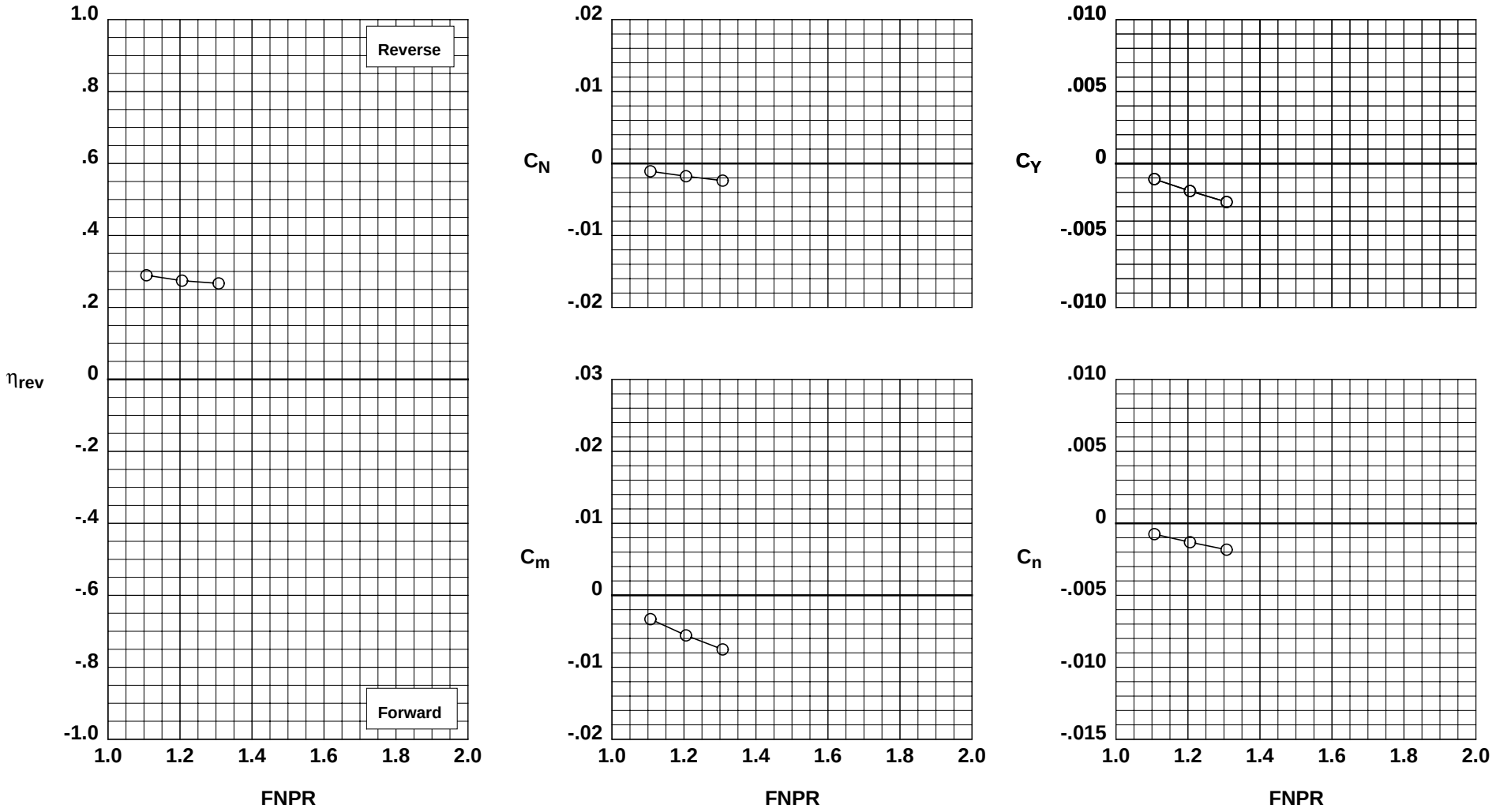

Figure H-28. Wing-mounted thrust reverser performance characteristics for configuration 728.

Operation Mode: Dual Flow
Deflector Mount Position: Parallel
Deflector Chord Lengths: Long/Long/Long
Deflector Angles: 15°/ 30°/30°
Deflector Fences: Installed
Ground Plane: Removed

	Test	Run	Configuration
○	1001	30	729

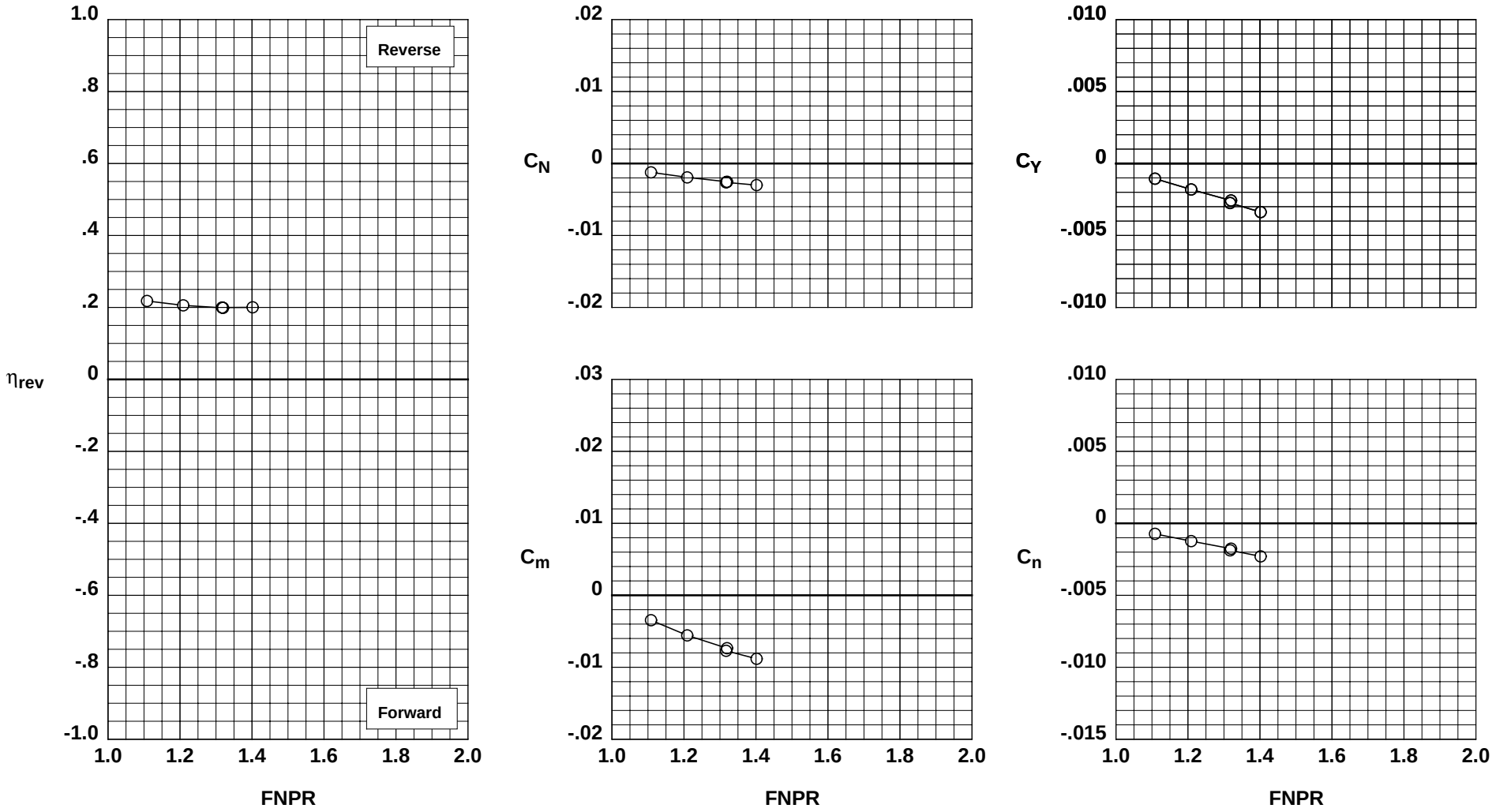

Figure H-29. Wing-mounted thrust reverser performance characteristics for configuration 729.

Operation Mode: Dual Flow
Deflector Mount Position: Parallel
Deflector Chord Lengths: Long/Long/Long
Deflector Angles: 15°/ 45°/45°
Deflector Fences: Installed
Ground Plane: Removed

	Test	Run	Configuration
○	1001	29	730

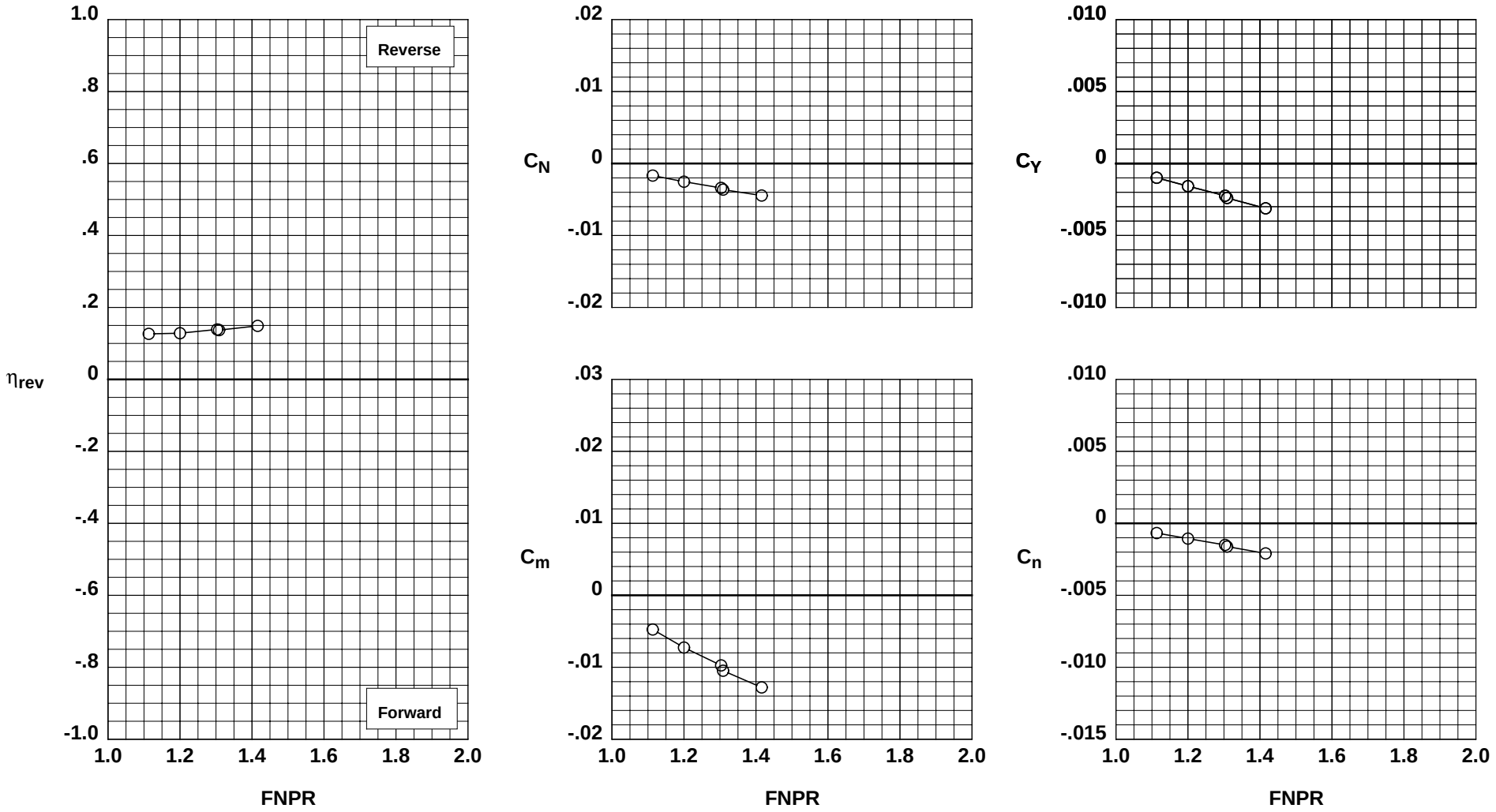

Figure H-30. Wing-mounted thrust reverser performance characteristics for configuration 730.

Operation Mode: Dual Flow
Deflector Mount Position: Parallel
Deflector Chord Lengths: Long/Long/Long
Deflector Angles: 30°/ 15°/30°
Deflector Fences: Removed
Ground Plane: Removed

	Test	Run	Configuration
○	1001	55	731

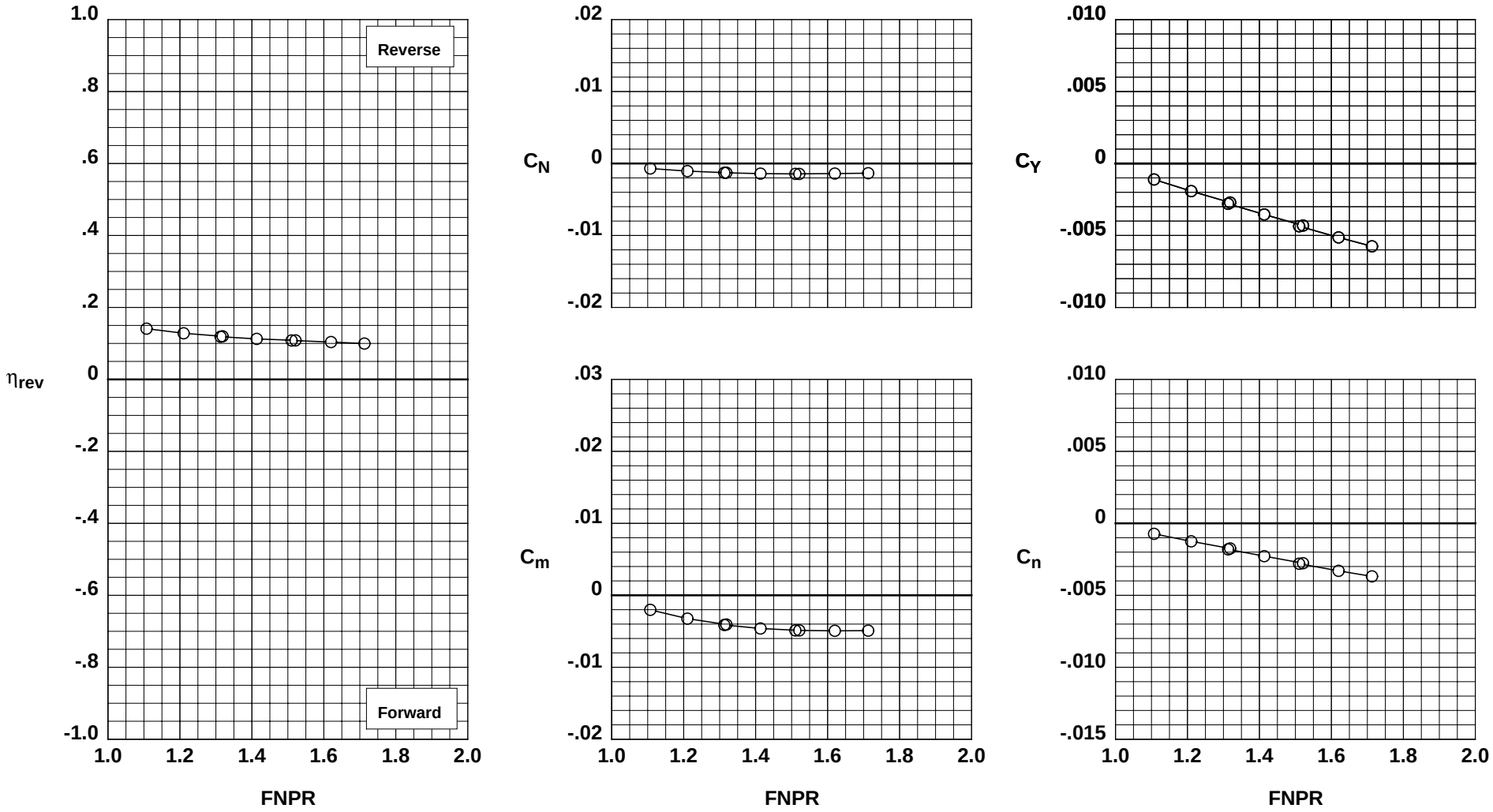

Figure H-31. Wing-mounted thrust reverser performance characteristics for configuration 731.

Operation Mode: Dual Flow
Deflector Mount Position: Parallel
Deflector Chord Lengths: Long/Long/Long
Deflector Angles: 45°/ 0°/30°
Deflector Fences: Removed
Ground Plane: Removed

	Test	Run	Configuration
○	1001	56	732

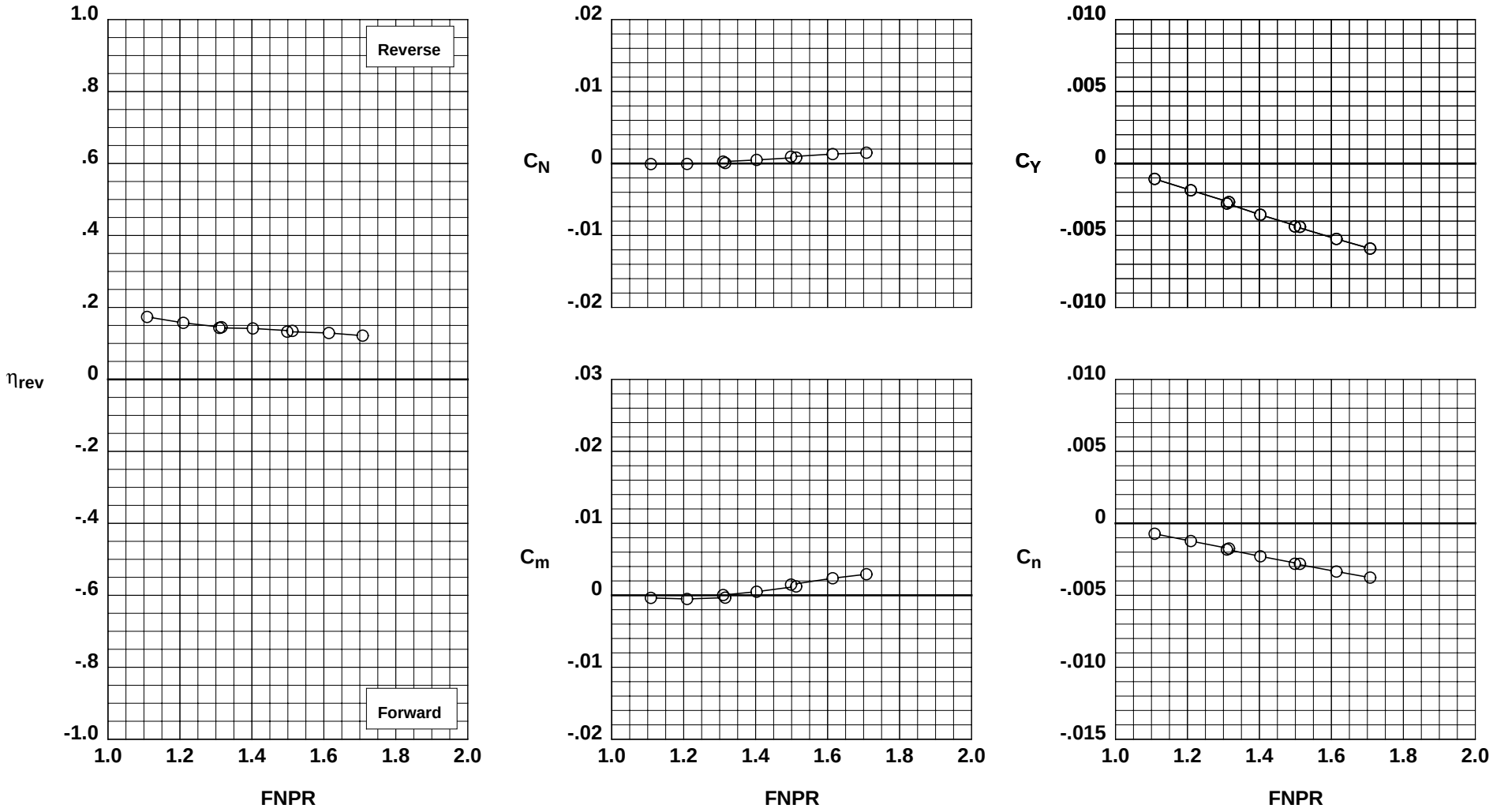

Figure H-32. Wing-mounted thrust reverser performance characteristics for configuration 732.

Operation Mode: Dual Flow
Deflector Mount Position: Parallel
Deflector Chord Lengths: Long/Long/Long
Deflector Angles: 60°/ 0°/30°
Deflector Fences: Removed
Ground Plane: Removed

	Test	Run	Configuration
○	1001	57	733

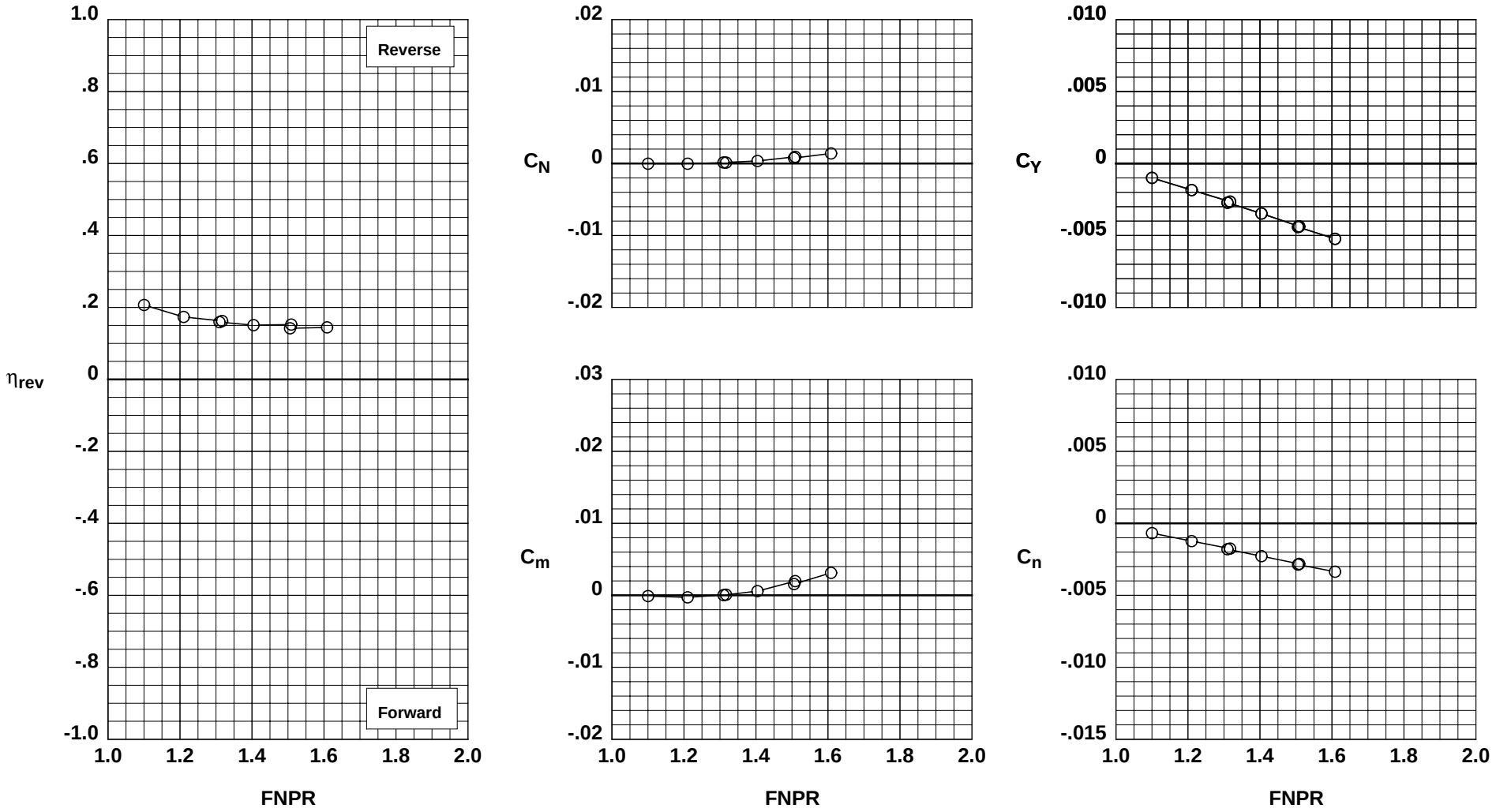

Figure H-33. Wing-mounted thrust reverser performance characteristics for configuration 733.

Operation Mode: Dual Flow
Deflector Mount Position: Parallel
Deflector Chord Lengths: Long/Long/Long
Deflector Angles: 60°/-15°/30°
Deflector Fences: Removed
Ground Plane: Removed

	Test	Run	Configuration
○	1001	58	734

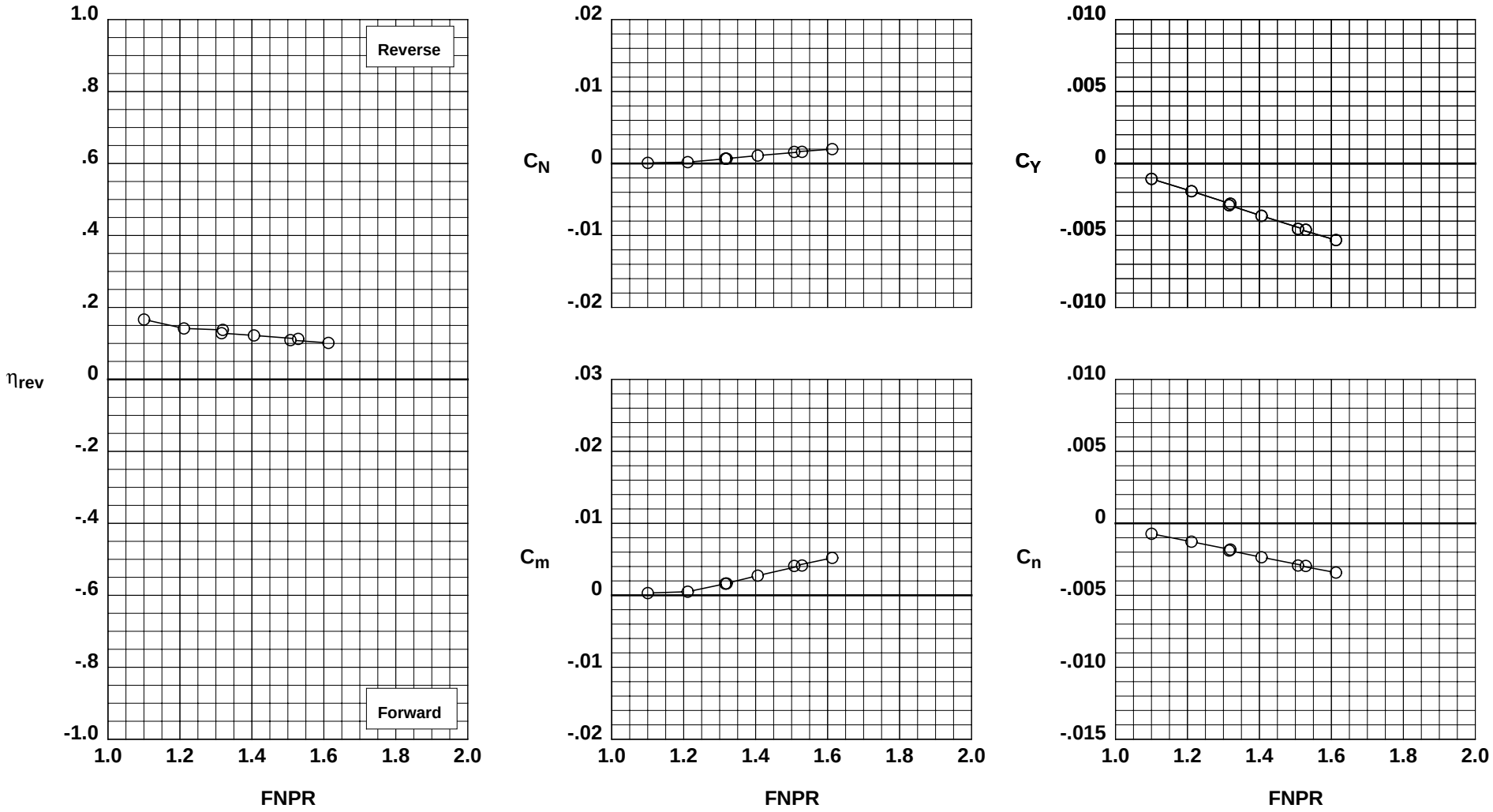

Figure H-34. Wing-mounted thrust reverser performance characteristics for configuration 734.

Operation Mode: Dual Flow
Deflector Mount Position: Parallel
Deflector Chord Lengths: Long/Long/Long
Deflector Angles: 45°/-15°/30°
Deflector Fences: Removed
Ground Plane: Removed

	Test	Run	Configuration
○	1001	59	735

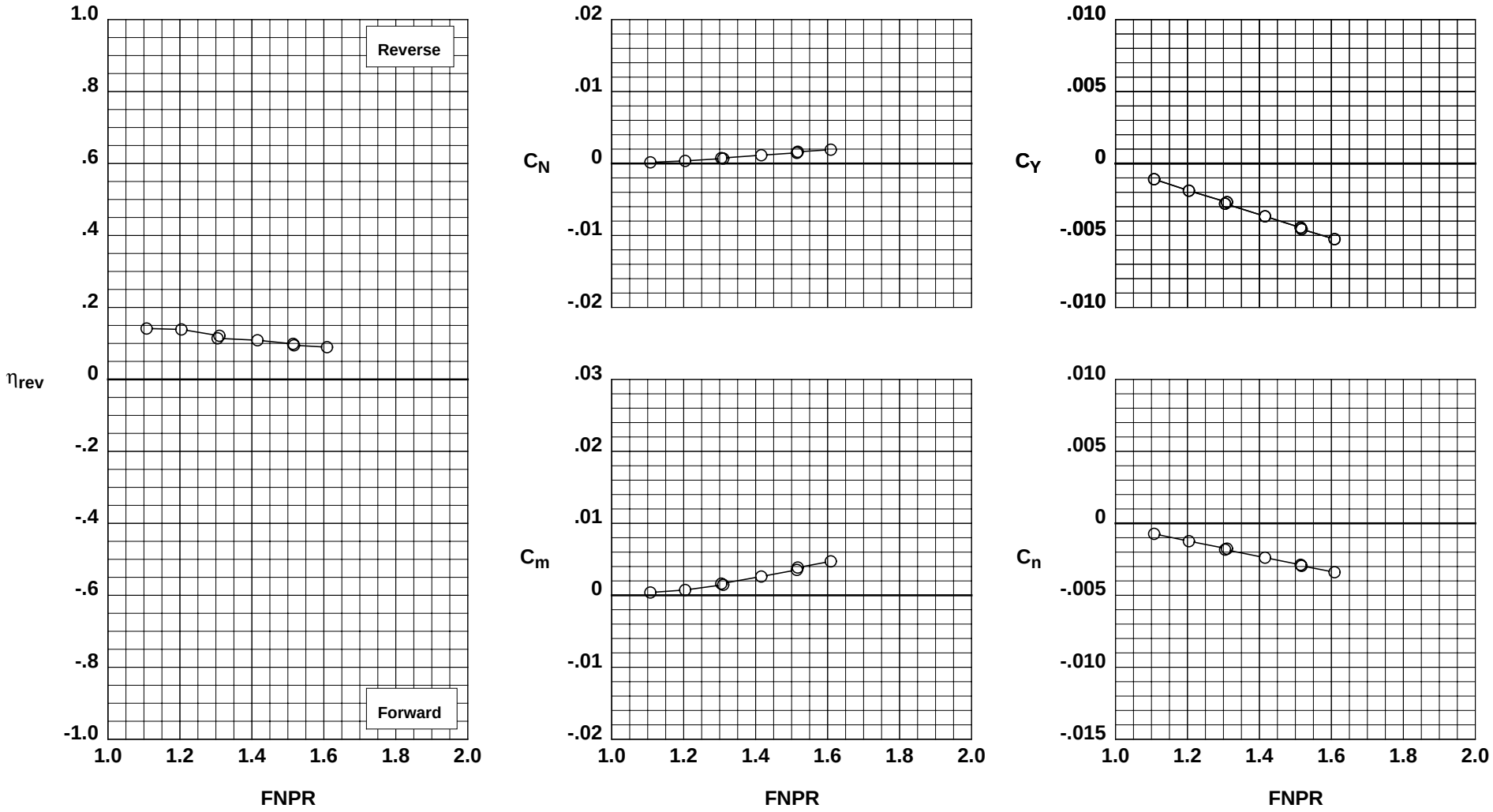

Figure H-35. Wing-mounted thrust reverser performance characteristics for configuration 735.

Operation Mode: Dual Flow
Deflector Mount Position: Normal
Deflector Chord Lengths: Long/Long/Long
Deflector Angles: 30°/ 15°/30°
Deflector Fences: Installed
Ground Plane: Removed

	Test	Run	Configuration
○	1001	64	736

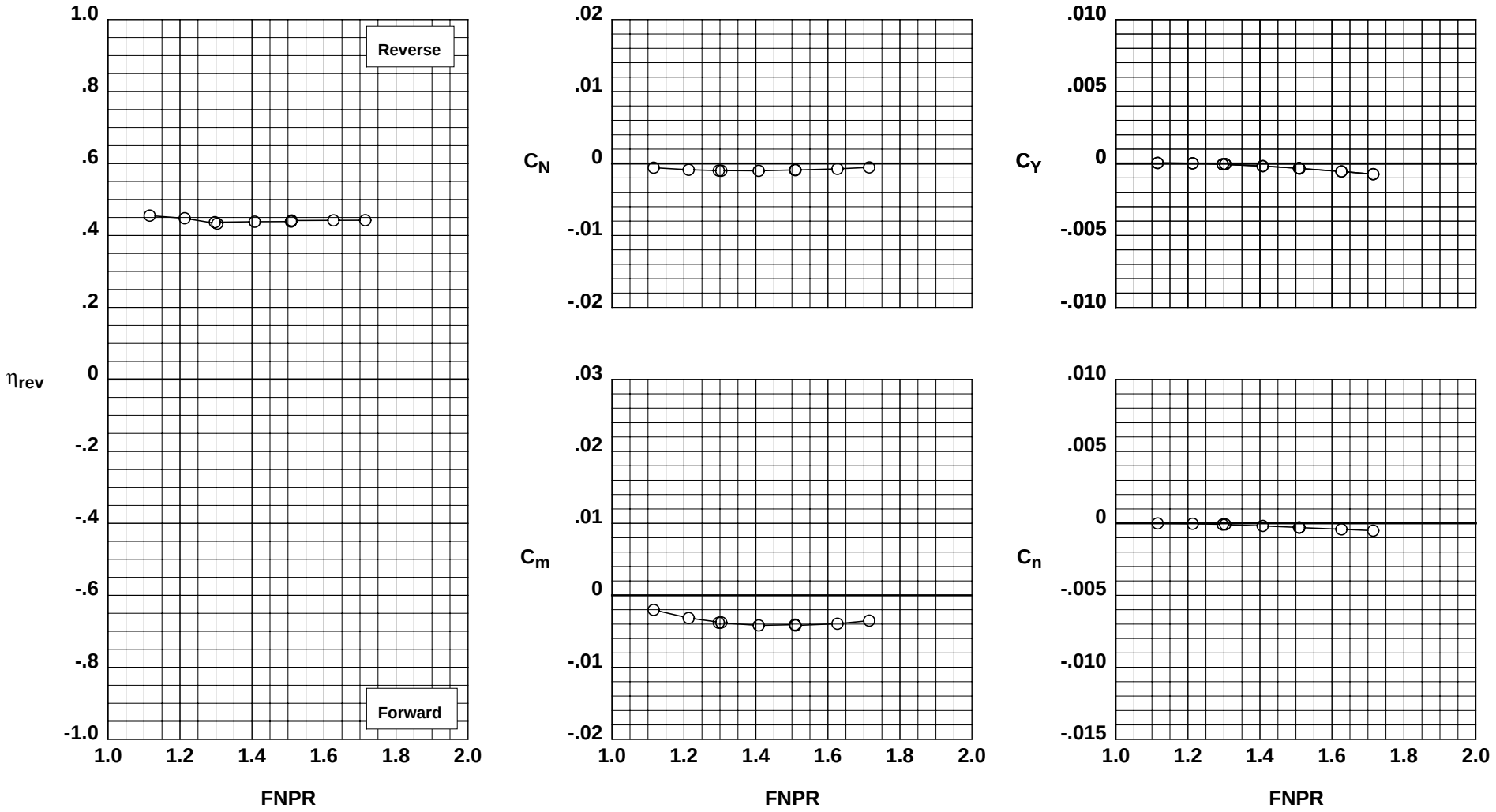

Figure H-36. Wing-mounted thrust reverser performance characteristics for configuration 736.

Operation Mode: Dual Flow
Deflector Mount Position: Normal
Deflector Chord Lengths: Long/Long/Long
Deflector Angles: 45°/ 0°/30°
Deflector Fences: Installed
Ground Plane: Removed

	Test	Run	Configuration
○	1001	61	737

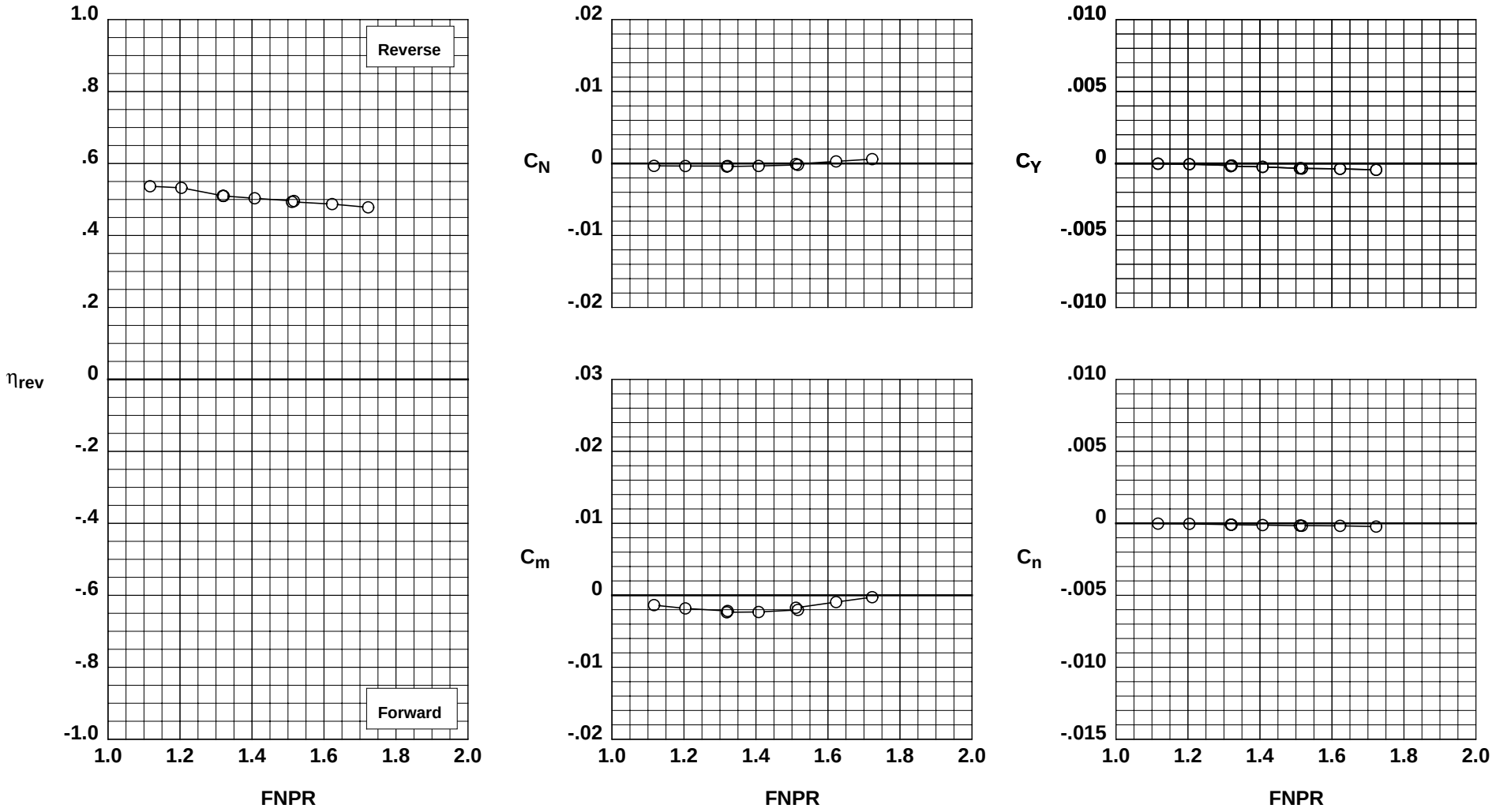

Figure H-37. Wing-mounted thrust reverser performance characteristics for configuration 737.

Operation Mode: Dual Flow
Deflector Mount Position: Normal
Deflector Chord Lengths: Long/Long/Long
Deflector Angles: 60°/ 0°/30°
Deflector Fences: Installed
Ground Plane: Removed

	Test	Run	Configuration
○	1001	62	738

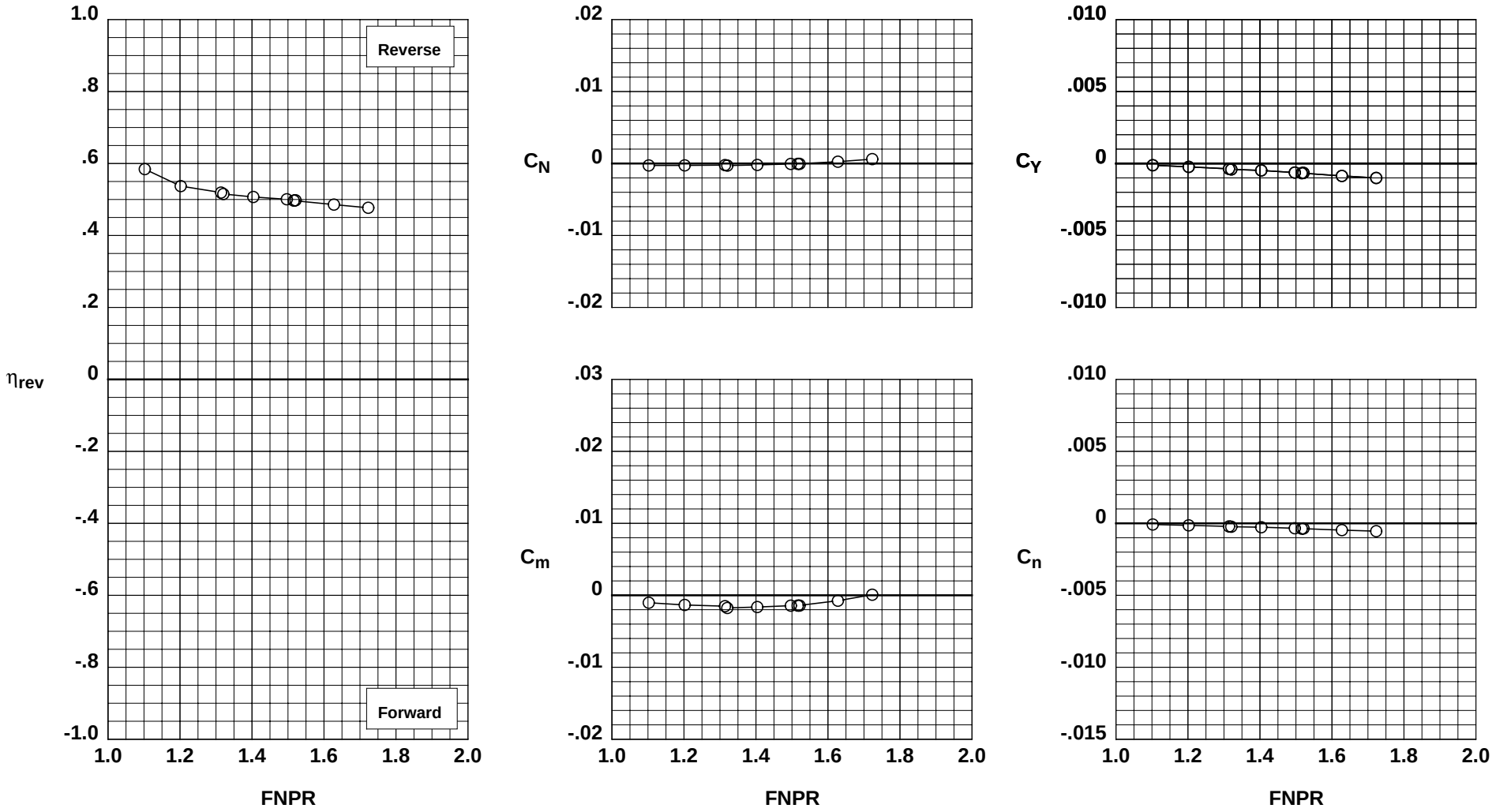

Figure H-38. Wing-mounted thrust reverser performance characteristics for configuration 738.

Operation Mode: Dual Flow
Deflector Mount Position: Normal
Deflector Chord Lengths: Long/Long/Long
Deflector Angles: 60°/-15°/30°
Deflector Fences: Removed
Ground Plane: Removed

	Test	Run	Configuration
○	1001	63	739

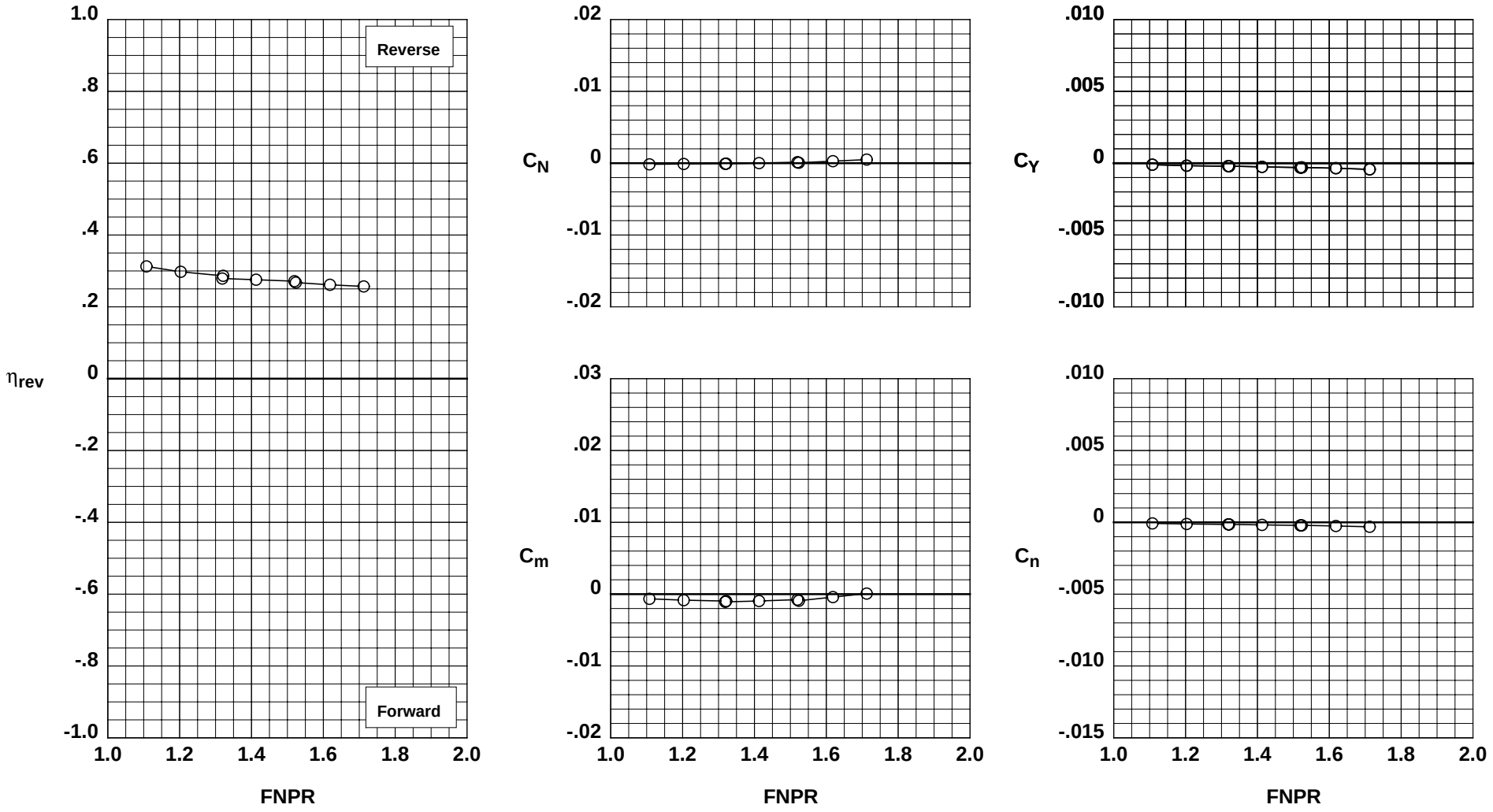

Figure H-39. Wing-mounted thrust reverser performance characteristics for configuration 739.

Operation Mode: Dual Flow
Deflector Mount Position: Normal
Deflector Chord Lengths: Long/Long/Long
Deflector Angles: 45°/-15°/30°
Deflector Fences: Installed
Ground Plane: Removed

	Test	Run	Configuration
○	1001	60	740

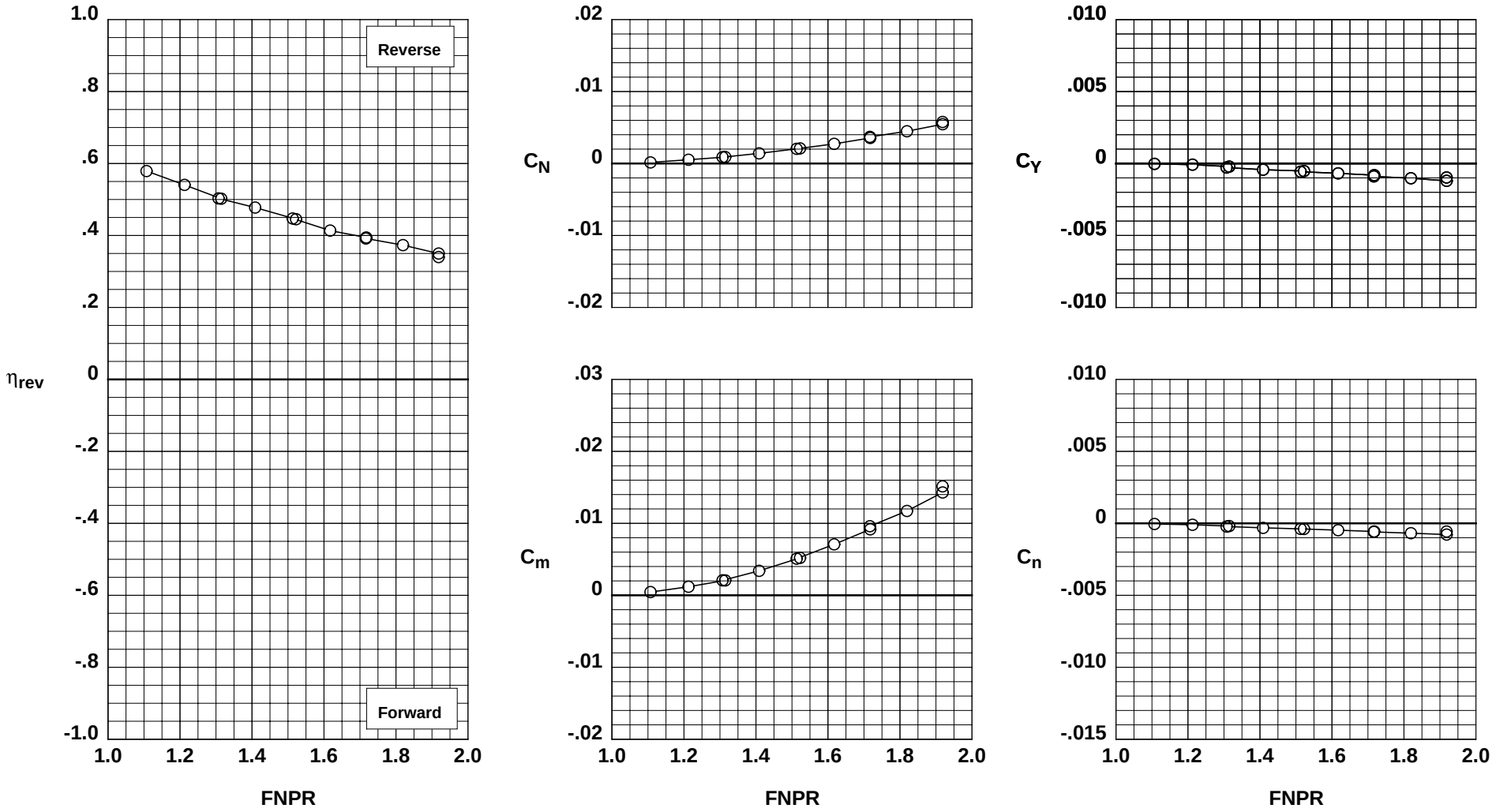

Figure H-40. Wing-mounted thrust reverser performance characteristics for configuration 740.

Operation Mode: Dual Flow
Deflector Mount Position: Parallel
Deflector Chord Lengths: Short/Short/Long
Deflector Angles: 60°/-15°/30°
Deflector Fences: Installed
Ground Plane: Removed

	Test	Run	Configuration
○	1001	70	741

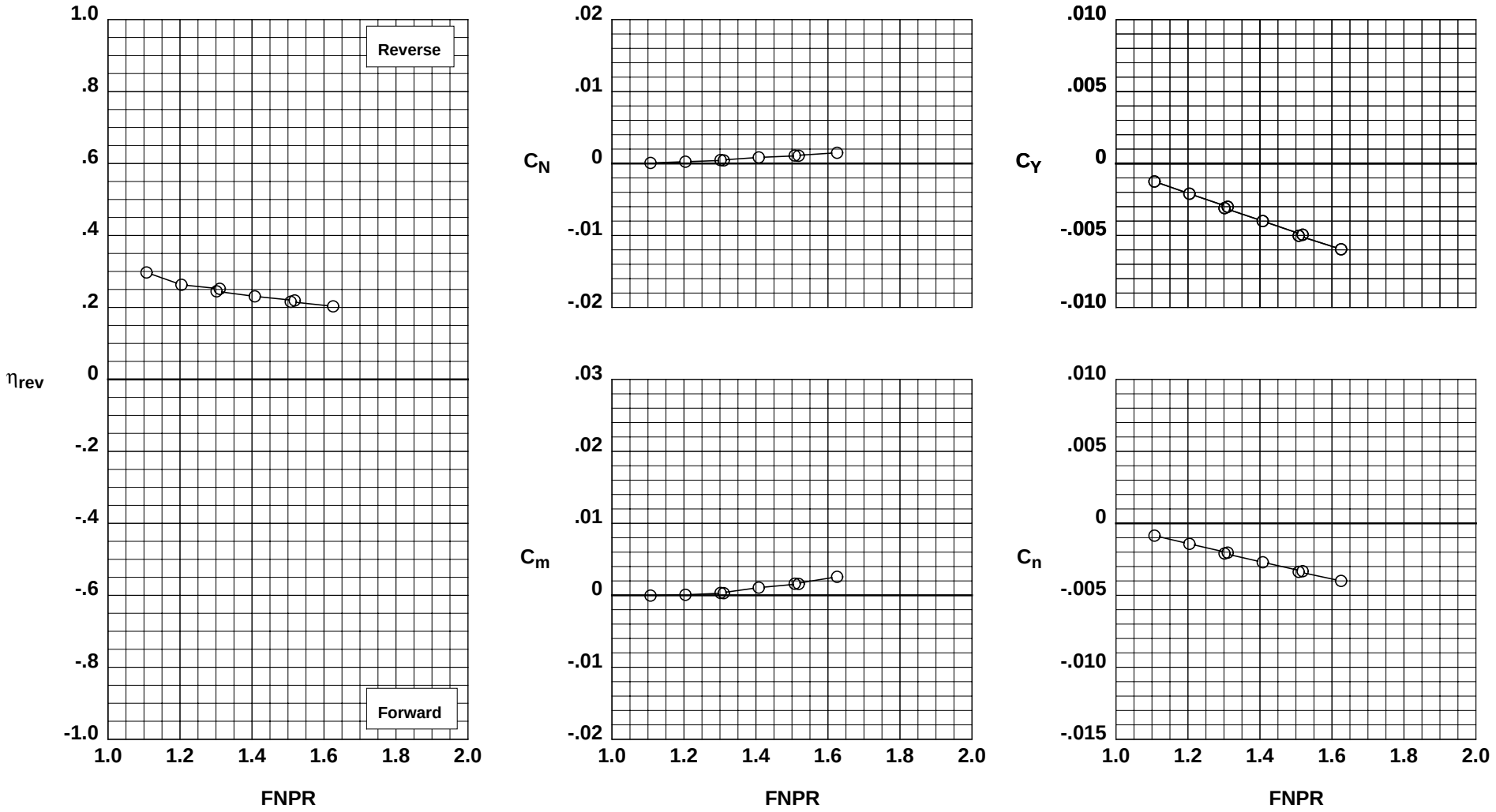

Figure H-41. Wing-mounted thrust reverser performance characteristics for configuration 741.

Operation Mode: Dual Flow
Deflector Mount Position: Parallel
Deflector Chord Lengths: Short/Short/Long
Deflector Angles: 45°/-15°/30°
Deflector Fences: Installed
Ground Plane: Removed

	Test	Run	Configuration
○	1001	71	742

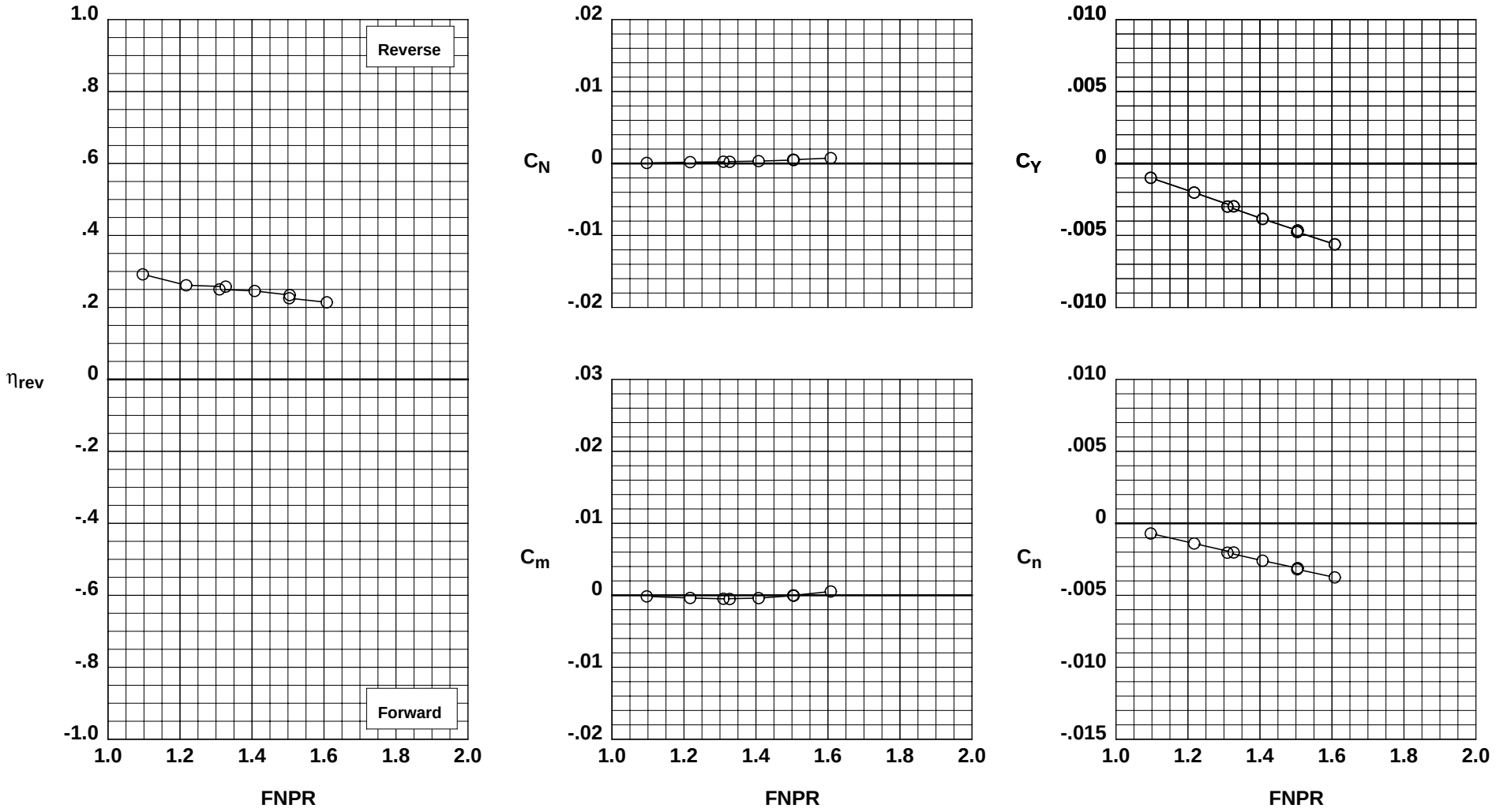

Figure H-42. Wing-mounted thrust reverser performance characteristics for configuration 742.

Operation Mode: Dual Flow
Deflector Mount Position: Parallel
Deflector Chord Lengths: Short/Short/Long
Deflector Angles: 60°/ 0°/30°
Deflector Fences: Installed
Ground Plane: Removed

	Test	Run	Configuration
○	1001	72	743

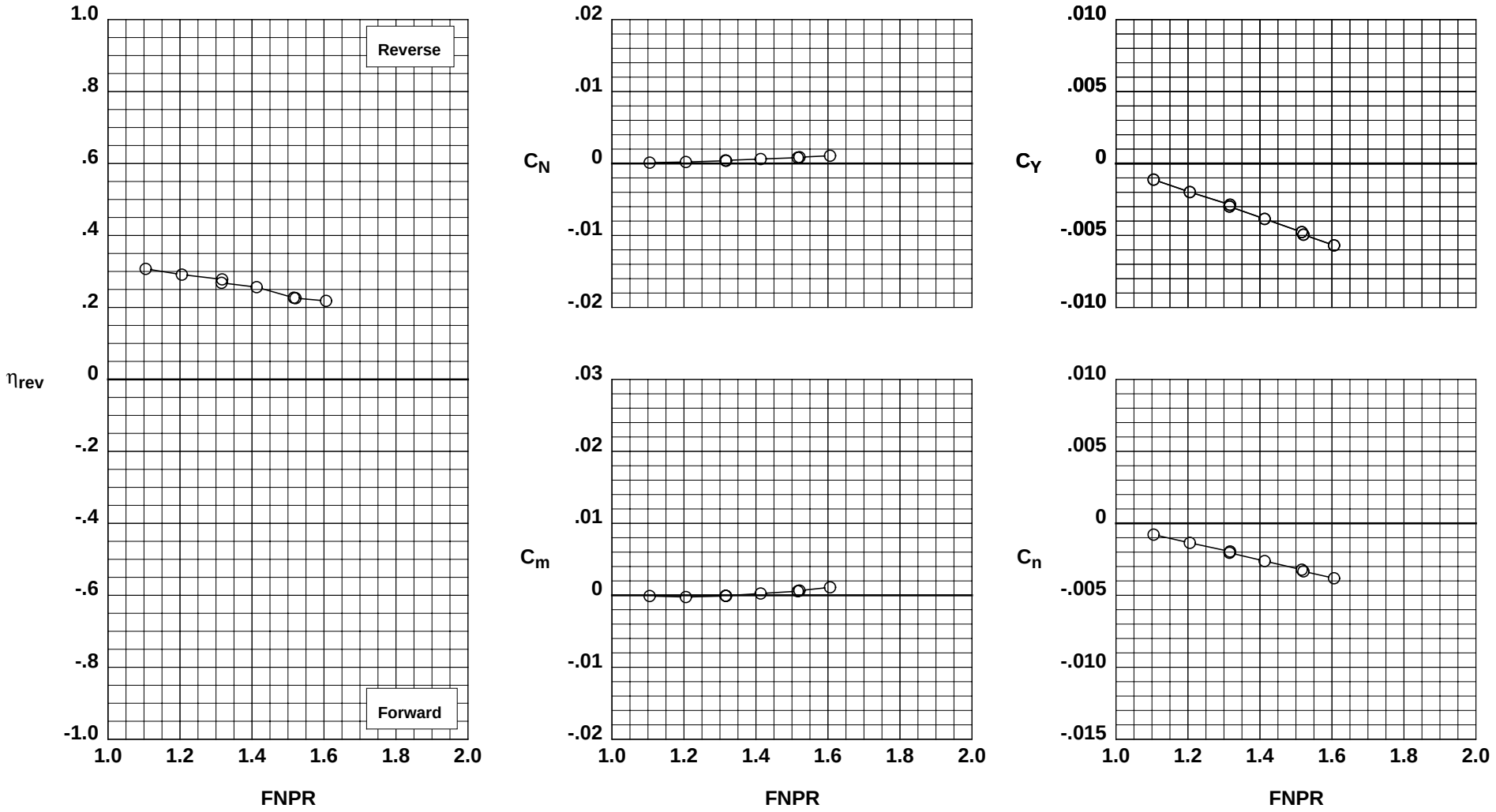

Figure H-43. Wing-mounted thrust reverser performance characteristics for configuration 743.

Operation Mode: Dual Flow
Deflector Mount Position: Parallel
Deflector Chord Lengths: Long/Long/Long
Deflector Angles: 60°/-15°/45°
Deflector Fences: Installed
Ground Plane: 36" FSE

	Test	Run	Configuration
○	1001	67	744

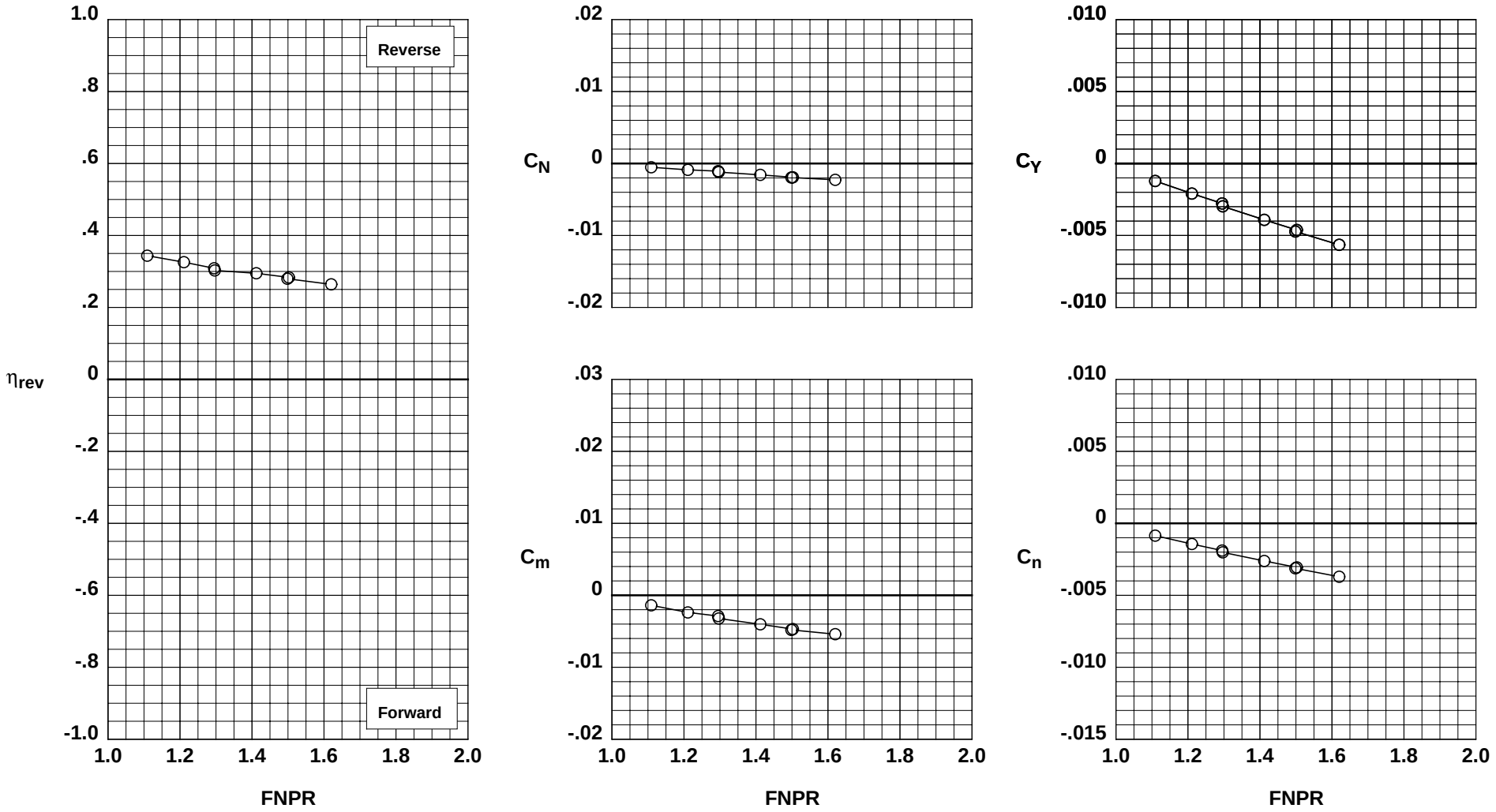

Figure H-44. Wing-mounted thrust reverser performance characteristics for configuration 744.

Operation Mode: Dual Flow
Deflector Mount Position: Parallel
Deflector Chord Lengths: Short/Short/Long
Deflector Angles: 60°/-15°/30°
Deflector Fences: Installed
Ground Plane: 36" FSE

	Test	Run	Configuration
○	1001	68	745

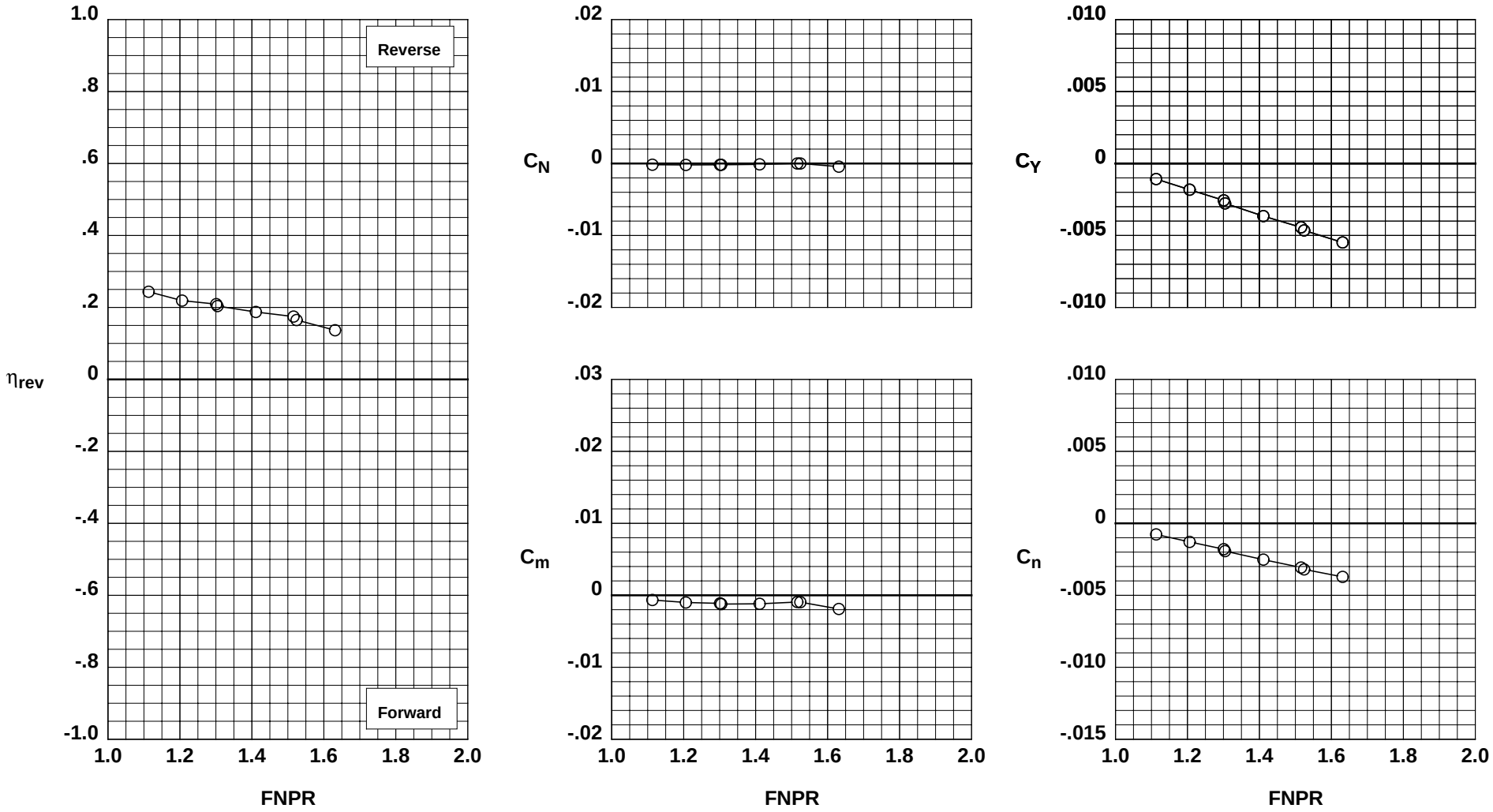

Figure H-45. Wing-mounted thrust reverser performance characteristics for configuration 745.

Operation Mode: Dual Flow
Deflector Mount Position: Parallel
Deflector Chord Lengths: Short/Short/Long
Deflector Angles: 60°/-15°/30°
Deflector Fences: Installed
Ground Plane: 18" FSE

	Test	Run	Configuration
○	1001	69	746

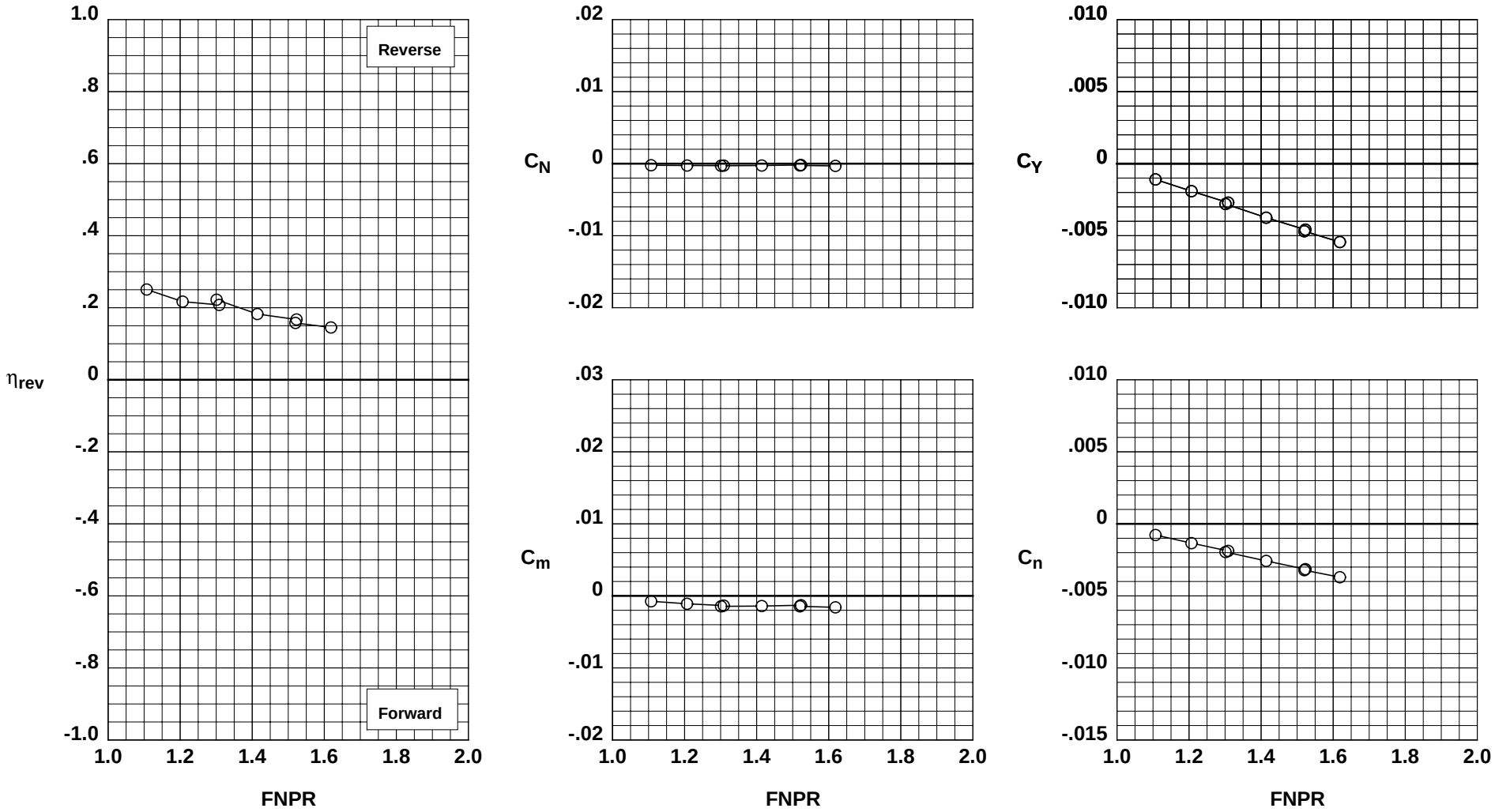

Figure H-46. Wing-mounted thrust reverser performance characteristics for configuration 746.

REPORT DOCUMENTATION PAGE

Form Approved
OMB No. 0704-0188

1. AGENCY USE ONLY (Leave blank)	2. REPORT DATE	3. REPORT TYPE AND DATES COVERED
	July 2000	Technical Memorandum

4. TITLE AND SUBTITLE
Static Performance of Six Innovative Thrust Reverser Concept for Subsonic Transport Applications, *Summary of the NASA Langley Innovative Thrust Reverser Test Program*

5. FUNDING NUMBERS
WU 522-25-31-01

6. AUTHOR(S)
Scott C. Asbury and Jeffrey A. Yetter

7. PERFORMING ORGANIZATION NAME(S) AND ADDRESS(ES)
NASA Langley Research Center
Hampton, VA 23681-2199

8. PERFORMING ORGANIZATION REPORT NUMBER
L-17975

9. SPONSORING/MONITORING AGENCY NAME(S) AND ADDRESS(ES)
National Aeronautics and Space Administration
Washington, DC 20546-0001

10. SPONSORING/MONITORING AGENCY REPORT NUMBER
NASA/TM-2000-210300

11. SUPPLEMENTARY NOTES

12a. DISTRIBUTION/AVAILABILITY STATEMENT
Unclassified-Unlimited
Subject Category 02 Distribution: Standard
Availability: NASA CASI (301) 621-0390

12b. DISTRIBUTION CODE

13. ABSTRACT *(Maximum 200 words)*

The NASA Langley Configuration Aerodynamics Branch has conducted an experimental investigation to study the static performance of innovative thrust reverser concepts applicable to high-bypass-ratio turbofan engines. Testing was conducted on a conventional separate-flow exhaust system configuration, a conventional cascade thrust reverser configuration, and six innovative thrust reverser configurations. The innovative thrust reverser configurations consisted of a cascade thrust reverser with porous fan-duct blocker, a blockerless thrust reverser, two core-mounted target thrust reversers, a multi-door crocodile thrust reverser, and a wing-mounted thrust reverser. Each of the innovative thrust reverser concepts offer potential weight savings and/or design simplifications over a conventional cascade thrust reverser design. Testing was conducted in the Jet-Exit Test Facility at NASA Langley Research Center using a 7.9%-scale exhaust system model with a fan-to-core bypass ratio of approximately 9.0. All tests were conducted with no external flow and cold, high-pressure air was used to simulate core and fan exhaust flows. Results show that the innovative thrust reverser concepts achieved thrust reverser performance levels which, when taking into account the potential for system simplification and reduced weight, may make them competitive with, or potentially more cost effective than current state-of-the-art thrust reverser systems.

14. SUBJECT TERMS	15. NUMBER OF PAGES
High-Bypass-Ratio, Reverser, Thrust Reverser, Turbofan Engines	369
	16. PRICE CODE: A16

17. SECURITY CLASSIFICATION OF REPORT	18. SECURITY CLASSIFICATION OF THIS PAGE	19. SECURITY CLASSIFICATION OF ABSTRACT	20. LIMITATION OF ABSTRACT
Unclassified	Unclassified	Unclassified	UL